can be used to advantage in formation flying if proper position is maintained. While downwash is induced between the wingtip vortices, upwash is induced outboard from the wingtips of any airplane in flight. Another airplane flying slightly aft and outboard from the wingtips of a lead airplane will be flying in a region of constant upwash. This upwash decreases induced drag and can significantly reduce the fuel consumed during a long flight for a large formation of airplanes. Migrating ducks and geese use this same strategy. Use the vortex model presented in Sec. 4.5 to develop an expression for the upwash angle that is induced outboard from the wingtip vortex shed from one semispan of an airplane's wing. Express this upwash angle as a function of the distance aft of the wing, the distance outboard from the center of shed vorticity, and any other parameters that you find to be important.

Chapter 6
Aircraft Controls and Maneuverability

6.1. Longitudinal Control and Maneuverability

From the material presented in the previous chapters, the student should now have a good understanding of the trim and static stability requirements for nonaccelerating flight. Both trim and static stability were defined only for an equilibrium flight condition. While the operation of an airplane in equilibrium flight is a very important consideration in aircraft design, it is also important to understand how aircraft controls are used to accelerate an airplane from one equilibrium state to another. The force that provides nearly all of the acceleration typically used to maneuver an airplane is the lift. For the most part, the aerodynamic controls of an airplane are designed to change the magnitude and direction of this force. Angle of attack governs the magnitude of the lift, and the elevator controls the angle of attack. The ailerons are used primarily to control the direction of the lift vector and the rudder is normally used only to coordinate the maneuver and eliminate the sideslip. Since the elevator provides pitch control, it controls the magnitude of the lift and is used in almost all airplane maneuvers.

In Chapter 4 we learned how the elevator is used to trim an airplane. To determine the elevator angle required for trim, we set the summation of normal forces and pitching moments both equal to zero. These two coupled equations are then solved for the equilibrium angle of attack and elevator deflection. Clearly, the elevator must be large enough to trim the airplane for any possible operating condition, with or without flaps deployed. However, simply being able to trim the airplane is not sufficient. The elevator must also be large enough to maneuver the airplane adequately over the full range of operating conditions as well.

While the elevator trim analysis was based on static equilibrium, for maneuverability analysis we consider accelerating flight. The elevator is used to accelerate the airplane in a direction normal to the flight path. Consider, for example, the constant-speed pull-up maneuver that is shown in Fig. 6.1.1. For this maneuver, the airspeed, V, is held constant but the airplane has an acceleration, a_N, that is normal to the flight path. This normal acceleration requires lift in excess of the weight. From Newton's second law we can write

$$\frac{W}{g} a_N = L - W \tag{6.1.1}$$

or

$$a_N = \left(\frac{L}{W} - 1\right) g \tag{6.1.2}$$

The ratio of the lift generated during an accelerating maneuver to the weight of the airplane is the load factor that was defined in Chapter 3. That is,

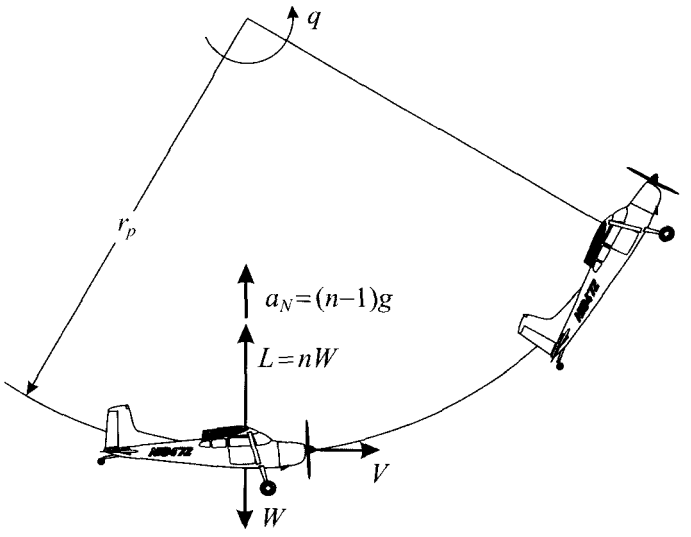


Figure 6.1.1. Constant-speed pull-up maneuver.

$$n \equiv \frac{L}{W} \tag{6.1.3}$$

Recall that load factor is usually stated in terms of g's. For example, a maneuver that produces a lift force that is five times the aircraft weight is said to be a "5-g maneuver." Using the definition of load factor with Eq. (6.1.2), the normal acceleration for the pull-up maneuver can be written

$$a_N = (n-1)g \tag{6.1.4}$$

The acceleration normal to the direction of flight can also be expressed in terms of the radius of curvature of the flight path and the airplane's forward airspeed,

$$a_N = \frac{V^2}{r_p} \tag{6.1.5}$$

where r_p is the radius of curvature for the pull-up maneuver. Using Eq. (6.1.4) to express the normal acceleration in terms of the load factor, Eq. (6.1.5) is solved for the radius of curvature,

$$r_p = \frac{V^2}{(n-1)g} \tag{6.1.6}$$

As the airplane travels this curved path it rotates in pitch, as can be seen in Fig. 6.1.1. This is where the elevator comes in. Elevator deflection is required to initiate and sustain

this rotation. The rate of pitching rotation about the aircraft center of gravity is called the *pitch rate* and is commonly given the symbol, q. If the airplane were to travel a curved path of radius r_p at constant speed for one complete revolution, the total rotation angle would be 2π radian. The distance traveled would be $2\pi r_p$ and the time of rotation would be $2\pi r_p/V$. Since the rotation rate is the rotation angle divided by the rotation time, the pitch rate is the forward velocity divided by the radius of curvature,

$$q = \frac{2\pi}{2\pi r_p/V} = \frac{V}{r_p} \tag{6.1.7}$$

Using Eq. (6.1.6) to eliminate the radius of curvature from Eq. (6.1.7), the pitch rate for a constant-speed pull-up maneuver can be expressed in terms of the airspeed and the load factor,

$$q = \frac{(n-1)g}{V} \tag{6.1.8}$$

As the airplane negotiates the pull-up maneuver, the center of gravity has a translational velocity, V, and the airplane is rotating about its center of gravity with an angular velocity, q. Since the airplane is traveling a curved path through the air, the relative airflow past the airplane is also curved, as shown in Fig. 6.1.2. This curvature changes the pressure distribution and the aerodynamic forces and moments acting on the airplane. As can be seen in Fig. 6.1.2, all points aft of the center of gravity experience an increase in angle of attack, while all points forward of the center of gravity experience a decrease in angle of attack. While this alters the pressure distribution over the entire airplane, by far the most significant effects on the aerodynamic forces and moments result from the change in the angle of attack for the horizontal surface and the wing. From Fig. 6.1.2, the change in angle of attack for the horizontal surface can be written as

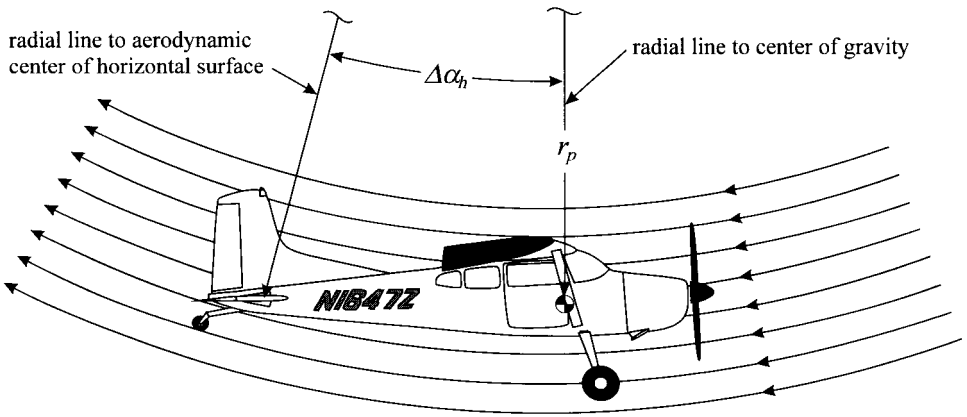


Figure 6.1.2. Airflow relative to the airplane during a pull-up maneuver.

$$\Delta\alpha_h = \tan^{-1}\left(\frac{l_h}{r_p}\right) \cong \frac{l_h}{r_p} \tag{6.1.9}$$

where again l_h is the distance that the aerodynamic center of the horizontal surface is aft of the center of gravity and r_p is the radius of curvature. For an aft tail, this change in angle of attack is positive, and for a forward canard, the change is negative. From Eq. (6.1.7), the radius of curvature is the forward velocity divided by the pitch rate. Thus, Eq. (6.1.9) can be written

$$\Delta\alpha_h = \frac{l_h q}{V} \tag{6.1.10}$$

Unlike the angle of attack, the pitch rate, q, is not dimensionless. Thus, in order to maintain all variables in dimensionless form, it is standard convention to define a dimensionless pitch rate to be

$$\overline{q} \equiv \frac{q\bar{c}_w/2}{V} \tag{6.1.11}$$

The choice of $\bar{c}_w/2$ as the characteristic length is the usual convention. However, this is arbitrary and has no real physical significance. Other characteristic lengths could and have been used. Using Eq. (6.1.11) in Eq. (6.1.10), we can write

$$\Delta\alpha_h = \frac{2l_h}{\bar{c}_w}\overline{q} \tag{6.1.12}$$

Similarly, for the wing we can write

$$\Delta\alpha_w = \frac{2l_w}{\bar{c}_w}\overline{q} \tag{6.1.13}$$

These changes in angle of attack affect both the lift and the pitching moment for the airplane. In the range of linear lift, the lift coefficients for the wing and the horizontal surface are, respectively,

$$C_{L_w} = C_{L_w,\alpha}(\alpha + \Delta\alpha_w + \alpha_{0w} - \alpha_{L0w}) \tag{6.1.14}$$

$$C_{L_h} = C_{L_h,\alpha}(\alpha + \Delta\alpha_h + \alpha_{0h} - \alpha_{L0h} - \varepsilon_d + \varepsilon_e\delta_e) \tag{6.1.15}$$

Thus, assuming no vertical offsets and using the effects of pitch rate from Eqs. (6.1.12) and (6.1.13), the total lift coefficient for the two surfaces combined is

$$\begin{aligned} C_L = {} & C_{L_w,\alpha}\left(\alpha + \frac{2l_w}{\bar{c}_w}\overline{q} + \alpha_{0w} - \alpha_{L0w}\right) \\ & + \frac{S_h}{S_w}\eta_h C_{L_h,\alpha}\left(\alpha + \frac{2l_h}{\bar{c}_w}\overline{q} + \alpha_{0h} - \alpha_{L0h} - \varepsilon_d + \varepsilon_e\delta_e\right) \end{aligned} \tag{6.1.16}$$

and the total moment coefficient is

$$\begin{aligned} C_m &= C_{m_w} - \frac{l_w}{\bar{c}_w} C_{L_w,\alpha}\left(\alpha + \frac{2l_w}{\bar{c}_w}\bar{q} + \alpha_{0w} - \alpha_{L0w}\right) \\ &+ \frac{S_h \bar{c}_h}{S_w \bar{c}_w}\eta_h (C_{m_h 0} + C_{m_h,\delta_e}\delta_e) \\ &- \frac{S_h l_h}{S_w \bar{c}_w}\eta_h C_{L_h,\alpha}\left(\alpha + \frac{2l_h}{\bar{c}_w}\bar{q} + \alpha_{0h} - \alpha_{L0h} - \varepsilon_d + \varepsilon_e\delta_e\right) \end{aligned} \tag{6.1.17}$$

These two equations can be written as

$$C_L = C_{L0} + C_{L,\alpha}\,\alpha + C_{L,\bar{q}}\,\bar{q} + C_{L,\delta_e}\,\delta_e \tag{6.1.18}$$

$$C_m = C_{m0} + C_{m,\alpha}\,\alpha + C_{m,\bar{q}}\,\bar{q} + C_{m,\delta_e}\,\delta_e \tag{6.1.19}$$

where

$$C_{L0} = C_{L_w,\alpha}\,(\alpha_{0w} - \alpha_{L0w}) + \frac{S_h}{S_w}\eta_h C_{L_h,\alpha}\,(\alpha_{0h} - \alpha_{L0h} - \varepsilon_{d0}) \tag{6.1.20}$$

$$C_{L,\alpha} = C_{L_w,\alpha} + \frac{S_h}{S_w}\eta_h C_{L_h,\alpha}(1 - \varepsilon_{d,\alpha}) \tag{6.1.21}$$

$$C_{L,\bar{q}} = 2\frac{l_w}{\bar{c}_w}C_{L_w,\alpha} + 2\frac{S_h l_h}{S_w \bar{c}_w}\eta_h C_{L_h,\alpha} \tag{6.1.22}$$

$$C_{L,\delta_e} = \frac{S_h}{S_w}\eta_h C_{L_h,\alpha}\varepsilon_e \tag{6.1.23}$$

$$\begin{aligned} C_{m0} &= C_{m_w} - \frac{l_w}{\bar{c}_w}C_{L_w,\alpha}\,(\alpha_{0w} - \alpha_{L0w}) + \frac{S_h \bar{c}_h}{S_w \bar{c}_w}\eta_h C_{m_h 0} \\ &- \frac{S_h l_h}{S_w \bar{c}_w}\eta_h C_{L_h,\alpha}\,(\alpha_{0h} - \alpha_{L0h} - \varepsilon_{d0}) \end{aligned} \tag{6.1.24}$$

$$C_{m,\alpha} = -\frac{l_w}{\bar{c}_w}C_{L_w,\alpha} - \frac{S_h l_h}{S_w \bar{c}_w}\eta_h C_{L_h,\alpha}(1 - \varepsilon_{d,\alpha}) \tag{6.1.25}$$

$$C_{m,\bar{q}} = -2\frac{l_w^2}{\bar{c}_w^2}C_{L_w,\alpha} - 2\frac{S_h l_h^2}{S_w \bar{c}_w^2}\eta_h C_{L_h,\alpha} \tag{6.1.26}$$

$$C_{m,\delta_e} = \frac{S_h \bar{c}_h}{S_w \bar{c}_w}\eta_h C_{m_h,\delta_e} - \frac{S_h l_h}{S_w \bar{c}_w}\eta_h C_{L_h,\alpha}\varepsilon_e \tag{6.1.27}$$

The coefficient $C_{m,\bar{q}}$ is the change in the pitching moment coefficient with respect to the dimensionless pitch rate. This is commonly referred to as the *pitch-damping derivative*. Notice that in unstalled flight, this derivative is always negative. In the absence of stall, the only parameters in Eq. (6.1.26) that can ever be negative are l_w and l_h. Since both of these parameters are squared in Eq. (6.1.26), the pitch-damping derivative is negative. This means that the contribution to the pitching moment that results from the pitch rate always opposes the pitching motion. A positive pitch rate will produce a negative pitching moment, and a negative pitch rate will produce a positive pitching moment.

When an airplane is flying in trimmed flight, the pitch rate is zero. As the pilot first introduces an elevator deflection to initiate a pull-up maneuver, a nonzero pitching moment is generated about the CG. This causes acceleration in pitch, which in turn produces an increasing pitch rate. As the pitch rate increases, the pitching moment decreases as a result of pitch damping. The acceleration in pitch quickly results in a pitch rate that returns the pitching moment to zero. At this point, the negative pitching moment that results from the positive pitch rate exactly balances the positive pitching moment produced by the added elevator deflection. Since there is no longer an imbalance in the total pitching moment, the pitch rate cannot increase farther without additional elevator deflection.

As a measure of the airplane's maneuverability in pitch, we wish to predict the maximum normal acceleration that could be sustained in a constant-speed pull-up maneuver with a given elevator deflection. To this end, we apply the definition of dimensionless pitch rate from Eq. (6.1.11) to the pitch rate relation expressed in Eq. (6.1.8). This gives

$$\bar{q} = (n-1)\frac{g\bar{c}_w}{2V^2} \tag{6.1.28}$$

This equation relates the maximum dimensionless pitch rate to the load factor for a constant-speed pull-up maneuver. From the definition of load factor, the lift coefficient for the maneuver is

$$C_L \equiv \frac{L}{\frac{1}{2}\rho V^2 S_w} = \frac{L}{W}\frac{W}{\frac{1}{2}\rho V^2 S_w} = nC_W \tag{6.1.29}$$

where C_W is sometimes called the *weight coefficient* and is defined as

$$C_W \equiv \frac{W}{\frac{1}{2}\rho V^2 S_w} \tag{6.1.30}$$

Maximum normal acceleration for any given elevator deflection occurs at maximum pitch rate, when the net pitching moment is zero. Thus, using Eqs. (6.1.28) and (6.1.29) in Eqs. (6.1.18) and (6.1.19) while setting the total pitching moment coefficient to zero gives

$$C_{L,\alpha}\,\alpha + C_{L,\delta_e}\,\delta_e = nC_W - C_{L0} - C_{L,\bar{q}}\,(n-1)\frac{g\bar{c}_w}{2V^2} \tag{6.1.31}$$

$$C_{m,\alpha}\,\alpha + C_{m,\delta_e}\,\delta_e = -C_{m0} - C_{m,\bar{q}}\,(n-1)\frac{g\bar{c}_w}{2V^2} \tag{6.1.32}$$

For any given load factor, these two equations are readily solved for the angle of attack and the elevator deflection,

$$\alpha = \frac{(nC_W - C_{L0})C_{m,\delta_e} + C_{L,\delta_e}\,C_{m0} + (C_{L,\delta_e}\,C_{m,\bar{q}} - C_{L,\bar{q}}\,C_{m,\delta_e})(n-1)(g\bar{c}_w/2V^2)}{C_{L,\alpha}\,C_{m,\delta_e} - C_{L,\delta_e}\,C_{m,\alpha}} \tag{6.1.33}$$

$$\delta_e = -\frac{(nC_W - C_{L0})C_{m,\alpha} + C_{L,\alpha}\,C_{m0} + (C_{L,\alpha}\,C_{m,\bar{q}} - C_{L,\bar{q}}\,C_{m,\alpha})(n-1)(g\bar{c}_w/2V^2)}{C_{L,\alpha}\,C_{m,\delta_e} - C_{L,\delta_e}\,C_{m,\alpha}} \tag{6.1.34}$$

Since trimmed flight can be viewed as a 1-g maneuver, the elevator deflection required for trim can be found as a special case of Eq. (6.1.34) with the load factor set to 1.0.

An important measure of maneuverability for an airplane is the increase in elevator deflection that is required to produce a given level of normal acceleration. This is typically specified as the elevator deflection that is required to produce a unit increase in load factor. This can be found by differentiating Eq. (6.1.34) with respect to n,

$$\frac{\partial \delta_e}{\partial n} = -\frac{C_W C_{m,\alpha} + (C_{L,\alpha}\,C_{m,\bar{q}} - C_{L,\bar{q}}\,C_{m,\alpha})(g\bar{c}_w/2V^2)}{C_{L,\alpha}\,C_{m,\delta_e} - C_{L,\delta_e}\,C_{m,\alpha}} \tag{6.1.35}$$

This derivative is commonly referred to as the *elevator angle per g*, because it specifies the elevator deflection required to sustain each additional g of normal acceleration, beyond the 1 g that is required to sustain trimmed flight. It provides a measure of airplane maneuverability. The smaller this derivative is, the more maneuverable the airplane. In other words, when this derivative is small, large accelerations are produced with small elevator deflections. While maneuverability is important, particularly for aerobatics and combat, if the elevator angle per g is too small, the airplane becomes difficult to fly.

We have previously seen that the location of the center of gravity has a profound effect on airplane stability. In a similar manner, the location of the CG also affects maneuverability. Since we are neglecting vertical offsets, from Eq. (4.4.13), the pitch stability derivative can be written in terms of the lift slope and the static margin,

$$C_{m,\alpha} = -\frac{l_{np}}{\bar{c}_w} C_{L,\alpha} \tag{6.1.36}$$

Using Eq. (6.1.36) to eliminate the pitch stability derivative, Eq. (6.1.35) can be written in the form

$$\frac{\partial \delta_e}{\partial n} = -\frac{C_W - C_{L,\bar{q}}\,(g\bar{c}_w/2V^2)}{C_{m,\delta_e} + C_{L,\delta_e}\,(l_{np}/\bar{c}_w)}\left[\frac{C_{m,\bar{q}}\,(g\bar{c}_w/2V^2)}{C_W - C_{L,\bar{q}}\,(g\bar{c}_w/2V^2)} - \frac{l_{np}}{\bar{c}_w}\right] \tag{6.1.37}$$

Following the development that was presented in Example 4.4.2, we let x denote the *aerodynamic coordinate* measured aft of some fixed point on the airplane. (Remember, the x-axis points aft and the x_b-axis points forward; see Figs. 1.1.1 and 5.1.1.) We then have

$$l_{np} = x_{np} - x_{CG} \tag{6.1.38}$$

Using this in Eq. (6.1.37) gives

$$\frac{\partial \delta_e}{\partial n} = -\frac{C_W - C_{L,\bar{q}}\,(g\bar{c}_w/2V^2)}{C_{m,\delta_e} + C_{L,\delta_e}\,[(x_{np} - x_{CG})/\bar{c}_w]}\left[\frac{C_{m,\bar{q}}\,(g\bar{c}_w/2V^2)}{C_W - C_{L,\bar{q}}\,(g\bar{c}_w/2V^2)} - \frac{x_{np}}{\bar{c}_w} + \frac{x_{CG}}{\bar{c}_w}\right] \tag{6.1.39}$$

By examining the three terms in the brackets on the right-hand side of Eq. (6.1.39), we see that there is some particular location for the center of gravity that will cause the elevator angle per g to go to zero. With the CG located at this point, an infinite acceleration would result from an infinitesimal elevator deflection. This would make it impossible to control the airplane. The CG location that causes the elevator angle per g to go to zero is commonly called the *stick-fixed maneuver point* and will be denoted as x_{mp}. From Eq. (6.1.39) we see that

$$\frac{x_{mp}}{\bar{c}_w} = \frac{x_{np}}{\bar{c}_w} - \frac{C_{m,\bar{q}}}{C_W\,(2V^2/g\bar{c}_w) - C_{L,\bar{q}}} \tag{6.1.40}$$

Similar to the stick-fixed static margin, the distance aft from the CG to the stick-fixed maneuver point, expressed as a fraction of the mean chord, is called the *stick-fixed maneuver margin*,

$$\frac{l_{mp}}{\bar{c}_w} \equiv \frac{x_{mp} - x_{CG}}{\bar{c}_w} = \frac{l_{np}}{\bar{c}_w} - \frac{C_{m,\bar{q}}}{C_W\,(2V^2/g\bar{c}_w) - C_{L,\bar{q}}} \tag{6.1.41}$$

Since both $C_{m,\bar{q}}$ and $C_{L,\bar{q}}$ depend on the location of the CG, finding the stick-fixed maneuver point and maneuver margin from Eqs. (6.1.40) and (6.1.41) is not quite as simple as it looks. However, we can deduce the relative position of the maneuver point by examining the signs of the various terms in Eq. (6.1.40).

The weight coefficient, C_W, is positive and the term $2V^2/g\bar{c}_w$ is positive and quite large. So, in general,

$$C_{L,\bar{q}} < C_W\,(2V^2/g\bar{c}_w)$$

and

$$C_W\,(2V^2/g\bar{c}_w) - C_{L,\bar{q}} > 0$$

As previously discussed, the pitch damping derivative is always negative in unstalled flight. Thus,

$$\frac{C_{m,\bar{q}}}{C_W\,(2V^2/g\bar{c}_w) - C_{L,\bar{q}}} < 0$$

Using this result with Eq. (6.1.40), we see that **the stick-fixed maneuver point is always aft of the stick-fixed neutral point**. Thus, the maneuver margin is always greater than the static margin, and if the airplane is statically stable, the maneuver margin will always be positive. Therefore, **it is not possible for a statically stable airplane to have a zero stick-fixed maneuver margin.**

Although a positive static margin will always assure a positive maneuver margin, many airplanes have been designed, built, and flown with a negative static margin. In fact, the 1903 Wright Flyer had a static margin that was slightly negative. While a positive static margin is desirable for good human handling qualities, it is possible for a human pilot to control an airplane with a static margin that is somewhat negative. Furthermore, to improve maneuverability, most modern fighters have a negative static margin. Such airplanes are typically fitted with computer control systems, which are called *stability augmentation systems*. A computer control system has a much faster reaction time than any human pilot does. Thus, a computer can control an airplane that would be much too unstable for a human pilot. However, even a computer cannot control an airplane with a zero maneuver margin. For this reason, **if an airplane is to be operated with a negative static margin, great care must be taken to assure that the center of gravity is always kept forward of the stick-fixed maneuver point.**

Because C_{m,δ_e}, $C_{m,\bar{q}}$, and $C_{L,\bar{q}}$ all depend on the position of the center of gravity, it is not at all obvious from Eq. (6.1.39) exactly how the elevator angle per g varies with the location of the center of gravity. This is examined in the following example.

EXAMPLE 6.1.1. For the wing-tail combination described in Example 4.4.2, plot the elevator angle per g at 80 mph and sea level as a function of the location of the CG measured relative to the quarter-chord of the main wing.

Solution. Let x denote the distance measured aft of the quarter-chord of the main wing. For this airplane we have

$$S_w = 180\ \text{ft}^2,\quad b_w = 33\ \text{ft},\quad C_{L_w,\alpha} = 4.44,\quad C_{m_w} = -0.053,\quad W = 2{,}700\ \text{lbf},$$
$$S_h = 36\ \text{ft}^2,\quad b_h = 12\ \text{ft},\quad C_{L_h,\alpha} = 3.97,\quad C_{m_h 0} = 0.0,\quad C_{m_h,\delta_e} = -0.55,$$
$$\varepsilon_e = 0.60,\quad x_h = 15\ \text{ft},\quad \eta_h = 1.0$$

From Example 4.4.2,

$$C_{L,\delta_e} = \frac{S_h}{S_w}\eta_h C_{L_h,\alpha}\,\varepsilon_e = 0.4764$$

and the weight coefficient is simply the lift coefficient required for steady level flight,

$$C_W = \frac{W}{\frac{1}{2}\rho V^2 S_w} = 0.9168$$

Also from Example 4.4.2, the change in pitching moment coefficient with respect to elevator deflection for this wing-tail combination is

$$C_{m,\delta_e} = \frac{S_h \bar{c}_h}{S_w \bar{c}_w}\eta_h C_{m_h,\delta_e} - \frac{S_h(x_h - x_{CG})}{S_w \bar{c}_w}\eta_h C_{L_h,\alpha}\varepsilon_e$$
$$= 0.4764\,\hat{x}_{CG} - 1.3706$$

where $\hat{x}_{CG} = x_{CG}/\bar{c}_w$. The position of the neutral point was found to be

$$\frac{x_{np}}{\bar{c}_w} = \frac{l_{np}}{\bar{c}_w} - \frac{l_w}{\bar{c}_w} = 0.2504$$

At 80 mph,

$$\frac{g\bar{c}_w}{2V^2} = \frac{32.2(180/33)}{2(80\times 5{,}280/3{,}600)^2} = 0.006379$$

From Eq. (6.1.22),

$$C_{L,\bar{q}} = 2\frac{-x_{CG}}{\bar{c}_w}C_{L_w,\alpha} + 2\eta_h \frac{S_h(x_h - x_{CG})}{S_w \bar{c}_w}C_{L_h,\alpha}$$
$$= 4.367 - 10.468\hat{x}_{CG}$$

and from Eq. (6.1.26),

$$C_{m,\bar{q}} = -2\frac{(-x_{CG})^2}{\bar{c}_w^2}C_{L_w,\alpha} - 2\eta_h \frac{S_h(x_h - x_{CG})^2}{S_w \bar{c}_w^2}C_{L_h,\alpha}$$
$$= -12.009 + 8.734\hat{x}_{CG} - 10.468\hat{x}_{CG}^2$$

Using these results in Eq. (6.1.39), the elevator angle per g can be written as

$$\frac{\partial \delta_e}{\partial n} = -\frac{C_W - C_{L,\bar{q}}\,(g\bar{c}_w/2V^2)}{C_{m,\delta_e} + C_{L,\delta_e}\,[(x_{np} - x_{CG})/\bar{c}_w]}\left[\frac{C_{m,\bar{q}}\,(g\bar{c}_w/2V^2)}{C_W - C_{L,\bar{q}}\,(g\bar{c}_w/2V^2)} - \frac{x_{np}}{\bar{c}_w} + \frac{x_{CG}}{\bar{c}_w}\right]$$

$$= -\frac{0.9168 - (4.367 - 10.468\hat{x}_{CG})(0.006379)}{0.4764\hat{x}_{CG} - 1.3706 + 0.4764(0.2504 - \hat{x}_{CG})}$$

$$\times\left[\frac{(-12.009 + 8.734\hat{x}_{CG} - 10.468\hat{x}_{CG}^2)(0.006379)}{0.9168 - (4.367 - 10.468\hat{x}_{CG})(0.006379)} - 0.2504 + \hat{x}_{CG}\right]$$

or after simplifying,

$$\frac{\partial \delta_e}{\partial n} = -\frac{139.35 + 10.468\hat{x}_{CG}}{-196.16}\left[\frac{-12.009 + 8.734\hat{x}_{CG} - 10.468\hat{x}_{CG}^2}{139.35 + 10.468\hat{x}_{CG}} + (-0.2504 + \hat{x}_{CG})\right]$$

$$= \frac{-12.009 + 8.734\hat{x}_{CG} - 10.468\hat{x}_{CG}^2 - 34.893 - 2.621\hat{x}_{CG} + 139.35\hat{x}_{CG} + 10.468\hat{x}_{CG}^2}{196.16}$$

$$= \frac{-46.902 + 145.463\hat{x}_{CG}}{196.16} = \underline{-0.2391 + 0.7416\hat{x}_{CG}}$$

So we see that within the approximations used for this example, the elevator angle per g is a linear function of CG location. This is not obvious from Eq. (6.1.39). Results for the particular wing-tail combination used in the present example are shown in Fig. 6.1.3 for airspeeds of 80, 120, and 160 mph.

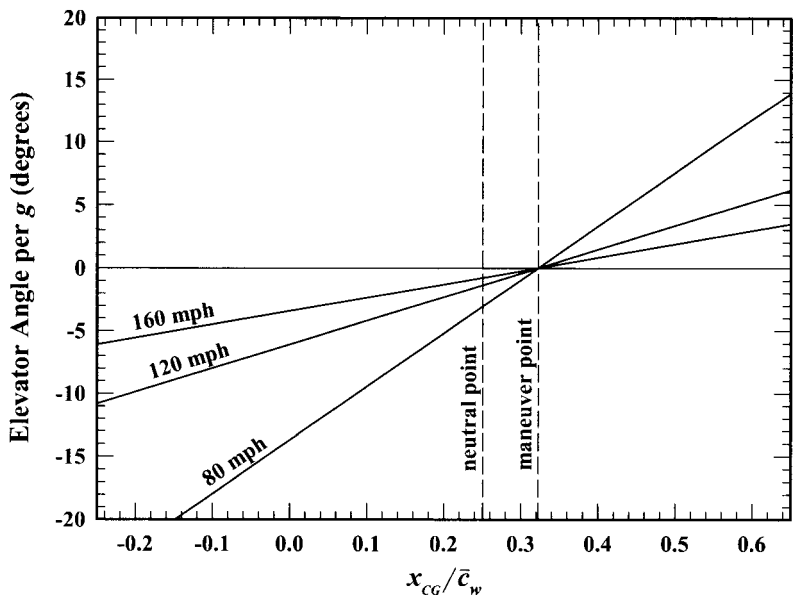


Figure 6.1.3. Elevator angle per g as a function of CG location measured aft of the wing quarter-chord for the airplane in Example 6.1.1.

From Example 6.1.1 we see that within the approximations used, the location of the stick-fixed maneuver point is independent of airspeed. We also see that for a stable aircraft, the elevator deflection required to produce a given normal acceleration increases as the airspeed is decreased. Moreover, as the CG is moved forward, the elevator deflection required for a given maneuver is increased. At low airspeed with the CG forward of the wing quarter-chord, large elevator deflections are required to maneuver the airplane. In Fig. 4.4.3, we saw that large negative elevator deflections are required just to trim the airplane under such conditions. Furthermore, with flaps fully deployed in landing configuration, this condition is further aggravated.

Also notice from Fig. 6.1.3 that as the CG is moved aft, the elevator control becomes more responsive, so the airplane becomes more maneuverable. That is, smaller elevator deflections are required to produce a given normal acceleration. With the CG located at the stick-fixed maneuver point, the elevator control becomes so sensitive that an infinitesimal elevator deflection will result in an infinite normal acceleration. With the CG located aft of the stick-fixed maneuver point, the elevator deflection required to produce a constant normal acceleration is reversed.

6.2. Effects of Structural Flexibility

To this point we have considered the airplane to be a rigid body. In reality, no structure is completely rigid. This is particularly true of an airplane. By necessity, airplanes are designed to be as light as possible, and elastic flexibility is a natural characteristic of lightweight structures. We have seen that even very small changes in airplane geometry (particularly angular changes) can have very significant effects on the aerodynamic forces and moments produced on the airplane. Furthermore, because of unavoidable elastic flexibility, the geometry of the airplane is not fixed but changes as the aerodynamic forces and moments are applied to the structure. For example, when an airplane is at rest on the ground, the fuselage supports the weight of the wings. When the airplane is in the air, the wings support the weight of the fuselage. The lift produced

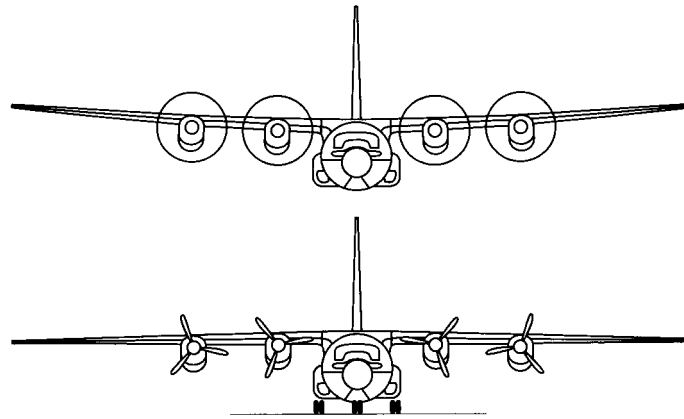


Figure 6.2.1. Elastic deformation of the wings resulting from aerodynamic lift.

by the wings results in significant elastic deformation, as shown in Fig. 6.2.1. In a large airplane, the wingtips can deflect several feet as a result of the applied lift. This deformation in turn affects the forces and moments acting on the airplane. This is only one of many ways in which an airplane can deform under aerodynamic loading.

The study of the coupling between the aerodynamic forces and moment and the elastic deformation of the airplane is a separate branch of aeronautical engineering known as *aeroelasticity*. Complete textbooks have been written on aeroelasticity and no attempt is made here to cover this topic in detail. However, to give the student an appreciation for the importance of the topic, a very simple example is considered. The serious student is encouraged to study the topic further, either through formal coursework or independent study.

Like the wings of an airplane, the structure supporting the tail is subject to elastic deformation. As shown schematically in Fig. 6.2.2, the stiffness of a typical tail boom is not constant but varies along the length of the boom, from the center of gravity to the aerodynamic center of the horizontal surface. Typically, the fuselage is quite stiff near the CG. However, the aft portion near the tail is usually much more flexible. The aerodynamic forces and moments produced on the tail cause the tail boom to deflect. This deflection changes the angle of attack for the horizontal surface, which in turn affects the aerodynamic load. For example, when the elevator is deflected downward, the lift on the tail is increased and the pitching moment becomes more negative. Thus, both the force and the moment resulting from a downward elevator deflection tend to deflect the tail boom upward and rotate the tail to a more negative angle of attack, as shown in Fig. 6.2.3. The reduction in tail angle of attack, which results from this elastic deformation, reduces the lift produced by the tail. Thus, flexibility in the tail boom

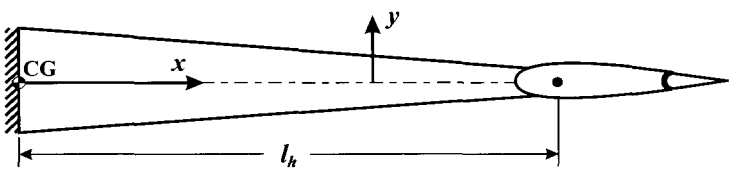


Figure 6.2.2. Schematic diagram of the structure supporting the aft tail of an airplane.

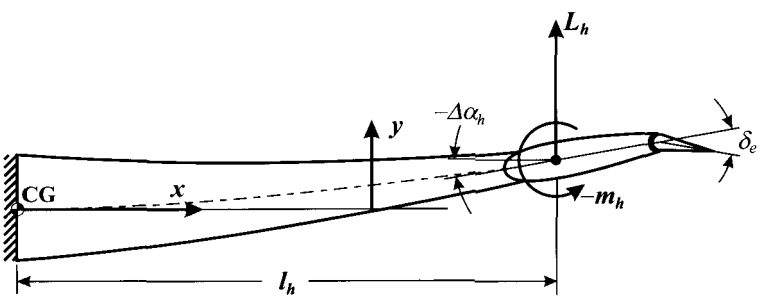


Figure 6.2.3. Deflection of the aft tail as a result of elevator deflection.

reduces the effectiveness of the elevator to produce the pitching moments necessary to trim and maneuver the airplane.

The elastic deflection of a beam can be found by relating the local curvature to the local bending moment and the local stiffness. The governing differential equation is

$$\frac{d^2y}{dx^2} = \frac{M_b}{EI} \tag{6.2.1}$$

where M_b is the local bending moment, E is the material modulus of elasticity, and I is the local area moment of inertia. In terms of the lift and pitching moment acting on the tail, this can be written as

$$\frac{d^2y}{dx^2} = \frac{L_h(l_h - x) - m_h}{EI} \tag{6.2.2}$$

The change in tail angle of attack that results from bending of the tail boom is found by integrating this equation from the center of gravity to the aerodynamic center of the tail. This gives

$$\Delta\alpha_h = -\left.\frac{dy}{dx}\right|_{x=l_h} = m_h \int_{x=0}^{l_h} \frac{1}{EI}\,dx - L_h \int_{x=0}^{l_h} \frac{l_h - x}{EI}\,dx \tag{6.2.3}$$

The lift and pitching moment acting on the horizontal tail can be written as

$$L_h = \tfrac{1}{2}\rho V^2 S_h \eta_h C_{L_h,\alpha}[(1-\varepsilon_{d,\alpha})\alpha + \Delta\alpha_h + \alpha_{0h} - \alpha_{L0h} - \varepsilon_{d0} + \varepsilon_e\delta_e] \tag{6.2.4}$$

$$m_h = \tfrac{1}{2}\rho V^2 S_h \bar{c}_h \eta_h (C_{m_h 0} + C_{m_h,\delta_e}\,\delta_e) \tag{6.2.5}$$

So the change in the tail angle of attack must satisfy the equation

$$\begin{aligned}\Delta\alpha_h = {} & \left(\tfrac{1}{2}\rho V^2 S_h \bar{c}_h \eta_h \int_{x=0}^{l_h} \frac{1}{EI}\,dx\right)(C_{m_h 0} + C_{m_h,\delta_e}\,\delta_e) \\ & - \left(\tfrac{1}{2}\rho V^2 S_h \eta_h \int_{x=0}^{l_h} \frac{l_h - x}{EI}\,dx\right) C_{L_h,\alpha}[(1-\varepsilon_{d,\alpha})\alpha + \Delta\alpha_h + \alpha_{0h} - \alpha_{L0h} - \varepsilon_{d0} + \varepsilon_e\delta_e]\end{aligned} \tag{6.2.6}$$

or

$$\begin{aligned}\Delta\alpha_h = {} & K_m (C_{m_h 0} + C_{m_h,\delta_e}\,\delta_e) \\ & - K_L\, C_{L_h,\alpha}[(1-\varepsilon_{d,\alpha})\alpha + \Delta\alpha_h + \alpha_{0h} - \alpha_{L0h} - \varepsilon_{d0} + \varepsilon_e\delta_e]\end{aligned} \tag{6.2.7}$$

where

$$K_m \equiv \tfrac{1}{2}\rho V^2 S_h \bar{c}_h \eta_h \int_{x=0}^{l_h} \frac{1}{EI}\,dx \tag{6.2.8}$$

$$K_L \equiv \tfrac{1}{2}\rho V^2 S_h \eta_h \int_{x=0}^{l_h} \frac{l_h - x}{EI}\,dx \tag{6.2.9}$$

The elastic deflection angle for the horizontal tail appears on both sides of Eq. (6.2.7). This is readily solved for the elastic deflection angle to give

$$\Delta\alpha_h = -\frac{K_L C_{L_h,\alpha}[(1-\varepsilon_{d,\alpha})\alpha + \alpha_{0h} - \alpha_{L0h} - \varepsilon_{d0} + \varepsilon_e\delta_e] - K_m(C_{m_h 0} + C_{m_h,\delta_e}\delta_e)}{1 + K_L C_{L_h,\alpha}} \tag{6.2.10}$$

Thus, the change in the elastic deflection angle with respect to elevator angle is

$$\frac{\partial\Delta\alpha_h}{\partial\delta_e} = -\frac{K_L C_{L_h,\alpha}\varepsilon_e - K_m C_{m_h,\delta_e}}{1 + K_L C_{L_h,\alpha}} \tag{6.2.11}$$

The contribution that the aft horizontal stabilizer makes to the aerodynamic pitching moment about the airplane center of gravity is given by

$$(\Delta m_{CG})_h = m_h - l_h L_h \tag{6.2.12}$$

Using Eqs. (6.2.4) and (6.2.5), this can be written as

$$\begin{aligned}(\Delta m_{CG})_h &= \tfrac{1}{2}\rho V^2 S_h \bar{c}_h \eta_h (C_{m_h 0} + C_{m_h,\delta_e}\delta_e) \\ &\quad -\tfrac{1}{2}\rho V^2 S_h l_h \eta_h C_{L_h,\alpha}[(1-\varepsilon_{d,\alpha})\alpha + \Delta\alpha_h + \alpha_{0h} - \alpha_{L0h} - \varepsilon_{d0} + \varepsilon_e\delta_e]\end{aligned} \tag{6.2.13}$$

In dimensionless form, this gives

$$\begin{aligned}(\Delta C_m)_h &= \frac{S_h\bar{c}_h}{S_w\bar{c}_w}\eta_h(C_{m_h 0} + C_{m_h,\delta_e}\delta_e) \\ &\quad -\frac{S_h l_h}{S_w\bar{c}_w}\eta_h C_{L_h,\alpha}[(1-\varepsilon_{d,\alpha})\alpha + \Delta\alpha_h + \alpha_{0h} - \alpha_{L0h} - \varepsilon_{d0} + \varepsilon_e\delta_e]\end{aligned} \tag{6.2.14}$$

The total change in the pitching moment coefficient with respect to elevator deflection, including the effect of elastic deformation of the fuselage, is found by differentiating Eq. (6.2.14) with respect to δ_e. This gives

$$C_{m,\delta_e} \equiv \frac{\partial C_m}{\partial\delta_e} = \frac{S_h\bar{c}_h}{S_w\bar{c}_w}\eta_h C_{m_h,\delta_e} - \frac{S_h l_h}{S_w\bar{c}_w}\eta_h C_{L_h,\alpha}\left(\frac{\partial\Delta\alpha_h}{\partial\delta_e} + \varepsilon_e\right) \tag{6.2.15}$$

or after using Eq. (6.2.11),

$$C_{m,\delta_e} = \frac{S_h \bar{c}_h}{S_w \bar{c}_w} \eta_h C_{m_h,\delta_e} - \frac{S_h l_h}{S_w \bar{c}_w} \eta_h C_{L_h,\alpha} \left(\varepsilon_e - \frac{K_L C_{L_h,\alpha} \varepsilon_e - K_m C_{m_h,\delta_e}}{1 + K_L C_{L_h,\alpha}} \right) \tag{6.2.16}$$

In Eq. (6.2.16), ε_e denotes the rigid-body elevator effectiveness. From Eqs. (6.2.8) and (6.2.9), we see that both K_m and K_L are zero for a rigid airframe. However, for an airframe of finite stiffness, both K_m and K_L increase with the square of the airspeed. Thus, as the airspeed is increased, the actual elevator effectiveness is reduced, due to the flexibility of the fuselage. This reduces the capacity of the elevator to control the pitching moment for the airplane. From Eq. (6.2.16), the reduction in the elevator control derivative that results from fuselage bending can be expressed as

$$\left(\Delta C_{m,\delta_e}\right)_{fb} = \frac{S_h l_h}{S_w \bar{c}_w} \eta_h C_{L_h,\alpha} \left(\frac{K_L C_{L_h,\alpha} \varepsilon_e - K_m C_{m_h,\delta_e}}{1 + K_L C_{L_h,\alpha}} \right) \tag{6.2.17}$$

In a similar manner, bending of the fuselage also reduces the stability of the airplane. The contribution that the aft tail makes to the pitch stability derivative is found by differentiating Eq. (6.2.14) with respect to the angle of attack. This gives

$$\left(\Delta C_{m,\alpha}\right)_h = -\frac{S_h l_h}{S_w \bar{c}_w} \eta_h C_{L_h,\alpha} \left(1 - \varepsilon_{d,\alpha} + \frac{\partial \Delta \alpha_h}{\partial \alpha} \right) \tag{6.2.18}$$

Differentiating Eq. (6.2.10) with respect to angle of attack, we have

$$\frac{\partial \Delta \alpha_h}{\partial \alpha} = -\frac{K_L C_{L_h,\alpha} (1 - \varepsilon_{d,\alpha})}{1 + K_L C_{L_h,\alpha}} \tag{6.2.19}$$

Using Eq. (6.2.19) in Eq. (6.2.18), the net contribution that the aft tail makes to the pitch stability derivative, including the effect of fuselage bending, is found to be

$$\left(\Delta C_{m,\alpha}\right)_h = -\frac{S_h l_h}{S_w \bar{c}_w} \eta_h C_{L_h,\alpha} (1 - \varepsilon_{d,\alpha}) \left(1 - \frac{K_L C_{L_h,\alpha}}{1 + K_L C_{L_h,\alpha}} \right) \tag{6.2.20}$$

Thus, we find that the contribution to the pitch stability derivative that results from fuselage bending is

$$\left(\Delta C_{m,\alpha}\right)_{fb} = \frac{S_h l_h}{S_w \bar{c}_w} \eta_h C_{L_h,\alpha} (1 - \varepsilon_{d,\alpha}) \left(\frac{K_L C_{L_h,\alpha}}{1 + K_L C_{L_h,\alpha}} \right) \tag{6.2.21}$$

From this result, we see that fuselage bending makes a positive contribution to the pitch stability derivative and is therefore destabilizing.

From Eq. (4.4.13), the static margin can be written in terms of the pitch stability derivative and the lift slope,

$$\frac{l_{np}}{\bar{c}_w} = -\frac{C_{m,\alpha}}{C_{L,\alpha}} \tag{6.2.22}$$

Since the tail has only a small effect on the net lift slope for the complete airplane, combining Eq. (6.2.21) with Eq. (6.2.22), the effect of fuselage bending on the static margin is approximated as

$$\left(\frac{\Delta l_{np}}{\bar{c}_w}\right)_{fb} \cong -\frac{S_h l_h}{S_w \bar{c}_w}\eta_h \frac{C_{L_h,\alpha}}{C_{L,\alpha}}(1-\varepsilon_{d,\alpha})\left(\frac{K_L C_{L_h,\alpha}}{1+K_L C_{L_h,\alpha}}\right) \tag{6.2.23}$$

From Eq. (6.2.23), we see that fuselage bending causes the neutral point to move forward, making the airplane less stable. Both the decrease in elevator effectiveness and the decrease in stability become more severe at higher airspeeds.

EXAMPLE 6.2.1. To demonstrate the effects of insufficient tail boom stiffness, consider the wing-tail combination that is described in Examples 4.3.1 through 4.4.2. Assume that the tail is attached to the wing with a thin-walled aluminum tube ($E = 10\times10^6$ psi) that extends from the tail to the center of gravity, which is located at the wing quarter-chord. The aluminum tube has a constant cross-section of 4-inch diameter and 0.125-inch wall thickness. Neglecting all effects of compressibility but accounting for tail boom bending, plot C_{m,δ_e} and $C_{m,\alpha}$ as a function of the airspeed at sea level from 80 to 600 mph.

Solution. For this airplane we have

$$S_w = 180 \text{ ft}^2, \quad b_w = 33 \text{ ft}, \quad l_w = 0.0 \text{ ft}, \quad C_{L_w,\alpha} = 4.44, \quad C_{m_w} = -0.053,$$
$$S_h = 36 \text{ ft}^2, \quad b_h = 12 \text{ ft}, \quad l_h = 15.0 \text{ ft}, \quad C_{L_h,\alpha} = 3.97, \quad C_{m_{h_0}} = 0.0,$$
$$\varepsilon_e = 0.60, \quad C_{m_h,\delta_e} = -0.55, \quad \varepsilon_{d,\alpha} = 0.44, \quad \eta_h = 1.0$$

From Example 4.3.1, assuming a rigid tail boom, we find that

$$(C_{m,\alpha})_{\text{rigid}} = -\frac{l_w}{\bar{c}_w}C_{L_w,\alpha} - \frac{S_h l_h}{S_w \bar{c}_w}\eta_h C_{L_h,\alpha}(1-\varepsilon_{d,\alpha}) = -1.22276$$

$$(C_{m,\delta_e})_{\text{rigid}} = \frac{S_h \bar{c}_h}{S_w \bar{c}_w}\eta_h C_{m_h,\delta_e} - \frac{S_h l_h}{S_w \bar{c}_w}\eta_h C_{L_h,\alpha}\varepsilon_e = -1.37060$$

For this wing-tail combination, the tail volume ratio multiplied by the tail lift slope is

$$\frac{S_h l_h}{S_w \bar{c}_w} \eta_h C_{L_h,\alpha} = \frac{36(15.0)}{180(180/33)} 1.0(3.97) = 2.1835$$

The moment of inertia for a thin-walled tube of radius, r, and wall thickness, t, is

$$I = \pi r^3 t = \pi(2/12)^3 0.125/12 = 0.0001515\,\text{ft}^4$$

Thus, the tail boom stiffness is

$$EI = (10\times144\times10^6\ \text{lbf/ft}^2)0.0001515\,\text{ft}^4 = 218{,}160\,\text{lbf}\cdot\text{ft}^2$$

From Eqs. (6.2.8) and (6.2.9),

$$K_m \equiv \tfrac{1}{2}\rho V^2 S_h \bar{c}_h \eta_h \int_{x=0}^{l_h} \frac{1}{EI} dx$$

$$K_L \equiv \tfrac{1}{2}\rho V^2 S_h \eta_h \int_{x=0}^{l_h} \frac{l_h - x}{EI} dx$$

For a tail boom of constant cross-section

$$\int_{x=0}^{l_h} \frac{1}{EI} dx = \frac{l_h}{EI}$$

$$\int_{x=0}^{l_h} \frac{l_h - x}{EI} dx = \frac{l_h^2}{2EI}$$

Thus,

$$K_m = \frac{\rho V^2 S_h \bar{c}_h l_h \eta_h}{2EI} = \frac{\rho V^2 (36\ \text{ft}^2)(3\ \text{ft})(15.0\ \text{ft})1.0}{2(218{,}160\ \text{lbf}\cdot\text{ft}^2)} = \frac{\rho V^2}{269.33\ \text{lbf/ft}^2}$$

$$K_L = \frac{\rho V^2 S_h l_h^2 \eta_h}{4EI} = \frac{\rho V^2 (36\ \text{ft}^2)(15.0\ \text{ft})^2 1.0}{4(218{,}160\ \text{lbf}\cdot\text{ft}^2)} = \frac{\rho V^2}{107.73\ \text{lbf/ft}^2}$$

For example, at 200 mph,

$$K_m = \frac{\rho V^2}{269.33\ \text{lbf/ft}^2} = \frac{0.0023769(200\times5{,}280/3{,}600)^2}{269.33} = 0.75935$$

$$K_L = \frac{\rho V^2}{107.73 \text{ lbf/ft}^2} = \frac{0.0023769(200\times 5{,}280/3{,}600)^2}{107.73} = 1.89838$$

Thus, from Eqs. (6.2.17) and (6.2.21),

$$\begin{aligned} C_{m,\delta_e} &= (C_{m,\delta_e})_{\text{rigid}} + (\Delta C_{m,\delta_e})_{fb} \\ &= (C_{m,\delta_e})_{\text{rigid}} + \frac{S_h l_h}{S_w \bar{c}_w}\eta_h C_{L_h,\alpha}\left(\frac{K_L C_{L_h,\alpha}\varepsilon_e - K_m C_{m_h,\delta_e}}{1+K_L C_{L_h,\alpha}}\right) \\ &= -1.37060 + 2.1835\left(\frac{1.89838(3.97)(0.60) - 0.75935(-0.55)}{1+1.89838(3.97)}\right) = \underline{-0.107} \end{aligned}$$

$$\begin{aligned} C_{m,\alpha} &= (C_{m,\alpha})_{\text{rigid}} + (\Delta C_{m,\alpha})_{fb} \\ &= (C_{m,\alpha})_{\text{rigid}} + \frac{S_h l_h}{S_w \bar{c}_w}\eta_h C_{L_h,\alpha}(1-\varepsilon_{d,\alpha})\left(\frac{K_L C_{L_h,\alpha}}{1+K_L C_{L_h,\alpha}}\right) \\ &= -1.22276 + 2.1835(1-0.44)\left(\frac{1.89838(3.97)}{1+1.89838(3.97)}\right) = \underline{-0.143} \end{aligned}$$

Repeating these calculations for airspeeds from 80 to 600 mph, the results shown in Fig. 6.2.4 are obtained.

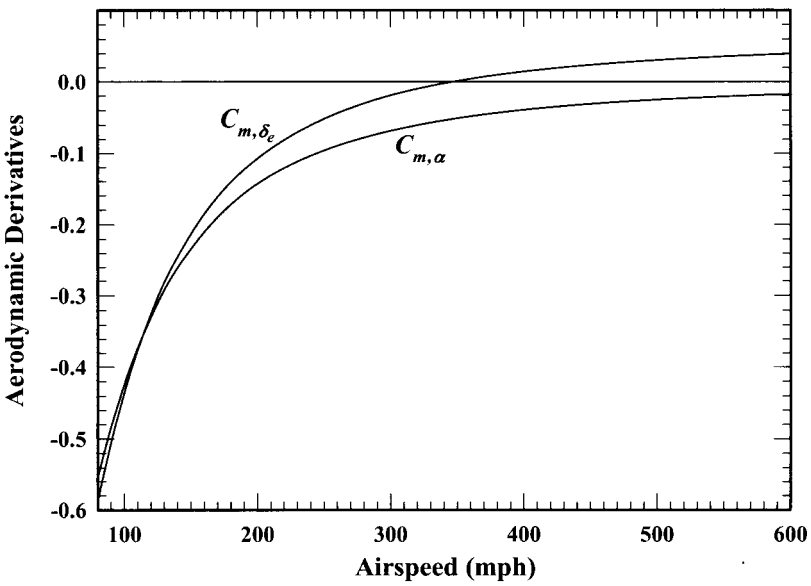


Figure 6.2.4. Effect of fuselage bending on stability and elevator effectiveness.

From Example 6.2.1, excluding compressibility effects, we have seen that both pitch stability and elevator control can be reduced drastically as a result of fuselage bending. Furthermore, from Fig. 6.2.4 we see that these effects are rapidly amplified as airspeed is increased. This could cause a very serious problem for an aircraft that enters a steep dive. The airplane might have adequate pitch stability and elevator power for normal flight conditions. However, if the tail boom stiffness is inadequate and the airplane enters a steep dive, as airspeed is quickly increased, both pitch stability and elevator power are reduced. This can cause the airplane to nose over or "tuck," which places the aircraft in an even steeper dive. With the ensuing reduction in elevator power, the airplane could become locked in the dive, and even with maximum elevator deflection, it may be impossible for the pilot to recover.

Compressibility effects at high subsonic airspeeds can amplify the tendency for an airplane to tuck under in a dive as a result of aeroelastic bending. When an airplane exceeds some critical Mach number, shock waves form on the upper surface of the wing. Such shock waves can induce premature flow separation, which increases the drag and decreases the lift. Since the downwash on an aft tail is directly related to the lift developed by the main wing, compressibility effects at high subsonic speeds can drastically reduce the downwash on an aft tail. This decrease in downwash causes an increase in the angle of attack for the tail and creates a nose-down pitching moment, which in turn aggravates any tendency for the airplane to tuck under in a dive.

Early versions of the Lockheed P-38 Lightning, shown in Fig. 6.2.5, were victims of such phenomena. Several pilots, including Ralph Virden, one of Lockheed's top test

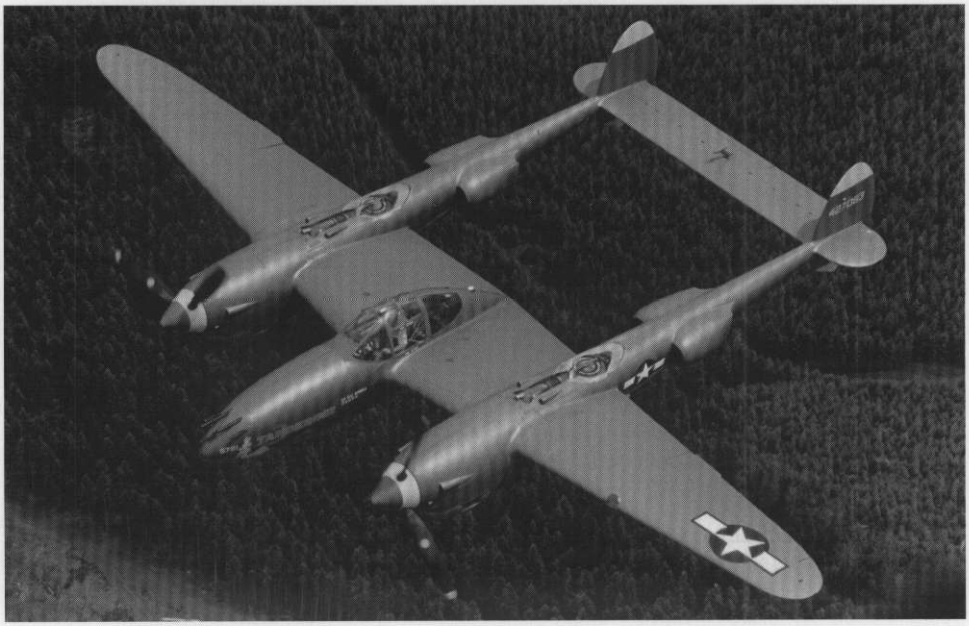


Figure 6.2.5. Lockheed P-38 Lightning. (Photograph by Terry Gleason)

pilots, were killed as a result of the Lightning's inability to recover from a steep dive. Enemy pilots soon learned of this flaw in the P-38 design and used the trait to their advantage. The problem was solved with the addition of dive recovery flaps on the lower surface of the main wing and a small fillet at the juncture between the wing leading edge and the canopy. When the dive recovery flaps were engaged in a high-speed dive, more lift was developed on the main wing, and as a result, the downwash was increased on the tail plane. This decreased the angle of attack for the horizontal tail, making it possible for the pilot to recover from the dive.

As shown in Fig. 6.2.4, under extreme conditions aeroelastic bending of the tail boom can result in elevator control reversal. As can be seen from Eqs. (6.2.8) and (6.2.9), both K_m and K_L are directly proportional to the airspeed squared and inversely proportional to the tail boom stiffness. From this fact combined with Eq. (6.2.16), we see that elevator control reversal occurs at an airspeed that is proportional to the square root of the tail boom stiffness. **The tail boom must be stiff enough so that the elevator control reversal speed exceeds the maximum airspeed that could ever be attained by the airplane.** A conservative rule for fixing the minimum tail boom stiffness is to allow no more than 10 percent control loss at the maximum allowable airspeed.

6.3. Control Force and Trim Tabs

We have now seen that an airplane's elevator must be large enough to trim and maneuver the craft in pitch, throughout the allowable flight envelope. We have also seen that the fuselage must be stiff enough to avoid substantial aeroelastic control loss at high airspeeds. These are not, however, the only constraints that must be placed on the pitch control system of an airplane. If we are to provide good handling qualities for a human pilot, consideration should also be given to the forces that must be exerted by the pilot to initiate and maintain the required elevator deflections.

The elevator of an airplane is actuated with the stick or control yoke. The control is pushed forward when a nose-down pitching moment is needed, and to provide a nose-up pitching moment, the pilot pulls back on the control. Obviously, the force required to move the stick or control yoke must fall within acceptable limits throughout the entire flight envelope of the airplane. FAR Part 23 allows a maximum temporary elevator-actuation-force of 60 pounds on a stick and 75 pounds on a control yoke. For prolonged application, the elevator-actuation force cannot exceed 10 pounds for either a stick or a control yoke.

In addition to limiting the maximum force required to provide needed elevator deflection, the variation in elevator control force with airplane trim speed must be sufficient to provide the pilot with a good "feel" for the trim attitude of the airplane. As we have seen, elevator deflection is used to control angle of attack and trim the airplane for level flight at any desired airspeed. To decrease the angle of attack and increase the trim speed, the pilot must push forward on the control. The control force should increase smoothly as the trim speed is increased beyond that associated with the neutral position of the control. Likewise, the pull force required to decrease the trim speed should increase smoothly as the trim speed is decreased. The change in elevator control force with respect to aircraft trim speed is commonly called the *control force gradient.*

For longitudinal maneuvers, like the pull-up or push-over maneuver, good handling qualities require a smooth increase in the stick force with increasing load factor. This gives the pilot a good feel for the severity of the maneuver being executed. In transport aircraft, the large elevator deflection needed to induce a rapid pull-up maneuver, near the structural limit of the aircraft, should require a fairly large stick force, near the FAR Part 23 limit. To provide good handling qualities for combat or stunt aircraft, a much lower stick force is needed. In combat, a *longitudinal stick force per g* between about 4 and 10 pounds per g is usually acceptable. Experienced pilots can easily adapt to lower stick force gradients, which make an airplane less tiring to fly in combat.

Large transports and modern fighter aircraft typically have irreversible hydraulic or electric systems for actuating the control surfaces. In these aircraft, the stick forces are provided artificially by a system commonly called a *control loader*. With such control systems, a motor provides the power required to move each control surface, and the control force felt by the pilot can be totally uncoupled from the aerodynamic hinge moment needed to deflect the control surface. There are many possible ways to provide such artificial feedback to the pilot, and the details of control loader design will not be discussed here.

For light aircraft, the power required to move the control surface is often supplied directly by the pilot, through a system of cables, pulleys, gears, rods, and levers. The range of options for mechanically connecting the cockpit controls to the aerodynamic control surfaces of an airplane is very great, and a detailed discussion of actual mechanisms would not be appropriate for this text. For our purpose, it is sufficient to understand that such control systems require a pilot-supplied control force that is in direct proportion to the aerodynamic hinge moment needed to deflect the control surface.

Whether the cockpit controls are linked to the aerodynamic control surfaces mechanically or through a modern "fly-by-wire" control system, knowledge of the control surface hinge moment is needed to properly design the aircraft control system. The moment that is required to rotate an airplane control surface about its hinge line is primarily a function of the aerodynamic pressure difference between the upper and lower surface. For example, consider the symmetric airfoil section of the horizontal tail that is shown schematically in Fig. 6.3.1. With no angle of attack and no elevator deflection, the aerodynamic pressure acting on the upper surface exactly balances that acting on the lower surface and no aerodynamic moment is produced about the hinge line. If this tail plane is given a positive angle of attack, the pressure on the upper surface is decreased and that on the lower surface is increased. This produces an aerodynamic hinge moment that must be countered by the control system to prevent the elevator from rotating upward. A negative angle of attack will produce an aerodynamic hinge moment in the opposite direction. Similarly, when the elevator is deflected downward, the pressure on the upper surface becomes less and the pressure on the lower surface becomes greater. This produces an aerodynamic hinge moment that opposes the downward rotation of the elevator. Likewise, an upward rotation of the elevator produces a downward acting hinge moment, which also opposes the rotation of the control surface. At any given angle of attack there is one elevator deflection angle that will result in a zero aerodynamic hinge moment. Elevator deflection in either direction from this neutral elevator position will produce an opposing aerodynamic hinge moment.

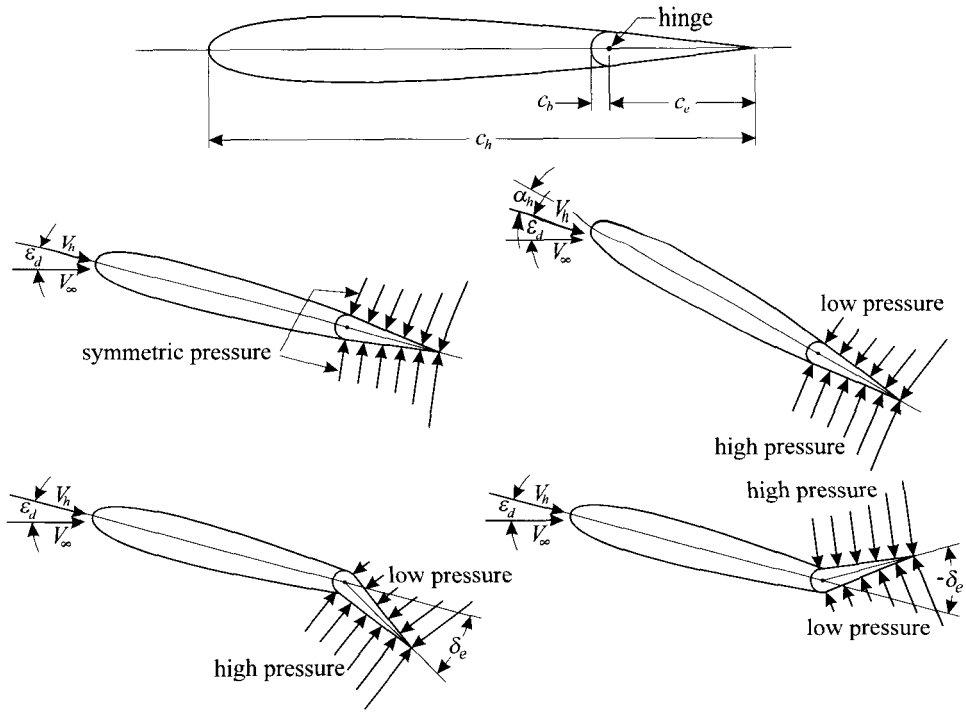


Figure 6.3.1. Aerodynamic hinge moment acting on the elevator of an aft tail.

Since elevator deflection controls the airplane angle of attack and trim speed, any airspeed that requires an elevator deflection that differs from the neutral position of the elevator will result in a nonzero elevator hinge moment. If the cockpit controls are mechanically connected to the elevator, the pilot must supply a control force proportional to this hinge moment. Suppose, for example, that an airplane with an aft tail is flying at some airspeed that produces steady level flight with absolutely no force on the control. If the pilot wishes to increase the airspeed to some faster level trim setting, she or he must increase the power in order to balance the thrust with the drag at this higher airspeed. However, if the angle of attack remains unchanged, the increased airspeed will produce lift in excess of the weight and the airplane will begin to climb. In order to maintain constant elevation, the pilot must also push forward on the control to deflect the aft elevator downward and rotate the airplane to a lower angle of attack. With the proper elevator deflection, the balance between lift and weight is reestablished at the higher airspeed. To balance the aerodynamic hinge moment produced on the elevator at this new trim speed, if no other trim adjustment is supplied, the pilot will need to maintain a continuous push force to hold the control at the new trim position. When flying at constant airspeed for a long period of time, it becomes uncomfortable for the pilot to maintain even a small force on the control. A trim tab, such as that shown in Fig. 6.3.2, can be used to relieve the pilot of this load.

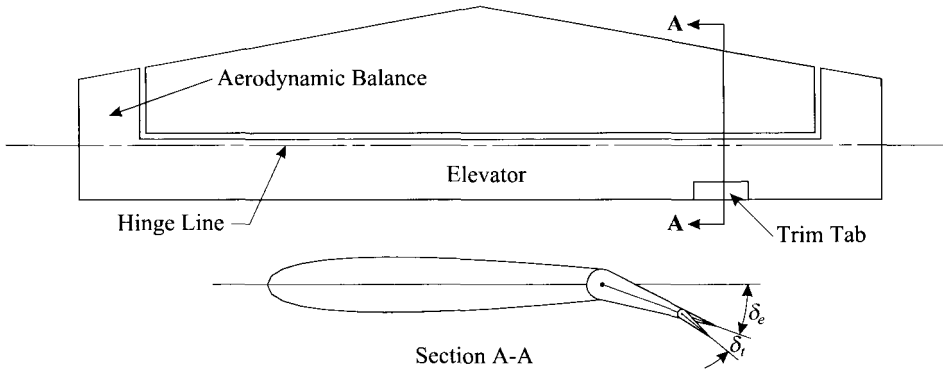


Figure 6.3.2. Elevator trim tab on an aft tail.

A trim tab is a small secondary control surface located somewhere along the trailing edge of the primary control surface. Since the planform area of the trim tab is very small, it usually has only a negligible effect on the lift produced by the aerodynamic surface to which it is attached. However, because there is a fairly large moment arm between the aerodynamic center of the trim tab and the hinge line of the primary control surface, deflection of the trim tab does have a significant effect on the aerodynamic hinge moment of the primary control surface. A downward deflection of the trim tab produces an alteration in the hinge moment that tends to deflect the primary control surface upward. Conversely, when the tab is deflected upward, a more downward-deflecting hinge moment is produced on the primary control surface.

The aerodynamic moment produced about the hinge line of an airplane's elevator depends on the local angle of attack for the horizontal surface, the deflection angle of the elevator itself, and the deflection angle of any trim tab. An elevator hinge moment coefficient is commonly defined as

$$C_{H_e} \equiv \frac{H_e}{\frac{1}{2}\rho V_h^2 S_e \bar{c}_e} \tag{6.3.1}$$

where, according to common notation, H_e is the aerodynamic elevator hinge moment, S_e is the planform area of that portion of the elevator that is aft of the hinge line, and $\bar{c}_e$ is the mean chord for that same portion of the elevator, aft of the hinge line. Since our sign convention defines a downward rotation of the elevator to be positive, a hinge moment that tends to rotate the elevator downward is also defined as positive. According to this convention, a positive elevator deflection usually tends to produce a negative hinge moment, and a negative elevator deflection will normally produce a positive hinge moment. In other words, the change in elevator hinge moment with respect to elevator deflection angle is typically negative.

Aerodynamic theory predicts that for small angles of attack and small control surface deflections, in both subsonic and supersonic flight, the hinge moment coefficient is very

nearly a linear function of the local angle of attack for the horizontal surface, the elevator deflection angle, and the trim tab deflection angle,

$$C_{H_e} = C_{H_e 0} + C_{H_e,\alpha_h}\alpha_h + C_{H_e,\delta_e}\delta_e + C_{H_e,\delta_t}\delta_t \tag{6.3.2}$$

where

$$C_{H_e,\alpha_h} \equiv \frac{\partial C_{H_e}}{\partial \alpha_h}$$

$$C_{H_e,\delta_e} \equiv \frac{\partial C_{H_e}}{\partial \delta_e}$$

$$C_{H_e,\delta_t} \equiv \frac{\partial C_{H_e}}{\partial \delta_t}$$

and $C_{H_e 0}$ is the elevator hinge moment coefficient with the local angle of attack, the elevator deflection angle, and the trim tab deflection angle all set at zero. In nearly all cases, an aft tail will have a symmetric airfoil section. Thus, $C_{H_e 0}$ is usually zero for an aft tail. For a canard, $C_{H_e 0}$ is typically negative.

While experiments confirm the linear relation given by Eq. (6.3.2) for small angles, the actual magnitudes of the coefficients cannot be accurately determined by analytical means. These constants depend in a very complex way on the section and planform geometry of the elevator, the horizontal surface, and the hinge. The coefficients are very sensitive to local boundary layer separation near the hinge and the state of the boundary layer near the trailing edge. These factors vary with Reynolds number. Typically, the coefficients in Eq. (6.3.2) are determined from wind tunnel tests.

From Eq. (6.3.2) we can show how a trim tab is used to zero the hinge moment at any desired elevator deflection angle and eliminate the pilot-supplied control force at any desired trim speed. Setting the hinge moment coefficient in Eq. (6.3.2) to zero and solving for the elevator deflection angle, we obtain

$$(\delta_e)_{H_e=0} = -\frac{C_{H_e 0}}{C_{H_e,\delta_e}} - \frac{C_{H_e,\alpha_h}}{C_{H_e,\delta_e}}\alpha_h - \frac{C_{H_e,\delta_t}}{C_{H_e,\delta_e}}\delta_t \tag{6.3.3}$$

From Eq. (6.3.3) we have

$$\left(\frac{\partial \delta_e}{\partial \delta_t}\right)_{H_e=0} = -\frac{C_{H_e,\delta_t}}{C_{H_e,\delta_e}} \tag{6.3.4}$$

Since C_{H_e,δ_e} and C_{H_e,δ_t} are both negative, we see that the change in the neutral elevator position with respect to the trim tab deflection angle is negative. In other words, a downward deflection of the trim tab will move the neutral elevator position upward, and an upward deflection of the tab will move the neutral elevator position downward.

The trim tab of a mechanical control system is typically held in position by an irreversible mechanism, such as a worm gear or jackscrew, that can be adjusted by the pilot but requires no pilot input to maintain. By adjusting the trim tab deflection angle, the pilot can change the neutral position of the elevator at any angle of attack. Thus, the pilot is able to zero out the elevator control force that is required to trim the airplane for any desired airspeed.

While a trim tab can be used to zero the stick force at trim, it does not significantly affect the force needed to deflect the elevator away from its neutral position. The magnitude of the force needed for such elevator deflection is also important to the handling qualities of an airplane, since the pilot will need to make temporary changes in elevator deflection to maneuver the airplane or simply to correct for disturbances caused by turbulence.

As the size of an airplane is increased, the size of the elevator and the power needed to deflect it from its neutral position, against the aerodynamic hinge moment, will typically increase as well. Within limits, the designer has some control over the aerodynamic hinge moment produced on an elevator of a given size. While that portion of the elevator aft of the hinge line produces a negative change in hinge moment with respect to deflection angle, any part of the elevator that is forward of the hinge line will tend to make this derivative more positive. The power required to deflect the elevator from neutral can be decreased by increasing the fraction of the total elevator area that is forward of the hinge line. When a significant portion of the elevator is forward of the hinge line, as shown in Fig. 6.3.2, it is commonly called an *aerodynamic balance.*

Two important control force derivatives are commonly used to quantify the stick force needed to deflect the elevator from its neutral position. The first of these derivatives is the *control force gradient*, which is defined to be the change in elevator control force with respect to airplane trim speed for a constant trim tab setting. The second of these important control force derivatives is the change in elevator control force with respect to load factor for the constant-speed pull-up maneuver. This derivative is commonly referred to as the *longitudinal control force per g.* To gain a better understanding for these stick force derivatives, we shall now examine the longitudinal control force in more detail.

When the cockpit controls are mechanically linked to the aerodynamic control surfaces, the pitch control force provided by the pilot, F_p, is proportional to the aerodynamic hinge moment produced on the elevator,

$$F_p = \frac{H_e}{l_g} = \frac{\frac{1}{2}\rho V_h^2 S_e \bar{c}_e C_{H_e}}{l_g} \tag{6.3.5}$$

where l_g is the length of the effective lever arm associated with the mechanism or *gearing* that links the cockpit control to the elevator. Using Eq. (6.3.2) in Eq. (6.3.5), the pitch control force can be written as

$$F_p = \frac{\frac{1}{2}\rho V^2 \eta_h S_e \bar{c}_e}{l_g}(C_{H_e 0} + C_{H_e,\alpha_h}\alpha_h + C_{H_e,\delta_e}\delta_e + C_{H_e,\delta_t}\delta_t) \tag{6.3.6}$$

where η_h is the usual dynamic pressure ratio for the horizontal surface and V is the airplane's true airspeed.

Including the effect of pitch rate given by Eq. (6.1.12), the local angle of attack for the horizontal surface can be written as

$$\alpha_h = \alpha_{0h} - \varepsilon_{d0} + (1 - \varepsilon_{d,\alpha})\alpha + \frac{2l_h}{\bar{c}_w}\bar{q} \tag{6.3.7}$$

where α_{0h} is the angle that the horizontal surface makes with the fuselage reference line, ε_{d0} is the downwash angle when the airplane angle of attack relative to the fuselage reference line is zero, $\varepsilon_{d,\alpha}$ is the downwash gradient, α is the airplane angle of attack relative to the fuselage reference line, and $\bar{q}$ is the dimensionless pitch rate that was defined in Eq. (6.1.11). Using Eq. (6.3.7) in Eq. (6.3.6), the pitch control force exerted by the pilot is

$$F_p = \frac{\frac{1}{2}\rho V^2 \eta_h S_e \bar{c}_e}{l_g} \times \left\{ C_{H_e 0} + C_{H_e,\alpha_h}\left[\alpha_{0h} - \varepsilon_{d0} + (1 - \varepsilon_{d,\alpha})\alpha + \frac{2l_h}{\bar{c}_w}\bar{q}\right] + C_{H_e,\delta_e}\delta_e + C_{H_e,\delta_t}\delta_t \right\} \tag{6.3.8}$$

The elevator deflection affects both the airplane angle of attack and the pitch rate. Recall from Sec. 6.1 that for constant airspeed and constant normal acceleration, the airplane angle of attack, α, the elevator deflection angle, δ_e, and the dimensionless pitch rate, $\bar{q}$, can all be related to the airspeed, V, and the load factor, n. From Eqs. (6.1.33), (6.1.34), and (6.1.28), we have

$$\alpha = \frac{(nC_W - C_{L0})C_{m,\delta_e} + C_{L,\delta_e} C_{m0} + (C_{L,\delta_e} C_{m,\bar{q}} - C_{L,\bar{q}} C_{m,\delta_e})(n-1)(g\bar{c}_w/2V^2)}{C_{L,\alpha} C_{m,\delta_e} - C_{L,\delta_e} C_{m,\alpha}} \tag{6.3.9}$$

$$\delta_e = -\frac{(nC_W - C_{L0})C_{m,\alpha} + C_{L,\alpha} C_{m0} + (C_{L,\alpha} C_{m,\bar{q}} - C_{L,\bar{q}} C_{m,\alpha})(n-1)(g\bar{c}_w/2V^2)}{C_{L,\alpha} C_{m,\delta_e} - C_{L,\delta_e} C_{m,\alpha}} \tag{6.3.10}$$

$$\bar{q} = (n-1)\frac{g\bar{c}_w}{2V^2} \tag{6.3.11}$$

Here it is important to remember that the weight coefficient, C_W, is a function of the airspeed,

$$C_W \equiv \frac{W}{\frac{1}{2}\rho V^2 S_w} \tag{6.3.12}$$

Using Eqs. (6.3.9) through (6.3.12) in Eq. (6.3.8), after some algebraic manipulation, the pitch control force can be written as

$$F_p = \eta_h \frac{S_e \bar{c}_e}{S_w l_g}\left[C_1 nW + C_2(n-1)\frac{\rho g S_w \bar{c}_w}{4} + (C_3 + C_{H_e,\delta_t}\delta_t)\left(\tfrac{1}{2}\rho V^2 S_w\right)\right] \quad (6.3.13)$$

where

$$C_1 = \frac{C_{m,\delta_e} C_{H_e,\alpha_h}(1-\varepsilon_{d,\alpha}) - C_{m,\alpha} C_{H_e,\delta_e}}{C_{L,\alpha} C_{m,\delta_e} - C_{L,\delta_e} C_{m,\alpha}} \quad (6.3.14)$$

$$C_2 = \frac{2l_h C_{H_e,\alpha_h}}{\bar{c}_w} + \frac{(C_{L,\delta_e} C_{m,\bar{q}} - C_{L,\bar{q}} C_{m,\delta_e}) C_{H_e,\alpha_h}(1-\varepsilon_{d,\alpha}) - (C_{L,\alpha} C_{m,\bar{q}} - C_{L,\bar{q}} C_{m,\alpha}) C_{H_e,\delta_e}}{C_{L,\alpha} C_{m,\delta_e} - C_{L,\delta_e} C_{m,\alpha}} \quad (6.3.15)$$

and

$$C_3 = C_{H_e 0} + C_{H_e,\alpha_h}(\alpha_{0h} - \varepsilon_{d0}) + \frac{(C_{m,\alpha} C_{L0} - C_{L,\alpha} C_{m0}) C_{H_e,\delta_e} - (C_{m,\delta_e} C_{L0} - C_{L,\delta_e} C_{m0}) C_{H_e,\alpha_h}(1-\varepsilon_{d,\alpha})}{C_{L,\alpha} C_{m,\delta_e} - C_{L,\delta_e} C_{m,\alpha}} \quad (6.3.16)$$

While the coefficients C_1, C_2, and C_3 are not affected by the cockpit controls, the trim tab setting can be used to adjust the value of δ_t so that the control force is zero at some desired airspeed. At level trim, the load factor is unity. Thus, if we let V_{trim} denote the airspeed that requires no pitch control force for level trimmed flight with a trim tab setting of δ_t, then Eq. (6.3.13) requires that

$$0 = \eta_h \frac{S_e \bar{c}_e}{S_w l_g}\left[C_1 W + (C_3 + C_{H_e,\delta_t}\delta_t)\left(\tfrac{1}{2}\rho V_{\text{trim}}^2 S_w\right)\right]$$

or

$$C_3 + C_{H_e,\delta_t}\delta_t = -\frac{W}{\frac{1}{2}\rho V_{\text{trim}}^2 S_w} C_1 \quad (6.3.17)$$

Using this result in Eq. (6.3.13), the **pitch control force required for constant airspeed and constant normal acceleration** is

$$F_p = \eta_h \frac{S_e \bar{c}_e}{S_w l_g}\left[C_1\left(n - \frac{V^2}{V_{\text{trim}}^2}\right)W + C_2(n-1)\frac{\rho g S_w \bar{c}_w}{4}\right] \quad (6.3.18)$$

In the absence of Reynolds number and Mach number effects, the **control force gradient** is obtained by differentiating Eq. (6.3.18) with respect to airspeed at constant load factor and evaluating the result at $V = V_{\text{trim}}$,

$$\left(\frac{\partial F_p}{\partial V}\right)_{\substack{n=\text{constant}\\ V=V_{\text{trim}}}} = -2\eta_h \frac{S_e \bar{c}_e}{S_w l_g} C_1 \frac{W}{V_{\text{trim}}} \tag{6.3.19}$$

Similarly, the **longitudinal control force per g** is found by differentiating Eq. (6.3.18) with respect to load factor at constant airspeed,

$$\left(\frac{\partial F_p}{\partial n}\right)_{V=\text{constant}} = \eta_h \frac{S_e \bar{c}_e}{S_w l_g}\left(C_1 W + C_2 \frac{\rho g S_w \bar{c}_w}{4}\right) \tag{6.3.20}$$

From Eq. (6.3.19) we see that the magnitude of the control force gradient is proportional to the aircraft gross weight, inversely proportional to the trim speed, and independent of altitude. Thus, the controls become heavier when gross weight is increased or trim speed is decreased. From Eq. (6.3.20) we see that the longitudinal control force per g also increases linearly with aircraft gross weight. However, apart from Mach number and Reynolds number effects, the control force per g is independent of airspeed. Altitude affects the control force per g only through the second term in Eq. (6.3.20). Comparing the two equations, we find that the change in the two control force derivatives with gross weight have opposite signs. The coefficient C_1 is positive, so the control force gradient decreases with gross weight, whereas the control force per g increases with gross weight. This is simply a result of our sign convention for the control force. This sign convention, which was implicitly stated in Eq. (6.3.5), specifies that a pull force is positive and a push force is negative. The difference in sign between Eqs. (6.3.19) and (6.3.20) results from the fact that increasing the trim speed requires a push force, whereas increasing the load factor requires a pull force.

Note that both control force derivatives are proportional to the ratio $S_e \bar{c}_e / S_w l_g$. For geometrically similar airplanes of different size, the ratio of elevator area to wing area does not change appreciably. Thus, in addition to the effect of weight, we see that aircraft size increases the control force derivatives in direct proportion to the elevator chord length, which is roughly proportional to the linear size of the airplane. When the effects of weight and linear size are combined, we see that the magnitudes of the mechanical control force derivatives increase very rapidly with increasing aircraft size.

Increasing the length of the lever arm associated with the mechanical gearing can decrease the magnitude of the control force derivatives. However, this is severely limited by the range of motion of the pilot's arms. When the aerodynamic control surfaces are connected to the cockpit controls with an all-mechanical linkage, the control force can be reduced by changing the gearing. However, this does not decrease the mechanical work required for a given control surface deflection. For example, if the control force were cut in half by doubling the mechanical gear ratio, the required displacement of the pilot's control would be doubled. The pilot can comfortably move the stick or control yoke only

through a limited range. Thus, the designer's ability to vary the control force with mechanical gearing is very limited. Since the mechanical control force increases rapidly with aircraft size, large airplanes typically utilize either power boost controls or complete fly-by-wire control systems.

Since several of the aerodynamic derivatives used in the definitions of C_1 and C_2 depend on the position of the center of gravity, the pitch control force is also CG dependent. The nature of this dependence is not obvious from Eq. (6.3.18). This is examined in the following example.

EXAMPLE 6.3.1. For the wing-tail combination that is described in Examples 4.4.2 and 6.1.1, plot the control force gradient and the longitudinal control force per g at sea level and 80 mph as a function of the location of the CG measured relative to the quarter-chord of the main wing. For this elevator and stabilizer the change in the hinge moment coefficient with angle of attack is –0.63 and the change in the hinge moment coefficient with elevator deflection is –0.97, based on a 12-ft^2 elevator with a mean chord of 1.1 ft. Assume that the mechanical linkage between the stick and the elevator has an effective lever arm of 2.0 ft.

Solution. Again we let x denote the distance measured aft of the wing quarter-chord. For this airplane we have

$$S_w = 180 \text{ ft}^2, \quad b_w = 33 \text{ ft}, \quad C_{L_w,\alpha} = 4.44, \quad C_{m_w} = -0.053, \quad W = 2{,}700 \text{ lbf},$$
$$S_h = 36 \text{ ft}^2, \quad b_h = 12 \text{ ft}, \quad C_{L_h,\alpha} = 3.97, \quad C_{m_{h0}} = 0.0, \quad C_{m_h,\delta_e} = -0.55,$$
$$S_e = 12 \text{ ft}^2, \quad \bar{c}_e = 1.1 \text{ ft}, \quad \varepsilon_e = 0.60, \quad x_h = 15 \text{ ft}, \quad \eta_h = 1.0, \quad \varepsilon_{d,\alpha} = 0.44,$$
$$C_{H_e,\alpha_h} = -0.63, \quad C_{H_e,\delta_e} = -0.97, \quad l_g = 2.0 \text{ ft}$$

By definition

$$l_w = x_w - x_{CG} = -x_{CG}$$

$$l_h = x_h - x_{CG}$$

Using results obtained in Examples 4.4.1, 4.4.2, and 6.1.1,

$$C_{L,\alpha} = C_{L_w,\alpha} + \frac{S_h}{S_w}\eta_h C_{L_h,\alpha}(1-\varepsilon_{d,\alpha}) = 4.8846$$

$$C_{L,\bar{q}} = 2\frac{-x_{CG}}{\bar{c}_w}C_{L_w,\alpha} + 2\eta_t \frac{S_t(x_t - x_{CG})}{S_w \bar{c}_w} C_{L_t,\alpha}$$
$$= 4.367 - 10.468\hat{x}_{CG}$$

$$C_{L,\delta_e} = \frac{S_h}{S_w}\eta_h C_{L_h,\alpha}\varepsilon_e = 0.4764$$

$$C_{m,\alpha} = -\frac{-x_{CG}}{\bar{c}_w} C_{L_w,\alpha} - \eta_t \frac{S_t(x_t - x_{CG})}{S_w \bar{c}_w} C_{L_t,\alpha}(1-\varepsilon_{d,\alpha})$$
$$= 4.8846\,\hat{x}_{CG} - 1.2228$$

$$C_{m,\bar{q}} = -2\frac{(-x_{CG})^2}{\bar{c}_w^2} C_{L_w,\alpha} - 2\eta_h \frac{S_h(x_h - x_{CG})^2}{S_w \bar{c}_w^2} C_{L_h,\alpha}$$
$$= -12.009 + 8.734\,\hat{x}_{CG} - 10.468\,\hat{x}_{CG}^2$$

$$C_{m,\delta_e} = \frac{S_h \bar{c}_h}{S_w \bar{c}_w} \eta_h C_{m_h,\delta_e} - \frac{S_h(x_h - x_{CG})}{S_w \bar{c}_w} \eta_h C_{L_h,\alpha} \varepsilon_e$$
$$= 0.4764\,\hat{x}_{CG} - 1.3706$$

where $\hat{x}_{CG} = x_{CG}/\bar{c}_w$. Using these results in Eq. (6.3.14), we obtain

$$C_1 = \frac{-0.3528(C_{m,\delta_e}) + 0.97(C_{m,\alpha})}{4.88464(C_{m,\delta_e}) - 0.4764(C_{m,\alpha})}$$
$$= \frac{-0.3528(0.4764\,\hat{x}_{CG} - 1.3706) + 0.97(4.8846\,\hat{x}_{CG} - 1.2228)}{4.8846(0.4764\,\hat{x}_{CG} - 1.3706) - 0.4764(4.8846\,\hat{x}_{CG} - 1.2228)}$$
$$= 0.11494 - 0.74767\,\hat{x}_{CG}$$

Similarly, using Eq. (6.3.15) with considerable algebraic manipulation gives

$$C_2 = 5.01202 - 0.80192\,\hat{x}_{CG}$$

For level trimmed flight at 80 mph, Eq. (6.3.19) results in

$$\left(\frac{\partial F_p}{\partial V}\right)_{\substack{n=\text{constant} \\ V=V_{\text{trim}}}} = -2\eta_h \frac{S_e \bar{c}_e}{S_w l_g} C_1 \frac{W}{V_{\text{trim}}}$$
$$= \underline{(-0.1940 + 1.262\,\hat{x}_{CG})\ \text{lbf}\cdot\text{s/ft}}$$

and at sea level, Eq. (6.3.20) reduces to

$$\left(\frac{\partial F_p}{\partial n}\right)_{V=\text{constant}} = \eta_h \frac{S_e \bar{c}_e}{S_w l_g}\left(C_1 W + C_2 \frac{\rho g S_w \bar{c}_w}{4}\right)$$
$$= \underline{(14.83 - 74.57\,\hat{x}_{CG})\ \text{lbf/}g}$$

Thus, within the approximations used for the present example, the control force derivatives vary linearly with the axial position of the CG. Results for the particular wing-tail combination used in this example are shown in Figs. 6.3.3 and 6.3.4 for trim speeds of 80, 120, and 160 mph.

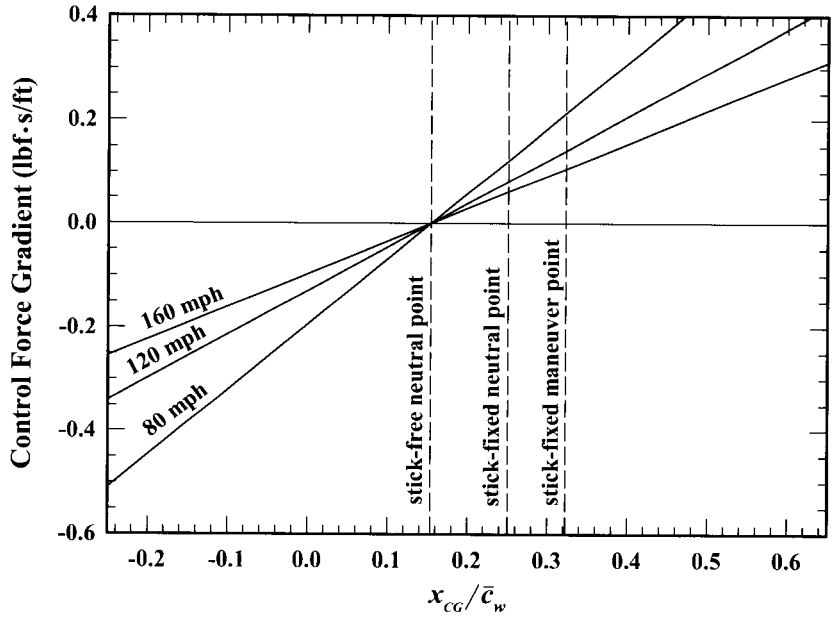


Figure 6.3.3. Control force gradient as a function of CG location measured aft of the wing quarter-chord for the airplane in Example 6.3.1.

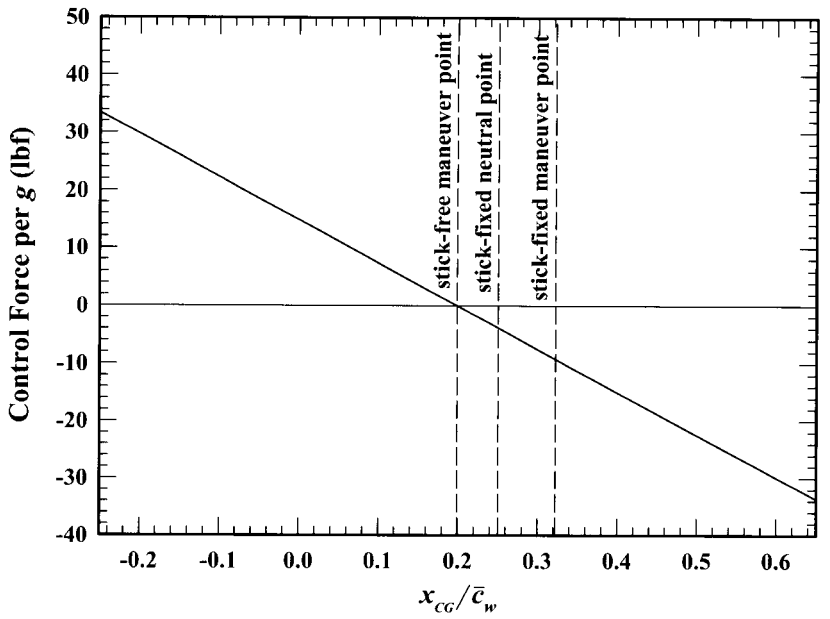


Figure 6.3.4. Longitudinal control force per g as a function of CG location measured aft of the wing quarter-chord for the airplane in Example 6.3.1.

The exact linear nature of the relations found in Example 6.3.1 is a direct result of neglecting the vertical offsets. If the vertical offsets were accounted for as described in Sec. 4.7, then the relations would no longer be exactly linear. However, the variation in pitch control force with the location of the center of gravity is very nearly linear for most airplanes.

For the airplane in Example 6.3.1, with the CG located near the wing quarter-chord, a stick force of about 15 pounds per g is required for the constant-speed pull-up maneuver. This means that executing a 4-g pull-up, which is near the structural limit of most general aviation airplanes, would require a stick force of about 60 pounds, which corresponds to the FAR Part 23 limit for a stick. With the CG so located, even at speeds above the maneuver speed, the pilot would need to exert considerable effort to initiate a pull-up that would damage the aircraft. It is not likely that such a maneuver could be initiated unintentionally.

In all cases, as the center of gravity is moved forward, the control becomes heavier, and as the CG is moved aft, the control becomes lighter. Notice that the control force gradient goes to zero for a CG location that is forward of the stick-fixed neutral point. The CG location that produces a zero longitudinal control force gradient is called the *stick-free neutral point*. The CG location that results in a zero longitudinal control force per g is aft of the stick-free neutral point but forward of the stick-fixed maneuver point. The CG location that gives a zero longitudinal control force per g is normally referred to as the *stick-free maneuver point*.

6.4. Stick-Free Neutral and Maneuver Points

The physical significance of the stick-free neutral point and stick-free maneuver point has often been misinterpreted. For this reason, some space has been devoted here to examining these two parameters. First, we discuss how the stick-free neutral point gets its name.

Consider a hypothetical elevator that has no mass and rotates about a frictionless hinge. Assume that this elevator is coupled to the cockpit control with a mechanical linkage that also has no mass and no friction. If no force were applied to the cockpit control of this hypothetical elevator, then the elevator deflection would always instantaneously take the value that would make the hinge moment go to zero. That is, from Eqs. (6.3.3) and (6.3.7),

$$(\delta_e)_{H_e=0} = -\frac{C_{H_e 0}}{C_{H_e,\delta_e}} - \frac{C_{H_e,\alpha_h}}{C_{H_e,\delta_e}}\left[\alpha_{0h} - \varepsilon_{d0} + (1-\varepsilon_{d,\alpha})\alpha + \frac{2l_h}{\bar{c}_w}\bar{q}\right] - \frac{C_{H_e,\delta_t}}{C_{H_e,\delta_e}}\delta_t \quad (6.4.1)$$

What is normally referred to as the lift slope for a complete airplane is defined to be the change in lift coefficient for the complete airplane differentiated with respect to angle of attack at constant elevator deflection. That is,

$$C_{L,\alpha} \equiv \left(\frac{\partial C_L}{\partial \alpha}\right)_{\delta_e=\text{constant}} \quad (6.4.2)$$

Similarly, what is commonly referred to as the *pitch stability derivative* is defined to be the change in pitching moment coefficient with respect to angle of attack at constant elevator deflection,

$$C_{m,\alpha} \equiv \left(\frac{\partial C_m}{\partial \alpha}\right)_{\delta_e=\text{constant}} \tag{6.4.3}$$

For our hypothetical massless and frictionless elevator, we can define a stick-free lift slope to be the change in lift coefficient with respect to angle of attack at zero hinge moment. From Eqs. (6.4.1) and (6.4.2), this gives

$$\begin{aligned} C'_{L,\alpha} \equiv \left(\frac{\partial C_L}{\partial \alpha}\right)_{H_e=0} &= \left(\frac{\partial C_L}{\partial \alpha}\right)_{\delta_e=\text{constant}} + \left(\frac{\partial C_L}{\partial \delta_e}\right)_{\alpha=\text{constant}} \left(\frac{\partial \delta_e}{\partial \alpha}\right)_{H_e=0} \\ &= C_{L,\alpha} - \frac{C_{L,\delta_e} C_{H_e,\alpha_h} (1-\varepsilon_{d,\alpha})}{C_{H_e,\delta_e}} \end{aligned} \tag{6.4.4}$$

Similarly, from Eqs. (6.4.1) and (6.4.3), we define the stick-free pitch stability derivative

$$\begin{aligned} C'_{m,\alpha} \equiv \left(\frac{\partial C_m}{\partial \alpha}\right)_{H_e=0} &= \left(\frac{\partial C_m}{\partial \alpha}\right)_{\delta_e=\text{constant}} + \left(\frac{\partial C_m}{\partial \delta_e}\right)_{\alpha=\text{constant}} \left(\frac{\partial \delta_e}{\partial \alpha}\right)_{H_e=0} \\ &= C_{m,\alpha} - \frac{C_{m,\delta_e} C_{H_e,\alpha_h} (1-\varepsilon_{d,\alpha})}{C_{H_e,\delta_e}} \end{aligned} \tag{6.4.5}$$

If we neglect the effects of vertical offsets, the stick-fixed neutral point is related to the lift slope and the pitch stability derivative according to Eq. (4.4.13),

$$\frac{l_{np}}{\bar{c}_w} = -\frac{C_{m,\alpha}}{C_{L,\alpha}} \tag{6.4.6}$$

For our hypothetical massless and frictionless elevator, we can define a stick-free neutral point as

$$\frac{l'_{np}}{\bar{c}_w} = -\frac{C'_{m,\alpha}}{C'_{L,\alpha}} \tag{6.4.7}$$

This is exactly the CG location where the longitudinal control force gradient goes to zero, as was shown in Fig. 6.3.3, hence the name.

The stick-free neutral point for an airplane is the aerodynamic center that the airplane would have with no pilot control force if the elevator and its mechanical linkage to the cockpit control had no mass and no friction. The mass and friction associated with any real elevator and mechanical control system will move the stick-free aerodynamic center of an airplane considerably aft of the point given by Eq. (6.4.7).

Thus, the name *stick-free neutral point* is somewhat misleading. **More appropriately, the stick-free neutral point should be thought of simply as that CG location for which the equilibrium stick force gradient goes to zero.**

The stick-fixed maneuver point for an airplane is that CG location for which the elevator angle per g goes to zero. In Sec. 6.1 it was stated that the elevator deflection required to produce constant normal acceleration is reversed when the center of gravity is located aft of the stick-fixed maneuver point. In that context, control reversal was implicitly defined in terms of elevator deflection. Under normal conditions, with the CG located forward of the stick-fixed maneuver point, downward rotation of an aft elevator, which occurs when the pilot moves the control stick forward, will result in a downward increment in the normal acceleration. Conversely, when the pilot moves the control stick back to rotate the aft elevator upward, the resulting increment in normal acceleration is upward. If the CG were located aft of the stick-fixed maneuver point, this relationship between control stick displacement and steady normal acceleration would be reversed.

With a normal CG location, the pilot exerts a pull force to move the control stick back and initiate upward acceleration from trimmed flight. Conversely, a push force is required to move the control stick forward and initiate a downward acceleration from trim. From the result shown in Fig. 6.3.4, one might conclude that when the CG is located aft of the stick-free maneuver point, this normal relation between control force and the initiation of normal acceleration is reversed. This is also misleading. We must remember that the control force per g, which is plotted in Fig. 6.3.4, is defined in terms of the *steady-state load factor*. That is, the control force required when the pitch damping moment exactly balances the pitching moment produced by the elevator deflection. This says nothing about the stick force required to initiate a normal acceleration from trimmed flight. **Even when the CG is located at the stick-free maneuver point, a pull force is typically required to initiate upward acceleration and a push force is required to initiate downward acceleration.** However, when the center of gravity is located near the stick-free maneuver point, these forces become very small.

In summary, the stick-free neutral point is defined to be that CG location for which the equilibrium stick force gradient goes to zero for an all-mechanical control system. The stick-free maneuver point is defined as that CG location for which the equilibrium stick force per g goes to zero for an all-mechanical control system. **Any interpretation of these parameters beyond those by which they were defined should be made with extreme caution.** The stick-free neutral and maneuver points for an airplane are of little or no importance in the design of a modern fly-by-wire control system.

6.5. Ground Effect, Elevator Sizing, and CG Limits

During takeoff and landing an airplane must briefly fly in very close proximity to the ground. Under such conditions the flow around the airplane is significantly modified by the presence of the ground. The resulting changes in lift and drag are commonly referred to as *ground effect*. The vorticity trailing aft of a lifting wing is substantially diminished in ground effect. This reduces the downwash that is induced on the wing and other components of the aircraft. The reduction in downwash increases the lift slope, decreases the induced drag, and shifts the neutral point aft.

The shift in the neutral point that results from ground effect has an important influence on aircraft controls. For a conventional airplane with an aft tail, there are three primary factors that contribute to this shift in the neutral point: an increase in lift slope for the wing, an increase in lift slope for the tail, and a reduction in the downwash induced on the tail by the main wing. All three of these factors arise directly from a reduction in downwash. The increase in wing lift slope will move the neutral point toward the aerodynamic center of the wing and the increase in lift slope for the horizontal stabilizer will move the neutral point toward the tail. These two effects tend to cancel. As can be seen from Eq. (4.4.3), if the lift slopes for the wing and horizontal stabilizer are increased in the same proportion, there is no net shift in the neutral point resulting directly from these lift slope changes. However, for most conventional airplanes, ground effect increases the lift slope for the wing by more than that for the horizontal stabilizer. Thus, lift slope changes resulting from ground effect will normally produce a slight forward shift in the neutral point. On the other hand, ground effect also reduces the downwash induced on the horizontal stabilizer by the main wing, and since this downwash is destabilizing, its reduction produces an aft shift in the neutral point. Typically, the aft shift caused by the decrease in $\varepsilon_{d,\alpha}$ is much greater than the forward shift caused by the change in lift slope. As a result, ground effect usually produces a substantial rearward shift in the neutral point for a conventional airplane.

Moving the neutral point farther aft affects the airplane controls in much the same way as moving the center of gravity forward. Thus, ground effect increases the amount of up elevator required to trim the airplane at low airspeeds. In a similar manner, ground effect also increases the magnitude of the control force gradient. For an airplane with an all-mechanical control system, this causes the control to become heavier as the airplane approaches the ground.

The fundamental analytical methods presented in this and the eariler chapters apply to airplanes in ground effect as well as in flight remote from the ground. The only significant difference is that some of the aerodynamic derivatives change as the airplane approaches the ground. Thus, the problem of evaluating stability and control for aircraft flying close to the ground is resolved into that of estimating the aerodynamic derivatives in ground effect. For the dimensions and airspeeds encountered in most atmospheric flight, ground effect is essentially an inviscid phenomenon. Thus, a potential flow solution will normally provide a satisfactory estimate for the aerodynamic changes produced by ground effect.

One convenient way to model an aircraft in ground effect for use with a potential flow algorithm is to replace the surface of the ground with an *image* of the aircraft, positioned and orientated as though it were reflected in the surface of the ground. Such a model is shown in Fig. 6.5.1. By design, the flow around this aircraft combined with its mirror image is symmetric across the plane of reflection. At any point on this plane of symmetry, the downwash generated by the aircraft will be exactly offset with upwash generated by its mirror image. Thus, there can be no net flow normal to the plane of reflection, which is accordingly a stream surface for the flow. This means that potential flow about the aircraft combined with its mirror image is identical to potential flow about the aircraft combined with a flat solid surface representing the ground. Since the two flows are identical, the associated aerodynamic forces will be identical as well.

From Eq. (4.5.11), the downwash induced on the horizontal stabilizer by the primary vortex system was found to be

$$(\varepsilon_d)_{\text{primary}} = \left(\frac{\kappa_v \kappa_p \kappa_s}{\kappa_b}\right)_{\text{primary}} \frac{C_{L_w}}{R_{A_w}} = \frac{1.035(0.433)1.015}{0.759} \frac{C_{L_w}}{R_{A_w}} = 0.599 \frac{C_{L_w}}{R_{A_w}}$$

As shown in Fig. 6.5.2, the mirror image of this vortex system is identical to the primary system, except for the direction of rotation and its position relative to the horizontal stabilizer of the actual airplane. The image vortex system is located a distance below the ground equal to the height of the wing above the ground. Thus, the height of the horizontal stabilizer above the image vortex system is twice the distance from the wing to the ground plus the distance that the horizontal stabilizer is above the primary vortex system. Therefore, relative to the image vortex system, we have

$$\bar{y} = (2 \times 4.0 + 3.4)/(33/2) = 0.691$$

From Eqs. (4.5.6) and (4.5.12), the position factor and sweep factor for the image vortex system are found to be

$$(\kappa_p)_{\text{image}} = 0.244, \quad (\kappa_s)_{\text{image}} = 1.001$$

The span factor, κ_b, for the image vortex system is the same as that for the primary system. Since the image vortex rotates in the opposite direction from the primary vortex, the strength factor, κ_v, for the image vortex is equal in magnitude but opposite in sign to that of the primary vortex. Thus, from Eq. (4.5.11), the downwash induced on the horizontal stabilizer by the image vortex system is

$$(\varepsilon_d)_{\text{image}} = \left(\frac{\kappa_v \kappa_p \kappa_s}{\kappa_b}\right)_{\text{image}} \frac{C_{L_w}}{R_{A_w}} = \frac{(-1.035)(0.244)1.001}{0.759} \frac{C_{L_w}}{R_{A_w}} = -0.333 \frac{C_{L_w}}{R_{A_w}}$$

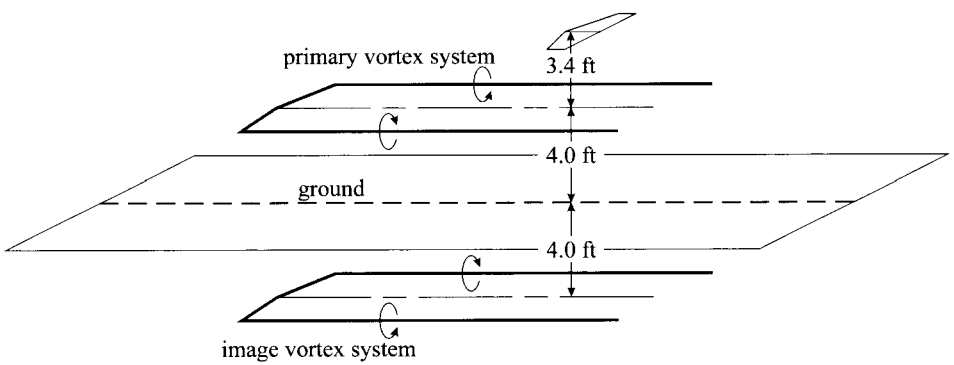


Figure 6.5.2. Vortex system and its mirror image for Example 6.5.1.

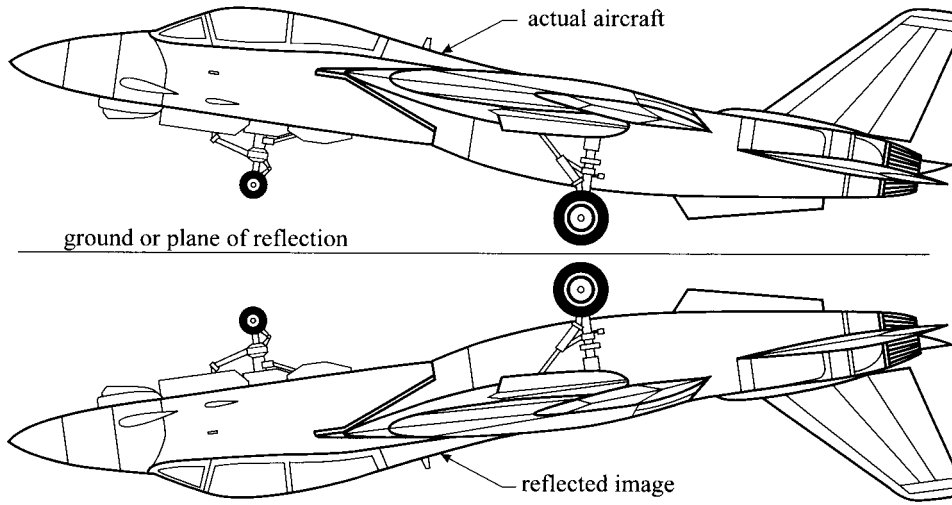


Figure 6.5.1. Mirror image model used to simulate ground effect.

The model shown in Fig. 6.5.1 can be used with either the vortex panel method or the vortex lifting-line method to obtain a detailed numerical estimate for the important aerodynamic derivatives, which affect an airplane's controls in ground effect. However, since lift slope effects for the wing and horizontal stabilizer tend to cancel, a reasonable first estimate can be obtained by considering only the reduction in downwash gradient induced on the tail by the main wing. This procedure is best demonstrated by example.

EXAMPLE 6.5.1. For the wing-tail combination that is described in Examples 4.3.1, 4.4.1, 4.4.2, and 4.5.1, estimate the downwash gradient induced on the horizontal stabilizer when the airplane is flying in ground effect with the main wing 4.0 feet above the ground. Also estimate the static margin.

Solution. For this estimate we will ignore changes in lift slope and will model the downwash using the vortex system described in Sec. 4.5. To account for ground effect, we combine this vortex system with an image of the vortex system that is positioned and orientated as though it were reflected in the surface of the ground, much like the image shown in Fig. 6.5.1. From Example 4.5.1, the geometry associated with the primary vortex system gives

$$S_w = 180\ \text{ft}^2, \quad b_w = 33\ \text{ft}, \quad R_{A_w} = 33^2/180 = 6.05, \quad C_{L_{w,\alpha}} = 4.44, \quad R_{T_w} = 0.40,$$
$$\Lambda = 10°, \quad l_h - l_w = 15\ \text{ft}, \quad \bar{x} = 15/(33/2) = 0.909, \quad \bar{y} = 3.4/(33/2) = 0.206$$

which was found to yield

$$\kappa_v = 1.035, \quad \kappa_b = 0.759, \quad \kappa_p = 0.433, \quad \kappa_s = 1.015$$

The net downwash in ground effect is then

$$\varepsilon_d = (\varepsilon_d)_{\text{primary}} + (\varepsilon_d)_{\text{image}} = (0.599 - 0.333)\frac{C_{L_w}}{R_{A_w}} = 0.266\frac{C_{L_w}}{R_{A_w}}$$

For this first approximation we are neglecting the change in lift slope caused by ground effect. Thus, the downwash gradient in ground effect is estimated to be

$$\varepsilon_{d,\alpha} = 0.266\frac{C_{L_w,\alpha}}{R_{A_w}} = 0.266\frac{4.44}{6.05} = \underline{0.195}$$

From Example 4.4.1, the center of gravity is located 0.71 feet aft of the aerodynamic center of the wing. Thus we have

$$S_w = 180\ \text{ft}^2, \quad b_w = 33\ \text{ft}, \quad C_{L_w,\alpha} = 4.44, \quad l_w = -0.71\ \text{ft},$$
$$S_h = 36\ \text{ft}^2, \quad b_h = 12\ \text{ft}, \quad C_{L_h,\alpha} = 3.97, \quad l_h = 14.29\ \text{ft}, \quad \eta_h = 1.0$$

Using these values combined with the downwash gradient that was predicted for the horizontal stabilizer in ground effect and following Example 4.4.1, the static margin in ground effect is estimated to be

$$\frac{l_{np}}{\bar{c}_w} = \frac{l_w C_{L_w,\alpha} + \dfrac{S_h l_h}{S_w}\eta_h C_{L_h,\alpha}(1-\varepsilon_{d,\alpha})}{\bar{c}_w\left[C_{L_w,\alpha} + \dfrac{S_h}{S_w}\eta_h C_{L_h,\alpha}(1-\varepsilon_{d,\alpha})\right]} = 0.2158 = \underline{22\%}$$

For the particular geometry and flight condition that were used in Example 6.5.1, we see that ground effect reduces the downwash on the horizontal stabilizer by more than 50 percent and nearly doubles the static margin. Since the computations used in this example were made neglecting changes in lift slope, the estimated changes in downwash and static margin are somewhat greater than would be observed for this airplane in actual flight.

The decrease in downwash that results from ground effect increases the local angle of attack for the horizontal stabilizer. This increases the lift on the aft stabilizer and produces a negative pitching moment about the center of gravity. To counter this nose-down pitching moment and maintain trim, additional up elevator must be applied in ground effect. Again this is best demonstrated by example.

EXAMPLE 6.5.2. We wish to examine the near-ground trim requirements for the wing-tail combination described in Example 4.4.2. For the ground-effect operating condition described in Example 6.5.1, plot the elevator deflection required to trim the airplane for 80 mph at sea level as a function of the location of the center of gravity measured aft of the wing quarter-chord. Compare these results with those obtained in Example 4.4.2 for flight at the same airspeed and altitude but out of ground effect.

Solution. Again we let x denote the distance measured aft of the quarter-chord of the main wing and we shall continue to ignore changes in lift slope caused by ground effect. For this wing-tail combination we have

$$S_w = 180 \text{ ft}^2, \quad b_w = 33 \text{ ft}, \quad C_{L_w,\alpha} = 4.44, \quad C_{m_w} = -0.053, \quad W = 2{,}700 \text{ lbf},$$
$$S_h = 36 \text{ ft}^2, \quad b_h = 12 \text{ ft}, \quad C_{L_h,\alpha} = 3.97, \quad C_{m_h,\delta_e} = -0.55,$$
$$\varepsilon_e = 0.60, \quad x_h = 15 \text{ ft}, \quad \eta_h = 1.0,$$
$$\alpha_{L0w} = -2.20°, \quad \alpha_{0w} = 3.1°, \quad \alpha_{L0h} = 0.0°, \quad \alpha_{0h} = 2.3°$$

For this geometry, the lift coefficient for the main wing at zero fuselage angle of attack is

$$C_{L_w 0} = C_{L_w,\alpha}(\alpha_{0w} - \alpha_{L0w}) = 0.4107$$

Thus, from Example 6.5.1 for the specified ground-effect flight condition, the downwash angle for the horizontal stabilizer at zero fuselage angle of attack is

$$\varepsilon_{d0} = 0.266 \frac{C_{L_w 0}}{R_{A_w}} = 0.0181 = 1.03°$$

Following Example 4.4.2, we obtain

$$C_{L0} = C_{L_w,\alpha}(\alpha_{0w} - \alpha_{L0w}) + \frac{S_h}{S_w}\eta_h C_{L_h,\alpha}(\alpha_{0h} - \varepsilon_{d0}) = 0.4282$$

$$C_{L,\delta_e} = \frac{S_h}{S_w}\eta_h C_{L_h,\alpha}\varepsilon_e = 0.4764$$

$$C_L = \frac{W}{\frac{1}{2}\rho V_\infty^2 S_w} = 0.9168$$

For these sample calculations we continue to follow Example 4.4.2 for the case where the center of gravity is located at $x_{CG}/\bar{c}_w = 0.1$. In ground effect, we obtain

$$C_{m0} = C_{m_w} + \frac{x_{CG}}{\bar{c}_w} C_{L_w,\alpha}(\alpha_{0w} - \alpha_{L0w}) - \frac{S_h(x_h - x_{CG})}{S_w \bar{c}_w}\eta_h C_{L_h,\alpha}(\alpha_{0h} - \varepsilon_{d0})$$
$$= -0.05840$$

$$C_{m,\delta_e} = \frac{S_h \bar{c}_h}{S_w \bar{c}_w}\eta_h C_{m_h,\delta_e} - \frac{S_h(x_h - x_{CG})}{S_w \bar{c}_w}\eta_h C_{L_h,\alpha}\varepsilon_e = -1.3230$$

$$\frac{x_{np}}{\bar{c}_w} = \frac{x_w C_{L_w,\alpha} + \frac{S_h x_h}{S_w}\eta_h C_{L_h,\alpha}(1 - \varepsilon_{d,\alpha})}{\bar{c}_w\left[C_{L_w,\alpha} + \frac{S_h}{S_w}\eta_h C_{L_h,\alpha}(1 - \varepsilon_{d,\alpha})\right]} = 0.3460$$

$$(\delta_e)_{\text{trim}} = -\frac{C_{m0} - (C_L - C_{L0})[(x_{np} - x_{CG})/\bar{c}_w]}{C_{m,\delta_e} + C_{L,\delta_e}[(x_{np} - x_{CG})/\bar{c}_w]} = -0.1481 = \underline{-8.5°}$$

This compares to an elevator deflection of about –4 degrees for the same operating condition outside of ground effect.

Repeating the previous computations for several different values of $x_{CG}/\bar{c}_w$, we obtain the result shown in Fig. 6.5.3. It should be remembered that these computations are based on constant elevator effectiveness. In reality, elevator effectiveness decreases when the deflection angle exceeds about 10 degrees. Thus, even larger elevator deflections would be required for the most forward CG locations shown in Fig. 6.5.3.

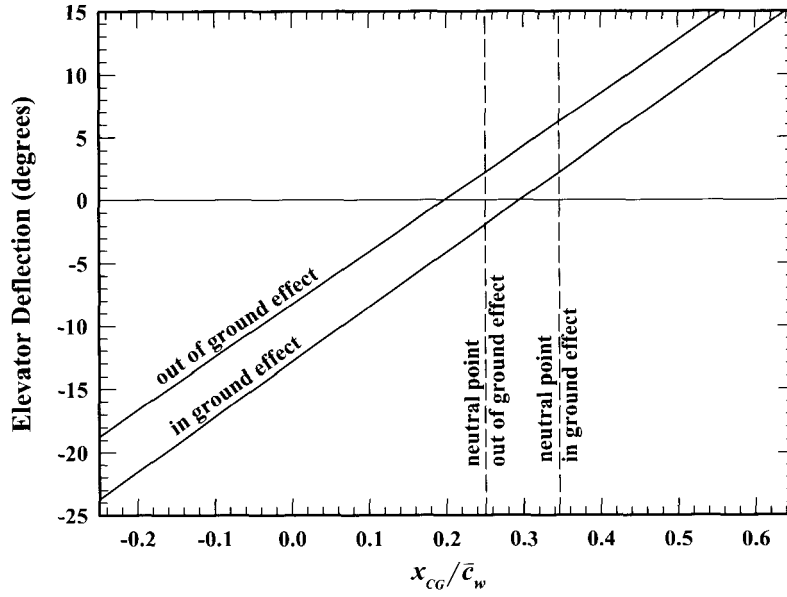


Figure 6.5.3. Elevator angle required for level trim at 80 mph and sea level as a function of CG location measured aft of the wing quarter-chord for the airplane in Example 6.5.2.

From Example 6.5.2 we see that trimming a conventional airplane in ground effect requires more up elevator than is required for the same operating condition remote from the ground. Additionally, from the results obtained in Example 4.4.2 and plotted in Fig. 4.4.3, we have seen that reducing airspeed also requires more up elevator for trim. Since it is desirable to land an airplane as slowly as possible, the combination of low airspeed and ground effect often make the landing case a critical constraint on elevator size and forward CG limit. In a perfect *full stall landing*, the airplane will stall just as the wheels touch the ground. Thus, the elevator must be sized and the forward CG limit set such that the elevator angle required to trim the airplane in ground effect for a lift

coefficient of $C_{L\max}$ does not exceed full up elevator. If the forward CG limit has been specified by some other means, this constraint can be used to size the elevator. On the other hand, for a given elevator geometry, the constraint could be used to specify the forward CG limit.

When a pilot sets up for landing, the airplane's trim setting is usually adjusted to zero the control force at the approach speed, which is below cruise but somewhat above landing speed. As the airplane is slowed from approach speed to landing speed, the pilot must apply a continuously increasing pull force to move the control back and provide the additional up elevator needed to maintain trim. Obviously, the control force required to land the airplane from the approach speed should not exceed that which can be applied comfortably by a human pilot. If the control force gradient were constant, the control force required to land would simply be the control force gradient multiplied by the difference between the approach speed and the landing speed. However, as the airplane approaches the ground, the control force gradient is increased by ground effect. This is readily demonstrated by repeating the computations in Example 6.3.1 for the ground-effect operating condition described in Example 6.5.1. The result of these computations is shown in Fig. 6.5.4. Notice that the stick-free neutral point is moved aft as a result of ground effect. When the center of gravity is forward of the stick-free neutral point, the magnitude of the control force gradient is increased in ground effect. This means that a greater pull force is required to reduce the trim speed in ground effect than would be required to achieve a similar speed reduction when the airplane is flying far from the ground.

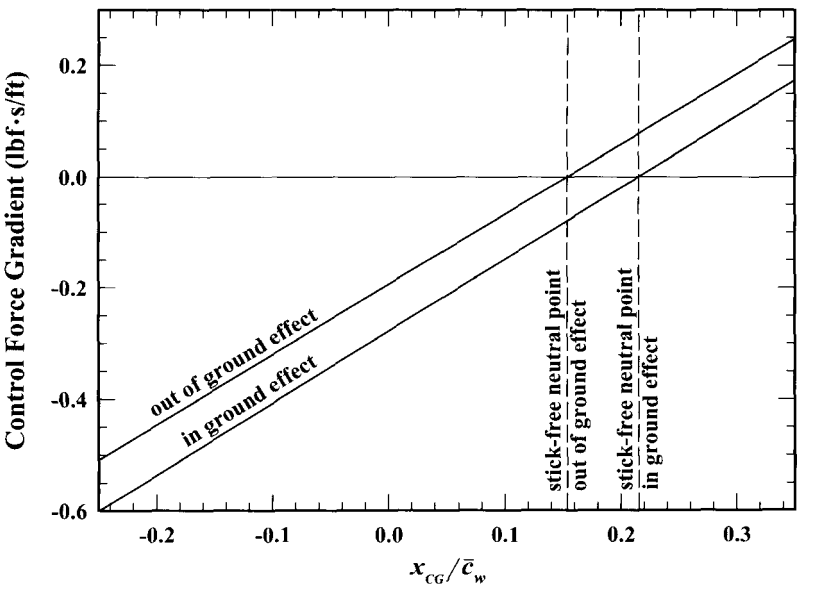


Figure 6.5.4. Control force gradient at 80 mph as a function of CG location measured aft of the wing quarter-chord for the airplane in Example 6.5.2.

EXAMPLE 6.5.3. For the wing-tail combination described in Example 6.3.1, we wish to estimate the control force required for a full stall landing from an approach speed of 80 mph, with the CG located 15 inches forward of the aerodynamic center of the wing. We will assume that the touchdown wing position relative to the ground is that described in Example 6.5.1. Using the trim tab setting, the control force is zeroed at the approach speed outside of ground effect, and the maximum lift coefficient for the wing-tail combination is 1.3.

Solution. For this wing-tail combination and CG location, we have

$$S_w = 180 \text{ ft}^2, \quad b_w = 33 \text{ ft}, \quad C_{L_w,\alpha} = 4.44, \quad C_{m_w} = -0.053, \quad W = 2{,}700 \text{ lbf},$$
$$S_h = 36 \text{ ft}^2, \quad b_h = 12 \text{ ft}, \quad C_{L_h,\alpha} = 3.97, \quad C_{m_h 0} = 0.0, \quad C_{m_h,\delta_e} = -0.55,$$
$$\alpha_{L0w} = -2.20°, \quad \alpha_{0w} = 3.1°, \quad \alpha_{L0h} = 0.0°, \quad \alpha_{0h} = 2.3°,$$
$$S_e = 12 \text{ ft}^2, \quad \bar{c}_e = 1.1 \text{ ft}, \quad \varepsilon_e = 0.60, \quad l_w = 1.25 \text{ ft}, \quad l_h = 16.25 \text{ ft}, \quad \eta_h = 1.0,$$
$$C_{H_e 0} = 0.00, \quad C_{H_e,\alpha_h} = -0.63, \quad C_{H_e,\delta_e} = -0.97, \quad l_g = 2.0 \text{ ft}$$

From Eq. (6.3.13) evaluated for a load factor of 1.0, the pitch control force required for level trim is

$$F_p = \eta_h \frac{S_e \bar{c}_e}{S_w l_g}\left[C_1 W + (C_3 + C_{H_e,\delta_t}\delta_t)\left(\tfrac{1}{2}\rho V^2 S_w\right)\right] \tag{6.5.1}$$

where

$$C_1 = \frac{C_{m,\delta_e} C_{H_e,\alpha_h}(1-\varepsilon_{d,\alpha}) - C_{m,\alpha} C_{H_e,\delta_e}}{C_{L,\alpha} C_{m,\delta_e} - C_{L,\delta_e} C_{m,\alpha}}$$

$$C_3 = C_{H_e 0} + C_{H_e,\alpha_h}(\alpha_{0h} - \varepsilon_{d0}) + \frac{(C_{m,\alpha} C_{L0} - C_{L,\alpha} C_{m0}) C_{H_e,\delta_e} - (C_{m,\delta_e} C_{L0} - C_{L,\delta_e} C_{m0}) C_{H_e,\alpha_h}(1-\varepsilon_{d,\alpha})}{C_{L,\alpha} C_{m,\delta_e} - C_{L,\delta_e} C_{m,\alpha}}$$

Since both C_1 and C_3 depend on the downwash induced on the horizontal stabilizer, these two coefficients change when the airplane enters ground effect. From Example 6.5.1, outside of ground effect the downwash angle for the horizontal stabilizer is given by

$$\varepsilon_d = 0.599 \frac{C_{L_w}}{R_{A_w}}$$

and we have

$$C_{L_w 0} = C_{L_w,\alpha}(\alpha_{0w} - \alpha_{L0w}) = 0.4107$$

$$\varepsilon_{d0} = 0.599\frac{C_{L_w 0}}{R_{A_w}} = 0.0407 = 2.33^\circ$$

$$\varepsilon_{d,\alpha} = 0.599\frac{C_{L_w,\alpha}}{R_{A_w}} = 0.4396$$

$$C_{L0} = C_{L_w,\alpha}(\alpha_{0w} - \alpha_{L0w}) + \frac{S_h}{S_w}\eta_h C_{L_h,\alpha}(\alpha_{0h} - \alpha_{L0h} - \varepsilon_{d0}) = 0.4103$$

$$C_{L,\alpha} = C_{L_w,\alpha} + \frac{S_h}{S_w}\eta_h C_{L_h,\alpha}(1 - \varepsilon_{d,\alpha}) = 4.8850$$

$$C_{L,\delta_e} = \frac{S_h}{S_w}\eta_h C_{L_h,\alpha}\varepsilon_e = 0.4764$$

$$C_{m0} = C_{m_w} - \frac{l_w}{\bar{c}_w}C_{L_w,\alpha}(\alpha_{0w} - \alpha_{L0w}) + \frac{S_h\bar{c}_h}{S_w\bar{c}_w}\eta_h C_{m_h 0} - \frac{S_h l_h}{S_w\bar{c}_w}\eta_h C_{L_h,\alpha}(\alpha_{0h} - \alpha_{L0h} - \varepsilon_{d0}) = -0.1459$$

$$C_{m,\alpha} = -\frac{l_w}{\bar{c}_w}C_{L_w,\alpha} - \frac{S_h l_h}{S_w\bar{c}_w}\eta_h C_{L_h,\alpha}(1 - \varepsilon_{d,\alpha}) = -2.3431$$

$$C_{m,\delta_e} = \frac{S_h\bar{c}_h}{S_w\bar{c}_w}\eta_h C_{m_h,\delta_e} - \frac{S_h l_h}{S_w\bar{c}_w}\eta_h C_{L_h,\alpha}\varepsilon_e = -1.4798$$

$$C_1 = \frac{C_{m,\delta_e}C_{H_e,\alpha_h}(1 - \varepsilon_{d,\alpha}) - C_{m,\alpha}C_{H_e,\delta_e}}{C_{L,\alpha}C_{m,\delta_e} - C_{L,\delta_e}C_{m,\alpha}} = 0.2864$$

$$C_3 = C_{H_e 0} + C_{H_e,\alpha_h}(\alpha_{0h} - \varepsilon_{d0}) + \frac{(C_{m,\alpha}C_{L0} - C_{L,\alpha}C_{m0})C_{H_e,\delta_e} - (C_{m,\delta_e}C_{L0} - C_{L,\delta_e}C_{m0})C_{H_e,\alpha_h}(1 - \varepsilon_{d,\alpha})}{C_{L,\alpha}C_{m,\delta_e} - C_{L,\delta_e}C_{m,\alpha}} = -0.0081$$

Since the pitch control force is set to zero when the airplane is trimmed for 80 mph out of ground effect, from Eq. (6.5.1) we have

$$C_{H_e,\delta_t}\delta_t = -C_1\frac{W}{\frac{1}{2}\rho V^2 S_w} - C_3 = -0.2544$$

For the full stall landing, the touchdown airspeed is

$$V_{\text{stall}} = \sqrt{\frac{2W}{\rho S_w C_{L\max}}} = 98.53 \text{ ft/sec}$$

From Example 6.5.1, in ground effect the downwash angle for the horizontal stabilizer is given by

$$\varepsilon_d = 0.266 \frac{C_{L_w}}{R_{A_w}}$$

Repeating the previous computations using the airspeed at stall and the downwash in ground effect gives

$$C_1 = 0.3402$$

$$C_3 = -0.0071$$

and from Eq. (6.5.1), the control force at touchdown is

$$F_p = \eta_h \frac{S_e \bar{c}_e}{S_w l_g}\left[C_1 W + (C_3 + C_{H_e,\delta_t}\delta_t)\left(\tfrac{1}{2}\rho V^2 S_w\right)\right] = \underline{13.8 \text{ lbf}}$$

If these same computations are carried out excluding the reduction in downwash produced by ground effect, we find that a control force of only 8.4 lbf is predicted to stall the airplane outside of ground effect.

In most cases, the increase in pitch control force that results from ground effect is not a critical concern to the designer. In fact, the slightly heavier pitch control gives the pilot increased sensory feedback at a time in the flight when maintaining precise pitch attitude is very critical. Since pilot effort and concentration is quite naturally increased as the airplane approaches the ground, most pilots are not aware of the increasing control force gradient.

Since trim requirements for landing often provides a critical constraint on elevator size and forward CG limit, it is important to understand how the airplane's landing configuration affects trim. Because the landing gear is always below the center of gravity, aerodynamic drag on the gear produces a nose-down pitching moment about the CG. Thus, when the landing gear is down, some additional up elevator is needed to compensate for the negative increment in pitching moment produced on the gear. Flaps and/or other high-lift devices are also commonly deployed for landing. The deployment of wing flaps gives rise to four significant aerodynamic changes; a positive increment in maximum lift coefficient, a negative increment in zero-lift angle of attack, a negative increment in wing pitching moment, and a positive increment in wing drag. The elevator angle required to trim the airplane for any given lift coefficient is significantly affected by the zero-lift angle of attack as well as the pitching moment produced on wing and the landing gear.

From Eqs. (6.1.33) and (6.1.34) evaluated for a load factor of 1.0 combined with the relation for static margin given by Eq. (4.4.13), the fuselage angle of attack and elevator angle at level trim can be estimated as

$$(\alpha)_{\text{trim}} = \frac{(C_W - C_{L0})C_{m,\delta_e} + C_{L,\delta_e} C_{m0}}{C_{L,\alpha}[C_{m,\delta_e} + C_{L,\delta_e}(l_{np}/\bar{c}_w)]} \tag{6.5.2}$$

$$(\delta_e)_{\text{trim}} = \frac{(C_W - C_{L0})(l_{np}/\bar{c}_w) - C_{m0}}{C_{m,\delta_e} + C_{L,\delta_e}(l_{np}/\bar{c}_w)} \tag{6.5.3}$$

When flaps are deployed for landing, C_{L0} is increased and except for the case of a very high wing, flaps and landing gear contribute to a negative increment in C_{m0}. The drag increment that results from deploying flaps on a high wing contributes to a positive increment in C_{m0}. If the flap deflection is not too large, deploying flaps and gear does not appreciably change the remaining terms in Eqs. (6.5.2) and (6.5.3). Thus, the increments in fuselage angle of attack and elevator angle at trim, which results from deploying the flaps and landing gear, are, respectively,

$$(\Delta\alpha)_{fg} = \frac{-C_{m,\delta_e}(\Delta C_{L0})_{fg} + C_{L,\delta_e}(\Delta C_{m0})_{fg}}{C_{L,\alpha}[C_{m,\delta_e} + C_{L,\delta_e}(l_{np}/\bar{c}_w)]} \tag{6.5.4}$$

$$(\Delta\delta_e)_{fg} = \frac{-(l_{np}/\bar{c}_w)(\Delta C_{L0})_{fg} - (\Delta C_{m0})_{fg}}{C_{m,\delta_e} + C_{L,\delta_e}(l_{np}/\bar{c}_w)} \tag{6.5.5}$$

where $(\Delta C_{L0})_{fg}$ and $(\Delta C_{m0})_{fg}$ are, respectively, the increments in C_{L0} and C_{m0} that result from deploying the flaps and gear.

The change in pitching moment coefficient with elevator deflection is negative and larger in magnitude than the change in lift coefficient with elevator deflection, which is positive. Thus, the denominators in Eqs. (6.5.4) and (6.5.5) are both negative. With this knowledge, inspection of the right-hand side of Eq. (6.5.4) reveals that the positive increment in C_{L0} produced by the flaps results in a decrease in fuselage angle of attack. On the other hand, the negative increment in C_{m0} will tend to increase fuselage angle of attack at trim. Since the change in lift coefficient with elevator deflection is typically small, the first term in the numerator of Eq. (6.5.4) dominates and the fuselage angle of attack is significantly reduced in landing configuration. From the pilot's point of view, this is perhaps the most important advantage of deploying flaps for landing, because it gives the pilot better visibility over the nose of the airplane.

In a similar manner, inspection of the right-hand side of Eq. (6.5.5) shows that when the CG is forward of the neutral point, the positive increment in C_{L0} produced by the flap deflection requires a positive increment in elevator deflection to maintain trim. However, the negative increment in C_{m0} requires a negative increment in elevator deflection. It is important to notice that the magnitude of the first term in the numerator of Eq. (6.5.5) increases as the CG is moved forward, while that of the second term remains constant. When the CG is located close to the neutral point, the second term in the numerator of Eq. (6.5.5) dominates and additional up elevator is needed to compensate for the nose-

down pitching moment produced by deploying the flaps and landing gear. As the CG is moved forward, the magnitude of the first term in the numerator of Eq. (6.5.5) increases and less up elevator is needed to compensate for flap and gear deployment. If the CG is moved far enough forward, some down elevator will be required to compensate for the net aerodynamic effects of deploying the flaps and gear.

Landing often provides a critical constraint on elevator size. To provide better pilot visibility and slower landing speed, airplanes are typically landed with flaps. However, at some point it may be necessary to land the airplane without flaps. Thus, the elevator should be sized large enough to trim the airplane at $C_{L\max}$, in ground effect, with the CG at its forward limit, and the landing gear down, both with and without flaps. Depending on the forward CG limit, either of these two cases could provide the critical constraint on elevator size. Demonstration of this point is left as an exercise for the student.

6.6. Stall Recovery

For the most part, the stability and control analysis that we have considered to this point has been based on a linear relation between angle of attack and lift. Furthermore, we have assumed a positive lift slope for all lifting surfaces. These assumptions are reasonable when the angle of attack is sufficiently below stall. However, as the angle of attack approaches stall, the variation in lift with angle of attack becomes nonlinear, and at angles of attack beyond stall, the lift slope becomes negative. Consequently, the post-stall stability and control characteristics of an aircraft are quite different from those at low angles of attack.

Fighter aircraft and stunt airplanes are commonly taken to angles of attack well beyond stall. The ability of a modern fighter to perform post-stall maneuvers, like the one shown in Fig. 3.9.7, is critical. Furthermore, missiles frequently operate at angles of attack that produce separated flow. For these reasons and many others, high angle of attack aerodynamics, stability, and control are of great interest, particularly to military aircraft designers.

While most transports and general aviation airplanes are not routinely flown at angles of attack beyond stall, the possibility of stall always exists. Hence, any airplane should be designed so that recovery from stall is at least possible. For most civilian airplanes, it is usually preferable if the airplane is designed to provide stall recovery with little or no control input from the pilot. In the most forgiving designs, the airplane will naturally recover from a stall if the pilot simply releases the controls.

At angles of attack beyond stall the airflow about an airplane is extremely complex and the aerodynamic forces and moments become highly nonlinear. At high angles of attack the drag forces acting on the wing and tail will contribute significantly to the aircraft's pitching moment, which adds to the nonlinear variation of pitching moment coefficient with angle of attack. Figure 6.6.1 shows how airplane lift, drag, and pitching moment coefficients vary with angle of attack for one particular geometry. The airplane used to generate this figure had a rectangular wing with no sweep and no geometric or aerodynamic twist. The airplane had a conventional aft tail and was trimmed for steady level flight with a fuselage angle of attack of about 4 degrees. The CG was located to provide a static margin of about 7 percent.

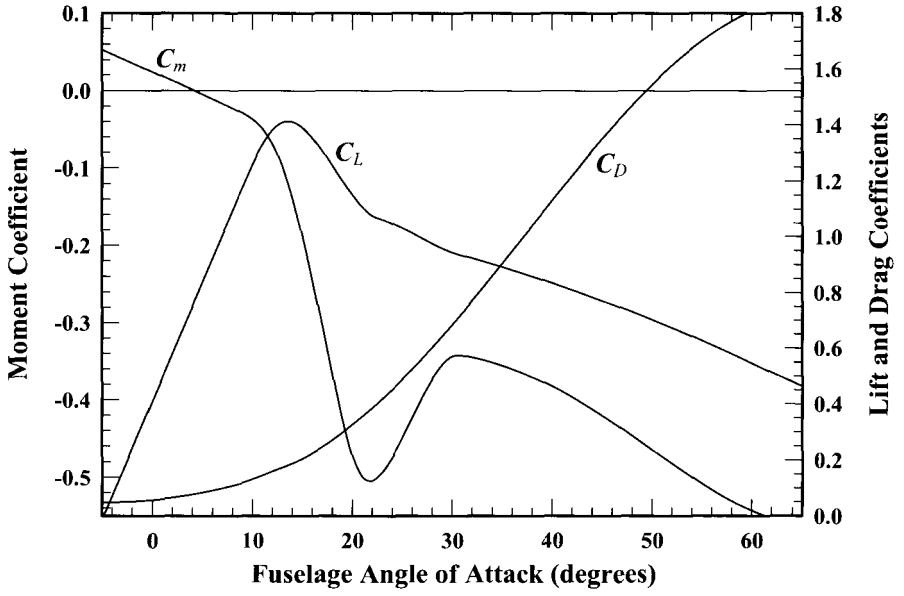


Figure 6.6.1. Lift, drag, and pitching moment coefficients for an airplane with an unswept rectangular wing and conventional aft tail.

Notice in Fig. 6.6.1 that for the region just to the right of $C_{L\max}$, the change in pitching moment coefficient with angle of attack becomes significantly more negative. This is primarily the result of two contributing factors. First of all, for this aircraft the CG was located somewhat aft of the aerodynamic center of the main wing, which makes the wing destabilizing when the lift slope is positive and the effects of drag are small. When the main wing stalls, its lift slope becomes negative and the contribution of wing lift becomes stabilizing (i.e., $C_{m,\alpha}$ becomes more negative).

The aft horizontal stabilizer also contributes to the more negative pitch stability derivative, which is seen in Fig. 6.6.1 for the region between 10 and 20 degrees angle of attack. As is often the case for an airplane with a conventional aft tail, the main wing of this airplane stalls before the horizontal stabilizer. Because downwash is induced on the aft tail by the main wing, the local angle of attack for the horizontal stabilizer is less than that for the main wing and stall of the stabilizer is postponed. We have seen that when the lift slope for the main wing is positive, this downwash reduces the stabilizing contribution that an aft tail makes to the pitch stability derivative. In a similar manner, when the lift slope for the main wing is negative, downwash increases the stabilizing contribution of an unstalled aft tail. When the main wing stalls, the decrease in lift reduces the downwash aft of the wing and increases the local angle of attack for the horizontal stabilizer. This increases the lift developed on the unstalled stabilizer and produces a greater nose-down pitching moment, which tends to reduce the angle of attack and return the airplane to unstalled flight. This increased contribution to pitch stability continues only as long as the horizontal stabilizer does not stall.

At the larger angles of attack shown in Fig. 6.6.1, both the wing and the horizontal stabilizer are stalled. From Eq. (4.7.6), for the special case where the vertical offset, h_h, is zero, the contribution of the horizontal stabilizer to the airplane pitching moment coefficient is

$$(\Delta C_m)_h = \frac{S_h \bar{c}_h}{S_w \bar{c}_w} \eta_h C_{m_h} - \frac{S_h l_h}{S_w \bar{c}_w} \eta_h \left[\cos(\alpha - \varepsilon_d) C_{L_h} + \sin(\alpha - \varepsilon_d) C_{D_h}\right] \quad (6.6.1)$$

When both the wing and the horizontal stabilizer are stalled, the downwash angle and lift coefficient decrease with increasing angle of attack, while the drag coefficient increases with angle of attack. With these facts in mind, from Eq. (6.6.1) we see that lift developed on this stalled aft stabilizer produces a nose-down pitching moment that decreases with increasing angle of attack. Drag, on the other hand, produces a nose-down pitching moment that increases with angle of attack. Thus, the lift developed on this stalled horizontal surface has a destabilizing effect on the moment slope, whereas the drag has a stabilizing effect. At angles of attack just slightly beyond the stabilizer stall point, the effects of lift are greater than the effects of drag and the aft horizontal surface is destabilizing in pitch. At somewhat higher angles of attack the drag term dominates and the horizontal surface again becomes stabilizing. This is the reason for the two changes in slope that are seen in the pitching moment curve of Fig. 6.6.1.

While the derivative of the pitching moment coefficient with respect to angle of attack is positive over a portion of the range shown in Fig. 6.6.1, the pitching moment coefficient is always negative at angles of attack beyond stall. This means that with the controls in this position, the stalled aircraft will always experience the nose-down pitching moment needed to recover from stall and return the airplane to trimmed flight. While post-stall stability characteristics similar to those shown in Fig. 6.6.1 are exhibited by many well-designed conventional airplanes, this is not necessarily the case for all airplanes and loading conditions.

The vertical position of the aircraft center of gravity relative to the wing and tail can have a significant effect on the post-stall stability characteristics of an airplane. This is demonstrated in Fig. 6.6.2. This figure shows the lift, drag, and pitching moment coefficients for the same airplane geometry that was used to generate Fig. 6.6.1. The only difference between the airplanes used for these two figures is the location of the center of gravity. For the results plotted in Fig. 6.6.2, the CG was lowered by a distance equal to one-half of the wing chord length, and the trim setting was adjusted to maintain the same level trim airspeed as that in Fig. 6.6.1. Notice that for the lower center of gravity, the destabilizing effect of the stalled aft tail is greater and extends over a larger range of angle of attack.

Wing sweep also affects the post-stall stability of an airplane. Figure 6.6.3 shows the lift, drag, and pitching moment coefficients for one particular airplane with a swept-back wing. The wing has a tapered planform with no geometric or aerodynamic twist. The airplane has the same conventional aft tail as that used for Fig. 6.6.1 and was trimmed for steady level flight at the same fuselage angle of attack. The center of gravity was located to provide the same static margin of about 7 percent, and the wing, horizontal stabilizer, and center of gravity were all placed on the fuselage reference line.

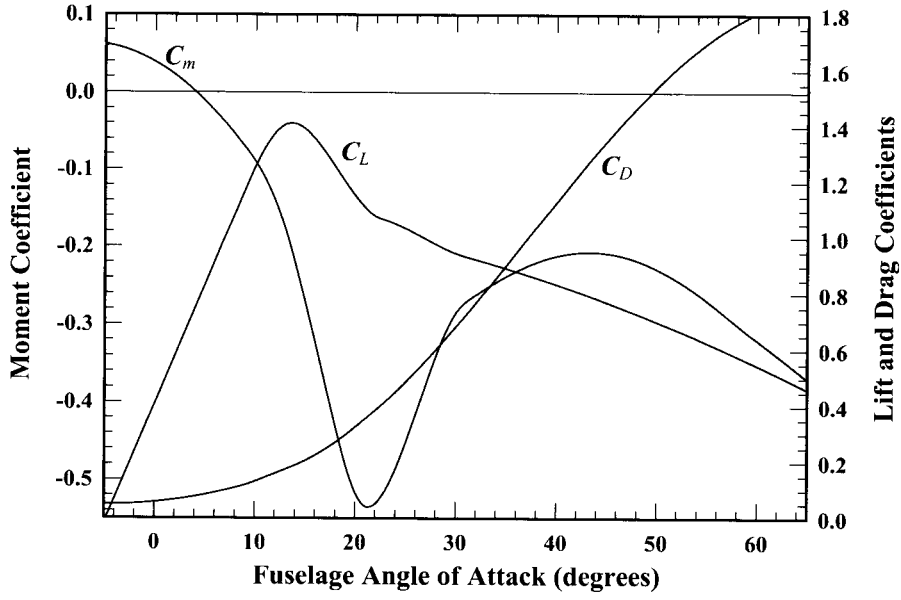


Figure 6.6.2. Lift, drag, and pitching moment coefficients for an airplane with an unswept rectangular wing, a conventional aft tail, and a low center of gravity.

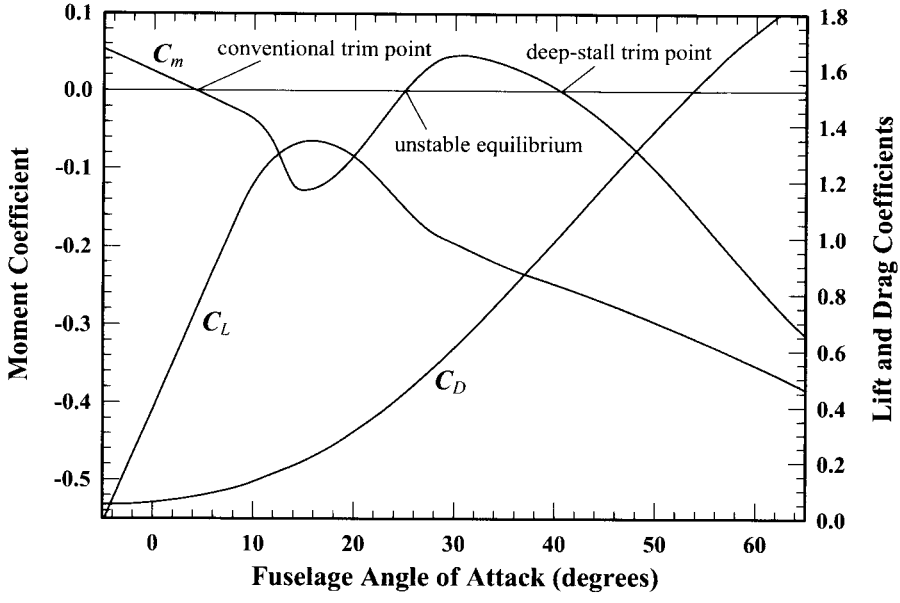


Figure 6.6.3. Lift, drag, and pitching moment coefficients for an airplane with a swept-back tapered wing and conventional aft tail.

Figure 6.6.3 demonstrates what can be a very significant problem for an airplane with a swept-back tapered wing. On a wing of this planform shape with no geometric or aerodynamic twist, the outboard wing sections will tend to stall before the sections near the root. As the angle of attack is increased from unstalled flight, the wingtips will stall first and the stall will progress inward and forward toward the root of the swept wing, as shown schematically in Fig. 6.6.4. Since positive sweep places the wingtips aft of the root, losing lift on the aft wingtips while retaining lift on the forward wing root produces a nose-up increment in the pitching moment, which tends to further increase the angle of attack and deepen the stall. This effect, combined with the destabilizing effects of a stalled aft tail, can cause the total airplane pitching moment to become positive over some range of angle of attack beyond stall. At even larger angles of attack, the pitching moment will again become negative, due to the stabilizing effects of drag. This behavior can be seen in Fig. 6.6.3.

Notice that for the pitching moment coefficient curve shown in Fig. 6.6.3, there are two stable trim points. The first occurs at an angle of attack of about 4 degrees and is the conventional trim point for unstalled flight. For this airplane, a second stable trim point occurs at about 40 degrees angle of attack. Since this point is well past stall, it is frequently called a *deep-stall trim point* or sometimes simply *deep stall.* An airplane

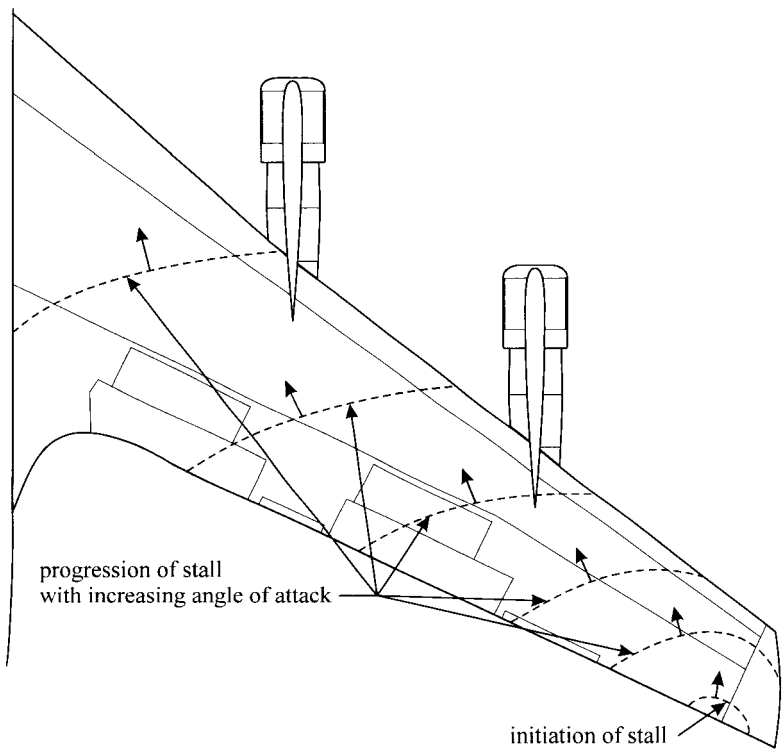


Figure 6.6.4. Stall progression on a tapered swept wing with no geometric or aerodynamic twist.

with the stall characteristics shown in Fig. 6.6.3 will recover from a shallow stall in much the same way as those shown in Figs. 6.6.1 and 6.6.2. For this particular case, as long as the angle of attack remains less than about 25 degrees, a nose-down pitching moment is created with the control in this position, and the airplane will recover from the shallow stall. However, if the angle of attack should ever exceed that of the 25-degree unstable equilibrium point with the control held in the same position that would result in recovery from a shallow stall, the airplane would quickly rotate to the deep-stall trim point. It can be difficult or even impossible to recover from this deep stall with conventional controls, because control surfaces may be immersed in the stalled wake and become ineffective. The T-tail can be particularly problematic in this regard.

One way to avoid the stall characteristic shown in Fig. 6.6.3 is through the use of washout in the swept wing. By decreasing the geometric angle of attack at the wingtips relative to that at the root, wingtip stall can be postponed to a higher angle of attack. If sufficient washout is used, the wing root will stall prior to the wingtips and the onset of stall will produce a nose-down pitching moment that counters the destabilizing effect of the lift developed on a stalled aft tail. Sometimes it is not possible to avoid the stall characteristic shown in Fig. 6.6.3 and still maintain the other characteristics needed to provide mission effectiveness. In such cases, some means must be provided for the pilot to recover from deep stall. Alternative controls such as movable canard surfaces, flaperons, and thrust vectoring are sometimes used for this purpose.

6.7. Lateral Control and Maneuverability

In Sec. 6.1 we examined how the elevator is used to control the normal acceleration of an aircraft in longitudinal motion. The elevator is used to control the angle of attack at which the pitching moment is zero. Thus, the elevator indirectly controls the magnitude of lift developed by the wing. If the lift does not equal the component of weight normal to the flight path, a normal acceleration will occur. Up to this point in the chapter, we have limited our study of aircraft maneuverability to the case where the normal acceleration is confined to the longitudinal plane.

To maneuver an aircraft outside the longitudinal plane, the ailerons and rudder are typically used in combination with the elevator to control not only the magnitude of the lift but also the direction in which the lift vector acts, thereby controlling both the direction and magnitude of acceleration for the maneuver. Consider, for example, the *steady coordinated turn* shown in Fig. 6.7.1. The term *steady* requires that both the airspeed and angular velocity are held constant. By definition, *a coordinated maneuver is one in which the controls are coordinated so that the vector sum of the airplane's acceleration and the acceleration of gravity produces an apparent body force that falls in the aircraft's plane of symmetry*. In other words, the apparent body force has no component in the spanwise direction. By definition, the turning axis for the steady coordinated turn is vertical, but the airplane may be climbing or descending during the turn. The climb angle, γ, is defined to be the angle that the airplane's velocity vector makes with the horizontal. For convenience, the body axis is chosen to align with the direction of flight, and the bank angle, ϕ, is the angle that the airplane is rolled about this velocity vector, as measured with respect to the upright "wings-level" orientation.

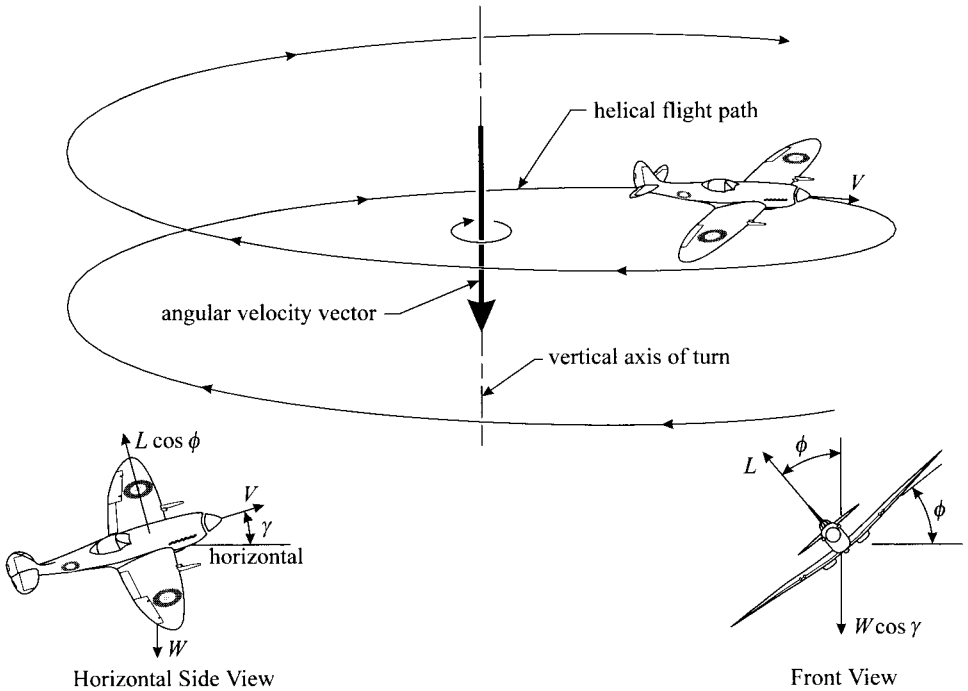


Figure 6.7.1. Steady coordinated turn.

We will use the (x_b, y_b, z_b) coordinate system shown in Fig. 5.1.1. The origin of this coordinate system is located at the aircraft center of gravity. For convenience, the x_b-axis is aligned with the direction of flight and the z_b-axis points downward in the aircraft plane of symmetry. To complete the right-hand coordinate system, the y_b-axis is then in the spanwise direction pointing to the pilot's right.

From Fig. 6.7.1, we see that the component of aircraft weight in the direction of flight is $-W\sin\gamma$ and the component of weight in the plane normal to the direction of flight is $W\cos\gamma$. The normal component of weight is easily resolved into a spanwise component, $W\cos\gamma\sin\phi$, and a component in the plane of symmetry, $W\cos\gamma\cos\phi$. Thus, the components of weight expressed in the (x_b, y_b, z_b) coordinate system are

$$\mathbf{W} = \begin{Bmatrix} -W\sin\gamma \\ W\cos\gamma\sin\phi \\ W\cos\gamma\cos\phi \end{Bmatrix} \tag{6.7.1}$$

The angular velocity vector for this steady coordinated turn is constant and parallel to the weight vector. Thus, using the same geometric relations that were used for the weight vector, the components of the airplane's angular velocity vector in (x_b, y_b, z_b) coordinates are

$$\boldsymbol{\Omega} = \begin{Bmatrix} -\Omega \sin\gamma \\ \Omega \cos\gamma \sin\phi \\ \Omega \cos\gamma \cos\phi \end{Bmatrix} \tag{6.7.2}$$

where Ω is the magnitude of the angular velocity vector. The (x_b, y_b, z_b) coordinate system was chosen so that the x_b-axis is aligned with the direction of flight. As a result, there is no velocity component in the y_b-z_b plane and the components of the translational velocity vector in the (x_b, y_b, z_b) coordinate system are

$$\mathbf{V} = \begin{Bmatrix} V \\ 0 \\ 0 \end{Bmatrix} \tag{6.7.3}$$

Since neither the translational velocity nor the angular velocity is changing with time, the only acceleration associated with the steady coordinated turn is the centripetal acceleration resulting from the changing direction of flight. Thus, from elementary rigid-body dynamics, the airplane's acceleration vector in the steady coordinated turn can be written as the cross product of the angular and translational velocity vectors,

$$\frac{d\mathbf{V}}{dt} = \boldsymbol{\Omega} \times \mathbf{V} = \begin{Bmatrix} 0 \\ \Omega V \cos\gamma \cos\phi \\ -\Omega V \cos\gamma \sin\phi \end{Bmatrix} \tag{6.7.4}$$

This acceleration vector includes the restriction that the turn is steady. However, an additional restriction is needed to account for the fact that the turn is also coordinated. The total apparent body force for this accelerating coordinate frame is the vector sum of that due to gravity and that due to the acceleration of the coordinate frame. Since an upward acceleration adds to the downward force of gravity, the apparent body force is

$$\mathbf{B} \equiv \mathbf{W} - \frac{W}{g}\frac{d\mathbf{V}}{dt} \tag{6.7.5}$$

Using Eqs. (6.7.1) and (6.7.4) in Eq. (6.7.5), the (x_b, y_b, z_b) components are

$$\mathbf{B} = W \begin{Bmatrix} -\sin\gamma \\ \cos\gamma \sin\phi \\ \cos\gamma \cos\phi \end{Bmatrix} - \frac{W}{g}\Omega V \begin{Bmatrix} 0 \\ \cos\gamma \cos\phi \\ -\cos\gamma \sin\phi \end{Bmatrix} \tag{6.7.6}$$

The definition of a coordinated maneuver requires that the spanwise component of this apparent body force must be zero, i.e.,

$$W \cos\gamma \sin\phi - (W\Omega V/g)\cos\gamma \cos\phi = 0 \tag{6.7.7}$$

This imposes a relation between the turning rate and the bank angle,

$$\Omega = \frac{g \tan \phi}{V} \tag{6.7.8}$$

Using Eq. (6.7.8) in Eq. (6.7.4), the acceleration for this steady coordinated turn is

$$\frac{d\mathbf{V}}{dt} = \begin{Bmatrix} 0 \\ g \cos\gamma \sin\phi \\ -g \cos\gamma \sin^2\phi / \cos\phi \end{Bmatrix} \tag{6.7.9}$$

The total force acting on the aircraft is the vector sum of the thrust force, the aerodynamic force, and the weight. Drag acts in the negative x_b-direction and lift acts in the negative z_b-direction. For this analysis we assume a thrust vector aligned with the x_b-axis and will let Y represent the side force acting in the positive y_b-direction. Thus, using Eqs. (6.7.1) and (6.7.9), Newton's second law requires that

$$\begin{Bmatrix} T-D \\ Y \\ -L \end{Bmatrix} + \begin{Bmatrix} -W \sin\gamma \\ W \cos\gamma \sin\phi \\ W \cos\gamma \cos\phi \end{Bmatrix} = \frac{W}{g} \begin{Bmatrix} 0 \\ g \cos\gamma \sin\phi \\ -g \cos\gamma \sin^2\phi / \cos\phi \end{Bmatrix} \tag{6.7.10}$$

or after rearranging and applying the trigonometric identity $\sin^2\phi + \cos^2\phi = 1$,

$$\begin{Bmatrix} T-D \\ Y \\ L \end{Bmatrix} = \begin{Bmatrix} W \sin\gamma \\ 0 \\ W \cos\gamma / \cos\phi \end{Bmatrix} \tag{6.7.11}$$

Because the turn is steady, the angular rates are constant. Furthermore, at the angular rates encountered in a coordinated turn, second-order angular momentum effects are negligible and the moments acting on the airplane are very close to zero:

$$\begin{Bmatrix} \ell \\ m \\ n \end{Bmatrix} = \begin{Bmatrix} 0 \\ 0 \\ 0 \end{Bmatrix} \tag{6.7.12}$$

Newton's second law, as expressed in Eqs. (6.7.11) and (6.7.12), provides six scalar equations that can be solved for the thrust, angle of attack, sideslip angle, and the three control surface deflections. From a conceptual point of view, this problem is identical to the longitudinal control problem considered in Sec. 6.1. Since longitudinal motion is two-dimensional, the longitudinal control problem involves only three degrees of freedom and three unknowns: the thrust, the angle of attack, and the elevator deflection. Because lateral motion is three-dimensional, the present problem involves six degrees of freedom and six unknowns, but is otherwise identical.

The first component of Eq. (6.7.11) allows us to determine the thrust needed to maintain constant airspeed at a specified climb angle, or if the thrust were specified, the climb angle could be determined from this relation. The remaining five components of Eqs. (6.7.11) and (6.7.12) will be used to determine the aerodynamic angles and control surface deflections. In traditional dimensionless form, these five scalar equations are

$$\begin{Bmatrix} C_L \\ C_Y \\ C_\ell \\ C_m \\ C_n \end{Bmatrix} = \begin{Bmatrix} C_W \cos\gamma/\cos\phi \\ 0 \\ 0 \\ 0 \\ 0 \end{Bmatrix} \tag{6.7.13}$$

From Eq. (6.1.18), the lift coefficient for the airplane can be written as

$$C_L = C_{L0} + C_{L,\alpha}\,\alpha + C_{L,\bar{q}}\,\bar{q} + C_{L,\delta_e}\,\delta_e \tag{6.7.14}$$

where $\bar{q}$ is the dimensionless pitching rate defined in Eq. (6.1.11). The pitching moment coefficient for pure longitudinal motion was given by Eq. (6.1.19). However, lateral motion allows sideslip and we have seen that a rotating propeller produces a pitching moment that is proportional to the sideslip angle. Thus, for turning flight, Eq. (6.1.19) should be modified to account for the change in the pitching moment coefficient with respect to sideslip angle,

$$C_m = C_{m0} + C_{m,\alpha}\,\alpha + C_{m,\beta}\,\beta + C_{m,\bar{q}}\,\bar{q} + C_{m,\delta_e}\,\delta_e \tag{6.7.15}$$

Just as the longitudinal forces and moment depend on the pitching rate, the lateral force and moments depend on the rolling and yawing rates. By standard convention, the rolling and yawing rates are given the symbols p and r, respectively, and they are traditionally nondimensionalized with respect to the forward velocity divided by the wing semispan,

$$\begin{Bmatrix} \bar{p} \\ \bar{q} \\ \bar{r} \end{Bmatrix} \equiv \begin{Bmatrix} pb_w/2V \\ q\bar{c}_w/2V \\ rb_w/2V \end{Bmatrix} \tag{6.7.16}$$

With these definitions, the lateral aerodynamic force and moments are written

$$C_Y = C_{Y,\beta}\,\beta + C_{Y,\bar{p}}\,\bar{p} + C_{Y,\bar{r}}\,\bar{r} + C_{Y,\delta_r}\,\delta_r \tag{6.7.17}$$

$$C_\ell = C_{\ell,\beta}\,\beta + C_{\ell,\bar{p}}\,\bar{p} + C_{\ell,\bar{r}}\,\bar{r} + C_{\ell,\delta_a}\,\delta_a + C_{\ell,\delta_r}\,\delta_r \tag{6.7.18}$$

$$C_n = C_{n,\alpha}\,\alpha + C_{n,\beta}\,\beta + C_{n,\bar{p}}\,\bar{p} + C_{n,\bar{r}}\,\bar{r} + C_{n,\delta_a}\,\delta_a + C_{n,\delta_r}\,\delta_r \tag{6.7.19}$$

Using Eqs. (6.7.14) through (6.7.19) in Eq. (6.7.13), we have

$$\begin{bmatrix} C_{L,\alpha} & 0 & 0 & C_{L,\delta_e} & 0 \\ 0 & C_{Y,\beta} & 0 & 0 & C_{Y,\delta_r} \\ 0 & C_{\ell,\beta} & C_{\ell,\delta_a} & 0 & C_{\ell,\delta_r} \\ C_{m,\alpha} & C_{m,\beta} & 0 & C_{m,\delta_e} & 0 \\ C_{n,\alpha} & C_{n,\beta} & C_{n,\delta_a} & 0 & C_{n,\delta_r} \end{bmatrix} \begin{Bmatrix} \alpha \\ \beta \\ \delta_a \\ \delta_e \\ \delta_r \end{Bmatrix} = \begin{Bmatrix} C_W \cos\gamma/\cos\phi - C_{L0} \\ 0 \\ 0 \\ -C_{m0} \\ 0 \end{Bmatrix} - \begin{bmatrix} 0 & C_{L,\bar{q}} & 0 \\ C_{Y,\bar{p}} & 0 & C_{Y,\bar{r}} \\ C_{\ell,\bar{p}} & 0 & C_{\ell,\bar{r}} \\ 0 & C_{m,\bar{q}} & 0 \\ C_{n,\bar{p}} & 0 & C_{n,\bar{r}} \end{bmatrix} \begin{Bmatrix} \bar{p} \\ \bar{q} \\ \bar{r} \end{Bmatrix} \tag{6.7.20}$$

From Eqs. (6.7.2), (6.7.8), and (6.7.16), we obtain

$$\begin{Bmatrix} \bar{p} \\ \bar{q} \\ \bar{r} \end{Bmatrix} = \begin{Bmatrix} -R_{gy} \sin\gamma \tan\phi \\ R_{gx} \cos\gamma \sin\phi \tan\phi \\ R_{gy} \cos\gamma \sin\phi \end{Bmatrix} \tag{6.7.21}$$

where

$$R_{gx} \equiv \frac{g\bar{c}_w}{2V^2} \tag{6.7.22}$$

$$R_{gy} \equiv \frac{gb_w}{2V^2} \tag{6.7.23}$$

Using Eq. (6.7.21) in Eq. (6.7.20) gives

$$\begin{bmatrix} C_{L,\alpha} & 0 & 0 & C_{L,\delta_e} & 0 \\ 0 & C_{Y,\beta} & 0 & 0 & C_{Y,\delta_r} \\ 0 & C_{\ell,\beta} & C_{\ell,\delta_a} & 0 & C_{\ell,\delta_r} \\ C_{m,\alpha} & C_{m,\beta} & 0 & C_{m,\delta_e} & 0 \\ C_{n,\alpha} & C_{n,\beta} & C_{n,\delta_a} & 0 & C_{n,\delta_r} \end{bmatrix} \begin{Bmatrix} \alpha \\ \beta \\ \delta_a \\ \delta_e \\ \delta_r \end{Bmatrix} = \begin{Bmatrix} C_W \cos\gamma/\cos\phi - C_{L0} - R_{gx} C_{L,\bar{q}} \cos\gamma \sin\phi \tan\phi \\ R_{gy}(C_{Y,\bar{p}} \sin\gamma \tan\phi - C_{Y,\bar{r}} \cos\gamma \sin\phi) \\ R_{gy}(C_{\ell,\bar{p}} \sin\gamma \tan\phi - C_{\ell,\bar{r}} \cos\gamma \sin\phi) \\ -C_{m0} - R_{gx} C_{m,\bar{q}} \cos\gamma \sin\phi \tan\phi \\ R_{gy}(C_{n,\bar{p}} \sin\gamma \tan\phi - C_{n,\bar{r}} \cos\gamma \sin\phi) \end{Bmatrix} \tag{6.7.24}$$

If the aerodynamic derivatives are all known, Eq. (6.7.24) can be solved for the control surface deflection angles required to maintain a steady coordinated turn with airspeed, V, climb angle, γ, and bank angle, ϕ. In this formulation, we have used the bank angle to characterize the severity of the turn. Other important measures that are commonly used to characterize a turn include the turning radius, the turning rate, and the load factor. In the steady coordinated turn, these four quantities are all related. If any one is known together with the climb angle and airspeed, the other three can easily be determined. From Eq. (3.9.6), the bank angle can be related to the turning radius, R,

$$\phi = \tan^{-1}\left(\frac{V^2 \cos\gamma}{Rg}\right) \tag{6.7.25}$$

Similarly, from Eq. (6.7.8), the bank angle can be computed from the turning rate, Ω,

$$\phi = \tan^{-1}\left(\frac{\Omega V}{g}\right) \tag{6.7.26}$$

and from Eq. (6.7.11), the bank angle can also be related to the load factor, L/W,

$$\phi = \cos^{-1}\left(\frac{\cos\gamma}{L/W}\right) \tag{6.7.27}$$

Here, the reader may recall that the traditional symbol used to denote load factor is n, which is also the symbol traditionally used to signify the yawing rate. This was a very unfortunate choice of notation, but it is well established in the literature and we must learn to live with it. Both load factor and yawing rate are important parameters in the analysis of turning flight and it is common to see the symbol, n, used to represent both of these parameters in the same formulation. It is usually left up to the reader to determine where n denotes load factor and where it denotes yawing rate. In this text, tradition will not be carried to that extreme. Whenever load factor and yawing rate are used in the same formulation, the more explicit notation, L/W, will be used for the load factor. However, the reader should be forewarned that this is not the norm.

EXAMPLE 6.7.1. Consider a level coordinated turn for the airplane described in Examples 5.2.1, 5.2.2, 5.5.1, and 6.1.1. All control surfaces are trimmed for steady level flight at 80 mph and sea level. Ignoring any possibility of stall, we wish to plot the change in aileron, elevator, and rudder deflection angles required to maintain the level coordinated turn, at the same airspeed and altitude, as a function bank angle. For this airplane and operating condition we will use

$$S_w = 180 \text{ ft}^2, \quad b_w = 33 \text{ ft}, \quad W = 2{,}700 \text{ lbf}, \quad V = 80 \text{ mph}, \quad C_W = 0.9168,$$
$$C_{L,\alpha} = 4.88, \quad C_{L,\delta_e} = 0.476, \quad C_{L,\bar{q}} = 3.00,$$
$$C_{Y,\beta} = -0.508, \quad C_{Y,\delta_r} = 0.131, \quad C_{Y,\bar{p}} = 0.00, \quad C_{Y,\bar{r}} = 0.142,$$

$$C_{\ell,\beta} = -0.050, \quad C_{\ell,\delta_a} = -0.134, \quad C_{\ell,\delta_r} = 0.012, \quad C_{\ell,\bar{p}} = -0.411,$$
$$C_{m,\alpha} = -0.587, \quad C_{m,\beta} = -0.031, \quad C_{m,\delta_e} = -1.31, \quad C_{m,\bar{q}} = -11.05,$$
$$C_{n,\alpha} = -0.0051, \quad C_{n,\beta} = 0.071, \quad C_{n,\delta_a} = 0.0035, \quad C_{n,\delta_r} = -0.059, \quad C_{n,\bar{p}} = -0.057,$$
$$C_{\ell,\bar{r}} = 0.020 + 0.25C_L, \quad C_{n,\bar{r}} = -0.114 - 0.024C_L^2,$$
$$R_{gx} \equiv g\bar{c}_w/2V^2 = 0.00637, \quad R_{gy} \equiv gb_w/2V^2 = 0.03856$$

Solution. Let the aerodynamic angles and control surface deflections for the steady level coordinated turn be expressed as

$$\begin{Bmatrix} \alpha \\ \beta \\ \delta_a \\ \delta_e \\ \delta_r \end{Bmatrix} = \begin{Bmatrix} \alpha \\ \beta \\ \delta_a \\ \delta_e \\ \delta_r \end{Bmatrix}_{\text{trim}} + \begin{Bmatrix} \Delta\alpha \\ \Delta\beta \\ \Delta\delta_a \\ \Delta\delta_e \\ \Delta\delta_r \end{Bmatrix} \tag{6.7.28}$$

where the trim condition is evaluated for steady level flight at the same airspeed and elevation. Steady level flight is a special case of the steady coordinated turn where both the bank angle and climb angle are zero. Thus, the trim condition must satisfy Eq. (6.7.24) with both ϕ and γ set to zero.

$$\begin{bmatrix} C_{L,\alpha} & 0 & 0 & C_{L,\delta_e} & 0 \\ 0 & C_{Y,\beta} & 0 & 0 & C_{Y,\delta_r} \\ 0 & C_{\ell,\beta} & C_{\ell,\delta_a} & 0 & C_{\ell,\delta_r} \\ C_{m,\alpha} & C_{m,\beta} & 0 & C_{m,\delta_e} & 0 \\ C_{n,\alpha} & C_{n,\beta} & C_{n,\delta_a} & 0 & C_{n,\delta_r} \end{bmatrix} \begin{Bmatrix} \alpha \\ \beta \\ \delta_a \\ \delta_e \\ \delta_r \end{Bmatrix}_{\text{trim}} = \begin{Bmatrix} C_W - C_{L0} \\ 0 \\ 0 \\ -C_{m0} \\ 0 \end{Bmatrix} \tag{6.7.29}$$

Using Eq. (6.7.28) in Eq. (6.7.24) and applying Eq. (6.7.29) gives

$$\begin{bmatrix} C_{L,\alpha} & 0 & 0 & C_{L,\delta_e} & 0 \\ 0 & C_{Y,\beta} & 0 & 0 & C_{Y,\delta_r} \\ 0 & C_{\ell,\beta} & C_{\ell,\delta_a} & 0 & C_{\ell,\delta_r} \\ C_{m,\alpha} & C_{m,\beta} & 0 & C_{m,\delta_e} & 0 \\ C_{n,\alpha} & C_{n,\beta} & C_{n,\delta_a} & 0 & C_{n,\delta_r} \end{bmatrix} \begin{Bmatrix} \Delta\alpha \\ \Delta\beta \\ \Delta\delta_a \\ \Delta\delta_e \\ \Delta\delta_r \end{Bmatrix}$$
$$= \begin{Bmatrix} C_W[(\cos\gamma/\cos\phi) - 1] - R_{gx}C_{L,\bar{q}}\cos\gamma\sin\phi\tan\phi \\ R_{gy}(C_{Y,\bar{p}}\sin\gamma\tan\phi - C_{Y,\bar{r}}\cos\gamma\sin\phi) \\ R_{gy}(C_{\ell,\bar{p}}\sin\gamma\tan\phi - C_{\ell,\bar{r}}\cos\gamma\sin\phi) \\ -R_{gx}C_{m,\bar{q}}\cos\gamma\sin\phi\tan\phi \\ R_{gy}(C_{n,\bar{p}}\sin\gamma\tan\phi - C_{n,\bar{r}}\cos\gamma\sin\phi) \end{Bmatrix} \tag{6.7.30}$$

Using the aerodynamic derivatives for this airplane, the 5×5 matrix on the left-hand side of Eq. (6.7.30) is

$$[\mathbf{A}] \equiv \begin{bmatrix} C_{L,\alpha} & 0 & 0 & C_{L,\delta_e} & 0 \\ 0 & C_{Y,\beta} & 0 & 0 & C_{Y,\delta_r} \\ 0 & C_{\ell,\beta} & C_{\ell,\delta_a} & 0 & C_{\ell,\delta_r} \\ C_{m,\alpha} & C_{m,\beta} & 0 & C_{m,\delta_e} & 0 \\ C_{n,\alpha} & C_{n,\beta} & C_{n,\delta_a} & 0 & C_{n,\delta_r} \end{bmatrix}$$

$$= \begin{bmatrix} 4.88 & 0 & 0 & 0.476 & 0 \\ 0 & -0.508 & 0 & 0 & 0.131 \\ 0 & -0.050 & -0.134 & 0 & 0.012 \\ -0.587 & -0.031 & 0 & -1.31 & 0 \\ -0.0051 & 0.071 & 0.0035 & 0 & -0.059 \end{bmatrix}$$

Since this matrix is independent of both climb angle and bank angle, the system of equations does not need to be solved separately for each value of bank angle to be used in the plot. The matrix need only be inverted once. The matrix can be inverted numerically to give

$$[\mathbf{A}]^{-1} = \begin{bmatrix} 0.21427 & -0.00685 & -0.00040 & 0.07786 & -0.01529 \\ -0.00692 & -2.83723 & -0.16542 & -0.00251 & -6.33325 \\ 0.00018 & 0.75698 & -7.45841 & 0.00007 & 0.16380 \\ -0.09585 & 0.07021 & 0.00409 & -0.79819 & 0.15672 \\ -0.02684 & -3.36879 & -0.64148 & -0.00975 & -24.55949 \end{bmatrix}$$

Choosing an example bank angle of 30 degrees and applying Eq. (6.7.11), the coordinated turn with $\gamma = 0$ at 80 mph and sea level gives

$$C_L = C_W \cos\gamma / \cos\phi = 1.05861$$

$$C_{\ell,\bar{r}} = 0.020 + 0.25 C_L = 0.28465$$

$$C_{n,\bar{r}} = -0.114 - 0.024 C_L^2 = -0.14090$$

$$\begin{Bmatrix} C_W[(\cos\gamma/\cos\phi) - 1] - R_{gx} C_{L,\bar{q}} \cos\gamma \sin\phi \tan\phi \\ R_{gy}(C_{Y,\bar{p}} \sin\gamma \tan\phi - C_{Y,\bar{r}} \cos\gamma \sin\phi) \\ R_{gy}(C_{\ell,\bar{p}} \sin\gamma \tan\phi - C_{\ell,\bar{r}} \cos\gamma \sin\phi) \\ -R_{gx} C_{m,\bar{q}} \cos\gamma \sin\phi \tan\phi \\ R_{gy}(C_{n,\bar{p}} \sin\gamma \tan\phi - C_{n,\bar{r}} \cos\gamma \sin\phi) \end{Bmatrix} = \begin{Bmatrix} 0.13631 \\ -0.00274 \\ -0.00549 \\ 0.02033 \\ 0.00272 \end{Bmatrix}$$

The changes in the aerodynamic angles and control surface deflections for this particular bank angle can now be found by multiplying this vector by the inverted matrix $[\mathbf{A}]^{-1}$,

$$\begin{Bmatrix} \Delta\alpha \\ \Delta\beta \\ \Delta\delta_a \\ \Delta\delta_e \\ \Delta\delta_r \end{Bmatrix}_{\phi=30^\circ} = [\mathbf{A}]^{-1} \begin{Bmatrix} 0.13631 \\ -0.00274 \\ -0.00549 \\ 0.02033 \\ 0.00272 \end{Bmatrix} = \begin{Bmatrix} 0.03077 \\ -0.00952 \\ 0.03933 \\ -0.02908 \\ -0.05782 \end{Bmatrix} = \begin{Bmatrix} 1.8^\circ \\ -0.5^\circ \\ 2.3^\circ \\ -1.7^\circ \\ -3.3^\circ \end{Bmatrix}$$

Similarly, a bank angle of −30 degrees requires that

$$\begin{Bmatrix} \Delta\alpha \\ \Delta\beta \\ \Delta\delta_a \\ \Delta\delta_e \\ \Delta\delta_r \end{Bmatrix}_{\phi=-30^\circ} = [\mathbf{A}]^{-1} \begin{Bmatrix} 0.13631 \\ 0.00274 \\ 0.00549 \\ 0.02033 \\ -0.00272 \end{Bmatrix} = \begin{Bmatrix} 0.03081 \\ 0.00753 \\ -0.03928 \\ -0.02950 \\ 0.05011 \end{Bmatrix} = \begin{Bmatrix} 1.8^\circ \\ 0.4^\circ \\ -2.3^\circ \\ -1.7^\circ \\ 2.9^\circ \end{Bmatrix}$$

Repeating these computations for a range of bank angles and neglecting the possibility of stall, we obtain the results that are plotted in Fig. 6.7.2.

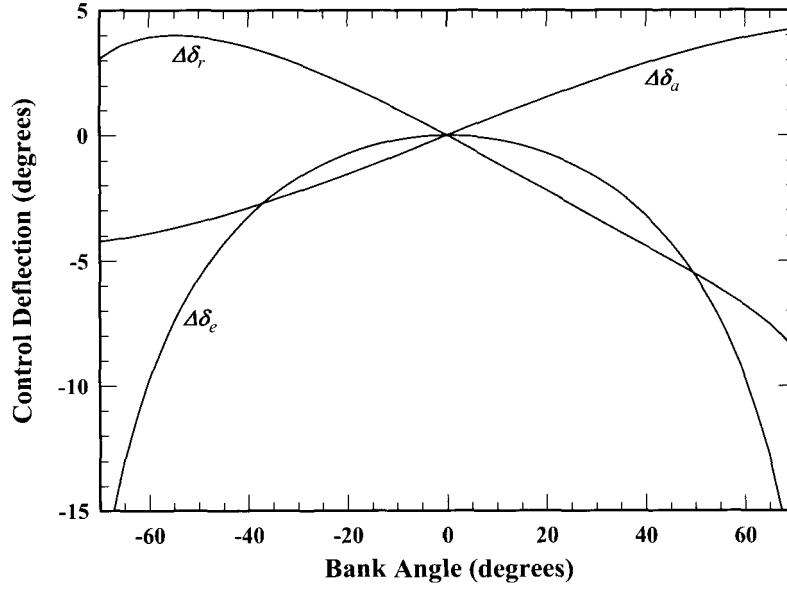


Figure 6.7.2. Control surface deflections for a steady coordinated turn, from Example 6.7.1.

Notice that for the airplane in Example 6.7.1, the rudder deflection is not symmetric with respect to right and left turns. This is a direct result of the yawing moment produced by the airplane's conventional right-hand propeller. When the airplane is turned either to the right or to the left, additional lift is needed to produce the turning acceleration. As seen in Fig. 6.7.2, an increment of up elevator (negative $\Delta\delta_e$) must be applied to increase the angle of attack and generate this added lift. However, the increase in angle of attack also produces an increased propeller yawing moment to the left. This must be countered with an increment of right rudder (negative $\Delta\delta_r$). If the airplane is being turned to the right (positive ϕ), the right rudder needed to compensate for the propeller yawing moment adds to the right rudder needed for the turn. If the airplane is being turned to the left, the right rudder needed to compensate for the propeller yawing moment decreases the left rudder needed for the turn.

It should also be noted from Fig. 6.7.2 that left aileron (positive $\Delta\delta_a$) is needed to maintain a right turn (positive ϕ). This may seem counterintuitive to some. From the sign convention and definitions presented in Sec. 5.6, it is clear that right aileron (negative $\Delta\delta_a$) is needed to initiate a roll to the right. Why then was left aileron predicted for the right turn in Example 6.7.1? To answer this question we must recognize that in a steady level coordinated turn, the bank angle is held constant and the airplane is not rolling. To initiate a right turn the pilot does need to provide right aileron input. This will start the airplane rolling to the right, increasing the bank angle. However, if the pilot continues to apply right aileron, the airplane will continue to roll and the bank angle will continue to increase. To stop the roll when the desired bank angle is reached, it seems reasonable that the pilot may need to briefly apply a little left aileron. Nevertheless, this still does not explain why left aileron should be needed to hold the bank angle constant in a coordinated right turn. This can be better understood by examining the reason that the rudder is needed to coordinate the turn.

The amount of right rudder needed to sustain a right turn depends primarily on the change in the yawing moment coefficient with respect to yawing rate, $C_{n,\bar{r}}$, which is commonly referred to as the *yaw-damping derivative*. As the airplane negotiates a right turn, the center of gravity follows a curved path and the airflow relative to the airplane is curved as shown in Fig. 6.7.3. This curvature of the relative wind has a significant effect on the yawing moment acting on the airplane. As seen in Fig. 6.7.3, this curvature produces sidewash on the vertical stabilizer, increases the airspeed over the outside wing semispan, and decreases the airspeed over the inside wing semispan. Thus, a right turn generates a side force to the right on the aft vertical stabilizer, increases the lift and drag on the left wing semispan, and decreases the lift and drag on the right wing semispan. For a conventional airplane with an aft vertical stabilizer having an aerodynamic center above the airplane's center of gravity, all of these effects tend to yaw the airplane to the left and roll it to the right. To counter the yawing moment produced by flight-path curvature in a right turn, some right rudder is required. Additionally, a left increment in the rolling moment is needed to compensate for the effects of flight-path curvature on the rolling moment produced in a right turn. Because of the roll-yaw coupling, right rudder will usually produce some left increment in the rolling moment, but this is almost never sufficient to counter the effects of flight-path curvature, and some left aileron is also typically needed.

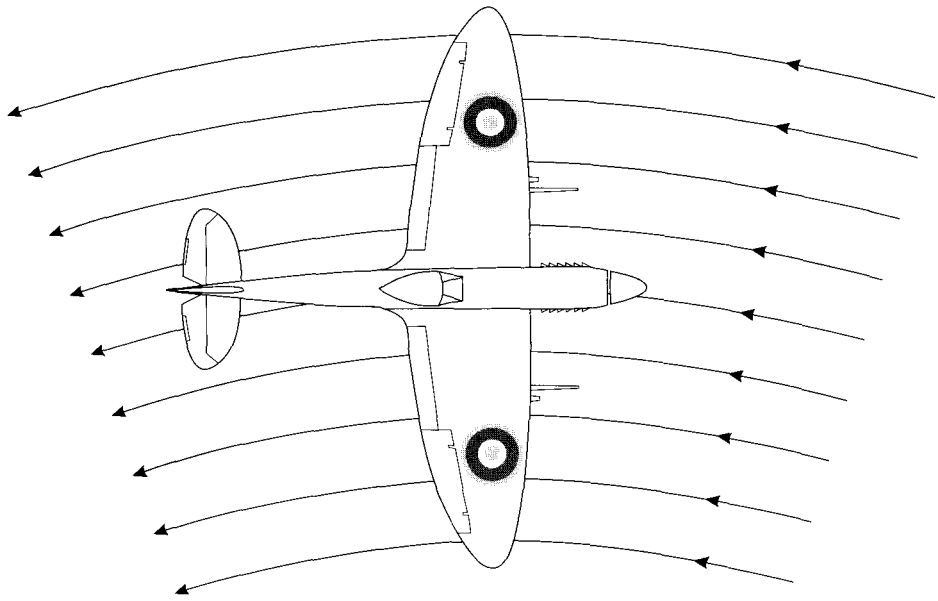


Figure 6.7.3. Top view of the airflow relative to an airplane in a right turn.

Example 6.7.1 was confined to the special case of a level turn (i.e., $\gamma = 0$). In a steady level coordinated turn the rolling rate is zero. This is not the case for a climbing or diving turn. Even though the bank angle remains constant in any steady turn, the airplane will experience a constant rolling rate when climbing or descending during a turn. As can be seen in Eq. (6.7.2), when climbing or descending while turning about the vertical axis, an airplane has a rolling rate that is proportional to the turning rate multiplied by the sine of the climb angle, $p = -\Omega \sin\gamma$. This rolling rate can have a significant effect on the control surface deflections required to sustain the turn, because the rolling rate substantially affects the aerodynamic moments. The investigation of these effects is left as an exercise for the student.

6.8. Aileron Reversal

In Sec. 6.2 we have seen that the lift developed on the horizontal stabilizer at a given fuselage angle of attack and the pitching moment created as the result of a given elevator deflection are reduced by aeroelastic bending of the fuselage. The aerodynamic forces and moments produced on the wing are also affected by deformation, which is caused by the aerodynamic loading. Aeroelastic bending of the wing causes a change in wing dihedral, as was shown in Fig. 6.2.1. However, the wing's bending stiffness typically has little effect on the rolling moment produced by the ailerons. The torsional stiffness of the wing, on the other hand, can significantly alter aileron effectiveness.

Flap deflection produces a pitching moment about the aerodynamic center of an airfoil section. Thus, when the right aileron is deflected down and the left aileron is

deflected up, the outboard wing sections on the right experience a negative increment in pitching moment while those on the left experience a positive increment in pitching moment. This differential pitching moment between the outboard sections of right and left semispans produces a twisting deformation of the wing, as shown in Fig. 6.8.1. The wing twist increases the angle of attack on the left and decreases it on the right, thereby reducing the rolling moment produced by the ailerons.

For small deflection angles, the aerodynamic twisting moment generated by aileron deflection is linearly proportional to the product of the dynamic pressure and the aileron deflection angle,

$$\Delta m_t = \tfrac{1}{2}\rho V^2 S_w \bar{c}_w C_{m_t,\delta_a}\delta_a \tag{6.8.1}$$

where C_{m_t,δ_a} can be simply viewed as an aerodynamic proportionality constant. From a structural viewpoint, the twisting moment on the wing must be linearly proportional to the twist deformation angle, τ,

$$\Delta m_t = k_t \tau \tag{6.8.2}$$

where k_t is a torsional stiffness coefficient. For small deflection angles, the net change in the rolling moment coefficient is linearly proportional to both the aileron deflection angle and the twist deformation angle,

$$\Delta C_\ell = \left(C_{\ell,\delta_a}\right)_{\text{rigid}}\delta_a - C_{\ell,\tau}\tau \tag{6.8.3}$$

Combining Eqs. (6.8.1) through (6.8.3), we obtain

$$\Delta C_\ell = \left[\left(C_{\ell,\delta_a}\right)_{\text{rigid}} - \tfrac{1}{2}\rho V^2 S_w \bar{c}_w C_{\ell,\tau} C_{m_t,\delta_a}/k_t\right]\delta_a \tag{6.8.4}$$

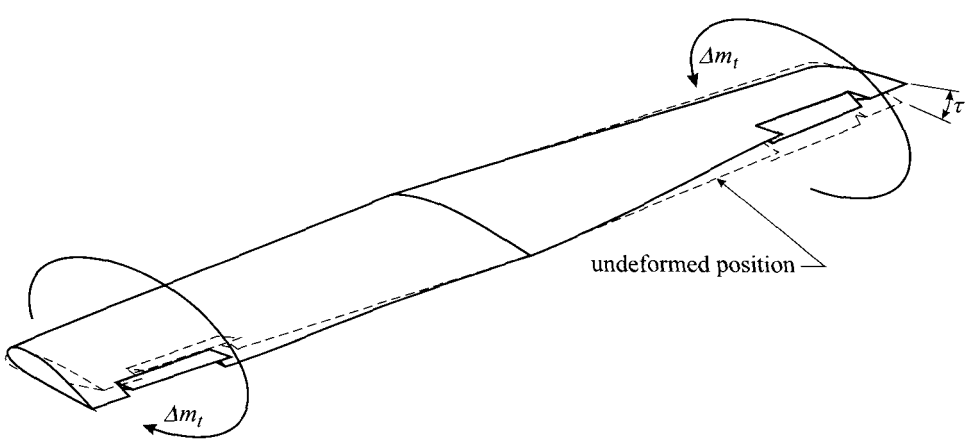


Figure 6.8.1. Deformation of a wing due to the twisting moment produced by aileron deflection.

From Eq. (6.8.4), we see that the net lateral control derivative, including the effect of wing twist, is given by

$$C_{\ell,\delta_a} = \left(C_{\ell,\delta_a}\right)_{\text{rigid}} - \frac{\rho V^2 S_w \bar{c}_w C_{\ell,\tau} C_{m_t,\delta_a}}{2k_t} \tag{6.8.5}$$

which shows that aileron effectiveness is decreased in direct proportion to the airspeed squared and in inverse proportion to the torsional stiffness of the wing. From this result we see that there is an aileron reversal speed that is proportional to the square root of the wing's torsional stiffness,

$$V_{ar} = \sqrt{\frac{2k_t\left(C_{\ell,\delta_a}\right)_{\text{rigid}}}{\rho S_w \bar{c}_w C_{\ell,\tau} C_{m_t,\delta_a}}} \tag{6.8.6}$$

At this airspeed, aileron deflection produces no rolling moment. At higher airspeeds, aileron control is reversed.

Because of the complex cross-sections used to construct the wing of an airplane, its torsional stiffness can only be determined experimentally or through the use of finite element analysis on a digital computer. Accurate estimation of the aerodynamic loading resulting from aileron deflection and wing twist also requires computer simulation. Since wing twist depends on aerodynamic loading and aerodynamic loading depends on wing twist, an iterative procedure must be used to estimate the change in rolling moment with respect to aileron deflection for a nonrigid wing. We can start by computing the aerodynamic loading for the undeformed or rigid wing. This loading is then used in a finite element structural analysis to determine the wing deformation. The aerodynamic computations are then repeated using the deformed geometry to obtain an improved estimate for the aerodynamic loading. The process is repeated until no further changes are observed.

All *fixed-wing* aircraft can be classified in one of two very broad categories, *rigid-wing* and *flex-wing* aircraft. Since aeroelastic deformation can never be eliminated in the lightweight structures required for flight, one might think that no airplane could ever be classified as a rigid-wing. However, this is not how the two categories are defined. **A rigid-wing aircraft is one in which the moments that result from the elastic deformation of the wing are less than those that result from control surface deflections.** On the other hand, **a flex-wing aircraft is one that derives the control moment primarily from elastic deformation of the wing.** When all things that fly are considered, most could be categorized as flex-wings. However, when we consider only those aircraft designed and built by humans, most are rigid-wings. **In a rigid-wing airplane, the wing should have sufficient torsional stiffness so that the aileron control reversal speed exceeds the maximum airspeed that could ever be attained by the airplane.**

When a wing is very flexible in torsion, as it is on birds and some ultralight aircraft such as hang gliders, the aileron control reversal speed for the wing could actually be less than the wing stall speed, and ailerons would not work at all in the conventional manner.

On such a wing, ailerons would work very much like trim tabs. A downward deflection of an aileron would twist the outboard sections of the wing semispan to sufficiently reduce the angle of attack so that a rolling moment would be produced in the same direction as the aileron deflection. This could still work as an aircraft control. However, the control derivative would be positive instead of negative and the ailerons would need to be linked to the stick or control yoke accordingly.

6.9. Other Control Surface Configurations

To this point we have treated trim, control, and maneuverability as though the airplane had fixed horizontal and vertical stabilizers combined with a control set composed of movable ailerons, elevator, and rudder, all with adjustable trim tabs. Alternative control surface configurations are commonly used. However, with suitable variable definitions, results obtained for these other configurations are very similar to those obtained for the conventional controls that have already been discussed.

Three different control surface configurations that are used for pitch control are shown in Fig. 6.9.1. The first is the conventional fixed stabilizer with movable elevator, which has already been treated. The second is often referred to as an *all-flying tail* and can be thought of as a special case of the stabilizer-elevator configuration with an elevator chord fraction of 1.0. The last configuration shown in Fig. 6.9.1 is called a *stabilator*. With this configuration, the entire horizontal surface is movable, but there is also an aft trailing-edge flap that moves relative to the forward portion of this surface.

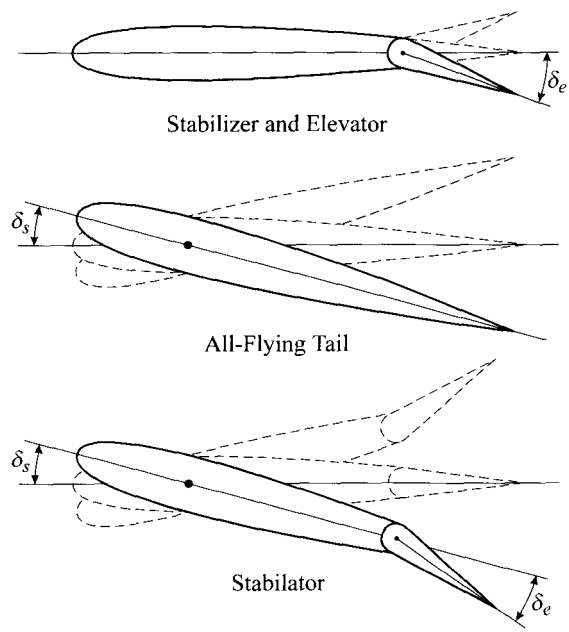


Figure 6.9.1. Three different configurations used for pitch control.

The Stabilator

Since both the stabilizer-elevator configuration and the all-flying tail can be viewed as special cases of the stabilator, this configuration is the most general of the three. From an external visual inspection, most people could not distinguish between a stabilator and a conventional stabilizer-elevator configuration. The external geometry is essentially the same. The difference is that there are two degrees of freedom associated with the deflection of a stabilator. The entire horizontal surface can be moved through a deflection angle that shall be denoted here as δ_s. Additionally, the trailing-edge flap can be deflected relative to the forward portion of the surface through a deflection angle indicated here by δ_e. The sign convention that will be used for both of these angles is positive with the leading edge up and the trailing edge down, as shown in Fig. 6.9.1.

While a stabilator has two deflection angles that could be controlled independently, the pilot has only one pitch control. To induce a nose-down pitching moment the pilot pushes the stick or control yoke forward, and pulling the control back creates a nose-up pitching moment. To maintain the conventional cockpit controls, the two stabilator deflection angles are linked together, either mechanically or electronically. The cockpit control is linked to the primary control surface deflection, δ_s, and the trailing-edge flap deflection, δ_e, is linked to the primary control surface deflection so that

$$\delta_e = k_{es}\delta_s + \delta_{et} \tag{6.9.1}$$

where the constant k_{es} can be varied by the designer but not usually by the pilot. In a mechanical system, k_{es} is fixed by the mechanical linkage between the primary control surface deflection and the trailing-edge flap deflection. The offset, δ_{et}, can usually be adjusted by the pilot as a trim setting to zero the control force at trim for some desired airspeed, much as a trim tab is used on a conventional elevator.

Following a procedure similar to that used to obtain Eqs. (6.1.16) and (6.1.17), the lift and pitching moment coefficients for a wing combined with a stabilator are

$$\begin{aligned} C_L &= C_{L_w,\alpha}\left(\alpha + \frac{2l_w}{\bar{c}_w}\bar{q} + \alpha_{0w} - \alpha_{L0w}\right) \\ &\quad + \frac{S_h}{S_w}\eta_h C_{L_h,\alpha}\left(\alpha + \frac{2l_h}{\bar{c}_w}\bar{q} + \alpha_{0h} - \alpha_{L0h} - \varepsilon_d + \delta_s + \varepsilon_e\delta_e\right) \end{aligned} \tag{6.9.2}$$

$$\begin{aligned} C_m &= C_{m_w} - \frac{l_w}{\bar{c}_w}C_{L_w,\alpha}\left(\alpha + \frac{2l_w}{\bar{c}_w}\bar{q} + \alpha_{0w} - \alpha_{L0w}\right) \\ &\quad + \frac{S_h\bar{c}_h}{S_w\bar{c}_w}\eta_h(C_{m_h0} + C_{m_h,\delta_e}\,\delta_e) \\ &\quad - \frac{S_h l_h}{S_w\bar{c}_w}\eta_h C_{L_h,\alpha}\left(\alpha + \frac{2l_h}{\bar{c}_w}\bar{q} + \alpha_{0h} - \alpha_{L0h} - \varepsilon_d + \delta_s + \varepsilon_e\delta_e\right) \end{aligned} \tag{6.9.3}$$

where the remaining notation is the same as that defined for the stabilizer-elevator configuration. Using Eq. (6.9.1), these two equations can be written as

$$C_L = C_{L0} + C_{L,\delta_e}\delta_{et} + C_{L,\alpha}\alpha + C_{L,\bar{q}}\bar{q} + C_{L,\delta_s}\delta_s \tag{6.9.4}$$

$$C_m = C_{m0} + C_{m,\delta_e}\delta_{et} + C_{m,\alpha}\alpha + C_{m,\bar{q}}\bar{q} + C_{m,\delta_s}\delta_s \tag{6.9.5}$$

where

$$C_{L,\delta_s} = \frac{S_h}{S_w}\eta_h C_{L_h,\alpha}(1+\varepsilon_e k_{es}) \tag{6.9.6}$$

$$C_{m,\delta_s} = \frac{S_h\bar{c}_h}{S_w\bar{c}_w}\eta_h C_{m_h,\delta_e}k_{es} - \frac{S_h l_h}{S_w\bar{c}_w}\eta_h C_{L_h,\alpha}(1+\varepsilon_e k_{es}) \tag{6.9.7}$$

and all of the other aerodynamic coefficients are the same as those for the stabilizer-elevator configuration as defined in Eqs. (6.1.20) through (6.1.27). Continuing to follow a development similar to that used for the stabilizer-elevator configuration, the fuselage angle of attack at level trim for the stabilator configuration is found to be

$$(\alpha)_{\text{trim}} = \frac{(C_W - C_{L0} - C_{L,\delta_e}\delta_{et})C_{m,\delta_s} + (C_{m0} + C_{m,\delta_e}\delta_{et})C_{L,\delta_s}}{C_{L,\alpha}C_{m,\delta_s} - C_{L,\delta_s}C_{m,\alpha}} \tag{6.9.8}$$

The stabilator angle at level trim is

$$(\delta_s)_{\text{trim}} = -\frac{(C_W - C_{L0} - C_{L,\delta_e}\delta_{et})C_{m,\alpha} + (C_{m0} + C_{m,\delta_e}\delta_{et})C_{L,\alpha}}{C_{L,\alpha}C_{m,\delta_s} - C_{L,\delta_s}C_{m,\alpha}} \tag{6.9.9}$$

Similarly, the stabilator angle per g is

$$\frac{\partial\delta_s}{\partial n} = -\frac{C_W C_{m,\alpha} + (C_{L,\alpha}C_{m,\bar{q}} - C_{L,\bar{q}}C_{m,\alpha})(g\bar{c}_w/2V^2)}{C_{L,\alpha}C_{m,\delta_s} - C_{L,\delta_s}C_{m,\alpha}} \tag{6.9.10}$$

Because the primary stabilator hinge is used to rotate the entire horizontal surface, the stabilator hinge moment coefficient is defined as

$$C_{H_s} \equiv \frac{H_s}{\frac{1}{2}\rho V_h^2 S_h\bar{c}_h} \tag{6.9.11}$$

where H_s is the hinge moment for the primary stabilator hinge. With this definition, the stabilator hinge moment coefficient can be written as

$$\begin{aligned} C_{H_s} &= C_{m_h 0} + C_{m_h,\delta_e}\delta_e \\ &\quad -\frac{l_{Hs}}{\bar{c}_h}C_{L_h,\alpha}\left(\alpha + \frac{2l_h}{\bar{c}_w}\bar{q} + \alpha_{0h} - \alpha_{L0h} - \varepsilon_d + \delta_s + \varepsilon_e\delta_e\right) \end{aligned} \tag{6.9.12}$$

where l_{Hs} is the distance that the aerodynamic center of the entire stabilator surface is aft of the primary hinge. The designer can vary this length, but it is typically set close to zero so that the pitch control force can be kept within allowable limits. Applying Eq. (6.9.1), Eq. (6.9.12) can be rearranged as

$$\begin{aligned} C_{H_s} &= C_{H_s 0} + C_{H_s,\alpha_h}[\alpha_{0h} - \varepsilon_{d0} + (1-\varepsilon_{d,\alpha})\alpha + \frac{2l_h}{\bar{c}_w}\bar{q}] \\ &\quad + C_{H_s,\delta_s}\delta_s + C_{H_s,\delta_e}\delta_{et} \end{aligned} \tag{6.9.13}$$

where

$$C_{H_s 0} = C_{m_h 0} + \frac{l_{Hs}}{\bar{c}_h} C_{L_h,\alpha}\,\alpha_{L0h} \tag{6.9.14}$$

$$C_{H_s,\alpha_h} = -\frac{l_{Hs}}{\bar{c}_h} C_{L_h,\alpha} \tag{6.9.15}$$

$$C_{H_s,\delta_s} = C_{m_h,\delta_e} k_{es} - \frac{l_{Hs}}{\bar{c}_h} C_{L_h,\alpha}(1+\varepsilon_e k_{es}) \tag{6.9.16}$$

$$C_{H_s,\delta_e} = C_{m_h,\delta_e} - \frac{l_{Hs}}{\bar{c}_h} C_{L_h,\alpha}\,\varepsilon_e \tag{6.9.17}$$

The pitch control force exerted by the pilot for a stabilator operated by an all-mechanical control system would then be

$$\begin{aligned} F_p &= \frac{H_s}{l_g} = \frac{\frac{1}{2}\rho V^2 \eta_h S_h \bar{c}_h}{l_g} \\ &\times \left\{ C_{H_s 0} + C_{H_s,\alpha_h}[\alpha_{0h} - \varepsilon_{d0} + (1-\varepsilon_{d,\alpha})\alpha + \frac{2l_h}{\bar{c}_w}\bar{q}] + C_{H_s,\delta_s}\delta_s + C_{H_s,\delta_e}\delta_{et} \right\} \end{aligned} \tag{6.9.18}$$

Notice that this has exactly the same form as Eq. (6.3.8).

Continuing to follow the development in Sec. 6.3, with a stabilator the pitch control force required for constant airspeed and constant normal acceleration is

$$F_p = \eta_h \frac{S_h \bar{c}_h}{S_w l_g}\left[C_1\left(n - \frac{V^2}{V_{\text{trim}}^2} \right) W + C_2 (n-1)\frac{\rho g S_w \bar{c}_w}{4} \right] \tag{6.9.19}$$

where

$$C_1 = \frac{C_{m,\delta_s} C_{H_s,\alpha_h}(1-\varepsilon_{d,\alpha}) - C_{m,\alpha} C_{H_s,\delta_s}}{C_{L,\alpha} C_{m,\delta_s} - C_{L,\delta_s} C_{m,\alpha}} \tag{6.9.20}$$

$$C_2 = \frac{2l_h C_{H_s,\alpha_h}}{\bar{c}_w} + \frac{(C_{L,\delta_s}C_{m,\bar{q}} - C_{L,\bar{q}}C_{m,\delta_s})C_{H_s,\alpha_h}(1-\varepsilon_{d,\alpha}) - (C_{L,\alpha}C_{m,\bar{q}} - C_{L,\bar{q}}C_{m,\alpha})C_{H_s,\delta_s}}{C_{L,\alpha}C_{m,\delta_s} - C_{L,\delta_s}C_{m,\alpha}} \tag{6.9.21}$$

The control force gradient and longitudinal control force per g for the stabilator are obtained from Eq. (6.9.19) in the same way that Eqs. (6.3.19) and (6.3.20) were obtained from Eq. (6.3.18).

The primary advantage of the stabilator over the stabilizer-elevator configuration is the extra flexibility afforded the designer in adjusting the control force derivatives for an all-mechanical control system. As discussed in Sec. 6.3, the mechanical control force for a stabilizer-elevator configuration increases rapidly with aircraft size. The added versatility of the stabilator allows the designer the possibility of using mechanical controls on larger airplanes. Investigation of this potential is left as an exercise for the student. A disadvantage of the stabilator is added complexity. An additional mechanism is required to link the primary hinge to the flap hinge. With all else being equal, increased complexity always translates to reduced reliability.

The All-Flying Tail

The all-movable or all-flying tail, which is also shown in Fig. 6.9.1, is hinged like the primary hinge of the stabilator, but it has no movable trailing-edge flap. For the purpose of analysis, the all-flying tail can be treated like an elevator having a flap chord fraction of 1.0. On the other hand, it could also be treated as a special case of the stabilator, having both k_{es} and δ_{et} set to zero. For these reasons, no additional analysis need be presented for this configuration.

Like the stabilator, the all-flying tail can provide an advantage for designs where it is difficult to keep the pitch control force within allowable limits and a mechanical control system is desired. If a symmetric airfoil is used and the hinge is located at the aerodynamic center, then the only moment needed to rotate the horizontal surface is that needed to overcome friction. With this design, the needed control force and trim adjustment could be provided by an adjustable spring mechanism. This allows a mechanical control system to be used on larger airplanes.

A disadvantage of this configuration, which is also shared by the stabilator, is that the hinge must carry all of the lift developed on the surface. The design of a freely moving hinge with adequate strength and stiffness for this purpose can be challenging but is not impossible. The problem is amplified by the fact that failure of the hinge would be catastrophic.

The Stabilizer-Elevator Configuration with All-Movable Trim Adjustment

There is a common variation of the stabilizer-elevator configuration that has exactly the same external geometry as the stabilator, which is shown in Fig. 6.9.1. The only difference between these two configurations is in how the pilot controls the two deflection angles. For this stabilizer-elevator configuration, the cockpit pitch control is linked to the elevator deflection, δ_e, just as it is in any stabilizer-elevator configuration.

However, instead of using a trim tab, the trim adjustment is linked to the stabilizer deflection angle, δ_s. This provides a broader range of trim adjustment than can be attained with a trim tab. With this type of trim adjustment the control force can be zeroed over a wider range airspeed, gross weight, and CG location. In addition to increased manufacturing cost, the price for this increased flexibility is linked to the possibility of failure. While the mechanism used to adjust the trim setting by changing the incidence angle of the stabilizer is probably no more likely to fail than a trim tab mechanism, the consequences of failure are very different. If the pilot looses the ability to adjust a trim tab, the result will be increased control forces over some portions of the flight. However, if the jack screw controlling an airplane's stabilizer incidence angle were to fail, the result would likely be complete control loss.

The V-Tail

A variation of the conventional aft tail with separate horizontal and vertical stabilizers is the v-tail, shown in Fig. 6.9.2. With this configuration, the vertical stabilizer is absent and the "horizontal" stabilizer has considerable dihedral, usually close to 45 degrees. The normal and spanwise components of lift developed on this v-shaped surface can be used to provide stability and control in both pitch and yaw.

Unlike the conventional elevator, the control surface on each side of a v-tail can be deflected separately. Each of these control surfaces is linked to both the stick or control

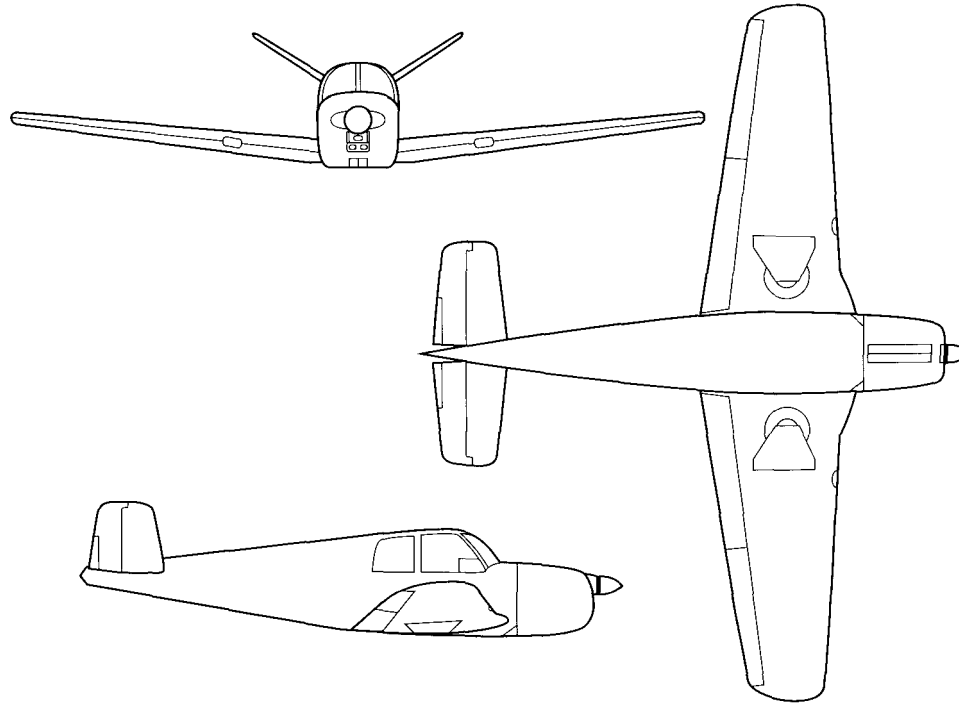


Figure 6.9.2. A general aviation airplane with the v-tail empennage.

yoke and to the rudder pedals. The position of the stick or control yoke determines the sum of the two deflection angles, and the position of the rudder pedals determines the difference. With the rudder pedals in the neutral position and the stick or control yoke pushed forward, both control surfaces are deflected downward through the same deflection angle, as shown in Fig. 6.9.3(a). With the pitch control in the neutral position and the left rudder pedal depresses, the control surface on the left is deflected downward and that on the right is deflected upward through the same deflection angle, as shown in Fig. 6.9.3(b). In addition to generating a yawing moment to the left, the control surface deflections that are shown in Fig. 6.9.3(b) will also produce a substantial rolling moment to the right.

Estimating the aerodynamic forces and moments developed by a v-tail as a function of angle of attack, sideslip angle, and control surface deflection angles is not a simple matter of using the results for a horizontal stabilizer multiplied by the appropriate sines and cosines. Lift developed on one side of the v-tail generates vorticity that produces downwash on the other side. This downwash affects the lift distribution over the entire empennage, and its effect depends significantly on the dihedral angle. The vortex interactions between the two sides of a v-tail are similar to those between the horizontal and vertical stabilizers of a conventional tail. This was discussed in Sec. 5.4 and shown schematically in Fig. 5.4.1. The classical infinite series solution to Prandtl's lifting-line theory cannot be used to estimate the forces and moments created by a v-tail, because this solution is only valid for lifting surfaces with no sweep or dihedral. In Sec. 5.5 an analytical method was developed for predicting the effects of dihedral and sideslip on the rolling moment coefficient. This method cannot be used for the v-tail, because it is based on the assumption of a small dihedral angle. The simplest analytical method that can be used to accurately estimate the aerodynamic forces and moments developed by a v-tail is the numerical lifting-line method.

The v-tail empennage has never been widely used. Perhaps the best known example of the v-tail design is the Beech Bonanza, which was the model for Fig. 6.9.2. The earliest versions of this airplane were manufactured in the late 1950s and early 1960s. Although many of these v-tail Bonanzas are still flying today, in later models the v-tail was replaced with a conventional aft tail. One possible reason for the dearth of v-tails is the inefficiency associated with producing control moments in this manner. When the control surfaces are deflected as shown in Fig. 6.9.3, only about 70 percent of the lift

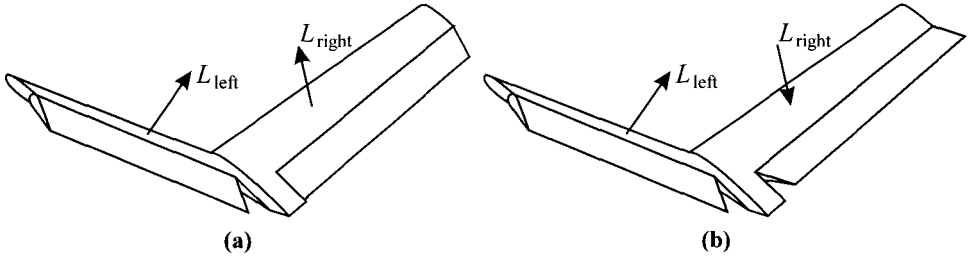


Figure 6.9.3. Control surface deflections for the v-tail empennage showing (a) down elevator equivalent and (b) left rudder equivalent.

developed on the empennage is useful in producing the desired moment. When the control surfaces are used to generate a pitching moment as shown in Fig. 6.9.3a, the horizontal components of lift on the right and left sides of the v-tail cancel. Only the vertical components of lift contribute to the pitching moment about the center of gravity. Similarly, when the control surfaces are used as shown in Fig. 6.9.3b to produce the equivalent of rudder deflection, only the horizontal components of lift contribute to the desired yawing moment and the vertical components cancel. The need to generate opposing components of lift on the two sides of a v-tail increases induced drag and reduces the maximum moment that can be produced by an empennage of any given size.

Ailerons, Spoilers, and Adverse Yaw

In Sec. 5.6 we learned that when conventional ailerons are used for roll control, an adverse yawing moment is generated as a result of the change in induced drag produced by aileron deflection. This tends to yaw the airplane in the direction opposite to the intended roll. The Frise aileron, shown in Fig. 6.9.4, can be used to reduce or eliminate this adverse yaw. These ailerons are shaped and hinged so that on the upward deflected aileron only, the leading edge projects out into the airflow. This increases the parasitic drag on the semispan with up aileron, producing a favorable yawing moment that counters the adverse yawing moment generated by the change in induced drag.

Aileron adverse yaw can also be avoided by using spoilers for roll control. A spoiler is a panel on the upper surface of a wing that can be raised into the airflow as shown in Fig. 6.9.5. The purpose of raising the spoiler is to induce flow separation, which destroys or "spoils" the lift on the wing sections involved. Raising a spoiler on the outboard sections of the left wing semispan produces a rolling moment to the left (negative ℓ). The raised left spoiler also increases the drag on the left semispan and produces a favorable yawing moment (negative n).

Spoilers could be used as the sole means of roll control, or they could be used in conjunction ailerons, as shown in Fig. 6.9.5. Since conventional ailerons produce adverse yaw and spoilers generate favorable yaw, aileron and spoiler deflection could be coordinated to produce a pure rolling moment. This could help to relieve the pilot of the need for careful aileron-rudder coordination in situations where maintaining precise aircraft attitude is critical.

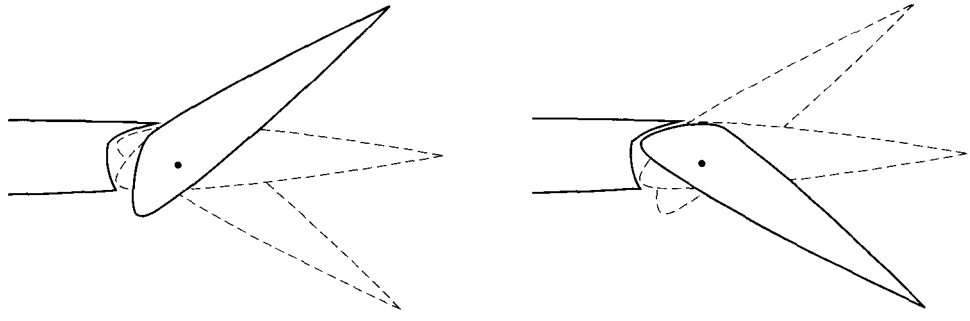


Figure 6.9.4. Frise ailerons used to eliminate adverse yaw.

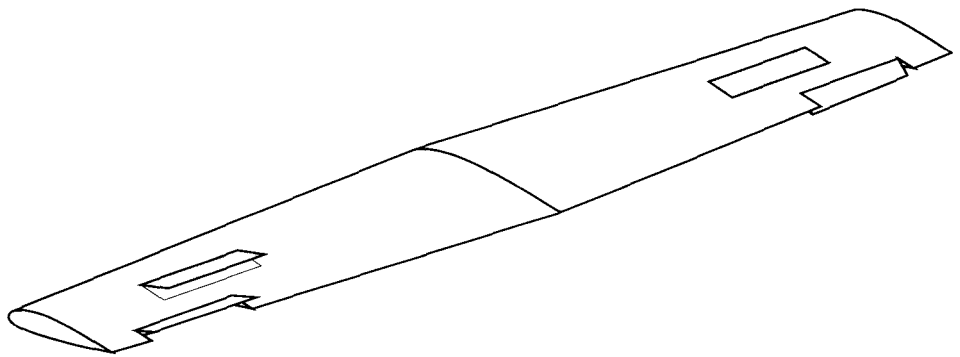


Figure 6.9.5. Spoilers used for roll control.

There are some objections to the use of spoilers as the primary source of roll control. For one, spoilers become ineffective at high angles of attack. Additionally, spoilers produce a nonlinear rolling moment, and they introduce hysteresis in the roll control because the boundary layer does not reattach as quickly as it separates. Another objection, which applies only to mechanical control systems, is the nonlinear hinge moment associated with spoiler deflection. Nevertheless, with proper attention to design detail, these difficulties can be circumvented, and spoilers are becoming more popular as a means of roll control.

With a modern fly-by-wire control system, it is possible to electronically reduce or eliminate coupling between the roll and yaw controls. This can be accomplished by "mixing" the electronic input signals. Output signals to determine aileron and rudder control surface deflections could be computed from input signals obtained from the pilot's cockpit controls according to the relation

$$\begin{Bmatrix} \delta_a \\ \delta_r \end{Bmatrix}_{\substack{\text{control} \\ \text{surface}}} = \begin{bmatrix} k_{aa} & k_{ar} \\ k_{ra} & k_{rr} \end{bmatrix} \begin{Bmatrix} \delta_a \\ \delta_r \end{Bmatrix}_{\substack{\text{pilot} \\ \text{input}}} \tag{6.9.22}$$

where k_{aa}, k_{ar}, k_{ra}, and k_{rr} are control system gain coefficients. For traditional "unmixed" control, both k_{ar} and k_{ra} would be zero. For small deflection angles, the contributions of control surface deflections to the rolling and yawing moment coefficients are

$$\begin{aligned} \begin{Bmatrix} \Delta C_\ell \\ \Delta C_n \end{Bmatrix}_{\text{control}} &= \begin{bmatrix} C_{\ell,\delta_a} & C_{\ell,\delta_r} \\ C_{n,\delta_a} & C_{n,\delta_r} \end{bmatrix} \begin{Bmatrix} \delta_a \\ \delta_r \end{Bmatrix}_{\substack{\text{control} \\ \text{surface}}} \\ &= \begin{bmatrix} C_{\ell,\delta_a} & C_{\ell,\delta_r} \\ C_{n,\delta_a} & C_{n,\delta_r} \end{bmatrix} \begin{bmatrix} k_{aa} & k_{ar} \\ k_{ra} & k_{rr} \end{bmatrix} \begin{Bmatrix} \delta_a \\ \delta_r \end{Bmatrix}_{\substack{\text{pilot} \\ \text{input}}} \\ &= \begin{bmatrix} (C_{\ell,\delta_a} k_{aa} + C_{\ell,\delta_r} k_{ra}) & (C_{\ell,\delta_a} k_{ar} + C_{\ell,\delta_r} k_{rr}) \\ (C_{n,\delta_a} k_{aa} + C_{n,\delta_r} k_{ra}) & (C_{n,\delta_a} k_{ar} + C_{n,\delta_r} k_{rr}) \end{bmatrix} \begin{Bmatrix} \delta_a \\ \delta_r \end{Bmatrix}_{\substack{\text{pilot} \\ \text{input}}} \end{aligned} \tag{6.9.23}$$

By choosing suitable values for the off-diagonal gain coefficients, the airplane could be made to "feel" as though the roll and yaw controls were uncoupled. Setting the off-diagonal terms on the far right-hand side Eq. (6.9.23) to zero, this requires that

$$\begin{Bmatrix} k_{ar} \\ k_{ra} \end{Bmatrix} = \begin{Bmatrix} -(C_{\ell,\delta_r}/C_{\ell,\delta_a})k_{rr} \\ -(C_{n,\delta_a}/C_{n,\delta_r})k_{aa} \end{Bmatrix} \tag{6.9.24}$$

The diagonal gain coefficients can be adjusted to give the desired sensitivity to the cockpit controls. One significant advantage of this approach to adverse yaw abatement is that the gain coefficients are easily modified to provide improved handling qualities, even after final design and flight testing. In fact, these gain coefficients could be varied with airspeed, altitude, and flap settings; or they could be adjusted by the pilot to provide improved handling qualities for a range of operating conditions and pilot preference.

6.10. Airplane Spin

In Sec. 6.6, airplane stall was treated as longitudinal motion. In reality, an airplane almost always has sufficient asymmetry to cause one wing to stall before the other. When one wing stalls, the asymmetric loss of lift produces a moment that rolls the airplane in the direction of the stalled wing. At stall, the fuselage angle of attack is typically quite high. When an airplane at a high angle of attack rolls about the fuselage axis, angle of attack is converted to sideslip. Since the airplane is stable in yaw, this sideslip will produce a moment that tends to yaw the airplane in the direction of the stalled wing. Because the wing typically stalls before the horizontal stabilizer, loss of lift on the wing also results in a nose-down pitching moment. These moments, combined with the force imbalance between lift and weight, cause the airplane to roll and yaw in the direction of the stalled wing while pitching nose down as it falls in response to the lost lift. This motion clearly involves all six degrees of freedom.

The yawing rate that is typically generated in an asymmetric stall can induce what is commonly called a *spin*. Airplane spin is a stalled motion in which the airplane rapidly descends while rotating about a nearly vertical axis that passes fairly close to the center of gravity. During the spinning descent, the airplane's center of gravity follows a helical path centered about the spin axis. As shown in Fig. 6.10.1, the spin can occur with the airplane in a rather steep nose-down attitude, or it can occur with the wings and fuselage closer to horizontal. The later case is called a *flat spin*. As shown in Fig. 6.10.1, the axis of a flat spin is closer to the center of gravity than that of a steep spin. In a flat spin, the wings of the airplane have a motion that is somewhat similar to that of the rotating blades of a helicopter, and in the limiting case, the spin axis may actually pass through the center of gravity. Because of the high descent rate, the wings of an airplane remain completely stalled in a spin. Both steep and flat spins can occur in either direction, right or left.

A spin can develop into stable motion. Spin rates on the order of 90 to 180 degrees per second can occur in the fully developed spin of a light aircraft. It can be difficult for the pilot to recover from a developed spin if the airplane is not specifically designed for spin recovery or spin resistance. Whether or not an airplane develops a stable spin depends on the airplane's inertia properties and aerodynamic moments.

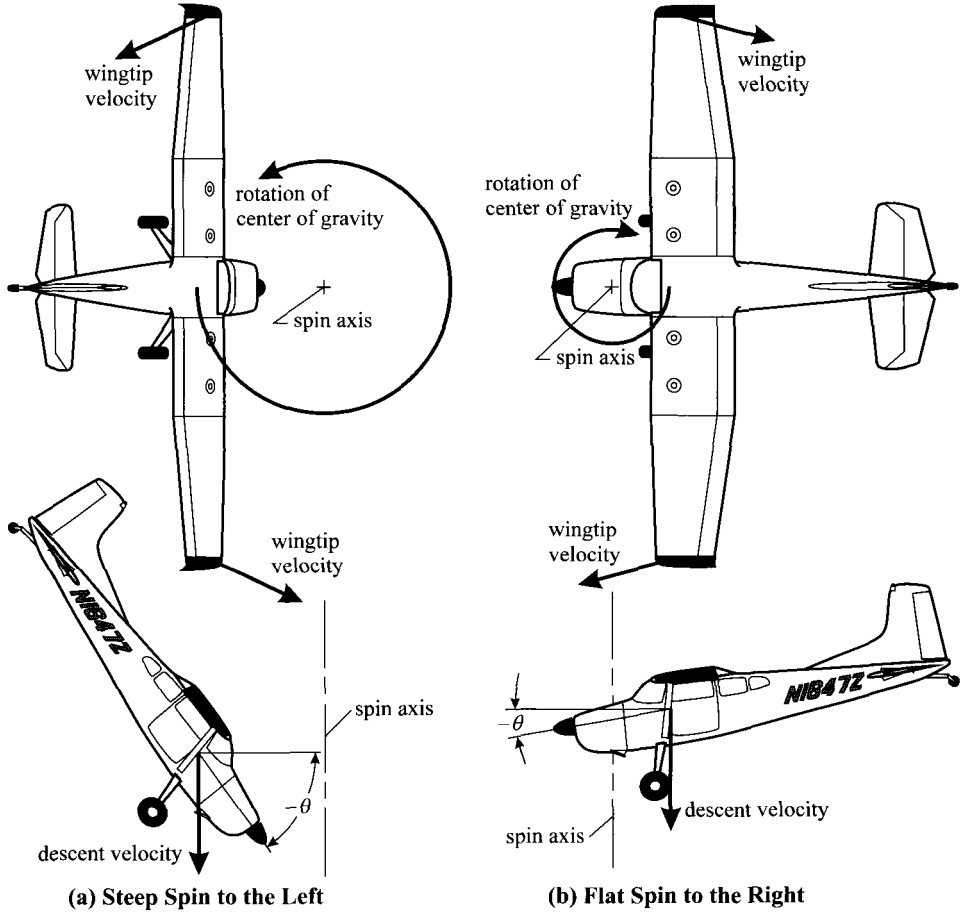


Figure 6.10.1. Top and side views of airplane pitch attitude and motion in steep and flat spins.

Airplane spin was encountered very early in the history of aviation. In the early days of flight, airplane spin was the cause of many fatal accidents. Even today, spin is one of the primary causes of accidents in general aviation. Since spin is always preceded by stall, the first solution to the spin problem was stall avoidance. Today, thanks to years of experimental investigation, most general aviation airplanes will recover from a spin if the pilot simply relinquishes control of the airplane. This does not mean that spins are not dangerous. FAR Part 23 requires that a single-engine airplane be able to recover from a one-turn spin in no more than one additional turn. Even so, because the airplane is descending very rapidly (100 to 200 ft/sec), a great deal of altitude is lost during any spin recovery. With insufficient altitude, the initiation of any spin will almost certainly be disastrous.

The aerodynamic forces and moments produced by the separated flow around a spinning airplane are highly nonlinear and quite complex. Thus, it is very difficult to

accurately predict the unsteady motion of a spinning airplane from theoretical analysis alone. Most of what is known about designing airplanes for spin resistance and spin recovery has been obtained from experimental investigation. Nevertheless, some insight into the physics of airplane spin can be gained by examining the equations of motion for a fully developed steady spin.

Development of the equations of motion for steady spin about a vertical axis is similar to that for the steady coordinated turn, which was presented in Sec. 6.7. In both cases the airplane's center of gravity traces a helical path centered about a vertical axis. The primary differences are the orientation of the aircraft and the radius of the helix. During the steady coordinated turn depicted in Fig. 6.7.1, the fuselage axis is nearly tangent to the flight path, and the radius of the helix is large compared to the wingspan. As shown schematically in Fig. 6.10.1, in a spin, the velocity vector for the airplane's center of gravity makes a rather large angle with the fuselage axis, and the radius of the helix is less than the wingspan. For simplicity, Fig. 6.10.1 was drawn with the bank angle set to zero. Although the bank angle can be small in a spin, it is not necessarily zero. Figure 6.10.2 shows a schematic of a spinning airplane with nonzero bank angle. In this figure, the spin radius has been somewhat enlarged for the sake of clarity. If the radius of the helix in Fig. 6.10.2 had been drawn to scale, the spin axis would pass through or very near the airplane, as was shown in Fig. 6.10.1.

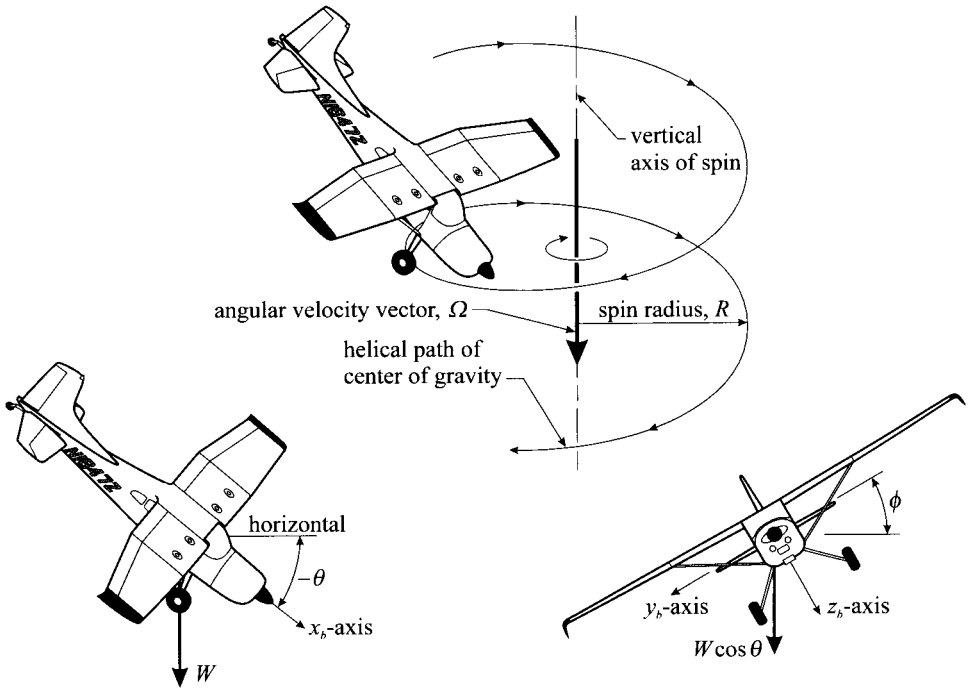


Figure 6.10.2. Airplane spin, showing the spin radius exaggerated for clarity.

Here again we shall use the (x_b, y_b, z_b) coordinate system that is shown in Fig. 5.1.1. For convenience in simplifying the angular momentum equations, we will choose this coordinate system to coincide with the primary inertial axes of the airplane. The angle that the fuselage axis makes with the horizontal, commonly called the *elevation angle*, is usually given the symbol θ. According to standard convention, θ is positive with the nose of the airplane above the horizontal. In a spin, the airplane has a nose-down attitude, which as shown in Fig. 6.10.2 corresponds to a negative elevation angle. As can be seen in Fig. 6.10.2, the airplane's weight can be resolved into components parallel with the x_b-axis, $W\sin(-\theta)$, and normal to the x_b-axis, $W\cos(-\theta)$. The component of weight normal to the x_b-axis can be resolved into components parallel with the y_b-axis, $W\cos(-\theta)\sin(\phi)$, and parallel with the z_b-axis, $W\cos(-\theta)\cos(\phi)$. Thus, the components of the weight vector expressed in our chosen coordinate system are

$$\mathbf{W} = \begin{Bmatrix} -W\sin\theta \\ W\cos\theta\sin\phi \\ W\cos\theta\cos\phi \end{Bmatrix} \tag{6.10.1}$$

Since the angular velocity vector is parallel with the weight vector, the airplane's angular velocity components can similarly be written in the same coordinate system as

$$\mathbf{\Omega} \equiv \begin{Bmatrix} p \\ q \\ r \end{Bmatrix} = \begin{Bmatrix} -\Omega\sin\theta \\ \Omega\cos\theta\sin\phi \\ \Omega\cos\theta\cos\phi \end{Bmatrix} \tag{6.10.2}$$

Likewise, the airplane's descent velocity, $\mathbf{V}_d$, is parallel to the weight vector and

$$\mathbf{V}_d = \begin{Bmatrix} -V_d\sin\theta \\ V_d\cos\theta\sin\phi \\ V_d\cos\theta\cos\phi \end{Bmatrix} \tag{6.10.3}$$

The total velocity of the airplane's center of gravity is the vector sum of the descent velocity and the circumferential velocity. By definition, the spin axis is vertical and the circumferential velocity is in the horizontal plane. In Fig. 6.10.1, the fuselage axis was drawn in the radial plane of the spin helix. We have no way of knowing a priori that this will be the case. In general, we must allow the fuselage axis to be rotated relative to the radial plane through some angle, σ, as shown in the top view of Fig. 6.10.3. The magnitude of the circumferential velocity is $R\Omega$, and as can be seen from Fig. 6.10.3, its x_b-, y_b-, and z_b-components are

$$\mathbf{V}_c = \begin{Bmatrix} -R\Omega\sin\sigma\cos\theta \\ R\Omega(-\cos\sigma\cos\phi - \sin\sigma\sin\theta\sin\phi) \\ R\Omega(\cos\sigma\sin\phi - \sin\sigma\sin\theta\cos\phi) \end{Bmatrix} \tag{6.10.4}$$

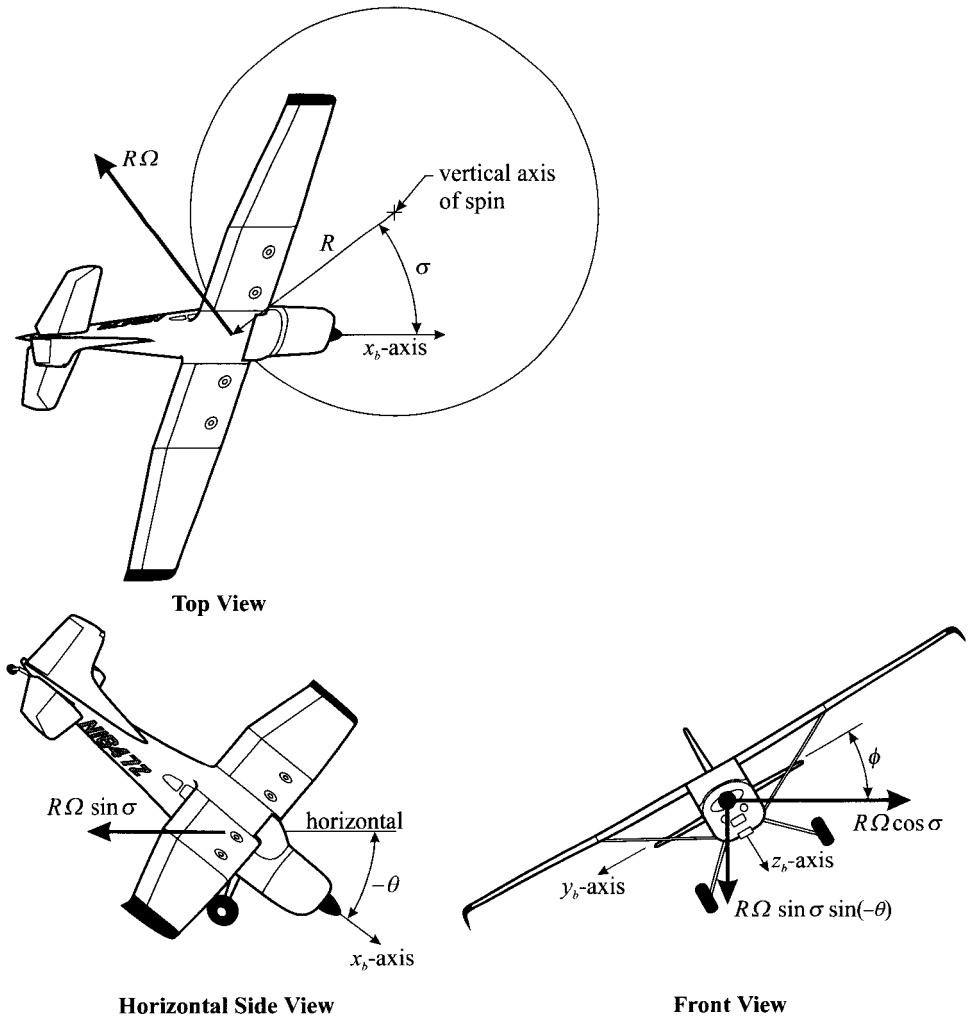


Figure 6.10.3. Top, side, and front views of an airplane's circumferential velocity in a spin.

Combining the components of Eq. (6.10.3) with those from Eq. (6.10.4), the total velocity of the airplane's center of gravity in our body-fixed coordinate system is

$$\mathbf{V} \equiv \begin{Bmatrix} u \\ v \\ w \end{Bmatrix} = \begin{Bmatrix} -V_d \sin\theta - R\Omega \sin\sigma \cos\theta \\ V_d \cos\theta \sin\phi - R\Omega(\cos\sigma \cos\phi + \sin\sigma \sin\theta \sin\phi) \\ V_d \cos\theta \cos\phi + R\Omega(\cos\sigma \sin\phi - \sin\sigma \sin\theta \cos\phi) \end{Bmatrix} \tag{6.10.5}$$

It is sometimes assumed that both ϕ and σ are zero in the developed spin of a conventional airplane. However, this cannot be justified in general.

Because we have chosen our coordinate system to coincide with the primary inertial axes of the airplane, the angular momentum vector can be written from Eq. (6.10.2) as

$$\mathbf{H} = \begin{Bmatrix} -I_{xx_b}\Omega\sin\theta \\ I_{yy_b}\Omega\cos\theta\sin\phi \\ I_{zz_b}\Omega\cos\theta\cos\phi \end{Bmatrix} \tag{6.10.6}$$

where I_{xx_b}, I_{yy_b}, and I_{zz_b} are, respectively, the x_b, y_b, and z_b moments of inertia.

By definition, we are considering the case of a fully developed steady spin. Thus, the translational velocity components in our body-fixed coordinate system are not changing with time. The only translational acceleration is the centripetal acceleration associated with the rotating coordinate system. From Eqs. (6.10.2) and (6.10.5), we have

$$\frac{d\mathbf{V}}{dt} = \boldsymbol{\Omega}\times\mathbf{V} = R\Omega^2\begin{Bmatrix} \cos\sigma\cos\theta \\ \cos\sigma\sin\theta\sin\phi - \sin\sigma\cos\phi \\ \cos\sigma\sin\theta\cos\phi + \sin\sigma\sin\phi \end{Bmatrix} \tag{6.10.7}$$

Similarly, the airplane's angular velocity components in this body-fixed coordinate system are constant and the only angular acceleration is that associated with coordinate system rotation. Using Eqs. (6.10.2) and (6.10.6) gives

$$\frac{d\mathbf{H}}{dt} = \boldsymbol{\Omega}\times\mathbf{H} = \Omega^2\begin{Bmatrix} (I_{zz_b} - I_{yy_b})\cos^2\theta\cos\phi\sin\phi \\ (I_{zz_b} - I_{xx_b})\cos\theta\sin\theta\cos\phi \\ (I_{xx_b} - I_{yy_b})\cos\theta\sin\theta\sin\phi \end{Bmatrix} \tag{6.10.8}$$

Applying Eqs. (6.10.1) and (6.10.7), the body-fixed components of the translational momentum equation are written as

$$\begin{Bmatrix} T+X \\ Y \\ Z \end{Bmatrix} + W\begin{Bmatrix} -\sin\theta \\ \cos\theta\sin\phi \\ \cos\theta\cos\phi \end{Bmatrix} = \frac{WR\Omega^2}{g}\begin{Bmatrix} \cos\sigma\cos\theta \\ \cos\sigma\sin\theta\sin\phi - \sin\sigma\cos\phi \\ \cos\sigma\sin\theta\cos\phi + \sin\sigma\sin\phi \end{Bmatrix} \tag{6.10.9}$$

where X, Y, and Z are, respectively, the x_b-, y_b-, and z_b-components of the aerodynamic force acting on the airplane and T is the thrust developed by the engine or engines. Here, we are assuming that the thrust vector is aligned with the x_b-axis. Similarly, assuming that the thrust vector passes through the airplane's center of gravity, using Eq. (6.10.8) the angular momentum equation requires that

$$\begin{Bmatrix} \ell \\ m \\ n \end{Bmatrix} = \Omega^2\begin{Bmatrix} (I_{zz_b} - I_{yy_b})\cos^2\theta\cos\phi\sin\phi \\ (I_{zz_b} - I_{xx_b})\cos\theta\sin\theta\cos\phi \\ (I_{xx_b} - I_{yy_b})\cos\theta\sin\theta\sin\phi \end{Bmatrix} \tag{6.10.10}$$

Equations (6.10.9) and (6.10.10) provide six scalar equations that relate the forces, moments, and mass properties of the airplane to the dynamic parameters of the spin. If we could express the forces and moments in terms of the translational and rotational velocity components, we would have six equations in six unknowns, ϕ, θ, σ, Ω, R, and V_d. The aerodynamic forces and moments depend on the relative wind. At any point on the airplane, the relative wind can be expressed in terms of the position relative to the center of gravity and the translational and rotational velocities. If we let $\mathbf{r}$ represent the position vector from the center of gravity to some arbitrary point on the airplane, using the definitions in Eqs. (6.10.2) and (6.10.5), the local relative wind can be expressed as

$$\mathbf{V}_r = -\mathbf{V} + \mathbf{r} \times \boldsymbol{\Omega} = -\begin{Bmatrix} u \\ v \\ w \end{Bmatrix} + \begin{Bmatrix} y_b r - z_b q \\ z_b p - x_b r \\ x_b q - y_b p \end{Bmatrix} \tag{6.10.11}$$

Since the wing is stalled, the force on the wing's surface dominates the aerodynamic force on the airplane. Furthermore, the force acting on a stalled surface is dominated by pressure, which acts normal to the surface. Thus, the total longitudinal force is closely aligned with the negative z_b-direction and is proportional to the square of the normal velocity, V_N, which is the negative z_b-component of relative wind,

$$V_N^2 = w^2 + 2y_b pw + y_b^2 p^2 - 2x_b qw - 2x_b y_b pq + x_b^2 q^2 \tag{6.10.12}$$

For example, the force and associated moments produced on the wing are then given by

$$\begin{aligned} \begin{Bmatrix} Z_w \\ \ell_w \\ m_w \end{Bmatrix} &= \tfrac{1}{2}\rho \widetilde{C}_w \int_{-b_w/2}^{b_w/2} \begin{Bmatrix} -V_N^2 \\ -y_b V_N^2 \\ x_b V_N^2 \end{Bmatrix} c_w dy_b \\ &= \tfrac{1}{2}\rho S_w \widetilde{C}_w \begin{Bmatrix} -w^2 - \overline{y_w^2} p^2 + 2\overline{x_w} qw - \overline{x_w^2} q^2 \\ -2\overline{y_w^2} pw + 2\overline{x_w y_w^2} pq \\ \overline{x_w} w^2 + \overline{x_w y_w^2} p^2 - 2\overline{x_w^2} qw + \overline{x_w^3} q^2 \end{Bmatrix} \end{aligned} \tag{6.10.13}$$

where $\widetilde{C}_w$ is the section normal force coefficient for the stalled wing (i.e., about 2.0 for a thin airfoil section), S_w is the planform area of the wing, and

$$\overline{f_w^k} \equiv \frac{1}{S_w} \int_{-b_w/2}^{b_w/2} f^k c_w dy_b \tag{6.10.14}$$

Similar results are obtained for the other surfaces of the airplane, with the side force and yawing moment being proportional to the square of the sideslip velocity.

As previously discussed, a rotating propeller produces a yawing moment that is proportional to the normal component of relative wind. Because an airplane's normal

velocity component is typically quite large in a spin, a rotating propeller can contribute significantly to the yawing moment needed to initiate and sustain the spin. If the propeller's rotational velocity is sufficiently large compared to the relative wind, the propeller yawing moment can be approximated according to Eq. (2.5.31). Using the negative z_b-component of Eq. (6.10.11) for the normal component of relative wind, this gives

$$n_p = \frac{\partial n_p}{\partial V_N} V_N \cong -\frac{TV_N}{\omega_p} = \frac{\partial n_p}{\partial V_N}(w + y_p p - x_p q) \cong -\frac{T}{\omega_p}(w + y_p p - x_p q) \quad (6.10.15)$$

where x_p and y_p are the x_b- and y_b-coordinate of the propeller axis and the propeller's angular velocity, ω_p, is positive for a conventional right-hand propeller and negative for a left-hand propeller. Notice from Eq. (6.10.15) that even balanced counterrotating propellers will produce a net yawing moment in a spin. For counterrotating propellers mounted equal distance on opposite sides of the CG, contributions from the first and third terms on the right-hand side of Eq. (6.10.15) will cancel, since ω_p will be positive for one propeller and negative for the other. However, the contributions from the second term on the right of Eq. (6.10.15) will add, because both ω_p and y_p have opposite signs.

Assuming the thrust to be a linear function of the forward velocity and combining contributions from the wing, horizontal stabilizer, vertical stabilizer, fuselage, propellers, and rudder, the net forces and moments are approximated as

$$\begin{Bmatrix} T+X \\ Y \\ Z \end{Bmatrix} = \tfrac{1}{2}\rho S_w \begin{Bmatrix} V_{T0}^2 + V_{T1}u + C_X u^2 \\ (C_{Y1}v^2 + 2C_{n1}b_w rv + C_{Y2}b_w^2 r^2 - 2C_{Y3}b_w pv \\ \qquad - 2C_{n3}b_w^2 pr + C_{Y4}b_w^2 p^2)\Omega/|\Omega| \\ -C_{N1}w^2 - C_{N2}b_w^2 p^2 + 2C_{m1}b_w qw - C_{N3}b_w^2 q^2 \end{Bmatrix} \quad (6.10.16)$$

$$\begin{Bmatrix} \ell \\ m \\ n \end{Bmatrix} = \tfrac{1}{2}\rho S_w b_w \begin{Bmatrix} -2C_{N2}b_w pw + 2C_{m2}b_w^2 pq \\ C_{m1}w^2 + C_{m2}b_w^2 p^2 - 2C_{N3}b_w qw + C_{m3}b_w^2 q^2 \\ [(C_{n1}v^2 + 2C_{Y2}b_w rv + C_{n2}b_w^2 r^2 - 2C_{n3}b_w pv - 2C_{n4}b_w^2 pr \\ + C_{n5}b_w^2 p^2)\Omega/|\Omega| - V_{p1}w - V_{p2}b_w p + V_{p3}b_w q + (\Delta C_n)_r u^2] \end{Bmatrix} \quad (6.10.17)$$

where

$$V_{T0}^2 \equiv \frac{2T_{u=0}}{\rho S_w},\ V_{T1} \equiv \frac{2}{\rho S_w}\frac{\partial T}{\partial u},\ C_X \equiv \frac{X}{\frac{1}{2}\rho S_w u^2},\ (\Delta C_n)_r \equiv \frac{(\Delta n)_r}{\frac{1}{2}\rho S_w b_w u^2},$$

$$C_{N1} \equiv \frac{S_w\widetilde{C}_w + S_h\widetilde{C}_h + S_{fh}\widetilde{C}_f}{S_w},\ C_{N2} \equiv \frac{S_w\widetilde{C}_w\overline{y_w^2} + S_h\widetilde{C}_h\overline{y_h^2} + S_{fh}\widetilde{C}_f\overline{y_{fh}^2}}{S_w b_w^2},$$

$$C_{N3} \equiv \frac{S_w\widetilde{C}_w\overline{x_w^2} + S_h\widetilde{C}_h\overline{x_h^2} + S_{fh}\widetilde{C}_f\overline{x_{fh}^2}}{S_w b_w^2},\ C_{Y1} \equiv \frac{\eta_v S_v\widetilde{C}_v + S_{fv}\widetilde{C}_f}{S_w},$$

$$C_{Y2} \equiv \frac{\eta_v S_v \widetilde{C}_v \overline{x_v^2} + S_{fv} \widetilde{C}_f \overline{x_{fv}^2}}{S_w b_w^2}, \quad C_{Y3} \equiv \frac{\eta_v S_v \widetilde{C}_v \overline{z_v} + S_{fv} \widetilde{C}_f \overline{z_{fv}}}{S_w b_w},$$

$$C_{Y4} \equiv \frac{\eta_v S_v \widetilde{C}_v \overline{z_v^2} + S_{fv} \widetilde{C}_f \overline{z_{fv}^2}}{S_w b_w^2}, \quad C_{m1} \equiv \frac{S_w \widetilde{C}_w \overline{x_w} + S_h \widetilde{C}_h \overline{x_h} + S_{fh} \widetilde{C}_f \overline{x_{fh}}}{S_w b_w},$$

$$C_{m2} \equiv \frac{S_w \widetilde{C}_w \overline{x_w y_w^2} + S_h \widetilde{C}_h \overline{x_h y_h^2} + S_{fh} \widetilde{C}_f \overline{x_{fh} y_{fh}^2}}{S_w b_w^3},$$

$$C_{m3} \equiv \frac{S_w \widetilde{C}_w \overline{x_w^3} + S_h \widetilde{C}_h \overline{x_h^3} + S_{fh} \widetilde{C}_f \overline{x_{fh}^3}}{S_w b_w^3}, \quad C_{n1} \equiv \frac{\eta_v S_v \widetilde{C}_v \overline{x_v} + S_{fv} \widetilde{C}_f \overline{x_{fv}}}{S_w b_w},$$

$$C_{n2} \equiv \frac{\eta_v S_v \widetilde{C}_v \overline{x_v^3} + S_{fv} \widetilde{C}_f \overline{x_{fv}^3}}{S_w b_w^3}, \quad C_{n3} \equiv \frac{\eta_v S_v \widetilde{C}_v \overline{x_v z_v} + S_{fv} \widetilde{C}_f \overline{x_{fv} z_{fv}}}{S_w b_w^2},$$

$$C_{n4} \equiv \frac{\eta_v S_v \widetilde{C}_v \overline{x_v^2 z_v} + S_{fv} \widetilde{C}_f \overline{x_{fv}^2 z_{fv}}}{S_w b_w^3}, \quad C_{n5} \equiv \frac{\eta_v S_v \widetilde{C}_v \overline{x_v z_v^2} + S_{fv} \widetilde{C}_f \overline{x_{fv} z_{fv}^2}}{S_w b_w^3},$$

$$V_{p1} = -\sum \frac{2}{\rho S_w b_w} \frac{\partial n_p}{\partial V_N}, \quad V_{p2} = -\sum \frac{2 y_p}{\rho S_w b_w^2} \frac{\partial n_p}{\partial V_N}, \quad V_{p3} = -\sum \frac{2 x_p}{\rho S_w b_w^2} \frac{\partial n_p}{\partial V_N}$$

The vertical stabilizer efficiency factor, η_v, is less than unity to account for the reduced yaw stability resulting from the vertical stabilizer being partly shadowed by the wake of the horizontal stabilizer as shown in Fig. 6.10.4. The vertical stabilizer efficiency factor can be approximated as the ratio of the unshadowed stabilizer area to the total stabilizer area. The 15-degree expansion angle shown in Fig. 6.10.4 is typical but depends somewhat on the section geometry of the horizontal stabilizer.

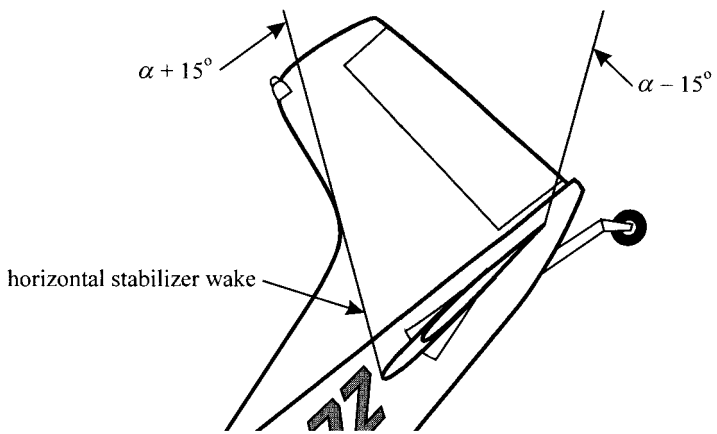


Figure 6.10.4. Schematic diagram showing the reduction in yaw stability due to the vertical stabilizer being partially shadowed by the wake of the horizontal stabilizer.

Starting with the definitions in Eqs. (6.10.2) and (6.10.5), then using Eqs. (6.10.16) and (6.10.17) in Eqs. (6.10.9) and (6.10.10), we have a complete formulation for the steady developed spin of a stalled airplane,

$$\begin{Bmatrix} u \\ v \\ w \end{Bmatrix} \equiv \begin{Bmatrix} -V_d \sin\theta - R\Omega \sin\sigma\cos\theta \\ V_d \cos\theta\sin\phi - R\Omega(\cos\sigma\cos\phi + \sin\sigma\sin\theta\sin\phi) \\ V_d \cos\theta\cos\phi + R\Omega(\cos\sigma\sin\phi - \sin\sigma\sin\theta\cos\phi) \end{Bmatrix}, \quad \begin{Bmatrix} p \\ q \\ r \end{Bmatrix} \equiv \begin{Bmatrix} -\Omega\sin\theta \\ \Omega\cos\theta\sin\phi \\ \Omega\cos\theta\cos\phi \end{Bmatrix}$$

$$\begin{aligned} \tfrac{1}{2}\rho S_w \begin{Bmatrix} V_{T0}^2 + V_{T1}u + C_X u^2 \\ (C_{Y1}v^2 + 2C_{n1}b_w rv + C_{Y2}b_w^2 r^2 - 2C_{Y3}b_w pv \\ \qquad - 2C_{n3}b_w^2 pr + C_{Y4}b_w^2 p^2)\,\Omega/|\Omega| \\ -C_{N1}w^2 - C_{N2}b_w^2 p^2 + 2C_{m1}b_w qw - C_{N3}b_w^2 q^2 \end{Bmatrix} + W\begin{Bmatrix} -\sin\theta \\ \cos\theta\sin\phi \\ \cos\theta\cos\phi \end{Bmatrix} \\ = \frac{WR\Omega^2}{g}\begin{Bmatrix} \cos\sigma\cos\theta \\ \cos\sigma\sin\theta\sin\phi - \sin\sigma\cos\phi \\ \cos\sigma\sin\theta\cos\phi + \sin\sigma\sin\phi \end{Bmatrix} \end{aligned} \tag{6.10.18}$$

$$\begin{aligned} \tfrac{1}{2}\rho S_w b_w \begin{Bmatrix} -2C_{N2}b_w pw + 2C_{m2}b_w^2 pq \\ C_{m1}w^2 + C_{m2}b_w^2 p^2 - 2C_{N3}b_w qw + C_{m3}b_w^2 q^2 \\ [(C_{n1}v^2 + 2C_{Y2}b_w rv + C_{n2}b_w^2 r^2 - 2C_{n3}b_w pv - 2C_{n4}b_w^2 pr \\ + C_{n5}b_w^2 p^2)\,\Omega/|\Omega| - V_{p1}w - V_{p2}b_w p + V_{p3}b_w q + (\Delta C_n)_r u^2] \end{Bmatrix} \\ = \Omega^2 \begin{Bmatrix} (I_{zz_b} - I_{yy_b})\cos^2\theta\cos\phi\sin\phi \\ (I_{zz_b} - I_{xx_b})\cos\theta\sin\theta\cos\phi \\ (I_{xx_b} - I_{yy_b})\cos\theta\sin\theta\sin\phi \end{Bmatrix} \end{aligned} \tag{6.10.19}$$

The six components of Eqs. (6.10.18) and (6.10.19) can be solved numerically for the six unknowns ϕ, θ, σ, Ω, R, and V_d. However, with some further assumptions it is possible to obtain an approximate solution in closed form.

The difference between the thrust and the axial component of drag is typically quite small compared to the normal force developed on the stalled wing. Furthermore, it is often assumed that both σ and ϕ are small in a spin. If we also assume that the wing and tail are in close vertical alignment with the center of gravity ($z_b \cong 0$), a reasonable first approximation for the aerodynamic forces and moments is obtained by using

$$V_{T0}^2 + V_{T1}u + C_X u^2 \cong C_{Y3} \cong C_{Y4} \cong C_{n3} \cong C_{n4} \cong C_{n5} \cong 0$$

$$\begin{Bmatrix} u \\ v \\ w \end{Bmatrix} \cong \begin{Bmatrix} -V_d \sin\theta \\ -R\Omega \\ V_d \cos\theta \end{Bmatrix}, \quad \begin{Bmatrix} p \\ q \\ r \end{Bmatrix} \cong \begin{Bmatrix} -\Omega\sin\theta \\ 0 \\ \Omega\cos\theta \end{Bmatrix}$$

Also applying the small-angle approximation for ϕ and σ, the formulation reduces to

$$\frac{1}{2}\rho S_w \begin{Bmatrix} 0 \\ (C_{Y1}R^2 - 2C_{n1}b_w R\cos\theta + C_{Y2}b_w^2\cos^2\theta)\Omega|\Omega| \\ -C_{N1}V_d^2\cos^2\theta - C_{N2}b_w^2\Omega^2\sin^2\theta \end{Bmatrix} + W\begin{Bmatrix} -\sin\theta \\ \phi\cos\theta \\ \cos\theta \end{Bmatrix} = \frac{WR\Omega^2}{g}\begin{Bmatrix} \cos\theta \\ \phi\sin\theta - \sigma \\ \sin\theta \end{Bmatrix} \tag{6.10.20}$$

$$\frac{1}{2}\rho S_w b_w \begin{Bmatrix} 2C_{N2}b_w\Omega V_d\cos\theta\sin\theta \\ C_{m1}V_d^2\cos^2\theta + C_{m2}b_w^2\Omega^2\sin^2\theta \\ [(C_{n1}R^2 - 2C_{Y2}b_w R\cos\theta + C_{n2}b_w^2\cos^2\theta)\Omega|\Omega| \\ -V_{p1}V_d\cos\theta + V_{p2}b_w\Omega\sin\theta + (\Delta C_n)_r V_d^2\sin^2\theta] \end{Bmatrix} = \Omega^2\begin{Bmatrix} (I_{zz_b} - I_{yy_b})\phi\cos^2\theta \\ (I_{zz_b} - I_{xx_b})\cos\theta\sin\theta \\ (I_{xx_b} - I_{yy_b})\phi\cos\theta\sin\theta \end{Bmatrix} \tag{6.10.21}$$

The yawing moment is very critical to the physics of airplane spin. Both spin initiation and spin recovery depend primarily on the magnitude and sign of the yawing moment. For positive spin ($\Omega > 0$), a positive yawing moment supports spin and a negative yawing moment opposes spin. From the definition of C_{Y2} it can be seen that the second yaw term on the left-hand side of Eq. (6.10.21) always opposes spin, while the definitions of C_{n1} and C_{n2} show that the first and third terms can either support or oppose spin, depending on airplane geometry. Since the vertical stabilizer is aft of the CG ($x_b < 0$), the aerodynamic yawing moment generated by the vertical stabilizer opposes spin. However, the aerodynamic center of the fuselage is typically forward of the CG and the yawing moment generated on the fuselage usually supports spin. If the vertical stabilizer is sufficiently shadowed by the wake of the horizontal stabilizer, the fuselage can dominate to produce a net yawing moment in support of the spin.

The fourth and fifth yaw terms on the left-hand side of Eq. (6.10.21) result from the propeller or propellers. For a single-engine airplane with the propeller axis in the plane of symmetry, only the first of these terms is nonzero and the sign of the propeller yawing moment is independent of the direction of airplane spin. In such configurations a conventional right-hand propeller supports negative spin, while a left-hand propeller supports positive spin. For a twin-engine configuration with counterrotating propellers, the first of the two propeller terms that appear in Eq. (6.10.21) is zero and the propeller-induced yawing moment is proportional to Ω. If the right-hand propeller has right-hand rotation and the left-hand propeller has left-hand rotation, the resulting yawing moment always opposes the spin (remember $\sin\theta < 0$), which makes the design more spin resistant. If each of these twin propellers were to rotate in the opposite direction, the propeller-induced yawing moment would support spin in either direction.

With algebraic manipulation, the six components of Eqs. (6.10.20) and (6.10.21) can be rearranged to eliminate ϕ and σ. Thus, the formulation can be reduced to a system of four nonlinear equations that can be directly solved for the spin rate, Ω, the spin radius, R, the sink rate, V_d, and the required yaw control coefficient, $(\Delta C_n)_r$, all as a function of the elevation angle, θ,

$$\Omega^2 = \frac{2W}{\rho S_w C_{N_1} \cos\theta \sin^2\theta}\left[\frac{2(I_{zz_b} - I_{xx_b})}{\rho S_w b_w C_{m_1} \tan\theta} - \frac{C_{m_2} b_w^2}{C_{m_1}} + \frac{C_{N_2} b_w^2}{C_{N_1}}\right]^{-1} \tag{6.10.22}$$

$$R = -\frac{g \tan\theta}{\Omega^2} \tag{6.10.23}$$

$$V_d^2 = \frac{2W}{\rho S_w C_{N_1} \cos^3\theta} - \frac{C_{N_2} b_w^2 \Omega^2 \tan^2\theta}{C_{N_1}} \tag{6.10.24}$$

$$\begin{aligned}(\Delta C_n)_r = {} & \frac{2C_{N_2}(I_{xx_b} - I_{yy_b}) b_w \Omega}{(I_{zz_b} - I_{yy_b}) V_d} + \frac{V_{p_1} \cos\theta}{V_d \sin^2\theta} - \frac{V_{p_2} b_w \Omega}{V_d^2 \sin\theta} \\ & - \left(\frac{C_{n_1} R^2}{\sin^2\theta} - \frac{2C_{Y_2} b_w R}{\sin\theta \tan\theta} + \frac{C_{n_2} b_w^2}{\tan^2\theta}\right)\frac{\Omega|\Omega|}{V_d^2}\end{aligned} \tag{6.10.25}$$

Typically, the elevation angle required to support a fully developed steady spin is not known a priori. Instead, the yaw control coefficient might be known for a given rudder deflection. For example, $(\Delta C_n)_r$ would be zero with no rudder deflection. After using Eqs. (6.10.22) through (6.10.24) to eliminate Ω, R, and V_d, Eq. (6.10.25) provides a single nonlinear equation for the unknown elevation angle, θ. The roots of this equation, if they exist, are the elevation angles that will support a fully developed steady spin, with the assumption that ϕ and σ are small.

Figure 6.10.5 shows an example of spin characteristics that were predicted from Eqs. (6.10.22) through (6.10.25) for a light aircraft having similar moments of inertia for roll and pitch. For these predictions, the normal force coefficient for the wing and both surfaces of the tail were assumed to be 2.0 and that for the fuselage was taken as 1.0. Several important observations can be made from Fig. 6.10.5. First of all, notice that the spin radius for a flat spin is much smaller than that for a steep spin. For a very flat spin, the spin radius approaches zero. For the more common steeper spins, which typically occur with the airplane's nose about 40 to 60 degrees below horizontal, the predicted spin radius is about 25 to 30 percent of the wingspan. Also notice that the predicted sink rate is much larger for a steep spin than for a flat spin. For the common elevation angle range between –40 and –60 degrees, the current analytical model predicts sink rates ranging from about 100 to 200 ft/sec, which is in good agreement with experimental data (see, for example, Stough, DiCarlo, and Patton 1985). For this same range of elevation angles, the predicted spin rate only varies from about 110 to 140 deg/sec. This is also in good agreement with experimental observation.

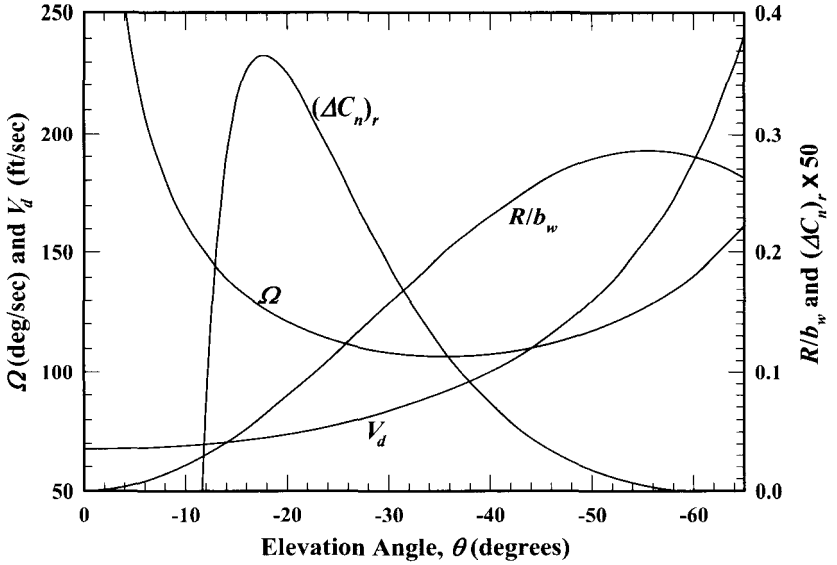


Figure 6.10.5. Example of spin characteristics for a light airplane, which is not spin resistant.

For the airplane used to generate Fig. 6.10.5, the analytical model predicts that there are two elevation angles that will support a steady developed spin with no rudder deflection, i.e., $(\Delta C_n)_r = 0$. These correspond to a flat spin at about –12 degrees and a steep spin at about –58 degrees. The flat spin would most likely be difficult to initiate, because the airplane's nose usually drops very rapidly when the wing stalls. However, if this flat spin were to develop, it could be difficult or impossible for the pilot to recover, because the rudder may be completely shadowed by the horizontal stabilizer unless the airplane is specifically designed for this contingency.

Today, unlike the airplane used to generate Fig. 6.10.5, most general aviation airplanes will not support a steady spin without maintained rudder deflection. In such spin-resistant airplanes a spin can usually be initiated by applying full rudder just as the wing stalls. If some rudder deflection is maintained, the airplane may develop a steady spin. However, when the controls are returned to neutral, the airplane will usually recover from the spin in less than one complete revolution. The spin characteristics predicted from Eqs. (6.10.22) through (6.10.25) for a typical general aviation airplane are shown in Fig. 6.10.6. Notice that a very large yaw control input would be required to maintain a flat spin. This is usually significantly more than can be achieved with a conventional rudder. In a steeper nose-down attitude there would be sufficient rudder power to stabilize the spin. However, the predicted rudder control moment required to support the spin only goes to zero in the limit as the elevation angle for the spin approaches –90 degrees. Such a steep maneuver is not a spin at all but a spiral dive, and the present analytical model does not apply because the angle of attack would be below stall. Furthermore, the present model does not account for compressibility effects, which become important in very steep spins and dives.

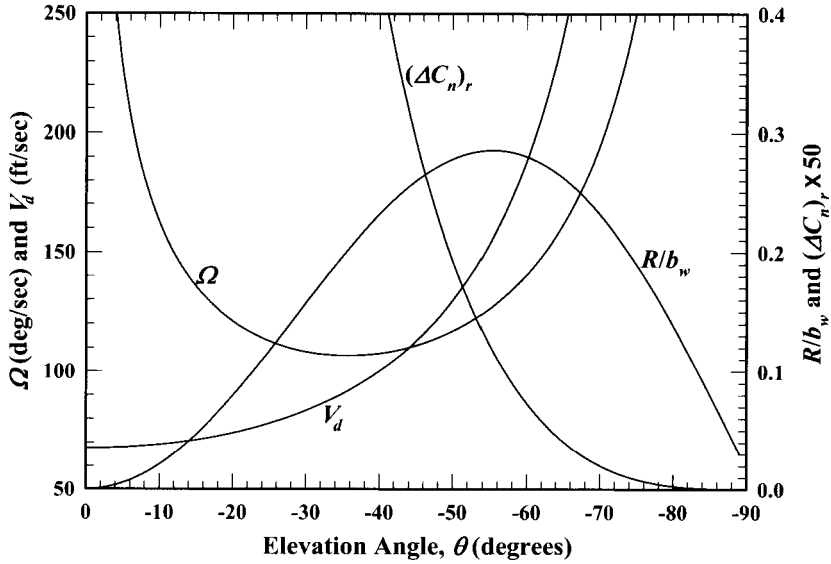


Figure 6.10.6. Example of predicted spin characteristics for a typical spin-resistant light airplane.

It should be reemphasized that Eqs. (6.10.22) through (6.10.25) are based on an approximation to the steady equations of motion for airplane spin. In reality, the net axial force will not be exactly zero in a spin. However, compared to the normal force generated on the stalled wing, this force is small. Furthermore, the angles σ and ϕ are not necessarily small in a spin. Thus, the model does not apply to all spins and all airplanes. The model is based on the assumption of large angle of attack and thus does not apply to extremely steep spins and spiral dives because the angle of attack becomes small in such cases. Also, the model does not account for compressibility effects, which become important in very steep spins and dives. Nevertheless, this approximate model can provide some valuable insight into the physics of airplane spin.

6.11. Problems

6.1. Consider the British Spitfire Mark XVIII that is described in problem 4.8. The wing and horizontal tail have the following properties:

$$S_w = 244 \text{ ft}^2, \quad b_w = 36.83 \text{ ft}, \quad C_{L_w,\alpha} = 4.62, \quad C_{m_w} = -0.053, \quad W = 8{,}375 \text{ lbf},$$
$$S_h = 31 \text{ ft}^2, \quad b_h = 10.64 \text{ ft}, \quad C_{L_h,\alpha} = 4.06, \quad C_{m_{h0}} = 0.00, \quad C_{m_h,\delta_e} = -0.55,$$
$$\varepsilon_e = 0.60, \quad l_h - l_w = 18.16 \text{ ft}, \quad \eta_h = 1.0$$

Including the effects of wing downwash but neglecting all effects of the propeller and fuselage, plot the elevator angle per g as a function of CG location relative to the wing quarter-chord. Use an airspeed of 100 miles per hour at sea level.

6.2. The small jet transport that is described in problem 4.16 has the following properties:

$$S_w = 950 \text{ ft}^2, \quad b_w = 75 \text{ ft}, \quad C_{L_w,\alpha} = 4.30, \quad C_{m_w} = -0.050, \quad W = 73{,}000 \text{ lbf},$$
$$S_h = 207 \text{ ft}^2, \quad b_h = 31 \text{ ft}, \quad C_{L_h,\alpha} = 4.00, \quad C_{m_{h0}} = 0.00, \quad C_{m_h,\delta_e} = -0.49,$$
$$\varepsilon_e = 0.51, \quad l_h - l_w = 42.5 \text{ ft}, \quad \eta_h = 1.0$$

Including the effects of wing downwash but neglecting effects of the thrust deck and fuselage, plot the elevator angle per g as a function of CG location relative to the wing quarter-chord. Use an airspeed of 300 miles per hour at sea level.

6.3. Consider the small jet transport that is described in problem 4.25. The wing and canard have the following properties:

$$S_w = 950 \text{ ft}^2, \quad b_w = 75 \text{ ft}, \quad C_{L_w,\alpha} = 4.30, \quad C_{m_w} = -0.050, \quad W = 73{,}000 \text{ lbf},$$
$$S_h = 219 \text{ ft}^2, \quad b_h = 36 \text{ ft}, \quad C_{L_h,\alpha} = 4.30, \quad C_{m_{h0}} = -0.050, \quad C_{m_h,\delta_e} = -0.49,$$
$$\varepsilon_e = 0.51, \quad l_h - l_w = -42.5 \text{ ft}, \quad \eta_h = 1.0$$

Including the effects of wing downwash but neglecting effects of the thrust deck and fuselage, plot the elevator angle per g as a function of CG location relative to the wing quarter-chord. Use an airspeed of 300 miles per hour at sea level.

6.4. The turboprop transport that is described in problem 4.32 has the following properties:

$$S_w = 1{,}745 \text{ ft}^2, \quad b_w = 132.6 \text{ ft}, \quad C_{L_w,\alpha} = 5.16, \quad C_{m_w} = -0.050, \quad W = 155{,}000 \text{ lbf},$$
$$S_h = 528 \text{ ft}^2, \quad b_h = 52.7 \text{ ft}, \quad C_{L_h,\alpha} = 4.52, \quad C_{m_{h0}} = 0.00, \quad C_{m_h,\delta_e} = -0.49,$$
$$\varepsilon_e = 0.58, \quad l_h - l_w = 47.0 \text{ ft}, \quad \eta_h = 1.0$$

Including the effects of wing downwash but neglecting effects of the propellers and fuselage, plot the elevator angle per g as a function of CG location relative to the wing quarter-chord. Use an airspeed of 200 miles per hour at sea level.

6.5. Consider the wing-tail combination that is described in Example 6.2.1. Assume that the tail is attached to the wing with a thin-walled aluminum tube that extends from the tail to the center of gravity, which is located at the wing quarter-chord. The aluminum tube has a constant circular cross-section and constant wall thickness. To avoid buckling, the ratio of tube diameter to wall thickness is kept less than or equal to 32. Neglecting all effects of compressibility but accounting for tail boom bending, what are the diameter, wall thickness, and weight of the lightest aluminum tube that would result in no more than 10 percent control loss with an airspeed of 400 mph at sea level?

6.6. The diameter of the thin-walled aluminum tube connecting the wing and tail in problem 6.5 is allowed to vary linearly along the length of the tube. To avoid buckling, the ratio of tube diameter to wall thickness is to be kept equal to 32 at every cross-section. Neglecting all effects of compressibility but accounting for tail boom bending, what are the maximum diameter, maximum wall thickness, taper ratio, and weight of the lightest tapered aluminum tube that would result in no more than 10 percent control loss with an airspeed of 400 mph at sea level?

6.7. For the Spitfire in problem 6.1, neglecting the effects of propeller and fuselage, plot the control force gradient at sea level and 100 mph as a function of CG location relative to the wing quarter-chord. The change in elevator hinge moment coefficient with angle of attack is –0.59 and the change in the hinge moment coefficient with elevator deflection is –0.90, based on a 14-ft^2 elevator with a mean chord of 1.4 ft. The mechanical linkage between the stick and elevator has an effective lever arm of 2.0 ft. Where is the stick-free neutral point?

6.8. For the British Spitfire Mark XVIII and operating conditions in problem 6.7, neglecting the effects of the propeller and fuselage, plot the longitudinal control force per g as a function of the location of the CG measured relative to the quarter-chord of the main wing. Also find the stick-free maneuver point.

6.9. For the small jet transport in problem 6.2, neglecting the effects of the thrust deck and fuselage, plot the control force gradient at sea level and 300 mph as a function of the location of the CG measured relative to the quarter-chord of the main wing. For this elevator and stabilizer the change in the hinge moment coefficient with angle of attack is –0.63 and the change in the hinge moment coefficient with elevator deflection is –0.97, based on a 69-ft^2 elevator with a mean chord of 2.5 ft. Assume a mechanical linkage between the control yoke and the elevator that has an effective lever arm of 2.0 ft. Also find the stick-free neutral point. Do you think that a mechanical control is feasible for this airplane?

6.10. For the small jet transport and operating conditions in problem 6.9, neglecting the effects of the thrust deck and fuselage, plot the longitudinal control force per g as a function of the location of the CG measured relative to the quarter-chord of the main wing. Also find the stick-free maneuver point.

6.11. For the small jet transport in problem 6.3, neglecting the effects of the thrust deck and fuselage, plot the control force gradient at sea level and 300 mph as a function of CG location measured relative to the quarter-chord of the main wing. For the control surface on the canard, the change in hinge moment coefficient with angle of attack is –0.63 and the change in the hinge moment coefficient with elevator deflection is –0.97, based on a 69-ft^2 control surface with a mean chord of 2.5 ft. Assume a mechanical linkage between the control yoke and the control surface that has an effective lever arm of 2.0 ft. Also find the stick-free neutral point. Do you think that a mechanical control is feasible for this airplane?

6.12. For the small jet transport and operating conditions in problem 6.11, neglecting the effects of the thrust deck and fuselage, plot the longitudinal control force per g as a function of the location of the CG measured relative to the quarter-chord of the main wing. Also find the stick-free maneuver point.

6.13. For the large turboprop transport described in problem 6.4, neglecting the effects of the propellers and fuselage, plot the control force gradient at sea level and 200 mph as a function of the location of the CG measured relative to the quarter-chord of the main wing. For this elevator and stabilizer, the change in the hinge moment coefficient with angle of attack is –0.63 and the change in the hinge moment coefficient with elevator deflection is –0.97, based on a 176-ft^2 elevator with a mean chord of 3.4 ft. Assume a mechanical linkage between the control yoke and the elevator that has an effective lever arm of 2.0 ft. Also find the stick-free neutral point. Do you think that a mechanical control is feasible for this airplane?

6.14. For the turboprop transport and operating conditions in problem 6.13, neglecting the effects of the propellers and fuselage, plot the longitudinal control force per g as a function of the location of the CG measured relative to the quarter-chord of the main wing. Also find the stick-free maneuver point.

6.15. For the British Spitfire Mark XVIII that is described in problems 4.3 and 4.5, estimate the downwash gradient induced on the aft horizontal stabilizer when the airplane is flying in ground effect with the tips of the main wing 4.0 feet above the ground.

6.16. For the small jet transport that is described in problem 4.14, estimate the downwash gradient induced on the horizontal stabilizer when the airplane is flying in ground effect with the main wing 8.0 feet above the ground.

6.17. For the turboprop transport that is described in problem 4.32, estimate the downwash gradient induced on the horizontal stabilizer when the airplane is flying in ground effect with the main wing 18.3 feet above the ground.

6.18. For the British Spitfire and the ground effect operating condition described in problem 6.15, plot the elevator deflection required to trim the airplane at 100 mph and sea level as a function of the location of the center of gravity measured aft of the wing quarter-chord. Compare this result with that obtained in problem 4.9 for flight at the same airspeed and altitude but out of ground effect.

6.19. For the turboprop transport and the ground effect operating condition described in problem 6.17, plot the elevator deflection required to trim the airplane for 200 mph at sea level as a function of the location of the center of gravity measured aft of the wing quarter-chord. Compare this result with that obtained in problem 4.33 for flight at the same airspeed and altitude but out of ground effect.

6.20. For the British Spitfire Mark XVIII in problem 6.7, estimate the control force required for a full stall landing from an approach speed of 120 mph, with the CG located at the aerodynamic center of the wing. Assume that the touchdown wing position relative to the ground is that described in problem 6.15. Using the trim tab setting, the control force is zeroed at the approach speed outside of ground effect and the maximum lift coefficient for the wing-tail combination is 1.4.

6.21. Rework Example 6.7.1 for the case of a climbing coordinated turn. Use a climb angle of 20 degrees. Assume that the airplane's engine has sufficient power to support the climbing turn. Ignore any possibility of stall and hold all parameters, except the climb angle, the same as those used in Example 6.7.1.

6.22. Rework Example 6.7.1 for the case of a descending coordinated turn. Use a climb angle of –20 degrees. Assume that the airplane's drag is sufficient to maintain the desired airspeed simply by throttling back the engine. Ignore any possibility of stall and hold all parameters, except the climb angle, the same as those used in Example 6.7.1.

6.23. Consider a level coordinated turn for the British Spitfire described in problem 6.1. All control surfaces are trimmed for steady level flight at 300 mph and sea level. Ignoring any possibility of stall, plot the change in aileron, elevator, and rudder deflection angles required to maintain the level coordinated turn, at the same airspeed and altitude, as a function bank angle. For this airplane and operating condition use

$$S_w = 244 \text{ ft}^2, \quad b_w = 36.83 \text{ ft}, \quad W = 8{,}375 \text{ lbf}, \quad V = 300 \text{ mph},$$
$$C_{L,\alpha} = 4.88, \quad C_{L,\delta_e} = 0.305, \quad C_{L,\bar{q}} = 2.83,$$
$$C_{Y,\beta} = -0.212, \quad C_{Y,\delta_r} = 0.209, \quad C_{Y,\bar{p}} = 0.045, \quad C_{Y,\bar{r}} = 0.282,$$
$$C_{\ell,\beta} = 0.00, \quad C_{\ell,\delta_a} = -0.201, \quad C_{\ell,\delta_r} = 0.019, \quad C_{\ell,\bar{p}} = -0.889,$$
$$C_{m,\alpha} = -0.469, \quad C_{m,\beta} = 0.0085, \quad C_{m,\delta_e} = -0.879, \quad C_{m,\bar{q}} = -7.75,$$
$$C_{n,\alpha} = 0.0018, \quad C_{n,\beta} = 0.095, \quad C_{n,\delta_a} = 0.0053, \quad C_{n,\delta_r} = -0.094,$$
$$C_{n,\bar{p}} = -0.0186, \quad C_{\ell,\bar{r}} = 0.017 + 0.148C_L, \quad C_{n,\bar{r}} = -0.137 - 0.0274C_L^2$$

Discuss the differences that you observe between the results predicted for this airplane and the one in Example 6.7.1.

6.24. A later version of the British Spitfire eliminated the propeller torque problem by using twin coaxial-contrarotating propellers. Repeat problem 6.23 assuming that all parameters remain the same except that $C_{n,\alpha} = C_{m,\beta} = 0$.

6.25. Following a procedure similar to that used in Sec. 6.1 for the stabilizer-elevator configuration, show that the stabilator configuration leads to the results given in Eqs. (6.9.8), (6.9.9), and (6.9.10).

6.26. Following a procedure similar to that used in Sec. 6.3 for the stabilizer-elevator configuration, show that the stabilator configuration leads to the results given in Eqs. (6.9.19), (6.9.20), and (6.9.21).

6.27. Following a procedure similar to that used in Sec. 6.3 for the stabilizer-elevator configuration, show that the trim setting, δ_{et}, for the stabilator configuration varies with level flight trim speed according to the relation

$$\delta_{et} = -[C_1(W/\tfrac{1}{2}\rho V_{\text{trim}}^2 S_w) + C_3]/C_4$$

where C_1 is given by Eq. (6.9.20) and

$$C_3 = C_{H_s 0} + C_{H_s,\alpha_h}(\alpha_{0h} - \varepsilon_{d0}) + \frac{(C_{m,\alpha}C_{L0} - C_{L,\alpha}C_{m0})C_{H_s,\delta_s} - (C_{m,\delta_s}C_{L0} - C_{L,\delta_s}C_{m0})C_{H_s,\alpha_h}(1-\varepsilon_{d,\alpha})}{C_{L,\alpha}C_{m,\delta_s} - C_{L,\delta_s}C_{m,\alpha}}$$

$$C_4 = C_{H_s,\delta_e} + \frac{(C_{m,\alpha}C_{L,\delta_e} - C_{L,\alpha}C_{m,\delta_e})C_{H_s,\delta_s} - (C_{m,\delta_s}C_{L,\delta_e} - C_{L,\delta_s}C_{m,\delta_e})C_{H_s,\alpha_h}(1-\varepsilon_{d,\alpha})}{C_{L,\alpha}C_{m,\delta_s} - C_{L,\delta_s}C_{m,\alpha}}$$

6.28. Consider replacing the aft stabilizer and elevator of the airplane described in Example 6.3.1 with a stabilator having exactly the same geometry. Assume that the primary hinge of the stabilator will pass through the aerodynamic center of this horizontal surface. The trailing-edge flap will be mechanically linked to the stabilator so that k_{es} will be 0.50. Assume a mechanical linkage between the stick and the stabilator having an effective lever arm of 2.0 ft. For this stabilator, repeat the computations that were carried out in Example 6.3.1 for the stabilizer-elevator configuration and compare the results.

6.29 One advantage of using the stabilator configuration for pitch control is that the hinge location, l_{Hs}, and the linkage coefficient between the stabilator and the trailing-edge flap, k_{es}, can be varied by the designer to adjust the control forces. In the absence of Reynolds number and Mach number effects, show that a desired control force gradient, $F_{p,V}$, can be attained at a specified trim speed, V_{trim}, by enforcing the relation

$$\frac{l_{Hs}}{\bar{c}_h} = \frac{C_1(C_{L,\alpha}C_{m,\delta_s} - C_{L,\delta_s}C_{m,\alpha}) + C_{m_h,\delta_e}C_{m,\alpha}k_{es}}{C_{L_h,\alpha}[C_{m,\alpha}(1+\varepsilon_e k_{es}) - C_{m,\delta_s}(1-\varepsilon_{d,\alpha})]}$$

where

$$C_1 = -\frac{S_w l_g F_{p,V} V_{\text{trim}}}{2\eta_h S_h \bar{c}_h W}$$

6.30. For the airplane and stabilator that is described in problem 6.28, use the result obtained in problem 6.29 to estimate the stabilator hinge location that would be required to provide a control force gradient of –0.20 lbf·sec/ft at a trim speed of 80 mph. Assume that the trailing-edge flap is mechanically linked to the stabilator so that k_{es} is 0.50, and that the CG is located 10 percent forward of the wing quarter-chord.

6.31 The designer can also adjust the control forces for an airplane with a mechanical stabilator by changing the gear ratio for the linkage between the main hinge of the stabilator and the trailing-edge flap. Starting with the result obtained in problem 6.29, develop a relation for the linkage coefficient, k_{es}, that is required to attain a desired control force gradient at a specified trim speed for a fixed location of the main stabilator hinge.

6.32. For the airplane and stabilator described in problem 6.28, use the result obtained in problem 6.31 to estimate the linkage coefficient, k_{es}, that would be required to provide a control force gradient of –0.20 lbf·sec/ft at a trim speed of 80 mph. Assume that the primary hinge of the stabilator passes through the aerodynamic center of the horizontal surface, and that the CG is located 10 percent forward of the wing quarter-chord.

6.33. For a light airplane with the properties listed below, use the approximate model for airplane spin that is given by Eqs. (6.10.22) through (6.10.25) to plot the fully developed spin rate, spin radius, and sink rate as a function of elevation angle. Assume standard sea-level air density and neglect the yawing moment produced by the airplane's propeller.

$$I_{xx_b} = 1{,}000 \text{ slug}\cdot\text{ft}^2, \quad I_{yy_b} = 1{,}000 \text{ slug}\cdot\text{ft}^2, \quad I_{zz_b} = 3{,}300 \text{ slug}\cdot\text{ft}^2,$$

$$S_w = 180 \text{ ft}^2, \quad b_w = 33 \text{ ft}, \quad \widetilde{C}_w = 2.0, \quad x_w = 0.71 \text{ ft}, \quad W = 2{,}700 \text{ lbf},$$

$$S_h = 36 \text{ ft}^2, \quad b_h = 12 \text{ ft}, \quad \widetilde{C}_h = 2.0, \quad x_h = -14.29 \text{ ft},$$

$$S_v = 11.9 \text{ ft}^2, \quad \widetilde{C}_v = 2.0, \quad x_v = -14.81 \text{ ft}, \quad \eta_v = 0.1,$$

$$S_{fh} = 63.8 \text{ ft}^2, \quad C_f = 1.0, \quad \overline{x_{fh}} = 3.5 \text{ ft},$$

$$S_{fv} = 80.2 \text{ ft}^2, \quad \overline{x_{fv}} = 3.5 \text{ ft}, \quad \overline{x_{fv}^2} = 22.3 \text{ ft}^2, \quad \overline{x_{fv}^3} = 149 \text{ ft}^3$$

6.34. For the steady coordinated turn analysis presented in Sec. 6.7, it was assumed that the angular rate was sufficiently small so that the angular acceleration associated with the rotating coordinate system could be ignored. Because the angular rate is much higher in a spin, this assumption was not made for the spin analysis presented in Sec. 6.10. Assume that the body-fixed coordinate system coincides with the primary inertial axes of the airplane and follow a procedure similar to that used in Sec. 6.10 to add the angular acceleration terms to the steady coordinated turn analysis presented in Sec. 6.7.

6.35. Using the more general formulation developed in problem 6.34, repeat the computations in problem 6.22, accounting for the angular acceleration terms. Use the following moments of inertia,

$$I_{xx_b} = 1{,}000 \text{ slug}\cdot\text{ft}^2, \quad I_{yy_b} = 3{,}000 \text{ slug}\cdot\text{ft}^2, \quad I_{zz_b} = 3{,}500 \text{ slug}\cdot\text{ft}^2$$

Compare your results with those obtained in problem 6.22. Do you think that angular acceleration would ever be significant in a typical steady coordinated turn?

6.36 The XP-38 prototype for the P-38 Lightning had propellers that turned opposite to those of the later production models. Based on spin considerations and the photograph of the production model that is shown in Fig. 5.9.2, can you suggest a reason why the direction of propeller rotation may have been changed in going from the prototype to the production model?

6.37 Supersonic flow is characteristically very different from subsonic flow. Recall that camber does not contribute to the section lift developed on a thin airfoil at supersonic airspeeds. As a result, control surface effectiveness is reduced at Mach numbers greater than 1. Consider, for example, the symmetric diamond-wedge airfoil section with trailing-edge flap shown in Fig. 6.11.1. The thickness distribution increases linearly from zero at the leading edge to the point of maximum thickness located at the half-chord. The thickness then decreases linearly from the half-chord to the sharp trailing edge. Recall that the pressure coefficient at any point in the flow over a thin airfoil at supersonic airspeeds depends only on the freestream Mach number and the slope of the local streamline relative to the freestream, i.e.,

$$C_p \equiv \frac{p - p_\infty}{\frac{1}{2}\rho_\infty V_\infty^2} = \pm \frac{2}{\sqrt{M_\infty^2 - 1}} \left(\frac{\partial y}{\partial x} \right)_{\text{streamline}}$$

where the positive sign applies above the airfoil and the negative sign applies below. With the maximum thickness denoted as t and assuming that all angles are small, start with this result and develop an expression for the ideal section flap effectiveness.

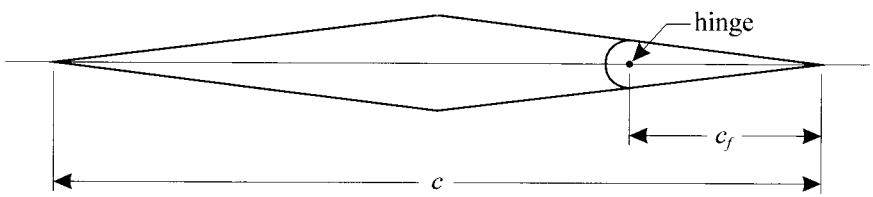


Figure 6.11.1. Diamond-wedge supersonic airfoil and trailing-edge flap used in problem 6.37.

6.38 For the supersonic airfoil section that was described in problem 6.37, develop a small-angle expression for the half-chord section moment coefficient as a function of the flap deflection angle and the angle of attack measured relative to the undeflected chord line.

6.39 For the supersonic airfoil section that was described in problem 6.37, develop a small-angle expression for the section wave drag coefficient as a function of the flap deflection angle and the angle of attack measured relative to the undeflected chord line.

6.40 A trim tab with chord length c_t is added to the supersonic airfoil section that was described in problem 6.37 (see Fig. 6.11.2). Develop a small-angle expression for the section hinge moment coefficient as a function of the flap deflection angle, trim tab deflection angle, and angle of attack measured relative to the undeflected chord line.

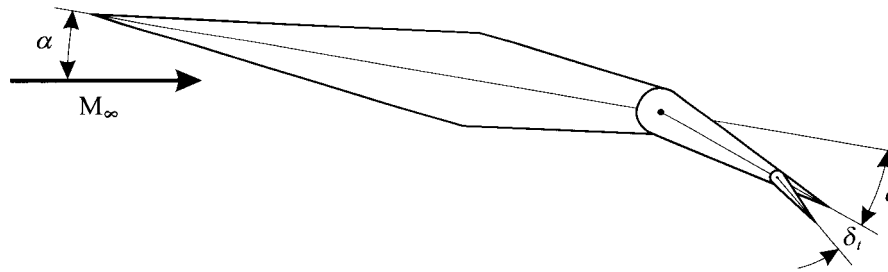


Figure 6.11.2. Diamond-wedge supersonic airfoil section with trailing-edge flap and trim tab used in problem 6.40.

Chapter 7
Aircraft Equations of Motion

7.1. Introduction

The process involved in carrying out any engineering analysis can be divided into two phases, problem formulation and problem solution. The formulation phase requires understanding the physics of an engineering problem and converting that physics into a consistent set of mathematical equations. The solution phase involves applying the rules of mathematics and/or numerical methods to obtain a solution to the system of equations that was developed in the formulation phase. Both phases are equally important. A system of equations is of little direct use in engineering analysis unless it can be accurately solved. Likewise, a mathematical solution is of no use unless the formulation from which it came provides a reasonable description for the physics of the original engineering problem.

In Chapters 3 through 6 of this text, the formulation and solution for many flight mechanics problems were obtained starting from fundamental principles of Newtonian mechanics. In each case we started with the physics of a particular engineering problem and applied all appropriate simplifications as the governing mathematical equations were being developed. This approach minimizes mathematical complexity and emphasizes understanding the physics of each engineering problem. This approach also allows us to begin with simple problems, like those associated with steady level flight, and progress toward more complex problems, such as the analysis of turns and spins. However, as the reader has probably observed, there is a great deal of repetition involved in formulating different but related problems in this manner. For most students, this repetition and the progression from the simple to more complex are helpful in building an understanding of new material.

Once an engineer has developed a good understanding of the physics associated with a particular discipline, there is another approach that can be used for the formulation of engineering problems, that is, starting with a very general formulation and obtaining the formulation for more restricted problems by direct mathematical reduction. For example, had we begun our study of flight mechanics with analysis of the steady coordinated turn, the formulation for steady level flight could have been obtained from the more general formulation by simply setting the climb angle and bank angle to zero. The obvious advantage of this method is reduced formulation time once the more general formulation has been developed. There is a less obvious disadvantage. **No formulation has ever been completely general.** Human limitations being what they are, we all have a tendency to forget the restrictions that apply to a "general" formulation. Sooner or later most engineers have used a so-called "general formulation" for a problem to which it does not apply. Nevertheless, if the engineer exercises appropriate care, the advantage of using this method of formulation outweighs the disadvantage.

In this chapter we develop a *more general* formulation of the rigid-body equations of motion. Since the chapter could serve as a starting point for a second-semester course in flight mechanics, it includes a review of coordinate systems and mathematical

notation that were introduced gradually throughout Chapters 3 through 6. This chapter was deliberately written to be more or less independent of the presentation in Chapters 3 through 6. Thus, a student or practicing engineer who is already familiar with the principles of static stability and control could start with this chapter to begin a study of aircraft dynamics.

Before the equations of motion for a physical system can be formulated mathematically, a coordinate system must be chosen. Furthermore, this choice of coordinate system can have a profound effect on the complexity of the ensuing mathematical formulation. Thus, before developing the more general rigid-body equations of motion for an aircraft in flight, it is worth spending some time considering the advantages and disadvantages of the coordinate systems that could be used. Here we discuss the advantages and disadvantages of some common coordinate systems and settle on three different coordinate systems to be used in our development of the aircraft equations of motion.

Study of aerodynamics typically begins with the consideration of two-dimensional flows, such as the flow around airfoils and long cylinders. When formulating any two-dimensional problem in Cartesian coordinates, it is conventional to use an x-y coordinate system. When considering flow over an airfoil, it was quite convenient to have the x-axis aligned with the chord, pointing in the general direction of flow with the origin at the leading edge. The y-axis was quite naturally chosen normal to the x-axis in the upward direction. It was also quite natural to choose the angle of attack to be positive with the leading edge high, since increasing the angle of attack in this direction increases the lift produced by the airfoil. Once the sign convention for angle of attack was established, both the pitching moment and the pitching rate were naturally defined to be positive in the direction of increasing angle of attack.

When the study of aerodynamics is extended to include three-dimensional flow around finite wings, retaining the original x-y coordinate system and choosing a conventional right-handed system requires the z-axis to be pointing in the spanwise direction from right to left, as shown in Fig. 7.1.1. Here, this coordinate system is

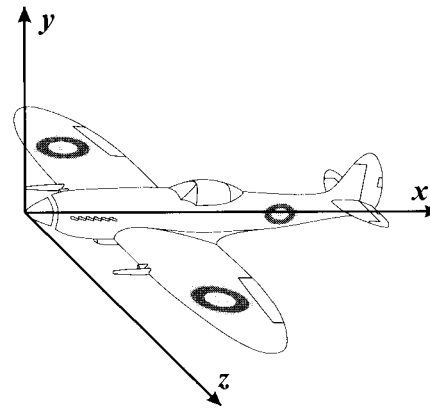


Figure 7.1.1. The aerodynamic coordinate system.

referred to as *aerodynamic coordinates*. When using aerodynamic coordinates it is conventional to choose the origin to be at the leading edge of the object of study, in this case the nose of an airplane, with the x-axis lying along a somewhat arbitrary fuselage reference line.

There are two primary objections to continuing with aerodynamic coordinates as the sole coordinate system to be used in our study of aircraft dynamics. First, because the aerodynamic coordinate system is fixed to the aircraft, the position and orientation of the aircraft cannot be conveniently described in terms of aerodynamic coordinates. Second, the sign convention for the moment and angular velocity components used with aerodynamic coordinates does not follow the conventional right-hand rule.

To describe the position and orientation of an aircraft relative to the Earth, we normally use a coordinate system fixed to the Earth. Position relative to the Earth is usually described in terms of latitude, longitude, and elevation above mean sea level. However, because this coordinate system is not a Cartesian system, it introduces unnecessary complexities to the dynamic formulation. Since the radius of the Earth is large compared to the distance traveled by an airplane in the relatively short time periods that characterize aircraft motion, the formulation can be greatly simplified by using a Cartesian coordinate system fixed to the Earth. For all practical purposes, such a Cartesian system can be considered to be an inertial coordinate system. Of course, this so-called "flat Earth" approximation is not appropriate for tracking the position of an aircraft over long distances.

While an Earth-fixed coordinate system allows us to conveniently describe aircraft position and orientation, the components of the inertia tensor become time dependent in Earth-fixed coordinates. The complexity associated with carrying a time-dependent inertia tensor in the equations of motion is almost prohibitive. The mathematical description of the inertia tensor can be greatly simplified by formulating the angular momentum equation in terms of a coordinate system that is fixed to the aircraft with the origin located at the aircraft's center of gravity.

The aerodynamic forces and moments acting on an aircraft depend not on the velocity of the aircraft relative to the ground, but rather, on the velocity relative to the surrounding air. Thus, these forces and moments are most conveniently described in terms of a coordinate system fixed to the atmosphere. The atmosphere can have motion relative to the Earth, i.e., wind. In our development of the aircraft equations of motion we shall consider the atmosphere in the immediate vicinity of the aircraft to be moving at a constant velocity relative to the Earth. Thus, within this approximation, an atmosphere-fixed coordinate system can also be considered to be an inertial coordinate system.

In summary, position and orientation are best described in terms of an Earth-fixed coordinate system; the inertia tensor is most conveniently described in terms of a body-fixed coordinate system; and forces and moments are more easily described in terms of an atmosphere-fixed coordinate system. For this reason, these three different coordinate systems will all be used in developing the aircraft equations of motion. Furthermore, it is desirable to define the body-fixed system such that the usual sign conventions for the moment and angular velocity components follow the conventional right-hand rule. The Earth-fixed and body-fixed Cartesian coordinate systems commonly used for this purpose are shown in Fig. 7.1.2.

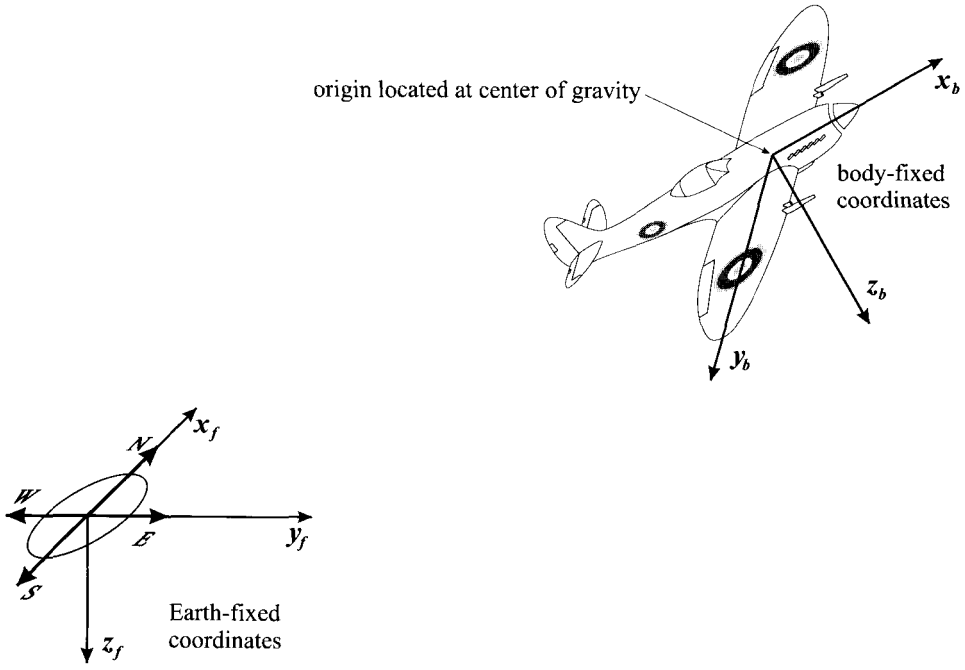


Figure 7.1.2. The body-fixed and Earth-fixed coordinate systems.

The **body-fixed coordinate system** has the origin located at the aircraft center of gravity. The x-axis points forward along some convenient axis of the fuselage in the aircraft's plane of symmetry. The y-axis is normal to the plane of symmetry pointing in the direction of the right wing. The z-axis then points downward in the aircraft plane of symmetry, completing the right-handed Cartesian system. In the present text, (x_b, y_b, z_b) will always denote this particular body-fixed coordinate system and it will often be referred to simply as body coordinates. In this coordinate system, a positive angle of attack corresponds to a positive z_b-component of the airplane's velocity vector relative to the surrounding atmosphere. Similarly, a positive sideslip angle corresponds to a positive y_b-component of airspeed. Also, the sign conventions for roll, pitch, and yaw all follow the right-hand rule relative to the x_b-, y_b-, and z_b-axes, respectively.

For the **Earth-fixed coordinate system** shown in Fig. 7.1.2, the x-y plane is normal to the local gravitational vector with the x-axis pointing north and the y-axis pointing east. The z-axis then points down, completing the right-handed Cartesian system. In the present text, this coordinate system will be designated (x_f, y_f, z_f) and will normally be referred to simply as *fixed coordinates*. While the student may find a downward-pointing z-axis to be somewhat unconventional, when the aircraft heading or azimuth angle is described in terms of a conventional right-handed angular rotation about the z_f-axis, the heading angles conform to conventional compass headings, that is, a heading angle measured clockwise from north with east being 90 degrees, south being 180 degrees, west being 270 degrees, and north being either 0 or 360 degrees.

The **atmosphere-fixed coordinate system** is denoted (x_a, y_a, z_a) and defined such that all three axes are always parallel to those of the Earth-fixed coordinate system. However, the atmosphere-fixed system moves at a constant velocity relative to the Earth-fixed system. The atmosphere-fixed and Earth-fixed systems are defined to be coincident at time equal to zero. The atmosphere-fixed coordinate system will be used only temporarily, in the development of the aircraft equations of motion. The final equations will be expressed completely in terms of Earth-fixed and body-fixed coordinates.

The vector $\mathbf{V}_g$ will denote the velocity of the body-fixed coordinate frame relative to the Earth-fixed coordinate frame. The magnitude of this velocity vector is commonly termed the *ground speed*, which is simply the speed of the aircraft relative to the ground. The velocity of the body-fixed coordinate frame relative to the atmosphere-fixed coordinate frame is denoted here simply as $\mathbf{V}$, and its magnitude is commonly termed the *airspeed*. Ground speed and airspeed are related through the simple vector equation

$$\mathbf{V}_g = \mathbf{V} + \mathbf{V}_w \tag{7.1.1}$$

where $\mathbf{V}_w$ is the velocity of the atmosphere relative to the Earth, which is commonly called the *wind*.

The aerodynamic forces and moments acting on an aircraft could be expressed as functions of the translational and rotational velocity components relative to the surrounding air. However, in the study of aerodynamic forces and moments, it is more convenient to express the translational dependence in terms of total airspeed, angle of attack, and sideslip angle. Of course, the velocity vector relative to the surrounding air can be equivalently described either in terms of three velocity components or in terms of a magnitude and any two independent aerodynamic angles. The total airspeed is readily expressed in terms of the body-fixed components according to the relation

$$V \equiv \sqrt{V_{x_b}^2 + V_{y_b}^2 + V_{z_b}^2} \tag{7.1.2}$$

As standard convention, angle of attack has always traditionally been defined according to the mathematical relation

$$\alpha \equiv \tan^{-1}\left(\frac{V_{z_b}}{V_{x_b}}\right) \tag{7.1.3}$$

Unfortunately, there are two different mathematical definitions for the sideslip angle that are sometimes used in the determination of aerodynamic forces.

In Chapter 5, the side force and yawing moment contributed by the vertical stabilizer were estimated from the sideslip angle and section properties of the vertical stabilizer in the same way that the lift and pitching moment were estimated from the angle of attack and section properties for the wing and horizontal stabilizer. This method of estimating the aerodynamic forces and moments tacitly assumes that the sideslip angle is related to a vertical surface in the same way that the angle of attack is related to a horizontal surface. This implies a mathematical definition of sideslip angle analogous to Eq. (7.1.3), i.e.,

$$\beta_a \equiv \tan^{-1}\left(\frac{V_{y_b}}{V_{x_b}}\right) \tag{7.1.4}$$

Here the subscript a is used with this definition of sideslip angle because the definition is most convenient for the *analytical* estimation of aerodynamic forces and moments.

For the experimental determination of aerodynamic forces and moments, another definition of sideslip angle is used almost exclusively. This definition comes about as a result of the way in which data are gathered in a wind tunnel. Typically, the rotational mechanism used to adjust the angle of attack is mounted on a turntable, which is used to set the sideslip angle. When this gimbal mechanism is used to orient a model in a wind tunnel, one of two gimbal angles is exactly the angle of attack as defined by Eq. (7.1.3). However, the other gimbal angle is not that defined by Eq. (7.1.4). The angle set by the turntable of such a mechanism is related to the body-fixed velocity components by

$$\beta_e \equiv \sin^{-1}\left(\frac{V_{y_b}}{\sqrt{V_{x_b}^2 + V_{y_b}^2 + V_{z_b}^2}}\right) \tag{7.1.5}$$

where the subscript e is used here to indicate the definition that is most convenient for *experimental* determination of aerodynamic forces and moments. The definitions given by Eqs. (7.1.4) and (7.1.5) are identical only when the angle of attack is zero. Of course, these two definitions are essentially equivalent for small angles of attack, but as the angle of attack becomes large, the difference becomes significant.

Clearly, both the aerodynamic angle defined by Eq. (7.1.4) and that defined by Eq. (7.1.5) are independent of the angle of attack defined by Eq. (7.1.3). Thus, either of these two sideslip definitions could be combined with the angle of attack and the total airspeed to uniquely describe the velocity vector relative to the air. However, the aerodynamic angle defined by Eq. (7.1.4) has the same geometric relationship to a vertical surface as the angle of attack has to a horizontal surface. This cannot be said of the aerodynamic angle defined by Eq. (7.1.5). Most textbooks define the sideslip angle only in terms of Eq. (7.1.5), but for analytical predictions this angle is often used as if it were defined according to Eq. (7.1.4).

The sideslip angle defined by Eq. (7.1.5) depends on the z_b-velocity component, while the angle of attack as defined from Eq. (7.1.3) does not depend on the y_b-velocity component. This asymmetry in the two definitions is not at all attractive from a physical point of view, especially when considering large angles of attack. For example, consider an aircraft that is symmetric about both the x_b-y_b and the x_b-z_b planes, such as a rocket with four identical tail fins. Let the velocity of this aircraft be such that the x_b-, y_b-, and z_b-components of velocity are all equal. From Eqs. (7.1.3), (7.1.4), and (7.1.5) we have $\alpha = 45°$, $\beta_a = 45°$, and $\beta_e = 35.26°$. If the sideslip angle were used to obtain the side force in the same way that the angle of attack is used to obtain the normal force, the aerodynamic angles defined by Eqs. (7.1.3) and (7.1.5) would result in an asymmetric aerodynamic loading produced by this completely symmetric flight condition. This is clearly not consistent with reality.

One reason commonly given for defining the sideslip angle according to Eq. (7.1.5) is that this definition gives a sideslip angle that is completely independent of the orientation of the x_b-axis within the x_b-z_b plane of symmetry. Clearly, the side force should not depend on our choice for the direction of the x_b-axis within this plane. However, the sweep angle that any vertical surface makes with the z_b-axis does depend on the x_b-axis orientation. Thus, the sideslip angle should also vary with the x_b-axis orientation, such that the combined effects of sweep and sideslip make the airflow relative to a vertical surface independent of the x_b-axis orientation within the x_b-z_b plane of symmetry. The definition of sideslip angle that is given by Eq. (7.1.4) satisfies this requirement, while that given by Eq. (7.1.5) does not. Thus, the definition in Eq. (7.1.5) is not nearly as convenient for analytical prediction as that in Eq. (7.1.4).

Either of these two definitions for sideslip angle may be used in a formulation of the rigid-body equations of motion for aircraft dynamics. **The important thing to remember is to be consistent.** Whenever a relation for some particular aerodynamic coefficient has been obtained using one definition of sideslip angle, it should be applied using that same definition. It is easy to violate this requirement unintentionally if some aerodynamic coefficients are estimated analytically from airfoil section properties, while others are taken from experimental data.

During most of the flight of a conventional airplane the aerodynamic angles remain relatively small and the difference between the two definitions for sideslip angle is insignificant. However, **for flight conditions that may involve large aerodynamic angles, care should be taken to avoid the common pitfall of using one definition for sideslip angle in a relation that was developed using the other**.

The transformation equations given by Eqs. (7.1.2) through (7.1.4) can readily be rearranged to yield an inverse transformation, which can be used to compute the three body-fixed velocity components from known values of V, α, and β_a. We start by solving Eq. (7.1.2) for the x_b-velocity component. This gives

$$V_{x_b} = \sqrt{V^2 - V_{y_b}^2 - V_{z_b}^2} \tag{7.1.6}$$

Solving Eq. (7.1.3) for the z_b-velocity component yields

$$V_{z_b} = V_{x_b} \tan\alpha = V_{x_b} \frac{\sin\alpha}{\cos\alpha} \tag{7.1.7}$$

and solving Eq. (7.1.4) for the y_b-velocity component results in

$$V_{y_b} = V_{x_b} \tan\beta_a = V_{x_b} \frac{\sin\beta_a}{\cos\beta_a} \tag{7.1.8}$$

Using Eqs. (7.1.7) and (7.1.8) in Eq. (7.1.6), we obtain

$$V_{x_b} = \sqrt{V^2 - V_{x_b}^2 \tan^2\beta_a - V_{x_b}^2 \tan^2\alpha} = \sqrt{V^2 - V_{x_b}^2 \frac{\sin^2\beta_a}{\cos^2\beta_a} - V_{x_b}^2 \frac{\sin^2\alpha}{\cos^2\alpha}} \tag{7.1.9}$$

Solving Eq. (7.1.9) for the x_b-component of velocity and using the result in Eqs. (7.1.7) and (7.1.8), we obtain the inverse transformation equations

$$V_{x_b} = V\frac{1}{\sqrt{1+\tan^2\alpha+\tan^2\beta_a}} = V\frac{\cos\alpha\cos\beta_a}{\sqrt{1-\sin^2\alpha\,\sin^2\beta_a}} \tag{7.1.10}$$

$$V_{y_b} = V\frac{\tan\beta_a}{\sqrt{1+\tan^2\alpha+\tan^2\beta_a}} = V\frac{\cos\alpha\sin\beta_a}{\sqrt{1-\sin^2\alpha\,\sin^2\beta_a}} \tag{7.1.11}$$

$$V_{z_b} = V\frac{\tan\alpha}{\sqrt{1+\tan^2\alpha+\tan^2\beta_a}} = V\frac{\sin\alpha\cos\beta_a}{\sqrt{1-\sin^2\alpha\,\sin^2\beta_a}} \tag{7.1.12}$$

Similarly, if Eq. (7.1.5) is used for the sideslip angle, the inverse transformation is

$$V_{x_b} = V\cos\alpha\cos\beta_e \tag{7.1.13}$$

$$V_{y_b} = V\sin\beta_e \tag{7.1.14}$$

$$V_{z_b} = V\sin\alpha\cos\beta_e \tag{7.1.15}$$

Notice the symmetry that exists between Eqs. (7.1.11) and (7.1.12). There is no such symmetry between Eqs. (7.1.14) and (7.1.15).

EXAMPLE 7.1.1. A rocket is flying at an airspeed of 1,000 ft/sec. The angle of attack is 30 degrees and the sideslip angle, β_a, is 20 degrees. Determine the axial, sideslip, and normal velocity components.

Solution. From Eqs. (7.1.10), (7.1.11), and (7.1.12), the velocity components are

$$V_{x_b} = \frac{V}{\sqrt{1+\tan^2\alpha+\tan^2\beta_a}} = \frac{1{,}000\text{ ft/sec}}{\sqrt{1+(0.577350)^2+(0.363970)^2}}$$
$$= \underline{825.96\text{ ft/sec}}$$

$$V_{y_b} = \frac{V\tan\beta_a}{\sqrt{1+\tan^2\alpha+\tan^2\beta_a}} = \frac{1{,}000\text{ ft/sec}(0.363970)}{\sqrt{1+(0.577350)^2+(0.363970)^2}}$$
$$= \underline{300.63\text{ ft/sec}}$$

$$V_{z_b} = \frac{V\tan\alpha}{\sqrt{1+\tan^2\alpha+\tan^2\beta_a}} = \frac{1{,}000\text{ ft/sec}(0.577350)}{\sqrt{1+(0.577350)^2+(0.363970)^2}}$$
$$= \underline{476.87\text{ ft/sec}}$$

EXAMPLE 7.1.2. A rocket is flying at an airspeed of 1,000 ft/sec. The angle of attack is 30 degrees and the sideslip angle, β_e, is 20 degrees. Determine the axial, sideslip, and normal velocity components.

Solution. From Eqs. (7.1.13), (7.1.14), and (7.1.15), the velocity components are

$$V_{x_b} = V\cos\alpha\cos\beta_e = 1{,}000 \text{ ft/sec}(0.866025)(0.939693) = \underline{813.80 \text{ ft/sec}}$$

$$V_{y_b} = V\sin\beta_e = 1{,}000 \text{ ft/sec}(0.342020) = \underline{342.02 \text{ ft/sec}}$$

$$V_{z_b} = V\sin\alpha\cos\beta_e = 1{,}000 \text{ ft/sec}(0.500000)(0.939693) = \underline{469.85 \text{ ft/sec}}$$

In certain situations it may be necessary to estimate some aerodynamic coefficients using airfoil section properties and the definition given by Eq. (7.1.4), while others may be taken from experimental results that were obtained using the definition in Eq. (7.1.5). In such cases it is convenient to be able to transform results from one definition to the other. The mathematical relation between β_a and β_e can readily be established by using Eqs. (7.1.13) and (7.1.14) in Eq. (7.1.4). This results in

$$\tan\beta_a = \frac{\tan\beta_e}{\cos\alpha} \tag{7.1.16}$$

Now consider some aerodynamic coefficient, C, that is somehow known as a function of V, α, and β_e. Suppose that we also know the partial derivative of C with respect to β_e at constant V and α. The partial derivative of C with respect to β_a at constant V and α can then be expressed as

$$\frac{\partial C}{\partial \beta_a} = \frac{\partial C}{\partial \beta_e}\frac{\partial \beta_e}{\partial \beta_a} \tag{7.1.17}$$

Differentiating both sides of Eq. (7.1.16) with respect to β_a and rearranging, it is readily shown that

$$\frac{\partial \beta_e}{\partial \beta_a} = \frac{\cos\alpha\cos^2\beta_e}{\cos^2\beta_a}$$

After applying the trigonometric identity, $\cos^2\beta_e = 1/(1+\tan^2\beta_e)$, and using Eq. (7.1.16) to eliminate $\tan\beta_e$, we have

$$\frac{\partial \beta_e}{\partial \beta_a} = \frac{\cos\alpha}{\cos^2\beta_a + \cos^2\alpha\sin^2\beta_a} \tag{7.1.18}$$

Using Eq. (7.1.18) in Eq. (7.1.17) results in

$$\frac{\partial C}{\partial \beta_a} = \frac{\cos\alpha}{\cos^2\beta_a + \cos^2\alpha \sin^2\beta_a} \frac{\partial C}{\partial \beta_e} \tag{7.1.19}$$

In a similar manner, it can be shown that

$$\frac{\partial C}{\partial \beta_e} = \frac{\cos\alpha}{\sin^2\beta_e + \cos^2\alpha \cos^2\beta_e} \frac{\partial C}{\partial \beta_a} \tag{7.1.20}$$

EXAMPLE 7.1.3. An airplane model is mounted in a wind tunnel with the angle of attack set at 12.0 degrees and the sideslip angle, β_e, set to 8.0 degrees. By varying β_e slightly to both sides from this orientation, the change in the yawing moment coefficient with respect to β_e is estimated to be 0.250. Find the angle, β_a, and estimate the change in the yawing moment coefficient with respect to β_a.

Solution. From Eq. (7.1.16),

$$\beta_a = \tan^{-1}\left(\frac{\tan\beta_e}{\cos\alpha}\right) = \tan^{-1}\left(\frac{0.140541}{0.978148}\right) = 0.142704 = \underline{8.2^\circ}$$

Using this in Eq. (7.1.19) yields

$$\frac{\partial C}{\partial \beta_a} = \frac{\cos\alpha}{\cos^2\beta_a + \cos^2\alpha \sin^2\beta_a} \frac{\partial C}{\partial \beta_e}$$

$$= \frac{0.978148}{(0.989835)^2 + (0.978148)^2 (0.142220)^2} 0.250 = \underline{0.245}$$

EXAMPLE 7.1.4. An airplane model is mounted in a wind tunnel with the angle of attack set at 40 degrees and the sideslip angle, β_e, set to 30 degrees. By varying β_e slightly to both sides from this orientation, the change in the yawing moment coefficient with respect to β_e is estimated to be 0.250. Find the angle, β_a, and estimate the change in the yawing moment coefficient with respect to β_a.

Solution. From Eq. (7.1.16),

$$\beta_a = \tan^{-1}\left(\frac{\tan\beta_e}{\cos\alpha}\right) = \tan^{-1}\left(\frac{0.577350}{0.766044}\right) = 0.645850 = \underline{37^\circ}$$

Using this in Eq. (7.1.19) yields

$$\frac{\partial C}{\partial \beta_a} = \frac{\cos\alpha}{\cos^2\beta_a + \cos^2\alpha \sin^2\beta_a} \frac{\partial C}{\partial \beta_e}$$

$$= \frac{0.766044}{(0.798588)^2 + (0.766044)^2 (0.601878)^2} 0.250 = \underline{0.225}$$

From the results of Example 7.1.3 it can be seen that at angles of attack below stall, there is no significant difference between our two definitions for sideslip angle. Even for the relatively high angles used in Example 7.1.4, the difference between C_{n,β_e} and C_{n,β_a} is only about 10 percent. This should not be taken as a general license for carelessness with regard to sideslip angle definition. There are important applications where angles of attack can approach or even exceed 90 degrees. For such cases, the difference between the definitions in Eqs. (7.1.4) and (7.1.5) is quite large. For instance, when the angle of attack is 80 degrees, a value for β_e of 30 degrees corresponds to a value of β_a of approximately 73 degrees. Nevertheless, in the vast majority of all flight, the angle of attack remains small. For analysis of such flight the subscript on β will be dropped and no distinction will be made.

7.2. Newton's Second Law for Rigid-Body Dynamics

The foundation for the formulation of most problems in flight mechanics is Newton's second law (often stated as $F=ma$). Newton's second law applied to a rigid body requires that the summation of forces must equal the time rate of change of translational momentum, and the summation of moments must equal the time rate of change of angular momentum. Application of this principle is not always as simple as it sounds. For the present formulation, we will be using a body-fixed coordinate system and allowing both translational and angular acceleration. At this point you may wish to review the chapter on accelerating coordinate systems in your introductory dynamics textbook.

Newton's second law for rigid-body motion can be expressed in the following vector equations, which are written in terms of a body-fixed coordinate system (see, for example, Hibbeler 1998 or Beer and Johnston 1997),

$$\mathbf{F}_S + \mathbf{W} = \frac{d}{dt}(m\mathbf{V}) + \boldsymbol{\omega} \times (m\mathbf{V}) \tag{7.2.1}$$

$$\mathbf{M}_S = \frac{d}{dt}([\mathbf{I}]\,\boldsymbol{\omega}) + \boldsymbol{\omega} \times ([\mathbf{I}]\,\boldsymbol{\omega}) \tag{7.2.2}$$

where $\mathbf{F}_S$ is the net surface force vector, $\mathbf{W}$ is the weight vector, $\mathbf{M}_S$ is the net moment vector about the body-fixed origin (i.e., the CG), m is the mass, $[\mathbf{I}]$ is the inertia tensor,

$$[\mathbf{I}] = \begin{bmatrix} I_{xx_b} & -I_{xy_b} & -I_{xz_b} \\ -I_{yx_b} & I_{yy_b} & -I_{yz_b} \\ -I_{zx_b} & -I_{zy_b} & I_{zz_b} \end{bmatrix} \tag{7.2.3}$$

$$I_{xx_b} = \iiint_m (y_b^2 + z_b^2)\,dm \tag{7.2.4}$$

$$I_{yy_b} = \iiint_m (x_b^2 + z_b^2)\,dm \tag{7.2.5}$$

$$I_{zz_b} = \iiint_m (x_b^2 + y_b^2)dm \tag{7.2.6}$$

$$I_{xy_b} = I_{yx_b} = \iiint_m x_b y_b dm \tag{7.2.7}$$

$$I_{yz_b} = I_{zy_b} = \iiint_m y_b z_b dm \tag{7.2.8}$$

$$I_{xz_b} = I_{zx_b} = \iiint_m x_b z_b dm \tag{7.2.9}$$

and $\mathbf{V}$ and $\boldsymbol{\omega}$ are, respectively, the translational and rotational velocities of the body-fixed coordinate frame relative to some inertial reference frame. For convenience in describing the aerodynamic forces and moments, the atmosphere-fixed coordinate system is selected as our inertial reference frame.

Mass is a scalar, so the second term on the right-hand side of Eq. (7.2.1) is written

$$\boldsymbol{\omega}\times(m\mathbf{V}) = m\begin{vmatrix} \mathbf{i}_{x_b} & \mathbf{i}_{y_b} & \mathbf{i}_{z_b} \\ \omega_{x_b} & \omega_{y_b} & \omega_{z_b} \\ V_{x_b} & V_{y_b} & V_{z_b} \end{vmatrix} = m\begin{Bmatrix} \omega_{y_b}V_{z_b} - \omega_{z_b}V_{y_b} \\ \omega_{z_b}V_{x_b} - \omega_{x_b}V_{z_b} \\ \omega_{x_b}V_{y_b} - \omega_{y_b}V_{x_b} \end{Bmatrix} \tag{7.2.10}$$

Equation (7.2.10) can be used in Eq. (7.2.1) to yield the body-fixed Cartesian components of the translational momentum equation,

$$\frac{d}{dt}\left(m\begin{Bmatrix} V_{x_b} \\ V_{y_b} \\ V_{z_b} \end{Bmatrix}\right) = \begin{Bmatrix} F_{Sx_b} + W_{x_b} - m\omega_{y_b}V_{z_b} + m\omega_{z_b}V_{y_b} \\ F_{Sy_b} + W_{y_b} - m\omega_{z_b}V_{x_b} + m\omega_{x_b}V_{z_b} \\ F_{Sz_b} + W_{z_b} - m\omega_{x_b}V_{y_b} + m\omega_{y_b}V_{x_b} \end{Bmatrix} \tag{7.2.11}$$

The total surface force, $\mathbf{F}_S$, is simply the vector sum of all pressure and shear forces acting on the surface of the control volume enclosing the aircraft.

Aircraft mass typically changes with time as a result of fuel burn. Furthermore, fuel weight can be a very significant fraction of total aircraft weight, and the mass of an aircraft can change very rapidly with time. For example, a rocket may burn off a large fraction of its total weight in fuel within just a few seconds. During midair refueling, the mass of both airplanes can change quite rapidly. Also, bombers, crop dusters, and fire-fighting aircraft can drop a large fraction of their total mass in a very short time.

When mass exits an aircraft, it carries momentum with it. Any mass that leaves an aircraft (or enters, in the case of an aircraft being refueled) could have velocity different from that of the aircraft. With a jet or rocket, the fuel mass leaves at a velocity that is significantly higher than the velocity of the aircraft. However, the difference between the exit velocity and the aircraft velocity is commonly included in the thrust force. Care must be taken to see that this momentum flux is not counted twice when formulating Newton's second law. Thus, including mass transfer, Eq. (7.2.11) is written as

$$m\frac{\partial}{\partial t}\begin{Bmatrix} V_{x_b} \\ V_{y_b} \\ V_{z_b} \end{Bmatrix} + \begin{Bmatrix} V_{x_b} \\ V_{y_b} \\ V_{z_b} \end{Bmatrix}\frac{\partial m}{\partial t} + \dot{m}_e \begin{Bmatrix} V_{ex_b} \\ V_{ey_b} \\ V_{ez_b} \end{Bmatrix} = \begin{Bmatrix} F_{Sx_b} + W_{x_b} - m\omega_{y_b}V_{z_b} + m\omega_{z_b}V_{y_b} \\ F_{Sy_b} + W_{y_b} - m\omega_{z_b}V_{x_b} + m\omega_{x_b}V_{z_b} \\ F_{Sz_b} + W_{z_b} - m\omega_{x_b}V_{y_b} + m\omega_{y_b}V_{x_b} \end{Bmatrix} \tag{7.2.12}$$

where $\dot{m}_e$ is the mass flow rate leaving the aircraft and $\mathbf{V}_e$ is the velocity of the mass leaving or entering the aircraft, as measured relative to the inertial coordinate system. The mass flow rate, $\dot{m}_e$, is negative for an aircraft being refueled.

In addition to Newton's second law, we must also assure that mass is conserved. The continuity equation requires that

$$\frac{\partial m}{\partial t} + \dot{m}_e = 0 \tag{7.2.13}$$

Using Eq. (7.2.13) in Eq. (7.2.12), the body-fixed Cartesian components of the translational momentum equation can be written

$$m\begin{Bmatrix} \dot{V}_{x_b} \\ \dot{V}_{y_b} \\ \dot{V}_{z_b} \end{Bmatrix} = \begin{Bmatrix} F_{x_b} + W_{x_b} - m\omega_{y_b}V_{z_b} + m\omega_{z_b}V_{y_b} \\ F_{y_b} + W_{y_b} - m\omega_{z_b}V_{x_b} + m\omega_{x_b}V_{z_b} \\ F_{z_b} + W_{z_b} - m\omega_{x_b}V_{y_b} + m\omega_{y_b}V_{x_b} \end{Bmatrix} \tag{7.2.14}$$

where $\mathbf{F}$ is a pseudo aerodynamic force including thrust, $\mathbf{F} = \mathbf{F}_S - \dot{m}(\mathbf{V}_e - \mathbf{V})$, and the dot indicates a time derivative. **It is important to recognize that Eq. (7.2.14) is not based on the assumption that aircraft mass does not change with time. This equation is valid regardless of how rapidly the aircraft mass is changing, provided that the pseudo thrust force accounts for any difference between the exit velocity and the velocity of the aircraft.**

As discussed in the preceding section, the Cartesian body-fixed coordinate system, which is commonly used in aircraft dynamics, has the x_b-axis pointing forward from the center of mass along some convenient body-fixed axis in the aircraft plane of symmetry. The y_b-axis is normal to the plane of symmetry pointing out the right-hand side of the aircraft, and the z_b-axis points downward in the aircraft plane of symmetry. Here the designation (x_b, y_b, z_b) always refers to this body-fixed coordinate system. Since the coordinate system was chosen so that the airplane is symmetric in y_b, we have

$$I_{xy_b} = I_{yx_b} = I_{yz_b} = I_{zy_b} = 0 \tag{7.2.15}$$

and

$$[\mathbf{I}] = \begin{bmatrix} I_{xx_b} & 0 & -I_{xz_b} \\ 0 & I_{yy_b} & 0 \\ -I_{zx_b} & 0 & I_{zz_b} \end{bmatrix} \tag{7.2.16}$$

The product of inertia terms in Eq. (7.2.15) could be carried through the analysis. However, virtually all aircraft possess this symmetry, which simplifies the linearized equations of motion. With this symmetry, the angular momentum vector, $\mathbf{H}$, is

$$\mathbf{H} \equiv [\mathbf{I}]\boldsymbol{\omega} = \begin{bmatrix} I_{xx_b} & 0 & -I_{xz_b} \\ 0 & I_{yy_b} & 0 \\ -I_{zx_b} & 0 & I_{zz_b} \end{bmatrix} \begin{Bmatrix} \omega_{x_b} \\ \omega_{y_b} \\ \omega_{z_b} \end{Bmatrix} = \begin{Bmatrix} I_{xx_b}\omega_{x_b} - I_{xz_b}\omega_{z_b} \\ I_{yy_b}\omega_{y_b} \\ I_{zz_b}\omega_{z_b} - I_{xz_b}\omega_{x_b} \end{Bmatrix}$$

$$\boldsymbol{\omega}\times([\mathbf{I}]\boldsymbol{\omega}) = \boldsymbol{\omega}\times\mathbf{H}$$

$$= \begin{vmatrix} \mathbf{i}_{x_b} & \mathbf{i}_{y_b} & \mathbf{i}_{z_b} \\ \omega_{x_b} & \omega_{y_b} & \omega_{z_b} \\ H_{x_b} & H_{y_b} & H_{z_b} \end{vmatrix} = \begin{Bmatrix} \omega_{y_b}H_{z_b} - \omega_{z_b}H_{y_b} \\ \omega_{z_b}H_{x_b} - \omega_{x_b}H_{z_b} \\ \omega_{x_b}H_{y_b} - \omega_{y_b}H_{x_b} \end{Bmatrix} = \begin{Bmatrix} (I_{zz_b} - I_{yy_b})\omega_{y_b}\omega_{z_b} - I_{xz_b}\omega_{x_b}\omega_{y_b} \\ (I_{xx_b} - I_{zz_b})\omega_{x_b}\omega_{z_b} + I_{xz_b}(\omega_{x_b}^2 - \omega_{z_b}^2) \\ (I_{yy_b} - I_{xx_b})\omega_{x_b}\omega_{y_b} + I_{xz_b}\omega_{y_b}\omega_{z_b} \end{Bmatrix} \tag{7.2.17}$$

Using Eq. (7.2.17), the body-fixed Cartesian components of Eq. (7.2.2) are

$$\frac{d}{dt}\left(\begin{bmatrix} I_{xx_b} & 0 & -I_{xz_b} \\ 0 & I_{yy_b} & 0 \\ -I_{zx_b} & 0 & I_{zz_b} \end{bmatrix} \begin{Bmatrix} \omega_{x_b} \\ \omega_{y_b} \\ \omega_{z_b} \end{Bmatrix} \right) = \begin{Bmatrix} M_{Sx_b} + (I_{yy_b} - I_{zz_b})\omega_{y_b}\omega_{z_b} + I_{xz_b}\omega_{x_b}\omega_{y_b} \\ M_{Sy_b} + (I_{zz_b} - I_{xx_b})\omega_{x_b}\omega_{z_b} + I_{xz_b}(\omega_{z_b}^2 - \omega_{x_b}^2) \\ M_{Sz_b} + (I_{xx_b} - I_{yy_b})\omega_{x_b}\omega_{y_b} - I_{xz_b}\omega_{y_b}\omega_{z_b} \end{Bmatrix} \tag{7.2.18}$$

As aircraft mass changes with time, so does the moment of inertia. However, when mass is expelled from an aircraft, it can carry angular momentum with it. Thus, including the effects of mass transfer and applying conservation of mass in a manner similar to that used for translational momentum, Eq. (7.2.18) can be written as

$$\begin{bmatrix} I_{xx_b} & 0 & -I_{xz_b} \\ 0 & I_{yy_b} & 0 \\ -I_{zx_b} & 0 & I_{zz_b} \end{bmatrix} \begin{Bmatrix} \dot{\omega}_{x_b} \\ \dot{\omega}_{y_b} \\ \dot{\omega}_{z_b} \end{Bmatrix} = \begin{Bmatrix} M_{x_b} + (I_{yy_b} - I_{zz_b})\omega_{y_b}\omega_{z_b} + I_{xz_b}\omega_{x_b}\omega_{y_b} \\ M_{y_b} + (I_{zz_b} - I_{xx_b})\omega_{x_b}\omega_{z_b} + I_{xz_b}(\omega_{z_b}^2 - \omega_{x_b}^2) \\ M_{z_b} + (I_{xx_b} - I_{yy_b})\omega_{x_b}\omega_{y_b} - I_{xz_b}\omega_{y_b}\omega_{z_b} \end{Bmatrix} \tag{7.2.19}$$

where **M** is a pseudo aerodynamic moment including any and all effects of thrust. **This pseudo moment accounts for all the effects of mass leaving or entering the aircraft. Equation (7.2.19) does not require constant moment of inertia.**

The explicit notation (V_{x_b}, V_{y_b}, V_{z_b}) and (ω_{x_b}, ω_{y_b}, ω_{z_b}), which is commonly used in classical dynamics for the components of the translational and angular velocity vectors in body-fixed coordinates, is not normally used in the field of aircraft flight dynamics. The notation that is used almost exclusively by the aircraft community is

$$\begin{Bmatrix} u \\ v \\ w \end{Bmatrix} \equiv \begin{Bmatrix} V_{x_b} \\ V_{y_b} \\ V_{z_b} \end{Bmatrix} = \begin{Bmatrix} \text{the axial velocity} \\ \text{the sideslip velocity} \\ \text{the normal velocity} \end{Bmatrix}, \quad \begin{Bmatrix} p \\ q \\ r \end{Bmatrix} \equiv \begin{Bmatrix} \omega_{x_b} \\ \omega_{y_b} \\ \omega_{z_b} \end{Bmatrix} = \begin{Bmatrix} \text{the rolling rate} \\ \text{the pitching rate} \\ \text{the yawing rate} \end{Bmatrix}$$

This notation has always had the potential for causing some confusion with new students. However, the notation is well established in the literature and it should be memorized. **Be careful not to confuse the rolling rate with the pressure and remember that *p* does not stand for pitch and *r* does not stand for roll.**

As a memory aid, notice that p, q, and r are in alphabetical order, as are the rotation axes x_b, y_b, and z_b. If we think of the rotation triad "roll, pitch, and yaw," in that order, the symbols used for the angular velocity components and the axes of rotation form alphabetic triads in the same order.

There is another potential confusion associated with using lowercase m for mass, as is commonly done in classical dynamics. This is because in the field of aerodynamics, lowercase m is normally used to signify the aerodynamic pitching moment. To avoid this confusion, the x_b-, y_b-, and z_b-components of the aerodynamic moment vector (excluding the effects of thrust) are denoted ℓ, m, and n, whereas the mass is designated as W/g with W denoting the weight and g signifying the acceleration of gravity.

The flight mechanics community sometimes uses the symbols L, M, and N to designate the x_b-, y_b-, and z_b-components of the total moment vector, including any moment produced by the thrust vector, which in some cases may not act through the center of gravity. This has been extremely confusing to new students, since L is also used to signify lift and N is commonly used to denote the normal force. In at least one textbook, the author has seen the symbol L used twice in the same equation, once to represent lift and once to represent the rolling moment. In the present text, we shall not carry tradition quite that far. Here we shall continue to use M_{x_b}, M_{y_b}, and M_{z_b} to designate the body-fixed components of the total moment vector.

In the remainder of our development of the aircraft equations of motion we shall use the following notation:

u	$\equiv$	x_b-component of aircraft translational velocity relative to surrounding air.
v	$\equiv$	y_b-component of aircraft translational velocity relative to surrounding air.
w	$\equiv$	z_b-component of aircraft translational velocity relative to surrounding air.
p	$\equiv$	x_b-component of aircraft rotational velocity (rolling rate).
q	$\equiv$	y_b-component of aircraft rotational velocity (pitching rate).
r	$\equiv$	z_b-component of aircraft rotational velocity (yawing rate).
F_{x_b}	$\equiv$	x_b-component of total pseudo aerodynamic force vector, including thrust.
F_{y_b}	$\equiv$	y_b-component of total pseudo aerodynamic force vector, including thrust.
F_{z_b}	$\equiv$	z_b-component of total pseudo aerodynamic force vector, including thrust.
M_{x_b}	$\equiv$	x_b-component of total pseudo aerodynamic moment vector, including thrust.
M_{y_b}	$\equiv$	y_b-component of total pseudo aerodynamic moment vector, including thrust.
M_{z_b}	$\equiv$	z_b-component of total pseudo aerodynamic moment vector, including thrust.
X	$\equiv$	x_b-component of aerodynamic force, excluding thrust (axial force).
Y	$\equiv$	y_b-component of aerodynamic force, excluding thrust (side force).
Z	$\equiv$	z_b-component of aerodynamic force, excluding thrust (normal force).
ℓ	$\equiv$	x_b-component of aerodynamic moment, excluding thrust (rolling moment).
m	$\equiv$	y_b-component of aerodynamic moment, excluding thrust (pitching moment).
n	$\equiv$	z_b-component of aerodynamic moment, excluding thrust (yawing moment).

Students should memorize this notation before proceeding with their study of this and the following chapters.

Substituting the aircraft notation just defined into Eqs. (7.2.14) and (7.2.19), we have a system of six first-order differential equations for the six components of aircraft velocity relative to the surrounding atmosphere. These are the velocity components associated with the six degrees of freedom for the aircraft treated as a rigid body. This is our statement of **Newton's second law**,

$$\begin{bmatrix} W/g & 0 & 0 \\ 0 & W/g & 0 \\ 0 & 0 & W/g \end{bmatrix} \begin{Bmatrix} \dot{u} \\ \dot{v} \\ \dot{w} \end{Bmatrix} = \begin{Bmatrix} F_{x_b} + W_{x_b} + (rv - qw)W/g \\ F_{y_b} + W_{y_b} + (pw - ru)W/g \\ F_{z_b} + W_{z_b} + (qu - pv)W/g \end{Bmatrix}$$

$$\begin{bmatrix} I_{xx_b} & 0 & -I_{xz_b} \\ 0 & I_{yy_b} & 0 \\ -I_{zx_b} & 0 & I_{zz_b} \end{bmatrix} \begin{Bmatrix} \dot{p} \\ \dot{q} \\ \dot{r} \end{Bmatrix} = \begin{Bmatrix} M_{x_b} + (I_{yy_b} - I_{zz_b})qr + I_{xz_b} pq \\ M_{y_b} + (I_{zz_b} - I_{xx_b})pr + I_{xz_b}(r^2 - p^2) \\ M_{z_b} + (I_{xx_b} - I_{yy_b})pq - I_{xz_b} qr \end{Bmatrix} \tag{7.2.20}$$

where W_{x_b}, W_{y_b}, and W_{z_b} are body-fixed components of aircraft weight. It is important to keep in mind that the forces and moments listed in Eq. (7.2.20) represent the total summation of forces and moments, including those due to thrust and gravity. Thrust can contribute to both the net force and the net moment if the thrust vector does not act through the center of gravity. The gravitational force can never contribute to the net moment, since by definition it always acts through the center of gravity.

When an aircraft is operating in steady flight, with some equilibrium airspeed, V_o, some equilibrium angle of attack, α_o, no sideslip velocity, and no angular velocity, the summation of forces and moments will vanish and the terms on the right-hand side of Eq. (7.2.20) will be zero. For example, in steady level flight with the thrust vector aligned with the direction of flight, the lift is equal to the weight, the thrust is equal to the drag, and the summation of moments must be zero. If any of the parameters on the right deviate from the equilibrium values, the aircraft will accelerate and the translational and rotational velocities will change. The terms on the right may be thought of as disturbances to steady equilibrium flight. These disturbances are usually divided into two categories. The disturbances that affect the motion only in the x_b-z_b plane are called the *longitudinal disturbances*,

$$u - V_o \cos(\alpha_o),\ w - V_o \sin(\alpha_o),\ q,\ F_{x_b} + W_{x_b},\ F_{z_b} + W_{z_b},\ M_{y_b}$$

The remaining disturbances are called the *lateral disturbances*,

$$v,\ p,\ r,\ F_{y_b} + W_{y_b},\ M_{x_b},\ M_{z_b}$$

If all of the lateral disturbances are zero,

$$v = p = r = F_{y_b} + W_{y_b} = M_{x_b} = M_{z_b} = 0 \tag{7.2.21}$$

and Eq. (7.2.20) becomes

$$\begin{bmatrix} W/g & 0 & 0 & 0 & 0 & 0 \\ 0 & W/g & 0 & 0 & 0 & 0 \\ 0 & 0 & W/g & 0 & 0 & 0 \\ 0 & 0 & 0 & I_{xx_b} & 0 & -I_{xz_b} \\ 0 & 0 & 0 & 0 & I_{yy_b} & 0 \\ 0 & 0 & 0 & -I_{xz_b} & 0 & I_{zz_b} \end{bmatrix} \begin{Bmatrix} \dot{u} \\ \dot{v} \\ \dot{w} \\ \dot{p} \\ \dot{q} \\ \dot{r} \end{Bmatrix} = \begin{Bmatrix} F_{x_b} + W_{x_b} - qwW/g \\ 0 \\ F_{z_b} + W_{z_b} + quW/g \\ 0 \\ M_{y_b} \\ 0 \end{Bmatrix} \tag{7.2.22}$$

From Eq. (7.2.22), we see that the longitudinal disturbances affect only the longitudinal velocity components, u, w, and q. The longitudinal disturbances produce no change in the lateral velocity components, v, p, and r. This results from the assumed symmetry of the aircraft about the x_b-z_b plane. Eliminating the trivial results, $\dot{v} = \dot{p} = \dot{r} = 0$, which are easily obtained from the second, fourth, and sixth rows of Eq. (7.2.22), the longitudinal equations of motion for the aircraft reduce to

$$\begin{bmatrix} W/g & 0 & 0 \\ 0 & W/g & 0 \\ 0 & 0 & I_{yy_b} \end{bmatrix} \begin{Bmatrix} \dot{u} \\ \dot{w} \\ \dot{q} \end{Bmatrix} = \begin{Bmatrix} F_{x_b} + W_{x_b} - qwW/g \\ F_{z_b} + W_{z_b} + quW/g \\ M_{y_b} \end{Bmatrix} \tag{7.2.23}$$

If, on the other hand, all of the longitudinal disturbances are zero,

$$\begin{aligned} u - V_o\cos(\alpha_o) &= w - V_o\sin(\alpha_o) = q \\ &= F_{x_b} + W_{x_b} = F_{z_b} + W_{z_b} = M_{y_b} = 0 \end{aligned} \tag{7.2.24}$$

and Eq. (7.2.20) becomes

$$\begin{bmatrix} W/g & 0 & 0 & 0 & 0 & 0 \\ 0 & W/g & 0 & 0 & 0 & 0 \\ 0 & 0 & W/g & 0 & 0 & 0 \\ 0 & 0 & 0 & I_{xx_b} & 0 & -I_{xz_b} \\ 0 & 0 & 0 & 0 & I_{yy_b} & 0 \\ 0 & 0 & 0 & -I_{xz_b} & 0 & I_{zz_b} \end{bmatrix} \begin{Bmatrix} \dot{u} \\ \dot{v} \\ \dot{w} \\ \dot{p} \\ \dot{q} \\ \dot{r} \end{Bmatrix}$$

$$= \begin{Bmatrix} rvW/g \\ F_{y_b} + W_{y_b} + [pV_o\sin(\alpha_o) - rV_o\cos(\alpha_o)]W/g \\ -pvW/g \\ M_{x_b} \\ (I_{zz_b} - I_{xx_b})pr + I_{xz_b}(r^2 - p^2) \\ M_{z_b} \end{Bmatrix} \tag{7.2.25}$$

Thus we see that while the longitudinal disturbances affect only the longitudinal velocity components, the lateral disturbances have an effect on both the lateral and the longitudinal velocity components. It should be noted that longitudinal motion (axial translation, normal translation, and pitching rotation) is simple planar motion confined to the x_b-z_b plane. On the other hand, lateral motion (sideslip translation, rolling rotation, and yawing rotation) is not a simple planar motion at all. Roll is rotation in the y_b-z_b plane and yaw is rotation in the x_b-y_b plane. The longitudinal velocity components are directly affected by the lateral velocity components, in part because of the Coriolis accelerations. For example, sideslip combined with a yawing rate results in a Coriolis acceleration in the axial direction. Similarly, sideslip combined with a rolling rate produces a normal Coriolis acceleration. Rolling and yawing rates also produce a pitching acceleration that results from the asymmetry of the aircraft in the x_b-z_b plane. The latter coupling term is usually referred to as the *inertial cross coupling*.

EXAMPLE 7.2.1. Consider an object moving through space with no forces of any kind acting on the body. The body is initially moving relative to an inertial coordinate system with a velocity of V_0 and is rotating about an axis normal to the velocity vector with an angular velocity of ω_0. We wish to use Newton's second law to determine the translational and rotational velocity of this object as a function of time. This problem is, of course, trivial to solve using an inertial coordinate system. However, to gain some familiarity and confidence in working with body-fixed coordinates, we wish to solve this simple problem using only body-fixed coordinates.

Solution. Because the rotation vector is normal to the translation vector, this is planar motion. Choosing the body-fixed coordinate system so that at time $t = 0$ the x_b-axis coincides with the direction of motion and the y_b-axis coincides with the axis of rotation, the motion is planar longitudinal motion. Newton's second law is given by Eq. (7.2.23) with all forces and moments set to zero,

$$\begin{bmatrix} W/g & 0 & 0 \\ 0 & W/g & 0 \\ 0 & 0 & I_{yy_b} \end{bmatrix} \begin{Bmatrix} \dot{u} \\ \dot{w} \\ \dot{q} \end{Bmatrix} = \begin{Bmatrix} -qwW/g \\ quW/g \\ 0 \end{Bmatrix} \tag{7.2.26}$$

The initial conditions for this first-order system of differential equations is

$$\begin{Bmatrix} u \\ w \\ q \end{Bmatrix}_{t=0} = \begin{Bmatrix} V_0 \\ 0 \\ \omega_0 \end{Bmatrix} \tag{7.2.27}$$

The third equation in Eq. (7.2.26) is not coupled to the other two. This equation is easily integrated subject to the third initial condition in Eq. (7.2.27) to give

$$q = \omega_0$$

Using this result in the remaining two equations from Eq. (7.2.26), we have

$$\begin{bmatrix} 1 & 0 \\ 0 & 1 \end{bmatrix} \begin{Bmatrix} \dot{u} \\ \dot{w} \end{Bmatrix} + \begin{bmatrix} 0 & \omega_0 \\ -\omega_0 & 0 \end{bmatrix} \begin{Bmatrix} u \\ w \end{Bmatrix} = \begin{Bmatrix} 0 \\ 0 \end{Bmatrix}$$

This is a homogeneous system of first-order linear differential equations. At this point students may wish to review the chapter on systems of linear differential equations from their introductory course on ordinary differential equations. Rewriting this system of equations in the usual differential operator notation, we have

$$\begin{bmatrix} D & \omega_0 \\ -\omega_0 & D \end{bmatrix} \begin{Bmatrix} u \\ w \end{Bmatrix} = \begin{Bmatrix} 0 \\ 0 \end{Bmatrix} \tag{7.2.28}$$

where D the differential operator. Differentiating the first equation and multiplying the second equation by ω_0 gives

$$\begin{bmatrix} D^2 & \omega_0 D \\ -\omega_0^2 & \omega_0 D \end{bmatrix} \begin{Bmatrix} u \\ w \end{Bmatrix} = \begin{Bmatrix} 0 \\ 0 \end{Bmatrix}$$

Subtracting the second equation from the first, we have

$$\begin{bmatrix} (D^2 + \omega_0^2) & 0 \\ -\omega_0^2 & \omega_0 D \end{bmatrix} \begin{Bmatrix} u \\ w \end{Bmatrix} = \begin{Bmatrix} 0 \\ 0 \end{Bmatrix}$$

In a similar manner the system can be further reduced to yield

$$\begin{bmatrix} (D^2 + \omega_0^2) & 0 \\ 0 & (D^2 + \omega_0^2) \end{bmatrix} \begin{Bmatrix} u \\ w \end{Bmatrix} = \begin{Bmatrix} 0 \\ 0 \end{Bmatrix}$$

We have now reduced a system of two coupled first-order equations to a system of two uncoupled second-order equations. Each of these are easily solved separately to give

$$\begin{Bmatrix} u \\ w \end{Bmatrix} = \begin{Bmatrix} C_1 \sin(\omega_0 t) + C_2 \cos(\omega_0 t) \\ C_3 \sin(\omega_0 t) + C_4 \cos(\omega_0 t) \end{Bmatrix} \tag{7.2.29}$$

Using this result in Eq. (7.2.28), we have

$$\begin{Bmatrix} C_1\omega_0 \cos(\omega_0 t) - C_2\omega_0 \sin(\omega_0 t) + C_3\omega_0 \sin(\omega_0 t) + C_4\omega_0 \cos(\omega_0 t) \\ -C_1\omega_0 \sin(\omega_0 t) - C_2\omega_0 \cos(\omega_0 t) + C_3\omega_0 \cos(\omega_0 t) - C_4\omega_0 \sin(\omega_0 t) \end{Bmatrix} = \begin{Bmatrix} 0 \\ 0 \end{Bmatrix}$$

which requires that

$$\begin{Bmatrix} C_3 \\ C_4 \end{Bmatrix} = \begin{Bmatrix} C_2 \\ -C_1 \end{Bmatrix} \tag{7.2.30}$$

Using Eq. (7.2.30) in Eq. (7.2.29) gives

$$\begin{Bmatrix} u \\ w \end{Bmatrix} = \begin{Bmatrix} C_1 \sin(\omega_0 t) + C_2 \cos(\omega_0 t) \\ C_2 \sin(\omega_0 t) - C_1 \cos(\omega_0 t) \end{Bmatrix} \tag{7.2.31}$$

Applying the initial conditions,

$$\begin{Bmatrix} u(0) \\ w(0) \end{Bmatrix} = \begin{Bmatrix} V_0 \\ 0 \end{Bmatrix}$$

we obtain

$$\begin{Bmatrix} C_1 \\ C_2 \end{Bmatrix} = \begin{Bmatrix} 0 \\ V_0 \end{Bmatrix} \tag{7.2.32}$$

Using Eq. (7.2.32) in Eq. (7.2.31) and including the result obtained for the angular velocity gives the complete solution,

$$\begin{Bmatrix} u \\ w \\ q \end{Bmatrix} = \begin{Bmatrix} V_0 \cos(\omega_0 t) \\ V_0 \sin(\omega_0 t) \\ \omega_0 \end{Bmatrix}$$

This problem is, of course, trivial to solve relative to an inertial coordinate system. For an inertial coordinate system, Eq. (7.2.26) reduces to the completely uncoupled system,

$$\begin{bmatrix} W/g & 0 & 0 \\ 0 & W/g & 0 \\ 0 & 0 & I_{yy_b} \end{bmatrix} \begin{Bmatrix} \dot{V}_{x_f} \\ \dot{V}_{z_f} \\ \dot{\omega}_{y_f} \end{Bmatrix} = \begin{Bmatrix} 0 \\ 0 \\ 0 \end{Bmatrix}$$

which can be directly integrated subject to the initial conditions to give

$$\begin{Bmatrix} V_{x_f} \\ V_{z_f} \\ \omega_{y_f} \end{Bmatrix} = \begin{Bmatrix} V_0 \\ 0 \\ \omega_0 \end{Bmatrix}$$

Thus, to a fixed observer in the inertial coordinate system, the velocity of the object appears to be constant with time. On the other hand, to an observer in the body-fixed coordinate system, the velocity appears to be changing sinusoidal with time. These are simply two equivalent ways to describe exactly the same motion.

The advantage of using the body-fixed coordinate system is not at all obvious from Example 7.2.1. This very simple problem is much easier to solve using the inertial coordinate system. We do see, however, that Newton's second law can be stated and solved either in terms of inertial coordinates or in terms of body-fixed coordinates. The advantage of using a body-fixed coordinate system will become more apparent in the following sections.

7.3. Position and Orientation: The Euler Angle Formulation

In the preceding section, Newton's second law was written in terms of a coordinate system fixed to the aircraft. For complex geometry and/or complex motion, this coordinate system can simplify the equations of motion by making the inertia tensor independent of time. Furthermore, onboard instruments report flight parameters only as viewed from a body-fixed coordinate system. Thus, the body-fixed coordinate system extends considerable utility to the study of aircraft dynamics. Unfortunately, this moving coordinate system cannot easily be used for describing the position and orientation of the airplane. The aircraft position and orientation are most conveniently described in terms of a coordinate system fixed to the Earth.

The position of an aircraft relative to the Earth is normally described in terms of latitude, longitude, and elevation. However, over short time periods, the distance traveled is small compared to the radius of the Earth and we can describe position in terms of a Cartesian system. As previously discussed, the Cartesian system commonly used has the x-axis pointing north, the y-axis pointing east, and the z-axis pointing down. This Earth-fixed coordinate system has been designated (x_f, y_f, z_f). The position of the aircraft is specified by the location of the origin of the body-fixed coordinate frame relative to the Earth-fixed coordinate frame.

The orientation of an aircraft relative to the Earth can be described in terms of what are called *Euler angles*. The orientation of the body-fixed coordinate frame, (x_b, y_b, z_b), relative to the Earth-fixed coordinate frame, (x_f, y_f, z_f), is described in terms of three consecutive rotations through three Euler angles, in the specific order as follows:

a) Rotate the (x_f, y_f, z_f) coordinate system about the z_f-axis through an angle ψ to the coordinate system (x_1, y_1, z_1), as shown in Fig. 7.3.1a.

b) Rotate the (x_1, y_1, z_1) coordinate system about the y_1-axis through an angle θ to the coordinate system (x_2, y_2, z_2), as shown in Fig. 7.3.1b.

c) Rotate the (x_2, y_2, z_2) coordinate system about the x_2-axis through an angle ϕ to the coordinate system (x_b, y_b, z_b), as shown in Fig. 7.3.1c.

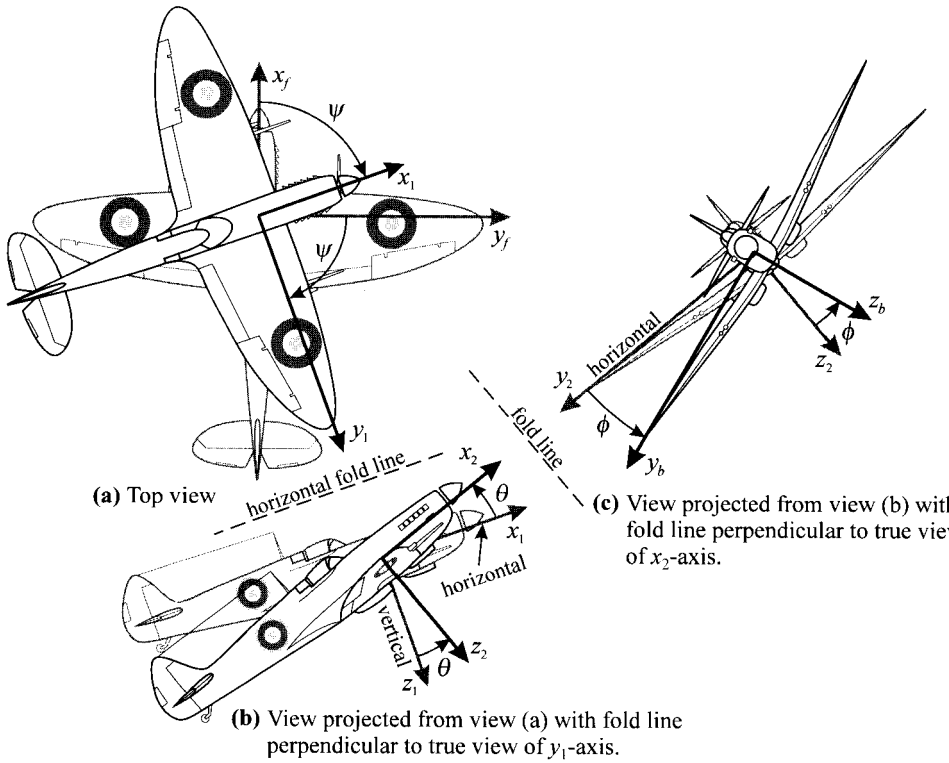


Figure 7.3.1. True views of the three Euler angles shown following the standard conventions of engineering graphics and descriptive geometry.

An isometric view of these three rotations is shown in Fig. 7.3.2. The order of rotation is very important. In general, if these three rotations were to take place in a different order, the final orientation would be different.

The three Euler angles, ϕ, θ, and ψ are, respectively, called the bank angle, the elevation angle, and the azimuth angle or heading. These three angles are sometimes incorrectly referred to as the roll, pitch, and yaw. There is a subtle but very important difference between the Euler angles and roll, pitch, and yaw. The azimuth angle is a rotation about the z_f-axis and yaw is a rotation about the z_b-axis. Similarly, the elevation angle is a rotation about the y_1-axis and pitch is a rotation about the y_b-axis. Roll, pitch, and yaw are orthogonal. The Euler angles are not.

The Euler angles can be related to roll, pitch, and yaw, but this is not a one-to-one relationship. For example, it is possible to change the bank angle of an aircraft without using any roll input whatsoever. To demonstrate this, consider an airplane in a level attitude with all three Euler angles at zero, as shown in Fig. 7.3.3. Now let the airplane move through a pitch angle of 90 degrees, followed by a yaw angle of 90 degrees and a pitch angle of –90 degrees. The airplane now has a bank angle of 90 degrees, but there was no roll input throughout the process. Try it with a model.

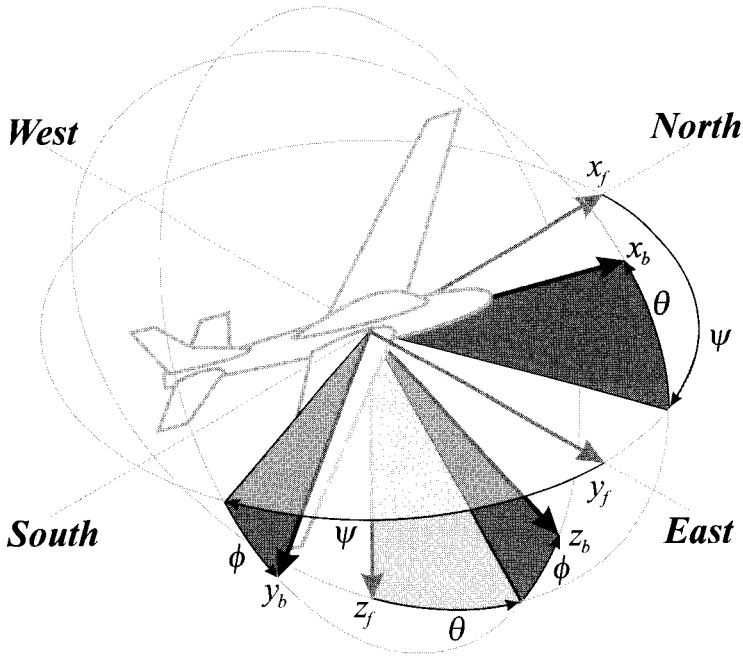


Figure 7.3.2. Euler angles shown in an isometric view.

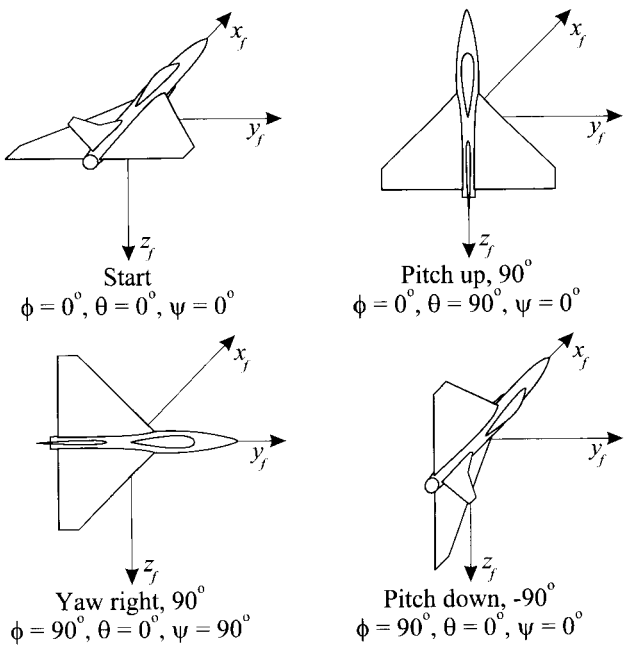


Figure 7.3.3. Relationship between Euler angles and roll, pitch, and yaw.

Any set of three Euler angles describes a unique orientation of the aircraft (i.e., no two different orientations have the same three Euler angles). A specific set of Euler angles specifies an instantaneous orientation that does not depend in any way on how the aircraft came to be so orientated. While a given set of Euler angles specifies a unique orientation for the aircraft, orientation is a periodic function of the Euler angles. Thus, any orientation of an aircraft could be described by more than one set of Euler angles. Clearly, adding 360 degrees to any one of the Euler angles will result in a different but equivalent set of Euler angles. If we are to define the Euler angles so that any given orientation has a unique set of Euler angles, then we must restrict each Euler angle to fall within some range including no more than 360 degrees. However, even this is not sufficient. This is demonstrated in Fig. 7.3.4. In this figure we start with an airplane pointed due north with both the wing span and the fuselage reference line parallel to the ground. Normally, we would specify this orientation as having all three Euler angles equal to zero. From this starting point, shown in Fig. 7.3.4a, we let the airplane move through a pitch angle of 180 degrees to the orientation shown in Fig. 7.3.4b. Clearly, this orientation could be described as having a bank angle of zero, an elevation angle of 180 degrees, and azimuth angle of zero. The airplane could be placed in this same

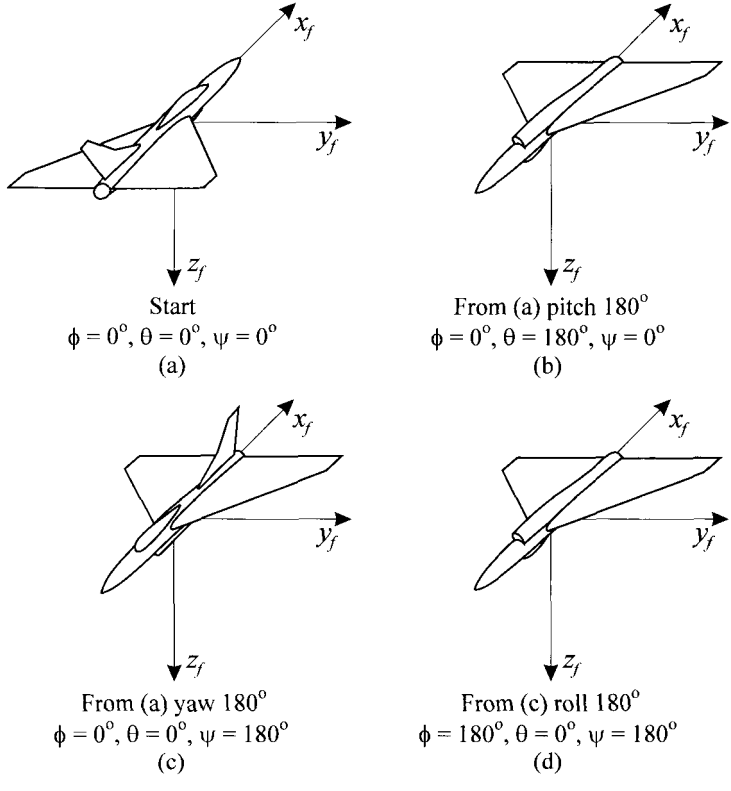


Figure 7.3.4. Two equivalent Euler angle descriptions for the same aircraft orientation.

orientation by starting with all Euler angles at zero and rotating the airplane through a yaw angle of 180 degrees to the orientation shown in Fig. 7.3.4c. From this point the airplane is rolled through 180 degrees to the orientation shown in Fig. 7.3.4d. This final orientation could be described as having a bank angle of 180 degrees, an elevation angle of zero, and an azimuth angle of 180 degrees. Since the orientation shown in Fig. 7.3.4b is identical to that shown in Fig. 7.3.4d, the Euler angle set $\phi = 0°$, $\theta = 180°$, and $\psi = 0°$ is obviously equivalent to the set $\phi = 180°$, $\theta = 0°$, and $\psi = 180°$. To avoid this duality and make the Euler angle definitions unique, the Euler angles are by standard convention usually restricted to the range $-180° < \phi \leq 180°$, $-90° \leq \theta \leq 90°$, and $0° \leq \psi < 360°$.

To obtain the transformations between coordinate systems (x_b, y_b, z_b) and (x_f, y_f, z_f), we now review some principles from calculus and analytic geometry. In terms of the three Euler angle rotations shown in Fig. 7.3.1, we wish to develop two transformation matrices, one to transform from body-fixed to Earth-fixed coordinates and another to transform from Earth-fixed to body-fixed coordinates. We first consider each of the three rotations shown in Fig. 7.3.1 as a separate transformation and then combine the three transformations into one transformation matrix.

Consider first an arbitrary vector $\mathbf{v}$ having components $(v_{x_1}, v_{y_1}, v_{z_1})$ in coordinate system (x_1, y_1, z_1) and having components $(v_{x_f}, v_{y_f}, v_{z_f})$ in the (x_f, y_f, z_f) coordinate system. From the geometry in Fig. 7.3.1a, we see that the x-component of the vector $\mathbf{v}$ in coordinate system 1 can be broken up into two components in coordinate system f. Thus we have

$$v_{x_1}\mathbf{i}_{x_1} = v_{x_1}\cos(\psi)\mathbf{i}_{x_f} + v_{x_1}\sin(\psi)\mathbf{i}_{y_f} \tag{7.3.1}$$

Similarly, the y-component transforms as

$$v_{y_1}\mathbf{i}_{y_1} = -v_{y_1}\sin(\psi)\mathbf{i}_{x_f} + v_{y_1}\cos(\psi)\mathbf{i}_{y_f} \tag{7.3.2}$$

and the z-component transforms as

$$v_{z_1}\mathbf{i}_{z_1} = v_{z_1}\mathbf{i}_{z_f} \tag{7.3.3}$$

Combining Eqs. (7.3.1) through (7.3.3), we obtain the transformation equation

$$\begin{Bmatrix} v_{x_f} \\ v_{y_f} \\ v_{z_f} \end{Bmatrix} = \begin{bmatrix} \cos(\psi) & -\sin(\psi) & 0 \\ \sin(\psi) & \cos(\psi) & 0 \\ 0 & 0 & 1 \end{bmatrix} \begin{Bmatrix} v_{x_1} \\ v_{y_1} \\ v_{z_1} \end{Bmatrix} \tag{7.3.4}$$

In a similar manner, the inverse transformation can be written

$$\begin{Bmatrix} v_{x_1} \\ v_{y_1} \\ v_{z_1} \end{Bmatrix} = \begin{bmatrix} \cos(\psi) & \sin(\psi) & 0 \\ -\sin(\psi) & \cos(\psi) & 0 \\ 0 & 0 & 1 \end{bmatrix} \begin{Bmatrix} v_{x_f} \\ v_{y_f} \\ v_{z_f} \end{Bmatrix} \tag{7.3.5}$$

Likewise, from Fig. 7.3.1b, $(v_{x_1}, v_{y_1}, v_{z_1})$ can be expressed in terms of $(v_{x_2}, v_{y_2}, v_{z_2})$,

$$\begin{Bmatrix} v_{x_1} \\ v_{y_1} \\ v_{z_1} \end{Bmatrix} = \begin{bmatrix} \cos(\theta) & 0 & \sin(\theta) \\ 0 & 1 & 0 \\ -\sin(\theta) & 0 & \cos(\theta) \end{bmatrix} \begin{Bmatrix} v_{x_2} \\ v_{y_2} \\ v_{z_2} \end{Bmatrix} \tag{7.3.6}$$

and the inverse transformation is found to be

$$\begin{Bmatrix} v_{x_2} \\ v_{y_2} \\ v_{z_2} \end{Bmatrix} = \begin{bmatrix} \cos(\theta) & 0 & -\sin(\theta) \\ 0 & 1 & 0 \\ \sin(\theta) & 0 & \cos(\theta) \end{bmatrix} \begin{Bmatrix} v_{x_1} \\ v_{y_1} \\ v_{z_1} \end{Bmatrix} \tag{7.3.7}$$

From Fig. 7.3.1c we obtain

$$\begin{Bmatrix} v_{x_2} \\ v_{y_2} \\ v_{z_2} \end{Bmatrix} = \begin{bmatrix} 1 & 0 & 0 \\ 0 & \cos(\phi) & -\sin(\phi) \\ 0 & \sin(\phi) & \cos(\phi) \end{bmatrix} \begin{Bmatrix} v_{x_b} \\ v_{y_b} \\ v_{z_b} \end{Bmatrix} \tag{7.3.8}$$

and

$$\begin{Bmatrix} v_{x_b} \\ v_{y_b} \\ v_{z_b} \end{Bmatrix} = \begin{bmatrix} 1 & 0 & 0 \\ 0 & \cos(\phi) & \sin(\phi) \\ 0 & -\sin(\phi) & \cos(\phi) \end{bmatrix} \begin{Bmatrix} v_{x_2} \\ v_{y_2} \\ v_{z_2} \end{Bmatrix} \tag{7.3.9}$$

Combining Eqs. (7.3.4), (7.3.6), and (7.3.8), we have

$$\begin{Bmatrix} v_{x_f} \\ v_{y_f} \\ v_{z_f} \end{Bmatrix} = \begin{bmatrix} \cos(\psi) & -\sin(\psi) & 0 \\ \sin(\psi) & \cos(\psi) & 0 \\ 0 & 0 & 1 \end{bmatrix} \begin{bmatrix} \cos(\theta) & 0 & \sin(\theta) \\ 0 & 1 & 0 \\ -\sin(\theta) & 0 & \cos(\theta) \end{bmatrix} \begin{bmatrix} 1 & 0 & 0 \\ 0 & \cos(\phi) & -\sin(\phi) \\ 0 & \sin(\phi) & \cos(\phi) \end{bmatrix} \begin{Bmatrix} v_{x_b} \\ v_{y_b} \\ v_{z_b} \end{Bmatrix} \tag{7.3.10}$$

and combining Eqs. (7.3.5), (7.3.7), and (7.3.9), gives the inverse transformation,

$$\begin{Bmatrix} v_{x_b} \\ v_{y_b} \\ v_{z_b} \end{Bmatrix} = \begin{bmatrix} 1 & 0 & 0 \\ 0 & \cos(\phi) & \sin(\phi) \\ 0 & -\sin(\phi) & \cos(\phi) \end{bmatrix} \begin{bmatrix} \cos(\theta) & 0 & -\sin(\theta) \\ 0 & 1 & 0 \\ \sin(\theta) & 0 & \cos(\theta) \end{bmatrix} \begin{bmatrix} \cos(\psi) & \sin(\psi) & 0 \\ -\sin(\psi) & \cos(\psi) & 0 \\ 0 & 0 & 1 \end{bmatrix} \begin{Bmatrix} v_{x_f} \\ v_{y_f} \\ v_{z_f} \end{Bmatrix} \tag{7.3.11}$$

The three individual transformation matrices in Eq. (7.3.10) and Eq. (7.3.11) may be multiplied together to obtain a single transformation matrix for each equation. Using the shorthand notation $S_\phi = \sin(\phi)$, $C_\phi = \cos(\phi)$, $S_\theta = \sin(\theta)$, $C_\theta = \cos(\theta)$, $S_\psi = \sin(\psi)$, and $C_\psi = \cos(\psi)$, from Eq. (7.3.10), we have the transformation equation,

$$\begin{Bmatrix} v_{x_f} \\ v_{y_f} \\ v_{z_f} \end{Bmatrix} = \begin{bmatrix} C_\theta C_\psi & S_\phi S_\theta C_\psi - C_\phi S_\psi & C_\phi S_\theta C_\psi + S_\phi S_\psi \\ C_\theta S_\psi & S_\phi S_\theta S_\psi + C_\phi C_\psi & C_\phi S_\theta S_\psi - S_\phi C_\psi \\ -S_\theta & S_\phi C_\theta & C_\phi C_\theta \end{bmatrix} \begin{Bmatrix} v_{x_b} \\ v_{y_b} \\ v_{z_b} \end{Bmatrix} \tag{7.3.12}$$

and from Eq. (7.3.11) we obtain the inverse transformation equation,

$$\begin{Bmatrix} v_{x_b} \\ v_{y_b} \\ v_{z_b} \end{Bmatrix} = \begin{bmatrix} C_\theta C_\psi & C_\theta S_\psi & -S_\theta \\ S_\phi S_\theta C_\psi - C_\phi S_\psi & S_\phi S_\theta S_\psi + C_\phi C_\psi & S_\phi C_\theta \\ C_\phi S_\theta C_\psi + S_\phi S_\psi & C_\phi S_\theta S_\psi - S_\phi C_\psi & C_\phi C_\theta \end{bmatrix} \begin{Bmatrix} v_{x_f} \\ v_{y_f} \\ v_{z_f} \end{Bmatrix} \tag{7.3.13}$$

Equation (7.3.12) can be used to transform the components of any vector from body-fixed to Earth-fixed coordinates, and Eq. (7.3.13) can be used to transform vector components from Earth-fixed to body-fixed coordinates. **It should be noted that the inverse of the transformation matrix in Eq. (7.3.12) is its transpose.**

In body-fixed coordinates, the velocity of the aircraft relative to the surrounding air has been designated (u, v, w), and in Earth-fixed coordinates, the velocity of the aircraft relative to the Earth is the time rate of change of the position vector ($\dot{x}_f$, $\dot{y}_f$, $\dot{z}_f$). The airspeed is related to the ground speed and the wind through Eq. (7.1.1). Thus, combining Eqs. (7.1.1) and (7.3.12), we can write

$$\begin{Bmatrix} \dot{x}_f \\ \dot{y}_f \\ \dot{z}_f \end{Bmatrix} = \begin{bmatrix} C_\theta C_\psi & S_\phi S_\theta C_\psi - C_\phi S_\psi & C_\phi S_\theta C_\psi + S_\phi S_\psi \\ C_\theta S_\psi & S_\phi S_\theta S_\psi + C_\phi C_\psi & C_\phi S_\theta S_\psi - S_\phi C_\psi \\ -S_\theta & S_\phi C_\theta & C_\phi C_\theta \end{bmatrix} \begin{Bmatrix} u \\ v \\ w \end{Bmatrix} + \begin{Bmatrix} V_{wx_f} \\ V_{wy_f} \\ V_{wz_f} \end{Bmatrix} \tag{7.3.14}$$

where V_{wx_f}, V_{wy_f}, and V_{wz_f} are the components of the wind in Earth-fixed coordinates. Integration of this equation will yield the airplane's position as a function of time, relative to the Earth-fixed coordinate system.

Since we are using Newton's second law in body-fixed coordinates, we must express the gravitational force in body-fixed coordinates as well. In Earth-fixed coordinates, the representation of the gravitational force vector is (0, 0, W). Thus, from Eq. (7.3.13), the **gravitational force vector in body-fixed coordinates** is represented as

$$\begin{Bmatrix} W_{x_b} \\ W_{y_b} \\ W_{z_b} \end{Bmatrix} = W \begin{Bmatrix} -\sin(\theta) \\ \sin(\phi)\cos(\theta) \\ \cos(\phi)\cos(\theta) \end{Bmatrix} \tag{7.3.15}$$

In a similar manner, the time derivatives of the Euler angles, ($\dot{\phi}$, $\dot{\theta}$, $\dot{\psi}$), are related to the body-fixed components of the angular velocity vector, (p, q, r). However, we must remember that each of the Euler angles is defined relative to a different coordinate system. The bank angle, ϕ, is defined relative to the coordinate system (x_2, y_2, z_2), the elevation angle, θ, is defined relative to (x_1, y_1, z_1), and the azimuth angle, ψ, is defined relative to (x_f, y_f, z_f). Thus, using Eqs. (7.3.5), (7.3.7), and (7.3.9), we can write

$$\begin{Bmatrix} p \\ q \\ r \end{Bmatrix} = \begin{bmatrix} 1 & 0 & 0 \\ 0 & C_\phi & S_\phi \\ 0 & -S_\phi & C_\phi \end{bmatrix} \begin{Bmatrix} \dot{\phi} \\ 0 \\ 0 \end{Bmatrix} + \begin{bmatrix} 1 & 0 & 0 \\ 0 & C_\phi & S_\phi \\ 0 & -S_\phi & C_\phi \end{bmatrix} \begin{bmatrix} C_\theta & 0 & -S_\theta \\ 0 & 1 & 0 \\ S_\theta & 0 & C_\theta \end{bmatrix} \begin{Bmatrix} 0 \\ \dot{\theta} \\ 0 \end{Bmatrix} + \begin{bmatrix} 1 & 0 & 0 \\ 0 & C_\phi & S_\phi \\ 0 & -S_\phi & C_\phi \end{bmatrix} \begin{bmatrix} C_\theta & 0 & -S_\theta \\ 0 & 1 & 0 \\ S_\theta & 0 & C_\theta \end{bmatrix} \begin{bmatrix} C_\psi & S_\psi & 0 \\ -S_\psi & C_\psi & 0 \\ 0 & 0 & 1 \end{bmatrix} \begin{Bmatrix} 0 \\ 0 \\ \dot{\psi} \end{Bmatrix} \tag{7.3.16}$$

or after combining terms,

$$\begin{Bmatrix} p \\ q \\ r \end{Bmatrix} = \begin{bmatrix} 1 & 0 & -S_\theta \\ 0 & C_\phi & S_\phi C_\theta \\ 0 & -S_\phi & C_\phi C_\theta \end{bmatrix} \begin{Bmatrix} \dot{\phi} \\ \dot{\theta} \\ \dot{\psi} \end{Bmatrix} \tag{7.3.17}$$

Inverting Eq. (7.3.17), we get the Euler rates in terms of the roll, pitch, and yaw rates,

$$\begin{Bmatrix} \dot{\phi} \\ \dot{\theta} \\ \dot{\psi} \end{Bmatrix} = \begin{bmatrix} 1 & S_\phi S_\theta / C_\theta & C_\phi S_\theta / C_\theta \\ 0 & C_\phi & -S_\phi \\ 0 & S_\phi / C_\theta & C_\phi / C_\theta \end{bmatrix} \begin{Bmatrix} p \\ q \\ r \end{Bmatrix} \tag{7.3.18}$$

Here, we see that **the inverse of the matrix in Eq. (7.3.17) is not its transpose.** Integration of this equation will yield the airplane's orientation as a function of time in terms of the Euler angles ϕ, θ, and ψ.

Combining Eqs. (7.3.14) and (7.3.18), we have a system of six first-order differential equations that relate the time rate of change of the position and orientation of the aircraft in Earth-fixed coordinates to the translational and rotational velocity components, relative to the surrounding air, in body-fixed coordinates,

$$\begin{Bmatrix} \dot{x}_f \\ \dot{y}_f \\ \dot{z}_f \end{Bmatrix} = \begin{bmatrix} C_\theta C_\psi & S_\phi S_\theta C_\psi - C_\phi S_\psi & C_\phi S_\theta C_\psi + S_\phi S_\psi \\ C_\theta S_\psi & S_\phi S_\theta S_\psi + C_\phi C_\psi & C_\phi S_\theta S_\psi - S_\phi C_\psi \\ -S_\theta & S_\phi C_\theta & C_\phi C_\theta \end{bmatrix} \begin{Bmatrix} u \\ v \\ w \end{Bmatrix} + \begin{Bmatrix} V_{wx_f} \\ V_{wy_f} \\ V_{wz_f} \end{Bmatrix}$$

$$\begin{Bmatrix} \dot{\phi} \\ \dot{\theta} \\ \dot{\psi} \end{Bmatrix} = \begin{bmatrix} 1 & S_\phi S_\theta / C_\theta & C_\phi S_\theta / C_\theta \\ 0 & C_\phi & -S_\phi \\ 0 & S_\phi / C_\theta & C_\phi / C_\theta \end{bmatrix} \begin{Bmatrix} p \\ q \\ r \end{Bmatrix} \tag{7.3.19}$$

These six equations are called the **kinematic transformation equations**, in terms of Euler angles. This transformation contains a singularity. This singularity can be seen in the last two terms in both the fourth and sixth equations in Eq. (7.3.19). Clearly, these four terms become singular when the Euler angle, θ, is $\pm 90°$ and $\cos\theta$ becomes zero. At

these points the transformation breaks down, and integration of the Euler angles becomes indeterminate. This singularity in the integration of the Euler angles is commonly known as *gimbal lock*. Due to its existence, virtually no commercial or widely used six-degree-of-freedom code (6-DOF) employs the transformation given by Eq. (7.3.19) for determination of the Euler angles. Rather, other methods are generally employed, which avoids these singularities through the use of either a *quaternion transformation* or a *direction cosine transformation*. However, the Euler angle transformation is widely used in the linearized equations of motion. Clearly, under normal operation, most airplanes stay within the range of motion that can be described by Eq. (7.3.19). Except for vertical launch vehicles, fighter aircraft, and stunt planes that might pass through these attitudes, the Euler angle singularities at ±90° are not a problem. The main disadvantage of using the quaternion formulation for aircraft attitude is the increased complexity of the physical interpretation. Thus, the student should have a good understanding of the Euler angles discussed in this section before attempting to understand the quaternion formulation to be presented later in this text.

For pure longitudinal motion, the bank angle is typically zero and the azimuth angle must remain constant. For simplicity, we could align the x_f-axis of the Earth-fixed coordinate system with the x_b-z_b plane of the body-fixed coordinate system and make the assumption of no wind. Thus, we can write

$$v = p = r = \phi = \psi = 0 \tag{7.3.20}$$

For this pure longitudinal motion, from Eq. (7.3.15), the gravitational force described in body-fixed coordinates reduces to

$$\begin{Bmatrix} W_{x_b} \\ W_{y_b} \\ W_{z_b} \end{Bmatrix} = W \begin{Bmatrix} -\sin(\theta) \\ 0 \\ \cos(\theta) \end{Bmatrix} \tag{7.3.21}$$

and Eq. (7.3.19) becomes

$$\begin{Bmatrix} \dot{x}_f \\ \dot{y}_f \\ \dot{z}_f \\ \dot{\phi} \\ \dot{\theta} \\ \dot{\psi} \end{Bmatrix} = \begin{bmatrix} C_\theta & 0 & S_\theta & 0 & 0 & 0 \\ 0 & 1 & 0 & 0 & 0 & 0 \\ -S_\theta & 0 & C_\theta & 0 & 0 & 0 \\ 0 & 0 & 0 & 1 & 0 & S_\theta / C_\theta \\ 0 & 0 & 0 & 0 & 1 & 0 \\ 0 & 0 & 0 & 0 & 0 & 1/C_\theta \end{bmatrix} \begin{Bmatrix} u \\ 0 \\ w \\ 0 \\ q \\ 0 \end{Bmatrix} \tag{7.3.22}$$

Here again we see that longitudinal motion has no tendency to introduce lateral motion. Eliminating the trivial results, $W_{y_b} = \dot{y}_f = \dot{\phi} = \dot{\psi} = 0$, longitudinal motion requires that

$$\begin{Bmatrix} W_{x_b} \\ W_{z_b} \end{Bmatrix} = W \begin{Bmatrix} -\sin(\theta) \\ \cos(\theta) \end{Bmatrix} \tag{7.3.23}$$

$$\begin{Bmatrix} \dot{x}_f \\ \dot{z}_f \\ \dot{\theta} \end{Bmatrix} = \begin{bmatrix} \cos(\theta) & \sin(\theta) & 0 \\ -\sin(\theta) & \cos(\theta) & 0 \\ 0 & 0 & 1 \end{bmatrix} \begin{Bmatrix} u \\ w \\ q \end{Bmatrix} \tag{7.3.24}$$

For pure lateral motion, the axial velocity, normal velocity, and elevation angle must remain constant and the y_b-component of the angular velocity must be zero. For simplicity, we shall neglect wind and consider the special case of lateral motion relative to an equilibrium flight path where the elevation angle is zero. Thus, we can write

$$u - V_o \cos(\alpha_o) = w - V_o \sin(\alpha_o) = q = \theta = 0 \tag{7.3.25}$$

Thus, for this pure lateral motion, Eqs. (7.3.15) and (7.3.19) become

$$\begin{Bmatrix} W_{x_b} \\ W_{y_b} \\ W_{z_b} \end{Bmatrix} = W \begin{Bmatrix} 0 \\ \sin(\phi) \\ \cos(\phi) \end{Bmatrix} \tag{7.3.26}$$

$$\begin{Bmatrix} \dot{x}_f \\ \dot{y}_f \\ \dot{z}_f \\ \dot{\phi} \\ \dot{\theta} \\ \dot{\psi} \end{Bmatrix} = \begin{bmatrix} C_\psi & -C_\phi S_\psi & S_\phi S_\psi & 0 & 0 & 0 \\ S_\psi & C_\phi C_\psi & -S_\phi C_\psi & 0 & 0 & 0 \\ 0 & S_\phi & C_\phi & 0 & 0 & 0 \\ 0 & 0 & 0 & 1 & 0 & 0 \\ 0 & 0 & 0 & 0 & C_\phi & -S_\phi \\ 0 & 0 & 0 & 0 & S_\phi & C_\phi \end{bmatrix} \begin{Bmatrix} V_o \cos(\alpha_o) \\ V_{y_b} \\ V_o \sin(\alpha_o) \\ p \\ 0 \\ r \end{Bmatrix} \tag{7.3.27}$$

Here again we find that while the longitudinal disturbances affect only the longitudinal motion, the lateral disturbances have an effect on both the lateral and the longitudinal motion.

EXAMPLE 7.3.1. Determine the position and orientation of the object in Example 7.2.1 as a function of time. Starting with the body-fixed solution to Example 7.2.1, describe the position in terms of Earth-fixed coordinates, and the orientation in terms of Euler angles.

Solution. From the solution to Example 7.2.1,

$$\begin{Bmatrix} u \\ w \\ q \end{Bmatrix} = \begin{Bmatrix} V_0 \cos(\omega_0 t) \\ V_0 \sin(\omega_0 t) \\ \omega_0 \end{Bmatrix}$$

Since this is longitudinal motion, we can apply this result to Eq. (7.3.24):

$$\begin{Bmatrix} \dot{x}_f \\ \dot{z}_f \\ \dot{\theta} \end{Bmatrix} = \begin{bmatrix} \cos(\theta) & \sin(\theta) & 0 \\ -\sin(\theta) & \cos(\theta) & 0 \\ 0 & 0 & 1 \end{bmatrix} \begin{Bmatrix} V_0 \cos(\omega_0 t) \\ V_0 \sin(\omega_0 t) \\ \omega_0 \end{Bmatrix} \tag{7.3.28}$$

The initial conditions are

$$\begin{Bmatrix} x_f \\ z_f \\ \theta \end{Bmatrix}_{t=0} = \begin{Bmatrix} 0 \\ 0 \\ 0 \end{Bmatrix} \tag{7.3.29}$$

The third equation in Eq. (7.3.28) is easily integrated subject to the third initial condition in Eq. (7.3.29) to yield

$$\theta = \omega_0 t$$

Using this result in the first two equations in Eq. (7.3.28), we have

$$\begin{Bmatrix} \dot{x}_f \\ \dot{z}_f \end{Bmatrix} = \begin{bmatrix} \cos(\omega_0 t) & \sin(\omega_0 t) \\ -\sin(\omega_0 t) & \cos(\omega_0 t) \end{bmatrix} \begin{Bmatrix} V_0 \cos(\omega_0 t) \\ V_0 \sin(\omega_0 t) \end{Bmatrix}$$

Performing the indicated multiplication gives

$$\begin{Bmatrix} \dot{x}_f \\ \dot{z}_f \end{Bmatrix} = \begin{Bmatrix} V_0 \cos^2(\omega_0 t) + V_0 \sin^2(\omega_0 t) \\ -V_0 \cos(\omega_0 t)\sin(\omega_0 t) + V_0 \sin(\omega_0 t)\cos(\omega_0 t) \end{Bmatrix} = \begin{Bmatrix} V_0 \\ 0 \end{Bmatrix}$$

Integrating this result subject to Eq. (7.3.29), the complete solution is

$$\begin{Bmatrix} x_f \\ z_f \\ \theta \end{Bmatrix} = \begin{Bmatrix} V_0 t \\ 0 \\ \omega_0 t \end{Bmatrix}$$

EXAMPLE 7.3.2. The rocket in Example 7.1.1 has a bank angle of 40 degrees, an elevation angle of 20 degrees, and an azimuth angle of 70 degrees. Assuming no wind, what is its velocity in Earth-fixed coordinates?

Solution. From Example 7.1.1,

$$\begin{Bmatrix} V_{x_b} \\ V_{y_b} \\ V_{z_b} \end{Bmatrix} \equiv \begin{Bmatrix} u \\ v \\ w \end{Bmatrix} = \begin{Bmatrix} 825.96 \text{ ft/sec} \\ 300.63 \text{ ft/sec} \\ 476.87 \text{ ft/sec} \end{Bmatrix}$$

From Eq. (7.3.19),

$$\begin{Bmatrix} V_{x_f} \\ V_{y_f} \\ V_{z_f} \end{Bmatrix} = \begin{bmatrix} C_\theta C_\psi & S_\phi S_\theta C_\psi - C_\phi S_\psi & C_\phi S_\theta C_\psi + S_\phi S_\psi \\ C_\theta S_\psi & S_\phi S_\theta S_\psi + C_\phi C_\psi & C_\phi S_\theta S_\psi - S_\phi C_\psi \\ -S_\theta & S_\phi C_\theta & C_\phi C_\theta \end{bmatrix} \begin{Bmatrix} u \\ v \\ w \end{Bmatrix}$$

For this example,

$$\begin{aligned} C_\phi &= \cos 40^\circ = 0.766044, \quad S_\phi = \sin 40^\circ = 0.642788, \\ C_\theta &= \cos 20^\circ = 0.939693, \quad S_\theta = \sin 20^\circ = 0.342020, \\ C_\psi &= \cos 70^\circ = 0.342020, \quad S_\psi = \sin 70^\circ = 0.939693 \end{aligned}$$

Substituting, we have

$$\begin{Bmatrix} V_{x_f} \\ V_{y_f} \\ V_{z_f} \end{Bmatrix} = \begin{bmatrix} 0.321394 & -0.644654 & 0.693633 \\ 0.883022 & 0.468591 & 0.026356 \\ -0.342020 & 0.604023 & 0.719846 \end{bmatrix} \begin{Bmatrix} 825.96 \text{ ft/sec} \\ 300.63 \text{ ft/sec} \\ 476.87 \text{ ft/sec} \end{Bmatrix}$$

and the matrix multiplication gives

$$\begin{Bmatrix} V_{x_f} \\ V_{y_f} \\ V_{z_f} \end{Bmatrix} = \begin{Bmatrix} 402.43 \text{ ft/sec} \\ 882.78 \text{ ft/sec} \\ 242.37 \text{ ft/sec} \end{Bmatrix}$$

As a cross-check on our math we can compute the magnitude of this vector. It should be the same as the magnitude in body-fixed coordinates, 1,000 ft/sec.

$$V = \sqrt{V_{x_f}^2 + V_{y_f}^2 + V_{z_f}^2} = \sqrt{402.43^2 + 882.78^2 + 242.37^2} \text{ ft/sec} = 1{,}000.00 \text{ ft/sec}$$

EXAMPLE 7.3.3. The flight of a stable projectile, such as an arrow or a stable bomb, can be approximated as pure longitudinal motion. If the projectile is stable enough, the angle of attack remains small and we can approximate the longitudinal aerodynamic forces and moment as

$$X \cong -\tfrac{1}{2}\rho u^2 S_r \left(k_0 + k_1 \alpha^2\right) \tag{7.3.30}$$

$$Z \cong -\tfrac{1}{2}\rho u^2 S_r k_2 \alpha \tag{7.3.31}$$

$$m \cong -\tfrac{1}{2}\rho u^2 S_r l_r \left(k_3 \alpha + k_4 l_r \, q/u\right) \tag{7.3.32}$$

where X is the x_b-component of the aerodynamic force, Z is the z_b-component of the aerodynamic force, m is the aerodynamic pitching moment, k_0, k_1, k_2, k_3, and k_4 are dimensionless constants, S_r is a reference area, l_r is a reference length, and α is the angle of attack, which can be approximated as

$$\alpha \cong \frac{w}{u} \tag{7.3.33}$$

Using these approximations and assuming no wind, we wish to determine the position and orientation of the projectile as a function of time. Formulate the problem in a manner suitable for solution by fourth-order Runge-Kutta. Assume that at time equal zero, the position and orientation are (x_0, z_0, θ_0), the magnitude of the velocity is V_0, while the angle of attack and angular velocity are both zero.

Solution. Fourth-order Runge-Kutta requires a system of first-order differential equations and initial conditions in the form

$$\begin{aligned} \dot{y}_i &= f_i(y_1, y_2, y_3, ..., y_n, t) \\ y_i(0) &= Y_i \end{aligned}, \quad i = 1,2,3,...,n$$

Using Eq. (7.3.33) in Eqs. (7.3.30) through (7.3.32), we can write

$$\begin{Bmatrix} X \\ Z \\ m \end{Bmatrix} = -\tfrac{1}{2}\rho S_r \begin{Bmatrix} k_0 u^2 + k_1 w^2 \\ k_2 u w \\ k_3 l_r u w + k_4 l_r^2 q u \end{Bmatrix}$$

The total force is the aerodynamic force plus the gravitational force. Since this is longitudinal motion, we can apply this result along with Eq. (7.3.23) to Eq. (7.2.23),

$$\begin{bmatrix} W/g & 0 & 0 \\ 0 & W/g & 0 \\ 0 & 0 & I_{yy_b} \end{bmatrix} \begin{Bmatrix} \dot{u} \\ \dot{w} \\ \dot{q} \end{Bmatrix}$$

$$= -\tfrac{1}{2}\rho S_r \begin{Bmatrix} k_0 u^2 + k_1 w^2 \\ k_2 u w \\ k_3 l_r u w + k_4 l_r^2 q u \end{Bmatrix} + \begin{Bmatrix} -W\sin(\theta) \\ W\cos(\theta) \\ 0 \end{Bmatrix} + \begin{Bmatrix} -q w W/g \\ q u W/g \\ 0 \end{Bmatrix}$$

Solving for the time derivatives, we have

$$\begin{Bmatrix} \dot{u} \\ \dot{w} \\ \dot{q} \end{Bmatrix} = \begin{Bmatrix} -K_0 u^2 - K_1 w^2 - g\sin(\theta) - q w \\ -K_2 u w + g\cos(\theta) + q u \\ -K_3 u w - K_4 q u \end{Bmatrix} \tag{7.3.34}$$

where

$$\begin{Bmatrix} K_0 \\ K_1 \\ K_2 \\ K_3 \\ K_4 \end{Bmatrix} \equiv \begin{Bmatrix} \frac{1}{2}\rho S_r k_0 g/W \\ \frac{1}{2}\rho S_r k_1 g/W \\ \frac{1}{2}\rho S_r k_2 g/W \\ \frac{1}{2}\rho S_r l_r k_3/I_{yy_b} \\ \frac{1}{2}\rho S_r l_r^2 k_4/I_{yy_b} \end{Bmatrix}$$

Combining Eq. (7.3.24) with Eq. (7.3.34), we obtain a complete system of first-order differential equations in a form suitable for solution by fourth-order Runge-Kutta,

$$\begin{Bmatrix} \dot{u} \\ \dot{w} \\ \dot{q} \\ \dot{x}_f \\ \dot{z}_f \\ \dot{\theta} \end{Bmatrix} = \begin{Bmatrix} -K_0 u^2 - K_1 w^2 - g\sin\theta - q w \\ -K_2 u w + g\cos\theta + q u \\ -K_3 u w - K_4 q u \\ u\cos\theta + w\sin\theta \\ w\cos\theta - u\sin\theta \\ q \end{Bmatrix} \tag{7.3.35}$$

The appropriate initial conditions are

$$\begin{Bmatrix} u(0) \\ w(0) \\ q(0) \\ x_f(0) \\ z_f(0) \\ \theta(0) \end{Bmatrix} = \begin{Bmatrix} V_0 \\ 0 \\ 0 \\ x_0 \\ z_0 \\ \theta_0 \end{Bmatrix} \tag{7.3.36}$$

Starting with the initial values given in Eq. (7.3.36), Eq. (7.3.35) can be integrated forward in time using fourth-order Runge-Kutta. After the first four steps the computation time can be decreased with no loss of accuracy by switching to the fourth-order Adams-Moulton method. The details of the fourth-order Runge-Kutta and the fourth-order Adams-Moulton numerical methods can be found in any undergraduate text on numerical methods (see, for example, Hoffman 1992). The details of obtaining this solution are left as an exercise for the student.

EXAMPLE 7.3.4. An arrow is shot from a bow with a velocity of 210 ft/sec and an elevation angle of 5.0 degrees. Using the formulation developed in Example 7.3.3, we wish to obtain the position, orientation, and airspeed of the arrow 100 yards downrange. For this arrow the aerodynamic coefficients that were defined following Eq. (7.3.34) in Example 7.3.3 are $K_0 = 0.00061$ ft^{-1}, $K_1 = 0.14$ ft^{-1},

$K_2 = 0.00059\ \text{ft}^{-1}$, $K_3 = 0.0016\ \text{ft}^{-2}$, and $K_4 = 0.0064\ \text{ft}^{-1}$. Also plot the elevation of the arrow in inches above the starting point, its airspeed in feet per second, its elevation angle in degrees, and its angle of attack in degrees as a function of horizontal distance downrange in yards, from zero to 100 yards.

Solution. The details of obtaining a Runge-Kutta solution are straightforward and left as an exercise for the student. However, the formulation given by Eq. (7.3.35) is written with time as the independent variable and we wish to obtain a solution for a specified downrange distance of 100 yards. We have no way of knowing, a priori, the length of time required for the arrow to travel 100 yards. Since x_f is a monotonically increasing function of time, rather than using the formulation with time as the independent variable, which requires stepping forward in time, it would be convenient to have x_f as the independent variable, so that we could step forward in range. To facilitate this change of variables, we recognize that

$$\frac{d\mathcal{F}}{dx_f} = \frac{d\mathcal{F}}{dt} \Big/ \frac{dx_f}{dt}$$

where $\mathcal{F}$ could be any one of the dependent variables. The change in x_f with respect to time is given by the fourth equation in Eq. (7.3.35). Thus we can write

$$\frac{d\mathcal{F}}{dx_f} = \frac{d\mathcal{F}}{dt} \Big/ (u\cos\theta + w\sin\theta) \tag{7.3.37}$$

Using this result in Eq. (7.3.35) gives

$$\begin{Bmatrix} u' \\ w' \\ q' \\ x_f' \\ z_f' \\ \theta' \end{Bmatrix} = \left(\frac{1}{u\cos\theta + w\sin\theta} \right) \begin{Bmatrix} -K_0 u^2 - K_1 w^2 - g\sin\theta - q w \\ -K_2 uw + g\cos\theta + q u \\ -K_3 u w - K_4 q u \\ u\cos\theta + w\sin\theta \\ w\cos\theta - u\sin\theta \\ q \end{Bmatrix}$$

where the prime indicates differentiation with respect to x_f. With this change of variables, the fourth equation becomes trivial, and if we do not care about time, we can reduce the order of the system from six to five. However, since computation time is of no concern with this very simple system, we could as well compute time as a dependent variable. Using Eq. (7.3.37) for $\mathcal{F} = t$, we have

$$\frac{dt}{dx_f} = \frac{dt}{dt} \Big/ \frac{dx_f}{dt} = \frac{1}{u\cos\theta + w\sin\theta}$$

Replacing the fourth equation with this result, we obtain the complete system of first-order differential equations with x_f as the independent variable,

$$\begin{Bmatrix} u' \\ w' \\ q' \\ t' \\ z_f' \\ \theta' \end{Bmatrix} = \left(\frac{1}{u\cos\theta + w\sin\theta} \right) \begin{Bmatrix} -K_0 u^2 - K_1 w^2 - g\sin\theta - q w \\ -K_2 u w + g\cos\theta + q u \\ -K_3 u w - K_4 q u \\ 1 \\ w\cos\theta - u\sin\theta \\ q \end{Bmatrix} \tag{7.3.38}$$

The appropriate initial conditions are

$$\begin{Bmatrix} u(0) \\ w(0) \\ q(0) \\ t(0) \\ z_f(0) \\ \theta(0) \end{Bmatrix} = \begin{Bmatrix} V_0 \\ 0 \\ 0 \\ 0 \\ 0 \\ \theta_0 \end{Bmatrix} \tag{7.3.39}$$

We can now use fourth-order Runge-Kutta to step the solution in horizontal position rather than time. Using a specified change in horizontal position, say δx_f, we can integrate numerically from zero to some specified downrange distance, say $x_{\max}$, as demonstrated in the following algorithm:

$g = 32.2$
$u = V_0$
$w = 0.0$
$q = 0.0$
$t = 0.0$
$z_f = 0.0$
$\theta = \theta_0$
$\alpha = \tan^{-1}(w/u)$
$V = \sqrt{u^2 + w^2}$
print $t,\ x_f/3.,\ -12.z_f,\ V,\ 57.2957795\theta,\ 57.2957795\alpha$
do $x_f = 0.0, x_{\max}, \delta x_f$
    call Runge-Kutta for range step δx_f to find u, w, q, t, z_f, θ
    $\alpha = \tan^{-1}(w/u)$
    $V = \sqrt{u^2 + w^2}$
    print $t,\ x_f/3.,\ -12.z_f,\ V,\ 57.2957795\theta,\ 57.2957795\alpha$
end do

Using this algorithm with $\delta x_f = 3$ ft and $x_{max} = 300$ ft, we obtain the following numerical results, which are plotted in Figs. 7.3.5 and 7.3.6. For comparison, Fig. 7.3.5 also shows the elevation and airspeed of the projectile for the classical solution corresponding to the case of no drag.

Time (sec)	Range (yd)	Elevation (in.)	Speed (ft/sec)	θ (degrees)	α (degrees)
0.000000	0.000	0.000	210.000	5.000000	0.000000
0.014353	1.000	3.110	209.575	4.999698	0.125461
0.028733	2.000	6.140	209.150	4.997596	0.249642
⋮	⋮	⋮	⋮	⋮	⋮
1.543669	98.000	−125.007	176.654	−10.014533	−0.126531
1.560924	99.000	−131.340	176.422	−10.156230	−0.090636
1.578210	100.000	−137.788	176.192	−10.294110	−0.050468

Example 7.3.4 demonstrates how to compute the free trajectory of an aerodynamically stable object moving through a fluid. The object, in this case an arrow, is given some initial velocity in some initial direction. In free trajectory problems, the only forces acting on the moving object are the gravitational force and the aerodynamic force. The force of gravity tends to give the object a constant acceleration in the positive z_f-direction. If there were no aerodynamic force, the trajectory would be a parabola, as is shown in Fig. 7.3.5. Since the aerodynamic force on a streamlined body such as an arrow is quite small compared to the weight, the trajectory does not deviate

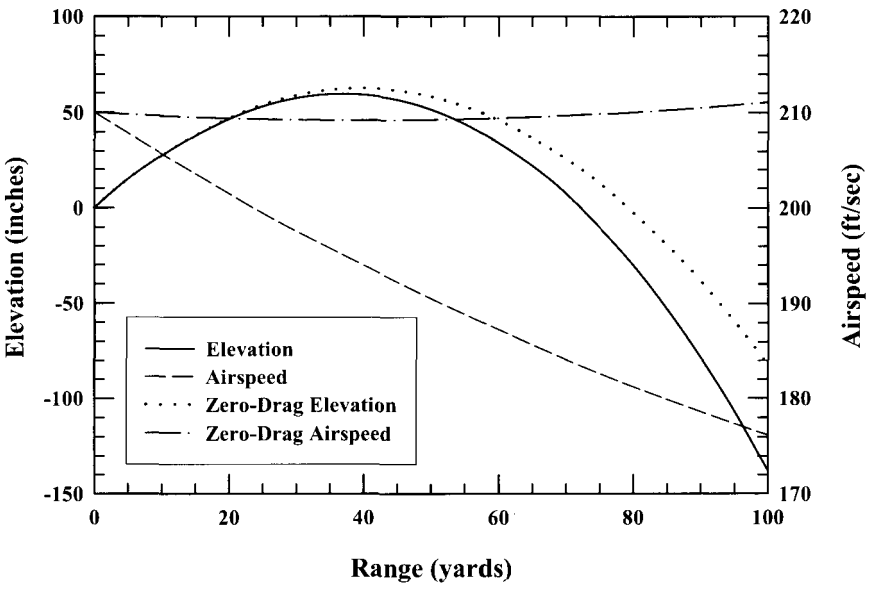


Figure 7.3.5. Elevation and airspeed as a function of range for the trajectory of an arrow.

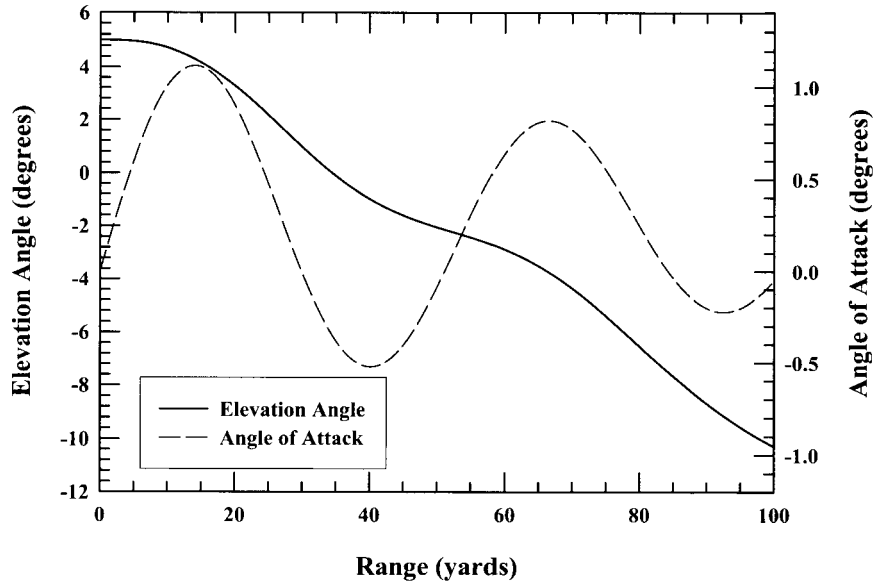


Figure 7.3.6. Elevation angle and angle of attack as a function of range for the trajectory of an arrow.

dramatically from the zero-drag parabola, but the deviation is significant. Most readers will probably find nothing surprising in the results that are shown in Fig. 7.3.5.

This problem would be very difficult to solve using only Earth-fixed coordinates. Because the object is aerodynamically stable, it rotates as it moves, weathervaning into the relative wind as the force of gravity curves its trajectory. This change in orientation causes the inertia tensor to change with time in Earth-fixed coordinates. In addition, the aerodynamic force and moment components were much easier to describe in body-fixed coordinates than they would be in Earth-fixed coordinates. The change in orientation of the arrow as it moves over the ground is shown in Fig. 7.3.6.

This figure also shows something that the reader may not have expected. The angle of attack oscillates as the arrow moves through the air. This is our first look at a phenomenon that can affect any object in stable flight. The reader may ask, why should the angle of attack oscillate? The answer is linked directly to the same aerodynamic forces and moments that make the arrow stable in flight. When the angle of attack deviates from zero, an aerodynamic lift force is generated on the vanes of the arrow. Since the vanes are well aft of the center of gravity, the center of pressure is aft of the center of gravity, and this lift produces a moment that tends to restore the angle of attack toward zero. This restoring moment acts like an *aerodynamic torsional spring*, since the restoring moment increases with angle of attack. Whenever a torsional spring force is applied to an object with a finite mass moment of inertia there is always the possibility of oscillating angular motion. Similar oscillating motion can occur in any aircraft and is discussed in greater detail in later chapters.

7.4. Rigid-Body 6-DOF Equations of Motion

Starting at a time when we know the airplane's position, orientation, translational velocity, and rotational velocity, we can determine the airspeed and the aerodynamic angles from the translational velocity components,

$$V = \sqrt{u^2 + v^2 + w^2} \tag{7.4.1}$$

$$\alpha = \tan^{-1}\left(\frac{w}{u}\right) \tag{7.4.2}$$

$$\beta_a = \tan^{-1}\left(\frac{v}{u}\right) \text{ and/or } \beta_e = \sin^{-1}\left(v/\sqrt{u^2 + v^2 + w^2}\right) \tag{7.4.3}$$

From the known airspeed, aerodynamic angles, and angular velocity components, we can compute the aerodynamic forces and moments, including thrust. We can then compute the time derivatives from Newton's second law and the kinematic transformation equations. For a spanwise symmetric aircraft, the **Euler angle formulation** is

$$\begin{Bmatrix} \dot{u} \\ \dot{v} \\ \dot{w} \end{Bmatrix} = \frac{g}{W}\begin{Bmatrix} F_{x_b} \\ F_{y_b} \\ F_{z_b} \end{Bmatrix} + g\begin{Bmatrix} -S_\theta \\ S_\phi C_\theta \\ C_\phi C_\theta \end{Bmatrix} + \begin{Bmatrix} rv - qw \\ pw - ru \\ qu - pv \end{Bmatrix} \tag{7.4.4}$$

$$\begin{Bmatrix} \dot{p} \\ \dot{q} \\ \dot{r} \end{Bmatrix} = \begin{bmatrix} I_{xx_b} & 0 & -I_{xz_b} \\ 0 & I_{yy_b} & 0 \\ -I_{zx_b} & 0 & I_{zz_b} \end{bmatrix}^{-1} \begin{Bmatrix} M_{x_b} + (I_{yy_b} - I_{zz_b})qr + I_{xz_b}pq \\ M_{y_b} + (I_{zz_b} - I_{xx_b})pr + I_{xz_b}(r^2 - p^2) \\ M_{z_b} + (I_{xx_b} - I_{yy_b})pq - I_{xz_b}qr \end{Bmatrix} \tag{7.4.5}$$

$$\begin{Bmatrix} \dot{x}_f \\ \dot{y}_f \\ \dot{z}_f \end{Bmatrix} = \begin{bmatrix} C_\theta C_\psi & S_\phi S_\theta C_\psi - C_\phi S_\psi & C_\phi S_\theta C_\psi + S_\phi S_\psi \\ C_\theta S_\psi & S_\phi S_\theta S_\psi + C_\phi C_\psi & C_\phi S_\theta S_\psi - S_\phi C_\psi \\ -S_\theta & S_\phi C_\theta & C_\phi C_\theta \end{bmatrix} \begin{Bmatrix} u \\ v \\ w \end{Bmatrix} + \begin{Bmatrix} V_{wx_f} \\ V_{wy_f} \\ V_{wz_f} \end{Bmatrix} \tag{7.4.6}$$

$$\begin{Bmatrix} \dot{\phi} \\ \dot{\theta} \\ \dot{\psi} \end{Bmatrix} = \begin{bmatrix} 1 & S_\phi S_\theta / C_\theta & C_\phi S_\theta / C_\theta \\ 0 & C_\phi & -S_\phi \\ 0 & S_\phi / C_\theta & C_\phi / C_\theta \end{bmatrix} \begin{Bmatrix} p \\ q \\ r \end{Bmatrix} \tag{7.4.7}$$

where F_{x_b}, F_{y_b}, F_{z_b}, M_{x_b}, M_{y_b}, and M_{z_b} are the body-fixed components of the aerodynamic force and moment vectors, including thrust. This system of 12 equations can be integrated numerically to yield the position vector, Euler angles, translational velocity, and rotational velocity of the aircraft as a function of time.

7.5. Linearized Equations of Motion

The rigid-body 6-DOF equations of motion, summarized in Sec. 7.4, are nonlinear. Solutions can only be obtained numerically, for all but the most trivial conditions. However, the dynamics of aircraft motion depend on many aircraft design and operating parameters, and the nature of this dependence is not easily observable from a numerical solution. For this reason, closed-form solutions that accurately describe the essential features of aircraft dynamics are desirable. In addition, closed-form solutions are useful for the optimization of aircraft control systems. In most cases, closed-form solutions can be obtained only for linear systems of equations.

In this section we simplify the rigid-body equations of motion by applying a very powerful analytical tool, which is widely used in almost every field of engineering and science. Since this analytical technique, known as *small-disturbance theory*, has broad application outside the field of flight mechanics, the student should strive to understand the method at a fundamental level. To help facilitate this understanding, we shall begin by examining how small-disturbance theory is applied to a simple one-dimensional problem.

For example, consider some function of time, $x(t)$, that is governed by a nonlinear second-order differential equation of the form

$$\ddot{x} = f(\dot{x}, x, t)$$

Now suppose that there is a known particular solution to this problem, $x_o(t)$. Expanding the differential equation in a Taylor series about this particular solution gives

$$\ddot{x} = f(\dot{x}_o, x_o, t) + \left.\frac{\partial f}{\partial \dot{x}}\right|_{\substack{\dot{x}=\dot{x}_o \\ x=x_o}} (\dot{x} - \dot{x}_o) + \left.\frac{\partial f}{\partial x}\right|_{\substack{\dot{x}=\dot{x}_o \\ x=x_o}} (x - x_o) + \cdots$$

If we assume that the general solution does not deviate greatly from the particular solution, then the higher-order terms in the Taylor series can be ignored. Since the particular solution satisfies $\ddot{x}_o = f(\dot{x}_o, x_o, t)$, any small disturbances from the particular solution must satisfy the differential equation

$$\Delta\ddot{x} = \left.\frac{\partial f}{\partial \dot{x}}\right|_{\substack{\dot{x}=\dot{x}_o \\ x=x_o}} \Delta\dot{x} + \left.\frac{\partial f}{\partial x}\right|_{\substack{\dot{x}=\dot{x}_o \\ x=x_o}} \Delta x$$

where Δx is the deviation from the particular solution, $\Delta x = x - x_o$. Since the derivatives of f with respect to $\dot{x}$ and x in this approximate differential equation are evaluated for the known particular solution, the approximate equation is linear in Δx.

EXAMPLE 7.5.1. Consider a tractor pulling a trailer of mass m. The trailer is attached to the tractor with an elastic tongue having a spring constant k. The tractor is moving along a straight and level roadway with constant velocity V_o. Assuming that the total resistance force on the trailer is proportional to velocity squared, obtain a linearized differential equation for the position of the trailer.

Solution. Newton's second law governs the motion of the trailer. This requires that the mass of the trailer multiplied by its acceleration must equal the net force acting on the trailer. There are two forces acting along the axis of motion, the force applied to the tongue by the tractor and the resistance force between the trailer and its surroundings. Because of the elastic tongue, the force between the tractor and trailer varies linearly with the distance between them. Since the tractor is moving with a constant velocity, its position is changing linearly with time. Letting x denote the position of the trailer relative to some convenient origin, you should be able to draw a free-body diagram of the trailer and show that the governing differential equation is

$$m\ddot{x} = k(V_o t - x) - C\dot{x}^2$$

where C is the proportionality constant between the resistance force acting on the trailer and its velocity squared.

Physics dictates that there should be a steady solution, $x_o(t)$, for which the trailer velocity is constant and equal to the tractor velocity. From the governing differential equation this requires that

$$0 = k(V_o t - x_o) - CV_o^2$$

or

$$x_o = V_o t - \frac{CV_o^2}{k}$$

which requires that

$$\dot{x}_o = V_o$$

We now define the position disturbance to be the difference between the general solution, $x(t)$, and this static equilibrium solution, $x_o(t)$,

$$\Delta x \equiv x - x_o = x - V_o t + \frac{CV_o^2}{k}$$

Since the trailer is attached to the tractor by the elastic tongue, its position cannot deviate far from the equilibrium position. Thus, assuming the disturbance to be small, the governing differential equation is expanded in a Taylor series with all but the first-order terms neglected. This gives

$$m\Delta\ddot{x} = \frac{\partial}{\partial\dot{x}}\left[k(V_o t - x) - C\dot{x}^2\right]\Bigg|_{\substack{\dot{x}=\dot{x}_o \\ x=x_o}} \Delta\dot{x} + \frac{\partial}{\partial x}\left[k(V_o t - x) - C\dot{x}^2\right]\Bigg|_{\substack{\dot{x}=\dot{x}_o \\ x=x_o}} \Delta x$$

or

$$m\Delta\ddot{x} = -2CV_o\Delta\dot{x} - k\Delta x$$

This is the linearized second-order differential equation that governs the small disturbance motion of the trailer relative to its equilibrium position behind the moving tractor.

Small-disturbance theory can also be applied to systems of differential equations. The rigid-body 6-DOF equations of motion, written in terms of Euler angles, consist of 12 coupled nonlinear differential equations in 12 unknowns. Using small-disturbance theory, these equations can be linearized. The small-disturbance approximation requires that the motion of the aircraft be confined to small deviations about some steady equilibrium flight condition. Under normal operating conditions, the forces and moments acting on an aircraft change slowly and do not deviate far from equilibrium. Thus, small-disturbance theory can be applied to aircraft motion for many commonly encountered flight conditions.

In the application of small-disturbance theory to aircraft dynamics, we write each variable in the equations of motion as its value at the equilibrium reference state plus a small disturbance from that equilibrium state,

$$\begin{array}{lll}
u = u_o + \Delta u & v = v_o + \Delta v & w = w_o + \Delta w \\
p = p_o + \Delta p & q = q_o + \Delta q & r = r_o + \Delta r \\
x_f = x_o + \Delta x_f & y_f = y_o + \Delta y_f & z_f = z_o + \Delta z_f \\
\phi = \phi_o + \Delta\phi & \theta = \theta_o + \Delta\theta & \psi = \psi_o + \Delta\psi \\
F_{x_b} = F_{x_bo} + \Delta F_{x_b} & F_{y_b} = F_{y_bo} + \Delta F_{y_b} & F_{z_b} = F_{z_bo} + \Delta F_{z_b} \\
W_{x_b} = W_{x_bo} + \Delta W_{x_b} & W_{y_b} = W_{y_bo} + \Delta W_{y_b} & W_{z_b} = W_{z_bo} + \Delta W_{z_b} \\
M_{x_b} = M_{x_bo} + \Delta M_{x_b} & M_{y_b} = M_{y_bo} + \Delta M_{y_b} & M_{z_b} = M_{z_bo} + \Delta M_{z_b} \\
\delta_a = \delta_{ao} + \Delta\delta_a & \delta_e = \delta_{eo} + \Delta\delta_e & \delta_r = \delta_{ro} + \Delta\delta_r
\end{array} \qquad (7.5.1)$$

The first 12 variables in Eq. (7.5.1) are commonly known as the *state variables*, because they define the instantaneous state of the aircraft in terms of velocity, position, and orientation. Since there are only 12 scalar components in Eqs. (7.4.4) through (7.4.7), the remaining 12 variables must somehow be known as functions of the state variables and pilot control inputs.

Here we consider the reference condition to be steady flight, at some equilibrium airspeed, V_o, with no sideslip, no bank angle, and no angular velocity. Since the alignment of the axes is arbitrary, we shall align the x_b-axis with the aircraft's equilibrium direction of flight and place the x_f-axis so that the equilibrium azimuth angle is zero. Furthermore, since the summation of forces is zero in steady flight, we have

$$u_o = V_o,\ x_o = (V_{wx_f} + V_o\cos\theta_o)t,\ y_o = V_{wy_f}t,\ z_o = (V_{wz_f} - V_o\sin\theta_o)t, \qquad (7.5.2)$$

$$F_{x_bo} = -W_{x_bo},\ F_{z_bo} = -W_{z_bo},\ v_o = w_o = p_o = q_o = r_o = \phi_o = \psi_o = F_{y_bo} = W_{y_bo} = \mathbf{M}_o = 0$$

By substituting the results from Eq. (7.5.2) for the equilibrium values in Eq. (7.5.1), the system variables are expanded in terms of the disturbances from this equilibrium flight condition. This gives

$$
\begin{aligned}
u &= V_o + \Delta u & v &= \Delta v & w &= \Delta w \\
p &= \Delta p & q &= \Delta q & r &= \Delta r \\
x_f &= (V_{wx_f} + V_o \cos\theta_o)t + \Delta x_f & y_f &= V_{wy_f} t + \Delta y_f & z_f &= (V_{wz_f} - V_o \sin\theta_o)t + \Delta z_f \\
\phi &= \Delta\phi & \theta &= \theta_o + \Delta\theta & \psi &= \Delta\psi \\
F_{x_b} &= -W_{x_b o} + \Delta F_{x_b} & F_{y_b} &= \Delta F_{y_b} & F_{z_b} &= -W_{z_b o} + \Delta F_{z_b} \\
W_{x_b} &= W_{x_b o} + \Delta W_{x_b} & W_{y_b} &= \Delta W_{y_b} & W_{z_b} &= W_{z_b o} + \Delta W_{z_b} \\
M_{x_b} &= \Delta M_{x_b} & M_{y_b} &= \Delta M_{y_b} & M_{z_b} &= \Delta M_{z_b} \\
\delta_a &= \delta_{ao} + \Delta\delta_a & \delta_r &= \delta_{ro} + \Delta\delta_r & \delta_e &= \delta_{eo} + \Delta\delta_e
\end{aligned}
\tag{7.5.3}
$$

Newton's second law of motion can be written in terms of the disturbance variables by using Eq. (7.5.3) in Eq. (7.2.20). Since the disturbances are assumed small, we can neglect the product of disturbances, and Newton's second law can be approximated as

$$
\begin{bmatrix}
W/g & 0 & 0 & 0 & 0 & 0 \\
0 & W/g & 0 & 0 & 0 & 0 \\
0 & 0 & W/g & 0 & 0 & 0 \\
0 & 0 & 0 & I_{xx_b} & 0 & -I_{xz_b} \\
0 & 0 & 0 & 0 & I_{yy_b} & 0 \\
0 & 0 & 0 & -I_{xz_b} & 0 & I_{zz_b}
\end{bmatrix}
\begin{Bmatrix} \Delta\dot{u} \\ \Delta\dot{v} \\ \Delta\dot{w} \\ \Delta\dot{p} \\ \Delta\dot{q} \\ \Delta\dot{r} \end{Bmatrix}
=
\begin{Bmatrix}
\Delta F_{x_b} + \Delta W_{x_b} \\
\Delta F_{y_b} + \Delta W_{y_b} - \Delta r V_o W/g \\
\Delta F_{z_b} + \Delta W_{z_b} + \Delta q V_o W/g \\
\Delta M_{x_b} \\
\Delta M_{y_b} \\
\Delta M_{z_b}
\end{Bmatrix}
\tag{7.5.4}
$$

The aerodynamic forces and moments are functions of the translational and rotational velocities, the translational acceleration, and the deflection of the control surfaces. Thus, for small-disturbance theory, the aerodynamic force is approximated as

$$
\begin{aligned}
\begin{Bmatrix} \Delta F_{x_b} \\ \Delta F_{y_b} \\ \Delta F_{z_b} \end{Bmatrix}
&=
\begin{bmatrix}
\dfrac{\partial F_{x_b}}{\partial u} & \dfrac{\partial F_{x_b}}{\partial v} & \dfrac{\partial F_{x_b}}{\partial w} \\
\dfrac{\partial F_{y_b}}{\partial u} & \dfrac{\partial F_{y_b}}{\partial v} & \dfrac{\partial F_{y_b}}{\partial w} \\
\dfrac{\partial F_{z_b}}{\partial u} & \dfrac{\partial F_{z_b}}{\partial v} & \dfrac{\partial F_{z_b}}{\partial w}
\end{bmatrix}
\begin{Bmatrix} \Delta u \\ \Delta v \\ \Delta w \end{Bmatrix}
+
\begin{bmatrix}
\dfrac{\partial F_{x_b}}{\partial p} & \dfrac{\partial F_{x_b}}{\partial q} & \dfrac{\partial F_{x_b}}{\partial r} \\
\dfrac{\partial F_{y_b}}{\partial p} & \dfrac{\partial F_{y_b}}{\partial q} & \dfrac{\partial F_{y_b}}{\partial r} \\
\dfrac{\partial F_{z_b}}{\partial p} & \dfrac{\partial F_{z_b}}{\partial q} & \dfrac{\partial F_{z_b}}{\partial r}
\end{bmatrix}
\begin{Bmatrix} \Delta p \\ \Delta q \\ \Delta r \end{Bmatrix} \\
&+
\begin{bmatrix}
\dfrac{\partial F_{x_b}}{\partial \dot{u}} & \dfrac{\partial F_{x_b}}{\partial \dot{v}} & \dfrac{\partial F_{x_b}}{\partial \dot{w}} \\
\dfrac{\partial F_{y_b}}{\partial \dot{u}} & \dfrac{\partial F_{y_b}}{\partial \dot{v}} & \dfrac{\partial F_{y_b}}{\partial \dot{w}} \\
\dfrac{\partial F_{z_b}}{\partial \dot{u}} & \dfrac{\partial F_{z_b}}{\partial \dot{v}} & \dfrac{\partial F_{z_b}}{\partial \dot{w}}
\end{bmatrix}
\begin{Bmatrix} \Delta\dot{u} \\ \Delta\dot{v} \\ \Delta\dot{w} \end{Bmatrix}
+
\begin{bmatrix}
\dfrac{\partial F_{x_b}}{\partial \delta_a} & \dfrac{\partial F_{x_b}}{\partial \delta_e} & \dfrac{\partial F_{x_b}}{\partial \delta_r} \\
\dfrac{\partial F_{y_b}}{\partial \delta_a} & \dfrac{\partial F_{y_b}}{\partial \delta_e} & \dfrac{\partial F_{y_b}}{\partial \delta_r} \\
\dfrac{\partial F_{z_b}}{\partial \delta_a} & \dfrac{\partial F_{z_b}}{\partial \delta_e} & \dfrac{\partial F_{z_b}}{\partial \delta_r}
\end{bmatrix}
\begin{Bmatrix} \Delta\delta_a \\ \Delta\delta_e \\ \Delta\delta_r \end{Bmatrix}
\end{aligned}
\tag{7.5.5}
$$

and for the aerodynamic moment we use the approximation

$$\begin{Bmatrix} \Delta M_{x_b} \\ \Delta M_{y_b} \\ \Delta M_{z_b} \end{Bmatrix} = \begin{bmatrix} \frac{\partial M_{x_b}}{\partial u} & \frac{\partial M_{x_b}}{\partial v} & \frac{\partial M_{x_b}}{\partial w} \\ \frac{\partial M_{y_b}}{\partial u} & \frac{\partial M_{y_b}}{\partial v} & \frac{\partial M_{y_b}}{\partial w} \\ \frac{\partial M_{z_b}}{\partial u} & \frac{\partial M_{z_b}}{\partial v} & \frac{\partial M_{z_b}}{\partial w} \end{bmatrix} \begin{Bmatrix} \Delta u \\ \Delta v \\ \Delta w \end{Bmatrix} + \begin{bmatrix} \frac{\partial M_{x_b}}{\partial p} & \frac{\partial M_{x_b}}{\partial q} & \frac{\partial M_{x_b}}{\partial r} \\ \frac{\partial M_{y_b}}{\partial p} & \frac{\partial M_{y_b}}{\partial q} & \frac{\partial M_{y_b}}{\partial r} \\ \frac{\partial M_{z_b}}{\partial p} & \frac{\partial M_{z_b}}{\partial q} & \frac{\partial M_{z_b}}{\partial r} \end{bmatrix} \begin{Bmatrix} \Delta p \\ \Delta q \\ \Delta r \end{Bmatrix}$$
$$+ \begin{bmatrix} \frac{\partial M_{x_b}}{\partial \dot{u}} & \frac{\partial M_{x_b}}{\partial \dot{v}} & \frac{\partial M_{x_b}}{\partial \dot{w}} \\ \frac{\partial M_{y_b}}{\partial \dot{u}} & \frac{\partial M_{y_b}}{\partial \dot{v}} & \frac{\partial M_{y_b}}{\partial \dot{w}} \\ \frac{\partial M_{z_b}}{\partial \dot{u}} & \frac{\partial M_{z_b}}{\partial \dot{v}} & \frac{\partial M_{z_b}}{\partial \dot{w}} \end{bmatrix} \begin{Bmatrix} \Delta \dot{u} \\ \Delta \dot{v} \\ \Delta \dot{w} \end{Bmatrix} + \begin{bmatrix} \frac{\partial M_{x_b}}{\partial \delta_a} & \frac{\partial M_{x_b}}{\partial \delta_e} & \frac{\partial M_{x_b}}{\partial \delta_r} \\ \frac{\partial M_{y_b}}{\partial \delta_a} & \frac{\partial M_{y_b}}{\partial \delta_e} & \frac{\partial M_{y_b}}{\partial \delta_r} \\ \frac{\partial M_{z_b}}{\partial \delta_a} & \frac{\partial M_{z_b}}{\partial \delta_e} & \frac{\partial M_{z_b}}{\partial \delta_r} \end{bmatrix} \begin{Bmatrix} \Delta \delta_a \\ \Delta \delta_e \\ \Delta \delta_r \end{Bmatrix} \tag{7.5.6}$$

where all derivatives are evaluated at the equilibrium flight condition.

The body-fixed aerodynamic force and moment components, which are expressed in Eqs. (7.5.5) and (7.5.6), are shown as independent of the Euler angles. The aerodynamic force and moment components in body-fixed coordinates do not depend on the aircraft orientation relative to the Earth, but only on the motion of the aircraft relative to the surrounding air. This is why atmosphere-fixed coordinates were chosen as the inertial coordinate system in the formulation of Newton's second law.

In Eqs. (7.5.5) and (7.5.6) we have assumed that the force and moment components depend on the translational acceleration components. The forces and moments depend on the translational accelerations because the vorticity generated by the wing requires a finite time to travel from the wing to the tail. As the angle of attack changes, the lift and vorticity generated by the wing also change. This change in vorticity alters the downwash at the tail and hence alters the forces and moments produced by the tail. However, since the vorticity travels from the wing to the tail at the speed of the aircraft, it takes a finite time for the altered downwash to reach the tail. Since sideslip has little effect on lift or vorticity, the sideslip acceleration terms are not significant. In addition, several of the remaining terms can be eliminated on the basis of symmetry. Thus, for the linearized equations of motion we shall use

$$\frac{\partial F_{y_b}}{\partial \dot{u}} = \frac{\partial F_{x_b}}{\partial \dot{v}} = \frac{\partial F_{y_b}}{\partial \dot{v}} = \frac{\partial F_{z_b}}{\partial \dot{v}} = \frac{\partial F_{y_b}}{\partial \dot{w}} = 0$$
$$\frac{\partial M_{x_b}}{\partial \dot{u}} = \frac{\partial M_{z_b}}{\partial \dot{u}} = \frac{\partial M_{x_b}}{\partial \dot{v}} = \frac{\partial M_{y_b}}{\partial \dot{v}} = \frac{\partial M_{z_b}}{\partial \dot{v}} = \frac{\partial M_{x_b}}{\partial \dot{w}} = \frac{\partial M_{z_b}}{\partial \dot{w}} = 0 \tag{7.5.7}$$

Several more of the derivatives in Eqs. (7.5.5) and (7.5.6) can be eliminated on the basis of symmetry. For example, at the equilibrium flight condition, the change in axial force with respect to the sideslip velocity must be zero, because the aircraft is assumed symmetric about the x_b-z_b plane and the equilibrium sideslip velocity is zero. Keep in

mind that the derivatives in Eqs. (7.5.5) and (7.5.6) are all evaluated at the equilibrium flight condition. Clearly, the axial force is not totally independent of sideslip. However, from the assumed symmetry, a positive sideslip should have the same effect on the axial force as a negative sideslip. Thus, the axial force must be a symmetric function of sideslip, and the change in axial force with respect to sideslip velocity must be zero, when the sideslip velocity is zero. By similar reasoning we can eliminate all of the following derivatives evaluated at the reference flight condition:

$$
\begin{gathered}
\frac{\partial F_{x_b}}{\partial v}=\frac{\partial F_{y_b}}{\partial u}=\frac{\partial F_{y_b}}{\partial w}=\frac{\partial F_{z_b}}{\partial v}=0 \\
\frac{\partial M_{x_b}}{\partial u}=\frac{\partial M_{x_b}}{\partial w}=\frac{\partial M_{y_b}}{\partial v}=\frac{\partial M_{z_b}}{\partial u}=\frac{\partial M_{z_b}}{\partial w}=0 \\
\frac{\partial F_{x_b}}{\partial p}=\frac{\partial F_{x_b}}{\partial r}=\frac{\partial F_{y_b}}{\partial q}=\frac{\partial F_{z_b}}{\partial p}=\frac{\partial F_{z_b}}{\partial r}=0 \\
\frac{\partial M_{x_b}}{\partial q}=\frac{\partial M_{y_b}}{\partial p}=\frac{\partial M_{y_b}}{\partial r}=\frac{\partial M_{z_b}}{\partial q}=0 \\
\frac{\partial F_{x_b}}{\partial \delta_a}=\frac{\partial F_{x_b}}{\partial \delta_r}=\frac{\partial F_{y_b}}{\partial \delta_e}=\frac{\partial F_{z_b}}{\partial \delta_a}=\frac{\partial F_{z_b}}{\partial \delta_r}=0 \\
\frac{\partial M_{x_b}}{\partial \delta_e}=\frac{\partial M_{y_b}}{\partial \delta_a}=\frac{\partial M_{y_b}}{\partial \delta_r}=\frac{\partial M_{z_b}}{\partial \delta_e}=0
\end{gathered}
\tag{7.5.8}
$$

The body-fixed components of the gravitational force vector change with aircraft orientation. Since the body-fixed gravitational components only depend on the Euler angles, from Eq. (7.3.15) we have

$$
\begin{Bmatrix} W_{x_b} \\ W_{y_b} \\ W_{z_b} \end{Bmatrix} = W \begin{Bmatrix} -\sin(\theta) \\ \sin(\phi)\cos(\theta) \\ \cos(\phi)\cos(\theta) \end{Bmatrix} \tag{7.5.9}
$$

which at the equilibrium flight condition gives

$$
\begin{Bmatrix} \Delta W_{x_b} \\ \Delta W_{y_b} \\ \Delta W_{z_b} \end{Bmatrix} = \begin{bmatrix} \dfrac{\partial W_{x_b}}{\partial \phi} & \dfrac{\partial W_{x_b}}{\partial \theta} & \dfrac{\partial W_{x_b}}{\partial \psi} \\ \dfrac{\partial W_{y_b}}{\partial \phi} & \dfrac{\partial W_{y_b}}{\partial \theta} & \dfrac{\partial W_{y_b}}{\partial \psi} \\ \dfrac{\partial W_{z_b}}{\partial \phi} & \dfrac{\partial W_{z_b}}{\partial \theta} & \dfrac{\partial W_{z_b}}{\partial \psi} \end{bmatrix} \begin{Bmatrix} \Delta\phi \\ \Delta\theta \\ \Delta\psi \end{Bmatrix} = \begin{bmatrix} 0 & -W\cos\theta_0 & 0 \\ W\cos\theta_0 & 0 & 0 \\ 0 & -W\sin\theta_0 & 0 \end{bmatrix} \begin{Bmatrix} \Delta\phi \\ \Delta\theta \\ \Delta\psi \end{Bmatrix} \tag{7.5.10}
$$

By definition, the gravitational force does not produce a moment about the CG.

Using Eqs. (7.5.7) and (7.5.8) in Eqs. (7.5.5) and (7.5.6) and adding Eq. (7.5.10), the small-disturbance force approximations are given by

$$\begin{Bmatrix} \Delta F_{x_b} + \Delta W_{x_b} \\ \Delta F_{y_b} + \Delta W_{y_b} \\ \Delta F_{z_b} + \Delta W_{z_b} \end{Bmatrix} = \begin{bmatrix} F_{x_b,u} & 0 & F_{x_b,w} \\ 0 & F_{y_b,v} & 0 \\ F_{z_b,u} & 0 & F_{z_b,w} \end{bmatrix} \begin{Bmatrix} \Delta u \\ \Delta v \\ \Delta w \end{Bmatrix} + \begin{bmatrix} 0 & F_{x_b,q} & 0 \\ F_{y_b,p} & 0 & F_{y_b,r} \\ 0 & F_{z_b,q} & 0 \end{bmatrix} \begin{Bmatrix} \Delta p \\ \Delta q \\ \Delta r \end{Bmatrix}$$
$$+ \begin{bmatrix} F_{x_b,\dot{u}} & 0 & F_{x_b,\dot{w}} \\ 0 & 0 & 0 \\ F_{z_b,\dot{u}} & 0 & F_{z_b,\dot{w}} \end{bmatrix} \begin{Bmatrix} \Delta \dot{u} \\ \Delta \dot{v} \\ \Delta \dot{w} \end{Bmatrix} + \begin{bmatrix} 0 & F_{x_b,\delta_e} & 0 \\ F_{y_b,\delta_a} & 0 & F_{y_b,\delta_r} \\ 0 & F_{z_b,\delta_e} & 0 \end{bmatrix} \begin{Bmatrix} \Delta \delta_a \\ \Delta \delta_e \\ \Delta \delta_r \end{Bmatrix} \tag{7.5.11}$$
$$+ \begin{bmatrix} 0 & -W\cos\theta_0 & 0 \\ W\cos\theta_0 & 0 & 0 \\ 0 & -W\sin\theta_0 & 0 \end{bmatrix} \begin{Bmatrix} \Delta \phi \\ \Delta \theta \\ \Delta \psi \end{Bmatrix}$$

and the small-disturbance moment approximations become

$$\begin{Bmatrix} \Delta M_{x_b} \\ \Delta M_{y_b} \\ \Delta M_{z_b} \end{Bmatrix} = \begin{bmatrix} 0 & M_{x_b,v} & 0 \\ M_{y_b,u} & 0 & M_{y_b,w} \\ 0 & M_{z_b,v} & 0 \end{bmatrix} \begin{Bmatrix} \Delta u \\ \Delta v \\ \Delta w \end{Bmatrix} + \begin{bmatrix} M_{x_b,p} & 0 & M_{x_b,r} \\ 0 & M_{y_b,q} & 0 \\ M_{z_b,p} & 0 & M_{z_b,r} \end{bmatrix} \begin{Bmatrix} \Delta p \\ \Delta q \\ \Delta r \end{Bmatrix}$$
$$+ \begin{bmatrix} 0 & 0 & 0 \\ M_{y_b,\dot{u}} & 0 & M_{y_b,\dot{w}} \\ 0 & 0 & 0 \end{bmatrix} \begin{Bmatrix} \Delta \dot{u} \\ \Delta \dot{v} \\ \Delta \dot{w} \end{Bmatrix} + \begin{bmatrix} M_{x_b,\delta_a} & 0 & M_{x_b,\delta_r} \\ 0 & M_{y_b,\delta_e} & 0 \\ M_{z_b,\delta_a} & 0 & M_{z_b,\delta_r} \end{bmatrix} \begin{Bmatrix} \Delta \delta_a \\ \Delta \delta_e \\ \Delta \delta_r \end{Bmatrix} \tag{7.5.12}$$

Notice that within the accuracy of small-disturbance theory, ΔF_{x_b}, ΔF_{z_b}, ΔW_{x_b}, ΔW_{z_b}, and ΔM_{y_b} depend only on $\Delta \dot{u}$, $\Delta \dot{w}$, Δu, Δw, Δq, $\Delta \delta_e$, and $\Delta \theta$, while ΔF_{y_b}, ΔW_{y_b}, ΔM_{x_b}, and ΔM_{z_b} depend only on Δv, Δp, Δr, $\Delta \delta_a$, $\Delta \delta_r$, and $\Delta \phi$.

Rearranging Eqs. (7.5.11) and (7.5.12), we have

$$\begin{Bmatrix} \Delta F_{x_b} + \Delta W_{x_b} \\ \Delta F_{z_b} + \Delta W_{z_b} \\ \Delta M_{y_b} \end{Bmatrix} = \begin{bmatrix} F_{x_b,\dot{u}} & F_{x_b,\dot{w}} & 0 \\ F_{z_b,\dot{u}} & F_{z_b,\dot{w}} & 0 \\ M_{y_b,\dot{u}} & M_{y_b,\dot{w}} & 0 \end{bmatrix} \begin{Bmatrix} \Delta \dot{u} \\ \Delta \dot{w} \\ \Delta \dot{q} \end{Bmatrix} + \begin{bmatrix} F_{x_b,u} & F_{x_b,w} & F_{x_b,q} \\ F_{z_b,u} & F_{z_b,w} & F_{z_b,q} \\ M_{y_b,u} & M_{y_b,w} & M_{y_b,q} \end{bmatrix} \begin{Bmatrix} \Delta u \\ \Delta w \\ \Delta q \end{Bmatrix}$$
$$+ \begin{Bmatrix} F_{x_b,\delta_e} \\ F_{z_b,\delta_e} \\ M_{y_b,\delta_e} \end{Bmatrix} \Delta \delta_e + \begin{Bmatrix} -W\cos(\theta_0) \\ -W\sin(\theta_0) \\ 0 \end{Bmatrix} \Delta \theta \tag{7.5.13}$$

$$\begin{Bmatrix} \Delta F_{y_b} + \Delta W_{y_b} \\ \Delta M_{x_b} \\ \Delta M_{z_b} \end{Bmatrix} = \begin{bmatrix} F_{y_b,v} & F_{y_b,p} & F_{y_b,r} \\ M_{x_b,v} & M_{x_b,p} & M_{x_b,r} \\ M_{z_b,v} & M_{z_b,p} & M_{z_b,r} \end{bmatrix} \begin{Bmatrix} \Delta v \\ \Delta p \\ \Delta r \end{Bmatrix} + \begin{bmatrix} F_{y_b,\delta_a} & F_{y_b,\delta_r} \\ M_{x_b,\delta_a} & M_{x_b,\delta_r} \\ M_{z_b,\delta_a} & M_{z_b,\delta_r} \end{bmatrix} \begin{Bmatrix} \Delta \delta_a \\ \Delta \delta_r \end{Bmatrix}$$
$$+ \begin{Bmatrix} W\cos(\theta_0) \\ 0 \\ 0 \end{Bmatrix} \Delta \phi \tag{7.5.14}$$

Applying these results, the system of six equations in Eq. (7.5.4) may be separated into two uncoupled systems, each containing three equations,

$$\begin{bmatrix} W/g & 0 & 0 \\ 0 & W/g & 0 \\ 0 & 0 & I_{yy_b} \end{bmatrix} \begin{Bmatrix} \Delta\dot{u} \\ \Delta\dot{w} \\ \Delta\dot{q} \end{Bmatrix} = \begin{Bmatrix} \Delta F_{x_b} + \Delta W_{x_b} \\ \Delta F_{z_b} + \Delta W_{z_b} + \Delta q V_o W/g \\ \Delta M_{y_b} \end{Bmatrix} \tag{7.5.15}$$

$$\begin{bmatrix} W/g & 0 & 0 \\ 0 & I_{xx_b} & -I_{xz_b} \\ 0 & -I_{xz_b} & I_{zz_b} \end{bmatrix} \begin{Bmatrix} \Delta\dot{v} \\ \Delta\dot{p} \\ \Delta\dot{r} \end{Bmatrix} = \begin{Bmatrix} \Delta F_{y_b} + \Delta W_{y_b} - \Delta r V_o W/g \\ \Delta M_{x_b} \\ \Delta M_{z_b} \end{Bmatrix} \tag{7.5.16}$$

or after using Eqs. (7.5.13) and (7.5.14),

$$\begin{aligned} &\begin{bmatrix} W/g - F_{x_b,\dot{u}} & -F_{x_b,\dot{w}} & 0 \\ -F_{z_b,\dot{u}} & W/g - F_{z_b,\dot{w}} & 0 \\ -M_{y_b,\dot{u}} & -M_{y_b,\dot{w}} & I_{yy_b} \end{bmatrix} \begin{Bmatrix} \Delta\dot{u} \\ \Delta\dot{w} \\ \Delta\dot{q} \end{Bmatrix} \\ &= \begin{bmatrix} F_{x_b,u} & F_{x_b,w} & F_{x_b,q} \\ F_{z_b,u} & F_{z_b,w} & F_{z_b,q} + V_o W/g \\ M_{y_b,u} & M_{y_b,w} & M_{y_b,q} \end{bmatrix} \begin{Bmatrix} \Delta u \\ \Delta w \\ \Delta q \end{Bmatrix} + \begin{Bmatrix} F_{x_b,\delta_e} \\ F_{z_b,\delta_e} \\ M_{y_b,\delta_e} \end{Bmatrix} \Delta\delta_e + \begin{Bmatrix} -W\cos(\theta_0) \\ -W\sin(\theta_0) \\ 0 \end{Bmatrix} \Delta\theta \end{aligned} \tag{7.5.17}$$

$$\begin{aligned} &\begin{bmatrix} W/g & 0 & 0 \\ 0 & I_{xx_b} & -I_{xz_b} \\ 0 & -I_{xz_b} & I_{zz_b} \end{bmatrix} \begin{Bmatrix} \Delta\dot{v} \\ \Delta\dot{\omega}_{x_b} \\ \Delta\dot{\omega}_{z_b} \end{Bmatrix} \\ &= \begin{bmatrix} F_{y_b,v} & F_{y_b,p} & F_{y_b,r} - V_o W/g \\ M_{x_b,v} & M_{x_b,p} & M_{x_b,r} \\ M_{z_b,v} & M_{z_b,p} & M_{z_b,r} \end{bmatrix} \begin{Bmatrix} \Delta v \\ \Delta p \\ \Delta r \end{Bmatrix} + \begin{bmatrix} F_{y_b,\delta_a} & F_{y_b,\delta_r} \\ M_{x_b,\delta_a} & M_{x_b,\delta_r} \\ M_{z_b,\delta_a} & M_{z_b,\delta_r} \end{bmatrix} \begin{Bmatrix} \Delta\delta_a \\ \Delta\delta_r \end{Bmatrix} \\ &\qquad + \begin{Bmatrix} W\cos(\theta_0) \\ 0 \\ 0 \end{Bmatrix} \Delta\phi \end{aligned} \tag{7.5.18}$$

Using the small-disturbance variables from Eq. (7.5.3), applying the small-angle approximations,

$$\begin{aligned} \sin(\phi) &\cong \Delta\phi & \sin(\theta) &\cong \sin(\theta_o) + \cos(\theta_o)\Delta\theta & \sin(\psi) &\cong \Delta\psi \\ \cos(\phi) &\cong 1 & \cos(\theta) &\cong \cos(\theta_o) - \sin(\theta_o)\Delta\theta & \cos(\psi) &\cong 1 \end{aligned} \tag{7.5.19}$$

and neglecting second-order terms in the kinematic transformation matrix, Eq. (7.3.19) reduces to

$$\begin{Bmatrix} V_{wx_f} + V_o C_{\theta_o} + \Delta\dot{x}_f \\ V_{wy_f} + \Delta\dot{y}_f \\ V_{wz_f} - V_o S_{\theta_o} + \Delta\dot{z}_f \end{Bmatrix} = \begin{bmatrix} C_{\theta_o} - S_{\theta_o}\Delta\theta & S_{\theta_o}\Delta\phi - \Delta\psi & S_{\theta_o} + C_{\theta_o}\Delta\theta \\ C_{\theta_o}\Delta\psi & 1 & S_{\theta_o}\Delta\psi - \Delta\phi \\ -S_{\theta_o} - C_{\theta_o}\Delta\theta & C_{\theta_o}\Delta\phi & C_{\theta_o} - S_{\theta_o}\Delta\theta \end{bmatrix} \begin{Bmatrix} V_o + \Delta u \\ \Delta v \\ \Delta w \end{Bmatrix} + \begin{Bmatrix} V_{wx_f} \\ V_{wy_f} \\ V_{wz_f} \end{Bmatrix} \tag{7.5.20}$$

$$\begin{Bmatrix} \Delta\dot{\phi} \\ \Delta\dot{\theta} \\ \Delta\dot{\psi} \end{Bmatrix} = \begin{bmatrix} 1 & S_{\theta_o}\Delta\phi/C_{\theta_o} & S_{\theta_o}/C_{\theta_o} + \Delta\theta/C_{\theta_o}^2 \\ 0 & 1 & -\Delta\phi \\ 0 & \Delta\phi/C_{\theta_o} & 1/C_{\theta_o} + S_{\theta_o}\Delta\theta/C_{\theta_o}^2 \end{bmatrix} \begin{Bmatrix} \Delta p \\ \Delta q \\ \Delta r \end{Bmatrix} \tag{7.5.21}$$

or, after eliminating the remaining second-order terms, we have

$$\begin{Bmatrix} \Delta\dot{x}_f \\ \Delta\dot{y}_f \\ \Delta\dot{z}_f \\ \Delta\dot{\phi} \\ \Delta\dot{\theta} \\ \Delta\dot{\psi} \end{Bmatrix} = \begin{bmatrix} \cos(\theta_o) & 0 & \sin(\theta_o) & 0 & 0 & 0 \\ 0 & 1 & 0 & 0 & 0 & 0 \\ -\sin(\theta_o) & 0 & \cos(\theta_o) & 0 & 0 & 0 \\ 0 & 0 & 0 & 1 & 0 & \tan(\theta_o) \\ 0 & 0 & 0 & 0 & 1 & 0 \\ 0 & 0 & 0 & 0 & 0 & \sec(\theta_o) \end{bmatrix} \begin{Bmatrix} \Delta u \\ \Delta v \\ \Delta w \\ \Delta p \\ \Delta q \\ \Delta r \end{Bmatrix} + \begin{bmatrix} 0 & -V_o\sin(\theta_o) & 0 \\ 0 & 0 & V_o\cos(\theta_o) \\ 0 & -V_o\cos(\theta_o) & 0 \\ 0 & 0 & 0 \\ 0 & 0 & 0 \\ 0 & 0 & 0 \end{bmatrix} \begin{Bmatrix} \Delta\phi \\ \Delta\theta \\ \Delta\psi \end{Bmatrix} \tag{7.5.22}$$

Equations (7.5.17), (7.5.18), and (7.5.22) provide 12 first-order linearized differential equations for the velocity and position associated with each of the six degrees of freedom that are possible in rigid-body flight. These include three translational degrees of freedom (axial, normal, and transverse) and three rotational degrees of freedom (roll, pitch, and yaw). We could solve this system of equations as a fully coupled system of 12 equations in 12 unknowns. However, this is not a fully coupled system of equations. The subsystem given by Eq. (7.5.17) provides three equations, which include only four of the 12 unknowns, Δu, Δw, Δq, and $\Delta\theta$. The subsystem in Eq. (7.5.18) provides three more equations in four entirely different unknowns, Δv, Δp, Δr, and $\Delta\phi$. Combining Eq. (7.5.17) with the first, third, and fifth equations from Eq. (7.5.22), we have a complete subsystem that can be solved for six of the 12 unknowns, independent of the other six. Similarly, by combining Eq. (7.5.18) with the second, fourth, and sixth equations from Eq. (7.5.22), we can solve for the remaining six of the 12 unknowns.

Thus, rearranging Eqs. (7.5.17), (7.5.18), and (7.5.22), we obtain two separate systems of six equations in six unknowns:

the **linearized longitudinal equations**,

$$\begin{bmatrix} W/g - F_{x_b,\dot{u}} & -F_{x_b,\dot{w}} & 0 & 0 & 0 & 0 \\ -F_{z_b,\dot{u}} & W/g - F_{z_b,\dot{w}} & 0 & 0 & 0 & 0 \\ -M_{y_b,\dot{u}} & -M_{y_b,\dot{w}} & I_{yy_b} & 0 & 0 & 0 \\ 0 & 0 & 0 & 1 & 0 & 0 \\ 0 & 0 & 0 & 0 & 1 & 0 \\ 0 & 0 & 0 & 0 & 0 & 1 \end{bmatrix} \begin{Bmatrix} \Delta\dot{u} \\ \Delta\dot{w} \\ \Delta\dot{q} \\ \Delta\dot{x}_f \\ \Delta\dot{z}_f \\ \Delta\dot{\theta} \end{Bmatrix} = \begin{Bmatrix} F_{x_b,\delta_e} \\ F_{z_b,\delta_e} \\ M_{y_b,\delta_e} \\ 0 \\ 0 \\ 0 \end{Bmatrix} \Delta\delta_e$$

$$+ \begin{bmatrix} F_{x_b,u} & F_{x_b,w} & F_{x_b,q} & 0 & 0 & -W\cos\theta_0 \\ F_{z_b,u} & F_{z_b,w} & F_{z_b,q} + V_o W/g & 0 & 0 & -W\sin\theta_0 \\ M_{y_b,u} & M_{y_b,w} & M_{y_b,q} & 0 & 0 & 0 \\ \cos\theta_o & \sin\theta_o & 0 & 0 & 0 & -V_o\sin\theta_o \\ -\sin\theta_o & \cos\theta_o & 0 & 0 & 0 & -V_o\cos\theta_o \\ 0 & 0 & 1 & 0 & 0 & 0 \end{bmatrix} \begin{Bmatrix} \Delta u \\ \Delta w \\ \Delta q \\ \Delta x_f \\ \Delta z_f \\ \Delta\theta \end{Bmatrix} \tag{7.5.23}$$

and the **linearized lateral equations**,

$$\begin{bmatrix} W/g & 0 & 0 & 0 & 0 & 0 \\ 0 & I_{xx_b} & -I_{xz_b} & 0 & 0 & 0 \\ 0 & -I_{xz_b} & I_{zz_b} & 0 & 0 & 0 \\ 0 & 0 & 0 & 1 & 0 & 0 \\ 0 & 0 & 0 & 0 & 1 & 0 \\ 0 & 0 & 0 & 0 & 0 & 1 \end{bmatrix} \begin{Bmatrix} \Delta\dot{v} \\ \Delta\dot{p} \\ \Delta\dot{r} \\ \Delta\dot{y}_f \\ \Delta\dot{\phi} \\ \Delta\dot{\psi} \end{Bmatrix} = \begin{bmatrix} F_{y_b,\delta_a} & F_{y_b,\delta_r} \\ M_{x_b,\delta_a} & M_{x_b,\delta_r} \\ M_{z_b,\delta_a} & M_{z_b,\delta_r} \\ 0 & 0 \\ 0 & 0 \\ 0 & 0 \end{bmatrix} \begin{Bmatrix} \Delta\delta_a \\ \Delta\delta_r \end{Bmatrix}$$

$$+ \begin{bmatrix} F_{y_b,v} & F_{y_b,p} & F_{y_b,r} - V_o W/g & 0 & W\cos\theta_0 & 0 \\ M_{x_b,v} & M_{x_b,p} & M_{x_b,r} & 0 & 0 & 0 \\ M_{z_b,v} & M_{z_b,p} & M_{z_b,r} & 0 & 0 & 0 \\ 1 & 0 & 0 & 0 & 0 & V_o\cos\theta_o \\ 0 & 1 & \tan\theta_o & 0 & 0 & 0 \\ 0 & 0 & \sec\theta_o & 0 & 0 & 0 \end{bmatrix} \begin{Bmatrix} \Delta v \\ \Delta p \\ \Delta r \\ \Delta y_f \\ \Delta\phi \\ \Delta\psi \end{Bmatrix} \tag{7.5.24}$$

Equations (7.5.23) and (7.5.24) combined are the linearized 6-DOF equations of motion. They provide a tremendous simplification over the general nonlinear 6-DOF equations. However, we must remember that these equations are valid only if the motion of the aircraft is confined to small deviations about some steady equilibrium flight condition. Larger deviations will introduce coupling between the lateral and longitudinal motions and nonlinearity in the aerodynamic forces and moments.

With this said, it should be pointed out that this linearized theory yields considerable information and many valuable insights with comparatively little effort. Furthermore, it gives good engineering accuracy over a surprisingly wide range of application. The small-disturbance model is actually valid for disturbance magnitudes that would seem quite violent to most passengers. In fact, after experiencing flight disturbances of a magnitude that is near the limit of applicability for small-disturbance theory, most individuals would not care to investigate a large-disturbance theory experimentally. Small-disturbance theory is valid for most commonly encountered flying situations. Nearly all of the flying time logged by commercial and private pilots is spent within the boundaries of the constraints imposed by small-disturbance theory. There are, of course, limitations. Small-disturbance theory is not applicable to spinning motion, stall recovery, or any other application that involves rapid maneuvers or large-amplitude oscillations.

EXAMPLE 7.5.2. Over a short distance, the flight of an arrow or other such projectile does not deviate a great deal from motion along a straight line at constant speed. Small-disturbance theory can be used to approximate such motion. Using small-disturbance theory, linearize the system of equations that was developed in Example 7.3.3. Linearize the equations relative to motion at constant speed, V_o, along a horizontal line. After the full system of equations has been linearized, solve the linear system for the special case where K_2 is zero and K_3 is infinity. Assume that initially the projectile starts from $x_f = 0$ and $z_f = 0$ with a speed of V_o and a small elevation angle of $\Delta\theta_0$.

Solution. From the solution to Example 7.3.3,

$$\begin{Bmatrix} \dot{u} \\ \dot{w} \\ \dot{q} \\ \dot{x}_f \\ \dot{z}_f \\ \dot{\theta} \end{Bmatrix} = \begin{Bmatrix} -K_0 u^2 - K_1 w^2 - g\sin\theta - q w \\ -K_2 u w + g\cos\theta + q u \\ -K_3 u w - K_4 q u \\ u\cos\theta + w\sin\theta \\ w\cos\theta - u\sin\theta \\ q \end{Bmatrix} \tag{7.5.25}$$

Expanding relative to horizontal motion at constant speed, we use

$$\begin{Bmatrix} u(t) \\ w(t) \\ q(t) \\ x_f(t) \\ z_f(t) \\ \theta(t) \end{Bmatrix} = \begin{Bmatrix} V_o + \Delta u(t) \\ \Delta w(t) \\ \Delta q(t) \\ V_o t + \Delta x_f(t) \\ \Delta z_f(t) \\ \Delta\theta(t) \end{Bmatrix} \tag{7.5.26}$$

Using these definitions in Eq. (7.5.25) gives

$$\begin{Bmatrix} \Delta\dot{u} \\ \Delta\dot{w} \\ \Delta\dot{q} \\ V_o + \Delta\dot{x}_f \\ \Delta\dot{z}_f \\ \Delta\dot{\theta} \end{Bmatrix} = \begin{Bmatrix} -K_0(V_o+\Delta u)^2 - K_1(\Delta w)^2 - g\sin(\Delta\theta) - \Delta q\Delta w \\ -K_2(V_o+\Delta u)\Delta w + g\cos(\Delta\theta) + \Delta q(V_o+\Delta u) \\ -K_3(V_o+\Delta u)\Delta w - K_4\Delta q(V_o+\Delta u) \\ (V_o+\Delta u)\cos(\Delta\theta) + \Delta w\sin(\Delta\theta) \\ \Delta w\cos(\Delta\theta) - (V_o+\Delta u)\sin(\Delta\theta) \\ \Delta q \end{Bmatrix}$$

Retaining only first-order terms, we have

$$\begin{Bmatrix} \Delta\dot{u} \\ \Delta\dot{w} \\ \Delta\dot{q} \\ V_o + \Delta\dot{x}_f \\ \Delta\dot{z}_f \\ \Delta\dot{\theta} \end{Bmatrix} = \begin{Bmatrix} -K_0(V_o^2 + 2V_o\Delta u) - g\Delta\theta \\ -K_2V_o\Delta w + g + V_o\Delta q \\ -K_3V_o\Delta w - K_4V_o\Delta q \\ V_o + \Delta u \\ \Delta w - V_o\Delta\theta \\ \Delta q \end{Bmatrix}$$

or

$$\begin{Bmatrix} \Delta\dot{u} \\ \Delta\dot{w} \\ \Delta\dot{q} \\ \Delta\dot{x}_f \\ \Delta\dot{z}_f \\ \Delta\dot{\theta} \end{Bmatrix} = \begin{bmatrix} -2K_0V_o & 0 & 0 & 0 & 0 & -g \\ 0 & -K_2V_o & V_o & 0 & 0 & 0 \\ 0 & -K_3V_o & -K_4V_o & 0 & 0 & 0 \\ 1 & 0 & 0 & 0 & 0 & 0 \\ 0 & 1 & 0 & 0 & 0 & -V_o \\ 0 & 0 & 1 & 0 & 0 & 0 \end{bmatrix} \begin{Bmatrix} \Delta u \\ \Delta w \\ \Delta q \\ \Delta x_f \\ \Delta z_f \\ \Delta\theta \end{Bmatrix} + \begin{Bmatrix} -K_0V_o^2 \\ g \\ 0 \\ 0 \\ 0 \\ 0 \end{Bmatrix}$$

This can be written in differential operator notation as

$$\begin{bmatrix} (D+2K_0V_o) & 0 & 0 & 0 & 0 & g \\ 0 & (D+K_2V_o) & -V_o & 0 & 0 & 0 \\ 0 & K_3V_o & (D+K_4V_o) & 0 & 0 & 0 \\ -1 & 0 & 0 & D & 0 & 0 \\ 0 & -1 & 0 & 0 & D & V_o \\ 0 & 0 & -1 & 0 & 0 & D \end{bmatrix} \begin{Bmatrix} \Delta u \\ \Delta w \\ \Delta q \\ \Delta x_f \\ \Delta z_f \\ \Delta\theta \end{Bmatrix} = \begin{Bmatrix} -K_0V_o^2 \\ g \\ 0 \\ 0 \\ 0 \\ 0 \end{Bmatrix}$$

This is the linearized system of differential equations that applies to the motion of a stable projectile having small deviations from motion along a horizontal line at constant speed. For a projectile such as an arrow that has a large static margin but does not have a large lifting surface, the lift force has little effect

on the motion, and the change in aerodynamic moment with respect to angle of attack is quite large. For such projectiles, we can assume that K_2 is very small and K_3 is very large.

Setting K_2 to zero and K_3 to infinity, this system becomes

$$\begin{bmatrix} (D+2K_0V_o) & 0 & 0 & 0 & 0 & g \\ 0 & D & -V_o & 0 & 0 & 0 \\ 0 & 1 & 0 & 0 & 0 & 0 \\ -1 & 0 & 0 & D & 0 & 0 \\ 0 & -1 & 0 & 0 & D & V_o \\ 0 & 0 & -1 & 0 & 0 & D \end{bmatrix} \begin{Bmatrix} \Delta u \\ \Delta w \\ \Delta q \\ \Delta x_f \\ \Delta z_f \\ \Delta\theta \end{Bmatrix} = \begin{Bmatrix} -K_0V_o^2 \\ g \\ 0 \\ 0 \\ 0 \\ 0 \end{Bmatrix} \tag{7.5.27}$$

The appropriate initial conditions are

$$\begin{Bmatrix} \Delta u(0) \\ \Delta x_f(0) \\ \Delta z_f(0) \\ \Delta\theta(0) \end{Bmatrix} = \begin{Bmatrix} 0 \\ 0 \\ 0 \\ \Delta\theta_0 \end{Bmatrix} \tag{7.5.28}$$

From the third equation in Eq. (7.5.27),

$$\Delta w = 0 \tag{7.5.29}$$

Using this result in the second equation in Eq. (7.5.27), we have

$$\Delta q = -\frac{g}{V_o} \tag{7.5.30}$$

Using this with the last equation in Eq. (7.5.27) gives

$$D\Delta\theta = -\frac{g}{V_o}$$

Integrating and applying the fourth initial condition from Eq. (7.5.28),

$$\Delta\theta = -\frac{g}{V_o}t + C_1$$

$$\Delta\theta = \Delta\theta_0 - \frac{g}{V_o}t \tag{7.5.31}$$

Using Eqs. (7.5.29) and (7.5.31) in the fifth equation in Eq. (7.5.27) results in

$$D\Delta z_f = gt - V_o\Delta\theta_0$$

Integrating and applying the third initial condition from Eq. (7.5.28) yields

$$\Delta z_f = \frac{g}{2}t^2 - V_o\Delta\theta_0 t \tag{7.5.32}$$

Using Eq. (7.5.31) in the first equation in Eq. (7.5.27) gives

$$(D + 2K_0V_o)\Delta u = \frac{g^2}{V_o}t - K_0V_o^2 - g\Delta\theta_0$$

Integrating this subject to the first initial condition from Eq. (7.5.28) yields

$$\Delta u = \left(\frac{V_o}{2} + \frac{g\Delta\theta_0}{2K_0V_o} + \frac{g^2}{4K_0^2V_o^3}\right)\left(e^{-2K_0V_ot} - 1\right) + \frac{g^2t}{2K_0V_o^2} \tag{7.5.33}$$

Using this result in the fourth equation in Eq. (7.5.27), we have

$$D\Delta x_f = \left(\frac{V_o}{2} + \frac{g\Delta\theta_0}{2K_0V_o} + \frac{g^2}{4K_0^2V_o^3}\right)\left(e^{-2K_0V_ot} - 1\right) + \frac{g^2t}{2K_0V_o^2}$$

Integrating subject to the second initial condition from Eq. (7.5.28) gives

$$\Delta x_f = \left(\frac{V_o}{2} + \frac{g\Delta\theta_0}{2K_0V_o} + \frac{g^2}{4K_0^2V_o^3}\right)\left(\frac{1 - e^{-2K_0V_ot}}{2K_0V_o} - t\right) + \frac{g^2t^2}{4K_0V_o^2} \tag{7.5.34}$$

Applying Eqs. (7.5.29) through (7.5.34) to Eq. (7.5.26), the full solution is

$$\begin{Bmatrix} u(t) \\ w(t) \\ q(t) \\ x_f(t) \\ z_f(t) \\ \theta(t) \end{Bmatrix} = \begin{Bmatrix} V_o + \left(\frac{V_o}{2} + \frac{g\Delta\theta_0}{2K_0V_o} + \frac{g^2}{4K_0^2V_o^3}\right)\left(e^{-2K_0V_ot} - 1\right) + \frac{g^2t}{2K_0V_o^2} \\ 0 \\ -\frac{g}{V_o} \\ V_ot + \left(\frac{V_o}{2} + \frac{g\Delta\theta_0}{2K_0V_o} + \frac{g^2}{4K_0^2V_o^3}\right)\left(\frac{1 - e^{-2K_0V_ot}}{2K_0V_o} - t\right) + \frac{g^2t^2}{4K_0V_o^2} \\ \frac{g}{2}t^2 - V_o\Delta\theta_0 t \\ \Delta\theta_0 - \frac{g}{V_o}t \end{Bmatrix}$$

7.6. Force and Moment Derivatives

While computer simulations or wind tunnel tests are required for accurate determination of aerodynamic derivatives, some first-order approximations can be made analytically. Formulation of the linearized equations of motion requires evaluation of the derivatives of the aerodynamic forces and moments with respect to the translational velocity components. However, in our study of aerodynamic forces and moments, we found it convenient to express these forces and moments in terms of total airspeed,

$$V = \sqrt{u^2 + v^2 + w^2} \tag{7.6.1}$$

angle of attack,

$$\alpha = \tan^{-1}\left(\frac{w}{u}\right) \cong \frac{w}{u} \tag{7.6.2}$$

and sideslip angle,

$$\beta \cong \beta_a = \tan^{-1}\left(\frac{v}{u}\right) \cong \beta_e = \sin^{-1}\left(\frac{v}{\sqrt{u^2 + v^2 + w^2}}\right) \cong \frac{v}{u} \tag{7.6.3}$$

The change in any function, $\mathcal{F}(V,\alpha,\beta)$, with respect to axial velocity component is

$$\frac{\partial \mathcal{F}}{\partial u} = \frac{\partial \mathcal{F}}{\partial V}\frac{\partial V}{\partial u} + \frac{\partial \mathcal{F}}{\partial \alpha}\frac{\partial \alpha}{\partial u} + \frac{\partial \mathcal{F}}{\partial \beta}\frac{\partial \beta}{\partial u} \tag{7.6.4}$$

Since the angle of attack is not a function of the sideslip velocity, a change with respect to the sideslip velocity component is

$$\frac{\partial \mathcal{F}}{\partial v} = \frac{\partial \mathcal{F}}{\partial V}\frac{\partial V}{\partial v} + \frac{\partial \mathcal{F}}{\partial \beta}\frac{\partial \beta}{\partial v} \tag{7.6.5}$$

Likewise, within the approximation of Eq. (7.6.3), the sideslip angle is not a function of normal velocity, so a change with respect to normal velocity component is given by

$$\frac{\partial \mathcal{F}}{\partial w} = \frac{\partial \mathcal{F}}{\partial V}\frac{\partial V}{\partial w} + \frac{\partial \mathcal{F}}{\partial \alpha}\frac{\partial \alpha}{\partial w} \tag{7.6.6}$$

From Eq. (7.6.1),

$$\frac{\partial V}{\partial u} = \frac{u}{\sqrt{u^2 + v^2 + w^2}} \tag{7.6.7}$$

$$\frac{\partial V}{\partial v} = \frac{v}{\sqrt{u^2 + v^2 + w^2}} \tag{7.6.8}$$

$$\frac{\partial V}{\partial w} = \frac{w}{\sqrt{u^2 + v^2 + w^2}} \tag{7.6.9}$$

For small angles, Eq. (7.6.2) gives

$$\frac{\partial \alpha}{\partial u} \cong -\frac{w}{u^2} \tag{7.6.10}$$

$$\frac{\partial \alpha}{\partial w} \cong \frac{1}{u} \tag{7.6.11}$$

and Eq. (7.6.3) results in

$$\frac{\partial \beta}{\partial u} \cong -\frac{v}{u^2} \tag{7.6.12}$$

$$\frac{\partial \beta}{\partial v} \cong \frac{1}{u} \tag{7.6.13}$$

The particular body-fixed coordinate system that we are using was chosen so that at the equilibrium reference state,

$$\begin{Bmatrix} u \\ v \\ w \end{Bmatrix} = \begin{Bmatrix} V_o \\ 0 \\ 0 \end{Bmatrix} \tag{7.6.14}$$

The result given by Eq. (7.6.14) is valid only for this particular body-fixed coordinate system, which is normally referred to as the *stability axes*. This particular coordinate system was chosen specifically to make the angle of attack zero at the reference flight condition. This choice of coordinate system simplifies the results considerably, just as it did for the static analysis.

Using Eq. (7.6.14) in Eqs. (7.6.7) through (7.6.13), at the reference state, we obtain the results

$$\frac{\partial V}{\partial u} = 1 \tag{7.6.15}$$

$$\frac{\partial \alpha}{\partial w} \cong \frac{\partial \beta}{\partial v} \cong \frac{1}{V_o} \tag{7.6.16}$$

$$\frac{\partial V}{\partial v} = \frac{\partial V}{\partial w} = \frac{\partial \alpha}{\partial u} = \frac{\partial \beta}{\partial u} = 0 \tag{7.6.17}$$

Using Eqs. (7.6.15) through (7.6.17) in Eqs. (7.6.4) through (7.6.6) results in

$$\frac{\partial \mathcal{F}}{\partial u} = \frac{\partial \mathcal{F}}{\partial V} \tag{7.6.18}$$

$$\frac{\partial \mathcal{F}}{\partial v} = \frac{1}{V_o}\frac{\partial \mathcal{F}}{\partial \beta} \tag{7.6.19}$$

and

$$\frac{\partial \mathcal{F}}{\partial w} = \frac{1}{V_o}\frac{\partial \mathcal{F}}{\partial \alpha} \tag{7.6.20}$$

The forces and moments acting on an aircraft are the sum of those due to gravity, aerodynamic loading, and thrust. Figure 7.6.1a shows the body-fixed components of the force due to gravity. Figure 7.6.1b shows the body-fixed components of the aerodynamic forces and moments. Finally, the thrust force, which acts in the plane of symmetry, is shown in Fig. 7.6.2 along with the longitudinal components of the aerodynamic and gravitational forces. Combining these, the total force and moment in body-fixed coordinates are given by

$$\bar{\mathbf{F}} + \bar{\mathbf{W}} = \tfrac{1}{2}\rho V^2 S_w \begin{Bmatrix} C_X \\ C_Y \\ C_Z \end{Bmatrix} + T \begin{Bmatrix} \cos(\alpha_{T0}) \\ 0 \\ -\sin(\alpha_{T0}) \end{Bmatrix} + W \begin{Bmatrix} -\sin(\theta) \\ \sin(\phi)\cos(\theta) \\ \cos(\phi)\cos(\theta) \end{Bmatrix} \tag{7.6.21}$$

$$\bar{\mathbf{M}} = \tfrac{1}{2}\rho V^2 S_w \begin{Bmatrix} b_w C_\ell \\ \bar{c}_w C_m \\ b_w C_n \end{Bmatrix} + T \begin{Bmatrix} 0 \\ z_T \cos(\alpha_{T0}) + x_T \sin(\alpha_{T0}) \\ 0 \end{Bmatrix} \tag{7.6.22}$$

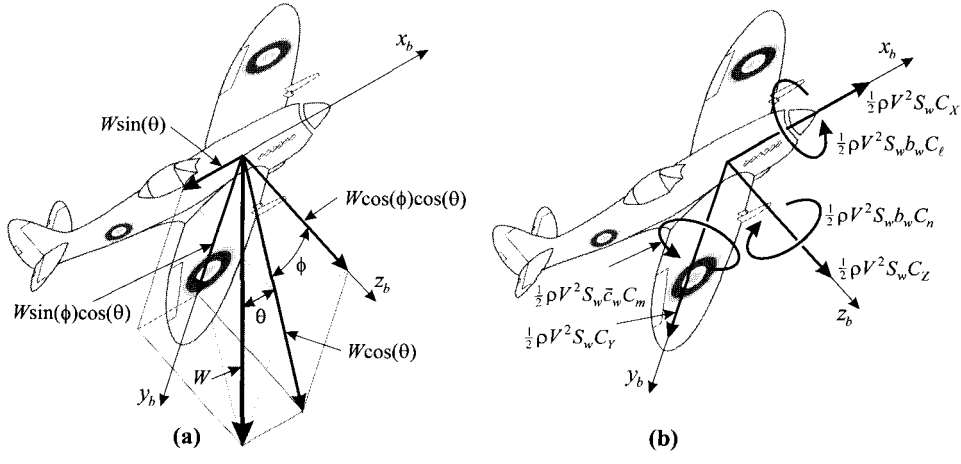


Figure 7.6.1. Gravitational and aerodynamic forces and moments in body-fixed coordinates.

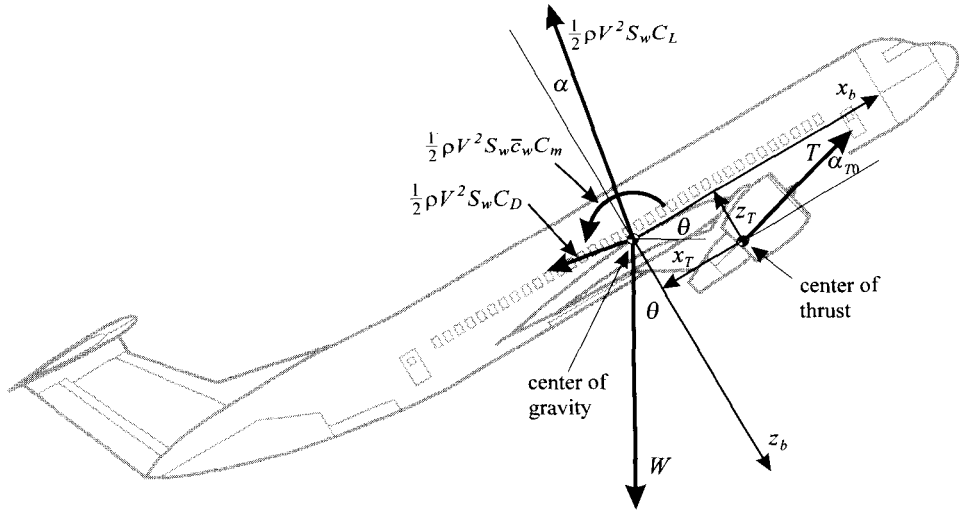


Figure 7.6.2. Longitudinal forces and moments acting in the aircraft plane of symmetry.

It is sometimes convenient to express the x_b- and z_b-components of the aerodynamic force in terms of lift and drag. As shown in Fig. 7.6.2, these two equivalent descriptions of the aerodynamic force are related through the angle of attack measured relative to the stability axes,

$$\tfrac{1}{2}\rho V^2 S_w \begin{Bmatrix} C_X \\ C_Y \\ C_Z \end{Bmatrix} = \tfrac{1}{2}\rho V^2 S_w \begin{Bmatrix} C_L \sin(\alpha) - C_D \cos(\alpha) \\ C_Y \\ -C_L \cos(\alpha) - C_D \sin(\alpha) \end{Bmatrix} \tag{7.6.23}$$

For the nonaccelerating reference state, the lift, drag, and aerodynamic pitching moment can be related to the weight and thrust. The fuselage reference line was defined so that α is zero at the equilibrium reference state. Thus at equilibrium, the drag force must balance the x_b-components of thrust and weight; the lift force must balance the z_b-components of thrust and weight; the aerodynamic pitching moment must balance the moment due to thrust; and the remaining aerodynamic force and moment components must vanish. Therefore, at the equilibrium reference state, we have

$$\tfrac{1}{2}\rho V_o^2 S_w \begin{Bmatrix} C_X \\ C_Y \\ C_Z \\ b_w C_\ell \\ \bar{c}_w C_m \\ b_w C_n \end{Bmatrix} = \tfrac{1}{2}\rho V_o^2 S_w \begin{Bmatrix} -C_D \\ 0 \\ -C_L \\ 0 \\ \bar{c}_w C_m \\ 0 \end{Bmatrix} = \begin{Bmatrix} -T\cos(\alpha_{T0}) + W\sin(\theta_o) \\ 0 \\ T\sin(\alpha_{T0}) - W\cos(\theta_o) \\ 0 \\ -z_T T\cos(\alpha_{T0}) - x_T T\sin(\alpha_{T0}) \\ 0 \end{Bmatrix} \tag{7.6.24}$$

An important and often used special case of this equilibrium force and moment balance occurs for level flight, with the thrust vector aligned with the center of gravity and the direction of flight. In this case, for nonaccelerating flight, the thrust must equal the drag; the lift must equal the weight; and the aerodynamic pitching moment must vanish along with the remaining force and moment components. The lift, weight, thrust, and drag are sometimes referred to as the *four forces of flight* and the relations *lift equals weight* and *thrust equals drag* are often used. However, we must keep in mind that these are only for the special case of steady level flight when the thrust vector is aligned with the direction of flight. A more general relation is provided by Eq. (7.6.24).

The force and moment derivatives with respect to total airspeed are obtained by differentiating Eqs. (7.6.21) and (7.6.22) with respect to V at constant angle of attack. Using Eq. (7.6.23) to replace the axial and normal coefficients, this gives

$$\begin{aligned}\frac{\partial F_{x_b}}{\partial V} &= \frac{\partial}{\partial V}\left[\tfrac{1}{2}\rho V^2 S_w C_X + T\cos(\alpha_{T0}) - W\sin(\theta)\right] \\ &= \rho V S_w\left(C_X + \frac{V}{2}\frac{\partial C_X}{\partial V}\right) + \frac{\partial T}{\partial V}\cos(\alpha_{T0}) \\ &= \rho V S_w\left[\left(C_L + \frac{V}{2}\frac{\partial C_L}{\partial V}\right)\sin(\alpha) - \left(C_D + \frac{V}{2}\frac{\partial C_D}{\partial V}\right)\cos(\alpha)\right] + \frac{\partial T}{\partial V}\cos(\alpha_{T0})\end{aligned} \tag{7.6.25}$$

$$\frac{\partial F_{y_b}}{\partial V} = \frac{\partial}{\partial V}\left[\tfrac{1}{2}\rho V^2 S_w C_Y + W\sin(\phi)\cos(\theta)\right] = \rho V S_w\left(C_Y + \frac{V}{2}\frac{\partial C_Y}{\partial V}\right) \tag{7.6.26}$$

$$\begin{aligned}\frac{\partial F_{z_b}}{\partial V} &= \frac{\partial}{\partial V}\left[\tfrac{1}{2}\rho V^2 S_w C_Z - T\sin(\alpha_{T0}) + W\cos(\phi)\cos(\theta)\right] \\ &= \rho V S_w\left(C_Z + \frac{V}{2}\frac{\partial C_Z}{\partial V}\right) - \frac{\partial T}{\partial V}\sin(\alpha_{T0}) \\ &= \rho V S_w\left[-\left(C_L + \frac{V}{2}\frac{\partial C_L}{\partial V}\right)\cos(\alpha) - \left(C_D + \frac{V}{2}\frac{\partial C_D}{\partial V}\right)\sin(\alpha)\right] - \frac{\partial T}{\partial V}\sin(\alpha_{T0})\end{aligned} \tag{7.6.27}$$

$$\frac{\partial M_{x_b}}{\partial V} = \frac{\partial}{\partial V}\left(\tfrac{1}{2}\rho V^2 S_w b_w C_\ell\right) = \rho V S_w b_w\left(C_\ell + \frac{V}{2}\frac{\partial C_\ell}{\partial V}\right) \tag{7.6.28}$$

$$\begin{aligned}\frac{\partial M_{y_b}}{\partial V} &= \frac{\partial}{\partial V}\left[\tfrac{1}{2}\rho V^2 S_w \bar{c}_w C_m + z_T T\cos(\alpha_{T0}) + x_T T\sin(\alpha_{T0})\right] \\ &= \rho V S_w \bar{c}_w\left(C_m + \frac{V}{2}\frac{\partial C_m}{\partial V}\right) + \frac{\partial T}{\partial V}\left[z_T\cos(\alpha_{T0}) + x_T\sin(\alpha_{T0})\right]\end{aligned} \tag{7.6.29}$$

$$\frac{\partial M_{z_b}}{\partial V} = \frac{\partial}{\partial V}\left(\tfrac{1}{2}\rho V^2 S_w b_w C_n\right) = \rho V S_w b_w\left(C_n + \frac{V}{2}\frac{\partial C_n}{\partial V}\right) \tag{7.6.30}$$

Remember, these derivatives are all evaluated at the reference flight condition.

The aerodynamic coefficients are generally functions of geometry, Reynolds number, and Mach number. Both the Reynolds number and the Mach number depend on the flight speed. In certain flow regimes, the effect of Reynolds number on the aerodynamic coefficients can be quite pronounced. The coefficients can change dramatically over the Reynolds number region that encompasses the transition from laminar to turbulent boundary layers. However, in other flow regimes, the effect of the Reynolds number is much less. As a result, aerodynamic coefficients are often considered to be rather weak functions of Reynolds number, R, and strong functions of the Mach number, M, and the aerodynamic angles, α and β. Furthermore, the drag coefficient, the lift coefficient, and the pitching moment coefficient can be considered functions only of R, M, and α, while the side force coefficient, the rolling moment coefficient, and the yawing moment coefficient can be taken as functions only of R, M, and β.

Aerodynamic data are generally computed analytically or collected in the wind tunnel as functions of Mach number and Reynolds number rather than the flight velocity. Thus, derivatives of the aerodynamic coefficients with respect to the flight velocity are not as convenient as derivatives with respect to Mach number and Reynolds number. However, if the Mach number and Reynolds number derivatives are known, the derivative of any aerodynamic coefficient with respect to flight velocity can easily be computed from the definition of Mach number and Reynolds number,

$$\mathrm{M} \equiv \frac{V}{a}$$

$$\mathrm{R} \equiv \frac{V l_{\mathrm{ref}}}{\nu}$$

where M is the Mach number, a is the speed of sound, R is the Reynolds number, l_{ref} is the reference length, and ν is the kinematic viscosity. From these definitions we have

$$V\frac{\partial C}{\partial V} = V\left(\frac{\partial \mathrm{M}}{\partial V}\frac{\partial C}{\partial \mathrm{M}} + \frac{\partial \mathrm{R}}{\partial V}\frac{\partial C}{\partial \mathrm{R}}\right) = V\left(\frac{1}{a}\frac{\partial C}{\partial \mathrm{M}} + \frac{l_{ref}}{\nu}\frac{\partial C}{\partial \mathrm{R}}\right) = \mathrm{M}\frac{\partial C}{\partial \mathrm{M}} + \mathrm{R}\frac{\partial C}{\partial \mathrm{R}} \qquad (7.6.31)$$

where C could be any one of the aerodynamic coefficients. In general, the derivatives of the aerodynamic coefficients with respect to Mach number and Reynolds number could be determined from wind tunnel tests or computer simulations. The results could then be used with Eq. (7.6.31) in Eqs. (7.6.25) through (7.6.30) to obtain the required derivatives with respect to forward velocity.

For applications with very low Mach number, the flow can be considered to be incompressible and the aerodynamic coefficients are independent of Mach number but may be strongly dependent on the Reynolds number. However, for most applications, the Reynolds numbers encountered in normal flight are quite large, and for large Reynolds number, the aerodynamic coefficients are nearly independent of Reynolds number. Thus, for most atmospheric flight we can neglect derivatives with respect to Reynolds number, and Eq. (7.6.31) can be approximated as

$$\frac{V}{2}\frac{\partial C}{\partial V} \cong \frac{\mathrm{M}}{2}\frac{\partial C}{\partial \mathrm{M}} \tag{7.6.32}$$

Applying Eq. (7.6.18) with Eqs. (7.6.25) through (7.6.30) and Eq. (13.7.32), **for high Reynolds number at the equilibrium reference state, the derivatives with respect to forward velocity** can be approximated as

$$\begin{aligned}
F_{x_b,u} &\equiv \frac{\partial F_{x_b}}{\partial u} = \frac{\partial F_{x_b}}{\partial V} = \rho V_o S_w\left(C_X + \frac{\mathrm{M}}{2}C_{X,\mathrm{M}}\right) + \frac{\partial T}{\partial V}\cos(\alpha_{T0}) \\
&= -\tfrac{1}{2}\rho V_o^2 S_w\left(2\frac{C_D}{V_o} + \frac{C_{D,\mathrm{M}}}{a}\right) + \frac{\partial T}{\partial V}\cos(\alpha_{T0}) \\
F_{y_b,u} &\equiv \frac{\partial F_{y_b}}{\partial u} = \frac{\partial F_{y_b}}{\partial V} = \rho V_o S_w\left(C_Y + \frac{\mathrm{M}}{2}C_{Y,\mathrm{M}}\right) = 0 \\
F_{z_b,u} &\equiv \frac{\partial F_{z_b}}{\partial u} = \frac{\partial F_{z_b}}{\partial V} = \rho V_o S_w\left(C_Z + \frac{\mathrm{M}}{2}C_{Z,\mathrm{M}}\right) - \frac{\partial T}{\partial V}\sin(\alpha_{T0}) \\
&= -\tfrac{1}{2}\rho V_o^2 S_w\left(2\frac{C_L}{V_o} + \frac{C_{L,\mathrm{M}}}{a}\right) - \frac{\partial T}{\partial V}\sin(\alpha_{T0}) \\
M_{x_b,u} &\equiv \frac{\partial M_{x_b}}{\partial u} = \frac{\partial M_{x_b}}{\partial V} = \rho V_o S_w b_w\left(C_\ell + \frac{\mathrm{M}}{2}C_{\ell,\mathrm{M}}\right) = 0 \\
M_{y_b,u} &\equiv \frac{\partial M_{y_b}}{\partial u} = \frac{\partial M_{y_b}}{\partial V} = \rho V_o S_w \bar{c}_w\left(C_m + \frac{\mathrm{M}}{2}C_{m,\mathrm{M}}\right) + z_{T0}\frac{\partial T}{\partial V} \\
&= \tfrac{1}{2}\rho V_o^2 S_w \bar{c}_w\left(2\frac{C_m}{V_o} + \frac{C_{m,\mathrm{M}}}{a}\right) + z_{T0}\frac{\partial T}{\partial V} \\
M_{z_b,u} &\equiv \frac{\partial M_{z_b}}{\partial u} = \frac{\partial M_{z_b}}{\partial V} = \rho V_o S_w b_w\left(C_n + \frac{\mathrm{M}}{2}C_{n,\mathrm{M}}\right) = 0
\end{aligned} \tag{7.6.33}$$

where z_{T0} is the perpendicular offset between the thrust vector and the CG,

$$z_{T0} \equiv z_T\cos(\alpha_{T0}) + x_T\sin(\alpha_{T0})$$

The derivatives of the aerodynamic coefficients with respect to Mach number can be determined from wind tunnel data, which are generally gathered as a function of the Mach number. The derivatives are estimated from the data using finite difference. However, the required wind tunnel tests are time consuming and expensive. Thus, for preliminary design, it is convenient to have a first-order approximation for these derivatives that can be used to estimate their values prior to wind tunnel testing.

When the flow around an airfoil section remains subsonic, thin airfoil theory with the Prandtl-Glauert compressibility correction predicts a section lift coefficient given by

$$\widetilde{C}_L = \frac{2\pi(\alpha - \alpha_{L0})}{\sqrt{1-\mathrm{M}^2}}$$

Within the limitations of thin airfoil theory, the section lift coefficient for a subsonic airfoil depends only on angle of attack, Mach number, and camber line shape.

At supersonic flight speeds, Ackeret's theory predicts that the section lift coefficient for thin airfoils at low angles of attack is determined from

$$\tilde{C}_L = \frac{4\alpha}{\sqrt{M^2 - 1}}$$

Within the accuracy of this theory, the supersonic section lift coefficient is found to be a function only of angle of attack and Mach number. Camber is predicted to have no effect on the supersonic section lift.

These theoretical results for thin airfoils in both subsonic and supersonic flow are plotted in Fig. 7.6.3. From this figure we see that the variation in lift coefficient with Mach number is negligible only for Mach numbers less than about 0.3. In the transonic region near Mach 1, both of these theories break down. There is no simple theory that is capable of predicting the variation in section lift coefficient with Mach number in the transonic region. At Mach numbers near 1, the flow around an airfoil is extremely complex and very sensitive to section shape. In the transonic region we must rely on experimental data.

At subsonic speeds, a first approximation for the variation in airplane lift coefficient with Mach number can be obtained by assuming that the Prandtl-Glauert compressibility correction for airfoils can be applied to the lift coefficient for a complete airplane. This approximation results in

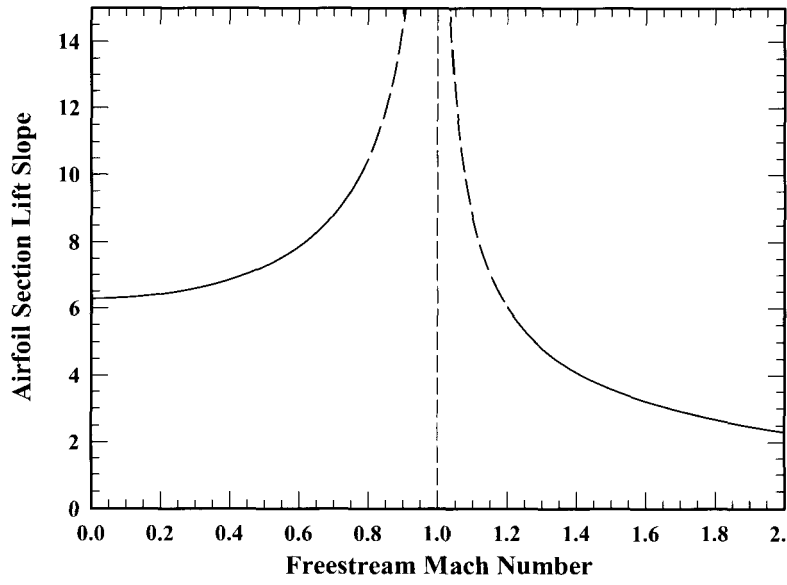


Figure 7.6.3. Theoretical lift slope for a thin airfoil as a function of freestream Mach number.

$$C_L \cong \frac{C_{L_{M=0}}}{\sqrt{1-M^2}} \tag{7.6.34}$$

where $C_{L_{M=0}}$ is the lift coefficient for incompressible flow. Equation (7.6.34) can easily be differentiated with respect to the Mach number to yield

$$C_{L,M} \cong \frac{M}{1-M^2} C_L \tag{7.6.35}$$

Equation (7.6.35) provides a reasonable first approximation for the change in lift coefficient with Mach number, which can be used in the absence of experimental data. However, it should be used with caution. Remember that Eq. (7.6.35) applies only for Mach numbers less than the critical Mach number, where sonic flow is first attained at some point around the airfoil. Furthermore, even below the critical Mach number, experimental observations show that Eq. (7.6.35) underestimates $C_{L,M}$ for some airfoil sections and overestimates it for others.

In a similar manner, subsonic thin airfoil theory predicts that the Prandtl-Glauert compressibility correction, which was used for the section lift coefficient, also applies directly to the section moment coefficient. Thus, by reasoning similar to that used for the lift coefficient, a first-order approximation for the subcritical derivative of the pitching moment coefficient with Mach number is given by

$$C_{m,M} \cong \frac{M}{1-M^2} C_m \tag{7.6.36}$$

Here again, this should be used with caution and only in absence of experimental data.

Unlike the lift and moment coefficients, which increase with subsonic Mach number, the zero-lift drag coefficient remains relatively constant with Mach number, up to the critical value at which sonic flow is first encountered at some location around the aircraft. The total drag is the zero-lift drag plus the drag due to lift. Using Eq. (7.6.34), the drag coefficient for subsonic flow can be approximated as

$$C_D = C_{D_{L0}} + C_{D_i} \cong C_{D_{L0}} + \frac{C_L^2}{\pi e R_A} \cong C_{D_{L0}} + \frac{C_{L_{M=0}}^2}{\pi e R_A (1-M^2)} \tag{7.6.37}$$

Differentiating this result with respect to Mach number gives a first approximation for the change in drag coefficient with Mach number, which can be used with caution for subcritical Mach numbers in the absence of experimental data,

$$C_{D,M} \cong \frac{2MC_{L_{M=0}}^2}{\pi e R_A (1-M^2)^2} = \frac{2M}{1-M^2} C_{D_i} \tag{7.6.38}$$

At some Mach number slightly above the critical, *drag divergence* is encountered and Eq. (7.6.38) becomes very inaccurate.

Using Eqs. (7.6.35), (7.6.36), and (7.6.38) together with the equilibrium requirement given by Eq. (7.6.24) in Eq. (7.6.33), we obtain a **first-order approximation for the derivatives with respect to forward velocity in subsonic flight**,

$$
\begin{aligned}
F_{x_b,u} &\cong -\tfrac{1}{2}\rho V_o^2 S_w\left(2+\frac{2\mathrm{M}^2}{1-\mathrm{M}^2}\frac{C_{D_i}}{C_D}\right)\frac{C_D}{V_o}+\frac{\partial T}{\partial V}\cos(\alpha_{T0}) \\
&= -\left(2+\frac{2\mathrm{M}^2}{1-\mathrm{M}^2}\frac{C_{D_i}}{C_D}\right)\frac{T\cos(\alpha_{T0})-W\sin(\theta_o)}{V_o}+\frac{\partial T}{\partial V}\cos(\alpha_{T0}) \\
F_{z_b,u} &\cong -\tfrac{1}{2}\rho V_o^2 S_w\frac{2-\mathrm{M}^2}{1-\mathrm{M}^2}\frac{C_L}{V_o}-\frac{\partial T}{\partial V}\sin(\alpha_{T0}) \\
&= -\frac{2-\mathrm{M}^2}{1-\mathrm{M}^2}\frac{W\cos(\theta_o)-T\sin(\alpha_{T0})}{V_o}-\frac{\partial T}{\partial V}\sin(\alpha_{T0}) \\
M_{y_b,u} &\cong \tfrac{1}{2}\rho V_o^2 S_w\bar{c}_w\frac{2-\mathrm{M}^2}{1-\mathrm{M}^2}\frac{C_m}{V_o}+\frac{\partial T}{\partial V}\left[z_T\cos(\alpha_{T0})+x_T\sin(\alpha_{T0})\right] \\
&= \left(-\frac{2-\mathrm{M}^2}{1-\mathrm{M}^2}\frac{T}{V_o}+\frac{\partial T}{\partial V}\right)\left[z_T\cos(\alpha_{T0})+x_T\sin(\alpha_{T0})\right] \\
F_{y_b,u} &= M_{x_b,u}=M_{z_b,u}=0
\end{aligned}
\tag{7.6.39}
$$

These approximations should only be used for subsonic flight below the critical Mach number and only for preliminary results in the absence of wind tunnel data.

In a similar manner, the force and moment derivatives with respect to angle of attack are obtained by differentiating Eqs. (7.6.21) and (7.6.22) with respect to α. Since only the axial force, the normal force, and the pitching moment depend on the angle of attack, we have

$$
\begin{aligned}
\frac{\partial F_{x_b}}{\partial\alpha} &= \frac{\partial}{\partial\alpha}\left[\tfrac{1}{2}\rho V^2 S_w C_X+T\cos(\alpha_{T0})-W\sin(\theta)\right]=\tfrac{1}{2}\rho V^2 S_w\frac{\partial C_X}{\partial\alpha} \\
&= \tfrac{1}{2}\rho V^2 S_w\left[\frac{\partial C_L}{\partial\alpha}\sin(\alpha)+C_L\cos(\alpha)-\frac{\partial C_D}{\partial\alpha}\cos(\alpha)+C_D\sin(\alpha)\right]
\end{aligned}
\tag{7.6.40}
$$

$$
\begin{aligned}
\frac{\partial F_{z_b}}{\partial\alpha} &= \frac{\partial}{\partial\alpha}\left[\tfrac{1}{2}\rho V^2 S_w C_Z-T\sin(\alpha_{T0})+W\cos(\phi)\cos(\theta)\right]=\tfrac{1}{2}\rho V^2 S_w\frac{\partial C_Z}{\partial\alpha} \\
&= \tfrac{1}{2}\rho V^2 S_w\left[-\frac{\partial C_L}{\partial\alpha}\cos(\alpha)+C_L\sin(\alpha)-\frac{\partial C_D}{\partial\alpha}\sin(\alpha)-C_D\cos(\alpha)\right]
\end{aligned}
\tag{7.6.41}
$$

$$
\begin{aligned}
\frac{\partial M_{y_b}}{\partial\alpha} &= \frac{\partial}{\partial\alpha}\left[\tfrac{1}{2}\rho V^2 S_w\bar{c}_w C_m+z_T T\cos(\alpha_{T0})+x_T T\sin(\alpha_{T0})\right] \\
&= \tfrac{1}{2}\rho V^2 S_w\bar{c}_w\frac{\partial C_m}{\partial\alpha}
\end{aligned}
\tag{7.6.42}
$$

The side force and the rolling and yawing moments do not depend on angle of attack. Thus, the derivatives of the remaining force and moment components with angle of attack are zero,

$$\frac{\partial F_{y_b}}{\partial \alpha} = \frac{\partial M_{x_b}}{\partial \alpha} = \frac{\partial M_{z_b}}{\partial \alpha} = 0$$

Using Eqs. (7.6.20), (7.6.24), and (7.6.40)-(7.6.42), the **derivatives with respect to normal velocity** evaluated at the reference flight condition are

$$\begin{aligned}
F_{x_b,w} &\equiv \frac{\partial F_{x_b}}{\partial w} = \frac{1}{V_o}\frac{\partial F_{x_b}}{\partial \alpha} = \frac{\rho V_o S_w}{2}\frac{\partial C_X}{\partial \alpha} = \frac{\rho V_o S_w}{2}\left(C_L - \frac{\partial C_D}{\partial \alpha}\right) \\
&= \frac{W\cos(\theta_o) - T\sin(\alpha_T)}{V_o} - \frac{\rho V_o S_w}{2}\frac{\partial C_D}{\partial \alpha} \\
F_{z_b,w} &\equiv \frac{\partial F_{z_b}}{\partial w} = \frac{1}{V_o}\frac{\partial F_{z_b}}{\partial \alpha} = \frac{\rho V_o S_w}{2}\frac{\partial C_Z}{\partial \alpha} = -\frac{\rho V_o S_w}{2}\left(\frac{\partial C_L}{\partial \alpha} + C_D\right) \\
&= -\frac{\rho V_o S_w}{2}\frac{\partial C_L}{\partial \alpha} - \frac{T\cos(\alpha_T) - W\sin(\theta_o)}{V_o} \\
M_{y_b,w} &\equiv \frac{\partial M_{y_b}}{\partial w} = \frac{1}{V_o}\frac{\partial M_{y_b}}{\partial \alpha} = \frac{\rho V_o S_w \bar{c}_w}{2}\frac{\partial C_m}{\partial \alpha} \\
F_{y_b,w} &= M_{z_b,w} = M_{x_b,w} = 0
\end{aligned} \tag{7.6.43}$$

Likewise, at the reference state, the **derivatives with respect to sideslip velocity** are

$$\begin{aligned}
F_{y_b,v} &\equiv \frac{\partial F_{y_b}}{\partial v} = \frac{1}{V_o}\frac{\partial F_{y_b}}{\partial \beta} = \frac{\rho V_o S_w}{2}\frac{\partial C_Y}{\partial \beta} \\
M_{x_b,v} &\equiv \frac{\partial M_{x_b}}{\partial v} = \frac{1}{V_o}\frac{\partial M_{x_b}}{\partial \beta} = \frac{\rho V_o S_w b_w}{2}\frac{\partial C_\ell}{\partial \beta} \\
M_{z_b,v} &\equiv \frac{\partial M_{z_b}}{\partial v} = \frac{1}{V_o}\frac{\partial M_{z_b}}{\partial \beta} = \frac{\rho V_o S_w b_w}{2}\frac{\partial C_n}{\partial \beta} \\
F_{x_b,v} &= F_{z_b,v} = M_{y_b,v} = 0
\end{aligned} \tag{7.6.44}$$

As we have seen previously, the aerodynamic forces and moments depend on the angular velocity components as well as the translational velocity components. As an aircraft rotates in roll, one wing moves down and experiences an increase in the z_b-component of velocity, while the other wing moves up, experiencing a decrease in the z_b-component of velocity. This results in a differential angle of attack between the two wings, as shown in Fig. 7.6.4. The rolling motion increasing the lift on the falling wing, decreases the lift on the rising wing, and creates a rolling moment that opposes the rolling rate. The change in the rolling moment with respect to the rolling rate is called the *roll-damping derivative*.

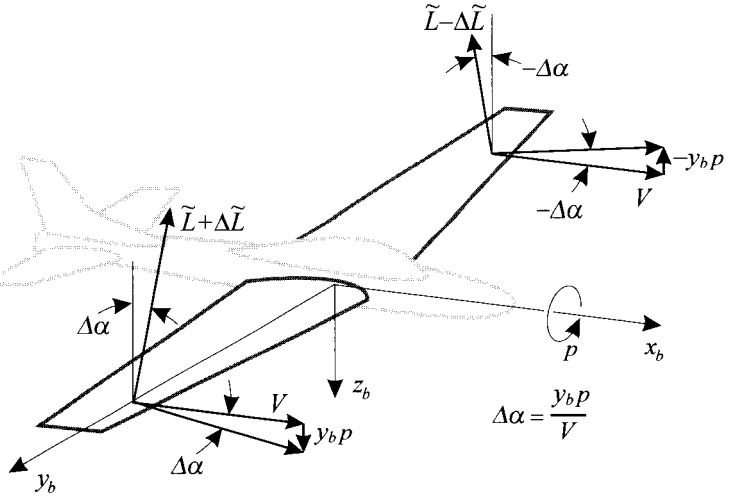


Figure 7.6.4. Effects of rolling rate on the local angle of attack and section lift.

The rolling rate also affects the yawing moment. The primary contribution to this yawing moment comes from the wing. The wing contribution arises from the increase in angle of attack on the falling wing and the decrease in angle of attack on the rising wing. Since the lift vector at any section of the wing must be perpendicular to the local freestream, the section lift vector on the falling wing $\tilde{L}+\Delta\tilde{L}$ is tilted forward and the section lift vector on the rising wing $\tilde{L}-\Delta\tilde{L}$ is tilted back, as is shown in Fig. 7.6.4. The result is the generation of a negative yawing moment from a positive rolling rate.

Using Prandtl's lifting-line theory, the change in the rolling and yawing moment coefficients with respect to rolling rate can be approximated as

$$\left(\frac{\partial C_\ell}{\partial p}\right)_{\text{wing}} \cong -\frac{\kappa_{\ell\bar{p}} b_w}{16 V_o}\frac{\partial C_{L_w}}{\partial \alpha} \tag{7.6.45}$$

$$\left(\frac{\partial C_n}{\partial p}\right)_{\text{wing}} \cong -\left(1-\frac{3\kappa_{\ell\bar{p}}}{\pi R_{A_w}}\frac{\partial C_{L_w}}{\partial \alpha}\right)\frac{b_w C_{L_w}}{16 V_o} \tag{7.6.46}$$

where b_w, R_{Aw}, and C_{Lw} are, respectively, the wingspan, aspect ratio, and lift coefficient for the wing at the equilibrium reference state. The coefficient $\kappa_{\ell\bar{p}}$ depends on wing planform and aspect ratio as described in Sec. 1.8 and shown in Fig. 1.8.25. Both the horizontal and vertical tail also contribute to the change in the rolling and yawing moments with respect to rolling rate. However, the tail contribution is small compared to that of the wing and is usually neglected in a first analysis.

If the wing has dihedral, then the lift differential between the right wing and the left wing that is caused by the roll rate will also produce a side force. However, this term is small and can be neglected as a first approximation.

Thus, for a first approximation, the **derivatives with respect to roll rate** evaluated at the reference flight condition are

$$
\begin{aligned}
F_{y_b,p} &\equiv \frac{\partial F_{y_b}}{\partial p} = \tfrac{1}{2}\rho V_o^2 S_w \frac{\partial C_Y}{\partial p} \cong 0 \\
M_{x_b,p} &\equiv \frac{\partial M_{x_b}}{\partial p} = \tfrac{1}{2}\rho V_o^2 S_w b_w \frac{\partial C_\ell}{\partial p} \cong -\rho V_o S_w b_w^2 \frac{\kappa_{\bar{fp}}}{32}\frac{\partial C_{L_w}}{\partial \alpha} \\
M_{z_b,p} &\equiv \frac{\partial M_{z_b}}{\partial p} = \tfrac{1}{2}\rho V_o^2 S_w b_w \frac{\partial C_n}{\partial p} \cong -\rho V_o S_w b_w^2 \left(1 - \frac{3\kappa_{\bar{fp}}}{\pi R_{A_w}}\frac{\partial C_{L_w}}{\partial \alpha}\right)\frac{C_{L_w}}{32} \\
F_{x_b,p} &= F_{z_b,p} = M_{y_b,p} = 0
\end{aligned}
\tag{7.6.47}
$$

The pitching rate affects the forces and moments on the aircraft primarily through the horizontal tail. As the aircraft rotates in pitch about the center of mass, an aft tail experiences an increase in the z_b-component of velocity that is equal to the product of the pitching rate and the distance the tail is aft of the center of mass (see Fig. 7.6.5). This increases the effective angle of attack for the horizontal tail, which produces a change in the lift force and the associated induced drag, as well as a pitching moment that opposes the pitching rate. The change in the pitching moment with respect to the pitching rate is called the *pitch-damping derivative*. The wing and the fuselage can also affect the pitch-damping derivative, but these effects are small and are often neglected in a first analysis.

The lift produced by the horizontal tail of a pitching aircraft is proportional to the local angle of attack, which is the sum of the geometric angle of attack and the angle of attack that is induced by the pitching rate $(-x_{bh}\,q/V_o)$. Thus, we can write

$$
\left(\frac{\partial C_Z}{\partial q}\right)_{\text{tail}} \cong \eta_h \frac{S_h x_{bh}}{S_w V_o}\frac{\partial C_{L_h}}{\partial \alpha} \tag{7.6.48}
$$

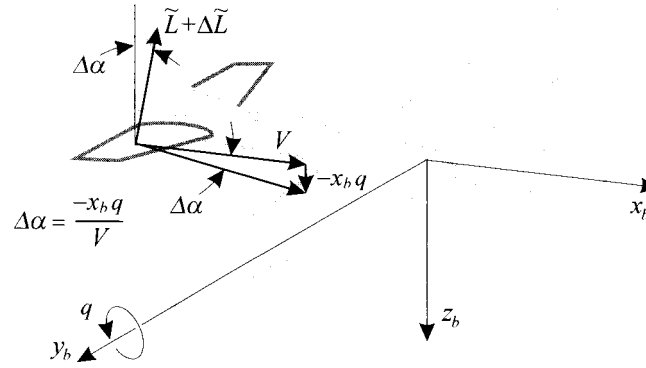


Figure 7.6.5. Effects of pitching rate on the local angle of attack at the tail.

and

$$\left(\frac{\partial C_m}{\partial q}\right)_{\text{tail}} \cong -\eta_h \frac{S_h x_{bh}^2}{S_w V_o \bar{c}_w} \frac{\partial C_{L_h}}{\partial \alpha} \tag{7.6.49}$$

where η_h, S_h, and x_{bh} are, respectively, the efficiency factor, area, and x_b-coordinate of the aerodynamic center for the horizontal tail. Because the pitching rate changes the lift on the horizontal tail, it also changes the induced drag. However, this effect is small and is usually neglected in a first analysis. The wing is included in the same manner.

As a first approximation the **derivatives with respect to pitch rate** evaluated at the reference flight condition are then given by

$$\begin{aligned}
F_{x_b,q} &\equiv \frac{\partial F_{x_b}}{\partial q} = -\tfrac{1}{2}\rho V_o^2 S_w \frac{\partial C_D}{\partial q} \cong 0 \\
F_{z_b,q} &\equiv \frac{\partial F_{z_b}}{\partial q} = -\tfrac{1}{2}\rho V_o^2 S_w \frac{\partial C_L}{\partial q} \cong \tfrac{1}{2}\rho V_o \left(S_w x_{bw} \frac{\partial C_{L_w}}{\partial \alpha} + \eta_h S_h x_{bh} \frac{\partial C_{L_h}}{\partial \alpha} \right) \\
M_{y_b,q} &\equiv \frac{\partial M_{y_b}}{\partial q} = \tfrac{1}{2}\rho V_o^2 S_w \bar{c}_w \frac{\partial C_m}{\partial q} \cong -\tfrac{1}{2}\rho V_o \left(S_w x_{bw}^2 \frac{\partial C_{L_w}}{\partial \alpha} + \eta_h S_h x_{bh}^2 \frac{\partial C_{L_h}}{\partial \alpha} \right) \\
F_{y_b,q} &= M_{x_b,q} = M_{z_b,q} = 0
\end{aligned} \tag{7.6.50}$$

In a similar manner, the yawing rate affects the side force, the rolling moment, and the yawing moment by changing the effective sideslip angle for the vertical tail, as shown in Fig. 7.6.6. Thus we have

$$\left(\frac{\partial C_Y}{\partial r}\right)_{\text{tail}} \cong -\eta_v \frac{S_v x_{bv}}{S_w V_o} \frac{\partial C_{L_v}}{\partial \beta} \tag{7.6.51}$$

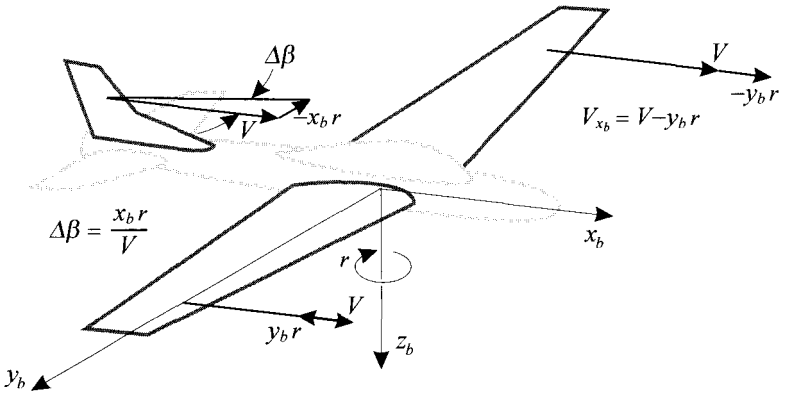


Figure 7.6.6. Effects of yawing rate on the sideslip angle at the tail and the local forward velocity of the wings.

$$\left(\frac{\partial C_\ell}{\partial r}\right)_{\text{tail}} \cong \eta_v \frac{S_v x_{bv} z_{bv}}{S_w b_w V_o} \frac{\partial C_{L_v}}{\partial \beta} \tag{7.6.52}$$

and

$$\left(\frac{\partial C_n}{\partial r}\right)_{\text{tail}} \cong -\eta_v \frac{S_v x_{bv}^2}{S_w b_w V_o} \frac{\partial C_{L_v}}{\partial \beta} \tag{7.6.53}$$

where η_v, S_v, x_{bv}, and z_{bv} are, respectively, the efficiency factor, area, x_b-coordinate, and z_b-coordinate of the aerodynamic center for the vertical tail. The change in the yawing moment with respect to the yawing rate is called the *yaw-damping derivative.*

The main wing also makes a significant contribution to the change in the rolling moment with respect to the yawing rate. If the airplane is rotating with a positive yawing rate, the forward speed of the left wing is increased and the forward speed of the right wing is decreased, as shown is in Fig. 7.6.6. This increases the lift on the left wing and decreases the lift on the right wing, creating a positive rolling moment. Again using Prandtl's lifting-line theory, the change in the wing's rolling moment coefficients with respect to yawing rate can be approximated as

$$\left(\frac{\partial C_\ell}{\partial r}\right)_{\text{wing}} \cong -2\left(\frac{\partial C_n}{\partial p}\right)_{\text{wing}} \cong \left(1 - \frac{3\kappa_{\ell\overline{p}}}{\pi R_{A_w}} \frac{\partial C_{L_w}}{\partial \alpha}\right) \frac{b_w C_{L_w}}{8 V_o} \tag{7.6.54}$$

Thus, at the reference state, **derivatives with respect to yaw rate** are approximated as

$$\begin{aligned}
F_{y_b,r} &\equiv \frac{\partial F_{y_b}}{\partial r} = \tfrac{1}{2}\rho V_o^2 S_w \frac{\partial C_Y}{\partial r} \cong -\tfrac{1}{2}\rho V_o \eta_v S_v x_{bv} \frac{\partial C_{L_v}}{\partial \beta} \\
M_{x_b,r} &\equiv \frac{\partial M_{x_b}}{\partial r} = \tfrac{1}{2}\rho V_o^2 S_w b_w \frac{\partial C_\ell}{\partial r} \\
&\cong \tfrac{1}{2}\rho V_o \left[\left(1 - \frac{3\kappa_{\ell\overline{p}}}{\pi R_{A_w}} \frac{\partial C_{L_w}}{\partial \alpha}\right) \frac{S_w b_w^2 C_{L_w}}{8} + \eta_v S_v x_{bv} z_{bv} \frac{\partial C_{L_v}}{\partial \beta}\right] \\
M_{z_b,r} &\equiv \frac{\partial M_{z_b}}{\partial r} = \tfrac{1}{2}\rho V_o^2 S_w b_w \frac{\partial C_n}{\partial r} \cong -\tfrac{1}{2}\rho V_o \eta_v S_v x_{bv}^2 \frac{\partial C_{L_v}}{\partial \beta} \\
F_{x_b,r} &= F_{z_b,r} = M_{y_b,r} = 0
\end{aligned} \tag{7.6.55}$$

As previously discussed, the longitudinal forces and the pitching moment also vary with translational acceleration, because a change in the vorticity generated by the wing requires a finite time to alter the downwash on the tail and fuselage. The aerodynamic derivatives with respect to the translational acceleration components are quite complex, depending on the shape and position of the wing, the tail, and the fuselage. In general, these derivatives would need to be determined from an unsteady fluid flow analysis. However, for a first estimate, the following quasi-steady approximations may be used with some caution.

From Prandtl's lifting-line theory, the downwash angle behind an elliptic wing in steady flight can be approximated as

$$\varepsilon_d \cong \frac{V_d}{V_o} \cong \frac{2S_w}{\pi b_w^2} C_{L_w} \tag{7.6.56}$$

The time required for the downwash generated by the wing to reach the tail is the distance from the wing to the tail, l_{wt}, divided by the forward velocity, V (see Fig. 7.6.7). During unsteady flight, this time lag can be approximated as $\Delta t = l_{wt}/V_o$ and the downwash angle at the tail can be approximated as

$$\begin{aligned} \varepsilon_d &\cong \frac{2S_w}{\pi b_w^2}\left(C_{L_w} - \frac{\partial C_{L_w}}{\partial t}\Delta t\right) = \frac{2S_w}{\pi b_w^2}\left(C_{L_w} - \frac{\partial C_{L_w}}{\partial t}\frac{l_{wt}}{V_o}\right) \\ &= \frac{2S_w}{\pi b_w^2}\left(C_{L_w} - \frac{\partial C_{L_w}}{\partial \alpha}\frac{\partial \alpha}{\partial t}\frac{l_{wt}}{V_o}\right) \end{aligned} \tag{7.6.57}$$

From Eq. (7.6.2),

$$\frac{\partial \alpha}{\partial t} = \frac{\partial \alpha}{\partial w}\frac{\partial w}{\partial t} + \frac{\partial \alpha}{\partial u}\frac{\partial u}{\partial t} \tag{7.6.58}$$

or using Eqs. (7.6.16) and (7.6.17),

$$\frac{\partial \alpha}{\partial t} = \frac{1}{V_o}\frac{\partial w}{\partial t} \equiv \frac{1}{V_o}\dot{w} \tag{7.6.59}$$

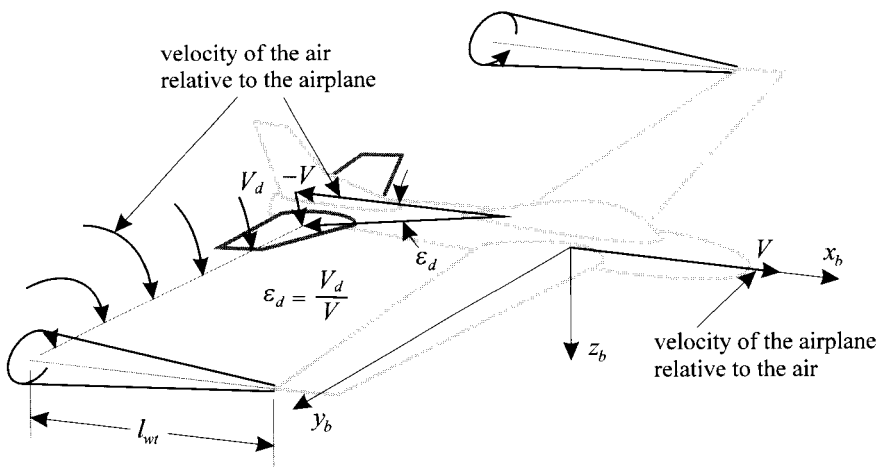


Figure 7.6.7. Effects of downwash from the wingtip vortices acting on the tail.

Using Eq. (7.6.59) in Eq. (7.6.57), we have

$$\varepsilon_d = \frac{2S_w}{\pi b_w^2}\left(C_{L_w} - \frac{\partial C_{L_w}}{\partial \alpha}\frac{l_{wf}}{V_o^2}\dot{w}\right) \tag{7.6.60}$$

The lift produced by the horizontal tail is proportional to its local angle of attack, which is the geometric angle of attack less the downwash angle,

$$(L)_{\text{tail}} = \eta_h\left(\tfrac{1}{2}\rho V_o^2 S_h\right)\frac{\partial C_{L_h}}{\partial \alpha}(\alpha_t - \varepsilon_d) \tag{7.6.61}$$

or in view of Eq. (7.6.60),

$$(L)_{\text{tail}} = \eta_h\left(\tfrac{1}{2}\rho V_o^2 S_h\right)\frac{\partial C_{L_h}}{\partial \alpha}\left[\alpha_t - \frac{2S_w}{\pi b_w^2}\left(C_{L_w} - \frac{\partial C_{L_w}}{\partial \alpha}\frac{l_{wf}}{V_o^2}\dot{w}\right)\right] \tag{7.6.62}$$

The pitching moment produced by the tail is the product of the lift developed on the horizontal tail and the moment arm between the aerodynamic center of the horizontal tail and the aircraft center of gravity,

$$\begin{aligned}(M_{y_b})_{\text{tail}} &= x_{bh}(L)_{\text{tail}} \\ &= \eta_h\left(\tfrac{1}{2}\rho V_o^2 S_h\right)\frac{\partial C_{L_h}}{\partial \alpha}\left[\alpha_t - \frac{2S_w}{\pi b_w^2}\left(C_{L_w} - \frac{\partial C_{L_w}}{\partial \alpha}\frac{l_{wf}}{V_o^2}\dot{w}\right)\right]x_{bh}\end{aligned} \tag{7.6.63}$$

Differentiating Eqs. (7.6.62) and (7.6.63) with respect to the normal acceleration, we have an approximation for the contribution that the horizontal tail makes to the change in normal force with respect to normal acceleration,

$$\left(\frac{\partial F_{z_h}}{\partial \dot{w}}\right)_{\text{tail}} = -\left(\frac{\partial L}{\partial \dot{w}}\right)_{\text{tail}} = -\eta_h\frac{\rho S_w S_h l_{wf}}{\pi b_w^2}\frac{\partial C_{L_w}}{\partial \alpha}\frac{\partial C_{L_h}}{\partial \alpha} \tag{7.6.64}$$

and the change in pitching moment with respect to normal acceleration,

$$\left(\frac{\partial M_{y_b}}{\partial \dot{w}}\right)_{\text{tail}} = \eta_h\frac{\rho S_w S_h l_{wf} x_{bh}}{\pi b_w^2}\frac{\partial C_{L_w}}{\partial \alpha}\frac{\partial C_{L_h}}{\partial \alpha} \tag{7.6.65}$$

To obtain an estimate of these derivatives for the complete aircraft, including the effects of the wing-fuselage interaction, it is recommended that these values be increased by 10 percent for an airplane with an aft tail and set to zero for an airplane with a forward canard. As a first approximation, the remaining longitudinal derivatives with respect to the translational acceleration components are usually assumed to be zero.

Thus, as a first estimate, the **longitudinal derivatives with respect to translational acceleration** can be approximated as

$$
\begin{aligned}
&F_{x_b,\dot{u}} \cong F_{z_b,\dot{u}} \cong M_{y_b,\dot{u}} \cong F_{x_b,\dot{w}} \cong 0 \\
&F_{z_b,\dot{w}} \equiv \frac{\partial F_{z_b}}{\partial \dot{w}} = \frac{1}{V_o}\frac{\partial F_{z_b}}{\partial \dot{\alpha}} = -\frac{\frac{1}{2}\rho V_o^2 S_w}{V_o}\frac{\partial C_L}{\partial \dot{\alpha}} \\
&\qquad \cong -\eta_h \frac{\rho S_w S_h l_{wt}}{\pi b_w^2}\frac{\partial C_{L_w}}{\partial \alpha}\frac{\partial C_{L_h}}{\partial \alpha} \\
&M_{y_b,\dot{w}} \equiv \frac{\partial M_{y_b}}{\partial \dot{w}} = \frac{1}{V_o}\frac{\partial M_{y_b}}{\partial \dot{\alpha}} = \frac{\frac{1}{2}\rho V_o^2 S_w \bar{c}_w}{V_o}\frac{\partial C_m}{\partial \dot{\alpha}} \\
&\qquad \cong \eta_H \frac{\rho S_w S_h l_{wt} x_{bh}}{\pi b_w^2}\frac{\partial C_{L_w}}{\partial \alpha}\frac{\partial C_{L_h}}{\partial \alpha} \\
&l_{wt} = \begin{cases} 1.1(x_{bw} - x_{bh}), & x_{bw} > x_{bh} \\ 0.0, & x_{bh} > x_{bw} \end{cases}
\end{aligned}
\tag{7.6.66}
$$

As previously mentioned, all of the **lateral derivatives with respect to translational acceleration are either zero or negligible.**

All of the aerodynamic derivatives that appear in the linearized equations of motion are complex functions of the shape and placement of the wing, tail, fuselage, and engines. For any given aircraft, these derivatives also vary with airspeed and other operating conditions. In general, these derivatives will need to be determined either from computer simulations or from wind tunnel tests. However, as a first estimate, the approximations given in this section may be used.

EXAMPLE 7.6.1. A large jet transport is flying at 30,000 ft with a steady level airspeed of 450 mph, which is the minimum drag airspeed for this altitude. This airplane has the following properties in cruise configuration:

$$
\begin{gathered}
S_w = 5{,}500 \text{ ft}^2, \quad b_w = 196 \text{ ft}, \quad \bar{c}_w = 28 \text{ ft}, \quad x_{bw} = 0, \quad C_{L_w,\alpha} = 4.67, \\
S_h = 1{,}300 \text{ ft}^2, \quad x_{bh} = -100 \text{ ft}, \quad l_{wt} = 55 \text{ ft}, \quad C_{L_h,\alpha} = 3.50, \\
W = 636{,}600 \text{ lbf}, \quad C_{L,\alpha} = 5.50, \quad C_{m,\alpha} = -1.26
\end{gathered}
$$

The maximum lift-to-drag ratio is 14. Assuming constant thrust aligned with the direction of flight and the center of gravity, estimate all dimensional longitudinal aerodynamic derivatives that appear in the homogeneous form of Eq. (7.5.23).

Solution. For this airplane the airspeed and the Mach number are

$$
V_o = 450\frac{5{,}280}{3{,}600} \text{ ft/sec} = 660 \text{ ft/sec}
$$

$$\mathrm{M} = \frac{V_o}{a} = \frac{660 \text{ ft/sec}}{994.85 \text{ ft/sec}} = 0.663$$

At the minimum drag airspeed the lift-to-drag ratio is equal to the maximum lift-to-drag ratio, and since the thrust is aligned with direction of flight, we have

$$\alpha_T = 0, \qquad L = W,$$
$$T = D = \frac{L}{L/D} = \frac{W}{L/D} = \frac{636{,}600 \text{ lbf}}{14} = 45{,}470 \text{ lbf}$$

At the minimum drag airspeed, the drag due to lift is approximately equal to the zero-lift drag. Thus, the drag due to lift is about half the total drag. Since we are assuming constant thrust, from Eq. (7.6.39), this level flight reference state gives

$$F_{x_b,u} \cong -\left(2 + \frac{2\mathrm{M}^2}{1-\mathrm{M}^2}\frac{C_{D_i}}{C_D}\right)\frac{T}{V_o} = -\left(2 + \frac{2(0.663)^2}{1-(0.663)^2}\frac{1}{2}\right)\frac{45{,}470 \text{ lbf}}{660 \text{ ft/sec}}$$
$$= \underline{-192 \text{ lbf}\cdot\text{sec/ft}}$$

$$F_{z_b,u} \cong -\frac{2-\mathrm{M}^2}{1-\mathrm{M}^2}\frac{W}{V_o} = -\left(\frac{2-(0.663)^2}{1-(0.663)^2}\right)\frac{636{,}600 \text{ lbf}}{660 \text{ ft/sec}} = \underline{-2{,}686 \text{ lbf}\cdot\text{sec/ft}}$$

Since the thrust is aligned with the direction of flight and the center of gravity, also from Eq. (7.6.39),

$$\alpha_{T0} = 0, \qquad z_T = 0,$$
$$M_{y_b,u} \cong -\frac{2-\mathrm{M}^2}{1-\mathrm{M}^2}\frac{T}{V_o}\left[z_T\cos(\alpha_{T0}) + x_T\sin(\alpha_{T0})\right] = \underline{0.0}$$

Since the total drag is the zero-lift drag plus the drag due to lift, the drag coefficient for subsonic flow can be approximated as

$$C_D = C_{D_{L0}} + C_{D_i} \cong C_{D_{L0}} + \frac{C_L^2}{\pi e R_A}$$

and the change in C_D with respect to angle of attack is approximated as

$$\frac{\partial C_D}{\partial \alpha} \cong \frac{2C_L}{\pi e R_A}\frac{\partial C_L}{\partial \alpha} = \frac{2C_{D_i}}{C_L}\frac{\partial C_L}{\partial \alpha}$$

At the minimum drag airspeed, the drag due to lift is approximately equal to the zero-lift drag. Thus, the drag due to lift is about half the total drag and

$$\frac{\partial C_D}{\partial \alpha} \cong \frac{2C_{D_i}}{C_L}\frac{\partial C_L}{\partial \alpha} \cong \frac{C_D}{C_L}\frac{\partial C_L}{\partial \alpha} = \frac{5.50}{14} = 0.393$$

Thus, from Eq. (7.6.43),

$$\begin{aligned} F_{x_b,w} &= \frac{W}{V_o} - \frac{\rho V_o S_w}{2}\frac{\partial C_D}{\partial \alpha} \\ &= \frac{636{,}600 \text{ lbf}}{660 \text{ ft/sec}} - \frac{0.00089068 \text{ slug/ft}^3 (660 \text{ ft/sec})(5{,}500 \text{ ft}^2)}{2} 0.393 \\ &= \underline{329 \text{ lbf}\cdot\text{sec/ft}} \end{aligned}$$

$$\begin{aligned} F_{z_b,w} &= -\frac{\rho V_o S_w}{2}\frac{\partial C_L}{\partial \alpha} - \frac{T}{V_o} \\ &= -\frac{0.00089068 \text{ slug/ft}^3 (660 \text{ ft/sec})(5{,}500 \text{ ft}^2)}{2} 5.50 - \frac{45{,}470 \text{ lbf}}{660 \text{ ft/sec}} \\ &= \underline{-8{,}960 \text{ lbf}\cdot\text{sec/ft}} \end{aligned}$$

$$\begin{aligned} M_{y_b,w} &= \frac{\rho V_o S_w \bar{c}_w}{2}\frac{\partial C_m}{\partial \alpha} \\ &= \frac{0.00089068 \text{ slug/ft}^3 (660 \text{ ft/sec})(5{,}500 \text{ ft}^2)(28 \text{ ft})}{2}(-1.26) \\ &= \underline{-57{,}033 \text{ lbf}\cdot\text{sec}} \end{aligned}$$

From Eq. (7.6.50), assuming $\eta_h = 1.0$, the derivatives with pitching rate are

$$F_{x_b,q} \cong \underline{0.0}$$

$$\begin{aligned} F_{z_b,q} &\cong \tfrac{1}{2}\rho V_o\left(S_w x_{bw}\frac{\partial C_{L_w}}{\partial \alpha} + \eta_h S_h x_{bh}\frac{\partial C_{L_h}}{\partial \alpha}\right) \\ &= \frac{0.00089068 \text{ slug/ft}^3 (660 \text{ ft/sec})}{2}\left[0.0 + 1.0(1{,}300 \text{ ft}^2)(-100 \text{ ft})3.50\right] \\ &= \underline{-133{,}700 \text{ lbf}\cdot\text{sec}} \end{aligned}$$

$$\begin{aligned} M_{y_b,q} &\cong -\tfrac{1}{2}\rho V_o\left(S_w x_{bw}^2\frac{\partial C_{L_w}}{\partial \alpha} + \eta_h S_h x_{bh}^2\frac{\partial C_{L_h}}{\partial \alpha}\right) \\ &= -\frac{0.00089068 \text{ slug/ft}^3 (660 \text{ ft/sec})}{2}\left[0.0 + 1.0(1{,}300 \text{ ft}^2)(-100 \text{ ft})^2 3.50\right] \\ &= \underline{-13{,}370{,}000 \text{ ft}\cdot\text{lbf}\cdot\text{sec}} \end{aligned}$$

From Eq. (7.6.66), the derivatives with respect to translational acceleration are

$$F_{x_b,\dot{u}} \cong F_{z_b,\dot{u}} \cong M_{y_b,\dot{u}} \cong F_{x_b,\dot{w}} \cong \underline{0.0}$$

$$F_{z_b,\dot{w}} \cong -\eta_h \frac{\rho S_w S_h l_{wt}}{\pi b_w^2} \frac{\partial C_{L_w}}{\partial \alpha} \frac{\partial C_{L_h}}{\partial \alpha}$$

$$= -1.0 \frac{0.00089068 \text{ slug/ft}^3 (5{,}500 \text{ ft}^2)(1{,}300 \text{ ft}^2)(55 \text{ ft})}{\pi (196 \text{ ft})^2} (4.67)(3.50)$$

$$= \underline{-47.4 \text{ slugs}}$$

$$M_{y_b,\dot{w}} \cong \eta_h \frac{\rho S_w S_h l_{wt} x_{bh}}{\pi b_w^2} \frac{\partial C_{L_w}}{\partial \alpha} \frac{\partial C_{L_h}}{\partial \alpha}$$

$$= 1.0 \frac{0.00089068 \text{ slug/ft}^3 (5{,}500 \text{ ft}^2)(1{,}300 \text{ ft}^2)(55 \text{ ft})(-100 \text{ ft})}{\pi (196 \text{ ft})^2} (4.67)(3.50)$$

$$= \underline{-4{,}740 \text{ slugs} \cdot \text{ft}}$$

Notice that for this example, the effect of the translational acceleration derivative on the z_b-component of the translational momentum equation is essentially equivalent to adding about 1,500 pounds of weight to the aircraft. This is hardly significant for an airplane that weights more than 300 tons. On the other hand, its effect on the pitching component of the angular momentum equation could be significant.

7.7. Nondimensional Linearized Equations of Motion

We can see from the results presented in the preceding section that even within the approximation of linear aerodynamics, most of the force and moment derivatives needed to fill out the matrices in Eqs. (7.5.23) and (7.5.24) are functions of airspeed and/or elevation angle as well as aircraft design. Furthermore, many of the derivatives in these linearized equations of motion are dimensional and thus dependent on the system of units being used. It is often more convenient to rearrange the equations of motion in a nondimensional form so that, as much as possible, the nondimensional force and moment derivatives are independent of airspeed, at least within the accuracy of the approximations used for linear aerodynamics.

To nondimensionalize the independent and dependent variables, we require only a characteristic length and velocity. One half the mean wing chord length is normally used as the characteristic length for longitudinal motion, and the wing semispan is ordinarily used as the characteristic length for the lateral motion. The equilibrium airspeed is quite naturally chosen as the characteristic velocity for both longitudinal and lateral motion. Thus, the three components of velocity disturbance are readily nondimensionalized with respect to the reference velocity. Within the approximation of small disturbance theory, the normal velocity disturbance divided by the reference velocity is simply the disturbance in angle of attack and the sideslip velocity disturbance divided by the reference velocity is the sideslip angle disturbance.

Thus, nondimensionalizing the three velocity components in this manner introduces only one new nondimensional variable, and we have

$$\begin{aligned} \Delta\mu &\equiv \frac{\Delta u}{V_o} \\ \Delta\beta &\cong \frac{\Delta v}{V_o} \\ \Delta\alpha &\cong \frac{\Delta w}{V_o} \end{aligned} \tag{7.7.1}$$

Angular velocity has dimensions of inverse time and is nondimensionalized with respect to the characteristic velocity divided by the characteristic length. Since we are using different characteristic lengths for longitudinal and lateral motion, we use

$$\begin{aligned} \Delta\hat{\alpha} &\equiv \frac{\Delta\dot{\alpha}\,\bar{c}_w}{2V_o} \\ \Delta\overline{p} &\equiv \frac{\Delta p\, b_w}{2V_o} \\ \Delta\overline{q} &\equiv \frac{\Delta q\,\bar{c}_w}{2V_o} \\ \Delta\overline{r} &\equiv \frac{\Delta r\, b_w}{2V_o} \end{aligned} \tag{7.7.2}$$

In a similar manner, the disturbances in aircraft position are nondimensionalized as

$$\begin{aligned} \Delta\xi_x &\equiv \frac{2\Delta x_f}{\bar{c}_w} \\ \Delta\xi_y &\equiv \frac{2\Delta y_f}{b_w} \\ \Delta\xi_z &\equiv \frac{2\Delta z_f}{\bar{c}_w} \end{aligned} \tag{7.7.3}$$

The Euler angles are already dimensionless, so no change in variables is required for describing the aircraft orientation.

Time is nondimensionalized with respect to the characteristic length divided by the characteristic velocity. Again, since we are using different characteristic lengths for longitudinal and lateral motion, the dimensionless time for longitudinal motion, τ_x, is not the same as the dimensionless time for lateral motion, τ_y,

$$\begin{aligned} \tau_x &\equiv \frac{2V_o t}{\bar{c}_w} \\ \tau_y &\equiv \frac{2V_o t}{b_w} \end{aligned} \tag{7.7.4}$$

Using the dimensionless variables that were defined in Eqs. (7.7.1) through (7.7.4), the linearized equations of motion that were given by Eqs. (7.5.23) and (7.5.24) may be written as:

the **nondimensional linearized longitudinal equations**,

$$\begin{bmatrix} (1-R_{x,\hat{u}}) & -R_{x,\hat{\alpha}} & 0 & 0 & 0 & 0 \\ -R_{z,\hat{u}} & (1-R_{z,\hat{\alpha}}) & 0 & 0 & 0 & 0 \\ -R_{m,\hat{u}} & -R_{m,\hat{\alpha}} & 1 & 0 & 0 & 0 \\ 0 & 0 & 0 & 1 & 0 & 0 \\ 0 & 0 & 0 & 0 & 1 & 0 \\ 0 & 0 & 0 & 0 & 0 & 1 \end{bmatrix} \begin{Bmatrix} \Delta\hat{u} \\ \Delta\hat{\alpha} \\ \Delta\hat{\bar{q}} \\ \Delta\hat{\xi}_x \\ \Delta\hat{\xi}_z \\ \Delta\hat{\theta} \end{Bmatrix}$$

$$= \begin{bmatrix} R_{x,\mu} & R_{x,\alpha} & R_{x,\bar{q}} & 0 & 0 & -R_{gx}\cos\theta_0 \\ R_{z,\mu} & R_{z,\alpha} & (R_{z,\bar{q}}+1) & 0 & 0 & -R_{gx}\sin\theta_0 \\ R_{m,\mu} & R_{m,\alpha} & R_{m,\bar{q}} & 0 & 0 & 0 \\ \cos\theta_o & \sin\theta_o & 0 & 0 & 0 & -\sin\theta_o \\ -\sin\theta_o & \cos\theta_o & 0 & 0 & 0 & -\cos\theta_o \\ 0 & 0 & 1 & 0 & 0 & 0 \end{bmatrix} \begin{Bmatrix} \Delta\mu \\ \Delta\alpha \\ \Delta\bar{q} \\ \Delta\xi_x \\ \Delta\xi_z \\ \Delta\theta \end{Bmatrix} + \begin{Bmatrix} R_{x,\delta_e} \\ R_{z,\delta_e} \\ R_{m,\delta_e} \\ 0 \\ 0 \\ 0 \end{Bmatrix} \Delta\delta_e \tag{7.7.5}$$

and the **nondimensional linearized lateral equations**,

$$\begin{bmatrix} 1 & 0 & 0 & 0 & 0 & 0 \\ 0 & 1 & -\iota_{xz} & 0 & 0 & 0 \\ 0 & -\iota_{zx} & 1 & 0 & 0 & 0 \\ 0 & 0 & 0 & 1 & 0 & 0 \\ 0 & 0 & 0 & 0 & 1 & 0 \\ 0 & 0 & 0 & 0 & 0 & 1 \end{bmatrix} \begin{Bmatrix} \Delta\hat{\beta} \\ \Delta\hat{\bar{p}} \\ \Delta\hat{\bar{r}} \\ \Delta\hat{\xi}_y \\ \Delta\hat{\phi} \\ \Delta\hat{\psi} \end{Bmatrix}$$

$$= \begin{bmatrix} R_{y,\beta} & R_{y,\bar{p}} & (R_{y,\bar{r}}-1) & 0 & R_{gy}\cos\theta_0 & 0 \\ R_{\ell,\beta} & R_{\ell,\bar{p}} & R_{\ell,\bar{r}} & 0 & 0 & 0 \\ R_{n,\beta} & R_{n,\bar{p}} & R_{n,\bar{r}} & 0 & 0 & 0 \\ 1 & 0 & 0 & 0 & 0 & \cos\theta_o \\ 0 & 1 & \tan\theta_o & 0 & 0 & 0 \\ 0 & 0 & \sec\theta_o & 0 & 0 & 0 \end{bmatrix} \begin{Bmatrix} \Delta\beta \\ \Delta\bar{p} \\ \Delta\bar{r} \\ \Delta\xi_y \\ \Delta\phi \\ \Delta\psi \end{Bmatrix} + \begin{bmatrix} R_{y,\delta_a} & R_{y,\delta_r} \\ R_{\ell,\delta_a} & R_{\ell,\delta_r} \\ R_{n,\delta_a} & R_{n,\delta_r} \\ 0 & 0 \\ 0 & 0 \\ 0 & 0 \end{bmatrix} \begin{Bmatrix} \Delta\delta_a \\ \Delta\delta_r \end{Bmatrix} \tag{7.7.6}$$

where we are using the notation for both longitudinal and lateral motion,

$$\hat{f} \equiv \frac{\partial f}{\partial \tau_x} \text{ for longitudinal motion and } \hat{f} \equiv \frac{\partial f}{\partial \tau_y} \text{ for lateral motion} \tag{7.7.7}$$

Here the nondimensional components of the coefficient matrices are those that arise naturally as a result of nondimensionalizing each of the 12 equations using the dimensionless variables defined in Eqs. (7.7.1) through (7.7.4). Thus we define

$$\iota_{xz} \equiv \frac{I_{xz_b}}{I_{xx_b}} \qquad \iota_{zx} \equiv \frac{I_{xz_b}}{I_{zz_b}} \qquad R_{gx} \equiv \frac{g\bar{c}_w}{2V_o^2} \qquad R_{gy} \equiv \frac{gb_w}{2V_o^2}$$

$$R_{x,\hat{u}} \equiv \frac{\rho S_w \bar{c}_w}{4W/g} C_{X,\hat{u}} \qquad R_{z,\hat{u}} \equiv \frac{\rho S_w \bar{c}_w}{4W/g} C_{Z,\hat{u}} \qquad R_{m,\hat{u}} \equiv \frac{\rho S_w \bar{c}_w^3}{8I_{yy_b}} C_{m,\hat{u}}$$

$$R_{x,\hat{\alpha}} \equiv \frac{\rho S_w \bar{c}_w}{4W/g} C_{X,\hat{\alpha}} \qquad R_{z,\hat{\alpha}} \equiv \frac{\rho S_w \bar{c}_w}{4W/g} C_{Z,\hat{\alpha}} \qquad R_{m,\hat{\alpha}} \equiv \frac{\rho S_w \bar{c}_w^3}{8I_{yy_b}} C_{m,\hat{\alpha}}$$

$$R_{x,\mu} \equiv \frac{\rho S_w \bar{c}_w}{4W/g}\left(2C_X + C_{X,\mu} + \frac{T_{,V}\cos(\alpha_{T0})}{\frac{1}{2}\rho V_o S_w}\right)$$

$$R_{z,\mu} \equiv \frac{\rho S_w \bar{c}_w}{4W/g}\left(2C_Z + C_{Z,\mu} - \frac{T_{,V}\sin(\alpha_{T0})}{\frac{1}{2}\rho V_o S_w}\right)$$

$$R_{m,\mu} \equiv \frac{\rho S_w \bar{c}_w^3}{8I_{yy_b}}\left(2C_m + C_{m,\mu} + \frac{T_{,V}[z_T\cos(\alpha_{T0}) + x_T\sin(\alpha_{T0})]}{\frac{1}{2}\rho V_o S_w \bar{c}_w}\right)$$

$$R_{x,\alpha} \equiv \frac{\rho S_w \bar{c}_w}{4W/g} C_{X,\alpha} \qquad R_{z,\alpha} \equiv \frac{\rho S_w \bar{c}_w}{4W/g} C_{Z,\alpha} \qquad R_{m,\alpha} \equiv \frac{\rho S_w \bar{c}_w^3}{8I_{yy_b}} C_{m,\alpha}$$

$$R_{y,\beta} \equiv \frac{\rho S_w b_w}{4W/g} C_{Y,\beta} \qquad R_{\ell,\beta} \equiv \frac{\rho S_w b_w^3}{8I_{xx_b}} C_{\ell,\beta} \qquad R_{n,\beta} \equiv \frac{\rho S_w b_w^3}{8I_{zz_b}} C_{n,\beta} \tag{7.7.8}$$

$$R_{y,\bar{p}} \equiv \frac{\rho S_w b_w}{4W/g} C_{Y,\bar{p}} \qquad R_{\ell,\bar{p}} \equiv \frac{\rho S_w b_w^3}{8I_{xx_b}} C_{\ell,\bar{p}} \qquad R_{n,\bar{p}} \equiv \frac{\rho S_w b_w^3}{8I_{zz_b}} C_{n,\bar{p}}$$

$$R_{x,\bar{q}} \equiv \frac{\rho S_w \bar{c}_w}{4W/g} C_{X,\bar{q}} \qquad R_{z,\bar{q}} \equiv \frac{\rho S_w \bar{c}_w}{4W/g} C_{Z,\bar{q}} \qquad R_{m,\bar{q}} \equiv \frac{\rho S_w \bar{c}_w^3}{8I_{yy_b}} C_{m,\bar{q}}$$

$$R_{y,\bar{r}} \equiv \frac{\rho S_w b_w}{4W/g} C_{Y,\bar{r}} \qquad R_{\ell,\bar{r}} \equiv \frac{\rho S_w b_w^3}{8I_{xx_b}} C_{\ell,\bar{r}} \qquad R_{n,\bar{r}} \equiv \frac{\rho S_w b_w^3}{8I_{zz_b}} C_{n,\bar{r}}$$

$$R_{y,\delta_a} \equiv \frac{\rho S_w b_w}{4W/g} C_{Y,\delta_a} \qquad R_{\ell,\delta_a} \equiv \frac{\rho S_w b_w^3}{8I_{xx_b}} C_{\ell,\delta_a} \qquad R_{n,\delta_a} \equiv \frac{\rho S_w b_w^3}{8I_{zz_b}} C_{n,\delta_a}$$

$$R_{x,\delta_e} \equiv \frac{\rho S_w \bar{c}_w}{4W/g} C_{X,\delta_e} \qquad R_{z,\delta_e} \equiv \frac{\rho S_w \bar{c}_w}{4W/g} C_{Z,\delta_e} \qquad R_{m,\delta_e} \equiv \frac{\rho S_w \bar{c}_w^3}{8I_{yy_b}} C_{m,\delta_e}$$

$$R_{y,\delta_r} \equiv \frac{\rho S_w b_w}{4W/g} C_{Y,\delta_r} \qquad R_{\ell,\delta_r} \equiv \frac{\rho S_w b_w^3}{8I_{xx_b}} C_{\ell,\delta_r} \qquad R_{n,\delta_r} \equiv \frac{\rho S_w b_w^3}{8I_{zz_b}} C_{n,\delta_r}$$

All of the dimensionless force and moment derivatives are expressed in terms of the usual force and moment coefficients and their derivatives with respect to the previously

defined dimensionless variables. Derivatives with respect to normal acceleration have been replaced by derivatives with respect to dimensionless rate of change in angle of attack. The normal and sideslip velocity derivatives are replaced with derivatives with respect to the aerodynamic angles, and the derivatives with respect to angular velocity are replaced with their nondimensional counterpart.

In this nondimensional form, many of the aerodynamic derivatives no longer depend on the airspeed. From Eq. (7.6.66), the approximate **nondimensional longitudinal derivatives with respect to translational acceleration** are

$$
\begin{aligned}
C_{X,\hat{\mu}} &\equiv \frac{\partial C_X}{\partial \hat{\mu}} \cong C_{Z,\hat{\mu}} \equiv \frac{\partial C_Z}{\partial \hat{\mu}} \cong C_{m,\hat{\mu}} \equiv \frac{\partial C_m}{\partial \hat{\mu}} \cong C_{X,\hat{\alpha}} \equiv \frac{\partial C_X}{\partial \hat{\alpha}} \cong 0 \\
C_{Z,\hat{\alpha}} &\equiv \frac{\partial C_Z}{\partial \hat{\alpha}} = -\frac{\partial C_L}{\partial \hat{\alpha}} = -\frac{2V_o}{\bar{c}_w}\frac{\partial C_L}{\partial \dot{\alpha}} \cong -\eta_h \frac{4S_h l_{wt}}{\pi b_w^2 \bar{c}_w}\frac{\partial C_{L_w}}{\partial \alpha}\frac{\partial C_{L_h}}{\partial \alpha} \\
C_{m,\hat{\alpha}} &\equiv \frac{\partial C_m}{\partial \hat{\alpha}} = \frac{2V_o}{\bar{c}_w}\frac{\partial C_m}{\partial \dot{\alpha}} \cong \eta_h \frac{4S_h l_{wt} x_{bh}}{\pi b_w^2 \bar{c}_w^2}\frac{\partial C_{L_w}}{\partial \alpha}\frac{\partial C_{L_h}}{\partial \alpha} \\
l_{wt} &= \begin{cases} 1.1(x_{bw} - x_{bh}), & x_{bw} > x_{bh} \\ 0.0, & x_{bh} > x_{bw} \end{cases}
\end{aligned}
\tag{7.7.9}
$$

In general, the aerodynamic forces and moments as well as the thrust are functions of forward velocity. However, for equilibrium flight, the change in side force with respect to forward velocity is zero. In addition, the derivatives of the rolling and yawing moments with forward velocity are also zero at equilibrium. Thus, from Eqs. (7.6.33) and (7.6.39), the **nondimensional derivatives with respect to forward velocity** are

$$
\begin{aligned}
2C_X + C_{X,\mu} + \frac{T_{,V}\cos(\alpha_{T0})}{\frac{1}{2}\rho V_o S_w} &= -2C_D - \mathrm{M}\,C_{D,\mathrm{M}} + \frac{T_{,V}\cos(\alpha_{T0})}{\frac{1}{2}\rho V_o S_w} \\
&\cong -\left(2 + \frac{2\mathrm{M}^2}{1-\mathrm{M}^2}\frac{C_{D_i}}{C_D}\right)C_D + \frac{T_{,V}\cos(\alpha_{T0})}{\frac{1}{2}\rho V_o S_w} \\
2C_Z + C_{Z,\mu} - \frac{T_{,V}\sin(\alpha_{T0})}{\frac{1}{2}\rho V_o S_w} &= -2C_L - \mathrm{M}\,C_{L,\mathrm{M}} - \frac{T_{,V}\sin(\alpha_{T0})}{\frac{1}{2}\rho V_o S_w} \\
&\cong -\left(\frac{2-\mathrm{M}^2}{1-\mathrm{M}^2}\right)C_L - \frac{T_{,V}\sin(\alpha_{T0})}{\frac{1}{2}\rho V_o S_w} \\
2C_m + C_{m,\mu} + \frac{T_{,V}[z_T\cos(\alpha_{T0}) + x_T\sin(\alpha_{T0})]}{\frac{1}{2}\rho V_o S_w \bar{c}_w} & \\
= 2C_m + \mathrm{M}\,C_{m,\mathrm{M}} + \frac{T_{,V}[z_T\cos(\alpha_{T0}) + x_T\sin(\alpha_{T0})]}{\frac{1}{2}\rho V_o S_w \bar{c}_w} & \\
\cong \left(\frac{2-\mathrm{M}^2}{1-\mathrm{M}^2}\right)C_m + \frac{T_{,V}[z_T\cos(\alpha_{T0}) + x_T\sin(\alpha_{T0})]}{\frac{1}{2}\rho V_o S_w \bar{c}_w} &
\end{aligned}
\tag{7.7.10}
$$

The stability derivatives with respect to angle of attack and sideslip angle were discussed in Chapters 4 and 5. From Eq. (7.6.43), the **nondimensional derivatives with respect to angle of attack** are

$$\begin{aligned} C_{X,\alpha} &\equiv \frac{\partial C_X}{\partial \alpha} = C_L - \frac{\partial C_D}{\partial \alpha} \\ C_{Z,\alpha} &\equiv \frac{\partial C_Z}{\partial \alpha} = -\frac{\partial C_L}{\partial \alpha} - C_D \\ C_{m,\alpha} &\equiv \frac{\partial C_m}{\partial \alpha} \end{aligned} \tag{7.7.11}$$

The pitch stability derivative, $C_{m,\alpha}$, can be estimated from the material presented in Chapter 4. From Eq. (7.6.44), the **nondimensional derivatives with respect to sideslip angle** are

$$\begin{aligned} C_{Y,\beta} &\equiv \frac{\partial C_Y}{\partial \beta} \\ C_{\ell,\beta} &\equiv \frac{\partial C_\ell}{\partial \beta} \\ C_{n,\beta} &\equiv \frac{\partial C_n}{\partial \beta} \end{aligned} \tag{7.7.12}$$

These lateral stability derivatives can be estimated from the material that was presented in Chapter 5. From Eq. (7.6.47), the approximate **nondimensional derivatives with respect to roll rate** are

$$\begin{aligned} C_{Y,\bar{p}} &\equiv \frac{\partial C_Y}{\partial \bar{p}} = \frac{2V_o}{b_w}\frac{\partial C_Y}{\partial p} \cong 0 \\ C_{\ell,\bar{p}} &\equiv \frac{\partial C_\ell}{\partial \bar{p}} = \frac{2V_o}{b_w}\frac{\partial C_\ell}{\partial p} \cong -\frac{\kappa_{\ell\bar{p}}}{8}\frac{\partial C_{L_w}}{\partial \alpha} \\ C_{n,\bar{p}} &\equiv \frac{\partial C_n}{\partial \bar{p}} = \frac{2V_o}{b_w}\frac{\partial C_n}{\partial p} \cong -\left(1 - \frac{3\kappa_{\ell\bar{p}}}{\pi R_{A_w}}\frac{\partial C_{L_w}}{\partial \alpha}\right)\frac{C_{L_w}}{8} \end{aligned} \tag{7.7.13}$$

From Eq. (7.6.50), the approximate **nondimensional derivatives with respect to pitch rate** are

$$\begin{aligned} C_{X,\bar{q}} &\equiv \frac{\partial C_X}{\partial \bar{q}} = -\frac{\partial C_D}{\partial \bar{q}} = -\frac{2V_o}{\bar{c}_w}\frac{\partial C_D}{\partial q} \cong 0 \\ C_{Z,\bar{q}} &\equiv \frac{\partial C_Z}{\partial \bar{q}} = -\frac{\partial C_L}{\partial \bar{q}} = -\frac{2V_o}{\bar{c}_w}\frac{\partial C_L}{\partial q} \cong \frac{2x_{bw}}{\bar{c}_w}\frac{\partial C_{L_w}}{\partial \alpha} + \eta_h \frac{2S_h x_{bh}}{S_w \bar{c}_w}\frac{\partial C_{L_h}}{\partial \alpha} \\ C_{m,\bar{q}} &\equiv \frac{\partial C_m}{\partial \bar{q}} = \frac{2V_o}{\bar{c}_w}\frac{\partial C_m}{\partial q} \cong -\frac{2x_{bw}^2}{\bar{c}_w^2}\frac{\partial C_{L_w}}{\partial \alpha} - \eta_h \frac{2S_h x_{bh}^2}{S_w \bar{c}_w^2}\frac{\partial C_{L_h}}{\partial \alpha} \end{aligned} \tag{7.7.14}$$

From Eq. (7.6.55), the approximate **nondimensional derivatives with respect to yaw rate** are

$$
\begin{aligned}
C_{Y,\bar{r}} &\equiv \frac{\partial C_Y}{\partial \bar{r}} = \frac{2V_o}{b_w}\frac{\partial C_Y}{\partial r} \cong -\eta_v \frac{2S_v x_{bv}}{S_w b_w}\frac{\partial C_{L_v}}{\partial \beta} \\
C_{\ell,\bar{r}} &\equiv \frac{\partial C_\ell}{\partial \bar{r}} = \frac{2V_o}{b_w}\frac{\partial C_\ell}{\partial r} \cong \left(1-\frac{3\kappa_{\ell\bar{p}}}{\pi R_{A_w}}\frac{\partial C_{L_w}}{\partial \alpha}\right)\frac{C_{L_w}}{4} + \eta_v \frac{2S_v x_{bv} z_{bv}}{S_w b_w^2}\frac{\partial C_{L_v}}{\partial \beta} \qquad (7.7.15) \\
C_{n,\bar{r}} &\equiv \frac{\partial C_n}{\partial \bar{r}} = \frac{2V_o}{b_w}\frac{\partial C_n}{\partial r} \cong -\eta_v \frac{2S_v x_{bv}^2}{S_w b_w^2}\frac{\partial C_{L_v}}{\partial \beta}
\end{aligned}
$$

Equations (7.7.5) and (7.7.6) are both nonhomogeneous systems of differential equations with constant coefficients. The general solution to such a system of equations is the sum of the homogeneous solution and a particular solution. The homogeneous solution is the solution to the system with all of the control inputs set to zero. The particular solution is any set of values for the state variables that when substituted into the nonhomogeneous system will satisfy all equations.

EXAMPLE 7.7.1. The large jet transport described in Example 7.6.1 has a pitching moment of inertia of 3.31×10^7 slug·ft^2. Using the same operating conditions and assumptions that were used in Example 7.6.1, fill out the nondimensional longitudinal coefficient matrices associated with the homogeneous form of Eq. (7.7.5).

Solution. From Example 7.6.1, for this airplane and flight condition we have

$$
\begin{gathered}
S_w = 5{,}500\ \text{ft}^2,\quad b_w = 196\ \text{ft},\quad \bar{c}_w = 28\ \text{ft},\quad x_{bw} = 0,\quad C_{L_w,\alpha} = 4.67, \\
W = 636{,}600\ \text{lbf},\quad C_{L,\alpha} = 5.50,\quad C_{m,\alpha} = -1.26,\quad C_{D,\alpha} = 0.393, \\
S_h = 1{,}300\ \text{ft}^2,\quad x_{bh} = -100\ \text{ft},\quad l_{wt} = 55\ \text{ft},\quad C_{L_h,\alpha} = 3.50, \\
V_o = 660\ \text{ft/sec},\quad \text{M} = 0.663,\quad C_L/C_D = 14,\quad C_{D_i}/C_D = 0.5, \\
I_{yy_b} = 3.31\times10^7\ \text{slug}\cdot\text{ft}^2
\end{gathered}
$$

At the minimum drag airspeed the lift-to-drag ratio is equal to the maximum lift-to-drag ratio, and since the thrust is aligned with direction of flight, we have

$$
\alpha_T = 0, \qquad L = W
$$

$$
C_L \equiv \frac{L}{\frac{1}{2}\rho V_o^2 S_w} = \frac{W}{\frac{1}{2}\rho V_o^2 S_w} = \frac{636{,}600\ \text{lbf}}{\frac{1}{2}(0.00089068\ \text{slug/ft}^3)(660\ \text{ft/sec})^2(5{,}500\ \text{ft}^2)} = 0.597
$$

$$
C_D = \frac{C_L}{C_L/C_D} = \frac{0.597}{14} = 0.0426
$$

Thus, from Eq. (7.7.9), the approximate nondimensional derivatives with respect to translational acceleration are

$$C_{X,\hat{\mu}} \cong C_{Z,\hat{\mu}} \cong C_{m,\hat{\mu}} \cong C_{X,\hat{\alpha}} \cong 0$$

$$C_{Z,\hat{\alpha}} \cong -\eta_h \frac{4S_h l_{wt}}{\pi b_w^2 \bar{c}_w} \frac{\partial C_{L_w}}{\partial \alpha} \frac{\partial C_{L_h}}{\partial \alpha} = -1.0 \frac{4(1{,}300\ \text{ft}^2)(55\ \text{ft})}{\pi (196\ \text{ft})^2 (28\ \text{ft})} (4.67) 3.50 = -1.38$$

$$C_{m,\hat{\alpha}} \cong \eta_h \frac{4S_h l_{wt} x_{bh}}{\pi b_w^2 \bar{c}_w^2} \frac{\partial C_{L_w}}{\partial \alpha} \frac{\partial C_{L_h}}{\partial \alpha} = 1.0 \frac{4(1{,}300\ \text{ft}^2)(55\ \text{ft})(-100\ \text{ft})}{\pi (196\ \text{ft})^2 (28\ \text{ft})^2} (4.67) 3.50$$
$$= -4.94$$

From Eq. (7.7.10), the approximate nondimensional derivatives with respect to forward velocity are

$$2C_X + C_{X,\mu} + \frac{T_{,V} \cos(\alpha_{T0})}{\frac{1}{2}\rho V_o S_w} = -2C_D - \mathrm{M} C_{D,\mathrm{M}} \cong -\left(2 + \frac{2\mathrm{M}^2}{1-\mathrm{M}^2} \frac{C_{D_i}}{C_D}\right) C_D$$
$$= -\left(2 + \frac{2(0.663)^2}{1-0.663^2} 0.5\right) 0.0426 = -0.1186$$

$$2C_Z + C_{Z,\mu} - \frac{T_{,V} \sin(\alpha_{T0})}{\frac{1}{2}\rho V_o S_w} = -2C_L - \mathrm{M} C_{L,\mathrm{M}} \cong -\left(\frac{2-\mathrm{M}^2}{1-\mathrm{M}^2}\right) C_L$$
$$= -\left(\frac{2-0.663^2}{1-0.663^2}\right) 0.597 = -1.662$$

and since the thrust is aligned with the center of gravity, the aerodynamic moment for the reference state must be zero:

$$2C_m + C_{m,\mu} + \frac{T_{,V}[z_T \cos(\alpha_{T0}) + x_T \sin(\alpha_{T0})]}{\frac{1}{2}\rho V_o S_w \bar{c}_w} \cong \left(\frac{2-\mathrm{M}^2}{1-\mathrm{M}^2}\right) C_m = 0.0$$

From Eq. (7.7.11), the nondimensional derivatives with respect to angle of attack are

$$C_{X,\alpha} = C_L - C_{D,\alpha} = 0.597 - 0.393 = 0.204$$

$$C_{Z,\alpha} = -C_{L,\alpha} - C_D = -5.50 - 0.0426 = -5.54$$

$$C_{m,\alpha} = -1.26$$

From Eq. (7.7.14), the nondimensional derivatives with respect to pitch rate are

$$C_{X,\bar{q}} \cong 0$$

$$C_{Z,\bar{q}} \cong \eta_h \frac{2S_h x_{bh}}{S_w \bar{c}_w} \frac{\partial C_{L_h}}{\partial \alpha} = 1.0 \frac{2(1{,}300 \text{ ft}^2)(-100 \text{ ft})}{5{,}500 \text{ ft}^2 (28 \text{ ft})} 3.50 = -5.91$$

$$C_{m,\bar{q}} \cong -\eta_h \frac{2S_h x_{bh}^2}{S_w \bar{c}_w^2} \frac{\partial C_{L_h}}{\partial \alpha} = -1.0 \frac{2(1{,}300 \text{ ft}^2)(-100 \text{ ft})^2}{5{,}500 \text{ ft}^2 (28 \text{ ft})^2} 3.50 = -21.10$$

From Eq. (7.7.8), we have

$$\frac{\rho S_w \bar{c}_w}{4W/g} = \frac{0.00089068 \text{ slug/ft}^3 (5{,}500 \text{ ft}^2)(28 \text{ ft})}{4(636{,}600/32.17) \text{ slug}} = 0.001733$$

$$\frac{\rho S_w \bar{c}_w^3}{8I_{yy_b}} = \frac{0.00089068 \text{ slug/ft}^3 (5{,}500 \text{ ft}^2)(28 \text{ ft})^3}{8(3.31 \times 10^7 \text{ slug} \cdot \text{ft}^2)} = 0.0004061$$

and

$$R_{gx} \equiv \frac{g\bar{c}_w}{2V_o^2} = \frac{32.17 \text{ ft/sec}^2 (28 \text{ ft})}{2(660 \text{ ft/sec})^2} = 0.00103$$

$$R_{x,\hat{\mu}} \equiv \frac{\rho S_w \bar{c}_w}{4W/g} C_{X,\hat{\mu}} \cong 0.0$$

$$R_{z,\hat{\mu}} \equiv \frac{\rho S_w \bar{c}_w}{4W/g} C_{Z,\hat{\mu}} \cong 0.0$$

$$R_{m,\hat{\mu}} \equiv \frac{\rho S_w \bar{c}_w^3}{8I_{yy_b}} C_{m,\hat{\mu}} \cong 0.0$$

$$R_{x,\hat{\alpha}} \equiv \frac{\rho S_w \bar{c}_w}{4W/g} C_{X,\hat{\alpha}} \cong 0.0$$

$$R_{z,\hat{\alpha}} \equiv \frac{\rho S_w \bar{c}_w}{4W/g} C_{Z,\hat{\alpha}} = 0.001733(-1.38) = -0.00239$$

$$R_{m,\hat{\alpha}} \equiv \frac{\rho S_w \bar{c}_w^3}{8I_{yy_b}} C_{m,\hat{\alpha}} = 0.0004061(-4.94) = -0.00201$$

$$R_{x,\mu} \equiv \frac{\rho S_w \bar{c}_w}{4W/g} \left(2C_X + C_{X,\mu} + \frac{T_{Y} \cos(\alpha_{T0})}{\frac{1}{2} \rho V_o S_w} \right) = 0.001733(-0.1186)$$

$$= -0.000206$$

$$R_{z,\mu} \equiv \frac{\rho S_w \bar{c}_w}{4W/g}\left(2C_Z + C_{Z,\mu} - \frac{T_{,V}\sin(\alpha_{T0})}{\frac{1}{2}\rho V_o S_w}\right) = 0.001733(-1.662)$$

$$= -0.00288$$

$$R_{m,\mu} \equiv \frac{\rho S_w \bar{c}_w^3}{8I_{yy_b}}\left(2C_m + C_{m,\mu} + \frac{T_{,V}[z_T\cos(\alpha_{T0}) + x_T\sin(\alpha_{T0})]}{\frac{1}{2}\rho V_o S_w \bar{c}_w}\right) = 0.0$$

$$R_{x,\alpha} \equiv \frac{\rho S_w \bar{c}_w}{4W/g} C_{X,\alpha} = 0.001733(0.204) = 0.000354$$

$$R_{z,\alpha} \equiv \frac{\rho S_w \bar{c}_w}{4W/g} C_{Z,\alpha} = 0.001733(-5.54) = -0.00960$$

$$R_{m,\alpha} \equiv \frac{\rho S_w \bar{c}_w^3}{8I_{yy_b}} C_{m,\alpha} = 0.0004061(-1.26) = -0.000512$$

$$R_{x,\bar{q}} \equiv \frac{\rho S_w \bar{c}_w}{4W/g} C_{X,\bar{q}} = 0.0$$

$$R_{z,\bar{q}} \equiv \frac{\rho S_w \bar{c}_w}{4W/g} C_{Z,\bar{q}} = 0.001733(-5.91) = -0.0102$$

$$R_{m,\bar{q}} \equiv \frac{\rho S_w \bar{c}_w^3}{8I_{yy_b}} C_{m,\bar{q}} = 0.0004061(-21.10) = -0.00857$$

Using these results in Eq. (7.7.5), the nondimensional form of the homogeneous linearized system of equations for longitudinal motion is

$$\begin{bmatrix} 1 & 0 & 0 & 0 & 0 & 0 \\ 0 & 1.00239 & 0 & 0 & 0 & 0 \\ 0 & 0.00201 & 1 & 0 & 0 & 0 \\ 0 & 0 & 0 & 1 & 0 & 0 \\ 0 & 0 & 0 & 0 & 1 & 0 \\ 0 & 0 & 0 & 0 & 0 & 1 \end{bmatrix} \begin{Bmatrix} \Delta\hat{\mu} \\ \Delta\hat{\alpha} \\ \Delta\hat{\bar{q}} \\ \Delta\hat{\xi}_x \\ \Delta\hat{\xi}_z \\ \Delta\hat{\theta} \end{Bmatrix}$$

$$= \begin{bmatrix} -0.000206 & 0.000354 & 0 & 0 & 0 & -0.00103 \\ -0.00288 & -0.00960 & 0.9898 & 0 & 0 & 0 \\ 0 & -0.000512 & -0.00857 & 0 & 0 & 0 \\ 1 & 0 & 0 & 0 & 0 & 0 \\ 0 & 1 & 0 & 0 & 0 & -1 \\ 0 & 0 & 1 & 0 & 0 & 0 \end{bmatrix} \begin{Bmatrix} \Delta\mu \\ \Delta\alpha \\ \Delta\bar{q} \\ \Delta\xi_x \\ \Delta\xi_z \\ \Delta\theta \end{Bmatrix}$$

7.8. Transformation of Stability Axes

In our original definition of the body-fixed coordinate system, the origin was fixed to the aircraft center of gravity; the x_b-axis was defined to point "forward" along "some convenient line" in the aircraft's plane of symmetry; and the z_b-axis was defined to point "downward" in the plane of symmetry. Thus, the y_b-axis is normal to the plane of symmetry pointing in the direction of the right wing. When developing the linearized equations of motion, we found that the most convenient orientation for the x_b-axis was pointing in the direction of the aircraft's equilibrium velocity relative to the surrounding air. This particular body-fixed coordinate system is usually called the *stability axes*.

Aligning our body-fixed coordinate system with the stability axes significantly simplifies the linearized equations of motion. However, since angle of attack is a function of aircraft operating parameters such as airspeed and elevation angle, the orientation of the stability axes within the plane of symmetry depends on the equilibrium operating conditions. The inertia tensor and the aerodynamic derivatives are measured relative to some reference body-fixed coordinate system, which may or may not be aligned with the stability axes for a given equilibrium operating condition. Thus, it is convenient to be able to transform the inertia tensor and the aerodynamic derivatives from one body-fixed coordinate system to another within the aircraft plane of symmetry.

Consider the two different body-fixed coordinate systems shown in Fig. 7.8.1. For both of these coordinate systems the x-z plane is coincident with the plane of symmetry. Thus, transformation from one of these coordinate systems to the other is a simple rotation about the y_b-axis. For an arbitrary vector, **v**, we can write

$$\begin{Bmatrix} v_{x_b} \\ v_{y_b} \\ v_{z_b} \end{Bmatrix} = \begin{bmatrix} \cos\varphi & 0 & \sin\varphi \\ 0 & 1 & 0 \\ -\sin\varphi & 0 & \cos\varphi \end{bmatrix} \begin{Bmatrix} v_{x_b'} \\ v_{y_b'} \\ v_{z_b'} \end{Bmatrix} \tag{7.8.1}$$

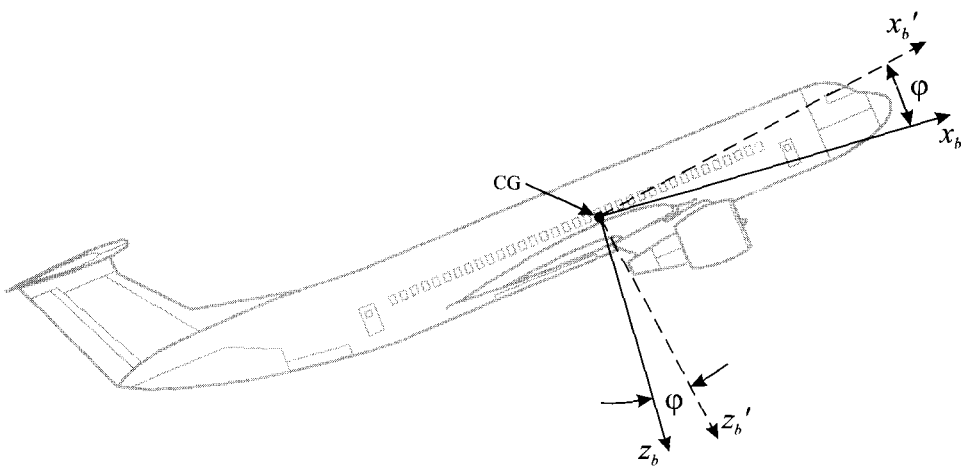


Figure 7.8.1. Two choices for the body-fixed coordinate system.

and

$$\begin{Bmatrix} v_{x_b'} \\ v_{y_b'} \\ v_{z_b'} \end{Bmatrix} = \begin{bmatrix} \cos\varphi & 0 & -\sin\varphi \\ 0 & 1 & 0 \\ \sin\varphi & 0 & \cos\varphi \end{bmatrix} \begin{Bmatrix} v_{x_b} \\ v_{y_b} \\ v_{z_b} \end{Bmatrix} \tag{7.8.2}$$

The angular momentum in the body-fixed coordinate system (x_b, y_b, z_b) is

$$\begin{Bmatrix} H_{x_b} \\ H_{y_b} \\ H_{z_b} \end{Bmatrix} = \begin{bmatrix} I_{xx_b} & 0 & -I_{xz_b} \\ 0 & I_{yy_b} & 0 \\ -I_{zx_b} & 0 & I_{zz_b} \end{bmatrix} \begin{Bmatrix} p \\ q \\ r \end{Bmatrix} \tag{7.8.3}$$

Transforming both sides of Eq. (7.8.3) using Eq. (7.8.2), we have

$$\begin{Bmatrix} H_{x_b'} \\ H_{y_b'} \\ H_{z_b'} \end{Bmatrix} = \begin{bmatrix} \cos\varphi & 0 & -\sin\varphi \\ 0 & 1 & 0 \\ \sin\varphi & 0 & \cos\varphi \end{bmatrix} \begin{bmatrix} I_{xx_b} & 0 & -I_{xz_b} \\ 0 & I_{yy_b} & 0 \\ -I_{zx_b} & 0 & I_{zz_b} \end{bmatrix} \begin{Bmatrix} p \\ q \\ r \end{Bmatrix} \tag{7.8.4}$$

The angular velocity vector on the right-hand side of Eq. (7.8.4) can be written in terms of the body-fixed coordinate system (x_b', y_b', z_b') by using Eq. (7.8.1),

$$\begin{Bmatrix} H_{x_b'} \\ H_{y_b'} \\ H_{z_b'} \end{Bmatrix} = \begin{bmatrix} \cos\varphi & 0 & -\sin\varphi \\ 0 & 1 & 0 \\ \sin\varphi & 0 & \cos\varphi \end{bmatrix} \begin{bmatrix} I_{xx_b} & 0 & -I_{xz_b} \\ 0 & I_{yy_b} & 0 \\ -I_{zx_b} & 0 & I_{zz_b} \end{bmatrix} \begin{bmatrix} \cos\varphi & 0 & \sin\varphi \\ 0 & 1 & 0 \\ -\sin\varphi & 0 & \cos\varphi \end{bmatrix} \begin{Bmatrix} p' \\ q' \\ r' \end{Bmatrix} \tag{7.8.5}$$

The angular momentum in the body-fixed coordinate system (x_b', y_b', z_b') can also be written in terms of the inertia tensor written in the same coordinate system,

$$\begin{Bmatrix} H_{x_b'} \\ H_{y_b'} \\ H_{z_b'} \end{Bmatrix} = [\mathbf{I}]' \begin{Bmatrix} p' \\ q' \\ r' \end{Bmatrix} = \begin{bmatrix} I_{xx_b} & 0 & -I_{xz_b} \\ 0 & I_{yy_b} & 0 \\ -I_{zx_b} & 0 & I_{zz_b} \end{bmatrix}' \begin{Bmatrix} p' \\ q' \\ r' \end{Bmatrix} \tag{7.8.6}$$

Combining Eqs. (7.8.5) and (7.8.6), we see that the inertia tensor written in the body-fixed coordinate system (x_b', y_b', z_b') can be found from

$$[\mathbf{I}]' = \begin{bmatrix} \cos\varphi & 0 & -\sin\varphi \\ 0 & 1 & 0 \\ \sin\varphi & 0 & \cos\varphi \end{bmatrix} \begin{bmatrix} I_{xx_b} & 0 & -I_{xz_b} \\ 0 & I_{yy_b} & 0 \\ -I_{zx_b} & 0 & I_{zz_b} \end{bmatrix} \begin{bmatrix} \cos\varphi & 0 & \sin\varphi \\ 0 & 1 & 0 \\ -\sin\varphi & 0 & \cos\varphi \end{bmatrix} \tag{7.8.7}$$

Equation (7.8.7) can be used to transform the inertia tensor from one body-fixed coordinate system to another whenever the two coordinate systems are related to each other through a simple rotation of φ about the y_b-axis from x_b to x_b'. Multiplying the three matrices on the right-hand side of Eq. (7.8.7), we obtain the component transformation equations

$$\begin{aligned}
\left(I_{xx_b}\right)' &= I_{xx_b}\cos^2\varphi + 2I_{xz_b}\cos\varphi\sin\varphi + I_{zz_b}\sin^2\varphi \\
\left(I_{yy_b}\right)' &= I_{yy_b} \\
\left(I_{zz_b}\right)' &= I_{zz_b}\cos^2\varphi - 2I_{xz_b}\cos\varphi\sin\varphi + I_{xx_b}\sin^2\varphi \\
\left(I_{xz_b}\right)' &= I_{xz_b}(\cos^2\varphi - \sin^2\varphi) + (I_{zz_b} - I_{xx_b})\cos\varphi\sin\varphi
\end{aligned} \tag{7.8.8}$$

The aerodynamic force and moment derivatives for the airplane can be transformed in a similar manner. In the linearized equations of motion, the aerodynamic force disturbances are written as

$$\begin{Bmatrix} \Delta F_{x_b} \\ \Delta F_{y_b} \\ \Delta F_{z_b} \end{Bmatrix} = \begin{bmatrix} F_{x_b,u} & 0 & F_{x_b,w} \\ 0 & F_{y_b,v} & 0 \\ F_{z_b,u} & 0 & F_{z_b,w} \end{bmatrix} \begin{Bmatrix} \Delta u \\ \Delta v \\ \Delta w \end{Bmatrix} + \begin{bmatrix} 0 & F_{x_b,q} & 0 \\ F_{y_b,p} & 0 & F_{y_b,r} \\ 0 & F_{z_b,q} & 0 \end{bmatrix} \begin{Bmatrix} \Delta p \\ \Delta q \\ \Delta r \end{Bmatrix}$$
$$+ \begin{bmatrix} F_{x_b,\dot{u}} & 0 & F_{x_b,\dot{w}} \\ 0 & 0 & 0 \\ F_{z_b,\dot{u}} & 0 & F_{z_b,\dot{w}} \end{bmatrix} \begin{Bmatrix} \Delta \dot{u} \\ \Delta \dot{v} \\ \Delta \dot{w} \end{Bmatrix} + \begin{bmatrix} 0 & F_{x_b,\delta_e} & 0 \\ F_{y_b,\delta_a} & 0 & F_{y_b,\delta_r} \\ 0 & F_{z_b,\delta_e} & 0 \end{bmatrix} \begin{Bmatrix} \Delta\delta_a \\ \Delta\delta_e \\ \Delta\delta_r \end{Bmatrix} \tag{7.8.9}$$

and the aerodynamic moment disturbances are

$$\begin{Bmatrix} \Delta M_{x_b} \\ \Delta M_{y_b} \\ \Delta M_{z_b} \end{Bmatrix} = \begin{bmatrix} 0 & M_{x_b,v} & 0 \\ M_{y_b,u} & 0 & M_{y_b,w} \\ 0 & M_{z_b,v} & 0 \end{bmatrix} \begin{Bmatrix} \Delta u \\ \Delta v \\ \Delta w \end{Bmatrix} + \begin{bmatrix} M_{x_b,p} & 0 & M_{x_b,r} \\ 0 & M_{y_b,q} & 0 \\ M_{z_b,p} & 0 & M_{z_b,r} \end{bmatrix} \begin{Bmatrix} \Delta p \\ \Delta q \\ \Delta r \end{Bmatrix}$$
$$+ \begin{bmatrix} 0 & 0 & 0 \\ M_{y_b,\dot{u}} & 0 & M_{y_b,\dot{w}} \\ 0 & 0 & 0 \end{bmatrix} \begin{Bmatrix} \Delta \dot{u} \\ \Delta \dot{v} \\ \Delta \dot{w} \end{Bmatrix} + \begin{bmatrix} M_{x_b,\delta_a} & 0 & M_{x_b,\delta_r} \\ 0 & M_{y_b,\delta_e} & 0 \\ M_{z_b,\delta_a} & 0 & M_{z_b,\delta_r} \end{bmatrix} \begin{Bmatrix} \Delta\delta_a \\ \Delta\delta_e \\ \Delta\delta_r \end{Bmatrix} \tag{7.8.10}$$

Each of the eight matrices in Eqs. (7.8.9) and (7.8.10) can be transformed using Eqs. (7.8.1) and (7.8.2) in a manner similar to that used to obtain Eq. (7.8.7). For example,

$$\begin{bmatrix} F_{x_b,\dot{u}} & 0 & F_{x_b,\dot{w}} \\ 0 & 0 & 0 \\ F_{z_b,\dot{u}} & 0 & F_{z_b,\dot{w}} \end{bmatrix}' = \begin{bmatrix} \cos\varphi & 0 & -\sin\varphi \\ 0 & 1 & 0 \\ \sin\varphi & 0 & \cos\varphi \end{bmatrix} \begin{bmatrix} F_{x_b,\dot{u}} & 0 & F_{x_b,\dot{w}} \\ 0 & 0 & 0 \\ F_{z_b,\dot{u}} & 0 & F_{z_b,\dot{w}} \end{bmatrix} \begin{bmatrix} \cos\varphi & 0 & \sin\varphi \\ 0 & 1 & 0 \\ -\sin\varphi & 0 & \cos\varphi \end{bmatrix} \tag{7.8.11}$$

and

$$\begin{bmatrix} 0 & F_{x_b,\delta_e} & 0 \\ F_{y_b,\delta_a} & 0 & F_{y_b,\delta_r} \\ 0 & F_{z_b,\delta_e} & 0 \end{bmatrix}' = \begin{bmatrix} \cos\varphi & 0 & -\sin\varphi \\ 0 & 1 & 0 \\ \sin\varphi & 0 & \cos\varphi \end{bmatrix} \begin{bmatrix} 0 & F_{x_b,\delta_e} & 0 \\ F_{y_b,\delta_a} & 0 & F_{y_b,\delta_r} \\ 0 & F_{z_b,\delta_e} & 0 \end{bmatrix} \tag{7.8.12}$$

When the matrix of aerodynamic derivatives in Eq. (7.8.12) is transformed, it is only premultiplied by the transformation matrix from Eq. (7.8.2). It is not postmultiplied by the transformation matrix from Eq. (7.8.1), because only the output vector for the last term in Eq. (7.8.9) depends on the coordinate system. The input vector of control surface deflections is the same in both coordinate systems. Similarly, we can also write

$$\begin{bmatrix} F_{x_b,u} & 0 & F_{x_b,w} \\ 0 & F_{y_b,v} & 0 \\ F_{z_b,u} & 0 & F_{z_b,w} \end{bmatrix}'$$

$$= \begin{bmatrix} \cos\varphi & 0 & -\sin\varphi \\ 0 & 1 & 0 \\ \sin\varphi & 0 & \cos\varphi \end{bmatrix} \begin{bmatrix} F_{x_b,u} & 0 & F_{x_b,w} \\ 0 & F_{y_b,v} & 0 \\ F_{z_b,u} & 0 & F_{z_b,w} \end{bmatrix} \begin{bmatrix} \cos\varphi & 0 & \sin\varphi \\ 0 & 1 & 0 \\ -\sin\varphi & 0 & \cos\varphi \end{bmatrix}$$

$$\begin{bmatrix} 0 & F_{x_b,q} & 0 \\ F_{y_b,p} & 0 & F_{y_b,r} \\ 0 & F_{z_b,q} & 0 \end{bmatrix}'$$

$$= \begin{bmatrix} \cos\varphi & 0 & -\sin\varphi \\ 0 & 1 & 0 \\ \sin\varphi & 0 & \cos\varphi \end{bmatrix} \begin{bmatrix} 0 & F_{x_b,q} & 0 \\ F_{y_b,p} & 0 & F_{y_b,r} \\ 0 & F_{z_b,q} & 0 \end{bmatrix} \begin{bmatrix} \cos\varphi & 0 & \sin\varphi \\ 0 & 1 & 0 \\ -\sin\varphi & 0 & \cos\varphi \end{bmatrix}$$

$$\begin{bmatrix} 0 & M_{x_b,v} & 0 \\ M_{y_b,u} & 0 & M_{y_b,w} \\ 0 & M_{z_b,v} & 0 \end{bmatrix}'$$

$$= \begin{bmatrix} \cos\varphi & 0 & -\sin\varphi \\ 0 & 1 & 0 \\ \sin\varphi & 0 & \cos\varphi \end{bmatrix} \begin{bmatrix} 0 & M_{x_b,v} & 0 \\ M_{y_b,u} & 0 & M_{y_b,w} \\ 0 & M_{z_b,v} & 0 \end{bmatrix} \begin{bmatrix} \cos\varphi & 0 & \sin\varphi \\ 0 & 1 & 0 \\ -\sin\varphi & 0 & \cos\varphi \end{bmatrix}$$

$$\begin{bmatrix} M_{x_b,\delta_a} & 0 & M_{x_b,\delta_r} \\ 0 & M_{y_b,\delta_e} & 0 \\ M_{z_b,\delta_a} & 0 & M_{z_b,\delta_r} \end{bmatrix}' = \begin{bmatrix} \cos\varphi & 0 & -\sin\varphi \\ 0 & 1 & 0 \\ \sin\varphi & 0 & \cos\varphi \end{bmatrix} \begin{bmatrix} M_{x_b,\delta_a} & 0 & M_{x_b,\delta_r} \\ 0 & M_{y_b,\delta_e} & 0 \\ M_{z_b,\delta_a} & 0 & M_{z_b,\delta_r} \end{bmatrix}$$

and so on.

By transforming each of the eight individual matrices in Eqs. (7.8.9) and (7.8.10), we obtain the component transformation equations for the **longitudinal aerodynamic derivatives**:

$$
\begin{aligned}
\left(F_{x_b,u}\right)' &= F_{x_b,u}\cos^2\varphi - \left(F_{x_b,w} + F_{z_b,u}\right)\cos\varphi\sin\varphi + F_{z_b,w}\sin^2\varphi \\
\left(F_{x_b,w}\right)' &= F_{x_b,w}\cos^2\varphi + \left(F_{x_b,u} - F_{z_b,w}\right)\cos\varphi\sin\varphi - F_{z_b,u}\sin^2\varphi \\
\left(F_{x_b,\dot{u}}\right)' &= F_{x_b,\dot{u}}\cos^2\varphi - \left(F_{x_b,\dot{w}} + F_{z_b,\dot{u}}\right)\cos\varphi\sin\varphi + F_{z_b,\dot{w}}\sin^2\varphi \\
\left(F_{x_b,\dot{w}}\right)' &= F_{x_b,\dot{w}}\cos^2\varphi + \left(F_{x_b,\dot{u}} - F_{z_b,\dot{w}}\right)\cos\varphi\sin\varphi - F_{z_b,\dot{u}}\sin^2\varphi \\
\left(F_{x_b,q}\right)' &= F_{x_b,q}\cos\varphi - F_{z_b,q}\sin\varphi \\
\left(F_{x_b,\delta_e}\right)' &= F_{x_b,\delta_e}\cos\varphi - F_{z_b,\delta_e}\sin\varphi \\
\left(F_{z_b,u}\right)' &= F_{z_b,u}\cos^2\varphi + \left(F_{x_b,u} - F_{z_b,w}\right)\cos\varphi\sin\varphi - F_{x_b,w}\sin^2\varphi \\
\left(F_{z_b,w}\right)' &= F_{z_b,w}\cos^2\varphi + \left(F_{x_b,w} + F_{z_b,u}\right)\cos\varphi\sin\varphi + F_{x_b,u}\sin^2\varphi \\
\left(F_{z_b,\dot{u}}\right)' &= F_{z_b,\dot{u}}\cos^2\varphi + \left(F_{x_b,\dot{u}} - F_{z_b,\dot{w}}\right)\cos\varphi\sin\varphi - F_{x_b,\dot{w}}\sin^2\varphi \\
\left(F_{z_b,\dot{w}}\right)' &= F_{z_b,\dot{w}}\cos^2\varphi + \left(F_{x_b,\dot{w}} + F_{z_b,\dot{u}}\right)\cos\varphi\sin\varphi + F_{x_b,\dot{u}}\sin^2\varphi \\
\left(F_{z_b,q}\right)' &= F_{z_b,q}\cos\varphi + F_{x_b,q}\sin\varphi \\
\left(F_{z_b,\delta_e}\right)' &= F_{z_b,\delta_e}\cos\varphi + F_{x_b,\delta_e}\sin\varphi \\
\left(M_{y_b,u}\right)' &= M_{y_b,u}\cos\varphi - M_{y_b,w}\sin\varphi \\
\left(M_{y_b,w}\right)' &= M_{y_b,w}\cos\varphi + M_{y_b,u}\sin\varphi \\
\left(M_{y_b,\dot{u}}\right)' &= M_{y_b,\dot{u}}\cos\varphi - M_{y_b,\dot{w}}\sin\varphi \\
\left(M_{y_b,\dot{w}}\right)' &= M_{y_b,\dot{w}}\cos\varphi + M_{y_b,\dot{u}}\sin\varphi \\
\left(M_{y_b,q}\right)' &= M_{y_b,q} \\
\left(M_{y_b,\delta_e}\right)' &= M_{y_b,\delta_e}
\end{aligned}
\tag{7.8.13}
$$

and the component transformation equations for the **lateral aerodynamic derivatives**:

$$\left(F_{y_b,v}\right)' = F_{y_b,v}$$

$$\left(F_{y_b,p}\right)' = F_{y_b,p}\cos\varphi - F_{y_b,r}\sin\varphi$$

$$\left(F_{y_b,r}\right)' = F_{y_b,r}\cos\varphi + F_{y_b,p}\sin\varphi$$

$$\left(F_{y_b,\delta_a}\right)' = F_{y_b,\delta_a}$$

$$\left(F_{y_b,\delta_r}\right)' = F_{y_b,\delta_r}$$

$$\left(M_{x_b,v}\right)' = M_{x_b,v}\cos\varphi - M_{z_b,v}\sin\varphi$$

$$\left(M_{x_b,p}\right)' = M_{x_b,p}\cos^2\varphi - \left(M_{x_b,r} + M_{z_b,p}\right)\cos\varphi\sin\varphi + M_{z_b,r}\sin^2\varphi$$

$$\left(M_{x_b,r}\right)' = M_{x_b,r}\cos^2\varphi + \left(M_{x_b,p} - M_{z_b,r}\right)\cos\varphi\sin\varphi - M_{z_b,p}\sin^2\varphi \qquad (7.8.14)$$

$$\left(M_{x_b,\delta_a}\right)' = M_{x_b,\delta_a}\cos\varphi - M_{z_b,\delta_a}\sin\varphi$$

$$\left(M_{x_b,\delta_r}\right)' = M_{x_b,\delta_r}\cos\varphi - M_{z_b,\delta_r}\sin\varphi$$

$$\left(M_{z_b,v}\right)' = M_{z_b,v}\cos\varphi + M_{x_b,v}\sin\varphi$$

$$\left(M_{z_b,p}\right)' = M_{z_b,p}\cos^2\varphi + \left(M_{x_b,p} - M_{z_b,r}\right)\cos\varphi\sin\varphi - M_{x_b,r}\sin^2\varphi$$

$$\left(M_{z_b,r}\right)' = M_{z_b,r}\cos^2\varphi + \left(M_{x_b,r} + M_{z_b,p}\right)\cos\varphi\sin\varphi + M_{x_b,p}\sin^2\varphi$$

$$\left(M_{z_b,\delta_a}\right)' = M_{z_b,\delta_a}\cos\varphi + M_{x_b,\delta_a}\sin\varphi$$

$$\left(M_{z_b,\delta_r}\right)' = M_{z_b,\delta_r}\cos\varphi + M_{x_b,\delta_r}\sin\varphi$$

The orientation of the stability axes for any given operating condition depends on some of the aerodynamic derivatives. Thus, we cannot know the exact orientation of the stability axes prior to determining these derivatives. For this reason, it is not convenient to directly measure the aerodynamic derivatives relative to the stability axes. However, the aerodynamic derivatives and inertia tensor can be measured relative to another convenient reference system, and the results can be transformed to the stability axes using Eqs. (7.8.8), (7.8.13), and (7.8.14).

EXAMPLE 7.8.1. The large jet transport described in Examples 7.6.1 and 7.7.1 has the following moments of inertia and product of inertia relative to the zero-lift axes of the airplane:

$$I_{xx_b} = 1.888\times10^7 \text{ slug}\cdot\text{ft}^2$$
$$I_{yy_b} = 3.310\times10^7 \text{ slug}\cdot\text{ft}^2$$
$$I_{zz_b} = 4.902\times10^7 \text{ slug}\cdot\text{ft}^2$$
$$I_{xz_b} = 4.075\times10^6 \text{ slug}\cdot\text{ft}^2$$

For the same flight condition used in Examples 7.6.1 and 7.7.1, estimate the components of the inertia tensor relative to the stability axes.

Solution. From Example 7.7.1, for this airplane and flight condition we have

$$C_L = 0.597, \quad C_{L,\alpha} = 5.50$$

Assuming the lift to be linear with angle of attack, we can approximate the equilibrium angle of attack relative to the zero-lift axes as

$$\alpha_o = \frac{C_L}{C_{L,\alpha}} = \frac{0.597}{5.50} = 0.1085 \text{ rad} = 6.22 \text{ degrees}$$

Since the equilibrium angle of attack is zero relative to the stability axes, the rotation about the y_b-axis from the zero-lift axes to the stability axes is

$$\varphi = -\alpha_o = -6.22 \text{ degrees}$$

Using Eq. (7.8.8), the four nonzero components of the inertia tensor relative to the stability axes are

$$\begin{aligned}(I_{xx_b})_s &= (I_{xx_b})_{L0}\cos^2\varphi + 2(I_{xz_b})_{L0}\cos\varphi\sin\varphi + (I_{zz_b})_{L0}\sin^2\varphi \\ &= 1.888\times10^7\cos^2\varphi + 2\left(4.075\times10^6\right)\cos\varphi\sin\varphi + 4.902\times10^7\sin^2\varphi \\ &= \underline{1.836\times10^7 \text{ slug}\cdot\text{ft}^2}\end{aligned}$$

$$(I_{yy_b})_s = (I_{yy_b})_{L0} = \underline{3.310\times10^7 \text{ slug}\cdot\text{ft}^2}$$

$$\begin{aligned}(I_{zz_b})_s &= (I_{zz_b})_{L0}\cos^2\varphi - 2(I_{xz_b})_{L0}\cos\varphi\sin\varphi + (I_{xx_b})_{L0}\sin^2\varphi \\ &= 4.902\times10^7\cos^2\varphi - 2\left(4.075\times10^6\right)\cos\varphi\sin\varphi + 1.888\times10^7\sin^2\varphi \\ &= \underline{4.954\times10^7 \text{ slug}\cdot\text{ft}^2}\end{aligned}$$

$$\begin{aligned}(I_{xz_b})_s &= (I_{xz_b})_{L0}(\cos^2\varphi - \sin^2\varphi) + \left[(I_{zz_b})_{L0} - (I_{xx_b})_{L0}\right]\cos\varphi\sin\varphi \\ &= \left(4.075\times10^6\right)\left(\cos^2\varphi - \sin^2\varphi\right) + \left(4.902\times10^7 - 1.888\times10^7\right)\cos\varphi\sin\varphi \\ &= \underline{7.330\times10^5 \text{ slug}\cdot\text{ft}^2}\end{aligned}$$

Notice that this transformation has little effect on the moments of inertia but has a large effect on the product of inertia.

7.9. Inertial and Gyroscopic Coupling

In our previous development of the rigid-body equations of motion, we assumed that the aircraft was symmetric about the x_b-z_b plane. It was this assumed symmetry that allowed us to uncouple the longitudinal equations from the lateral equations after applying the small disturbance approximation. While most aircraft possess this symmetry, it is not unusual for an aircraft to be flown in an asymmetrical configuration. For example, a military airplane might be flown with a missile under only one wing, and any airplane could be flown with more fuel in one wing than in the other. If the symmetry assumption is relaxed, the longitudinal and lateral equations become coupled, even within the approximation of small disturbance theory.

There is also another form of cross coupling that arises from the spinning rotors associated with aircraft power plants, i.e., turbines, compressors, and propellers. In treating the aircraft as a rigid body, we tacitly neglected the angular momentum of these rotors relative to the body-fixed coordinates. If we relax the rigid-body assumption to the extent that we allow some parts of the aircraft to be rotating relative to the body-fixed coordinate system, then additional terms appear on the right-hand side of the angular momentum equation, Eq. (7.2.2). These terms are called the *gyroscopic couples*.

Relaxing both the symmetry assumption and the rigid-body assumption as mentioned above, the angular momentum equation can be written as

$$\mathbf{M} = \frac{d\mathbf{H}}{dt} + \boldsymbol{\omega}\times\mathbf{H} \tag{7.9.1}$$

where

$$\mathbf{H} = [\mathbf{I}]\boldsymbol{\omega} + \mathbf{h} \tag{7.9.2}$$

$$[\mathbf{I}] = \begin{bmatrix} I_{xx_b} & -I_{xy_b} & -I_{xz_b} \\ -I_{yx_b} & I_{yy_b} & -I_{yz_b} \\ -I_{zx_b} & -I_{zy_b} & I_{zz_b} \end{bmatrix} \tag{7.9.3}$$

and $\mathbf{h}$ is the total angular momentum of all spinning rotors relative to the body-fixed coordinate system. If we assume all rotors to be spinning with a constant angular velocity relative to the aircraft, Eq. (7.9.1) can be written as

$$\mathbf{M} = \frac{d}{dt}\left([\mathbf{I}]\boldsymbol{\omega}\right) + \boldsymbol{\omega} \times \left([\mathbf{I}]\boldsymbol{\omega} + \mathbf{h}\right) \tag{7.9.4}$$

or after expanding and rearranging,

$$\begin{bmatrix} I_{xx_b} & -I_{xy_b} & -I_{xz_b} \\ -I_{xy_b} & I_{yy_b} & -I_{yz_b} \\ -I_{xz_b} & -I_{yz_b} & I_{zz_b} \end{bmatrix} \begin{Bmatrix} \dot{p} \\ \dot{q} \\ \dot{r} \end{Bmatrix} = \begin{Bmatrix} M_{x_b} \\ M_{y_b} \\ M_{z_b} \end{Bmatrix} + \begin{bmatrix} 0 & -h_{z_b} & h_{y_b} \\ h_{z_b} & 0 & -h_{x_b} \\ -h_{y_b} & h_{x_b} & 0 \end{bmatrix} \begin{Bmatrix} p \\ q \\ r \end{Bmatrix} + \begin{Bmatrix} (I_{yy_b} - I_{zz_b})qr + I_{yz_b}(q^2 - r^2) + I_{xz_b}pq - I_{xy_b}pr \\ (I_{zz_b} - I_{xx_b})pr + I_{xz_b}(r^2 - p^2) + I_{xy_b}qr - I_{yz_b}pq \\ (I_{xx_b} - I_{yy_b})pq + I_{xy_b}(p^2 - q^2) + I_{yz_b}pr - I_{xz_b}qr \end{Bmatrix} \tag{7.9.5}$$

From Eq. (7.9.5) we see that for this more general case, there is both linear and nonlinear coupling between the longitudinal and lateral degrees of freedom. These effects can be accounted for in the Euler angle formulation of the general 6-DOF equations of motion simply by replacing Eq. (7.4.5) with Eq. (7.9.5). This adds no significant complexity to the general nonlinear 6-DOF equations.

In steady linear flight, the first-order coupling between the longitudinal and lateral equations of motion results only from asymmetry about the x_b-z_b plane and/or from the gyroscopic effects of the spinning rotors. From Eq. (7.9.5), we see that both the rolling and yawing rates affect the pitching equation through the terms $-I_{xy_b}\dot{p}$ and $-I_{yz_b}\dot{r}$. Likewise, the pitching rate affects both the rolling and yawing equations through the terms $-I_{xy_b}\dot{q}$ and $-I_{yz_b}\dot{q}$. In conventional airplanes the spinning rotors are usually aligned very closely with the x_b-axis. In this case the gyroscopic effects result primarily in a coupling between pitch and yaw, through the terms $h_{x_b}q$ and $-h_{x_b}r$. For helicopters, the primary rotors are aligned more closely with the z_b-axis, which produces a roll-pitch coupling from the terms $h_{z_b}p$ and $-h_{z_b}q$.

During very rapid maneuvers, even the second-order terms in Eq. (7.9.5) can become significant. While pitching and yawing rates are not usually large, fighter aircraft routinely execute maneuvers with very high rolling rates. Such maneuvers can result in significant longitudinal-lateral coupling. Most notably, long slender aircraft have a moment of inertia about the roll axis that is much less than that about either the pitch or yaw axis. When such an aircraft executes a rapid rolling maneuver, the second-order term $(I_{zz_b} - I_{xx_b})pq$ can produce a pitching motion large enough to cause loss of control or even structural failure. Similarly, an aircraft with significant asymmetry will have significant product of inertia terms. A rapid rolling maneuver in this type of aircraft will also produce significant pitching motion as a result of the terms $I_{xz_b}(r^2 - p^2)$ and $-I_{yz_b}pq$. Such coupling between rolling and pitching motion is particularly important, since rolling rates can be very large in fighter aircraft and because pitching motion can result in rapid changes in angle of attack. These changes in angle of attack can have a profound and sometimes catastrophic effect on the aerodynamic forces. Fortunately, the angular rates in most flying situations are small and the second-order terms in Eq. (7.9.5) are not significant.

7.10. Problems

7.1. A rocket is flying with an axial velocity component of 1,000 ft/sec, a sideslip velocity component of 500 ft/sec, and a normal velocity component of 2,000 ft/sec. Determine the total airspeed in miles per hour and the angle of attack and sideslip angles β_a and β_e in degrees.

7.2. An aircraft has an airspeed of 400 ft/sec. The angle of attack is 20 degrees and the sideslip angle, β_a, is 10 degrees. Determine the axial velocity component, the sideslip velocity component, and the normal velocity component relative to the same body-fixed coordinate system.

7.3. An aircraft has an airspeed of 400 ft/sec. The angle of attack is 20 degrees and the sideslip angle, β_e, is 10 degrees. Determine the axial velocity component, the sideslip velocity component, and the normal velocity component relative to the same body-fixed coordinate system.

7.4. An aircraft has an airspeed of 800 ft/sec. The angle of attack is 75 degrees and the sideslip angle, β_a, is 60 degrees. Determine the axial velocity component, the sideslip velocity component, and the normal velocity component.

7.5. An aircraft has an airspeed of 800 ft/sec. The angle of attack is 75 degrees and the sideslip angle, β_e, is 60 degrees. Determine the axial velocity component, the sideslip velocity component, and the normal velocity component.

7.6. Consider some aerodynamic coefficient, C, that is somehow known as a function of V, α, and β_a. Using the definitions in Eqs. (7.1.2) through (7.1.4), obtain an expression for the change in C with respect to sideslip velocity in terms of the derivatives with respect to V, α, and β_a.

7.7. Consider some aerodynamic coefficient, C, that is somehow known as a function of V, α, and β_e. Using the definitions in Eqs. (7.1.2), (7.1.3), and (7.1.5), obtain an expression for the change in C with respect to sideslip velocity in terms of the derivatives with respect to V, α, and β_e.

7.8. Using Eqs. (7.1.16), (7.1.19), and (7.1.20), show that the results obtained in problems 7.6 and 7.7 are equivalent.

7.9. A rectangular solid of density ρ has length L_x in the x_b-direction, length L_y in the y_b-direction, and length L_z in the z_b-direction. Starting with Eqs. (7.2.3) through (7.2.9), obtain an expression for the inertia tensor for this object. Use a body-fixed coordinate system aligned with the primary axes of the body.

7.10. Starting with Eqs. (7.2.3) through (7.2.9), obtain an expression for the inertia tensor for a cylinder having density ρ, radius R, and length L. Use a body-fixed coordinate system aligned with the primary axes of the cylinder.

7.11. If the rocket in problem 7.1 has a bank angle of −30°, an elevation angle of 60°, and an azimuth angle of 230°, what is its velocity in Earth-fixed coordinates?

7.12. If the aircraft in problem 7.2 has a bank angle of 40°, an elevation angle of −20°, and an azimuth angle of 290°, what is its velocity in Earth-fixed coordinates?

7.13. An airplane has an angle of attack of 10 degrees and the sideslip angle, β_a, is 5 degrees. If the airplane has a bank angle of 60 degrees, an elevation angle of −30 degrees, and an azimuth angle of 0 degrees, what direction is the nose of the airplane pointing, and in what direction is the airplane moving?

7.14. An airplane has an angle of attack of 10 degrees and the sideslip angle, β_e, is 5 degrees. If the airplane has a bank angle of 60 degrees, an elevation angle of −30 degrees, and an azimuth angle of 0 degrees, what direction is the nose of the airplane pointing, and in what direction is the airplane moving?

7.15. During a post-stall maneuver, an airplane has an angle of attack of 80 degrees and the sideslip angle, β_a, is 30 degrees. If the airplane has a bank angle of 90 degrees, an elevation angle of 10 degrees, and an azimuth angle of 180 degrees, what direction is the nose of the airplane pointing, and in what direction is the airplane moving?

7.16. During a post-stall maneuver, an airplane has an angle of attack of 80 degrees and the sideslip angle, β_e, is 30 degrees. If the airplane has a bank angle of 90 degrees, an elevation angle of 10 degrees, and an azimuth angle of 180 degrees, what direction is the nose of the airplane pointing, and in what direction is the airplane moving?

7.17. Write a computer subroutine that uses fourth-order Runge-Kutta to solve the projectile equations developed in Example 7.3.4. Start with Eq. (7.3.38).

7.18. Using the subroutine from problem 7.17, obtain the Earth-fixed coordinates and airspeed at 25 and 100 yards downrange for an arrow having $K_0 = 0.00061$ ft^{-1}, $K_1 = 0.14$ ft^{-1}, $K_2 = 0.00059$ ft^{-1}, $K_3 = 0.0016$ ft^{-2}, and $K_4 = 0.0064$ ft^{-1}. The arrow starts at the Earth-fixed origin with a speed of 210 ft/sec, no angle of attack, no angular velocity, and an elevation angle of 0.0 degrees. How far is the arrow below the initial line of motion at 25 and 100 yards downrange?

7.19. Using the subroutine from problem 7.17, obtain the Earth-fixed coordinates and airspeed at 25 and 100 yards downrange for an arrow having $K_0 = 0.00061$ ft^{-1}, $K_1 = 0.14$ ft^{-1}, $K_2 = 0.00059$ ft^{-1}, $K_3 = 0.0016$ ft^{-2}, and $K_4 = 0.0064$ ft^{-1}. The arrow starts at the Earth-fixed origin with a speed of 210 ft/sec, no angle of attack, no angular velocity, and an elevation angle of 45 degrees. How far is the arrow below the initial line of motion at 25 and 100 yards downrange? Consider the downrange distance to be measured along the initial 45-degree flight line.

7.20. Modify the computer subroutine written for problem 7.17 so that time is used as the independent variable, i.e., use Eq. (7.3.35) instead of Eq. (7.3.38). Also account for the variation in air density with elevation.

7.21. A projectile is dropped from an aircraft flying at 10,000 ft with an airspeed of 500 ft/sec. At sea level, the projectile has $K_0 = 0.002$ ft^{-1}, $K_1 = 0.2$ ft^{-1}, $K_2 = 0.001$ ft^{-1}, $K_3 = 0.001$ ft^{-2}, and $K_4 = 0.01$ ft^{-1}. Use the subroutine written for problem 7.20 to determine the horizontal distance traveled by the projectile from the time it is dropped from the aircraft until it falls to sea level. What are the elevation angle and the angle of attack for the projectile when it reaches sea level? Assume that the projectile leaves the aircraft with no angular velocity and no angle of attack. Use a time step of 0.05 second and assume no wind.

7.22. Using the subroutine that was written for problem 7.20, plot the trajectory of the projectile in problem 7.21 from 10,000 feet to sea level.

7.23. Using the subroutine that was written for problem 7.20, plot both the horizontal and vertical components of velocity as a function of time for the projectile in problem 7.21.

7.24. Using the subroutine written for problem 7.20, plot the angle of attack as a function of time for the projectile in problem 7.21.

7.25. A spherical projectile 24 inches in diameter and weighing 50 pounds is dropped from an aircraft flying at 10,000 ft and 500 ft/sec. Use the subroutine written for problem 7.20 to determine the horizontal distance traveled by the projectile from the time it is dropped until it falls to sea level. Assume a constant drag coefficient of 1.0. Use a time step of 0.05 second and assume no wind.

7.26. Modify the computer subroutine written for problem 7.20 to account for the effects of wind. Assume constant headwind and no crosswind.

7.27. Using the subroutine written for problem 7.26, plot the trajectory of the projectile in problem 7.21 from 10,000 feet to sea level for the case of a constant headwind of 75 ft/sec.

7.28. Using the subroutine that was written for problem 7.26, plot the horizontal and vertical components of ground speed as a function of time for the projectile in problem 7.27.

7.29. For the arrow described in problem 7.18, use the fourth-order Runge-Kutta integration method with the linearized system of equations developed in Example 7.5.2 to plot the elevation and airspeed as a function of range from zero to 100 yards. Use a time step of 0.015 second. Compare your results to those obtained in problem 7.18.

7.30. In Example 7.5.2, the projectile equations developed in Example 7.3.3 were linearized relative to motion along a horizontal line at constant speed. We wish to develop a more general system of linearized projectile equations. Linearize the equations developed in Example 7.3.3 relative to constant-speed motion along a straight line having an elevation angle of θ_0.

7.31. For the arrow described in problem 7.19, use the linearized system of equations developed in problem 7.30 to plot the elevation and airspeed as a function of range from zero to 100 yards. Use a time step of 0.015 second. Compare your results to those obtained in problem 7.19.

7.32. For the airplane and flight conditions in Example 7.6.1, estimate all of the dimensional lateral aerodynamic derivatives that appear in the homogeneous form of Eq. (7.5.24). In addition to the properties given in Example 7.6.1, this airplane has the following properties:

$$(c_l/c_r)_w = 0.286, \quad S_v = 875 \text{ ft}^2, \quad x_{bv} = -96 \text{ ft}, \quad z_{bv} = -23 \text{ ft},$$
$$C_{L_v,\beta} = 3.30, \quad C_{Y,\beta} = -0.890, \quad C_{\ell,\beta} = -0.144, \quad C_{n,\beta} = 0.182$$

7.33. Repeat Example 7.6.1, for a thrust vector that is inclined upward at an angle of 9.0 degrees to the direction of flight and passes through a point that is 9.0 ft below the center of gravity. Assume that all other parameters, including the lift-to-drag ratio, remain unchanged.

7.34. For the airplane and flight conditions in problem 7.32, fill out the nondimensional lateral coefficient matrices associated with the homogeneous form of Eq. (7.7.6). For this airplane, the components of the inertia tensor relative to the stability axes were computed in Example 7.8.1.

7.35. For the airplane described in Example 7.8.1, what rotation angle about the y_b-axis is required to move from the zero-lift axes to the primary axes?

7.36. The Spitfire Mark XVIII that is shown in Figs. 4.11.1 and 4.11.2 is in level flight at sea level. Assume the following properties and operating conditions:

$$S_w = 244 \text{ ft}^2, \quad b_w = 36.83 \text{ ft}, \quad C_{L_w,\alpha} = 4.62, \quad C_{m_w} = -0.053,$$
$$\Lambda_w = 0.0°, \quad \alpha_{L0w} = -2.2°, \quad \alpha_{0w} = 3.0°, \quad l_w = 0.0 \text{ ft}, \quad h_w = -2.6 \text{ ft},$$
$$C_{D_{0w}} = 0.01, \quad C_{D_0,L_w} = 0.00, \quad e_w = 1.00,$$
$$S_h = 31 \text{ ft}^2, \quad b_h = 10.64 \text{ ft}, \quad C_{L_h,\alpha} = 4.06, \quad C_{m_h 0} = 0.000,$$
$$\Lambda_h = 0.0°, \quad \alpha_{L0h} = 0.0°, \quad \alpha_{0h} = 0.0°, \quad l_h = 18.16 \text{ ft}, \quad h_h = 0.0 \text{ ft},$$
$$C_{D_{0h}} = 0.01, \quad C_{D_0,L_h} = 0.00, \quad e_h = 1.00, \quad \eta_h = 1.0,$$
$$S_f = 15 \text{ ft}^2, \quad c_f = 32.67 \text{ ft}, \quad \alpha_{0f} = 0.0°, \quad l_f = -3.0 \text{ ft},$$

$$d_p = 132/12 \text{ ft}, \quad \omega/2\pi = 1350 \text{ rpm}, \quad C_{N_p,\alpha} = 0.390,$$
$$T_{,V} = -2.40 \text{ lbf}\cdot\text{sec/ft}, \quad \alpha_{0p} = 0.0°, \quad l_p = -9.33 \text{ ft}, \quad h_p = 0.0 \text{ ft},$$
$$W = 8{,}375 \text{ lbf}, \quad I_{yy_b} = 10{,}060 \text{ slug}\cdot\text{ft}^2, \quad V_o = 300 \text{ mph},$$
$$C_{L,\alpha} = 4.884, \quad C_{D_{L0}} = 0.0173, \quad C_{D_0,L} = 0.0, \quad e = 0.80, \quad C_{m,\alpha} = -0.3786$$

Estimate all of the dimensionless longitudinal aerodynamic derivatives and fill out the nondimensional longitudinal coefficient matrices associated with the homogeneous form of Eq. (7.7.5).

7.37. Two high-bypass-ratio turbofan engines power a small jet transport of the wing-canard design. The airplane is in level flight at 30,000 feet. Assume the following properties and operating conditions:

$$S_w = 950 \text{ ft}^2, \quad b_w = 75 \text{ ft}, \quad R_{T_w} = 0.35, \quad C_{L_w,\alpha} = 4.30, \quad C_{m_w} = -0.050,$$
$$\Lambda_w = 15°, \quad \alpha_{L0w} = -2.0°, \quad \alpha_{0w} = 1.5°, \quad l_w = 8.6 \text{ ft}, \quad h_w = -3.8 \text{ ft},$$
$$C_{D_{0w}} = 0.01, \quad C_{D_0,L_w} = 0.00, \quad e_w = 0.95,$$
$$S_h = 219 \text{ ft}^2, \quad b_h = 36 \text{ ft}, \quad R_{T_h} = 0.35, \quad C_{L_h,\alpha} = 4.30, \quad C_{m_h 0} = -0.050,$$
$$\Lambda_h = 15°, \quad \alpha_{L0h} = -2.0°, \quad \alpha_{0h} = 2.0°, \quad l_h = -33.9 \text{ ft}, \quad h_h = -3.8 \text{ ft},$$
$$C_{D_{0h}} = 0.01, \quad C_{D_0,L_h} = 0.00, \quad e_h = 0.95, \quad \eta_h = 1.0,$$
$$S_f = 52 \text{ ft}^2, \quad c_f = 78 \text{ ft}, \quad \alpha_{0f} = 0.0°, \quad l_f = -18.5 \text{ ft},$$
$$T_{,V} = -10.5 \text{ lbf}\cdot\text{sec/ft}, \quad \alpha_{0j} = 0.0°, \quad \eta_{p_i} = 0.64, \quad l_j = 9.4 \text{ ft}, \quad h_j = 2.4 \text{ ft},$$
$$W = 73{,}000 \text{ lbf}, \quad I_{yy_b} = 451{,}500 \text{ slug}\cdot\text{ft}^2, \quad V_o = 400 \text{ mph},$$
$$C_{L,\alpha} = 5.327, \quad C_{D_{L0}} = 0.020, \quad C_{D_0,L} = 0.0, \quad e = 0.67, \quad C_{m,\alpha} = -0.122$$

Estimate all of the dimensionless longitudinal aerodynamic derivatives and fill out the nondimensional longitudinal coefficient matrices associated with the homogeneous form of Eq. (7.7.5).

7.38. The turboprop transport that is shown in Fig. 4.11.3 is in level flight at sea level. Assume the following properties and operating conditions:

$$S_w = 1{,}745 \text{ ft}^2, \quad b_w = 132.6 \text{ ft}, \quad R_{T_w} = 0.57, \quad C_{L_w,\alpha} = 5.16, \quad C_{m_w} = -0.050,$$
$$\Lambda_w = 0.0°, \quad \alpha_{L0w} = -2.0°, \quad \alpha_{0w} = 0.0°, \quad l_w = -2.5 \text{ ft}, \quad h_w = 7.4 \text{ ft},$$
$$C_{D_{0w}} = 0.01, \quad C_{D_0,L_w} = 0.00, \quad e_w = 0.96,$$
$$S_h = 528 \text{ ft}^2, \quad b_h = 52.7 \text{ ft}, \quad R_{T_h} = 0.35, \quad C_{L_h,\alpha} = 4.52, \quad C_{m_h 0} = 0.000,$$
$$\Lambda_h = 7°, \quad \alpha_{L0h} = 0.0°, \quad \alpha_{0h} = -1.5°, \quad l_h = 44.5 \text{ ft}, \quad h_h = 7.4 \text{ ft},$$
$$C_{D_{0h}} = 0.01, \quad C_{D_0,L_h} = 0.00, \quad e_h = 0.97, \quad \eta_h = 1.0,$$
$$S_f = 173 \text{ ft}^2, \quad c_f = 87.9 \text{ ft}, \quad \alpha_{0f} = 0.0°, \quad l_f = -20.5 \text{ ft},$$

$$S_n = 28.7 \text{ ft}^2, \quad c_n = 23 \text{ ft}, \quad \alpha_{0n} = 0.0°, \quad l_n = -9.2 \text{ ft},$$
$$d_p = 162/12 \text{ ft}, \quad \omega/2\pi = 1020 \text{ rpm}, \quad C_{N_p,\alpha} = 0.721,$$
$$T_Y = -40.4 \text{ lbf}\cdot\text{sec/ft}, \quad \alpha_{0p} = 0.0°, \quad l_p = -11.9 \text{ ft}, \quad h_p = 6.2 \text{ ft},$$
$$W = 155{,}000 \text{ lbf}, \quad I_{yy_b} = 894{,}700 \text{ slug}\cdot\text{ft}^2, \quad V_o = 300 \text{ mph},$$
$$C_{L,\alpha} = 6.087, \quad C_{D_{L0}} = 0.031, \quad C_{D_0,L} = 0.0, \quad e = 0.65, \quad C_{m,\alpha} = -1.645$$

Estimate all of the dimensionless longitudinal aerodynamic derivatives and fill out the nondimensional longitudinal coefficient matrices associated with the homogeneous form of Eq. (7.7.5).

7.39. For the Spitfire Mark XVIII that is described in problem 7.36, fill out the nondimensional lateral coefficient matrices associated with the homogeneous form of Eq. (7.7.6). In addition to the properties and operating conditions listed in problem 7.36, assume the following:

$$I_{xx_b} = 1{,}500 \text{ slug}\cdot\text{ft}^2, \quad I_{zz_b} = 11{,}700 \text{ slug}\cdot\text{ft}^2, \quad I_{xz_b} = 100 \text{ slug}\cdot\text{ft}^2,$$
$$C_{Y,\beta} = -0.212, \quad C_{\ell,\beta} = 0.000, \quad C_{n,\beta} = 0.095,$$
$$C_{Y,\bar{p}} = 0.000, \quad C_{\ell,\bar{p}} = -0.8885, \quad C_{n,\bar{p}} = -0.0186,$$
$$C_{Y,\bar{r}} = 0.282, \quad C_{\ell,\bar{r}} = 0.037, \quad C_{n,\bar{r}} = -0.139$$

7.40. For the small jet transport that is described in problem 7.37, fill out the nondimensional lateral coefficient matrices associated with the homogeneous form of Eq. (7.7.6). In addition to the properties and operating conditions listed in problem 7.37, assume the following:

$$I_{xx_b} = 393{,}700 \text{ slug}\cdot\text{ft}^2, \quad I_{zz_b} = 808{,}200 \text{ slug}\cdot\text{ft}^2, \quad I_{xz_b} = 75{,}000 \text{ slug}\cdot\text{ft}^2,$$
$$C_{Y,\beta} = -0.735, \quad C_{\ell,\beta} = -0.220, \quad C_{n,\beta} = 0.135,$$
$$C_{Y,\bar{p}} = 0.000, \quad C_{\ell,\bar{p}} = -0.385, \quad C_{n,\bar{p}} = -0.049,$$
$$C_{Y,\bar{r}} = 0.092, \quad C_{\ell,\bar{r}} = 0.143, \quad C_{n,\bar{r}} = -0.165$$

7.41. For the turboprop transport that is described in problem 7.38, fill out the nondimensional lateral coefficient matrices associated with the homogeneous form of Eq. (7.7.6). In addition to the properties and operating conditions listed in problem 7.38, assume the following:

$$I_{xx_b} = 1{,}136{,}000 \text{ slug}\cdot\text{ft}^2, \quad I_{zz_b} = 1{,}860{,}000 \text{ slug}\cdot\text{ft}^2, \quad I_{xz_b} = 1{,}100 \text{ slug}\cdot\text{ft}^2,$$
$$C_{Y,\beta} = -0.362, \quad C_{\ell,\beta} = -0.125, \quad C_{n,\beta} = 0.101,$$
$$C_{Y,\bar{p}} = 0.000, \quad C_{\ell,\bar{p}} = -0.530, \quad C_{n,\bar{p}} = -0.037,$$
$$C_{Y,\bar{r}} = 0.082, \quad C_{\ell,\bar{r}} = 0.113, \quad C_{n,\bar{r}} = -0.171$$

Chapter 8
Linearized Longitudinal Dynamics

8.1. Fundamentals of Dynamics: Eigenproblems

The linearized 6-DOF equations of motion developed in Chapter 7 consist of 12 first-order linear differential equations with constant coefficients. These 12 first-order equations are equivalent to a system of six second-order equations for the six-degrees of freedom associated with rigid-body flight. Similar systems of second-order equations can be used to model many other physical phenomena. Systems of second-order differential equations with constant coefficients are frequently encountered in every branch of engineering. For this reason, such systems of equations have been studied at great length and their solutions are well understood. Because an understanding of second-order systems is prerequisite to an understanding of aircraft dynamics, here we review the characteristics of such systems in general before considering their application to dynamic aircraft stability and control.

First consider a one-degree-of-freedom system, modeled with a single second-order differential equation with constant coefficients. While several electrical and mechanical systems can be modeled with a single equation of this type, here we illustrate the problem by examining the motion of a one-degree-of-freedom spring-mass system with linearized viscous damping (see Fig 8.1.1). The equation of motion is developed by summing forces acting on the mass to obtain the second-order differential equation

$$m\frac{d^2x}{dt^2} + c\frac{dx}{dt} + k(x - x_o) = F(t) \tag{8.1.1}$$

where m is the mass, c is the damping coefficient, k is the spring constant, x_o is the equilibrium value of the x-position that results in no spring force, and $F(t)$ is a forcing function that may vary with time, t. The general solution to this equation, referred to as the *forced response*, is the sum of the homogeneous solution and a particular solution. The homogeneous solution, or *free response*, is the solution with the forcing function set

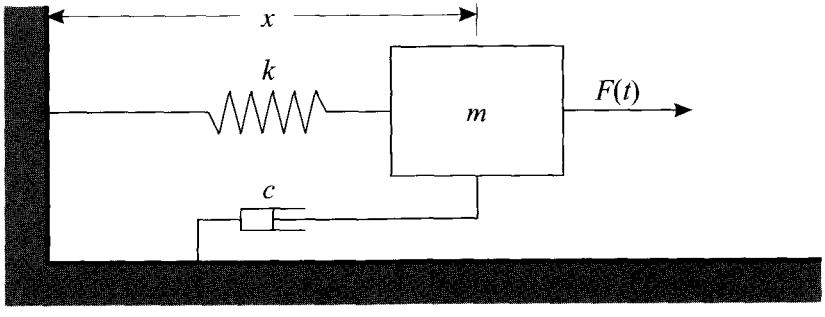


Figure 8.1.1. Damped spring-mass system with one degree of freedom.

to zero, and the particular solution is any solution that will satisfy the nonhomogeneous equation. Because system dynamics are characterized primarily by the free response, we start our discussion with a consideration of the homogeneous solution.

Equation (8.1.1) can be rewritten as

$$m\frac{d^2\Delta x}{dt^2}+c\frac{d\Delta x}{dt}+k\Delta x = F(t) \tag{8.1.2}$$

where Δx is the displacement from equilibrium, $\Delta x = x - x_o$. The reader should recognize the homogeneous solution to Eq. (8.1.2) from his or her introductory class on ordinary differential equations. The only existing solutions are given by

$$\Delta x(t) = C_1 e^{\lambda_1 t} + C_2 e^{\lambda_2 t} \tag{8.1.3}$$

where C_1 and C_2 are arbitrary constants, to be determined from the initial conditions, and λ_1 and λ_2 are the *eigenvalues*, which are the roots of the characteristic equation,

$$\lambda_{1,2} = \frac{-c \pm \sqrt{c^2 - 4mk}}{2m} = -\frac{c}{2m} \pm \sqrt{\left(\frac{c}{2m}\right)^2 - \frac{k}{m}} \tag{8.1.4}$$

The motion that occurs when the system is disturbed from equilibrium and then released will depend on the eigenvalues λ_1 and λ_2. The reader should be familiar with three types of motion that are shown in Fig 8.1.2. **Overdamped motion** occurs when the eigenvalues are real, negative, and distinct,

$$\left(\frac{c}{2m}\right)^2 > \frac{k}{m} \tag{8.1.5}$$

In this case any disturbance from equilibrium will result in a smooth exponential return to the equilibrium position with no oscillation or overshoot. **Underdamped motion** occurs when the eigenvalues are complex,

$$\left(\frac{c}{2m}\right)^2 < \frac{k}{m} \tag{8.1.6}$$

In this case, disturbance from equilibrium results in damped sinusoidal motion with a *damped natural frequency* equal to the magnitude of the eigenvalue's imaginary part,

$$\text{damped natural frequency} \equiv \omega_d = \left|\text{imag}(\lambda)\right| = \sqrt{\frac{k}{m} - \left(\frac{c}{2m}\right)^2} \tag{8.1.7}$$

and a *damping rate* equal to the negative of the real part of the eigenvalue,

$$\text{damping rate} \equiv \sigma = -\text{real}(\lambda) = \frac{c}{2m} \tag{8.1.8}$$

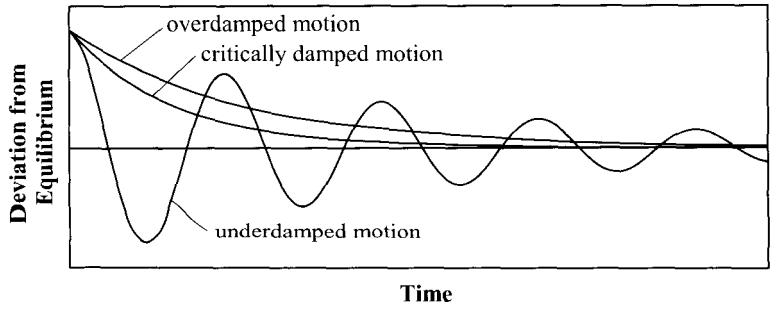


Figure 8.1.2. Overdamped, critically damped, and underdamped motion.

Critically damped motion occurs when the eigenvalues are real, negative, and identical,

$$\frac{c}{2m} = \sqrt{\frac{k}{m}} \tag{8.1.9}$$

This case is the boundary between overdamped exponential motion and underdamped sinusoidal motion. Critically damped motion provides the most rapid exponential return to equilibrium that is possible without inducing sinusoidal oscillations.

For an underdamped mode, the eigenvalues form a complex pair. This complex pair and the nature of the associated motion can be specified in terms of the damped natural frequency, ω_d, and the damping rate, σ, defined by Eqs. (8.1.7) and (8.1.8),

$$\lambda_{1,2} = -\sigma \pm \omega_d i \tag{8.1.10}$$

where $i = \sqrt{-1}$. For underdamped motion, both the damped natural frequency and the damping rate have rather obvious physical meanings. However, for overdamped or critically damped motion, the concept of damped natural frequency is meaningless. For this reason, it is often more convenient to describe an eigenvalue pair in terms of what are called the *undamped natural frequency* and the *damping ratio*. The undamped natural frequency is the frequency that the mode would exhibit if the damping were identically zero. This undamped natural frequency is related to the eigenvalue pair according to

$$\text{undamped natural frequency} \equiv \omega_n = \sqrt{\lambda_1 \lambda_2} \tag{8.1.11}$$

The damping ratio is the actual damping rate divided by the damping rate that would be required to make the mode critically damped. In general, to determine the damping ratio from the eigenvalue pair, we use

$$\text{damping ratio} \equiv \zeta = -\frac{\lambda_1 + \lambda_2}{2\sqrt{\lambda_1 \lambda_2}} \tag{8.1.12}$$

Using Eq. (8.1.10) in Eqs. (8.1.11) and (8.1.12), for an underdamped mode, the undamped natural frequency and the damping ratio can be related to the damped natural frequency and the damping rate. This gives

$$\omega_n = \sqrt{(-\sigma + \omega_d i)(-\sigma - \omega_d i)} = \sqrt{\sigma^2 + \omega_d^2} \tag{8.1.13}$$

$$\zeta = -\frac{-\sigma + \omega_d i - \sigma - \omega_d i}{2\sqrt{(-\sigma + \omega_d i)(-\sigma - \omega_d i)}} = \frac{\sigma}{\sqrt{\sigma^2 + \omega_d^2}} \tag{8.1.14}$$

While Eqs. (8.1.13) and (8.1.14) can only be applied to a mode that is underdamped, Eqs. (8.1.11) and (8.1.12) can be applied to underdamped, overdamped, and critically damped modes. For the damped spring-mass system that is shown in Fig 8.1.1, using Eq. (8.1.4) in Eq. (8.1.11) gives

$$\omega_n = \sqrt{k/m} \tag{8.1.15}$$

and using Eq. (8.1.4) in Eq. (8.1.12) results in

$$\zeta = c/\left(2\sqrt{km}\right) \tag{8.1.16}$$

Combining Eqs. (8.1.11) and (8.1.12), the eigenvalue pair can be expressed in terms of the undamped natural frequency and the damping ratio,

$$\lambda_{1,2} = -\zeta\omega_n \pm \omega_n\sqrt{\zeta^2 - 1} \tag{8.1.17}$$

If the damping ratio is less than 1.0, comparing Eq. (8.1.17) with Eq. (8.1.10), we see that the damping rate and the damped natural frequency are related to the damping ratio and the undamped natural frequency according to

$$\sigma = \zeta\omega_n \tag{8.1.18}$$

$$\omega_d = \omega_n\sqrt{1-\zeta^2} \tag{8.1.19}$$

When the eigenvalues are complex, using Eq. (8.1.10), the homogeneous solution given by Eq. (8.1.3) can also be written in terms of sinusoidal functions,

$$\Delta x(t) = e^{-\sigma t}[C_3 \sin(\omega_d t) + C_4 \cos(\omega_d t)] \tag{8.1.20}$$

where C_3 and C_4 are arbitrary constants, different from C_1 and C_2. In this form it is easy to see that the homogeneous solution is a sinusoidal oscillation with period $2\pi/\omega_d$. We also see that the amplitude of oscillation decreases exponentially with time. The rate at which the oscillations decay is sometimes specified by the *time constant*, which is $1/\sigma$ or the time required for the amplitude to be reduced by about 63 percent. Another common measure of the decay rate is the *time to half amplitude*, which is $-\ln(0.5)/\sigma$ or about 69 percent of the time constant.

In summary, the nature of the homogeneous solution to Eq. (8.1.2) depends on two constants, the eigenvalues λ_1 and λ_2, which can be either real or complex. In general, these eigenvalues can be written in terms of the damping ratio, ζ, and the undamped

natural frequency, ω_n, according to Eq. (8.1.17). If the damping ratio is less than 1.0, the eigenvalues are complex and can be written in terms of the damping rate, σ, and the damped natural frequency, ω_d, in accordance with Eq. (8.1.10). The homogeneous solution obtained from these eigenvalues is called the *free response*.

System motion resulting from the application of a time varying force is called the *forced response*. For example, consider the case where the forcing function, $F(t)$, is sinusoidal with frequency, ω_f, and amplitude, F_a. In this case Eq. (8.1.2) becomes

$$m\frac{d^2\Delta x}{dt^2} + c\frac{d\Delta x}{dt} + k\Delta x = F_a \sin(\omega_f t) \tag{8.1.21}$$

The general solution to this equation is the homogeneous solution in Eq. (8.1.3), plus a particular solution, which can be found using the method of undetermined coefficients,

$$\Delta x(t) = C_1 e^{\lambda_1 t} + C_2 e^{\lambda_2 t} + A_f \frac{F_a}{k}\sin(\omega_f t - \Psi) \tag{8.1.22}$$

where A_f is the amplification factor shown in Fig. 8.1.3 and given by

$$A_f = \frac{1}{\sqrt{\left[1-(\omega_f/\omega_n)^2\right]^2 + \left[2\zeta(\omega_f/\omega_n)\right]^2}} \tag{8.1.23}$$

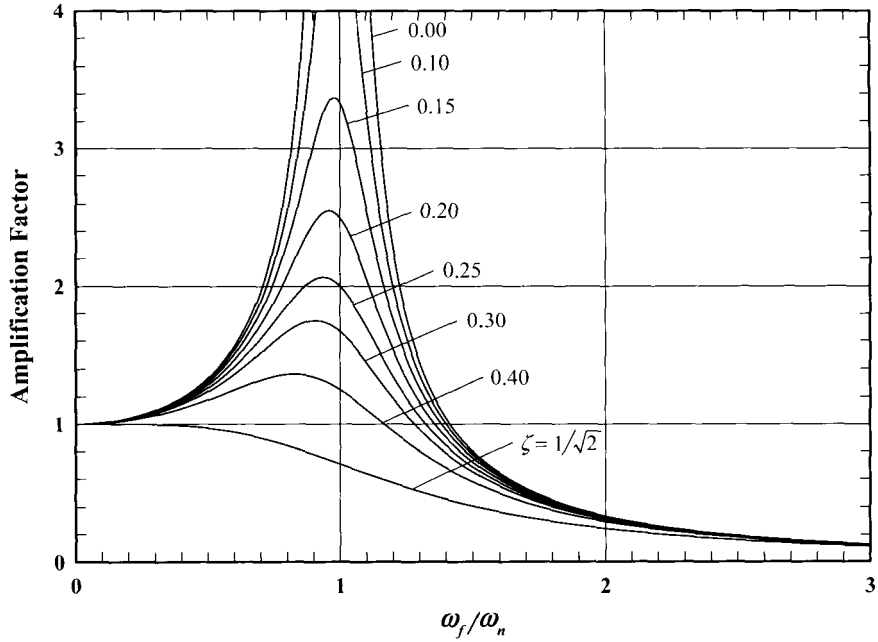


Figure 8.1.3. Amplification factor associated with the forced response.

and Ψ is the phase angle given by

$$\Psi = \frac{2\zeta(\omega_f/\omega_n)}{1-(\omega_f/\omega_n)^2} \tag{8.1.24}$$

Figure 8.1.3 shows the amplification factor, given by Eq. (8.1.23), plotted as a function of the forcing frequency, ω_f, divided by the undamped natural frequency, ω_n. In the limiting case of zero damping, the amplitude of the forced vibration is seen to approach infinity as the forcing frequency approaches the undamped natural frequency. This phenomenon is called *resonance*. The response amplitude of the forced vibration is maximum when the forcing frequency is somewhat less than the undamped natural frequency. The forcing frequency that results in maximum response amplification is found by differentiating the right-hand side of Eq. (8.1.23) with respect to ω_f and setting the result to zero. This gives

$$\text{maximum response frequency} \equiv \omega_m = \omega_n\sqrt{1-2\zeta^2} \tag{8.1.25}$$

Clearly, from Eq. (8.1.25) we see that the frequency of maximum response, ω_m, is less than the undamped natural frequency, ω_n. Furthermore, after comparing Eq. (8.1.25) with Eq. (8.1.19), we see that the frequency resulting in maximum response is also less than the damped natural frequency, ω_d.

For lightly damped systems when the forcing frequency is close to ω_m, the amplification factor is much greater than 1; when the forcing frequency is much less than ω_m, the amplification factor approaches 1; and for a forcing frequency much greater than ω_m, the amplification factor approaches zero. As the damping ratio is increased from zero, the amplification due to resonance is reduced. For damping ratios that are greater than $\zeta = \sqrt{1/2}$, all resonance amplification is eliminated.

Because the spring-mass system having one degree of freedom is modeled with a single second-order differential equation, the eigenvalues can be found analytically. However, this is not the case for systems with many degrees of freedom. For second-order systems having more than two degrees of freedom, the eigenvalues must be found numerically. To facilitate the numerical solution, it is convenient to express each second-order differential equation as two first-order equations. To demonstrate, we shall first apply this procedure to Eq. (8.1.2).

Defining a second dependent variable to be the time rate of change of the position disturbance, i.e., the velocity disturbance,

$$\Delta V \equiv \frac{d\Delta x}{dt} \tag{8.1.26}$$

we can rewrite the homogeneous form of Eq. (8.1.2) as

$$\begin{bmatrix} m & 0 \\ 0 & 1 \end{bmatrix} \begin{Bmatrix} \Delta\dot{V} \\ \Delta\dot{x} \end{Bmatrix} = \begin{bmatrix} -c & -k \\ 1 & 0 \end{bmatrix} \begin{Bmatrix} \Delta V \\ \Delta x \end{Bmatrix} \tag{8.1.27}$$

where the dot indicates a time derivative. Equation (8.1.27) is of the form

$$[\mathbf{B}]\{\dot{\mathbf{X}}\} = [\mathbf{A}]\{\mathbf{X}\} \tag{8.1.28}$$

where

$$\{\mathbf{X}\} = \begin{Bmatrix} \Delta V \\ \Delta x \end{Bmatrix} \tag{8.1.29}$$

$$[\mathbf{A}] = \begin{bmatrix} -c & -k \\ 1 & 0 \end{bmatrix} \tag{8.1.30}$$

$$[\mathbf{B}] = \begin{bmatrix} m & 0 \\ 0 & 1 \end{bmatrix} \tag{8.1.31}$$

The solutions to Eq. (8.1.28) are of the form

$$\{\mathbf{X}\} = C\{\boldsymbol{\chi}\}e^{\lambda t} \tag{8.1.32}$$

where C is an arbitrary scalar constant, $\{\boldsymbol{\chi}\}$ is a vector with explicit constant components, and λ is an explicit scalar constant. Using Eq. (8.1.32) in Eq. (8.1.28), we have

$$C\lambda[\mathbf{B}]\{\boldsymbol{\chi}\}e^{\lambda t} = C[\mathbf{A}]\{\boldsymbol{\chi}\}e^{\lambda t} \tag{8.1.33}$$

Equation (8.1.33) can be written in the alternative form

$$\left([\mathbf{A}] - \lambda[\mathbf{B}]\right)\{\boldsymbol{\chi}\} = 0 \tag{8.1.34}$$

Equation (8.1.34) represents a homogeneous system of linear algebraic equations. This is the *generalized eigenproblem*. Nontrivial solutions to this system of equation will exist only if the determinant of $[\mathbf{A}] - \lambda[\mathbf{B}]$ is zero. The values of λ that will force this determinant to be zero are the eigenvalues. There exists a pair of eigenvalues for each degree of freedom associated with the problem. A one-degree-of-freedom problem has two eigenvalues; a two-degree-of-freedom problem has four eigenvalues; and so on. For each eigenvalue there exists a nontrivial solution for $\{\boldsymbol{\chi}\}$ that will satisfy Eq. (8.1.34). These solution vectors are called *eigenvectors*. While the eigenvectors are nontrivial, they are not unique. Clearly, because Eq. (8.1.34) is homogeneous, any multiple of an eigenvector will also be an eigenvector.

In summary, the eigenvalues are found by obtaining the roots to the characteristic equation obtained by setting the determinant of $[\mathbf{A}] - \lambda[\mathbf{B}]$ to zero,

$$\left|[\mathbf{A}] - \lambda_i[\mathbf{B}]\right| = 0 \tag{8.1.35}$$

Each set of eigenvectors is found by using the corresponding eigenvalue in the system of equations given by

$$([\mathbf{A}] - \lambda_i [\mathbf{B}])\{\chi\}_i = 0 \tag{8.1.36}$$

Because the eigenvectors are unique only to within some arbitrary constant multiplier, they are commonly defined so that each eigenvector has a magnitude of unity, with the largest component being real,

$$\sqrt{\sum_{j=1}^{N} \left|\chi_j\right|_i^2} = 1, \qquad \text{imag}\left(\max(\chi_j)\right)_i = 0 \tag{8.1.37}$$

The *absolute value* or *magnitude* of any component of an eigenvector is defined to be the square root of the sum of the squares of its real and imaginary parts. Once any form of an eigenvector is found, it can easily be normalized according to Eq. (8.1.37). First, the component having the largest magnitude is found. All components of the eigenvector are then multiplied by the complex conjugate of this largest component. This makes the largest component real. Next, the magnitude of the entire eigenvector is found by taking the square root of the sum of the squares of the magnitudes of all components. Finally, all components of the eigenvector are divided by this magnitude, giving the final form of the eigenvector a magnitude of unity.

The two eigenvalues for a one-degree-of-freedom problem can easily be obtained analytically. Using Eqs. (8.1.30) and (8.1.31) in Eq. (8.1.35) and evaluating the determinate, we have

$$\left|[\mathbf{A}] - \lambda[\mathbf{B}]\right| = \left|\begin{bmatrix} -c & -k \\ 1 & 0 \end{bmatrix} - \lambda \begin{bmatrix} m & 0 \\ 0 & 1 \end{bmatrix}\right| = \begin{vmatrix} -(c+m\lambda) & -k \\ 1 & -\lambda \end{vmatrix} \tag{8.1.38}$$

$$= m\lambda^2 + c\lambda + k = 0$$

which gives the well-known solutions expressed in Eq. (8.1.4).

The eigenvalues and eigenvectors for systems with multiple degrees of freedom can readily be obtained numerically using a digital computer. Because of the importance of eigenproblems in all fields of engineering and science, algorithms for computing eigenvalues and eigenvectors are widely available. Most modern computer facilities will have subroutines available for determining eigenvalues and eigenvectors. In fact, today, most hand-held scientific calculators have preprogrammed algorithms for obtaining numerical solutions to eigenproblems.

The details associated with obtaining numerical solutions to eigenproblems can be found in any undergraduate text on engineering numerical methods (see, for example, Hoffman 1992 or Press et al., 1986). Since an introductory course in numerical methods is assumed to be a prerequisite to the material presented in this text, the details associated with implementing numerical solutions to the eigenproblem will not be repeated here.

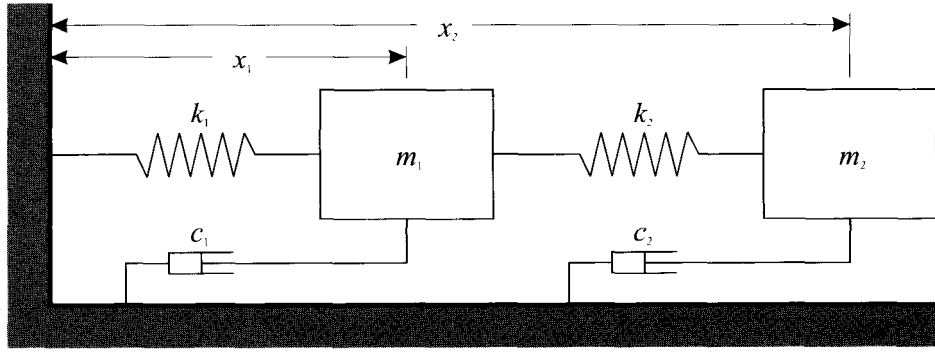


Figure 8.1.4. Damped spring-mass system with two degrees of freedom.

As an example of an eigenproblem with multiple degrees of freedom, consider the free response of the damped spring-mass system illustrated in Fig. 8.1.4. This system has two degrees of freedom, one associated with the independent translation of each mass. Applying Newton's second law of motion to this system, we have

$$m_1 \frac{d^2 x_1}{dt^2} = -c_1 \frac{dx_1}{dt} - k_1(x_1 - x_{1o}) + k_2[(x_2 - x_1) - (x_{2o} - x_{1o})] \tag{8.1.39}$$

$$m_2 \frac{d^2 x_2}{dt^2} = -c_2 \frac{dx_2}{dt} - k_2[(x_2 - x_1) - (x_{2o} - x_{1o})] \tag{8.1.40}$$

Equations (8.1.39) and (8.1.40) can be rewritten in terms of the axial displacement of each mass from equilibrium, $\Delta x_1 = x_1 - x_{1o}$ and $\Delta x_2 = x_2 - x_{2o}$,

$$m_1 \frac{d^2 \Delta x_1}{dt^2} + c_1 \frac{d\Delta x_1}{dt} + (k_1 + k_2)\Delta x_1 - k_2 \Delta x_2 = 0 \tag{8.1.41}$$

$$m_2 \frac{d^2 \Delta x_2}{dt^2} + c_2 \frac{d\Delta x_2}{dt} - k_2 \Delta x_1 + k_2 \Delta x_2 = 0 \tag{8.1.42}$$

Defining the dependent variables,

$$\Delta V_1 \equiv \frac{d\Delta x_1}{dt} \tag{8.1.43}$$

$$\Delta V_2 \equiv \frac{d\Delta x_2}{dt} \tag{8.1.44}$$

we can rewrite Eqs. (8.1.41) and (8.1.42) as

$$\begin{bmatrix} m_1 & 0 & 0 & 0 \\ 0 & m_2 & 0 & 0 \\ 0 & 0 & 1 & 0 \\ 0 & 0 & 0 & 1 \end{bmatrix} \begin{Bmatrix} \Delta\dot{V}_1 \\ \Delta\dot{V}_2 \\ \Delta\dot{x}_1 \\ \Delta\dot{x}_2 \end{Bmatrix} = \begin{bmatrix} -c_1 & 0 & -(k_1+k_2) & k_2 \\ 0 & -c_2 & k_2 & -k_2 \\ 1 & 0 & 0 & 0 \\ 0 & 1 & 0 & 0 \end{bmatrix} \begin{Bmatrix} \Delta V_1 \\ \Delta V_2 \\ \Delta x_1 \\ \Delta x_2 \end{Bmatrix} \tag{8.1.45}$$

In general, the solutions to the homogeneous system of equations given by Eq. (8.1.45) are all of the form

$$\begin{Bmatrix} \Delta V_1 \\ \Delta V_2 \\ \Delta x_1 \\ \Delta x_2 \end{Bmatrix} = C \begin{Bmatrix} \chi_{V_1} \\ \chi_{V_2} \\ \chi_{x_1} \\ \chi_{x_2} \end{Bmatrix} e^{\lambda t} \tag{8.1.46}$$

Using Eq. (8.1.46) in Eq. (8.1.45), we have

$$C\lambda \begin{bmatrix} m_1 & 0 & 0 & 0 \\ 0 & m_2 & 0 & 0 \\ 0 & 0 & 1 & 0 \\ 0 & 0 & 0 & 1 \end{bmatrix} \begin{Bmatrix} \chi_{V_1} \\ \chi_{V_2} \\ \chi_{x_1} \\ \chi_{x_2} \end{Bmatrix} e^{\lambda t} = C \begin{bmatrix} -c_1 & 0 & -(k_1+k_2) & k_2 \\ 0 & -c_2 & k_2 & -k_2 \\ 1 & 0 & 0 & 0 \\ 0 & 1 & 0 & 0 \end{bmatrix} \begin{Bmatrix} \chi_{V_1} \\ \chi_{V_2} \\ \chi_{x_1} \\ \chi_{x_2} \end{Bmatrix} e^{\lambda t} \tag{8.1.47}$$

or after rearranging,

$$\left(\begin{bmatrix} -c_1 & 0 & -(k_1+k_2) & k_2 \\ 0 & -c_2 & k_2 & -k_2 \\ 1 & 0 & 0 & 0 \\ 0 & 1 & 0 & 0 \end{bmatrix} - \lambda \begin{bmatrix} m_1 & 0 & 0 & 0 \\ 0 & m_2 & 0 & 0 \\ 0 & 0 & 1 & 0 \\ 0 & 0 & 0 & 1 \end{bmatrix} \right) \begin{Bmatrix} \chi_{V_1} \\ \chi_{V_2} \\ \chi_{x_1} \\ \chi_{x_2} \end{Bmatrix} = \begin{Bmatrix} 0 \\ 0 \\ 0 \\ 0 \end{Bmatrix} \tag{8.1.48}$$

This system of linear algebraic equations is in the form of the generalized eigenproblem given by Eq. (8.1.34), where

$$[\mathbf{A}] = \begin{bmatrix} -c_1 & 0 & -(k_1+k_2) & k_2 \\ 0 & -c_2 & k_2 & -k_2 \\ 1 & 0 & 0 & 0 \\ 0 & 1 & 0 & 0 \end{bmatrix} \tag{8.1.49}$$

$$[\mathbf{B}] = \begin{bmatrix} m_1 & 0 & 0 & 0 \\ 0 & m_2 & 0 & 0 \\ 0 & 0 & 1 & 0 \\ 0 & 0 & 0 & 1 \end{bmatrix} \tag{8.1.50}$$

If the masses, damping coefficients, and spring constants in Eq. (8.1.48) are all known, the eigenvalues and eigenvectors associated with the motion of this system can be found by using these matrices in any generalized eigensolver.

The character of each mode of motion associated with the free response of this system can be identified as being overdamped, underdamped, or critically damped, by examining the eigenvalues, just as was done for the one-degree-of-freedom problem. Any eigenvalue that is real, distinct, and negative corresponds to an overdamped mode, with the damping rate being equal to the negative of this real eigenvalue. A pair of eigenvalues that are real, identical, and negative corresponds to a critically damped mode, having a damping rate that is also equal to the negative of the real eigenvalue. When complex eigenvalues are found, they are always found in complex pairs. Each complex pair of eigenvalues corresponds to a mode that is underdamped. Such modes result in sinusoidal motion having a frequency equal to the magnitude of the imaginary part of the eigenvalue and a damping rate equal to the negative of the real part of the eigenvalue.

Most readers should be quite familiar with the foregoing interpretation of the eigenvalues, from their study of elementary dynamics with one degree of freedom. However, many readers may not be as familiar with the physical interpretation of the eigenvectors. Since a real number is a special case of a complex number, we shall first describe the interpretation of an eigenvector that is associated with a complex eigenvalue. The components of the eigenvectors associated with a complex pair of eigenvalues also form complex pairs. To demonstrate the physical meaning of such eigenvectors, consider the eigenvectors associated with a complex pair of eigenvalues that are solutions to Eq. (8.1.48). Let the eigenvalues be

$$\lambda_1, \lambda_2 = -\sigma \pm \omega_d i \tag{8.1.51}$$

and let the eigenvectors associated with these two eigenvalues be

$$\begin{Bmatrix} \chi_{V_1} \\ \chi_{V_2} \\ \chi_{x_1} \\ \chi_{x_2} \end{Bmatrix}_1, \begin{Bmatrix} \chi_{V_1} \\ \chi_{V_2} \\ \chi_{x_1} \\ \chi_{x_2} \end{Bmatrix}_2 = \begin{Bmatrix} R_{V_1} \pm I_{V_1} i \\ R_{V_2} \pm I_{V_2} i \\ R_{x_1} \pm I_{x_1} i \\ R_{x_2} \pm I_{x_2} i \end{Bmatrix} \tag{8.1.52}$$

where σ is the damping rate and ω_d is the damped natural frequency.

Recall that a complex number can be written in exponential form in terms of its amplitude and phase. Thus, Eq. (8.1.52) can be written as

$$\begin{Bmatrix} \chi_{V_1} \\ \chi_{V_2} \\ \chi_{x_1} \\ \chi_{x_2} \end{Bmatrix}_1, \begin{Bmatrix} \chi_{V_1} \\ \chi_{V_2} \\ \chi_{x_1} \\ \chi_{x_2} \end{Bmatrix}_2 = \begin{Bmatrix} A_{V_1} e^{\pm \Theta_{V_1} i} \\ A_{V_2} e^{\pm \Theta_{V_2} i} \\ A_{x_1} e^{\pm \Theta_{x_1} i} \\ A_{x_2} e^{\pm \Theta_{x_2} i} \end{Bmatrix} \tag{8.1.53}$$

where for each component of this complex pair of eigenvectors, the amplitude, A, and the phase angle, Θ, are related to the real part, R, and the imaginary part, I, according to the relations

$$A = \sqrt{R^2 + I^2} \tag{8.1.54}$$

and

$$\Theta = \tan^{-1}(I/R) \tag{8.1.55}$$

From Eq. (8.1.46), the general solution corresponding to this pair of eigenvalues can be written as

$$\begin{Bmatrix} \Delta V_1 \\ \Delta V_2 \\ \Delta x_1 \\ \Delta x_2 \end{Bmatrix} = C_1 \begin{Bmatrix} A_{V_1} e^{\Theta_{V_1} i} \\ A_{V_2} e^{\Theta_{V_2} i} \\ A_{x_1} e^{\Theta_{x_1} i} \\ A_{x_2} e^{\Theta_{x_2} i} \end{Bmatrix} e^{(-\sigma+\omega_d i)t} + C_2 \begin{Bmatrix} A_{V_1} e^{-\Theta_{V_1} i} \\ A_{V_2} e^{-\Theta_{V_2} i} \\ A_{x_1} e^{-\Theta_{x_1} i} \\ A_{x_2} e^{-\Theta_{x_2} i} \end{Bmatrix} e^{(-\sigma-\omega_d i)t} \tag{8.1.56}$$

or after rearranging,

$$\begin{Bmatrix} \Delta V_1 \\ \Delta V_2 \\ \Delta x_1 \\ \Delta x_2 \end{Bmatrix} = e^{-\sigma t} \left(C_1 \begin{Bmatrix} A_{V_1} e^{i(\omega_d t+\Theta_{V_1})} \\ A_{V_2} e^{i(\omega_d t+\Theta_{V_2})} \\ A_{x_1} e^{i(\omega_d t+\Theta_{x_1})} \\ A_{x_2} e^{i(\omega_d t+\Theta_{x_2})} \end{Bmatrix} + C_2 \begin{Bmatrix} A_{V_1} e^{-i(\omega_d t+\Theta_{V_1})} \\ A_{V_2} e^{-i(\omega_d t+\Theta_{V_2})} \\ A_{x_1} e^{-i(\omega_d t+\Theta_{x_1})} \\ A_{x_2} e^{-i(\omega_d t+\Theta_{x_2})} \end{Bmatrix} \right) \tag{8.1.57}$$

To facilitate writing the solution in terms of circular functions, Eq. (8.1.57) can be further rearranged to give

$$\begin{aligned} \begin{Bmatrix} \Delta V_1 \\ \Delta V_2 \\ \Delta x_1 \\ \Delta x_2 \end{Bmatrix} = {} & e^{-\sigma t} \left(\frac{C_1 + C_2}{2} \begin{Bmatrix} A_{V_1} e^{i(\omega_d t+\Theta_{V_1})} \\ A_{V_2} e^{i(\omega_d t+\Theta_{V_2})} \\ A_{x_1} e^{i(\omega_d t+\Theta_{x_1})} \\ A_{x_2} e^{i(\omega_d t+\Theta_{x_2})} \end{Bmatrix} + \frac{C_1 + C_2}{2} \begin{Bmatrix} A_{V_1} e^{-i(\omega_d t+\Theta_{V_1})} \\ A_{V_2} e^{-i(\omega_d t+\Theta_{V_2})} \\ A_{x_1} e^{-i(\omega_d t+\Theta_{x_1})} \\ A_{x_2} e^{-i(\omega_d t+\Theta_{x_2})} \end{Bmatrix} \right) \\ & + e^{-\sigma t} \left(\frac{C_1 - C_2}{2} \begin{Bmatrix} A_{V_1} e^{i(\omega_d t+\Theta_{V_1})} \\ A_{V_2} e^{i(\omega_d t+\Theta_{V_2})} \\ A_{x_1} e^{i(\omega_d t+\Theta_{x_1})} \\ A_{x_2} e^{i(\omega_d t+\Theta_{x_2})} \end{Bmatrix} - \frac{C_1 - C_2}{2} \begin{Bmatrix} A_{V_1} e^{-i(\omega_d t+\Theta_{V_1})} \\ A_{V_2} e^{-i(\omega_d t+\Theta_{V_2})} \\ A_{x_1} e^{-i(\omega_d t+\Theta_{x_1})} \\ A_{x_2} e^{-i(\omega_d t+\Theta_{x_2})} \end{Bmatrix} \right) \end{aligned} \tag{8.1.58}$$

Now, recalling the exponential definitions of the circular functions,

$$\cos x = \frac{e^{ix} + e^{-ix}}{2} \tag{8.1.59}$$

$$\sin x = \frac{e^{ix} - e^{-ix}}{2i} \tag{8.1.60}$$

Eq. (8.1.58) becomes

$$\begin{Bmatrix} \Delta V_1 \\ \Delta V_2 \\ \Delta x_1 \\ \Delta x_2 \end{Bmatrix} = (C_1 + C_2) e^{-\sigma t} \begin{Bmatrix} A_{V_1} \cos(\omega_d t + \Theta_{V_1}) \\ A_{V_2} \cos(\omega_d t + \Theta_{V_2}) \\ A_{x_1} \cos(\omega_d t + \Theta_{x_1}) \\ A_{x_2} \cos(\omega_d t + \Theta_{x_2}) \end{Bmatrix} + (C_1 - C_2) e^{-\sigma t} \begin{Bmatrix} A_{V_1} \sin(\omega_d t + \Theta_{V_1}) \\ A_{V_2} \sin(\omega_d t + \Theta_{V_2}) \\ A_{x_1} \sin(\omega_d t + \Theta_{x_1}) \\ A_{x_2} \sin(\omega_d t + \Theta_{x_2}) \end{Bmatrix} i \tag{8.1.61}$$

Here we see that this solution corresponds to damped sinusoidal oscillation. Each of the four dependent variables oscillates with exactly the same frequency. However, each dependent variable has a different amplitude and a different phase shift. The eigenvalues give us the damped natural frequency and the damping rate for all of the oscillation, while the components of the eigenvectors give us the amplitudes and the phase shifts. Since the sinusoidal terms are multiplied by arbitrary constants, the eigenvectors describe only relative amplitudes and phase shifts. If the eigenvector has been normalized according to Eq. (8.1.37), making the largest component real, from Eq. (8.1.55) we see that the phase angle for this component will be zero. Thus, an eigenvector in this form describes the phase of each component relative to the component having the largest magnitude.

Eigenvectors corresponding to purely real or purely imaginary eigenvalues can be viewed as special cases of the complex eigenvalue. Purely imaginary eigenvalues simply describe undamped sinusoidal motion, and the eigenvectors are interpreted exactly the same as those corresponding to complex eigenvalues. A purely real eigenvalue could be thought of as describing damped sinusoidal motion with a frequency of zero. All components of the eigenvector corresponding to a purely real eigenvalue are also real. Thus, the magnitude of each component of such an eigenvector is simply equal to its absolute value and the phase angle is either zero or 180 degrees. So we see that for a purely real eigenvalue, the components of the eigenvector also describe the relative amplitudes associated with the temporal variations of the dependent variables. The only difference between the results obtained from real eigenvalues and those obtained from complex eigenvalues is that the temporal variations associated with the real eigenvalues are exponential, while those associated with the complex eigenvalues represent damped sinusoidal motion.

Before proceeding with some example calculations, it is worth spending a few words talking about the *special eigenproblem*. The generalized eigenproblem specified by Eq. (8.1.34) contains two $n \times n$ matrices, **[A]** and **[B]**. No special requirements are placed on either **[A]** or **[B]**. In general, both of these matrices could have n^2 nonzero terms. However, many physical problems can readily be formulated in terms of a somewhat simpler system of equations called the *special eigenproblem*. For example, consider the spring-mass system shown in Fig. 8.1.4, which yields the eigenproblem specified by Eq. (8.1.48):

$$\left(\begin{bmatrix} -c_1 & 0 & -(k_1+k_2) & k_2 \\ 0 & -c_2 & k_2 & -k_2 \\ 1 & 0 & 0 & 0 \\ 0 & 1 & 0 & 0 \end{bmatrix} - \lambda \begin{bmatrix} m_1 & 0 & 0 & 0 \\ 0 & m_2 & 0 & 0 \\ 0 & 0 & 1 & 0 \\ 0 & 0 & 0 & 1 \end{bmatrix} \right) \begin{Bmatrix} \chi_{V_1} \\ \chi_{V_2} \\ \chi_{x_1} \\ \chi_{x_2} \end{Bmatrix} = \begin{Bmatrix} 0 \\ 0 \\ 0 \\ 0 \end{Bmatrix}$$

This eigenproblem can readily be rearranged to the form of the special eigenproblem. Dividing the first row by m_1 and the second row by m_2, we have

$$\left(\begin{bmatrix} -c_1/m_1 & 0 & -(k_1+k_2)/m_1 & k_2/m_1 \\ 0 & -c_2/m_2 & k_2/m_2 & -k_2/m_2 \\ 1 & 0 & 0 & 0 \\ 0 & 1 & 0 & 0 \end{bmatrix} - \lambda \begin{bmatrix} 1 & 0 & 0 & 0 \\ 0 & 1 & 0 & 0 \\ 0 & 0 & 1 & 0 \\ 0 & 0 & 0 & 1 \end{bmatrix} \right) \begin{Bmatrix} \chi_{V_1} \\ \chi_{V_2} \\ \chi_{x_1} \\ \chi_{x_2} \end{Bmatrix} = \begin{Bmatrix} 0 \\ 0 \\ 0 \\ 0 \end{Bmatrix} \tag{8.1.62}$$

This is exactly the form of the **special eigenproblem**, which is a special case of the generalized eigenproblem where the matrix **[B]** is exactly equal to the identity matrix **[i]**,

$$\left([\mathbf{A}] - \lambda [\mathbf{i}] \right) \{\chi\} = 0 \tag{8.1.63}$$

Eigensolvers for the special eigenproblem are more widely available than are those for the generalized eigenproblem. If you have an eigensolver that requires only one matrix as input, it is more than likely solving for the eigenvalues and eigenvectors associated with Eq. (8.1.63).

The specifications for a subroutine intended to solve the special eigenproblem might say that the subroutine finds the eigenvalues and eigenvectors of the matrix **[A]**. Strictly speaking, a single matrix **[A]** by itself does not have eigenvalues. Only when the matrix **[A]** is combined with a second matrix **[B]** and used in Eq. (8.1.34) to form a system of equations can we define the eigenvalues. Strictly speaking, it is the system of equations that has eigenvalues, not the matrix. However, in the usual manner of speaking,

whenever the second matrix **[B]** is not mentioned, it is assumed to be the identity matrix and it is assumed that we are solving the special eigenproblem given by Eq. (8.1.63).

The generalized eigenproblem can be reduced to the special eigenproblem. In the special case of Eq. (8.1.48) this was particularly easy because **[B]** was a diagonal matrix. In the more general case, a special eigenproblem can be obtained from a generalized eigenproblem by multiplying by the inverse of the matrix **[B]**. From Eq. (8.1.34) we can write

$$\left([\mathbf{B}]^{-1}[\mathbf{A}] - \lambda[\mathbf{B}]^{-1}[\mathbf{B}]\right)\{\chi\} = 0 \tag{8.1.64}$$

Since any matrix multiplied by its inverse is equal to the identity matrix, Eq. (8.1.64) is in the form of the special eigenproblem. The only difficulty comes in finding the inverse of **[B]**. If the matrix **[B]** is of a form that easily allows us to evaluate its inverse, then the generalized eigenproblem is easily reduced to the special eigenproblem. For example, if **[B]** is tridiagonal, the Thomas algorithm can be used to invert **[B]**. If **[B]** is diagonally dominant and otherwise quite sparse, it may be very simple to manually reduce the generalized eigenproblem to the special eigenproblem by using Gauss elimination. However, if a good generalized eigensolver is available, it is usually easier to leave the eigenproblem in the generalized form and let the computer do the work.

EXAMPLE 8.1.1. For the damped spring-mass system that is shown in Fig. 8.1.4, find the eigenvalues, the eigenvectors, the damping rate, the 99 percent damping time, and the damped natural frequency and period if underdamped, for each mode associated with the case:

$$\begin{aligned} m_1 &= 20.0 \text{ slugs}, & c_1 &= 30.0 \text{ lbf}\cdot\text{sec/ft}, & k_1 &= 2.0 \text{ lbf/ft}, \\ m_2 &= 20.0 \text{ slugs}, & c_2 &= 15.0 \text{ lbf}\cdot\text{sec/ft}, & k_2 &= 100.0 \text{ lbf/ft} \end{aligned}$$

For each pair of eigenvalues, compute the undamped natural frequency and the damping ratio. For each oscillatory mode, compute the amplitude and phase angle for each component of the eigenvector.

Solution. Using these values for the masses, damping coefficients, and spring constants in Eq. (8.1.48), the generalized eigenproblem for this system is

$$\left(\begin{bmatrix} -30.0 & 0 & -102.0 & 100.0 \\ 0 & -15.0 & 100.0 & -100.0 \\ 1 & 0 & 0 & 0 \\ 0 & 1 & 0 & 0 \end{bmatrix} - \lambda \begin{bmatrix} 20.0 & 0 & 0 & 0 \\ 0 & 20.0 & 0 & 0 \\ 0 & 0 & 1 & 0 \\ 0 & 0 & 0 & 1 \end{bmatrix}\right) \begin{Bmatrix} \chi_{V_1} \\ \chi_{V_2} \\ \chi_{x_1} \\ \chi_{x_2} \end{Bmatrix} = \begin{Bmatrix} 0 \\ 0 \\ 0 \\ 0 \end{Bmatrix}$$

The solution to this characteristic equation can be obtained numerically using a generalized eigensolver. This system of equations is also easily reduced to the special eigenproblem,

$$\left(\begin{bmatrix} -1.5 & 0 & -5.1 & 5.0 \\ 0 & -0.75 & 5.0 & -5.0 \\ 1 & 0 & 0 & 0 \\ 0 & 1 & 0 & 0 \end{bmatrix} - \lambda \begin{bmatrix} 1 & 0 & 0 & 0 \\ 0 & 1 & 0 & 0 \\ 0 & 0 & 1 & 0 \\ 0 & 0 & 0 & 1 \end{bmatrix}\right) \begin{Bmatrix} \chi_{V_1} \\ \chi_{V_2} \\ \chi_{x_1} \\ \chi_{x_2} \end{Bmatrix} = \begin{Bmatrix} 0 \\ 0 \\ 0 \\ 0 \end{Bmatrix}$$

The solution to either of these systems yields the eigenvalues and eigenvectors that correspond to the following modes:

Mode 1 ($\lambda_{1,2} = -0.556387\ \text{sec}^{-1} \pm 3.098306\, i\ \text{sec}^{-1}$)
From the eigenvectors associated with this mode, the corresponding homogeneous solutions are

$$\begin{Bmatrix} \Delta V_1 \\ \Delta V_2 \\ \Delta x_1 \\ \Delta x_2 \end{Bmatrix} = C_{1,2} \begin{Bmatrix} (-0.644717 \mp 0.153945\, i)\ \text{ft/sec} \\ 0.684817\ \text{ft/sec} \\ (-0.011934 \pm 0.210230\, i)\ \text{ft} \\ (-0.038452 \mp 0.214124\, i)\ \text{ft} \end{Bmatrix} \times \exp[(-0.556387 \pm 3.098306\, i)\, t/\text{sec}]$$

The damping rate is

$$\sigma = -\text{real}(\lambda) = 0.556387\ \text{sec}^{-1}$$

The 99 percent damping time is the time required for the amplitude of the oscillations to be reduced by 99 percent, in other words, the time required for the amplitude to be reduced to 1 percent of its original value. Thus, we can write

$$\frac{\exp(-\sigma t_{99})}{\exp(-\sigma 0.0)} = \exp(-\sigma t_{99}) = 0.01$$

$$99\%\ \text{damping time} = \frac{\ln(0.01)}{-\sigma} = \frac{\ln(0.01)}{-0.556387\ \text{sec}^{-1}} = 8.277\ \text{sec}$$

The damped natural frequency and period for this motion are

$$\omega_d = |\text{imag}(\lambda)| = 3.098306\ \text{rad/sec}$$

$$\text{period} = \frac{2\pi}{\omega_d} = \frac{2\pi}{3.098306\ \text{sec}^{-1}} = 2.028\ \text{sec}$$

For the pair of complex roots associated with this mode, the undamped natural frequency is

$$\omega_n = \sqrt{\lambda_1 \lambda_2} = \sqrt{(-0.556387 + 3.098306\,i)(-0.556387 - 3.098306\,i)}$$
$$= \sqrt{0.556387^2 + 3.098306^2} = 3.147867 \text{ rad/sec}$$

and the damping ratio is

$$\zeta = -\frac{\lambda_1 + \lambda_2}{2\sqrt{\lambda_1 \lambda_2}} = -\frac{-0.556387 + 3.098306\,i - 0.556387 - 3.098306\,i}{2\sqrt{(-0.556387 + 3.098306\,i)(-0.556387 - 3.098306\,i)}}$$
$$= \frac{0.556387}{\sqrt{0.556387^2 + 3.098306^2}} = 0.176750$$

Notice that for this mode, the frequency is decreased by less than 2 percent as a result of damping.

Mode 2 ($\lambda_3 = -1.090975 \text{ sec}^{-1}$)
From the eigenvector associated with this mode, the homogeneous solution that results from this real eigenvalue is

$$\begin{Bmatrix} \Delta V_1 \\ \Delta V_2 \\ \Delta x_1 \\ \Delta x_2 \end{Bmatrix} = C_3 \begin{Bmatrix} 0.539609 \text{ ft/sec} \\ 0.502243 \text{ ft/sec} \\ -0.494612 \text{ ft} \\ -0.460362 \text{ ft} \end{Bmatrix} \exp(-1.090975\, t/\text{sec})$$

Since the eigenvalue is real and negative, this is overdamped motion having a damping rate and 99 percent damping time of

$$\sigma = -\text{real}(\lambda) = 1.090975 \text{ sec}^{-1}$$

$$99\% \text{ damping time} = \frac{\ln(0.01)}{-\sigma} = \frac{\ln(0.01)}{-1.090975 \text{ sec}^{-1}} = 4.221 \text{ sec}$$

Mode 3 ($\lambda_4 = -0.046251 \text{ sec}^{-1}$)
From the associated eigenvector, the homogeneous solution for this overdamped mode is

$$\begin{Bmatrix} \Delta V_1 \\ \Delta V_2 \\ \Delta x_1 \\ \Delta x_2 \end{Bmatrix} = C_4 \begin{Bmatrix} -0.032563 \text{ ft/sec} \\ -0.032776 \text{ ft/sec} \\ 0.704041 \text{ ft} \\ 0.708654 \text{ ft} \end{Bmatrix} \exp(-0.046251\, t/\text{sec})$$

The damping rate and 99 percent damping time are

$$\sigma = -\text{real}(\lambda) = 0.046251\,\text{sec}^{-1}$$

$$99\%\ \text{damping time} = \frac{\ln(0.01)}{-\sigma} = \frac{\ln(0.01)}{-0.046251\,\text{sec}^{-1}} = 99.569\,\text{sec}$$

For the pair of roots that are associated with modes 2 and 3, the undamped natural frequency is

$$\omega_n = \sqrt{\lambda_3\lambda_4} = \sqrt{(-1.090975)(-0.046251)} = 0.224630\,\text{rad/sec}$$

and the damping ratio is

$$\zeta = -\frac{\lambda_3 + \lambda_4}{2\sqrt{\lambda_3\lambda_4}} = -\frac{-1.090975 - 0.046251}{2\sqrt{(-1.090975)(-0.046251)}} = 2.531330$$

For this eigenproblem, mode 1 is underdamped, while modes 2 and 3 are overdamped. Thus, mode 1 is the only oscillatory mode. The complex components of the eigenvectors associated with any complex pair of eigenvalues can be written in terms of amplitude and phase. The amplitude of each component is simply the magnitude of that complex number. Thus, for component χ_i,

$$\text{amplitude} = \sqrt{[\text{real}(\chi_i)]^2 + [\text{imag}(\chi_i)]^2}$$

The phase angle associated with each eigenvector component is the arctangent of the imaginary part divided by the real part. Thus, for component χ_i,

$$\text{phase} = \text{atan2}[\text{imag}(\chi_i), \text{real}(\chi_i)]$$

For mode 1, the amplitude and phase of the eigenvectors associated with the positive and negative frequencies are, respectively,

$$\text{amplitude}\begin{Bmatrix} \Delta V_1 \\ \Delta V_2 \\ \Delta x_1 \\ \Delta x_2 \end{Bmatrix} = C_{1,2}\begin{Bmatrix} 0.662842\ \text{ft/sec} \\ 0.684817\ \text{ft/sec} \\ 0.210569\ \text{ft} \\ 0.217549\ \text{ft} \end{Bmatrix}$$

$$\text{phase}\begin{Bmatrix} \Delta V_1 \\ \Delta V_2 \\ \Delta x_1 \\ \Delta x_2 \end{Bmatrix} = \pm\begin{Bmatrix} -2.9039 \\ 0.0000 \\ 1.6256 \\ -1.7466 \end{Bmatrix} = \pm\begin{Bmatrix} -166.38^\circ \\ 0.00^\circ \\ 93.14^\circ \\ -100.07^\circ \end{Bmatrix}$$

Thus, the homogeneous solutions associated with this pair of eigenvalues can be written as

$$\begin{Bmatrix} \Delta V_1 \\ \Delta V_2 \\ \Delta x_1 \\ \Delta x_2 \end{Bmatrix} = C_{1,2} \begin{Bmatrix} 0.662842 \exp[i(\mp 2.9039 \pm 3.098306\, t/\text{sec})]\ \text{ft/sec} \\ 0.684817 \exp[i(\pm 3.098306\, t/\text{sec})]\ \text{ft/sec} \\ 0.210568 \exp[i(\pm 1.6256 \pm 3.098306\, t/\text{sec})]\ \text{ft} \\ 0.217549 \exp[i(\mp 1.7466 \pm 3.098306\, t/\text{sec})]\ \text{ft} \end{Bmatrix} \times \exp(-0.556387\, t/\text{sec})$$

The damped spring-mass system in Example 8.1.1 is typical of systems that result in underdamped, overdamped, and/or critically damped motion, when disturbed from equilibrium. Underdamped modes produce sinusoidal oscillations in velocity and displacement for all degrees of freedom. The oscillations for each component of velocity and displacement can have a different amplitude and phase. Notice in Example 8.1.1 that the oscillations in Δx_1 and Δx_2 have similar amplitudes but are nearly 180° out of phase. In general, it is also possible for second-order systems to result in modes that are not underdamped, overdamped, or critically damped. One such mode, called a *rigid-body displacement mode*, is demonstrated in the following example.

EXAMPLE 8.1.2. Repeat Example 8.1.1 for the case

$$m_1 = 20.0 \text{ slugs}, \quad c_1 = 30.0 \text{ lbf}\cdot\text{sec/ft}, \quad k_1 = 0.0 \text{ lbf/ft},$$
$$m_2 = 20.0 \text{ slugs}, \quad c_2 = 15.0 \text{ lbf}\cdot\text{sec/ft}, \quad k_2 = 100.0 \text{ lbf/ft}$$

Solution. The generalized eigenproblem for this system is

$$\left(\begin{bmatrix} -30.0 & 0 & -100.0 & 100.0 \\ 0 & -15.0 & 100.0 & -100.0 \\ 1 & 0 & 0 & 0 \\ 0 & 1 & 0 & 0 \end{bmatrix} - \lambda \begin{bmatrix} 20.0 & 0 & 0 & 0 \\ 0 & 20.0 & 0 & 0 \\ 0 & 0 & 1 & 0 \\ 0 & 0 & 0 & 1 \end{bmatrix} \right) \begin{Bmatrix} \chi_{V_1} \\ \chi_{V_2} \\ \chi_{x_1} \\ \chi_{x_2} \end{Bmatrix} = \begin{Bmatrix} 0 \\ 0 \\ 0 \\ 0 \end{Bmatrix}$$

The numerical solution to this characteristic equation yields the eigenvalues and eigenvectors corresponding to the following modes:

Mode 1 $(\lambda_{1,2} = -0.554492\ \text{sec}^{-1} \pm 3.090658\, i\ \text{sec}^{-1})$

$$\begin{Bmatrix} \Delta V_1 \\ \Delta V_2 \\ \Delta x_1 \\ \Delta x_2 \end{Bmatrix} = C_{1,2} \begin{Bmatrix} (-0.641297 \mp 0.152667\, i)\ \text{ft/sec} \\ 0.688002\ \text{ft/sec} \\ (-0.011790 \pm 0.209611\, i)\ \text{ft} \\ (-0.038692 \mp 0.215665\, i)\ \text{ft} \end{Bmatrix} \times \exp[(-0.554492 \pm 3.090658\, i)\, t/\text{sec}]$$

$$\sigma = -\text{real}(\lambda) = 0.554492\ \text{sec}^{-1}$$

$$99\%\ \text{damping time} = \frac{\ln(0.01)}{-\sigma} = \frac{\ln(0.01)}{-0.554492\ \text{sec}^{-1}} = 8.305\ \text{sec}$$

$$\omega_d = |\text{imag}(\lambda)| = 3.090658\ \text{rad/sec}$$

$$\text{period} = \frac{2\pi}{\omega_d} = \frac{2\pi}{3.090658\ \text{sec}^{-1}} = 2.033\ \text{sec}$$

Following Example 8.1.1, the amplitudes for the four components of this pair of eigenvectors are

$$\text{amplitude}\begin{Bmatrix} \Delta V_1 \\ \Delta V_2 \\ \Delta x_1 \\ \Delta x_2 \end{Bmatrix} = C_{1,2}\begin{Bmatrix} 0.659219\ \text{ft/sec} \\ 0.688002\ \text{ft/sec} \\ 0.209942\ \text{ft} \\ 0.219109\ \text{ft} \end{Bmatrix}$$

and the phase shifts relative to ΔV_2 are

$$\text{phase}\begin{Bmatrix} \Delta V_1 \\ \Delta V_2 \\ \Delta x_1 \\ \Delta x_2 \end{Bmatrix} = \pm\begin{Bmatrix} -2.9045 \\ 0.0000 \\ 1.6251 \\ -1.7464 \end{Bmatrix} = \pm\begin{Bmatrix} -166.42^\circ \\ 0.00^\circ \\ 93.11^\circ \\ -100.06^\circ \end{Bmatrix}$$

Notice that this mode has changed very little from mode 1 in Example 8.1.1. This is because the mode primarily involves the vibration of only the second spring, which has not changed.

The undamped natural frequency for this mode is

$$\omega_n = \sqrt{\lambda_1\lambda_2} = \sqrt{(-0.554492 + 3.090658\,i)(-0.554492 - 3.090658\,i)}$$
$$= \sqrt{0.554492^{\,2} + 3.090658^{\,2}} = 3.140004\ \text{rad/sec}$$

and the damping ratio is

$$\zeta = -\frac{\lambda_1 + \lambda_2}{2\sqrt{\lambda_1\lambda_2}} = -\frac{-0.554492 + 3.090658\,i - 0.554492 - 3.090658\,i}{2\sqrt{(-0.554492 + 3.090658\,i)(-0.554492 - 3.090658\,i)}}$$
$$= \frac{0.556387}{\sqrt{0.554492^{\,2} + 3.090658^{\,2}}} = 0.176590$$

Mode 2 ($\lambda_3 = -1.141016\,\text{sec}^{-1}$)
This overdamped mode corresponds to the homogeneous solution

$$\begin{Bmatrix} \Delta V_1 \\ \Delta V_2 \\ \Delta x_1 \\ \Delta x_2 \end{Bmatrix} = C_3 \begin{Bmatrix} 0.553987\ \text{ft/sec} \\ 0.508604\ \text{ft/sec} \\ -0.485521\ \text{ft} \\ -0.445746\ \text{ft} \end{Bmatrix} \exp(-1.141016\, t/\text{sec})$$

$$\sigma = -\text{real}(\lambda) = 1.141016\,\text{sec}^{-1}$$

$$99\%\ \text{damping time} = \frac{\ln(0.01)}{-\sigma} = \frac{\ln(0.01)}{-1.141016\,\text{sec}^{-1}} = 4.036\,\text{sec}$$

Mode 3 ($\lambda_4 = 0.0\,\text{sec}^{-1}$)
This trivial mode results in

$$\begin{Bmatrix} \Delta V_1 \\ \Delta V_2 \\ \Delta x_1 \\ \Delta x_2 \end{Bmatrix} = C_4 \begin{Bmatrix} 0.0\ \text{ft/sec} \\ 0.0\ \text{ft/sec} \\ 0.707107\ \text{ft} \\ 0.707107\ \text{ft} \end{Bmatrix} \exp(0.0\, t/\text{sec})$$

For the pair of roots associated with modes 2 and 3, the undamped natural frequency is

$$\omega_n = \sqrt{\lambda_3 \lambda_4} = \sqrt{(-1.141016)(0.0)} = 0.0\,\text{rad/sec}$$

and the damping ratio is

$$\zeta = -\frac{\lambda_3 + \lambda_4}{2\sqrt{\lambda_3 \lambda_4}} = -\frac{-1.141016 + 0.0}{2\sqrt{(-1.141016)(0.0)}} = \infty$$

In Example 8.1.2, the eigenvalue for mode 3 is identically zero. This results in a constant solution with no velocity components and equal but arbitrary values for both displacements. This rather trivial mode arises from the fact that the spring constant, k_1, in Eq. (8.1.39) is zero. This is equivalent to removing the left-hand spring that is shown in Fig. 8.1.4. With this spring missing, there is no force that depends on the absolute position of the center of mass. The forces exerted on the components of the system depend only on the distance between the two masses and their respective velocities. Thus, the center of mass can be placed at any arbitrary position along the x-axis without changing the characteristics of the system response. This is simply a *rigid-body displacement* of the complete spring-mass system.

Many other physical systems exhibit one or more modes with eigenvalues of zero. Modes that have zero eigenvalues are called *rigid-body displacement modes*, since they correspond to simple rigid-body displacements of the system. Such a mode occurs whenever there is no force that depends on the displacement associated with a particular degree of freedom. The linearized rigid-body equations of motion for an aircraft exhibit four rigid-body displacement modes. In the linearized equations, there are no forces that depend on the translational displacements. Within the small displacement approximation, we neglect changes in air density and all forces are independent of longitude, latitude, and altitude. The aerodynamic forces depend only on the velocity components, and the gravitational forces depend only on orientation. Furthermore, while components of the gravitational force in body-fixed coordinates depend on the elevation angle and the bank angle, they do not depend on the azimuth angle. Thus, in the homogeneous solution to the linearized equations of motion for an aircraft, we should expect to find rigid-body displacement modes associated with four of the six degrees of freedom, x_f, y_f, z_f, and ψ.

There is yet another type of motion that can be associated with the free response of physical systems. This type of motion normally does not occur in simple spring-mass systems. Linearized viscous damping coefficients associated with conventional spring-mass systems are always positive or zero. As a result, the real part of each eigenvalue associated with such spring-mass systems will be either negative or zero. However, the analogous terms in systems of equations describing other physical phenomena, including aircraft dynamics, can result in eigenvalues with positive real parts. The motion associated with an eigenvalue having a positive real part is called a *divergent mode*. When a system having a divergent mode is disturbed from equilibrium, the disturbance will grow with time rather than decaying, as is shown in Fig 8.1.5. An aircraft can exhibit some divergent modes. In fact, divergence in some modes can be acceptable, provided that the time required to double the amplitude of a disturbance is not too short.

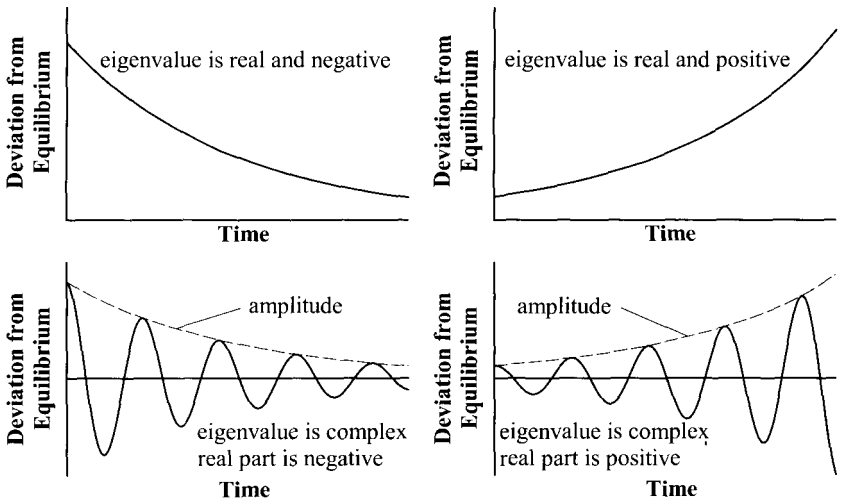


Figure 8.1.5. Types of motion associated with the free response.

In summary, the nature of the motion associated with the free response of a physical system, which is described by an eigenproblem, can be characterized by examining the eigenvalues and eigenvectors. The **eigenvalues** describe the form of the motion as shown in Fig. 8.1.5.

A **purely real eigenvalue** is associated with a **nonoscillatory mode**, having a damping rate equal to the negative of the eigenvalue.

If a **real eigenvalue is zero**, the solution corresponds to a **rigid-body mode**, describing a simple rigid-body displacement.

If a **real eigenvalue is negative**, the solution corresponds to a **convergent mode**, describing an exponential return to equilibrium following any disturbance.

If a **real eigenvalue is positive**, the solution corresponds to a **divergent mode**, describing an exponential deviation from equilibrium following any disturbance.

A **complex pair of eigenvalues** is associated with an **oscillatory mode**, having a damping rate equal to the negative of the real part of the eigenvalue and a damped natural frequency equal to the magnitude of the imaginary part of the eigenvalue.

If the **real part of the eigenvalue is zero**, the solution corresponds to an **undamped mode**, describing sinusoidal motion having constant amplitude.

If the **real part of the eigenvalue is negative**, the solution corresponds to a **damped mode**, describing sinusoidal motion having an amplitude that decreases exponentially with time.

If the **real part of the eigenvalue is positive**, the solution corresponds to a **divergent mode**, describing sinusoidal motion having an amplitude that increases exponentially with time.

The components of the eigenvector that is associated with any particular eigenvalue describe the relative participation of each dependent variable in the motion that is described by that eigenvalue. The **eigenvectors** are interpreted as follows:

A **purely real eigenvalue** always has a **purely real eigenvector**, whose components describe the relative amplitudes associated with the exponential motion.

For a real eigenvalue, the amplitude of the exponential variation in each dependent variable is proportional to the real component of the eigenvector that is associated with that dependent variable.

In general, a **complex eigenvalue** will result in an **eigenvector with complex components**, which describe the relative amplitudes and phase shifts associated with the sinusoidal motion.

For a complex eigenvalue, the amplitude of the sinusoidal variation in each dependent variable is proportional to the magnitude of the complex eigenvector component that is associated with that dependent variable.

For a complex eigenvalue, the phase of the sinusoidal variation in each dependent variable is equal to the arctangent of the imaginary part divided by the real part of the complex eigenvector component that is associated with that dependent variable. If the eigenvector is normalized to make the largest component real, then this phase is measured relative to the phase of the dependent variable having the largest amplitude.

In this section we have talked about three separate frequencies that can all be associated with any oscillatory mode, which represents a solution to an eigenproblem. These are the *undamped natural frequency*, ω_n, the *damped natural frequency*, ω_d, and the *maximum response frequency*, ω_m. In structural vibration problems these three frequencies are often used interchangeably, because structural damping is typically very light. With extremely light damping these three frequencies are, for all practical purposes, identical. However, **the modes encountered in aircraft dynamics are not all lightly damped. For this reason, we cannot use these three frequencies interchangeably** and the reader must be sure that he or she understands which of these three frequencies is being used in each case. Throughout this text an effort has been made to keep this distinction clear.

8.2. Longitudinal Motion: The Linearized Coupled Equations

The dynamic response of any real aircraft involves an extremely large number of degrees of freedom. An aircraft in flight has three translational degrees of freedom, three rotational degrees of freedom, and more elastic degrees of freedom than one would care to count. The equations of motion developed in Chapter 7 assume the aircraft to be a rigid body. This reduces the problem to one of six degrees of freedom. While the elastic degrees of freedom are important and cannot be completely neglected in aircraft design, much can be learned from the study of rigid-body aircraft dynamics. Thus, in this chapter we shall restrict our discussion entirely to the six degrees of freedom associated with rigid-body flight.

As we have seen, the general 6-DOF equations of motion are highly nonlinear. However, when the motion of the aircraft is confined to small deviations from steady equilibrium flight, the equations can be linearized. Furthermore, the linearized 6-DOF equations of motion can be separated into two subsystems, each with three degrees of freedom. These have been called the *linearized longitudinal equations* and the *linearized lateral equations*. For small deviations from equilibrium, there is no coupling between the longitudinal motion and the lateral motion. Thus, each of these three-degree-of-

freedom subsystems can be solved independently. In this section we examine the stick-fixed free response associated with linearized, longitudinal rigid-body motion. These results provide a reasonable description of longitudinal aircraft dynamics provided that the aircraft is not undergoing large-amplitude oscillations or rapid maneuvers.

The longitudinal motion comprises two translational degrees of freedom (axial and normal) and one rotational degree of freedom (pitch). Since this motion has three degrees of freedom, it is characterized by six eigenvalues. The eigenvalues associated with the linearized longitudinal motion of a typical airplane contain two complex pairs, corresponding to two oscillatory modes. One of these modes is lightly damped with a period on the order of 30 seconds or more and is called the *long-period* or *phugoid mode*. The other oscillatory mode is heavily damped with a much shorter period and is simply called the *short-period mode*. The remaining two longitudinal eigenvalues are always zero, corresponding to simple rigid-body displacement modes.

The free response of the longitudinal system is obtained from the homogeneous equations, with the control deviations set to zero. As indicated in Eq. (7.7.9), for all practical purposes, four of the derivatives with respect to the translational accelerations are zero,

$$R_{x,\dot{\mu}} \cong 0$$

$$R_{z,\dot{\mu}} \cong 0$$

$$R_{m,\dot{\mu}} \cong 0$$

$$R_{x,\dot{\alpha}} \cong 0$$

From Eq. (7.7.5), the homogeneous linearized longitudinal equations can then be written in the form

$$\begin{bmatrix} 1 & 0 & 0 & 0 & 0 & 0 \\ 0 & \left(1 - R_{z,\dot{\alpha}}\right) & 0 & 0 & 0 & 0 \\ 0 & -R_{m,\dot{\alpha}} & 1 & 0 & 0 & 0 \\ 0 & 0 & 0 & 1 & 0 & 0 \\ 0 & 0 & 0 & 0 & 1 & 0 \\ 0 & 0 & 0 & 0 & 0 & 1 \end{bmatrix} \begin{Bmatrix} \Delta\hat{\mu} \\ \Delta\hat{\alpha} \\ \Delta\hat{\bar{q}} \\ \Delta\hat{\xi}_x \\ \Delta\hat{\xi}_z \\ \Delta\hat{\theta} \end{Bmatrix}$$

$$- \begin{bmatrix} R_{x,\mu} & R_{x,\alpha} & R_{x,\bar{q}} & 0 & 0 & -R_{gx}\cos\theta_0 \\ R_{z,\mu} & R_{z,\alpha} & \left(1 + R_{z,\bar{q}}\right) & 0 & 0 & -R_{gx}\sin\theta_0 \\ R_{m,\mu} & R_{m,\alpha} & R_{m,\bar{q}} & 0 & 0 & 0 \\ \cos\theta_o & \sin\theta_o & 0 & 0 & 0 & -\sin\theta_o \\ -\sin\theta_o & \cos\theta_o & 0 & 0 & 0 & -\cos\theta_o \\ 0 & 0 & 1 & 0 & 0 & 0 \end{bmatrix} \begin{Bmatrix} \Delta\mu \\ \Delta\alpha \\ \Delta\bar{q} \\ \Delta\xi_x \\ \Delta\xi_z \\ \Delta\theta \end{Bmatrix} = \begin{Bmatrix} 0 \\ 0 \\ 0 \\ 0 \\ 0 \\ 0 \end{Bmatrix} \tag{8.2.1}$$

Equation (8.2.1) exactly fits the form of the eigenvalue problem given by Eq. (8.1.28). Thus, the **generalized eigenproblem for longitudinal motion** is

$$\left(\begin{bmatrix} R_{x,\mu} & R_{x,\alpha} & R_{x,\bar{q}} & 0 & 0 & -R_{gx}\cos\theta_0 \\ R_{z,\mu} & R_{z,\alpha} & \left(1+R_{z,\bar{q}}\right) & 0 & 0 & -R_{gx}\sin\theta_0 \\ R_{m,\mu} & R_{m,\alpha} & R_{m,\bar{q}} & 0 & 0 & 0 \\ \cos\theta_o & \sin\theta_o & 0 & 0 & 0 & -\sin\theta_o \\ -\sin\theta_o & \cos\theta_o & 0 & 0 & 0 & -\cos\theta_o \\ 0 & 0 & 1 & 0 & 0 & 0 \end{bmatrix} - \lambda \begin{bmatrix} 1 & 0 & 0 & 0 & 0 & 0 \\ 0 & \left(1-R_{z,\hat{\alpha}}\right) & 0 & 0 & 0 & 0 \\ 0 & -R_{m,\hat{\alpha}} & 1 & 0 & 0 & 0 \\ 0 & 0 & 0 & 1 & 0 & 0 \\ 0 & 0 & 0 & 0 & 1 & 0 \\ 0 & 0 & 0 & 0 & 0 & 1 \end{bmatrix}\right) \begin{Bmatrix} \chi_\mu \\ \chi_\alpha \\ \chi_{\bar{q}} \\ \chi_{\xi_x} \\ \chi_{\xi_z} \\ \chi_\theta \end{Bmatrix} = \begin{Bmatrix} 0 \\ 0 \\ 0 \\ 0 \\ 0 \\ 0 \end{Bmatrix} \tag{8.2.2}$$

The eigenvalues and eigenvectors associated with longitudinal motion can be found by solving Eq. (8.2.2) using a generalized eigensolver. If a generalized eigensolver is not available, this system of equations is easily rearranged to give the **special eigenproblem for longitudinal motion**:

$$\left(\begin{bmatrix} R_{x,\mu} & R_{x,\alpha} & R_{x,\bar{q}} & 0 & 0 & -R_{gx}\cos\theta_0 \\ \dfrac{R_{z,\mu}}{1-R_{z,\hat{\alpha}}} & \dfrac{R_{z,\alpha}}{1-R_{z,\hat{\alpha}}} & \dfrac{1+R_{z,\bar{q}}}{1-R_{z,\hat{\alpha}}} & 0 & 0 & -\dfrac{R_{gx}\sin\theta_0}{1-R_{z,\hat{\alpha}}} \\ R_{m,\mu}+\dfrac{R_{m,\hat{\alpha}}R_{z,\mu}}{1-R_{z,\hat{\alpha}}} & R_{m,\alpha}+\dfrac{R_{m,\hat{\alpha}}R_{z,\alpha}}{1-R_{z,\hat{\alpha}}} & R_{m,\bar{q}}+\dfrac{R_{m,\hat{\alpha}}\left(1+R_{z,\bar{q}}\right)}{1-R_{z,\hat{\alpha}}} & 0 & 0 & -\dfrac{R_{m,\hat{\alpha}}R_{gx}\sin\theta_0}{1-R_{z,\hat{\alpha}}} \\ \cos\theta_o & \sin\theta_o & 0 & 0 & 0 & -\sin\theta_o \\ -\sin\theta_o & \cos\theta_o & 0 & 0 & 0 & -\cos\theta_o \\ 0 & 0 & 1 & 0 & 0 & 0 \end{bmatrix} - \lambda \begin{bmatrix} 1 & 0 & 0 & 0 & 0 & 0 \\ 0 & 1 & 0 & 0 & 0 & 0 \\ 0 & 0 & 1 & 0 & 0 & 0 \\ 0 & 0 & 0 & 1 & 0 & 0 \\ 0 & 0 & 0 & 0 & 1 & 0 \\ 0 & 0 & 0 & 0 & 0 & 1 \end{bmatrix}\right) \begin{Bmatrix} \chi_\mu \\ \chi_\alpha \\ \chi_{\bar{q}} \\ \chi_{\xi_x} \\ \chi_{\xi_z} \\ \chi_\theta \end{Bmatrix} = \begin{Bmatrix} 0 \\ 0 \\ 0 \\ 0 \\ 0 \\ 0 \end{Bmatrix} \tag{8.2.3}$$

A variety of different numerical techniques are commonly used for finding eigenvalues and eigenvectors. The most popular of these techniques uses the method of Householder (1964) to transform the system to upper Hessenberg. The transformed system is then solved using the QR method. See Wilkinson (1965) for a discussion of the QR method.

From Eq. (8.2.2) or Eq. (8.2.3) we obtain dimensionless eigenvalues. To obtain the dimensional eigenvalues in terms of time, the dimensionless eigenvalues must be divided by the characteristic time, $\bar{c}_w/2V_o$.

Thus, the **damping rate for a longitudinal mode** is

$$\sigma = -\text{real}(\lambda)\frac{2V_o}{\bar{c}_w} \tag{8.2.4}$$

and the **damped natural frequency for a longitudinal mode** is

$$\omega_d = |\text{imag}(\lambda)|\frac{2V_o}{\bar{c}_w} \tag{8.2.5}$$

The **damping ratio** is

$$\zeta = -\frac{\lambda_1 + \lambda_2}{2\sqrt{\lambda_1\lambda_2}} \tag{8.2.6}$$

and the **undamped natural frequency for a longitudinal mode** is

$$\omega_n = \sqrt{\lambda_1\lambda_2}\,\frac{2V_o}{\bar{c}_w} \tag{8.2.7}$$

EXAMPLE 8.2.1. For steady level flight at sea level, find the dimensionless eigenvalues and eigenvectors, the damping rate, the 99 percent damping time, and the damped natural frequency and period if underdamped, for each longitudinal mode of the typical general aviation airplane with the characteristics listed below. For each pair of eigenvalues, find the undamped natural frequency and the damping ratio. For each oscillatory mode, compute the amplitude and phase for each component of the eigenvector associated with the positive frequency. Neglect the effects of compressibility and assume constant thrust aligned with the flight path and center of gravity.

$$S_w = 185\ \text{ft}^2,\quad b_w = 33\ \text{ft},\quad W = 2{,}800\ \text{lbf},\quad V_o = 180\ \text{ft/sec},\quad C_{Do} = 0.05,$$
$$I_{xx_b} = 1{,}000\ \text{slug}\cdot\text{ft}^2,\quad I_{yy_b} = 3{,}000\ \text{slug}\cdot\text{ft}^2,\quad I_{zz_b} = 3{,}500\ \text{slug}\cdot\text{ft}^2,$$
$$I_{xz_b} = 30\ \text{slug}\cdot\text{ft}^2,$$

$$C_{L,\alpha} = 4.40, \quad C_{D,\alpha} = 0.35, \quad C_{m,\alpha} = -0.68, \quad C_{L,\dot{\alpha}} = 1.60, \quad C_{m,\dot{\alpha}} = -4.35,$$
$$C_{Y,\beta} = -0.560, \quad C_{\ell,\beta} = -0.075, \quad C_{n,\beta} = 0.070,$$
$$C_{D,\bar{q}} \cong 0.0, \quad C_{L,\bar{q}} = 3.80, \quad C_{m,\bar{q}} = -9.95,$$
$$C_{Y,\bar{p}} \cong 0.0, \quad C_{\ell,\bar{p}} = -0.410, \quad C_{n,\bar{p}} = -0.0575,$$
$$C_{Y,\bar{r}} = 0.240, \quad C_{\ell,\bar{r}} = 0.105, \quad C_{n,\bar{r}} = -0.125$$

Solution. For this aircraft we have

$$W/g = 2800/32.17 = 87.04 \text{ slugs}$$

$$\bar{c}_w = S_w/b_w = 185/33 = 5.606 \text{ ft}$$

$$\frac{\rho S_w \bar{c}_w}{4W/g} = \frac{(0.0023769)(185)(5.606)}{4(87.04)} = 0.007080$$

$$\frac{\rho S_w \bar{c}_w^3}{8I_{yy_b}} = \frac{(0.0023769)(185)(5.606)^3}{8(3{,}000)} = 0.003228$$

$$R_{gx} \equiv \frac{g\bar{c}_w}{2V_o^2} = \frac{32.17(5.606)}{2(180)^2} = 0.00278$$

$$C_{Lo} = \frac{W\cos\theta_o}{\frac{1}{2}\rho V_o^2 S_w} = \frac{2{,}800(1.0)}{(0.5)(0.0023769)(180)^2(185)} = 0.393$$

$$R_{z,\dot{\alpha}} \equiv \frac{\rho S_w \bar{c}_w}{4W/g} C_{Z,\dot{\alpha}} = \frac{\rho S_w \bar{c}_w}{4W/g}\left(-C_{L,\dot{\alpha}}\right) = 0.007080(-1.60) = -0.01133$$

$$R_{m,\dot{\alpha}} \equiv \frac{\rho S_w \bar{c}_w^3}{8I_{yy_b}} C_{m,\dot{\alpha}} = 0.003228(-4.35) = -0.01404$$

$$R_{x,\mu} \equiv \frac{\rho S_w \bar{c}_w}{4W/g}\left(2C_{Xo}\right) = \frac{\rho S_w \bar{c}_w}{4W/g}\left(-2C_{Do}\right) = 0.007080(-2(0.05))$$
$$= -0.00071$$

$$R_{z,\mu} \equiv \frac{\rho S_w \bar{c}_w}{4W/g}\left(2C_{Zo}\right) = \frac{\rho S_w \bar{c}_w}{4W/g}\left(-2C_{Lo}\right) = 0.007080(-2(0.393))$$
$$= -0.00556$$

$$R_{m,\mu} \equiv \frac{\rho S_w \bar{c}_w^3}{4I_{yy_b}}\left(\frac{-2T_o + V_o T_{,V}}{\rho V_o^2 S_w}\right)\frac{\left[z_T\cos(\alpha_{T0}) + x_T\sin(\alpha_{T0})\right]}{\bar{c}_w} = 0.0$$

$$R_{x,\alpha} \equiv \frac{\rho S_w \bar{c}_w}{4W/g} C_{X,\alpha} = \frac{\rho S_w \bar{c}_w}{4W/g}\left(C_{Lo} - C_{D,\alpha}\right) = 0.007080(0.393 - 0.35)$$
$$= 0.00030$$

$$R_{z,\alpha} \equiv \frac{\rho S_w \bar{c}_w}{4W/g} C_{Z,\alpha} = \frac{\rho S_w \bar{c}_w}{4W/g}\left(-C_{L,\alpha} - C_{Do}\right) = 0.007080(-4.40 - 0.05)$$
$$= -0.03151$$

$$R_{m,\alpha} \equiv \frac{\rho S_w \bar{c}_w^3}{8I_{yy_b}} C_{m,\alpha} = 0.003228(-0.68) = -0.00220$$

$$R_{x,\bar{q}} \equiv \frac{\rho S_w \bar{c}_w}{4W/g} C_{X,\bar{q}} = \frac{\rho S_w \bar{c}_w}{4W/g}\left(-C_{D,\bar{q}}\right) = 0.007080(0.0) = 0.0$$

$$R_{z,\bar{q}} \equiv \frac{\rho S_w \bar{c}_w}{4W/g} C_{Z,\bar{q}} = \frac{\rho S_w \bar{c}_w}{4W/g}\left(-C_{L,\bar{q}}\right) = 0.007080(-3.80) = -0.02691$$

$$R_{m,\bar{q}} \equiv \frac{\rho S_w \bar{c}_w^3}{8I_{yy_b}} C_{m,\bar{q}} = 0.003228(-9.95) = -0.03212$$

For this level flight equilibrium condition, the characteristic equation given by Eq. (8.2.2) then becomes

$$\left(\begin{bmatrix} -0.00071 & 0.00030 & 0 & 0 & 0 & -0.00278 \\ -0.00556 & -0.03151 & 0.97309 & 0 & 0 & 0 \\ 0 & -0.00220 & -0.03212 & 0 & 0 & 0 \\ 1 & 0 & 0 & 0 & 0 & 0 \\ 0 & 1 & 0 & 0 & 0 & -1 \\ 0 & 0 & 1 & 0 & 0 & 0 \end{bmatrix}\right.$$
$$\left. -\lambda \begin{bmatrix} 1 & 0 & 0 & 0 & 0 & 0 \\ 0 & 1.01133 & 0 & 0 & 0 & 0 \\ 0 & 0.01404 & 1 & 0 & 0 & 0 \\ 0 & 0 & 0 & 1 & 0 & 0 \\ 0 & 0 & 0 & 0 & 1 & 0 \\ 0 & 0 & 0 & 0 & 0 & 1 \end{bmatrix}\right) \begin{Bmatrix} \chi_\mu \\ \chi_\alpha \\ \chi_{\bar{q}} \\ \chi_{\xi_x} \\ \chi_{\xi_z} \\ \chi_\theta \end{Bmatrix} = \begin{Bmatrix} 0 \\ 0 \\ 0 \\ 0 \\ 0 \\ 0 \end{Bmatrix}$$

Using a generalized numerical eigensolver, the dimensionless eigenvalues and eigenvectors for this eigenproblem are easily obtained. The solution to the characteristic equation results in two complex pairs of eigenvalues and two

eigenvalues that are identically zero. The two complex pairs describe the two oscillatory modes (the short-period mode and the long-period or phugoid mode) that are associated with the longitudinal free response of an aircraft in flight. The two zero eigenvalues correspond to two longitudinal rigid-body displacement modes (horizontal displacement and vertical displacement). From the numerical solution, these longitudinal modes are:

The short-period mode ($\lambda = -0.038484 \pm 0.040513\,i$)
The eigenvalue pair having the largest magnitude will always correspond to the short-period mode. In this case we have

$$\begin{Bmatrix} \Delta\mu \\ \Delta\alpha \\ \Delta\bar{q} \\ \Delta\xi_x \\ \Delta\xi_z \\ \Delta\theta \end{Bmatrix} = C_{1,2} \begin{Bmatrix} -0.000147 \pm 0.003381\,i \\ 0.010268 \pm 0.098873\,i \\ -0.004242 \mp 0.000301\,i \\ 0.045683 \mp 0.039762\,i \\ 0.990267 \\ 0.048378 \pm 0.058755\,i \end{Bmatrix} \exp[(-0.038484 \pm 0.040513\,i)\,\tau_x]$$

$$\sigma = -\text{real}(\lambda)\frac{2V_o}{\bar{c}_w} = 0.038484\frac{2(180)}{5.606} = 2.471324\ \text{sec}^{-1}$$

$$99\%\ \text{damping time} = \frac{\ln(0.01)}{-\sigma} = \frac{\ln(0.01)}{-2.471324\ \text{sec}^{-1}} = 1.86\ \text{sec}$$

$$\zeta = -\frac{\lambda_1 + \lambda_2}{2\sqrt{\lambda_1\lambda_2}} = -\frac{-0.038484 + 0.040513\,i - 0.038484 - 0.040513\,i}{2\sqrt{(-0.038484 + 0.040513\,i)(-0.038484 - 0.040513\,i)}}$$

$$= \frac{0.038484}{\sqrt{0.038484^{\,2} + 0.040513^{\,2}}} = 0.688718$$

$$\omega_d = |\text{imag}(\lambda)|\frac{2V_o}{\bar{c}_w} = 0.040513\frac{2(180)}{5.606} = 2.601620\ \text{rad/sec}$$

$$\text{period} = \frac{2\pi}{\omega_d} = \frac{2\pi}{2.601620\ \text{sec}^{-1}} = 2.42\ \text{sec}$$

$$\omega_n = \sqrt{\lambda_1\lambda_2}\,\frac{2V_o}{\bar{c}_w}$$

$$= \sqrt{(-0.038484 + 0.040513\,i)(-0.038484 - 0.040513\,i)}\,\frac{2(180)}{5.606}$$

$$= \sqrt{0.038484^{\,2} + 0.040513^{\,2}}\,\frac{2(180)}{5.606} = 3.588296\ \text{rad/sec}$$

The long-period (phugoid) mode ($\lambda = -0.000264 \pm 0.003272\,i$)

The second largest eigenvalue pair will always be associated with the phugoid. For the current example,

$$\begin{Bmatrix} \Delta\mu \\ \Delta\alpha \\ \Delta\overline{q} \\ \Delta\xi_x \\ \Delta\xi_z \\ \Delta\theta \end{Bmatrix} = C_{3,4} \begin{Bmatrix} 0.002090 \pm 0.000366\,i \\ -0.000118 \mp 0.000023\,i \\ 0.000008 \pm 0.000001\,i \\ 0.059947 \mp 0.643541\,i \\ 0.763053 \\ 0.000083 \mp 0.002520\,i \end{Bmatrix} \exp[(-0.000264 \pm 0.003272\,i)\,\tau_x]$$

$$\sigma = -\text{real}(\lambda)\frac{2V_o}{\bar{c}_w} = 0.000264\frac{2(180)}{5.606} = 0.016953\ \text{sec}^{-1}$$

$$99\%\ \text{damping time} = \frac{\ln(0.01)}{-\sigma} = \frac{\ln(0.01)}{-0.016953\ \text{sec}^{-1}} = 271.6\ \text{sec}$$

$$\zeta = -\frac{\lambda_1 + \lambda_2}{2\sqrt{\lambda_1\lambda_2}} = -\frac{-0.000264 + 0.003272\,i - 0.000264 - 0.003272\,i}{2\sqrt{(-0.000264 + 0.003272\,i)(-0.000264 - 0.003272\,i)}}$$

$$= \frac{0.000264}{\sqrt{0.000264^{\,2} + 0.003272^{\,2}}} = 0.080423$$

$$\omega_d = |\text{imag}(\lambda)|\frac{2V_o}{\bar{c}_w} = 0.003272\frac{2(180)}{5.606} = 0.210118\ \text{rad/sec}$$

$$\text{period} = \frac{2\pi}{\omega_d} = \frac{2\pi}{0.210118\ \text{sec}^{-1}} = 29.9\ \text{sec}$$

$$\omega_n = \sqrt{\lambda_1\lambda_2}\,\frac{2V_o}{\bar{c}_w}$$

$$= \sqrt{(-0.000264 + 0.003272\,i)(-0.000264 - 0.003272\,i)}\,\frac{2(180)}{5.606}$$

$$= \sqrt{0.000264^{\,2} + 0.003272^{\,2}}\,\frac{2(180)}{5.606} = 0.210801\ \text{rad/sec}$$

The amplitudes and phase shifts for both the short-period and long-period eigenvectors are listed in Table 8.2.1. The amplitudes in this table are normalized. In this case, for both short-period and long-period motion, the largest amplitude is associated with the oscillation in vertical displacement. Thus, all of the phase shifts listed in Table 8.2.1 are reported relative to the phase for the vertical displacement.

Eigenvector Component	Short-period		Long-period	
	Amplitude	Phase	Amplitude	Phase
$\Delta\mu$	0.003384	92.39°	0.002122	9.93°
$\Delta\alpha$	0.099405	83.97°	0.000121	−168.60°
$\Delta\overline{q}$	0.004253	−175.74°	0.000008	6.52°
$\Delta\xi_x$	0.060564	−40.99°	0.646327	−84.58°
$\Delta\xi_z$	0.990267	0.00°	0.763054	0.00°
$\Delta\theta$	0.076108	50.47°	0.002521	−88.00°

Table 8.2.1. Longitudinal eigenvectors for a typical general aviation airplane.

The rigid-body modes ($\lambda = 0.0, 0.0$)

$$\begin{Bmatrix} \Delta\mu \\ \Delta\alpha \\ \Delta\overline{q} \\ \Delta\xi_x \\ \Delta\xi_z \\ \Delta\theta \end{Bmatrix} = C_5 \begin{Bmatrix} 0 \\ 0 \\ 0 \\ 1 \\ 0 \\ 0 \end{Bmatrix} \exp(0.0\,\tau_x),\ C_6 \begin{Bmatrix} 0 \\ 0 \\ 0 \\ 0 \\ 1 \\ 0 \end{Bmatrix} \exp(0.0\,\tau_x)$$

These trivial rigid-body modes simply state the obvious fact that steady level flight can be maintained at different latitudes and/or different altitudes.

The two oscillatory longitudinal modes observed in Example 8.2.1 are illustrated in Figs. 8.2.1 through 8.2.3. These oscillatory modes are typical of the small-amplitude longitudinal modes associated with any airplane in flight. While the period and damping will vary with aircraft design and operating conditions, all airplanes exhibit these two modes of longitudinal motion.

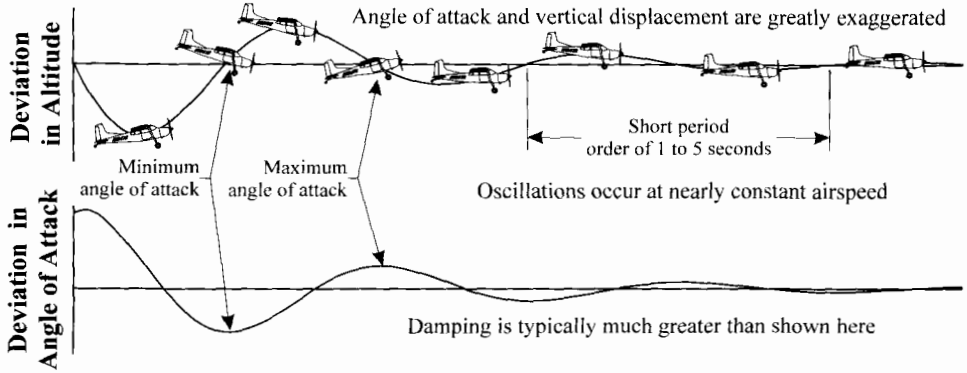


Figure 8.2.1. Short-period mode with reduced damping.

From examination of Example 8.2.1, several observations can be made. From this example we see that short-period motion is a heavily damped oscillatory mode that is composed of pitching motion with superimposed vertical oscillations. From the short-period eigenvector, we see that the amplitude for the dimensionless axial velocity deviation is small compared to that for the deviation in angle of attack. Thus, this mode is characterized by rapid changes in angle of attack and vertical position, with little change in axial velocity. Note that the deviation in angle of attack leads the deviation in vertical displacement by about 90° in phase. This can be seen in Fig. 8.2.1.

The motion depicted in Fig. 8.2.1 is shown starting from the left with the airplane moving downward from the equilibrium altitude to the point of maximum positive displacement in z_f (i.e., minimum altitude). At this point, the vertical velocity component is zero, but the angle of attack is somewhat greater than the equilibrium value. Thus, the lift is greater than the weight and the airplane is accelerated upward, back toward the equilibrium altitude. However, at the minimum altitude, the angle of attack is rapidly decreasing with time and the angular momentum of the aircraft causes the angle of attack to overshoot the equilibrium value. Once the angle of attack becomes less than the equilibrium value, the lift becomes less than the weight and the vertical velocity of the airplane begins to slow. As the airplane reaches its equilibrium altitude, the angle of attack approaches its minimum but the vertical velocity is still quite large. The vertical momentum of the airplane carries it above the equilibrium altitude as the angle of attack begins to increase. As the airplane reaches maximum altitude, the angle of attack is still less than the equilibrium value. So, the weight is still greater than the lift and the airplane accelerates back toward the equilibrium altitude once again. This oscillatory interchange between rotational kinetic energy and potential energy continues until it is damped out, primarily as a result of pitch damping.

In a well-designed airplane, the short-period damping is much greater than shown in Fig. 8.2.1. In this figure the damping was deliberately reduced to better show the physics of the oscillatory motion. Short-period motion with more typical damping is shown in Fig 8.2.2. Because short-period motion is heavily damped in most airplanes, it is not normally objectionable and most pilots are not even aware of its existence.

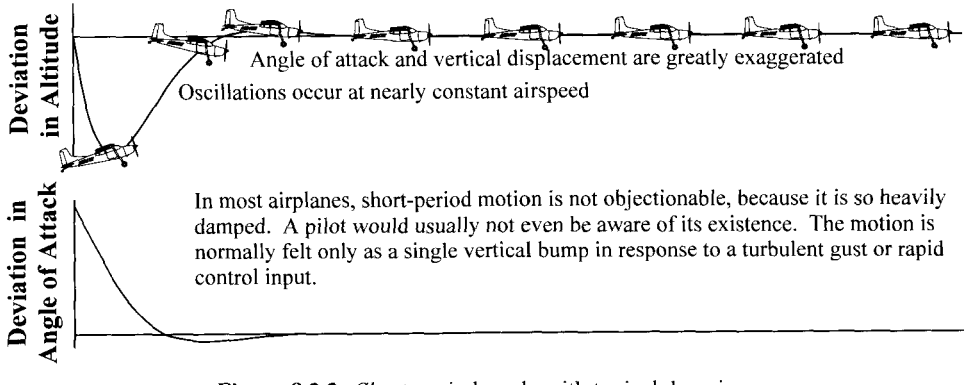


Figure 8.2.2. Short-period mode with typical damping.

While the short-period mode is a heavily damped oscillatory interchange between rotational kinetic energy and potential energy, the long-period or phugoid mode is a very lightly damped oscillatory interchange between translational kinetic energy and potential energy. From the long-period eigenvector, we see that the amplitude for the deviation in angle of attack is small compared to that for the dimensionless axial velocity deviation. This mode is then characterized by gradual changes in airspeed, altitude, and elevation angle, with very small changes in angle of attack. Notice that the axial velocity deviation is approximately 90° out of phase with the deviation in elevation angle, with the velocity leading the elevation angle. Also notice that the velocity deviation leads the deviation in vertical displacement by only a few degrees. This can be seen in Fig. 8.2.3.

The phugoid mode is, at best, very lightly damped, and some modern airplanes can have negative phugoid damping at certain airspeeds. Even so, this motion is usually not objectionable to VFR[1] pilots, because the period of the phugoid is so long. When a pilot is controlling an airplane using visual references, his or her response time is very short compared to the phugoid period and the pilot will normally correct for this motion without ever being cognizant of its existence. On the other hand, when flying an airplane solely from the references provided by instruments, the pilot's response to the gradual changes associated with phugoid motion is not nearly so rapid. Thus, IFR[2] pilots often find low phugoid damping to be very objectionable.

Once the aerodynamic derivatives for an aircraft are determined from wind tunnel tests or other means, the frequency and damping for both the short-period and phugoid modes can be evaluated by numerically determining the eigenvalues of Eq. (8.2.2). However, these eigenvalues depend on many aircraft design and operating parameters, and the nature of this dependence is not easily observable from a numerical solution. Thus, a closed-form solution that describes the essential features of these modes is desirable. In addition, closed-form solutions have always been useful for application to aircraft control systems. For this reason, we shall now proceed to the development of some closed-form approximations for the two modes of longitudinal motion.

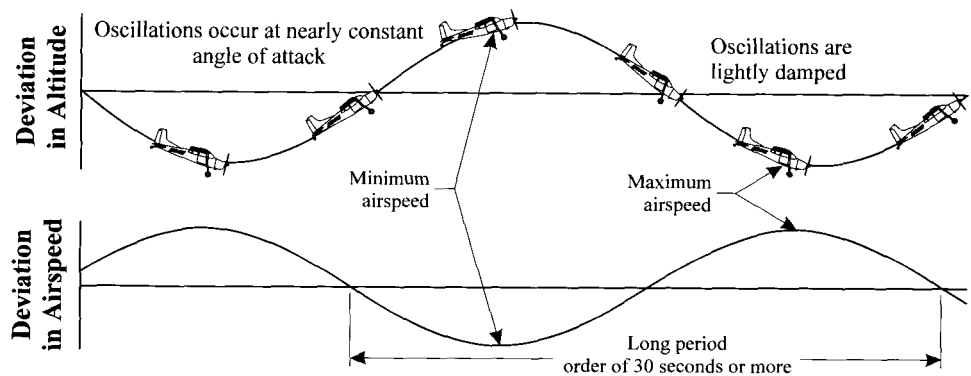


Figure 8.2.3. Phugoid or long-period mode.

[1] Visual Flight Rules. [2] Instrument Flight Rules.

8.3. Short-Period Approximation

For the short-period mode, the amplitude of the dimensionless axial velocity deviation is small compared to that for the deviation in angle of attack. Thus, an approximation for short-period motion can be obtained by neglecting changes in axial velocity and ignoring the x-momentum equation. For motion relative to steady level flight, assuming that

$$\Delta\mu = 0 \tag{8.3.1}$$

and replacing the x-momentum equation from Eq. (8.2.1) with Eq. (8.3.1) gives

$$\begin{bmatrix} 0 & 0 & 0 & 0 & 0 & 0 \\ 0 & (1-R_{z,\hat{\alpha}}) & 0 & 0 & 0 & 0 \\ 0 & -R_{m,\hat{\alpha}} & 1 & 0 & 0 & 0 \\ 0 & 0 & 0 & 1 & 0 & 0 \\ 0 & 0 & 0 & 0 & 1 & 0 \\ 0 & 0 & 0 & 0 & 0 & 1 \end{bmatrix} \begin{Bmatrix} \Delta\hat{\mu} \\ \Delta\hat{\alpha} \\ \Delta\hat{\bar{q}} \\ \Delta\hat{\xi}_x \\ \Delta\hat{\xi}_z \\ \Delta\hat{\theta} \end{Bmatrix} = \begin{bmatrix} 1 & 0 & 0 & 0 & 0 & 0 \\ 0 & R_{z,\alpha} & (R_{z,\bar{q}}+1) & 0 & 0 & 0 \\ 0 & R_{m,\alpha} & R_{m,\bar{q}} & 0 & 0 & 0 \\ 0 & 0 & 0 & 0 & 0 & 0 \\ 0 & 1 & 0 & 0 & 0 & -1 \\ 0 & 0 & 1 & 0 & 0 & 0 \end{bmatrix} \begin{Bmatrix} \Delta\mu \\ \Delta\alpha \\ \Delta\bar{q} \\ \Delta\xi_x \\ \Delta\xi_z \\ \Delta\theta \end{Bmatrix} \tag{8.3.2}$$

The z-force ratios, $R_{z,\hat{\alpha}}$ and $R_{z,\bar{q}}$, are much less than 1 and usually neglected, to give

$$\begin{bmatrix} 0 & 0 & 0 & 0 & 0 & 0 \\ 0 & 1 & 0 & 0 & 0 & 0 \\ 0 & -R_{m,\hat{\alpha}} & 1 & 0 & 0 & 0 \\ 0 & 0 & 0 & 1 & 0 & 0 \\ 0 & 0 & 0 & 0 & 1 & 0 \\ 0 & 0 & 0 & 0 & 0 & 1 \end{bmatrix} \begin{Bmatrix} \Delta\hat{\mu} \\ \Delta\hat{\alpha} \\ \Delta\hat{\bar{q}} \\ \Delta\hat{\xi}_x \\ \Delta\hat{\xi}_z \\ \Delta\hat{\theta} \end{Bmatrix} = \begin{bmatrix} 1 & 0 & 0 & 0 & 0 & 0 \\ 0 & R_{z,\alpha} & 1 & 0 & 0 & 0 \\ 0 & R_{m,\alpha} & R_{m,\bar{q}} & 0 & 0 & 0 \\ 0 & 0 & 0 & 0 & 0 & 0 \\ 0 & 1 & 0 & 0 & 0 & -1 \\ 0 & 0 & 1 & 0 & 0 & 0 \end{bmatrix} \begin{Bmatrix} \Delta\mu \\ \Delta\alpha \\ \Delta\bar{q} \\ \Delta\xi_x \\ \Delta\xi_z \\ \Delta\theta \end{Bmatrix} \tag{8.3.3}$$

The second and third equations in Eq. (8.3.3) are not coupled to any of the other four equations. Thus, Eq. (8.3.3) can be rearranged and separated to yield

$$\begin{bmatrix} 1 & 0 \\ -R_{m,\hat{\alpha}} & 1 \end{bmatrix} \begin{Bmatrix} \lambda\Delta\alpha \\ \lambda\Delta\bar{q} \end{Bmatrix} = \begin{bmatrix} R_{z,\alpha} & 1 \\ R_{m,\alpha} & R_{m,\bar{q}} \end{bmatrix} \begin{Bmatrix} \Delta\alpha \\ \Delta\bar{q} \end{Bmatrix} \tag{8.3.4}$$

and

$$\begin{Bmatrix} \Delta\mu \\ \Delta\alpha \\ \Delta\bar{q} \\ \Delta\xi_x \\ \Delta\theta \end{Bmatrix} = \frac{\lambda}{R_{z,\alpha}} \begin{Bmatrix} 0 \\ \lambda \\ \lambda(\lambda - R_{z,\alpha}) \\ 0 \\ \lambda - R_{z,\alpha} \end{Bmatrix} \Delta\xi_z \tag{8.3.5}$$

The eigenvalues are obtained from Eq. (8.3.4) and the eigenvectors from (8.3.5).

The eigenproblem associated with Eq. (8.3.4) is

$$\left(\begin{bmatrix} R_{z,\alpha} & 1 \\ R_{m,\alpha} & R_{m,\bar{q}} \end{bmatrix} - \lambda \begin{bmatrix} 1 & 0 \\ -R_{m,\dot{\alpha}} & 1 \end{bmatrix}\right) \begin{Bmatrix} \chi_\alpha \\ \chi_{\bar{q}} \end{Bmatrix} = \begin{Bmatrix} 0 \\ 0 \end{Bmatrix} \tag{8.3.6}$$

The eigenvalues are obtained from the roots of the characteristic equation, which is found by setting the determinate of the coefficient matrix on the left-hand side of Eq. (8.3.6) equal to zero,

$$\begin{vmatrix} (R_{z,\alpha} - \lambda) & 1 \\ (R_{m,\alpha} + R_{m,\dot{\alpha}}\lambda) & (R_{m,\bar{q}} - \lambda) \end{vmatrix} = 0 \tag{8.3.7}$$

Equation (8.3.7) can be expanded to yield

$$\lambda^2 - (R_{z,\alpha} + R_{m,\bar{q}} + R_{m,\dot{\alpha}})\lambda + (R_{z,\alpha}R_{m,\bar{q}} - R_{m,\alpha}) = 0 \tag{8.3.8}$$

From Eq. (8.3.8), the **dimensionless eigenvalues for the short-period approximation** are easily found to be

$$\lambda_{sp} = \left(\frac{R_{z,\alpha} + R_{m,\bar{q}} + R_{m,\dot{\alpha}}}{2}\right) \pm \sqrt{\left(\frac{R_{z,\alpha} + R_{m,\bar{q}} + R_{m,\dot{\alpha}}}{2}\right)^2 - (R_{z,\alpha}R_{m,\bar{q}} - R_{m,\alpha})} \tag{8.3.9}$$

which gives the approximate **short-period damped natural frequency**,

$$\omega_{d_{sp}} = \frac{2V_o}{\bar{c}_w}\left|\text{imag}(\lambda_{sp})\right| = \frac{2V_o}{\bar{c}_w}\sqrt{(R_{z,\alpha}R_{m,\bar{q}} - R_{m,\alpha}) - \left(\frac{R_{z,\alpha} + R_{m,\bar{q}} + R_{m,\dot{\alpha}}}{2}\right)^2} \tag{8.3.10}$$

and the approximate **short-period damping rate**,

$$\sigma_{sp} = -\frac{2V_o}{\bar{c}_w}\text{real}(\lambda_{sp}) = -\frac{V_o}{\bar{c}_w}(R_{z,\alpha} + R_{m,\bar{q}} + R_{m,\dot{\alpha}}) \tag{8.3.11}$$

The short-period approximation, as given by Eq. (8.3.9), agrees very closely with the exact solution for the short-period mode obtained from Eq. (8.2.2). This is demonstrated in the following example.

EXAMPLE 8.3.1. Using the short-period approximation given by Eq. (8.3.9), find the dimensionless eigenvalues and eigenvectors, the damping rate, and the damped natural frequency for the short-period mode of the typical general aviation airplane described in Example 8.2.1. Compare these approximate results with the fully coupled short-period solution that was obtained in Example 8.2.1.

Solution. From Example 8.2.1, for this general aviation airplane and operating conditions, we have

$$V_o = 180 \text{ ft/sec}, \qquad \bar{c}_w = 5.606 \text{ ft},$$
$$R_{z,\alpha} = -0.03151, \quad R_{m,\alpha} = -0.00220, \quad R_{m,\dot{\alpha}} = -0.01404, \quad R_{m,\bar{q}} = -0.03212$$

Using these values in Eq. (8.3.9), the short-period approximation gives the eigenvalues

$$\lambda_{sp} = \left(\frac{-0.03151-0.03212-0.01404}{2}\right)$$
$$\pm\sqrt{\left(\frac{-0.03151-0.03212-0.01404}{2}\right)^2 - [(-0.03151)(-0.03212)-(-0.00220)]}$$
$$= -0.038835 \pm 0.041279\, i$$

The damping rate is

$$\sigma = -\text{real}(\lambda)\frac{2V_o}{\bar{c}} = 0.038835\frac{2(180)}{5.606} = 2.493864 \text{ sec}^{-1}$$

and the damped natural frequency is

$$\omega_d = |\text{imag}(\lambda)|\frac{2V_o}{\bar{c}} = 0.041279\frac{2(180)}{5.606} = 2.650801 \text{ rad/sec}$$

The eigenvectors for the short-period approximation are found by using the complex eigenvalues in Eq. (8.3.5),

$$\begin{Bmatrix} \Delta\mu \\ \Delta\alpha \\ \Delta\bar{q} \\ \Delta\xi_x \\ \Delta\theta \end{Bmatrix} = \frac{\lambda}{R_{z,\alpha}}\begin{Bmatrix} 0 \\ \lambda \\ \lambda(\lambda - R_{z,\alpha}) \\ 0 \\ \lambda - R_{z,\alpha} \end{Bmatrix}\Delta\xi_z$$

The only requirement for the six components of this eigenvector is that they must satisfy these five equations. Thus, we can only determine the eigenvector to within an arbitrary constant. We can find one possible form for the eigenvector by setting $\Delta\xi_z$ equal to some arbitrary constant and then using the relations above to find the other five components. For example, in this particular case we can simplify the complex arithmetic by using

$$\Delta\xi_z = R_{z,\alpha}/\lambda$$

This gives the eigenvector

$$\begin{Bmatrix} \chi_\mu \\ \chi_\alpha \\ \chi_{\bar{q}} \\ \chi_{\xi_x} \\ \chi_{\xi_z} \\ \chi_\theta \end{Bmatrix} = \begin{Bmatrix} 0 \\ \lambda \\ \lambda(\lambda - R_{z,\alpha}) \\ 0 \\ R_{z,\alpha}/\lambda \\ \lambda - R_{z,\alpha} \end{Bmatrix}$$

or

$$\begin{Bmatrix} \chi_\mu \\ \chi_\alpha \\ \chi_{\bar{q}} \\ \chi_{\xi_x} \\ \chi_{\xi_z} \\ \chi_\theta \end{Bmatrix} = \begin{Bmatrix} 0 \\ -0.038835 \pm 0.041279\,i \\ (-0.038835 \pm 0.041279\,i)(-0.038835 \pm 0.041279\,i + 0.03151) \\ 0 \\ -0.03151/(-0.038835 \pm 0.041279\,i) \\ -0.038835 \pm 0.041279\,i + 0.03151 \end{Bmatrix}$$

After performing the complex arithmetic, this yields

$$\begin{Bmatrix} \chi_\mu \\ \chi_\alpha \\ \chi_{\bar{q}} \\ \chi_{\xi_x} \\ \chi_{\xi_z} \\ \chi_\theta \end{Bmatrix} = \begin{Bmatrix} 0 \\ -0.038835 \pm 0.041279\,i \\ -0.001419 \mp 0.001905\,i \\ 0 \\ 0.380963 \pm 0.404936\,i \\ -0.007325 \pm 0.041279\,i \end{Bmatrix}$$

To make the largest component real we multiply the entire eigenvector by the complex conjugate of the largest component,

$$\begin{Bmatrix} \chi_\mu \\ \chi_\alpha \\ \chi_{\bar{q}} \\ \chi_{\xi_x} \\ \chi_{\xi_z} \\ \chi_\theta \end{Bmatrix} = (0.380963 \mp 0.404936\,i) \begin{Bmatrix} 0 \\ -0.038835 \pm 0.041279\,i \\ -0.001419 \mp 0.001905\,i \\ 0 \\ 0.380963 \pm 0.404936\,i \\ -0.007325 \pm 0.041279\,i \end{Bmatrix}$$

This gives

$$\begin{Bmatrix} \chi_\mu \\ \chi_\alpha \\ \chi_{\bar{q}} \\ \chi_{\xi_x} \\ \chi_{\xi_z} \\ \chi_\theta \end{Bmatrix} = \begin{Bmatrix} 0 \\ 0.001921 \pm 0.031451\, i \\ -0.001312 \mp 0.000151\, i \\ 0 \\ 0.309106 \\ 0.013925 \pm 0.018692\, i \end{Bmatrix}$$

This eigenvector has a magnitude

$$\sqrt{\sum_{j=1}^{N} \left|\chi_j\right|_i^2} = 0.311584$$

Normalizing the eigenvector, we have

$$\begin{Bmatrix} \chi_\mu \\ \chi_\alpha \\ \chi_{\bar{q}} \\ \chi_{\xi_x} \\ \chi_{\xi_z} \\ \chi_\theta \end{Bmatrix} = \frac{1}{0.311584} \begin{Bmatrix} 0 \\ 0.001921 \pm 0.031451\, i \\ -0.001312 \mp 0.000151\, i \\ 0 \\ 0.309106 \\ 0.013925 \pm 0.018692\, i \end{Bmatrix} = \begin{Bmatrix} 0 \\ 0.006164 \pm 0.100940\, i \\ -0.004212 \mp 0.000485\, i \\ 0 \\ 0.992048 \\ 0.044690 \pm 0.059990\, i \end{Bmatrix}$$

This gives

$$\begin{Bmatrix} \Delta\mu \\ \Delta\alpha \\ \Delta\bar{q} \\ \Delta\xi_x \\ \Delta\xi_z \\ \Delta\theta \end{Bmatrix} = C_{1,2} \begin{Bmatrix} 0.000000 \\ 0.006164 \pm 0.100940\, i \\ -0.004212 \mp 0.000485\, i \\ 0.000000 \\ 0.992048 \\ 0.044690 \pm 0.059990\, i \end{Bmatrix} \exp[(-0.038835 \pm 0.041279\, i)\, \tau_x]$$

The exact solution from Example 8.2.1 is

$$\begin{Bmatrix} \Delta\mu \\ \Delta\alpha \\ \Delta\bar{q} \\ \Delta\xi_x \\ \Delta\xi_z \\ \Delta\theta \end{Bmatrix} = C_{1,2} \begin{Bmatrix} -0.000147 \pm 0.003381\, i \\ 0.010268 \pm 0.098873\, i \\ -0.004242 \mp 0.000301\, i \\ 0.045683 \mp 0.039762\, i \\ 0.990267 \\ 0.048378 \pm 0.058755\, i \end{Bmatrix} \exp[(-0.038484 \pm 0.040513\, i)\, \tau_x]$$

For the airplane and operating conditions used in Example 8.3.1, the eigenvalues computed from the short-period approximation agree with the exact solution to within about 2 percent. This result is quite typical of what can be expected from this short-period approximation.

8.4. Long-Period Approximation

The first closed-form solution for phugoid motion was developed by Lanchester (1908). In his original solution, Lanchester assumed no change in angle of attack and no change in the net axial force. With these assumptions, Lanchester obtained an approximation for the frequency of phugoid motion. However, this approximation predicts completely undamped sinusoidal motion and gives no information about the phugoid damping. A variation of Lanchester's solution, which does included an approximation for phugoid damping, has been widely used. In this approximation, Lanchester's original assumption of no change in axial force is dropped, but the assumption of no change in angle of attack is retained,

$$\Delta\alpha = 0 \tag{8.4.1}$$

Restricting the analysis to deviations about level flight and neglecting the force derivatives with respect to rate of change of angle of attack and pitching rate, the linearized longitudinal equations from Eq. (8.2.1) can be written as

$$\begin{bmatrix} 1 & 0 & 0 & 0 & 0 & 0 \\ 0 & 1 & 0 & 0 & 0 & 0 \\ 0 & -R_{m,\hat{\alpha}} & 1 & 0 & 0 & 0 \\ 0 & 0 & 0 & 1 & 0 & 0 \\ 0 & 0 & 0 & 0 & 1 & 0 \\ 0 & 0 & 0 & 0 & 0 & 1 \end{bmatrix} \begin{Bmatrix} \Delta\hat{\mu} \\ \Delta\hat{\alpha} \\ \Delta\hat{\bar{q}} \\ \Delta\hat{\xi}_x \\ \Delta\hat{\xi}_z \\ \Delta\hat{\theta} \end{Bmatrix} = \begin{bmatrix} R_{x,\mu} & R_{x,\alpha} & 0 & 0 & 0 & -R_{gx} \\ R_{z,\mu} & R_{z,\alpha} & 1 & 0 & 0 & 0 \\ R_{m,\mu} & R_{m,\alpha} & R_{m,\bar{q}} & 0 & 0 & 0 \\ 1 & 0 & 0 & 0 & 0 & 0 \\ 0 & 1 & 0 & 0 & 0 & -1 \\ 0 & 0 & 1 & 0 & 0 & 0 \end{bmatrix} \begin{Bmatrix} \Delta\mu \\ \Delta\alpha \\ \Delta\bar{q} \\ \Delta\xi_x \\ \Delta\xi_z \\ \Delta\theta \end{Bmatrix} \tag{8.4.2}$$

Applying Eq. (8.4.1) to Eq. (8.4.2) and then replacing the angular momentum equation with Eq. (8.4.1) yields

$$\begin{bmatrix} 1 & 0 & 0 & 0 & 0 & 0 \\ 0 & 0 & 0 & 0 & 0 & 0 \\ 0 & 0 & 0 & 0 & 0 & 0 \\ 0 & 0 & 0 & 1 & 0 & 0 \\ 0 & 0 & 0 & 0 & 1 & 0 \\ 0 & 0 & 0 & 0 & 0 & 1 \end{bmatrix} \begin{Bmatrix} \Delta\hat{\mu} \\ \Delta\hat{\alpha} \\ \Delta\hat{\bar{q}} \\ \Delta\hat{\xi}_x \\ \Delta\hat{\xi}_z \\ \Delta\hat{\theta} \end{Bmatrix} = \begin{bmatrix} R_{x,\mu} & 0 & 0 & 0 & 0 & -R_{gx} \\ R_{z,\mu} & 0 & 1 & 0 & 0 & 0 \\ 0 & 1 & 0 & 0 & 0 & 0 \\ 1 & 0 & 0 & 0 & 0 & 0 \\ 0 & 0 & 0 & 0 & 0 & -1 \\ 0 & 0 & 1 & 0 & 0 & 0 \end{bmatrix} \begin{Bmatrix} \Delta\mu \\ \Delta\alpha \\ \Delta\bar{q} \\ \Delta\xi_x \\ \Delta\xi_z \\ \Delta\theta \end{Bmatrix} \tag{8.4.3}$$

Notice that within this approximation, the second and third equations in Eq. (8.4.3) do not contain any derivative terms, and are thus algebraic.

Rewriting Eq. (8.4.3) after subtracting the second of these equations from the last gives the eigenproblem

$$\begin{bmatrix} 1 & 0 & 0 & 0 & 0 & 0 \\ 0 & 0 & 0 & 0 & 0 & 0 \\ 0 & 0 & 0 & 0 & 0 & 0 \\ 0 & 0 & 0 & 1 & 0 & 0 \\ 0 & 0 & 0 & 0 & 1 & 0 \\ 0 & 0 & 0 & 0 & 0 & 1 \end{bmatrix} \begin{Bmatrix} \Delta\hat{\mu} \\ \Delta\hat{\alpha} \\ \Delta\hat{\bar{q}} \\ \Delta\hat{\xi}_x \\ \Delta\hat{\xi}_z \\ \Delta\hat{\theta} \end{Bmatrix} = \begin{bmatrix} R_{x,\mu} & 0 & 0 & 0 & 0 & -R_{gx} \\ R_{z,\mu} & 0 & 1 & 0 & 0 & 0 \\ 0 & 1 & 0 & 0 & 0 & 0 \\ 1 & 0 & 0 & 0 & 0 & 0 \\ 0 & 0 & 0 & 0 & 0 & -1 \\ -R_{z,\mu} & 0 & 0 & 0 & 0 & 0 \end{bmatrix} \begin{Bmatrix} \Delta\mu \\ \Delta\alpha \\ \Delta\bar{q} \\ \Delta\xi_x \\ \Delta\xi_z \\ \Delta\theta \end{Bmatrix} \tag{8.4.4}$$

The first and last equations in Eq. (8.4.4) are not coupled to any of the other four equations. Thus, Eq. (8.4.4) can be rearranged and separated to yield

$$\begin{bmatrix} (R_{x,\mu} - \lambda) & -R_{gx} \\ -R_{z,\mu} & -\lambda \end{bmatrix} \begin{Bmatrix} \Delta\mu \\ \Delta\theta \end{Bmatrix} = \begin{Bmatrix} 0 \\ 0 \end{Bmatrix} \tag{8.4.5}$$

$$\begin{Bmatrix} \Delta\mu \\ \Delta\alpha \\ \Delta\bar{q} \\ \Delta\xi_z \\ \Delta\theta \end{Bmatrix} = \begin{Bmatrix} \lambda \\ 0 \\ -R_{z,\mu}\lambda \\ R_{z,\mu}/\lambda \\ -R_{z,\mu} \end{Bmatrix} \Delta\xi_x \tag{8.4.6}$$

The eigenvalues for Eq. (8.4.5) are obtained from the roots of the characteristic equation, which is readily expanded to give

$$\lambda^2 - R_{x,\mu}\lambda - R_{gx}R_{z,\mu} = 0 \tag{8.4.7}$$

Thus, from Eq. (8.4.7), the dimensionless eigenvalues for this phugoid approximation are given by

$$\lambda_p = \frac{R_{x,\mu}}{2} \pm \sqrt{\left(\frac{R_{x,\mu}}{2}\right)^2 + R_{gx}R_{z,\mu}} \tag{8.4.8}$$

which gives the approximate phugoid damping rate,

$$\sigma_p = -\frac{2V_o}{\bar{c}_w}\,\text{real}(\lambda_p) = -\frac{2V_o}{\bar{c}_w}\left(\frac{R_{x,\mu}}{2}\right) = -\frac{V_o}{\bar{c}_w}R_{x,\mu} \tag{8.4.9}$$

and the approximate phugoid damped natural frequency,

$$\begin{aligned}\omega_{d_p} &= \frac{2V_o}{\bar{c}_w}\left|\text{imag}(\lambda_p)\right| \\ &= \frac{2V_o}{\bar{c}_w}\sqrt{-R_{gx}R_{z,\mu}-\left(\frac{R_{x,\mu}}{2}\right)^2} = \frac{2V_o}{\bar{c}_w}\sqrt{-R_{gx}R_{z,\mu}}\sqrt{1+\frac{R_{x,\mu}^2}{4R_{gx}R_{z,\mu}}}\end{aligned} \tag{8.4.10}$$

If we also neglect compressibility and assume that the thrust is constant and aligned with the direction of flight, then from Eqs. (7.7.8) and (7.710), the equilibrium lift force must equal the weight and we can write

$$\begin{aligned}R_{z,\mu} &= \frac{\rho S_w \bar{c}_w}{2W/g}C_{Zo} = -\frac{\rho S_w \bar{c}_w}{2W/g}C_{Lo} \\ &= -\frac{\rho S_w \bar{c}_w}{2W/g}\left(\frac{W}{\frac{1}{2}\rho V_o^2 S_w}\right) = -\frac{g\bar{c}_w}{V_o^2} = -2R_{gx}\end{aligned} \tag{8.4.11}$$

and

$$R_{x,\mu} = \frac{\rho S_w \bar{c}_w}{2W/g}C_{Xo} = -\frac{\rho S_w \bar{c}_w}{2W/g}C_{Do} = -\frac{\rho S_w \bar{c}_w}{2W/g}C_{Lo}\frac{C_{Do}}{C_{Lo}} = -2R_{gx}\frac{C_{Do}}{C_{Lo}} \tag{8.4.12}$$

Using Eqs. (8.4.11) and (8.4.12), in Eq. (8.4.8), the dimensionless eigenvalues become

$$\lambda_p = R_{gx}\left[-\frac{C_{Do}}{C_{Lo}} \pm i\sqrt{2-\left(\frac{C_{Do}}{C_{Lo}}\right)^2}\right] = \frac{g\bar{c}_w}{2V_o^2}\left[-\frac{C_{Do}}{C_{Lo}} \pm i\sqrt{2-\left(\frac{C_{Do}}{C_{Lo}}\right)^2}\right] \tag{8.4.13}$$

The approximate phugoid damping rate then reduces to

$$\sigma_p = \frac{2V_o}{\bar{c}_w}\left(R_{gx}\frac{C_{Do}}{C_{Lo}}\right) = \frac{2V_o}{\bar{c}_w}\left(\frac{g\bar{c}_w}{2V_o^2}\right)\frac{C_{Do}}{C_{Lo}} = \frac{g}{V_o}\frac{C_{Do}}{C_{Lo}} \tag{8.4.14}$$

and the approximate phugoid damped natural frequency is

$$\begin{aligned}\omega_{d_p} &= \frac{2V_o}{\bar{c}_w}\left(\sqrt{2}R_{gx}\sqrt{1-\frac{1}{2}\left(\frac{C_{Do}}{C_{Lo}}\right)^2}\right) = \frac{2V_o}{\bar{c}_w}\left(\sqrt{2}\frac{g\bar{c}_w}{2V_o^2}\right)\sqrt{1-\frac{1}{2}\left(\frac{C_{Do}}{C_{Lo}}\right)^2} \\ &= \sqrt{2}\frac{g}{V_o}\sqrt{1-\frac{1}{2}\left(\frac{C_{Do}}{C_{Lo}}\right)^2}\end{aligned} \tag{8.4.15}$$

This approximation predicts the same undamped natural frequency as Lanchester's original approximation. This very simple result gives a phugoid frequency that depends

only on airspeed and not at all on the airplane or its altitude. The phugoid damping as predicted by Eq. (8.4.14) is also quite simple, depending only on the airspeed and the lift-to-drag ratio for the airplane.

The phugoid approximation, given by Eq. (8.4.13), is not nearly as accurate as the short-period approximation, given by Eq. (8.3.9). Furthermore, many of the fundamental characteristics of phugoid motion are not captured in Eq. (8.4.13) and the approximation can be quite misleading in some regards. This approximation has, however, been used extensively for many years as a first approximation for the frequency and damping associated with phugoid motion. The inaccuracy of this approximation is demonstrated in the following example.

EXAMPLE 8.4.1. Using the long-period approximation given by Eq. (8.4.13), find the dimensionless eigenvalues and eigenvectors, the damping rate, and the damped natural frequency for the phugoid mode of the typical general aviation airplane described in Example 8.2.1. Compare these approximate results with the long-period solution that was obtained in Example 8.2.1 from the fully coupled longitudinal equations.

Solution. From Example 8.2.1 we have

$$V_o = 180 \text{ ft/sec}, \qquad \bar{c}_w = 5.606 \text{ ft},$$
$$C_{Lo} = 0.393, \qquad C_{Do} = 0.050$$

Using these values in Eq. (8.4.13), the long-period approximation gives

$$\lambda_p = \frac{g\bar{c}_w}{2V_o^2}\left[-\frac{C_{Do}}{C_{Lo}} \pm i\sqrt{2-\left(\frac{C_{Do}}{C_{Lo}}\right)^2}\right]$$

$$= \frac{(32.17 \text{ ft/sec}^2)5.606 \text{ ft}}{2(180 \text{ ft/sec})^2}\left[-\frac{0.050}{0.393} \pm i\sqrt{2-\left(\frac{0.050}{0.393}\right)^2}\right]$$

$$= -0.000354 \pm 0.003920\, i$$

$$\sigma = -\text{real}(\lambda)\frac{2V_o}{\bar{c}_w} = \frac{C_{Do}}{C_{Lo}}\frac{g}{V_o} = \frac{0.050}{0.393}\frac{32.17}{180} = 0.022738 \text{ sec}^{-1}$$

$$\omega_d = |\text{imag}(\lambda)|\frac{2V_o}{\bar{c}_w} = \frac{g}{V_o}\sqrt{2-(C_{Do}/C_{Lo})^2}$$

$$= \frac{32.17}{180}\sqrt{2-(0.050/0.393)^2} = 0.251727 \text{ rad/sec}$$

The long-period eigenvectors for this first-order approximation, as are found from Eq. (8.4.6), give

$$\begin{Bmatrix} \Delta\mu \\ \Delta\alpha \\ \Delta\overline{q} \\ \Delta\xi_x \\ \Delta\xi_z \\ \Delta\theta \end{Bmatrix} = C_{1,2} \begin{Bmatrix} 0.002237 \pm 0.000408\,i \\ 0.000000 \\ 0.000012 \pm 0.000002\,i \\ 0.051978 \mp 0.575432\,i \\ 0.816187 \\ 0.000289 \mp 0.003199\,i \end{Bmatrix} \exp[(-0.000354 \pm 0.003920\,i)\,\tau_x]$$

The exact long-period solution from Example 8.2.1 is

$$\begin{Bmatrix} \Delta\mu \\ \Delta\alpha \\ \Delta\overline{q} \\ \Delta\xi_x \\ \Delta\xi_z \\ \Delta\theta \end{Bmatrix} = C_{3,4} \begin{Bmatrix} 0.002090 \pm 0.000366\,i \\ -0.000118 \mp 0.000023\,i \\ 0.000008 \pm 0.000001\,i \\ 0.059947 \mp 0.643541\,i \\ 0.763053 \\ 0.000083 \mp 0.002520\,i \end{Bmatrix} \exp[(-0.000264 \pm 0.003272\,i)\,\tau_x]$$

From this example we see that the phugoid eigenvalues, computed from Eq. (8.4.13), are significantly in error. For this example, the frequency from Eq. (8.4.13) is about 20 percent high and the damping is overpredicted by more than 33 percent. Furthermore, this type of aircraft, with low aspect ratio and high drag, is particularly flattering to this approximation. For high-performance aircraft, the result predicted by Eq. (8.4.13) is much worse. In fact, under certain conditions, this approximation does not even predict the correct sign for the phugoid damping. Since the gravitational acceleration, airspeed, lift coefficient, and drag coefficient are always positive, Eq. (8.4.14) will always predict a convergent phugoid mode. In reality, however, modern airplanes can exhibit a divergent phugoid at certain airspeeds.

The most restrictive approximation associated with the development of Eq. (8.4.13) comes from the assumption that all changes in angle of attack are exactly zero. Clearly, we have seen in Example 8.2.1 that phugoid motion does produce changes in angle of attack that are small compared to changes in the dimensionless axial velocity. On the other hand, we have also seen that even very small changes in angle of attack can have a significant effect on aircraft motion. In fact, angle of attack has such a profound effect on aircraft dynamics that one is usually ill advised to neglect changes in angle of attack under almost any circumstance.

Clearly, the approximation given by Eq. (8.4.13) does not accurately describe the phugoid motion under many conditions. Another closed-form approximation, which was first presented by Bairstow (1939), gives a much more accurate prediction of the phugoid frequency. However, this approximation was never widely used, since in most cases the damping predicted by Bairstow's approximation is less accurate than that predicted by Eq. (8.4.13). Here we shall use a closed-form approximation, which was developed by Phillips (2000a) and more accurately describes both the period and the damping for the long-period mode.

To this end, we recognize that phugoid motion is always underdamped. Thus, the eigenvalues describing the phugoid will always form a complex pair, $\lambda = \lambda_r \pm i\lambda_i$, where the imaginary part specifies the phugoid frequency and the real part specifies the damping. With this recognition, the eigenproblem associated with Eq. (8.4.2) could be written as

$$\begin{Bmatrix} (\lambda_r \pm i\lambda_i)\Delta\mu \\ (\lambda_r \pm i\lambda_i)\Delta\alpha \\ (\lambda_r \pm i\lambda_i)(\Delta\bar{q} - R_{m,\dot{\alpha}}\Delta\alpha) \\ (\lambda_r \pm i\lambda_i)\Delta\xi_x \\ (\lambda_r \pm i\lambda_i)\Delta\xi_z \\ (\lambda_r \pm i\lambda_i)\Delta\theta \end{Bmatrix} = \begin{bmatrix} R_{x,\mu} & R_{x,\alpha} & 0 & 0 & 0 & -R_{gx} \\ R_{z,\mu} & R_{z,\alpha} & 1 & 0 & 0 & 0 \\ R_{m,\mu} & R_{m,\alpha} & R_{m,\bar{q}} & 0 & 0 & 0 \\ 1 & 0 & 0 & 0 & 0 & 0 \\ 0 & 1 & 0 & 0 & 0 & -1 \\ 0 & 0 & 1 & 0 & 0 & 0 \end{bmatrix} \begin{Bmatrix} \Delta\mu \\ \Delta\alpha \\ \Delta\bar{q} \\ \Delta\xi_x \\ \Delta\xi_z \\ \Delta\theta \end{Bmatrix} \tag{8.4.16}$$

Since phugoid motion is lightly damped, the real part of the phugoid eigenvalue pair is very small. Furthermore, while both the angle of attack and the pitching rate change significantly with time, the amplitudes for these changes are also very small. Thus, the products $\lambda_r\Delta\alpha$ and $\lambda_r\Delta\bar{q}$ are extremely small and can be ignored. This means that we can approximate the variation in angle of attack and pitching rate as undamped sinusoidal motion,

$$(\lambda_r \pm i\lambda_i)\Delta\alpha \cong \pm i\varpi_n\Delta\alpha \tag{8.4.17}$$

$$(\lambda_r \pm i\lambda_i)\Delta\bar{q} \cong \pm i\varpi_n\Delta\bar{q} \tag{8.4.18}$$

where ϖ_n is the dimensionless undamped natural frequency. Because the rate of change of angle of attack is very small, we also neglect the change in pitching moment with respect to the time rate of change of angle of attack. Furthermore, we shall assume that the thrust force is aligned with the center of gravity so that the equilibrium aerodynamic pitching moment is zero. With these approximations, Eqs. (7.6.24) and (7.7.8) require that $R_{m,\mu} = 0$ and Eq. (8.4.16) reduces to

$$\begin{Bmatrix} \lambda\Delta\mu \\ \pm i\varpi_n\Delta\alpha \\ \pm i\varpi_n\Delta\bar{q} \\ \lambda\Delta\xi_x \\ \lambda\Delta\xi_z \\ \lambda\Delta\theta \end{Bmatrix} = \begin{bmatrix} R_{x,\mu} & R_{x,\alpha} & 0 & 0 & 0 & -R_{gx} \\ R_{z,\mu} & R_{z,\alpha} & 1 & 0 & 0 & 0 \\ 0 & R_{m,\alpha} & R_{m,\bar{q}} & 0 & 0 & 0 \\ 1 & 0 & 0 & 0 & 0 & 0 \\ 0 & 1 & 0 & 0 & 0 & -1 \\ 0 & 0 & 1 & 0 & 0 & 0 \end{bmatrix} \begin{Bmatrix} \Delta\mu \\ \Delta\alpha \\ \Delta\bar{q} \\ \Delta\xi_x \\ \Delta\xi_z \\ \Delta\theta \end{Bmatrix} \tag{8.4.19}$$

The second and third equations in Eq. (8.4.19) provide an algebraic system that can be used to relate the deviation in angle of attack and pitching rate to the deviation in forward velocity,

$$\begin{bmatrix} (R_{z,\alpha} \mp i\varpi_n) & 1 \\ R_{m,\alpha} & (R_{m,\bar{q}} \mp i\varpi_n) \end{bmatrix} \begin{Bmatrix} \Delta\alpha \\ \Delta\bar{q} \end{Bmatrix} = \begin{Bmatrix} -R_{z,\mu}\Delta\mu \\ 0 \end{Bmatrix} \tag{8.4.20}$$

The remaining four equations form the eigenproblem,

$$\begin{Bmatrix} \lambda\Delta\mu \\ \lambda\Delta\xi_x \\ \lambda\Delta\xi_z \\ \lambda\Delta\theta \end{Bmatrix} = \begin{bmatrix} R_{x,\mu} & R_{x,\alpha} & 0 & -R_{gx} \\ 1 & 0 & 0 & 0 \\ 0 & 1 & 0 & -1 \\ 0 & 0 & 1 & 0 \end{bmatrix} \begin{Bmatrix} \Delta\mu \\ \Delta\alpha \\ \Delta\bar{q} \\ \Delta\theta \end{Bmatrix} \tag{8.4.21}$$

The algebraic solution to Eq. (8.4.20) is rather straightforward and gives

$$\begin{Bmatrix} \Delta\alpha \\ \Delta\bar{q} \end{Bmatrix} = \begin{Bmatrix} R_{xc} \\ R_{zc} \end{Bmatrix} \Delta\mu \tag{8.4.22}$$

where the complex coefficients R_{xc} and R_{zc} are defined as

$$R_{xc} \equiv \frac{R_{z,\mu}(R_{m,\bar{q}} \mp i\varpi_n)}{R_{m,\alpha} - R_{z,\alpha}R_{m,\bar{q}} + \varpi_n^2 \pm i\varpi_n(R_{z,\alpha} + R_{m,\bar{q}})} \tag{8.4.23}$$

and

$$R_{zc} \equiv \frac{-R_{z,\mu}R_{m,\alpha}}{R_{m,\alpha} - R_{z,\alpha}R_{m,\bar{q}} + \varpi_n^2 \pm i\varpi_n(R_{z,\alpha} + R_{m,\bar{q}})} \tag{8.4.24}$$

Equation (8.4.22) describes both the amplitude and phase relationships between the angle of attack, pitching rate, and dimensionless axial velocity deviation. Using Eq. (8.4.22) in Eq. (8.4.21) to eliminate the angle of attack from the first equation and the pitching rate from the last equation, we obtain

$$\begin{Bmatrix} \lambda\Delta\mu \\ \lambda\Delta\xi_x \\ \lambda\Delta\xi_z \\ \lambda\Delta\theta \end{Bmatrix} = \begin{bmatrix} (R_{x,\mu} + R_{x,\alpha}R_{xc}) & 0 & 0 & -R_{gx} \\ 1 & 0 & 0 & 0 \\ 0 & 1 & 0 & -1 \\ R_{zc} & 0 & 0 & 0 \end{bmatrix} \begin{Bmatrix} \Delta\mu \\ \Delta\alpha \\ \Delta\bar{q} \\ \Delta\theta \end{Bmatrix} \tag{8.4.25}$$

The first and fourth equations in Eq. (8.4.25) contain only the forward velocity deviation and the elevation angle. Thus, these two equations can be separated from the other two equations to give

$$\begin{bmatrix} (R_{x,\mu} + R_{x,\alpha}R_{xc} - \lambda) & -R_{gx} \\ R_{zc} & -\lambda \end{bmatrix} \begin{Bmatrix} \Delta\mu \\ \Delta\theta \end{Bmatrix} = \begin{Bmatrix} 0 \\ 0 \end{Bmatrix} \tag{8.4.26}$$

Combining Eqs. (8.4.22) and (8.4.25) and rearranging, we also have

$$\begin{Bmatrix} \Delta\mu \\ \Delta\alpha \\ \Delta\bar{q} \\ \Delta\xi_z \\ \Delta\theta \end{Bmatrix} = \begin{Bmatrix} \lambda \\ R_{xc}\lambda \\ R_{zc}\lambda \\ R_{xc} - R_{zc}/\lambda \\ R_{zc} \end{Bmatrix} \Delta\xi_x \tag{8.4.27}$$

Equation (8.4.26) can be used to solve for the phugoid eigenvalues, and the resulting complex eigenvalues can then be used in Eq. (8.4.27) to obtain the eigenvectors. The characteristic equation associated with Eq. (8.4.26) is

$$\lambda^2 - \left(R_{x,\mu} + R_{x,\alpha} R_{xc}\right)\lambda + R_{gx} R_{zc} = 0 \tag{8.4.28}$$

and the eigenvalues are the roots of this quadratic equation,

$$\lambda = \frac{R_{x,\mu} + R_{x,\alpha} R_{xc}}{2} \pm \sqrt{\left(\frac{R_{x,\mu} + R_{x,\alpha} R_{xc}}{2}\right)^2 - R_{gx} R_{zc}} \tag{8.4.29}$$

Because the phugoid frequency is very low, we can neglect terms in Eqs. (8.4.23) and (8.4.24) that contain the phugoid frequency raised to any power greater than 1. Thus, these complex coefficients can be approximated as

$$R_{xc} \cong \frac{R_{z,\mu} R_{m,\bar{q}}}{R_{m,\alpha} - R_{z,\alpha} R_{m,\bar{q}}} \left(1 \mp i \frac{\varpi_n}{R_{m,\bar{q}}}\right)\left(1 \mp i \frac{\varpi_n \left(R_{z,\alpha} + R_{m,\bar{q}}\right)}{R_{m,\alpha} - R_{z,\alpha} R_{m,\bar{q}}}\right) \cong R_{xa}\left(1 \mp i \varpi_n R_{xp}\right) \tag{8.4.30}$$

$$R_{zc} \cong \frac{-R_{z,\mu} R_{m,\alpha}}{R_{m,\alpha} - R_{z,\alpha} R_{m,\bar{q}}} \left(1 \mp i \frac{\varpi_n \left(R_{z,\alpha} + R_{m,\bar{q}}\right)}{R_{m,\alpha} - R_{z,\alpha} R_{m,\bar{q}}}\right) \cong R_{za}\left(1 \mp i \varpi_n R_{zp}\right) \tag{8.4.31}$$

where R_{xa}, R_{za}, R_{xp}, and R_{zp} are defined,

$$R_{xa} \equiv \frac{R_{z,\mu} R_{m,\bar{q}}}{R_{m,\alpha} - R_{z,\alpha} R_{m,\bar{q}}} \tag{8.4.32}$$

$$R_{za} \equiv \frac{-R_{z,\mu} R_{m,\alpha}}{R_{m,\alpha} - R_{z,\alpha} R_{m,\bar{q}}} \tag{8.4.33}$$

$$R_{xp} \equiv \frac{R_{m,\alpha} + R_{m,\bar{q}}^2}{R_{m,\bar{q}}\left(R_{m,\alpha} - R_{z,\alpha} R_{m,\bar{q}}\right)} \tag{8.4.34}$$

$$R_{zp} \equiv \frac{R_{z,\alpha} + R_{m,\bar{q}}}{R_{m,\alpha} - R_{z,\alpha} R_{m,\bar{q}}} \tag{8.4.35}$$

Using the approximations that are given by Eqs. (8.4.30) and (8.4.31) in Eq. (8.4.29), the phugoid eigenvalues can be approximated as

$$\lambda \cong \frac{R_{x,\mu} + R_{x,\alpha} R_{xa}\left(1 \mp i\varpi_n R_{xp}\right)}{2} \pm \sqrt{\left(\frac{R_{x,\mu} + R_{x,\alpha} R_{xa}\left(1 \mp i\varpi_n R_{xp}\right)}{2}\right)^2 - R_{gx} R_{za}\left(1 \mp i\varpi_n R_{zp}\right)} \tag{8.4.36}$$

The imaginary components of the complex coefficients R_{xc} and R_{zc} are very small. The result of this very small phase shift is to transfer a small fraction of the imaginary part of the eigenvalue to the real part and to transfer a small fraction of the real part to the imaginary part. Because phugoid motion is so lightly damped, the small fraction of the real part that is phase-shifted to the imaginary part can be neglected. However, when a very small fraction of the much larger imaginary part is phase-shifted to the real part, it becomes significant.

Thus, ignoring the phase shift in R_{xc}, Eq. (8.4.36) can be written

$$\lambda \cong \frac{R_{x,\mu} + R_{x,\alpha} R_{xa}}{2} \pm \sqrt{\left(\frac{R_{x,\mu} + R_{x,\alpha} R_{xa}}{2}\right)^2 - R_{gx} R_{za}\left(1 \mp i\varpi_n R_{zp}\right)} \tag{8.4.37}$$

or

$$\lambda \cong \frac{R_{x,\mu} + R_{x,\alpha} R_{xa}}{2} \pm i\sqrt{R_{gx} R_{za}} \sqrt{1 \mp i\varpi_n R_{zp} - \frac{\left(R_{x,\mu} + R_{x,\alpha} R_{xa}\right)^2}{4 R_{gx} R_{za}}} \tag{8.4.38}$$

Since both the phase shift and the square of the damping term are very small, we can further approximate Eq. (8.4.38) as

$$\lambda \cong \frac{R_{x,\mu} + R_{x,\alpha} R_{xa}}{2} \pm i\sqrt{R_{gx} R_{za}}\left[1 \mp i\frac{\varpi_n R_{zp}}{2} - \frac{\left(R_{x,\mu} + R_{x,\alpha} R_{xa}\right)^2}{8 R_{gx} R_{za}}\right] \tag{8.4.39}$$

which can be rearranged to give

$$\lambda \cong \frac{R_{x,\mu} + R_{x,\alpha} R_{xa}}{2} + (\pm i)(\mp i)\frac{\varpi_n R_{zp}\sqrt{R_{gx} R_{za}}}{2} \pm i\sqrt{R_{gx} R_{za}}\left[1 - \frac{\left(R_{x,\mu} + R_{x,\alpha} R_{xa}\right)^2}{8 R_{gx} R_{za}}\right] \tag{8.4.40}$$

or

$$\lambda \cong \frac{R_{x,\mu} + R_{x,\alpha} R_{xa}}{2} + \frac{\varpi_n R_{zp} \sqrt{R_{gx} R_{za}}}{2} \pm i \sqrt{R_{gx} R_{za} - \left(\frac{R_{x,\mu} + R_{x,\alpha} R_{xa}}{2} \right)^2} \tag{8.4.41}$$

From Eq. (8.4.41) it is clearly seen that there is a component of phugoid damping that is related to the phugoid frequency. This will be called *phase damping*, because it results from the phase shift between angle of attack, pitching rate, and forward velocity. As will be shown, the phase damping contribution to the real component of the eigenvalue is always positive and tends to reduce the total phugoid damping. In fact, under certain circumstances, the phase damping can result in a large enough positive contribution to render the phugoid divergent.

The dimensionless undamped natural frequency, ϖ_n, has to this point been unknown. We can now evaluate this frequency by neglecting the damping terms in Eq. (8.4.41). This gives

$$\varpi_n = \sqrt{R_{gx} R_{za}} \tag{8.4.42}$$

Using Eq. (8.4.42) in Eq. (8.4.41), the phugoid eigenvalues can be expressed as

$$\lambda \cong \frac{R_{x,\mu} + R_{x,\alpha} R_{xa}}{2} + \frac{R_{zp} R_{gx} R_{za}}{2} \pm i \sqrt{R_{gx} R_{za} - \left(\frac{R_{x,\mu} + R_{x,\alpha} R_{xa}}{2} \right)^2} \tag{8.4.43}$$

Thus, for this approximation, the dimensionless **phugoid eigenvalues** can be written as

$$\lambda_p \cong \frac{R_{z,\mu}}{2} \left[\left(\frac{R_{x,\mu}}{R_{z,\mu}} + R_d - R_p \right) \pm i \sqrt{-\frac{4R_{gx}}{R_{z,\mu}} R_s - \left(\frac{R_{x,\mu}}{R_{z,\mu}} + R_d \right)^2} \right] \tag{8.4.44}$$

where we define the **phugoid stability ratio**,

$$R_s \equiv -\frac{R_{za}}{R_{z,\mu}} = \frac{R_{m,\alpha}}{R_{m,\alpha} - R_{z,\alpha} R_{m,\bar{q}}} \tag{8.4.45}$$

the **phugoid pitch-damping ratio**,

$$R_d \equiv \frac{R_{x,\alpha} R_{xa}}{R_{z,\mu}} = \frac{R_{x,\alpha} R_{m,\bar{q}}}{R_{m,\alpha} - R_{z,\alpha} R_{m,\bar{q}}} \tag{8.4.46}$$

and the **phugoid phase-divergence ratio**,

$$R_p \equiv -\frac{R_{zp} R_{gx} R_{za}}{R_z} = R_{gx} R_s \left(\frac{R_{z,\alpha} + R_{m,\bar{q}}}{R_{m,\alpha} - R_{z,\alpha} R_{m,\bar{q}}} \right) \tag{8.4.47}$$

This gives the approximate **phugoid damped natural frequency**,

$$\omega_{d_p} = \frac{2V_o}{\bar{c}_w}\left|\text{imag}(\lambda_p)\right| \cong \frac{2V_o}{\bar{c}_w}\left[\frac{R_{z,\mu}}{2}\sqrt{-\frac{4R_{gx}}{R_{z,\mu}}R_s - \left(\frac{R_{x,\mu}}{R_{z,\mu}} + R_d\right)^2}\right] \tag{8.4.48}$$

and the approximate **phugoid damping rate**,

$$\sigma_p = -\frac{2V_o}{\bar{c}_w}\text{real}(\lambda_p) \cong -\frac{2V_o}{\bar{c}_w}\left[\frac{R_{z,\mu}}{2}\left(\frac{R_{x,\mu}}{R_{z,\mu}} + R_d - R_p\right)\right] \tag{8.4.49}$$

If the flow is incompressible and the thrust is independent of airspeed and aligned with the direction of flight, the approximation can be somewhat simplified by invoking Eqs. (8.4.11) and (8.4.12). From these equations we can write

$$\frac{R_{z,\mu}}{2} = -R_{gx} = -\frac{g\bar{c}_w}{2V_o^2} \tag{8.4.50}$$

$$\frac{R_{x,\mu}}{R_{z,\mu}} = \frac{C_{Do}}{C_{Lo}} \tag{8.4.51}$$

Thus, for **incompressible flow and constant thrust aligned with the direction of flight**, the approximate dimensionless **phugoid eigenvalues** can be written as

$$\lambda_p \cong \frac{g\bar{c}_w}{2V_o^2}\left[\left(-\frac{C_{Do}}{C_{Lo}} - R_d + R_p\right) \pm i\sqrt{2R_s - \left(\frac{C_{Do}}{C_{Lo}} + R_d\right)^2}\right] \tag{8.4.52}$$

This gives the approximate **phugoid damped natural frequency**,

$$\omega_{d_p} \cong \frac{2V_o}{\bar{c}_w}\left[\frac{g\bar{c}_w}{2V_o^2}\sqrt{2R_s - \left(\frac{C_{Do}}{C_{Lo}} + R_d\right)^2}\right] = \sqrt{2}\frac{g}{V_o}\sqrt{R_s - \frac{1}{2}\left(\frac{C_{Do}}{C_{Lo}} + R_d\right)^2} \tag{8.4.53}$$

and the approximate **phugoid damping rate**,

$$\sigma_p \cong -\frac{2V_o}{\bar{c}_w}\left[\frac{g\bar{c}}{2V_o^2}\left(-\frac{C_{Do}}{C_{Lo}} - R_d + R_p\right)\right] = \frac{g}{V_o}\left(\frac{C_{Do}}{C_{Lo}} + R_d - R_p\right) \tag{8.4.54}$$

The eigenvalues and eigenvectors predicted using Eq. (8.4.44) or Eq. (8.4.52) are greatly improved over those predicted from Eq. (8.4.13). This is demonstrated in the following example.

EXAMPLE 8.4.2. Repeat Example 8.4.1 using Eq. (8.4.52). Again, compare the results obtained from this approximation with the long-period solution that was obtained in Example 8.2.1.

Solution. From Example 8.2.1, we have

$$V_o = 180 \text{ ft/sec}, \quad \bar{c}_w = 5.606 \text{ ft}, \quad R_{gx} = 0.00278, \quad C_{Lo} = 0.393, \quad C_{Do} = 0.050,$$
$$R_{x,\alpha} = 0.00030, \quad R_{z,\alpha} = -0.03151, \quad R_{m,\alpha} = -0.00220, \quad R_{m,\bar{q}} = -0.03212$$

From Eq. (8.4.45), the pitch-stability ratio is

$$R_s \equiv \frac{R_{m,\alpha}}{R_{m,\alpha} - R_{z,\alpha} R_{m,\bar{q}}} = \frac{-0.00220}{-0.00220 - (-0.03151)(-0.03212)} = 0.684910$$

From Eq. (8.4.46), the pitch-damping ratio is

$$R_d \equiv \frac{R_{x,\alpha} R_{m,\bar{q}}}{R_{m,\alpha} - R_{z,\alpha} R_{m,\bar{q}}} = \frac{0.00030(-0.03212)}{-0.00220 - (-0.03151)(-0.03212)} = 0.003000$$

From Eq. (8.4.47), the phase-divergence ratio is

$$R_p \equiv R_{gx} R_s \left(\frac{R_{z,\alpha} + R_{m,\bar{q}}}{R_{m,\alpha} - R_{z,\alpha} R_{m,\bar{q}}} \right)$$
$$= 0.00278(0.684910)\left(\frac{-0.03151 - 0.03212}{-0.00220 - (-0.03151)(-0.03212)} \right) = 0.037718$$

From Eq. (8.4.52), we have

$$\lambda_p \cong R_{gx}\left[\left(-\frac{C_{Do}}{C_{Lo}} - R_d + R_p \right) \pm i\sqrt{2R_s - \left(\frac{C_{Do}}{C_{Lo}} + R_d \right)^2} \right]$$
$$= 0.00278\left[\left(-\frac{0.050}{0.393} - 0.003000 + 0.037718 \right) \right.$$
$$\left. \pm i\sqrt{2(0.684910) - \left(\frac{0.050}{0.393} + 0.003000 \right)^2} \right] = -0.000257 \pm 0.003233\, i$$

$$\sigma = -\text{real}(\lambda)\frac{2V_o}{\bar{c}_w} = 0.000257\frac{2(180)}{5.606} = 0.016504 \text{ sec}^{-1}$$

$$\omega_d = |\text{imag}(\lambda)|\frac{2V_o}{\bar{c}_w} = 0.003233\frac{2(180)}{5.606} = 0.207613 \text{ rad/sec}$$

From Eqs. (8.4.32) through (8.4.35),

$$R_{xa} \equiv \frac{R_{z,\mu} R_{m,\bar{q}}}{R_{m,\alpha} - R_{z,\alpha} R_{m,\bar{q}}} = -0.055598$$

$$R_{za} \equiv \frac{-R_{z,\mu} R_{m,\alpha}}{R_{m,\alpha} - R_{z,\alpha} R_{m,\bar{q}}} = 0.003808$$

$$R_{xp} \equiv \frac{R_{m,\alpha} + R_{m,\bar{q}}^2}{R_{m,\bar{q}} (R_{m,\alpha} - R_{z,\alpha} R_{m,\bar{q}})} = -11.323787$$

$$R_{zp} \equiv \frac{R_{z,\alpha} + R_{m,\bar{q}}}{R_{m,\alpha} - R_{z,\alpha} R_{m,\bar{q}}} = 19.809463$$

From Eqs. (8.4.30), (8.4.31), and (8.4.42),

$$\varpi_n = \sqrt{R_{gx} R_{za}} = \sqrt{0.00278\,(0.003808)} = 0.003254$$

$$R_{xc} \cong R_{xa}\left(1 \mp i \varpi_n R_{xp}\right) = -0.055598 \mp i 0.002049$$

$$R_{zc} \cong R_{za}\left(1 \mp i \varpi_n R_{zp}\right) = 0.003808 \mp i 0.000245$$

Using these results in Eq. (8.4.27), the eigenvectors for this long-period approximation are

$$\begin{Bmatrix} \Delta\mu \\ \Delta\alpha \\ \Delta\bar{q} \\ \Delta\xi_x \\ \Delta\xi_z \\ \Delta\theta \end{Bmatrix} = C_{1,2} \begin{Bmatrix} 0.002077 \pm 0.000370\,i \\ -0.000115 \mp 0.000025\,i \\ 0.000008 \pm 0.000001\,i \\ 0.062894 \mp 0.647399\,i \\ 0.759545 \\ 0.000081 \mp 0.002481\,i \end{Bmatrix} \exp[(-0.000257 \pm 0.003233\,i)\,\tau_x]$$

The exact long-period solution from Example 8.2.1 is

$$\begin{Bmatrix} \Delta\mu \\ \Delta\alpha \\ \Delta\bar{q} \\ \Delta\xi_x \\ \Delta\xi_z \\ \Delta\theta \end{Bmatrix} = C_{3,4} \begin{Bmatrix} 0.002090 \pm 0.000366\,i \\ -0.000118 \mp 0.000023\,i \\ 0.000008 \pm 0.000001\,i \\ 0.059947 \mp 0.643541\,i \\ 0.763053 \\ 0.000083 \mp 0.002520\,i \end{Bmatrix} \exp[(-0.000264 \pm 0.003272\,i)\,\tau_x]$$

From Example 8.4.2 we see that the long-period eigenvalues that are computed from Eq. (8.4.52) are in excellent agreement with the fully coupled solution. For this example, the frequency prediction from Eq. (8.4.52) is accurate to within about 1 percent and the damping error is less than 3 percent. Furthermore, all components of the eigenvectors predicted from this approximation are in good agreement with the exact solution. Figures 8.4.1 through 8.4.3 show how this approximation compares with Eq. (8.4.13) and the exact solution over a broad range of aerodynamic parameters.

Here it should be noted that as the pitch-stability derivative approaches infinity, the phugoid stability ratio approaches unity, while both the phugoid pitch-damping ratio and the phugoid phase-divergence ratio approach zero. So we see that in the limit of infinite pitch stability, the result given by Eq. (8.4.52) reduces exactly to Eq. (8.4.13). Thus, Eq. (8.4.13) represents an asymptotic solution for very large pitch stability. This can be

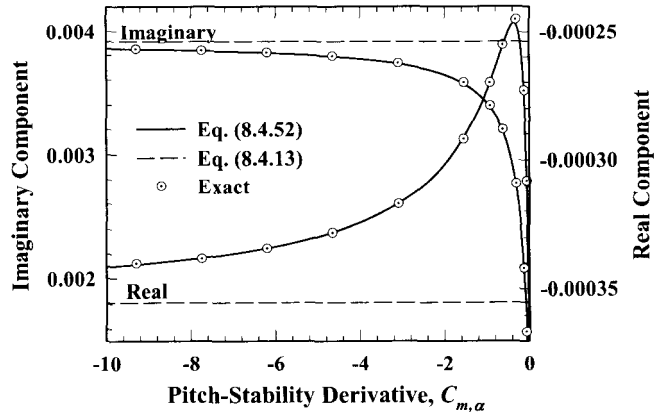


Figure 8.4.1. Effect of pitch stability on the dimensionless phugoid eigenvalues.

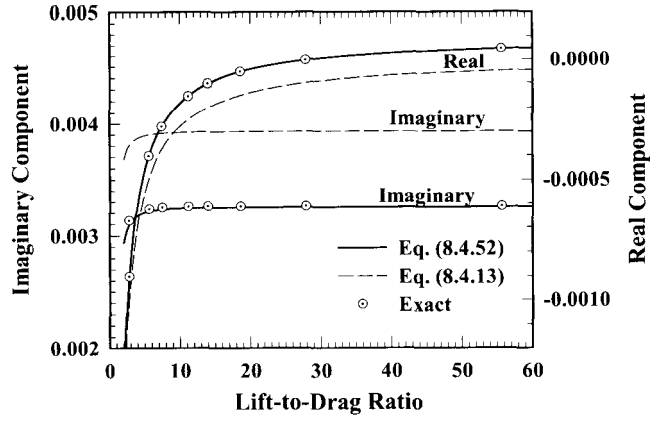


Figure 8.4.2. Effect of lift-to-drag ratio on the dimensionless phugoid eigenvalues.

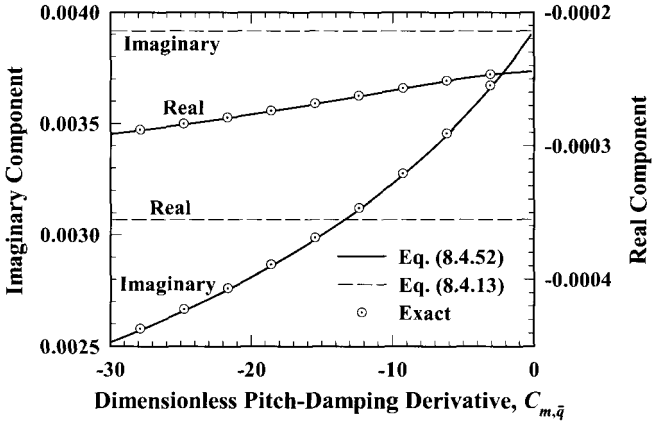


Figure 8.4.3. Effect of pitch damping on the dimensionless phugoid eigenvalues.

seen graphically in Fig. 8.4.1. Notice that as the pitch stability is increased, the result predicted by Eq. (8.4.52) approaches that predicted by Eq. (8.4.13). In this figure all parameters except the pitch stability ratio have been held constant at those values given in Example 8.2.1. In Fig 8.4.2, a comparison between Eq. (8.4.13), Eq. (8.4.52), and the exact solution is shown for a broad range of lift-to-drag ratio. A similar comparison showing the effect of pitch damping is displayed in Fig. 8.4.3.

This approximate closed-form solution allows us to more easily examine how the aerodynamic coefficients and stability derivatives affect phugoid motion. As we have seen, damping has very little effect on the phugoid frequency. Thus, neglecting the damping in Eq. (8.4.53) and applying the definition of the phugoid stability ratio from Eq. (8.4.45), the undamped natural frequency for phugoid motion is

$$\omega_n = \sqrt{2}\frac{g}{V_o}\sqrt{R_s} = \sqrt{2}\frac{g}{V_o}\sqrt{\frac{R_{m,\alpha}}{R_{m,\alpha} - R_{z,\alpha}R_{m,\bar{q}}}} = \sqrt{2}\frac{g}{V_o}\sqrt{\frac{\dfrac{4W/g}{\rho S_w \bar{c}_w}C_{m,\alpha}}{\dfrac{4W/g}{\rho S_w \bar{c}_w}C_{m,\alpha} - C_{Z,\alpha}C_{m,\bar{q}}}} \tag{8.4.55}$$

From Eq. (8.4.55), we first notice the well-known fact that the phugoid frequency is inversely proportional to forward speed. In addition, there are four other parameters that affect the phugoid frequency, the dimensionless mass, the change in pitching moment with respect to angle of attack, the change in z-force with respect to angle of attack, and the change in pitching moment with respect to pitching rate. For a stable aircraft, all of these parameters except the dimensionless mass are negative. Thus, the phugoid stability ratio is always between zero and unity. From this term we see that the phugoid frequency increases with dimensionless aircraft mass and pitch stability, while it decreases with lift slope and pitch damping. As the product of dimensionless mass and pitch stability becomes large compared to the product of lift slope and pitch damping, the

phugoid stability ratio approaches unity and the undamped phugoid frequency predicted from Eq. (8.4.55) reduces to that predicted by Eq. (8.4.15). Conversely, as the product of pitch stability and dimensionless mass approaches zero, so do the phugoid stability ratio and phugoid frequency.

From Eq. (8.4.54) we see that there are three distinct components to phugoid damping. Here these are called the *drag damping*, the *pitch damping*, and the *phase damping*. In most cases the drag damping is the largest of these three components. From Eq. (8.4.54), we define

$$\text{drag damping} \equiv \frac{g}{V_o}\frac{C_{Do}}{C_{Lo}} \tag{8.4.56}$$

Clearly, since the velocity, drag coefficient, and lift coefficient are all positive, the drag damping is always positive. The total drag is the sum of the parasitic drag and the induced drag. The parasitic drag coefficient is very nearly constant. The induced drag coefficient is proportional to the lift coefficient squared, and the lift coefficient is inversely proportional to the velocity squared. Thus, we can write

$$\begin{aligned}\text{drag damping} &\cong \frac{g}{V_o}\frac{C_{D_{Lo}} + C_{Lo}^2/\pi e R_A}{C_{Lo}} = \frac{g}{V_o}\left(\frac{C_{D_{Lo}}}{C_{Lo}} + \frac{C_{Lo}}{\pi e R_A}\right) \\ &= \frac{g}{V_o}\left(\frac{C_{D_{Lo}}(\frac{1}{2}\rho V_o^2 S_w)}{W} + \frac{W}{\pi e R_A(\frac{1}{2}\rho V_o^2 S_w)}\right)\end{aligned} \tag{8.4.57}$$

At very high airspeeds the parasitic drag dominates, the drag-to-lift ratio is proportional to velocity squared, and the phugoid drag damping increases linearly with forward velocity. At very low airspeeds the induced drag dominates, the drag-to-lift ratio is inversely proportional to velocity squared, and the phugoid drag damping varies inversely with the forward velocity cubed. At some intermediate airspeed, phugoid drag damping will exhibit a minimum. The airspeed that results in minimum phugoid drag damping is somewhat faster than the minimum drag airspeed.

The phugoid pitch damping is defined from Eqs. (8.4.54) and(8.4.46) to be

$$\text{pitch damping} \equiv \frac{g}{V_o}R_d = \frac{g}{V_o}\left(\frac{R_{x,\alpha}R_{m,\bar{q}}}{R_{m,\alpha} - R_{z,\alpha}R_{m,\bar{q}}}\right) = \frac{g}{V_o}\left(\frac{C_{X,\alpha}C_{m,\bar{q}}}{\frac{4W/g}{\rho S_w \bar{c}_w}C_{m,\alpha} - C_{Z,\alpha}C_{m,\bar{q}}}\right) \tag{8.4.58}$$

To determine the sign of the phugoid pitch damping, we note that the dimensionless mass is positive, while the pitch-stability derivative, the z-force derivative, and the pitch-damping derivative are all negative. Thus, the phugoid pitch damping will have the same sign as the change in axial force with respect to angle of attack. Depending on the airplane design, this axial force derivative can be either positive or negative.

The change in the x-force coefficient with respect to angle of attack can be written in terms of the lift and drag coefficients,

$$\begin{aligned} C_{X,\alpha} &= \frac{\partial}{\partial\alpha}\left(C_L \sin\alpha - C_D \cos\alpha\right) \\ &= C_L \cos\alpha + C_{L,\alpha} \sin\alpha + C_D \sin\alpha - C_{D,\alpha} \cos\alpha \cong C_{Lo} - C_{D,\alpha} \end{aligned} \tag{8.4.59}$$

The change in drag coefficient with angle of attack can be approximated as

$$C_{D,\alpha} \cong \frac{\partial C_D}{\partial C_L}\frac{\partial C_L}{\partial \alpha} = \frac{\partial}{\partial C_L}\left(C_{D_{f0}} + \frac{C_L^2}{\pi e R_A}\right) C_{L,\alpha} = \frac{2C_{L,\alpha}}{\pi e R_A} C_L \tag{8.4.60}$$

Using Eq. (8.4.60) in Eq. (8.4.59), we have

$$C_{X,\alpha} \cong C_{Lo}\left(1 - \frac{2C_{L,\alpha}}{\pi e R_A}\right) = \frac{W}{\frac{1}{2}\rho V_o^2 S_w}\left(1 - \frac{2C_{L,\alpha}}{\pi e R_A}\right) \tag{8.4.61}$$

Using Eq. (8.4.61) in Eq. (8.4.58), the phugoid pitch damping can be expressed as

$$\text{pitch damping} \cong \frac{gW}{\frac{1}{2}\rho V_o^3 S_w}\left(1 - \frac{2C_{L,\alpha}}{\pi e R_A}\right)\left(\frac{C_{m,\bar{q}}}{\frac{4W/g}{\rho S_w \bar{c}_w} C_{m,\alpha} - C_{Z,\alpha} C_{m,\bar{q}}}\right) \tag{8.4.62}$$

From Eq. (8.4.62), we see that phugoid pitch damping is inversely proportional to the cube of the forward velocity; it increases with the pitch-damping derivative; and it decreases with increasing pitch stability. We also see that phugoid pitch damping can be either positive or negative. Furthermore, the pitch damping is more negative for planes with low aspect ratio and low Oswald efficiency, and it is more positive for planes with high aspect ratio and Oswald efficiency. This may seem counterintuitive. However, the total phugoid damping is the sum of the drag damping, the pitch damping, and the phase damping. Lowering the aspect ratio or Oswald efficiency factor will increase the drag damping more than it will decrease the pitch damping. Thus, total phugoid damping will increase with decreasing aerodynamic efficiency, as expected.

Because lift slope decreases with decreasing aspect ratio, phugoid pitch damping can be negative only for airplanes with very low aspect ratio. For example, Prandtl's lifting-line theory combined with thin airfoil theory predicts that for an elliptic wing,

$$\frac{2C_{L,\alpha}}{\pi e R_A} \cong \frac{4}{R_A + 2} \tag{8.4.63}$$

If we were to use this result in Eq. (8.4.62), it would predict that phugoid pitch damping would be negative only for an airplane having an aspect ratio less than 2. Of course,

Prandtl's lifting-line theory does not apply to wings having an aspect ratio as low as 2. However, Eq. (8.4.63) does show that phugoid pitch damping will be positive for typical subsonic airplanes, which usually have aspect ratios of 5 or above.

Using Eq. (8.4.47) in Eq. (8.4.54), the phugoid phase damping is defined as

$$\begin{aligned}\text{phase damping} \equiv -\frac{g}{V_o}R_p &= -\frac{g}{V_o}R_{gx}R_s\left(\frac{R_{z,\alpha}+R_{m,\bar{q}}}{R_{m,\alpha}-R_{z,\alpha}R_{m,\bar{q}}}\right)\\ &= -\frac{g^2\bar{c}_w}{2V_o^3}R_s\left(\frac{\dfrac{8I_{yy_b}}{\rho S_w\bar{c}_w^3}C_{Z,\alpha}+\dfrac{4W/g}{\rho S_w\bar{c}_w}C_{m,\bar{q}}}{\dfrac{4W/g}{\rho S_w\bar{c}_w}C_{m,\alpha}-C_{Z,\alpha}C_{m,\bar{q}}}\right)\end{aligned} \tag{8.4.64}$$

We have already seen that the phugoid stability ratio can vary from zero to positive unity. The dimensionless mass and moment of inertia are always positive, while the pitch-stability derivative, the pitch-damping derivative, and the z-force derivative are all negative. Thus, for a stable aircraft, the phugoid phase damping is always negative, tending to decrease the total phugoid damping. In fact, under certain circumstances, it is possible for this negative phase damping to overpower the drag and pitch damping, which makes the phugoid divergent. Since the phugoid phase damping is inversely proportional to the forward velocity cubed, this condition is aggravated at low airspeed.

The phugoid approximation given by Eq. (8.4.13) predicts that only by increasing drag can we increase phugoid damping. Increasing aircraft drag to improve phugoid damping is obviously not a particularly desirable solution. From the present improved approximation, we see that phugoid damping can in fact be increased without increasing aircraft drag. This can be done by either increasing the phugoid pitch damping or by decreasing the magnitude of the negative phugoid phase damping.

8.5. Pure Pitching Motion

In addition to the short-period and long-period modes associated with free flight, there is a third type of oscillatory longitudinal motion that does not occur in free flight, but which has implications for wind tunnel testing. While it is not practical to perform free flight tests in a wind tunnel, it is possible to obtain much information about the free-flight characteristics of an aircraft from wind tunnel tests.

Here we shall consider the case in which the airplane's center of gravity is fixed in the wind tunnel. The airplane is constrained so that the lateral motions (sideslip, roll, and yaw) are all maintained at zero. In addition, the airplane's center of gravity cannot move axially or vertically within the wind tunnel. The aircraft is, however, free to rotate in pitch about the center of gravity. A model constrained in this manner has only one degree of freedom, rotation in pitch. Figure 8.5.1 shows a schematic drawing of a wind tunnel model so constrained. The oscillatory motion that can develop in such a wind tunnel test is *pure pitching motion*.

The equations of motion for this model can be obtained by applying the following constraints to the general longitudinal equations:

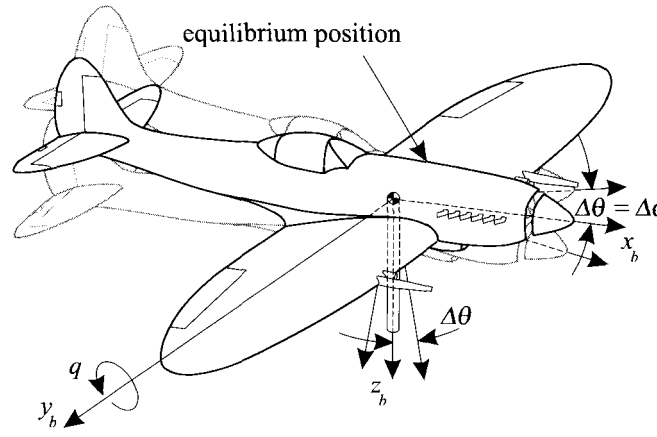


Figure 8.5.1. Wind tunnel model constrained to pure pitching motion.

$$\Delta\mu = \Delta\xi_x = \Delta\xi_z = 0 \tag{8.5.1}$$

$$\Delta\theta = \Delta\alpha \tag{8.5.2}$$

Because the axial and vertical motion is constrained, we can disregard the axial and vertical momentum equations. Thus, applying Eqs. (8.5.1) and (8.5.2) to Eq. (8.2.1) and eliminating the trivial equations, we have

$$\begin{bmatrix} -R_{m,\hat{\alpha}} & 1 \\ 1 & 0 \end{bmatrix} \begin{Bmatrix} \Delta\hat{\alpha} \\ \Delta\hat{\bar{q}} \end{Bmatrix} = \begin{bmatrix} R_{m,\alpha} & R_{m,\bar{q}} \\ 0 & 1 \end{bmatrix} \begin{Bmatrix} \Delta\alpha \\ \Delta\bar{q} \end{Bmatrix} \tag{8.5.3}$$

The eigenproblem associated with Eq. (8.5.3) is

$$\left(\begin{bmatrix} R_{m,\alpha} & R_{m,\bar{q}} \\ 0 & 1 \end{bmatrix} - \lambda \begin{bmatrix} -R_{m,\hat{\alpha}} & 1 \\ 1 & 0 \end{bmatrix} \right) \begin{Bmatrix} \chi_\alpha \\ \chi_{\bar{q}} \end{Bmatrix} = \begin{Bmatrix} 0 \\ 0 \end{Bmatrix} \tag{8.5.4}$$

The characteristic equation is

$$\begin{vmatrix} \left(R_{m,\alpha} + R_{m,\hat{\alpha}}\lambda\right) & \left(R_{m,\bar{q}} - \lambda\right) \\ -\lambda & 1 \end{vmatrix} = 0 \tag{8.5.5}$$

or

$$\lambda^2 - \left(R_{m,\bar{q}} + R_{m,\hat{\alpha}}\right)\lambda - R_{m,\alpha} = 0 \tag{8.5.6}$$

The **eigenvalues for pure pitching motion**, as obtained from Eq. (8.5.6), are then

$$\lambda = \frac{R_{m,\bar{q}} + R_{m,\dot{\alpha}}}{2} \pm \sqrt{\left(\frac{R_{m,\bar{q}} + R_{m,\dot{\alpha}}}{2}\right)^2 + R_{m,\alpha}} \tag{8.5.7}$$

Equation (8.5.7) looks very similar to Eq. (8.3.9), which expresses an approximate relationship for the eigenvalues associated with short-period motion in free flight. In fact, if we allow the mass to approach infinity, the z-force ratio in Eq. (8.3.9) goes to zero and Eq. (8.3.9) reduces to Eq. (8.5.7). Thus we see that as the dimensionless mass becomes large compared to the dimensionless moment of inertia, the short-period motion associated with free flight becomes pure pitching motion.

By performing wind tunnel tests on an aircraft model that is constrained to pure pitching motion, we could determine the eigenvalues experimentally. The model's moment of inertia should be adjusted to produce underdamped pitching motion. In the wind tunnel, the model is displaced in pitch from the equilibrium angle of attack and then released. The resulting oscillatory pitching motion is then recorded as a function of time. By measuring the period of oscillation and the time required to reduce the amplitude of oscillation by one-half, we could determine the sum of the two pitch-damping derivatives as well as the pitch-stability derivative.

From Eq. (8.5.7), the 50 percent damping time and the period for this pure pitching motion are given by

$$\begin{aligned}
50\%\ \text{damping time} \equiv t_{50} &= \frac{\bar{c}_w}{2V_o}\frac{\ln(0.50)}{\text{real}(\lambda)} = \frac{\bar{c}_w}{2V_o}\frac{\ln(0.50)}{\frac{1}{2}(R_{m,\bar{q}} + R_{m,\dot{\alpha}})} \\
&= \frac{\bar{c}_w}{2V_o}\frac{\ln(0.50)}{\frac{1}{2}\frac{\rho S_w \bar{c}_w^3}{8I_{yy_b}}(C_{m,\bar{q}} + C_{m,\dot{\alpha}})} = \left(\frac{8I_{yy_b}}{\rho S_w \bar{c}_w^2 V_o}\right)\frac{\ln(0.50)}{C_{m,\bar{q}} + C_{m,\dot{\alpha}}}
\end{aligned} \tag{8.5.8}$$

$$\begin{aligned}
\text{period} \equiv t_p &= \frac{\bar{c}_w}{2V_o}\frac{2\pi}{|\text{imag}(\lambda)|} = \frac{\pi \bar{c}_w / V_o}{\sqrt{-R_{m,\alpha} - \left(\frac{R_{m,\bar{q}} + R_{m,\dot{\alpha}}}{2}\right)^2}} \\
&= \frac{\pi \bar{c}_w / V_o}{\sqrt{-\left(\frac{\rho S_w \bar{c}^3}{8I_{yy_b}}\right)C_{m,\alpha} - \left(\frac{\rho S_w \bar{c}^3}{8I_{yy_b}}\frac{C_{m,\bar{q}} + C_{m,\dot{\alpha}}}{2}\right)^2}} \\
&= \frac{\frac{16\pi I_{yy_b}}{\rho S_w \bar{c}_w^2 V_o}}{\sqrt{-\left(\frac{32I_{yy_b}}{\rho S_w \bar{c}_w^3}\right)C_{m,\alpha} - \left(C_{m,\bar{q}} + C_{m,\dot{\alpha}}\right)^2}}
\end{aligned} \tag{8.5.9}$$

Rearranging Eqs. (8.5.8) and (8.5.9), we have

$$C_{m,\bar{q}} + C_{m,\dot{\alpha}} = \frac{8I_{yy_b} \ln(0.50)}{\rho S_w \bar{c}^2 V_o t_{50}} \tag{8.5.10}$$

and

$$C_{m,\alpha} = -\frac{2I_{yy_b}}{\rho S_w \bar{c} V_o^2}\left[\left(\frac{2\pi}{t_p}\right)^2 + \left(\frac{\ln(0.50)}{t_{50}}\right)^2\right] \tag{8.5.11}$$

Using Eqs. (8.5.10) and (8.5.11), we can determine the sum of the two pitch-damping derivatives as well as the pitch-stability derivative from the measured period and damping time, provided that we know the wind tunnel airspeed and density, along with the geometry and moment of inertia for the aircraft model. While the airflow and geometric parameters are readily determined, the mass moment of inertia is more easily resolved from a separate but related experiment.

The components of the mass moment of inertia tensor for any object could be determined using the concept of a simple torsional pendulum. To determine the pitching moment of inertia, the model is suspended from a wire as shown in Fig. 8.5.2. One end of the wire is rigidly attached to the model at the center of gravity, while the other end is rigidly attached to a supporting member. To determine the pitching moment of inertia,

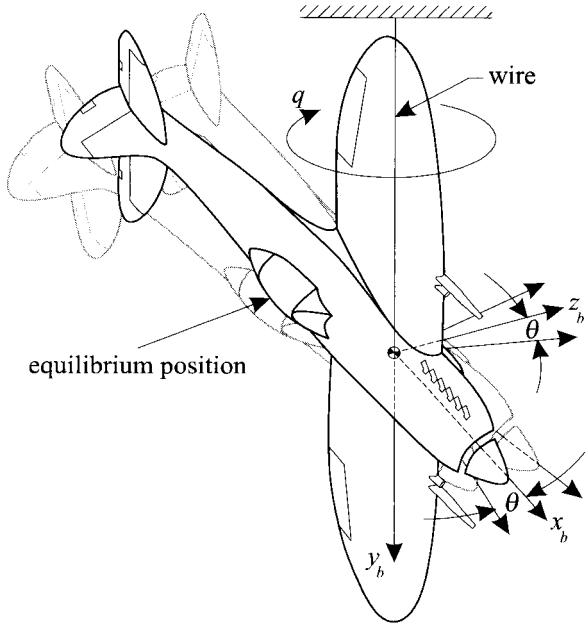


Figure 8.5.2. Aircraft model suspended as a torsional pendulum relative to the pitch axis.

the model is suspended so that the axis of the wire is coincident with the axis of pitch. The wire can pass through a small eyelet on the wing to help keep it aligned with the pitch axis. Thus, when the model is rotated about the pitch axis, the wire is loaded in pure torsion. The diameter and length of the wire can be adjusted to control the natural frequency of this torsional pendulum. The frequency should be low enough so that any aerodynamic forces on the model are negligible compared with the torsional force exerted by the wire. In addition, the diameter of the wire will be small enough so that the moment of inertia of the wire is small compared to that of the model.

Neglecting aerodynamic forces, Newton's second law for this torsional pendulum is

$$I_{yy_b}\frac{d^2\theta}{dt^2} + k_t\theta = 0 \tag{8.5.12}$$

where k_t is the torsional spring constant for the wire, which the student should be able to evaluate using elementary principles of solid mechanics for a known wire diameter, length, and modulus of elasticity. The eigenvalues from this second-order equation predict undamped torsional oscillations with a natural frequency of

$$\omega_n = \sqrt{\frac{k_t}{I_{yy_b}}} \tag{8.5.13}$$

In the real experiment, of course, there will be some damping. However, this damping will have little effect on the frequency. Thus, by measuring the natural frequency and determining the torsional spring constant, the mass moment of inertia about the axis of pitch is found to be

$$I_{yy_b} = \frac{k_t}{\omega_n^2} \tag{8.5.14}$$

The pitching moment of inertia so determined can be used in Eqs. (8.5.10) and (8.5.11) to obtain the related aerodynamic derivatives. Other components of the moment of inertia tensor can be obtained in a similar manner, by suspending the model in different orientations.

8.6. Summary

In this chapter we have examined the stick-fixed longitudinal dynamics of an aircraft in free flight. Our analysis was based on the assumptions of rigid-body motion and small deviations from equilibrium. We found that the same aerodynamic forces and moment that make an airplane statically stable in trimmed flight, will tend to produce oscillations in the aircraft operating parameters, such as airspeed and angle of attack, whenever the aircraft is disturbed from equilibrium. Furthermore, we found that under certain conditions it is possible for these oscillations to be dynamically unstable (i.e., divergent), even though the aircraft is statically stable in all regards. For a divergent mode, the amplitude of oscillation grows exponentially with time, if uncontrolled.

Two longitudinal modes of oscillation were found for a rigid airplane in free flight. These are the short-period mode and the phugoid or long-period mode. The short-period mode is composed of relatively high-frequency oscillations primarily in angle of attack and vertical displacement, with little change in airspeed. The short-period mode is typically heavily damped, with a period and 99 percent damping time both on the order of 1 to 5 seconds. The phugoid, on the other hand, is a low-frequency oscillation composed primarily of changes in airspeed and altitude, with little variation in angle of attack. The phugoid is usually very lightly damped and may even be divergent for some airplanes at certain airspeeds. The period for the phugoid is typically on the order of 30 seconds or more, and even when the mode is convergent, the 99 percent damping time is usually on the order of several minutes. The frequency and damping for both the short-period mode and the phugoid are determined form the eigenvalues, which are obtained from the linearized longitudinal equations of motion. The eigenvectors obtained from this system of equations tell us the relative amplitudes and phase shifts for the oscillations in each of the longitudinal flight variables.

These natural modes of oscillation for an aircraft in free flight are like the natural frequencies of vibration for a spring-mass system. If periodic flight disturbances are encountered of a frequency close to either that of the short-period mode or the phugoid, the oscillations associated with the affected mode can be excited in a manner similar to what is called resonance in a spring-mass system. With an aircraft, as with a spring-mass system, there are two ways to avoid resonance. One way is to make sure that the natural frequency of oscillation is not close to the frequency of any periodic disturbances that may be encountered. The other way is to provide sufficient damping in the oscillatory mode so that resonance does not produce significant amplification. For the longitudinal modes of a typical airplane, resonance is not usually a problem, because the short-period mode is heavily damped and the phugoid frequency is far below the frequency of any disturbances that are normally encountered in flight.

The material presented in this chapter is based on the assumption that the aircraft is a rigid body. Of course, in reality, airplanes are not rigid and have many modes of elastic vibration in addition to the two longitudinal flight modes discussed in this chapter. The flight modes are not significantly affected by the elastic modes provided that frequencies are not too closely aligned. The study of the effect of elastic deflection on the dynamics and aerodynamics of flight is a branch of aeronautical engineering called *aeroelasticity*. This is normally taught as a complete course, separate from flight mechanics, and many books have been written on the subject. The coupling between the elastic vibration modes of an airplane and the dynamic flight modes is beyond the scope of this textbook and is not covered here in any detail.

The reader should never lose sight of the fact that the material presented in this chapter is based on the assumption of small deviations from equilibrium flight. This approximation is quite good for the low angle of attack conditions that are encountered in nearly all flight of commercial and general aviation aircraft. However, fighter aircraft and stunt airplanes routinely execute maneuvers that involve high angles of attack, large angular rates, and substantial deviation from equilibrium flight. Dynamic analysis of such aircraft motion requires a much more sophisticated analysis than the application of linear theory that is presented in this chapter.

8.7. Problems

8.1. Use a numerical eigensolver to find the eigenvalues and eigenvectors for the spring-mass system described in Example 8.1.1. Verify that the results obtained from your solver agree with the results presented in Example 8.1.1. The solution may be obtained using either a generalized or a special eigensolver.

8.2. Use a numerical eigensolver to find the eigenvalues and eigenvectors for the spring-mass system described in Example 8.1.2. Verify that the results obtained from your solver agree with the results presented in Example 8.1.2.

8.3. Use a numerical eigensolver to find the eigenvalues and eigenvectors associated with the longitudinal modes of the typical general aviation airplane described in Example 8.2.1. Verify that the results obtained from your solver agree with the results presented in Example 8.2.1.

8.4. For the large jet transport and flight conditions in Examples 7.6.1 and 7.7.1, find the eigenvalues, the eigenvectors, the 99 percent damping time, and the period, if underdamped, for each longitudinal mode. For each oscillatory mode, compute the amplitude and phase for each component of the eigenvector associated with the positive frequency.

8.5. For the large jet transport and flight conditions in Examples 7.6.1 and 7.7.1, using the short-period eigenvalue approximation given by Eq. (8.3.9), find the eigenvalues, the 99 percent damping time, and the period for the short-period mode. Compare these approximate results with the fully coupled short-period solution that was obtained in problem 8.4.

8.6. For the large jet transport and flight conditions in Examples 7.6.1 and 7.7.1, using the short-period eigenvector approximation given by Eq. (8.3.5), find the eigenvectors for the short-period mode. Normalize these eigenvectors according to Eq. (8.1.37). Compare these approximate eigenvectors with the fully coupled short-period solution that was obtained in problem 8.4.

8.7. For the large jet transport and flight conditions in Examples 7.6.1 and 7.7.1, using the phugoid eigenvalue approximation given by Eq. (8.4.8), find the dimensionless phugoid eigenvalues, the 99 percent damping time, and the period for the long-period mode. Compare these approximate results with the fully coupled long-period solution that was obtained in problem 8.4.

8.8. For the large jet transport and flight conditions in Examples 7.6.1 and 7.7.1, using the phugoid eigenvector approximation given by Eq. (8.4.6), find the dimensionless phugoid eigenvectors for the long-period mode. Normalize these eigenvectors according to Eq. (8.1.37). Compare these approximate eigenvectors with those obtained from the fully coupled long-period solution that was obtained in problem 8.4.

8.9. For the large jet transport and flight conditions in Examples 7.6.1 and 7.7.1, using the phugoid eigenvalue approximation given by Eq. (8.4.44), find the dimensionless phugoid eigenvalues, the 99 percent damping time, and the period for the long-period mode. Compare these approximate results with the fully coupled long-period solution that was obtained in problem 8.4.

8.10. For the large jet transport and flight conditions in Examples 7.6.1 and 7.7.1, using the phugoid eigenvector approximation given by Eq. (8.4.27), find the dimensionless phugoid eigenvectors for the long-period mode. Normalize these eigenvectors according to Eq. (8.1.37). Compare these approximate eigenvectors with the fully coupled long-period solution that was obtained in problem 8.4.

8.11. For the large jet transport in Examples 7.6.1 and 7.7.1, the level flight airspeed is changed from 450 mph to 350 mph. All other operating conditions remain unchanged. Find the eigenvalues, the eigenvectors, the 99 percent damping time, and the period, if underdamped, for each longitudinal mode. For each oscillatory mode, compute the amplitude and phase for each component of the eigenvector associated with the positive frequency. Compare these results with those that were obtained for an airspeed of 450 mph in problem 8.4.

8.12. For the large jet transport in Examples 7.6.1 and 7.7.1, the airspeed is maintained at 450 mph while the aircraft is climbing at 2,000 ft/min. All other operating conditions remain unchanged. Find the eigenvalues, the eigenvectors, the 99 percent damping time, and the period, if underdamped, for each longitudinal mode. For each oscillatory mode, compute the amplitude and phase for each component of the eigenvector associated with the positive frequency. Compare the results with those obtained for level flight at 450 mph in problem 8.4.

8.13. For the Spitfire Mark XVIII and flight conditions described in problem 7.36, find the eigenvalues, the eigenvectors, the 99 percent damping time, and the period, if underdamped, for each longitudinal mode. For each oscillatory mode, compute the amplitude and phase for each component of the eigenvector associated with the positive frequency.

8.14. For the Spitfire Mark XVIII and flight conditions described in problem 7.36, using the short-period eigenvalue approximation given by Eq. (8.3.9), find the eigenvalues, the 99 percent damping time, and the period for the short-period mode. Compare these approximate results with the fully coupled short-period solution that was obtained in problem 8.13.

8.15. For the Spitfire Mark XVIII and flight conditions described in problem 7.36, using the short-period eigenvector approximation given by Eq. (8.3.5), find the eigenvectors for the short-period mode. Normalize these eigenvectors according to Eq. (8.1.37). Compare these approximate eigenvectors with the fully coupled short-period solution that was obtained in problem 8.13.

8.16. For the Spitfire Mark XVIII and flight conditions described in problem 7.36, using the phugoid eigenvalue approximation given by Eq. (8.4.8), find the dimensionless phugoid eigenvalues, the 99 percent damping time, and the period for the long-period mode. Compare these approximate results with the fully coupled long-period solution that was obtained in problem 8.13.

8.17. For the Spitfire Mark XVIII and flight conditions described in problem 7.36, using the phugoid eigenvector approximation given by Eq. (8.4.6), find the dimensionless phugoid eigenvectors for the long-period mode. Normalize these eigenvectors according to Eq. (8.1.37). Compare these approximate eigenvectors with those obtained from the fully coupled long-period solution that was obtained in problem 8.13.

8.18. For the Spitfire Mark XVIII and flight conditions described in problem 7.36, using the phugoid eigenvalue approximation given by Eq. (8.4.44), find the dimensionless phugoid eigenvalues, the 99 percent damping time, and the period for the long-period mode. Compare these approximate results with the fully coupled long-period solution that was obtained in problem 8.13.

8.19. For the Spitfire Mark XVIII and flight conditions described in problem 7.36, using the phugoid eigenvector approximation given by Eq. (8.4.27), find the dimensionless phugoid eigenvectors for the long-period mode. Normalize these eigenvectors according to Eq. (8.1.37). Compare these approximate eigenvectors with the fully coupled long-period solution that was obtained in problem 8.13.

8.20. For the Spitfire Mark XVIII described in problem 7.36, the level-flight airspeed is changed from 300 mph to 200 mph. All other operating conditions remain unchanged. Find the eigenvalues, the eigenvectors, the 99 percent damping time, and the period, if underdamped, for each longitudinal mode. For each oscillatory mode, compute the amplitude and phase for each component of the eigenvector associated with the positive frequency. Compare these results with those that were obtained for an airspeed of 300 mph in problem 8.13.

8.21. For the Spitfire Mark XVIII described in problem 7.36, the airspeed is maintained at 300 mph while the aircraft is climbing at 5,000 ft/min. All other operating conditions remain unchanged. Find the eigenvalues, the eigenvectors, the 99 percent damping time, and the period, if underdamped, for each longitudinal mode. For each oscillatory mode, compute the amplitude and phase for each component of the eigenvector associated with the positive frequency. Compare the results with those obtained for level flight at 300 mph in problem 8.13.

8.22. For the jet transport and flight conditions that are described in problem 7.37, find the eigenvalues, the eigenvectors, the 99 percent damping time, and the period, if underdamped, for each longitudinal mode. For each oscillatory mode, compute the amplitude and phase for each component of the eigenvector associated with the positive frequency.

8.23. For the jet transport and flight conditions that are described in problem 7.37, using the short-period eigenvalue approximation given by Eq. (8.3.9), find the eigenvalues, the 99 percent damping time, and the period for the short-period mode. Compare these approximate results with those obtained from the fully coupled short-period solution that was obtained in problem 8.22.

8.24. For the jet transport and flight conditions that are described in problem 7.37, using the short-period eigenvector approximation given by Eq. (8.3.5), find the eigenvectors for the short-period mode. Normalize these eigenvectors according to Eq. (8.1.37). Compare these approximate eigenvectors with the fully coupled short-period solution that was obtained in problem 8.22.

8.25. For the jet transport and flight conditions that are described in problem 7.37, using the phugoid eigenvalue approximation given by Eq. (8.4.8), find the dimensionless phugoid eigenvalues, the 99 percent damping time, and the period for the long-period mode. Compare these approximate results with the fully coupled long-period solution that was obtained in problem 8.22.

8.26. For the jet transport and flight conditions that are described in problem 7.37, using the phugoid eigenvector approximation given by Eq. (8.4.6), find the dimensionless phugoid eigenvectors for the long-period mode. Normalize these eigenvectors according to Eq. (8.1.37). Compare these approximate eigenvectors with those obtained from the fully coupled long-period solution that was obtained in problem 8.22.

8.27. For the jet transport and flight conditions that are described in problem 7.37, using the phugoid eigenvalue approximation given by Eq. (8.4.44), find the dimensionless phugoid eigenvalues, the 99 percent damping time, and the period for the long-period mode. Compare these approximate results with the fully coupled long-period solution that was obtained in problem 8.22.

8.28. For the jet transport and flight conditions that are described in problem 7.37, using the phugoid eigenvector approximation given by Eq. (8.4.27), find the dimensionless phugoid eigenvectors for the long-period mode. Normalize these eigenvectors according to Eq. (8.1.37). Compare these approximate eigenvectors with those obtained from the fully coupled long-period solution that was obtained in problem 8.22.

8.29. For the jet transport described in problem 7.37, assume that the pitch-stability and pitch-damping derivatives are doubled while all other parameters remain unchanged. Find the eigenvalues, the eigenvectors, the 99 percent damping time, and the period, if underdamped, for each longitudinal mode. For each oscillatory mode, compute the amplitude and phase for each component of the eigenvector associated with the positive frequency. Compare these results with those that were obtained in problem 8.22.

8.30. The jet transport described in problem 7.37 is climbing at 2,000 ft/min. Assume that the airspeed and all aerodynamic derivatives remain unchanged. Find the eigenvalues, the eigenvectors, the 99 percent damping time, and the period, if underdamped, for each longitudinal mode. For each oscillatory mode, compute the amplitude and phase for each component of the eigenvector associated with the positive frequency. Compare these results with those that were obtained for level flight in problem 8.22.

8.31. For the turboprop transport and flight conditions described in problem 7.38, find the eigenvalues, the eigenvectors, the 99 percent damping time, and the period, if underdamped, for each longitudinal mode. For each oscillatory mode, compute the amplitude and phase for each component of the eigenvector associated with the positive frequency.

8.32. For the turboprop transport and flight conditions described in problem 7.38, using the short-period eigenvalue approximation given by Eq. (8.3.9), find the eigenvalues, the 99 percent damping time, and the period for the short-period mode. Compare these approximate results with the fully coupled short-period solution that was obtained in problem 8.31.

8.33. For the turboprop transport and flight conditions described in problem 7.38, using the short-period eigenvector approximation given by Eq. (8.3.5), find the eigenvectors for the short-period mode. Normalize these eigenvectors according to Eq. (8.1.37). Compare these approximate eigenvectors with those from the exact solution for the fully coupled short-period mode, which was obtained in problem 8.31.

8.34. For the turboprop transport and flight conditions described in problem 7.38, using the phugoid eigenvalue approximation given by Eq. (8.4.8), find the dimensionless phugoid eigenvalues, the 99 percent damping time, and the period for the long-period mode. Compare these approximate results with the fully coupled long-period solution that was obtained in problem 8.31.

8.35. For the turboprop transport and flight conditions described in problem 7.38, using the phugoid eigenvector approximation given by Eq. (8.4.6), find the dimensionless phugoid eigenvectors for the long-period mode. Normalize these eigenvectors according to Eq. (8.1.37). Compare these approximate eigenvectors with those from the fully coupled long-period solution, which was obtained in problem 8.31.

8.36. For the turboprop transport and flight conditions described in problem 7.38, using the phugoid eigenvalue approximation given by Eq. (8.4.44), find the dimensionless phugoid eigenvalues, the 99 percent damping time, and the period for the long-period mode. Compare these approximate results with the fully coupled long-period solution that was obtained in problem 8.31.

8.37. For the turboprop transport and flight conditions described in problem 7.38, using the phugoid eigenvector approximation given by Eq. (8.4.27), find the dimensionless phugoid eigenvectors for the long-period mode. Normalize these eigenvectors according to Eq. (8.1.37). Compare these approximate eigenvectors with those from the fully coupled long-period solution, which was obtained in problem 8.31.

8.38. For the turboprop transport described in problem 7.38, assume that $R_{m,\mu}$ is doubled while all other aerodynamic derivatives and operating conditions remain unchanged. Find the eigenvalues, the eigenvectors, the 99 percent damping time, and the period, if underdamped, for each longitudinal mode. For each oscillatory mode, compute the amplitude and phase for each component of the eigenvector associated with the positive frequency. Compare these results with those that were obtained in problem 8.31.

8.39. The turboprop transport described in problem 7.38 is climbing at 5,000 ft/min. Assume that the airspeed and all aerodynamic derivatives remain unchanged. Find the eigenvalues, the eigenvectors, the 99 percent damping time, and the period, if underdamped, for each longitudinal mode. For each oscillatory mode, compute the amplitude and phase for each component of the eigenvector associated with the positive frequency. Compare these results with those obtained for level flight in problem 8.31.

Chapter 9
Linearized Lateral Dynamics

9.1. Introduction

If one understands the material presented in Chapter 8 it should be fairly easy to understand the material presented in this chapter, at least from an analytical point of view. Mathematically speaking, there is little difference between linearized lateral dynamics and linearized longitudinal dynamics. In each case we are dealing with an eigenproblem associated with a homogeneous system of six first-order linear differential equations. In both cases the six first-order equations were obtained from a second-order system representing uncontrolled motion with three degrees of freedom. It is a matter of little wonder that the homogeneous solutions for lateral aircraft dynamics have much in common with those for longitudinal dynamics. There are, however, some significant differences between the uncontrolled dynamic response of an aircraft to a lateral disturbance and its response to a similar longitudinal disturbance. In studying the material in this chapter, the student should strive to understand both the similarities and the differences between longitudinal and lateral aircraft dynamics.

A significant difference between lateral and longitudinal motion is that longitudinal motion is true two-dimensional motion, involving two translational degrees of freedom and one rotational degree of freedom. Lateral motion, however, is three-dimensional, involving two rotational degrees of freedom and one translational degree of freedom. Pure longitudinal motion can exist in free flight, even outside the approximation of small disturbance theory. Because longitudinal motion is two-dimensional, there is no tendency for a longitudinal disturbance to induce lateral motion in a perfectly symmetric aircraft, even if the disturbance is large. On the other hand, recall that the lateral equations of motion were separated from the longitudinal equations only as a result of the small disturbance approximation. Thus, lateral motion is only an approximation that can never truly exist in the world of finite disturbance. The actual response of an aircraft to a finite lateral disturbance will always involve all six degrees of freedom. Nevertheless, the lateral approximation to be studied in this chapter is very close to the response of a real aircraft for the disturbance magnitudes that are encountered in normal flight.

9.2. Lateral Motion: The Linearized Coupled Equations

The lateral dynamic response of an aircraft disturbed from equilibrium flight involves a complex combination of sideslip, roll, and yaw. These three degrees of freedom are very closely coupled. As we have already seen, sideslip produces both rolling and yawing moments, which in turn produce rolling and yawing rates. The rolling rate produces a significant yawing moment in addition to the rolling moment, and the yawing rate generates a side force and a rolling moment as well as a yawing moment. In general, the sideslip, roll, and yaw are also coupled to the longitudinal and elastic degrees of freedom. However, in this chapter we are restricting our discussion to the six degrees of freedom associated with rigid-body flight and we are confining the aircraft

motion to small deviations from steady equilibrium flight. For small deviations from equilibrium, the lateral motion is not coupled to the longitudinal motion and the lateral equations can be solved independently. In this section we examine the stick-fixed free response associated with linearized, lateral, rigid-body motion. Here again, these results provide a reasonable description of lateral aircraft dynamics provided that the aircraft is not undergoing large-amplitude oscillations or rapid maneuvers. We should also keep in mind that the separation of the longitudinal and lateral equations of motion depended on our neglecting the angular momentum of the spinning rotors in the aircraft's engines. In conventional airplanes, such gyroscopic effects can sometimes cause significant yaw-pitch coupling.

Since rigid-body lateral motion has three degrees of freedom (sideslip, roll, and yaw), it is characterized by six eigenvalues. The eigenvalues associated with the linearized lateral motion of a typical airplane contain two distinct real roots, one complex pair, and two identical zero roots. The real and distinct roots correspond to two nonoscillatory modes, one heavily damped motion called the *roll mode* and one lightly damped or divergent motion called the *spiral mode*. The complex pair describes a damped oscillatory motion that is called *Dutch roll*. The remaining two zero eigenvalues correspond to simple rigid-body displacement modes. The roll mode is so heavily damped that it is of no concern to pilots or passengers. As we shall see, the nonoscillatory spiral mode can be divergent even in an aircraft with a high degree of directional stability. However, in most aircraft, the spiral mode is convergent or so slowly divergent that it does not create significant problems for either the pilot or the designer. The Dutch roll mode is an out-of-phase combination of sideslipping, rolling, and yawing oscillations that can be very objectionable. In this section we examine these coupled lateral motions in detail.

The free response of a conventional airplane to small lateral disturbances is obtained from the linearized homogeneous system of lateral equations, with both lateral control inputs set to zero. From Eq. (7.7.6), the homogeneous linearized lateral equations can be written as

$$\begin{bmatrix} 1 & 0 & 0 & 0 & 0 & 0 \\ 0 & 1 & -\iota_{xz} & 0 & 0 & 0 \\ 0 & -\iota_{zx} & 1 & 0 & 0 & 0 \\ 0 & 0 & 0 & 1 & 0 & 0 \\ 0 & 0 & 0 & 0 & 1 & 0 \\ 0 & 0 & 0 & 0 & 0 & 1 \end{bmatrix} \begin{Bmatrix} \Delta\hat{\beta} \\ \Delta\hat{\bar{p}} \\ \Delta\hat{\bar{r}} \\ \Delta\hat{\xi}_y \\ \Delta\hat{\phi} \\ \Delta\hat{\psi} \end{Bmatrix}$$

$$- \begin{bmatrix} R_{y,\beta} & R_{y,\bar{p}} & (R_{y,\bar{r}} - 1) & 0 & R_{gy}\cos\theta_0 & 0 \\ R_{\ell,\beta} & R_{\ell,\bar{p}} & R_{\ell,\bar{r}} & 0 & 0 & 0 \\ R_{n,\beta} & R_{n,\bar{p}} & R_{n,\bar{r}} & 0 & 0 & 0 \\ 1 & 0 & 0 & 0 & 0 & \cos\theta_o \\ 0 & 1 & \tan\theta_o & 0 & 0 & 0 \\ 0 & 0 & \sec\theta_o & 0 & 0 & 0 \end{bmatrix} \begin{Bmatrix} \Delta\beta \\ \Delta\bar{p} \\ \Delta\bar{r} \\ \Delta\xi_y \\ \Delta\phi \\ \Delta\psi \end{Bmatrix} = \begin{Bmatrix} 0 \\ 0 \\ 0 \\ 0 \\ 0 \\ 0 \end{Bmatrix} \tag{9.2.1}$$

Here again, Eq. (9.2.1) exactly fits the form of the eigenvalue problem that was given by Eq. (8.1.28), and the **generalized eigenproblem for lateral motion** is

$$\left(\begin{bmatrix} R_{y,\beta} & R_{y,\bar{p}} & (R_{y,\bar{r}}-1) & 0 & R_{gy}\cos\theta_0 & 0 \\ R_{\ell,\beta} & R_{\ell,\bar{p}} & R_{\ell,\bar{r}} & 0 & 0 & 0 \\ R_{n,\beta} & R_{n,\bar{p}} & R_{n,\bar{r}} & 0 & 0 & 0 \\ 1 & 0 & 0 & 0 & 0 & \cos\theta_o \\ 0 & 1 & \tan\theta_o & 0 & 0 & 0 \\ 0 & 0 & \sec\theta_o & 0 & 0 & 0 \end{bmatrix} - \lambda \begin{bmatrix} 1 & 0 & 0 & 0 & 0 & 0 \\ 0 & 1 & -\iota_{xz} & 0 & 0 & 0 \\ 0 & -\iota_{zx} & 1 & 0 & 0 & 0 \\ 0 & 0 & 0 & 1 & 0 & 0 \\ 0 & 0 & 0 & 0 & 1 & 0 \\ 0 & 0 & 0 & 0 & 0 & 1 \end{bmatrix}\right) \begin{Bmatrix} \chi_\beta \\ \chi_{\bar{p}} \\ \chi_{\bar{r}} \\ \chi_{\xi_v} \\ \chi_\phi \\ \chi_\psi \end{Bmatrix} = \begin{Bmatrix} 0 \\ 0 \\ 0 \\ 0 \\ 0 \\ 0 \end{Bmatrix} \tag{9.2.2}$$

The eigenvalues and eigenvectors associated with linearized lateral aircraft motion can be found by solving Eq. (9.2.2) using a generalized eigensolver. If a generalized eigensolver is not available, the system can easily be rearranged to give the **special eigenproblem for lateral motion**:

$$\left(\begin{bmatrix} R_{y,\beta} & R_{y,\bar{p}} & (R_{y,\bar{r}}-1) & 0 & R_{gy}\cos\theta_0 & 0 \\ \dfrac{R_{\ell,\beta}+\iota_{xz}R_{n,\beta}}{1-\iota_{xz}\iota_{zx}} & \dfrac{R_{\ell,\bar{p}}+\iota_{xz}R_{n,\bar{p}}}{1-\iota_{xz}\iota_{zx}} & \dfrac{R_{\ell,\bar{r}}+\iota_{xz}R_{n,\bar{r}}}{1-\iota_{xz}\iota_{zx}} & 0 & 0 & 0 \\ \dfrac{R_{n,\beta}+\iota_{zx}R_{\ell,\beta}}{1-\iota_{xz}\iota_{zx}} & \dfrac{R_{n,\bar{p}}+\iota_{zx}R_{\ell,\bar{p}}}{1-\iota_{xz}\iota_{zx}} & \dfrac{R_{n,\bar{r}}+\iota_{zx}R_{\ell,\bar{r}}}{1-\iota_{xz}\iota_{zx}} & 0 & 0 & 0 \\ 1 & 0 & 0 & 0 & 0 & \cos\theta_o \\ 0 & 1 & \tan\theta_o & 0 & 0 & 0 \\ 0 & 0 & \sec\theta_o & 0 & 0 & 0 \end{bmatrix} - \lambda \begin{bmatrix} 1 & 0 & 0 & 0 & 0 & 0 \\ 0 & 1 & 0 & 0 & 0 & 0 \\ 0 & 0 & 1 & 0 & 0 & 0 \\ 0 & 0 & 0 & 1 & 0 & 0 \\ 0 & 0 & 0 & 0 & 1 & 0 \\ 0 & 0 & 0 & 0 & 0 & 1 \end{bmatrix}\right) \begin{Bmatrix} \chi_\beta \\ \chi_{\bar{p}} \\ \chi_{\bar{r}} \\ \chi_{\xi_v} \\ \chi_\phi \\ \chi_\psi \end{Bmatrix} = \begin{Bmatrix} 0 \\ 0 \\ 0 \\ 0 \\ 0 \\ 0 \end{Bmatrix} \tag{9.2.3}$$

From Eq. (9.2.2) or Eq. (9.2.3), we obtain dimensionless eigenvalues. To obtain the dimensional eigenvalues in terms of time, the dimensionless eigenvalues must be divided by the characteristic time, $b_w/2V_o$.

Thus, the **damping rate for a lateral mode** is

$$\sigma = -\text{real}(\lambda)\frac{2V_o}{b_w} \tag{9.2.4}$$

and the **damped natural frequency for a lateral mode** is

$$\omega_d = |\text{imag}(\lambda)|\frac{2V_o}{b_w} \tag{9.2.5}$$

The **damping ratio** is

$$\zeta = -\frac{\lambda_1 + \lambda_2}{2\sqrt{\lambda_1\lambda_2}} \tag{9.2.6}$$

and the **undamped natural frequency for a lateral mode** is

$$\omega_n = \sqrt{\lambda_1\lambda_2}\,\frac{2V_o}{b_w} \tag{9.2.7}$$

EXAMPLE 9.2.1. For steady level flight at sea level, find the dimensionless eigenvalues and eigenvectors, the damping rate, the 99 percent damping time, and the damped natural frequency and period, if underdamped, for each lateral mode of the typical general aviation airplane described in Example 8.2.1. For each pair of eigenvalues, find the undamped natural frequency and the damping ratio. For the oscillatory mode, compute the amplitude and phase. The characteristics of this airplane are again listed below.

$$S_w = 185\,\text{ft}^2, \quad b_w = 33\,\text{ft}, \quad W = 2800\,\text{lbf}, \quad V_o = 180\,\text{ft/sec}, \quad C_{Do} = 0.05,$$
$$I_{xx_b} = 1000\,\text{slug·ft}^2, \quad I_{yy_b} = 3000\,\text{slug·ft}^2, \quad I_{zz_b} = 3500\,\text{slug·ft}^2,$$
$$I_{xz_b} = 30\,\text{slug·ft}^2,$$
$$C_{L,\alpha} = 4.40, \quad C_{D,\alpha} = 0.35, \quad C_{m,\alpha} = -0.68, \quad C_{L,\dot{\alpha}} = 1.60, \quad C_{m,\dot{\alpha}} = -4.35,$$
$$C_{Y,\beta} = -0.560, \quad C_{\ell,\beta} = -0.075, \quad C_{n,\beta} = 0.070,$$
$$C_{D,\bar{q}} \cong 0.0, \quad C_{L,\bar{q}} = 3.80, \quad C_{m,\bar{q}} = -9.95,$$
$$C_{Y,\bar{p}} \cong 0.0, \quad C_{\ell,\bar{p}} = -0.410, \quad C_{n,\bar{p}} = -0.0575,$$
$$C_{Y,\bar{r}} = 0.240, \quad C_{\ell,\bar{r}} = 0.105, \quad C_{n,\bar{r}} = -0.125$$

Solution. The additional parameters that affect the lateral eigenvalues and eigenvectors for this aircraft are:

$$\iota_{xz} \equiv I_{xz_b}/I_{xx_b} = 0.0300, \qquad \iota_{zx} \equiv I_{xz_b}/I_{zz_b} = 0.0086,$$

$$\frac{\rho S_w b_w}{4W/g} = 0.041679, \qquad \frac{\rho S_w b_w^3}{8I_{xx_b}} = 1.975306, \qquad \frac{\rho S_w b_w^3}{8I_{zz_b}} = 0.564373,$$

$$R_{y,\beta} \equiv \frac{\rho S_w b_w}{4W/g} C_{Y,\beta} = -0.0233, \qquad R_{\ell,\beta} \equiv \frac{\rho S_w b_w^3}{8I_{xx_b}} C_{\ell,\beta} = -0.1481,$$

$$R_{n,\beta} \equiv \frac{\rho S_w b_w^3}{8I_{zz_b}} C_{n,\beta} = 0.0395, \qquad R_{y,\bar{p}} \equiv \frac{\rho S_w b_w}{4W/g} C_{Y,\bar{p}} = 0.0,$$

$$R_{\ell,\bar{p}} \equiv \frac{\rho S_w b_w^3}{8I_{xx_b}} C_{\ell,\bar{p}} = -0.8099, \qquad R_{n,\bar{p}} \equiv \frac{\rho S_w b_w^3}{8I_{zz_b}} C_{n,\bar{p}} = -0.0325,$$

$$R_{y,\bar{r}} \equiv \frac{\rho S_w b_w}{4W/g} C_{Y,\bar{r}} = 0.0100, \qquad R_{\ell,\bar{r}} \equiv \frac{\rho S_w b_w^3}{8I_{xx_b}} C_{\ell,\bar{r}} = 0.2074,$$

$$R_{n,\bar{r}} \equiv \frac{\rho S_w b_w^3}{8I_{zz_b}} C_{n,\bar{r}} = -0.0705, \qquad R_{gv} \equiv \frac{g b_w}{2V_o^2} = 0.0164$$

For this level-flight equilibrium condition, the cosine of the equilibrium elevation angle is unity while the tangent is zero. Thus, for this aircraft and flight condition, the eigenproblem given by Eq. (9.2.2) becomes

$$\left(\begin{bmatrix} -0.0233 & 0 & -0.9900 & 0 & 0.0164 & 0 \\ -0.1481 & -0.8099 & 0.2074 & 0 & 0 & 0 \\ 0.0395 & -0.0325 & -0.0705 & 0 & 0 & 0 \\ 1 & 0 & 0 & 0 & 0 & 1 \\ 0 & 1 & 0 & 0 & 0 & 0 \\ 0 & 0 & 1 & 0 & 0 & 0 \end{bmatrix} - \lambda \begin{bmatrix} 1 & 0 & 0 & 0 & 0 & 0 \\ 0 & 1 & -0.0300 & 0 & 0 & 0 \\ 0 & -0.0086 & 1 & 0 & 0 & 0 \\ 0 & 0 & 0 & 1 & 0 & 0 \\ 0 & 0 & 0 & 0 & 1 & 0 \\ 0 & 0 & 0 & 0 & 0 & 1 \end{bmatrix} \right) \begin{Bmatrix} \chi_\beta \\ \chi_{\bar{p}} \\ \chi_{\bar{r}} \\ \chi_y \\ \chi_\phi \\ \chi_\psi \end{Bmatrix} = \begin{Bmatrix} 0 \\ 0 \\ 0 \\ 0 \\ 0 \\ 0 \end{Bmatrix}$$

The solution to this characteristic equation yields one pair of distinct real eigenvalues, one complex pair of eigenvalues, and two eigenvalues that are identically zero. These roots describe two nonoscillatory modes, one oscillatory mode, and two rigid-body displacement modes that are associated with lateral motion. These modes are:

The roll mode ($\lambda_1 = -0.813797$)

$$\begin{Bmatrix} \Delta\beta \\ \Delta\bar{p} \\ \Delta\bar{r} \\ \Delta\xi_y \\ \Delta\phi \\ \Delta\psi \end{Bmatrix} = C_1 \begin{Bmatrix} -0.054317 \\ -0.629391 \\ -0.030559 \\ 0.020602 \\ 0.773401 \\ 0.037551 \end{Bmatrix} \exp(-0.813797\,\tau_y)$$

The damping rate is

$$\sigma = -\text{real}(\lambda)\frac{2V_o}{b_w} = 0.813797\frac{2(180)}{33} = 8.877785\ \text{sec}^{-1}$$

and the 99 percent damping time is

$$99\%\ \text{damping time} = \frac{\ln(0.01)}{-\sigma} = \frac{\ln(0.01)}{-8.877785\ \text{sec}^{-1}} = 0.519\ \text{sec}$$

The spiral mode ($\lambda_2 = -0.000918$)

$$\begin{Bmatrix} \Delta\beta \\ \Delta\bar{p} \\ \Delta\bar{r} \\ \Delta\xi_y \\ \Delta\phi \\ \Delta\psi \end{Bmatrix} = C_2 \begin{Bmatrix} 0.000001 \\ 0.000000 \\ 0.000001 \\ 0.999999 \\ 0.000053 \\ -0.000920 \end{Bmatrix} \exp(-0.000918\,\tau_y)$$

The damping rate and the 99 percent damping time are

$$\sigma = -\text{real}(\lambda)\frac{2V_o}{b_w} = 0.000918\frac{2(180)}{33} = 0.010015\ \text{sec}^{-1}$$

$$99\%\ \text{damping time} = \frac{\ln(0.01)}{-\sigma} = \frac{\ln(0.01)}{-0.010015\ \text{sec}^{-1}} = 460\ \text{sec}$$

The eigenvalues for the roll and spiral modes form a mathematical pair. For this roll-spiral pair, the undamped natural frequency is

$$\omega_n = \sqrt{\lambda_1\lambda_2}\,\frac{2V_o}{b_w} = \sqrt{(-0.813797)(-0.000918)}\,\frac{2(180)}{33} = 0.298173 \text{ rad/sec}$$

and the damping ratio is

$$\zeta = -\frac{\lambda_1+\lambda_2}{2\sqrt{\lambda_1\lambda_2}} = -\frac{-0.813797-0.000918}{2\sqrt{(-0.813797)(-0.000918)}} = 14.9038$$

The Dutch roll mode $(\lambda_{3,4} = -0.044202 \pm 0.217908\,i)$

$$\begin{Bmatrix} \Delta\beta \\ \Delta\bar{p} \\ \Delta\bar{r} \\ \Delta\xi_y \\ \Delta\phi \\ \Delta\psi \end{Bmatrix} = C_{3,4} \begin{Bmatrix} 0.589580 \\ -0.109648 \mp 0.001442\,i \\ 0.013967 \mp 0.121744\,i \\ 0.172251 \mp 0.220690\,i \\ 0.091681 \pm 0.484586\,i \\ -0.549104 \pm 0.047290\,i \end{Bmatrix} \exp[(-0.044202 \pm 0.217908\,i)\,\tau_y]$$

The damping rate for the Dutch roll mode is

$$\sigma = -\text{real}(\lambda)\frac{2V_o}{b_w} = 0.044202\frac{2(180)}{33} = 0.482204 \text{ sec}^{-1}$$

The 99 percent damping time is

$$99\% \text{ damping time} = \frac{\ln(0.01)}{-\sigma} = \frac{\ln(0.01)}{-0.482204} = 9.55 \text{ sec}$$

and the damping ratio for this mode is

$$\zeta = -\frac{\lambda_3+\lambda_4}{2\sqrt{\lambda_3\lambda_4}} = -\frac{-0.044202+0.217908\,i-0.044202-0.217908\,i}{2\sqrt{(-0.044202+0.217908\,i)(-0.044202-0.217908\,i)}}$$

$$= \frac{0.044202}{\sqrt{0.044202^{\,2}+0.217908^{\,2}}} = 0.198798$$

The damped natural frequency for the Dutch roll oscillations is

$$\omega_d = |\text{imag}(\lambda)|\frac{2V_o}{b_w} = 0.217908\frac{2(180)}{33} = 2.377178 \text{ rad/sec}$$

and the period is

$$\text{period} = \frac{2\pi}{\omega_d} = \frac{2\pi}{2.377178} = 2.64 \text{ sec}$$

The undamped natural frequency for the Dutch roll mode is

$$\begin{aligned}\omega_n &= \sqrt{\lambda_3\lambda_4}\,\frac{2V_o}{b_w} \\ &= \sqrt{(-0.044202+0.217908\,i)(-0.044202-0.217908\,i)}\,\frac{2(180)}{33} \\ &= \sqrt{0.044202^{\,2}+0.217908^{\,2}}\,\frac{2(180)}{33} = 2.425592 \text{ rad/sec}\end{aligned}$$

Notice that for this airplane and these operating conditions, damping reduces the Dutch roll frequency by about 2 percent.

The rigid-body modes ($\lambda_{5,6} = 0.0, 0.0$)

$$\begin{Bmatrix} \Delta\beta \\ \Delta\bar{p} \\ \Delta\bar{r} \\ \Delta\xi_y \\ \Delta\phi \\ \Delta\psi \end{Bmatrix} = C_5 \begin{Bmatrix} 0 \\ 0 \\ 0 \\ 1 \\ 0 \\ 0 \end{Bmatrix} \exp(0.0\,\tau_y),\; C_6 \begin{Bmatrix} 0 \\ 0 \\ 0 \\ 0 \\ 0 \\ 1 \end{Bmatrix} \exp(0.0\,\tau_y)$$

The trivial rigid-body displacement modes simply state the fact that steady level flight can be maintained, with no change in dynamic characteristics, at different longitudes and/or at different headings. These modes arise from the fact that the forces and moments are independent of ξ_y and ψ. The eigenvectors for the nontrivial modes are summarized in Table 9.2.1.

Eigenvector Component	Roll Mode Amplitude	Spiral Mode Amplitude	Dutch Roll	
			Amplitude	Phase
$\Delta\beta$	0.054317	0.000001	0.589580	0.00°
$\Delta\bar{p}$	0.629391	0.000000	0.109657	−179.04°
$\Delta\bar{r}$	0.030559	0.000001	0.122543	−83.36°
$\Delta\xi_y$	0.020602	0.999999	0.279954	−51.97°
$\Delta\phi$	0.773401	0.000053	0.493182	79.20°
$\Delta\psi$	0.037551	0.000920	0.551136	174.88°

Table 9.2.1. Lateral eigenvectors for a typical general aviation airplane.

The lateral modes observed in Example 9.2.1 are quite typical of the small-amplitude lateral motions associated with any conventional airplane in flight. While the damping associated with all of the nontrivial modes and the period associated with Dutch roll can vary with aircraft design and operating conditions, all conventional airplanes exhibit these three modes of lateral motion.

In this example we see that the roll mode is a heavily overdamped motion, which has a rolling rate that is much greater than the yawing rate. The significance of the roll mode is best explained in connection with the airplane's response to aileron deflection. Recall that the solutions given in Example 9.2.1 are homogeneous solutions, obtained from the linearized lateral equations with all control inputs set to zero. The aileron deflection enters the lateral equations of motion as a nonhomogeneity. The solution to any nonhomogeneous linear system of equations is obtained by adding a particular solution to the homogeneous solution. The particular solution is a steady-state solution. If the motion is convergent, after some time the homogeneous solution approaches zero and the nonhomogeneous solution approaches the particular solution. The roll response of a typical airplane to a step change in aileron deflection is shown in Fig. 9.2.1. In this figure the initial bank angle and initial rolling rate are both zero. At time $t = 0$, a step change in deflection is applied to the ailerons. Notice that as time increases, the rolling rate approaches a constant value. The time required for the rolling motion to approach a constant rate is determined by the roll mode eigenvalue. Since the roll mode for typical fixed-wing aircraft is overdamped and highly convergent, transients in roll are very quickly damped out. Thus, when an airplane responds to a change in aileron input, the transient time is very short and the airplane quickly approaches a steady rolling rate.

The spiral mode is characterized primarily by changes in heading and direction of travel. For conventional airplanes, this root is real but is usually only slowly convergent or even somewhat divergent. A slightly divergent spiral mode is acceptable provided that the time required to double the amplitude is not too short. The uncontrolled motion resulting from a divergent spiral mode is shown in Fig. 9.2.2. Since the lateral motion is uncoupled from the longitudinal motion only for small deviations from equilibrium,

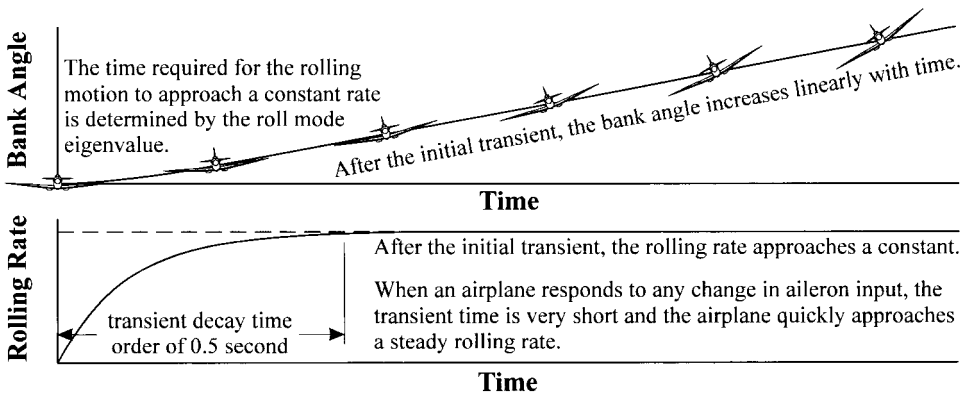


Figure 9.2.1. Roll response to a step change in aileron deflection.

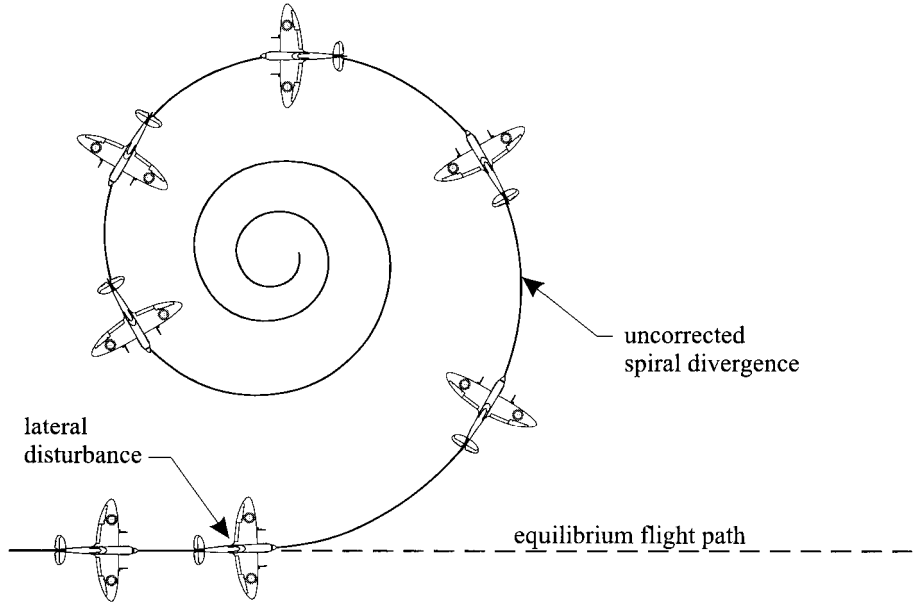


Figure 9.2.2. Spiral divergence.

as the spiral deviation becomes large, longitudinal motion is also induced. When an airplane with a divergent spiral mode is disturbed laterally from trimmed flight, the airplane will begin a slow spiral in the direction of the disturbance. If uncorrected, this spiral will continue to tighten as the airplane gradually enters an ever-tightening high-speed spiral dive. However, since the spiral mode is normally only slowly divergent, the time required to double the amplitude is long compared to the reaction time of either a VFR or an IFR pilot. Thus, even though the airplane is unstable, the pilot will usually not be aware of this instability and will instinctively provide the control inputs necessary to maintain straight and level flight.

Although an airplane with spiral instability is not considered dangerous in the hands of a qualified pilot, spiral divergence can result in extreme attitude changes and even structural failure if for some reason pilot control is absent for a few minutes. If a pilot without proper working instruments and the ability to use them should fly into a cloud, he or she would lose all visual reference with which to control the airplane. In this situation spiral divergence will prove catastrophic if the airplane does not emerge from the cloud very quickly.

While the spiral mode and the roll mode seem very different in character, they are mathematically quite closely related. Since the equations of motion are second order in each of the six degrees of freedom, the eigenvalues always occur in pairs. The eigenvalues for the roll and spiral modes together form one of these pairs. Because complex eigenvalues can occur only in complex pairs, if one of these roots is real, they both must be real. The large wing area of conventional airplanes inherently produces

ample roll damping, causing the eigenvalues for both the roll and spiral modes to be real. However, some modern aircraft have very little wing area and the roll damping for such aircraft can be quite low. For aircraft of this type, it is occasionally possible for the eigenvalues associated with the usual roll and spiral modes to combine, forming a complex pair. In this case, the aircraft will exhibit a long-period lateral oscillation similar to the phugoid mode associated with longitudinal dynamics.

Dutch roll is the lateral counterpart to the short-period mode associated with longitudinal dynamics. As shown in Fig. 9.2.3, Dutch roll is a damped oscillatory motion that is characterized by a combination of rolling, yawing, and sideslip. This yawing and rolling motion is similar to the rolling and twisting gait of an ice skater. Hence, the mode derives its name from the country well known for ice-skating. Here again, the lateral equations become coupled to the longitudinal equations for all but very small lateral oscillations. Thus, when the Dutch roll amplitude becomes large, longitudinal motions are also induced. Since the period for this motion is typically on the order of a few seconds, Dutch roll motion can be very annoying to both passengers and pilots. For well-designed airplanes, Dutch roll is not objectionable because the damping is large. However, this motion can be quite noticeable in flight and has been very objectionable in some aircraft, because of light damping. When flying an airplane with a lightly damped Dutch roll mode, the pilot will experience an unpleasant feel to the aircraft. Because of the large yaw component in the Dutch roll oscillations, this feel sometimes gives the impression that the tail of the airplane is trying to pass the nose. If the Dutch roll damping is extremely light, the airplane can be quite difficult to handle and very uncomfortable for passengers.

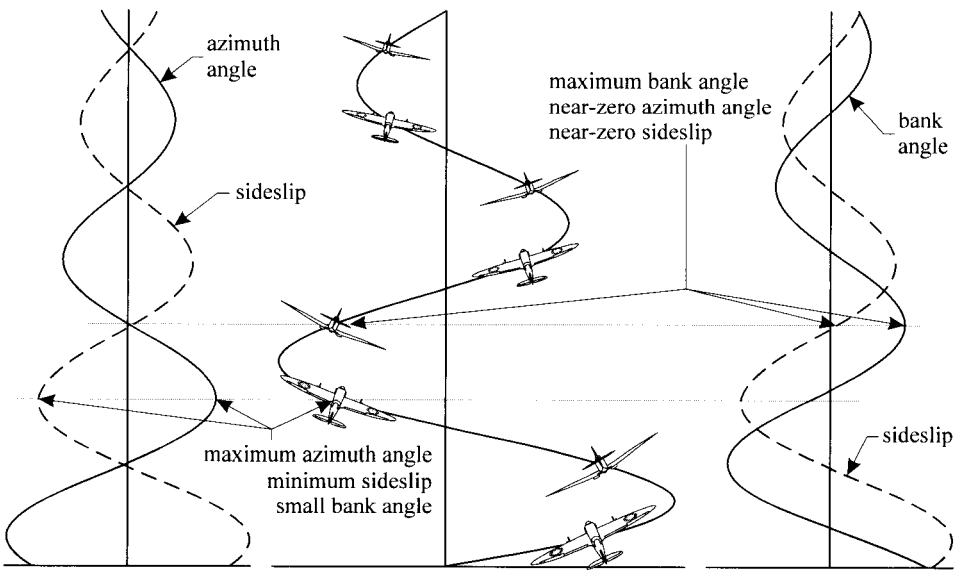


Figure 9.2.3. Dutch roll mode.

9.3. Roll Approximation

For the roll mode, the sideslip angle and yawing rate are small compared to the rolling rate. Thus, an approximation for the roll mode can be obtained by neglecting the rolling and yawing moments that result from the sideslip and yawing rate compared to those generated from the rolling rate. Since the yawing rate is much less than the rolling rate, we can also neglect the x-z product of inertia in the x-component of the angular momentum equation. The side force derivatives with respect to sideslip and yawing rate are also neglected, since they have little effect on the roll motion. Using these approximations for motion relative to steady level flight, Eq. (9.2.1) can be written

$$\begin{bmatrix} 1 & 0 & 0 & 0 & 0 & 0 \\ 0 & 1 & 0 & 0 & 0 & 0 \\ 0 & -\iota_{zx} & 1 & 0 & 0 & 0 \\ 0 & 0 & 0 & 1 & 0 & 0 \\ 0 & 0 & 0 & 0 & 1 & 0 \\ 0 & 0 & 0 & 0 & 0 & 1 \end{bmatrix} \begin{Bmatrix} \Delta\hat{\beta} \\ \Delta\hat{\bar{p}} \\ \Delta\hat{\bar{r}} \\ \Delta\hat{\xi}_y \\ \Delta\hat{\phi} \\ \Delta\hat{\psi} \end{Bmatrix} = \begin{bmatrix} 0 & R_{y,\bar{p}} & -1 & 0 & R_{gy} & 0 \\ 0 & R_{\ell,\bar{p}} & 0 & 0 & 0 & 0 \\ 0 & R_{n,\bar{p}} & 0 & 0 & 0 & 0 \\ 1 & 0 & 0 & 0 & 0 & 1 \\ 0 & 1 & 0 & 0 & 0 & 0 \\ 0 & 0 & 1 & 0 & 0 & 0 \end{bmatrix} \begin{Bmatrix} \Delta\beta \\ \Delta\bar{p} \\ \Delta\bar{r} \\ \Delta\xi_y \\ \Delta\phi \\ \Delta\psi \end{Bmatrix} \tag{9.3.1}$$

The second equation in Eq. (9.3.1) is uncoupled from the remaining five,

$$\Delta\hat{\bar{p}} = R_{\ell,\bar{p}}\Delta\bar{p} \tag{9.3.2}$$

and can be solved directly to give

the dimensionless **eigenvalue for the roll mode approximation**,

$$\lambda_r \cong R_{\ell,\bar{p}} \tag{9.3.3}$$

and the approximate **roll mode damping rate**,

$$\sigma_r \cong -\frac{2V_o}{b_w} R_{\ell,\bar{p}} = -\frac{2V_o}{b_w}\left(\frac{\rho S_w b_w^3}{8I_{xx_b}} C_{\ell,\bar{p}}\right) = -\frac{\rho S_w b_w^2 V_o}{4I_{xx_b}} C_{\ell,\bar{p}} \tag{9.3.4}$$

Since the eigenvalue is now known, the remaining five equations in Eq. (9.3.1) can be written in algebraic form,

$$\begin{Bmatrix} \lambda\Delta\beta \\ \lambda\Delta\bar{r} - \iota_{zx}\lambda\Delta\bar{p} \\ \lambda\Delta\xi_y \\ \lambda\Delta\phi \\ \lambda\Delta\psi \end{Bmatrix} = \begin{bmatrix} 0 & R_{y,\bar{p}} & -1 & R_{gy} & 0 \\ 0 & R_{n,\bar{p}} & 0 & 0 & 0 \\ 1 & 0 & 0 & 0 & 1 \\ 0 & 1 & 0 & 0 & 0 \\ 0 & 0 & 1 & 0 & 0 \end{bmatrix} \begin{Bmatrix} \Delta\beta \\ \Delta\bar{p} \\ \Delta\bar{r} \\ \Delta\phi \\ \Delta\psi \end{Bmatrix} \tag{9.3.5}$$

Equation (9.3.5) can be rearranged to yield

$$\begin{Bmatrix} \Delta\beta \\ \Delta\bar{p} \\ \Delta\bar{r} \\ \Delta\xi_y \\ \Delta\psi \end{Bmatrix} = \begin{Bmatrix} R_{y,\bar{p}} - \iota_{zx} + \left(R_{gy} - R_{n,\bar{p}}\right)/\lambda \\ \lambda \\ \iota_{zx}\lambda + R_{n,\bar{p}} \\ R_{y,\bar{p}}/\lambda + R_{gy}/\lambda^2 \\ \iota_{zx} + R_{n,\bar{p}}/\lambda \end{Bmatrix} \Delta\phi \tag{9.3.6}$$

The roll mode eigenvalue is determined from Eq. (9.3.3), and the eigenvector is found from Eq. (9.3.6).

The roll approximation given by Eq. (9.3.3) agrees closely with the exact solution for the roll mode obtained from Eq. (9.2.2). For the typical general aviation airplane in Example 9.2.1, this roll mode approximation results in

$$\begin{Bmatrix} \Delta\beta \\ \Delta\bar{p} \\ \Delta\bar{r} \\ \Delta\xi_y \\ \Delta\phi \\ \Delta\psi \end{Bmatrix} = C \begin{Bmatrix} -0.053453 \\ -0.627612 \\ -0.030583 \\ 0.019375 \\ 0.774925 \\ 0.037761 \end{Bmatrix} \exp(-0.809900\,\tau_y)$$

The details of obtaining this result are left as an exercise for the reader. The exact roll mode solution obtained in Example 9.2.1 is

$$\begin{Bmatrix} \Delta\beta \\ \Delta\bar{p} \\ \Delta\bar{r} \\ \Delta\xi_y \\ \Delta\phi \\ \Delta\psi \end{Bmatrix} = C_1 \begin{Bmatrix} -0.054317 \\ -0.629391 \\ -0.030559 \\ 0.020602 \\ 0.773401 \\ 0.037551 \end{Bmatrix} \exp(-0.813797\,\tau_y)$$

For this airplane, the approximate roll mode eigenvalue is accurate to within one-half of 1 percent, which is typical of what can be expected for most conventional airplanes.

9.4. Spiral Approximation

The spiral mode is characterized primarily by changes in heading and direction of travel. This mode is either slowly convergent or slowly divergent. Because the magnitude of the eigenvalue is so small, the change in heading occurs very slowly, with very little sideslip. The rolling and yawing rates also remain very low during spiral motion. The usual approximation for the spiral mode is obtained by neglecting the product of inertia,

rolling rate, bank angle, and sideslip momentum equation. With these approximations, Eq. (9.2.1) reduces to

$$\begin{bmatrix} 0 & 0 & 0 & 0 & 0 & 0 \\ 0 & 1 & 0 & 0 & 0 & 0 \\ 0 & 0 & 1 & 0 & 0 & 0 \\ 0 & 0 & 0 & 1 & 0 & 0 \\ 0 & 0 & 0 & 0 & 1 & 0 \\ 0 & 0 & 0 & 0 & 0 & 1 \end{bmatrix} \begin{Bmatrix} 0 \\ 0 \\ \Delta\hat{\bar{r}} \\ \Delta\hat{\xi}_y \\ 0 \\ \Delta\hat{\psi} \end{Bmatrix} = \begin{bmatrix} 0 & 1 & 0 & 0 & 0 & 0 \\ R_{\ell,\beta} & 0 & R_{\ell,\bar{r}} & 0 & 0 & 0 \\ R_{n,\beta} & 0 & R_{n,\bar{r}} & 0 & 0 & 0 \\ 1 & 0 & 0 & 0 & 0 & 1 \\ 0 & 0 & 0 & 0 & 1 & 0 \\ 0 & 0 & 1 & 0 & 0 & 0 \end{bmatrix} \begin{Bmatrix} \Delta\beta \\ \Delta\bar{p} \\ \Delta\bar{r} \\ \Delta\xi_y \\ \Delta\phi \\ \Delta\psi \end{Bmatrix} \tag{9.4.1}$$

Using the second equation in Eq. (9.4.1) to eliminate the sideslip angle from the third equations, Eq. (9.4.1) becomes

$$\begin{Bmatrix} 0 \\ 0 \\ \Delta\hat{\bar{r}} \\ \Delta\hat{\xi}_y \\ 0 \\ \Delta\hat{\psi} \end{Bmatrix} = \begin{bmatrix} 0 & 1 & 0 & 0 & 0 & 0 \\ R_{\ell,\beta} & 0 & R_{\ell,\bar{r}} & 0 & 0 & 0 \\ 0 & 0 & \left(\dfrac{R_{\ell,\beta}R_{n,\bar{r}} - R_{\ell,\bar{r}}R_{n,\beta}}{R_{\ell,\beta}}\right) & 0 & 0 & 0 \\ 1 & 0 & 0 & 0 & 0 & 1 \\ 0 & 0 & 0 & 0 & 1 & 0 \\ 0 & 0 & 1 & 0 & 0 & 0 \end{bmatrix} \begin{Bmatrix} \Delta\beta \\ \Delta\bar{p} \\ \Delta\bar{r} \\ \Delta\xi_y \\ \Delta\phi \\ \Delta\psi \end{Bmatrix} \tag{9.4.2}$$

The third equation in Eq. (9.4.2) can be solved directly for the characteristic root,

$$\lambda_s \cong \frac{R_{\ell,\beta}R_{n,\bar{r}} - R_{\ell,\bar{r}}R_{n,\beta}}{R_{\ell,\beta}} \tag{9.4.3}$$

The remaining equations in Eq. (9.4.2) can be combined with Eq. (9.4.3) to obtain the spiral mode eigenvector for this approximation. Rearranging Eq. (9.4.2), we have

$$\begin{Bmatrix} \Delta\beta \\ \Delta\bar{p} \\ \Delta\bar{r} \\ \Delta\xi_y \\ \Delta\phi \end{Bmatrix} = \begin{Bmatrix} -R_{\ell,\bar{r}}\lambda/R_{\ell,\beta} \\ 0 \\ \lambda \\ 1/\lambda - R_{\ell,\bar{r}}/R_{\ell,\beta} \\ 0 \end{Bmatrix} \Delta\psi \tag{9.4.4}$$

Using the definitions from Eq. (7.7.8) in Eq. (9.4.3), the dimensionless spiral mode eigenvalue for this approximation can be written

$$\lambda_s \cong \frac{\rho S_w b_w^3}{8I_{zz_b}}\left(\frac{C_{\ell,\beta}C_{n,\bar{r}} - C_{\ell,\bar{r}}C_{n,\beta}}{C_{\ell,\beta}}\right) \tag{9.4.5}$$

and the approximate spiral mode damping rate is

$$\sigma_s \cong -\frac{2V_o}{b_w}\lambda_s = \frac{\rho S_w b_w^2 V_o}{4I_{zz_b}}\left(\frac{C_{\ell,\bar{r}}C_{n,\beta} - C_{\ell,\beta}C_{n,\bar{r}}}{C_{\ell,\beta}}\right) \tag{9.4.6}$$

Equation (9.4.5) has been widely used as a spiral mode approximation. However, the accuracy of this approximation is very poor. The eigenvalue and some components of the eigenvector obtained form this approximation can be in error by more than two orders of magnitude. Furthermore, Eq. (9.4.6) predicts a damping rate that is directly proportional to airspeed, when in fact, the damping rate for spiral motion decreases with airspeed. A more realistic closed-form approximation for the spiral mode can be obtained by retaining the sideslip momentum equation and including the effects of rolling rate and bank angle.

While changes in rolling rate and bank angle are significant for spiral motion, the damping rate is very low, so all changes occur very slowly. Thus, for the spiral mode approximation, we neglect all acceleration terms in the lateral equations of motion,

$$\Delta\hat{\beta} \cong \Delta\hat{\bar{p}} \cong \Delta\hat{\bar{r}} \cong 0 \tag{9.4.7}$$

The side force derivatives with respect to sideslip, rolling rate, and yawing rate are also neglected in the spiral approximation, since they have little effect on spiral motion. Using these approximations for lateral motion relative to steady level flight, Eq. (9.2.1) reduces to

$$\begin{bmatrix} 1 & 0 & 0 & 0 & 0 & 0 \\ 0 & 1 & -\iota_{xz} & 0 & 0 & 0 \\ 0 & -\iota_{zx} & 1 & 0 & 0 & 0 \\ 0 & 0 & 0 & 1 & 0 & 0 \\ 0 & 0 & 0 & 0 & 1 & 0 \\ 0 & 0 & 0 & 0 & 0 & 1 \end{bmatrix} \begin{Bmatrix} 0 \\ 0 \\ 0 \\ \Delta\hat{\xi}_y \\ \Delta\hat{\phi} \\ \Delta\hat{\psi} \end{Bmatrix} = \begin{bmatrix} 0 & 0 & -1 & 0 & R_{gy} & 0 \\ R_{\ell,\beta} & R_{\ell,\bar{p}} & R_{\ell,\bar{r}} & 0 & 0 & 0 \\ R_{n,\beta} & R_{n,\bar{p}} & R_{n,\bar{r}} & 0 & 0 & 0 \\ 1 & 0 & 0 & 0 & 0 & 1 \\ 0 & 1 & 0 & 0 & 0 & 0 \\ 0 & 0 & 1 & 0 & 0 & 0 \end{bmatrix} \begin{Bmatrix} \Delta\beta \\ \Delta\bar{p} \\ \Delta\bar{r} \\ \Delta\xi_y \\ \Delta\phi \\ \Delta\psi \end{Bmatrix} \tag{9.4.8}$$

These approximate lateral equations contain only three differential equations. The remaining three equations are algebraic. These three algebraic equations can be combined to express the rolling rate in terms of the bank angle. This result can be used in the right-hand side of the fifth equation in Eq. (9.4.8) to obtain a single first-order differential equation containing only one dependent variable, the bank angle,

$$\Delta\hat{\phi} = -R_{gy}\left(\frac{R_{\ell,\beta}R_{n,\bar{r}} - R_{\ell,\bar{r}}R_{n,\beta}}{R_{\ell,\beta}R_{n,\bar{p}} - R_{\ell,\bar{p}}R_{n,\beta}}\right)\Delta\phi \tag{9.4.9}$$

Equation (9.4.9) can be used to obtain the spiral mode eigenvalue and the remaining five equations in Eq. (9.4.8) can be rearranged to obtain the eigenvector,

$$\begin{Bmatrix} \Delta\beta \\ \Delta\bar{p} \\ \Delta\bar{r} \\ \Delta\xi_y \\ \Delta\psi \end{Bmatrix} = \begin{Bmatrix} -\left(R_{n,\bar{p}}\,\lambda + R_{n,\bar{r}}\,R_{gy}\right)/R_{n,\beta} \\ \lambda \\ R_{gy} \\ R_{gy}/\lambda^2 - \left(R_{n,\bar{p}}\,\lambda + R_{n,\bar{r}}\,R_{gy}\right)/\left(R_{n,\beta}\,\lambda\right) \\ R_{gy}/\lambda \end{Bmatrix} \Delta\phi \tag{9.4.10}$$

From Eq. (9.4.9) the **approximate dimensionless spiral mode eigenvalue** is

$$\lambda_s \cong -R_{gy}\left(\frac{R_{\ell,\beta}\,R_{n,\bar{r}} - R_{\ell,\bar{r}}\,R_{n,\beta}}{R_{\ell,\beta}\,R_{n,\bar{p}} - R_{\ell,\bar{p}}\,R_{n,\beta}}\right) = -\frac{gb_w}{2V_o^2}\left(\frac{C_{\ell,\beta}\,C_{n,\bar{r}} - C_{\ell,\bar{r}}\,C_{n,\beta}}{C_{\ell,\beta}\,C_{n,\bar{p}} - C_{\ell,\bar{p}}\,C_{n,\beta}}\right) \tag{9.4.11}$$

and the **approximate spiral mode damping rate** is

$$\sigma_s \cong -\frac{2V_o}{b_w}\lambda_s = \frac{g}{V_o}\left(\frac{C_{\ell,\beta}\,C_{n,\bar{r}} - C_{\ell,\bar{r}}\,C_{n,\beta}}{C_{\ell,\beta}\,C_{n,\bar{p}} - C_{\ell,\bar{p}}\,C_{n,\beta}}\right) \tag{9.4.12}$$

The spiral mode approximation given by Eq. (9.4.11) agrees with the exact solution obtained from Eq. (9.2.2) to within about 10 percent. For the typical general aviation airplane in Example 9.2.1, obtaining the eigenvalue from Eq. (9.4.11) and using the result in Eq. (9.4.10) to obtain the eigenvector results in

$$\begin{Bmatrix} \Delta\beta \\ \Delta\bar{p} \\ \Delta\bar{r} \\ \Delta\xi_y \\ \Delta\phi \\ \Delta\psi \end{Bmatrix} = C \begin{Bmatrix} 0.000002 \\ 0.000000 \\ 0.000001 \\ 0.999999 \\ 0.000061 \\ -0.001004 \end{Bmatrix} \exp(-0.001002\,\tau_y)$$

The exact solution for the spiral mode from Example 9.2.1 is

$$\begin{Bmatrix} \Delta\beta \\ \Delta\bar{p} \\ \Delta\bar{r} \\ \Delta\xi_y \\ \Delta\phi \\ \Delta\psi \end{Bmatrix} = C_2 \begin{Bmatrix} 0.000001 \\ 0.000000 \\ 0.000001 \\ 0.999999 \\ 0.000053 \\ -0.000920 \end{Bmatrix} \exp(-0.000918\,\tau_y)$$

For this same airplane, the spiral mode approximation that is given by Eq. (9.4.5) yields the very different result

$$\begin{Bmatrix} \Delta\beta \\ \Delta\bar{p} \\ \Delta\bar{r} \\ \Delta\xi_y \\ \Delta\phi \\ \Delta\psi \end{Bmatrix} = C \begin{Bmatrix} 0.000330 \\ 0.000000 \\ 0.000236 \\ 0.999880 \\ 0.000000 \\ -0.015512 \end{Bmatrix} \exp(-0.015184\,\tau_y)$$

The details of this numerical comparison are left as an exercise for the reader.

Clearly, the spiral mode approximation expressed in Eq. (9.4.11) represents a tremendous improvement over Eq. (9.4.5). The most serious inaccuracy in the approximations associated with obtaining Eq. (9.4.5) is neglecting the effects of bank angle. The bank angle component of the eigenvector for spiral motion is one to two orders of magnitude larger than either the sideslip angle or the dimensionless yawing rate, both of which were retained in the earlier approximation. In fact, the change in bank angle provides the primary driving force associated with spiral motion.

Comparing spiral mode damping rate from Eq. (9.4.6) with that from Eq. (9.4.12) shows some similarity in dependence on stability and damping derivatives. However, these two approximations show a very different dependence on other aircraft design and operating parameters. The spiral approximation given by Eq. (9.4.6) predicts a damping rate that is proportional to airspeed, whereas Eq. (9.4.12) shows an inverse relation between airspeed and spiral mode damping rate. Equation (9.4.6) predicts a spiral mode damping rate that is directly proportional to air density, wing area, and the square of the wing span, while being inversely proportional to the yawing moment of inertia. On the other hand, Eq. (9.4.12) predicts no dependence on any of these parameters. Results obtained from Eq. (9.4.12) are much more consistent with reality.

EXAMPLE 9.4.1. The general aviation airplane described in Example 9.2.1 is modified so that the directional stability is doubled,

$$C_{n,\beta} = +0.140$$

All other parameters affecting lateral motion are unchanged. For this modified airplane, use Eq. (9.2.2) to find the eigenvalue and eigenvector corresponding to the spiral mode. Compare this exact solution with the spiral mode approximation given by Eq. (9.4.11).

Solution. For the modified airplane, we have

$$R_{\ell,\beta} \equiv \frac{\rho S_w b_w^3}{8 I_{xx_b}} C_{\ell,\beta} = -0.1481, \qquad R_{n,\beta} \equiv \frac{\rho S_w b_w^3}{8 I_{zz_b}} C_{n,\beta} = 0.0790,$$

$$R_{\ell,\bar{p}} \equiv \frac{\rho S_w b_w^3}{8 I_{xx_b}} C_{\ell,\bar{p}} = -0.8099, \qquad R_{n,\bar{p}} \equiv \frac{\rho S_w b_w^3}{8 I_{zz_b}} C_{n,\bar{p}} = -0.0325,$$

$$R_{\ell,\bar{r}} \equiv \frac{\rho S_w b_w^3}{8 I_{xx_b}} C_{\ell,\bar{r}} = 0.2074, \qquad R_{n,\bar{r}} \equiv \frac{\rho S_w b_w^3}{8 I_{zz_b}} C_{n,\bar{r}} = -0.0705,$$

$$R_{gy} \equiv \frac{g b_w}{2 V_o^2} = 0.0164$$

With this design change, the eigenproblem given by Eq. (9.2.2) is the same as that in Example 9.2.1, with the exception that the first term in the third row of the first matrix is doubled,

$$\left(\begin{bmatrix} -0.0233 & 0 & -0.9900 & 0 & 0.0164 & 0 \\ -0.1481 & -0.8099 & 0.2074 & 0 & 0 & 0 \\ 0.0790 & -0.0325 & -0.0705 & 0 & 0 & 0 \\ 1 & 0 & 0 & 0 & 0 & 1 \\ 0 & 1 & 0 & 0 & 0 & 0 \\ 0 & 0 & 1 & 0 & 0 & 0 \end{bmatrix} - \lambda \begin{bmatrix} 1 & 0 & 0 & 0 & 0 & 0 \\ 0 & 1 & -0.0300 & 0 & 0 & 0 \\ 0 & -0.0086 & 1 & 0 & 0 & 0 \\ 0 & 0 & 0 & 1 & 0 & 0 \\ 0 & 0 & 0 & 0 & 1 & 0 \\ 0 & 0 & 0 & 0 & 0 & 1 \end{bmatrix} \right) \begin{Bmatrix} \chi_\beta \\ \chi_{\bar{p}} \\ \chi_{\bar{r}} \\ \chi_{\xi_y} \\ \chi_\phi \\ \chi_\psi \end{Bmatrix} = \begin{Bmatrix} 0 \\ 0 \\ 0 \\ 0 \\ 0 \\ 0 \end{Bmatrix}$$

and the spiral mode solution is

$$\begin{Bmatrix} \Delta\beta \\ \Delta\bar{p} \\ \Delta\bar{r} \\ \Delta\xi_y \\ \Delta\phi \\ \Delta\psi \end{Bmatrix} = C_2 \begin{Bmatrix} 0.000002 \\ 0.000000 \\ 0.000002 \\ 0.999999 \\ 0.000112 \\ 0.001346 \end{Bmatrix} \exp(+0.001348\,\tau_y)$$

Using the parameters for the modified aircraft in Eq. (9.4.11), the approximate spiral mode eigenvalue is

$$\lambda_s = -R_{gy}\left(\frac{R_{\ell,\beta} R_{n,\bar{r}} - R_{\ell,\bar{r}} R_{n,\beta}}{R_{\ell,\beta} R_{n,\bar{p}} - R_{\ell,\bar{p}} R_{n,\beta}} \right)$$

$$= -0.0164\left(\frac{(-0.1481)(-0.0705) - (0.2074)(0.0790)}{(-0.1481)(-0.0325) - (-0.8099)(0.0790)} \right) = +0.001417$$

Applying this result to Eq. (9.4.10), we have

$$\begin{Bmatrix} \Delta\beta \\ \Delta\bar{p} \\ \Delta\bar{r} \\ \Delta\xi_y \\ \Delta\psi \end{Bmatrix} = \begin{Bmatrix} -\left(R_{n,\bar{p}}\,\lambda + R_{n,\bar{r}}\,R_{gy}\right)/R_{n,\beta} \\ \lambda \\ R_{gy} \\ R_{gy}/\lambda^2 - \left(R_{n,\bar{p}}\,\lambda + R_{n,\bar{r}}\,R_{gy}\right)/\left(R_{n,\beta}\,\lambda\right) \\ R_{gy}/\lambda \end{Bmatrix} \Delta\phi$$

$$= \begin{Bmatrix} -\left[-0.0325(0.001417) + 0.0164(-0.0705)\right]/0.0790 \\ 0.001417 \\ 0.0164 \\ 0.0164/(0.001417)^2 + 0.015218/0.001417 \\ 0.0164/0.001417 \end{Bmatrix} \Delta\phi = \begin{Bmatrix} 0.015218 \\ 0.001417 \\ 0.016400 \\ 8178.5220 \\ 11.573747 \end{Bmatrix} \Delta\phi$$

which gives the normalized solution,

$$\begin{Bmatrix} \Delta\beta \\ \Delta\bar{p} \\ \Delta\bar{r} \\ \Delta\xi_y \\ \Delta\phi \\ \Delta\psi \end{Bmatrix} = C \begin{Bmatrix} 0.000002 \\ 0.000000 \\ 0.000002 \\ 0.999999 \\ 0.000122 \\ 0.001415 \end{Bmatrix} \exp(+0.001417\,\tau_y)$$

For comparison, using Eq. (9.4.5) with Eq. (9.4.4) gives the very different result

$$\begin{Bmatrix} \Delta\beta \\ \Delta\bar{p} \\ \Delta\bar{r} \\ \Delta\xi_y \\ \Delta\phi \\ \Delta\psi \end{Bmatrix} = C \begin{Bmatrix} 0.002134 \\ 0.000000 \\ 0.001524 \\ 0.999276 \\ 0.000000 \\ 0.037969 \end{Bmatrix} \exp(+0.040132\,\tau_y)$$

From Example 9.4.1, we see that doubling the directional stability of this particular aircraft will change the spiral motion from slowly convergent to slowly divergent. This may seem counterintuitive at first thought. Because divergent spiral motion is characterized primarily by changes in heading and direction of travel, with a seemingly insignificant rolling rate, it could be thought of as some type of directional instability. With this line of reasoning, it may seem natural to think that increasing the directional stability should improve the convergence of the spiral mode. To understand why this is not so, one must understand that spiral motion is not caused directly by a disturbance in

yaw, but rather by a disturbance in roll. This is not to say that a disturbance in yaw will not induce spiral motion. Quite the contrary, because of the roll-yaw coupling, any disturbance in yaw will induce a disturbance in roll, and even the slightest roll disturbance can induce spiral motion.

To continue with our explanation of what was observed in Example 9.4.1, let us consider exactly how a disturbance in roll induces spiral motion. Even the smallest disturbance in roll will tend to induce some sideslip, because it results in a component of gravity in the y_b-direction. If the airplane is stable in both roll and yaw, this sideslip will tend to return the bank angle to zero, but it will also tend to yaw the aircraft in the direction of sideslip, in an attempt to return the sideslip angle to zero. If the directional stability is large enough, or the roll stability is low enough, the yaw correction will occur faster than the roll correction, and the airplane's heading will change continuously in the direction of the original roll disturbance, unless corrected with control input. Under such conditions the spiral motion is divergent. If the directional stability is low enough compared to the roll stability, then the roll correction will occur faster than the yaw correction and the spiral mode will be convergent. Thus, we see why increasing directional stability makes the spiral mode more divergent. A comparison between directional divergence and spiral divergence for a conventional airplane is shown in Fig. 9.4.1.

From this description of spiral motion, we also see why the commonly used spiral approximation given by Eq. (9.4.5) is so poor. This approximation totally neglects all changes in rolling rate and bank angle. In so doing, the approximation neglects the very essence of the spiral motion that it is attempting to capture. This can be seen more dramatically by considering an aircraft with neutral roll stability. From Eq. (9.4.5) we see that if the change in rolling moment with respect to yawing rate has the usual positive sign and the aircraft is stable in yaw, then this approximation predicts infinite spiral convergence for neutral roll stability. This is not consistent with reality. In fact, neutral roll stability normally produces spiral divergence.

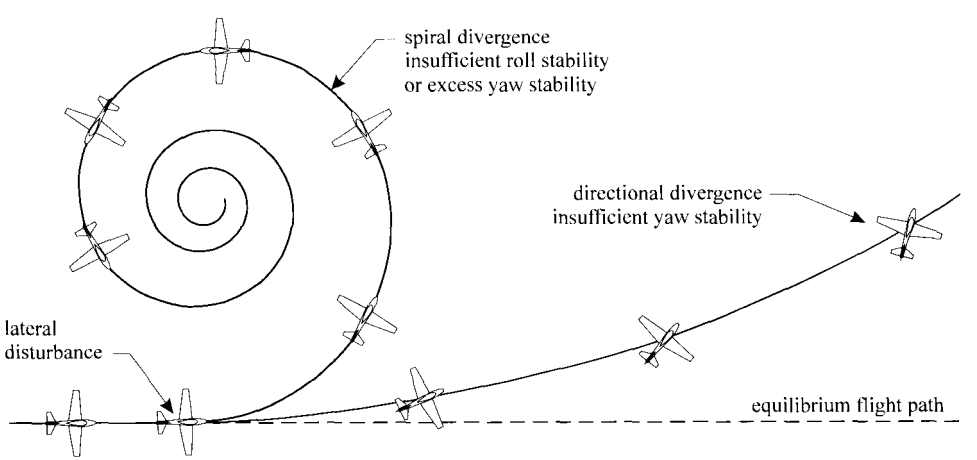


Figure 9.4.1. Comparison between directional divergence and spiral divergence.

If the aircraft in Example 9.2.1 is modified so that the roll stability becomes neutral while all other parameters remain unchanged, we have

$$R_{\ell,\beta} = 0.0$$

and the exact solution for the spiral mode becomes

$$\begin{Bmatrix} \Delta\beta \\ \Delta\bar{p} \\ \Delta\bar{r} \\ \Delta\xi_y \\ \Delta\phi \\ \Delta\psi \end{Bmatrix} = C \begin{Bmatrix} 0.000033 \\ 0.000004 \\ 0.000016 \\ 0.999992 \\ 0.001010 \\ 0.003960 \end{Bmatrix} \exp(+0.003993\,\tau_y)$$

For this case, the approximate spiral mode solution given by Eq. (9.4.11) gives

$$\begin{Bmatrix} \Delta\beta \\ \Delta\bar{p} \\ \Delta\bar{r} \\ \Delta\xi_y \\ \Delta\phi \\ \Delta\psi \end{Bmatrix} = C \begin{Bmatrix} 0.000035 \\ 0.000004 \\ 0.000017 \\ 0.999991 \\ 0.001067 \\ 0.004165 \end{Bmatrix} \exp(+0.004200\,\tau_y)$$

As mentioned previously, with neutral roll stability, the spiral mode approximation from Eq. (9.4.5) gives

$$\begin{Bmatrix} \Delta\beta \\ \Delta\bar{p} \\ \Delta\bar{r} \\ \Delta\xi_y \\ \Delta\phi \\ \Delta\psi \end{Bmatrix} = C\exp(-\infty\,\tau_y) = 0.0$$

Here again, we see that the spiral approximation given by Eq. (9.4.11) agrees closely with the exact solution while Eq. (9.4.5) predicts a much different result. In this case, the eigenvalue predicted by Eq. (9.4.5) does not even have the correct sign.

The spiral mode approximation given by Eq. (9.4.5) should never be used. It is based on a mathematical approximation that is not consistent with physical reality and is very misleading. It has been included here for historical reasons only and because the reader may encounter this approximation in the literature.

9.5. Dutch Roll Approximation

As noted previously, Dutch roll is a damped oscillatory motion that is characterized by a combination of sideslip, roll, and yaw. Nevertheless, the usual approximation for Dutch roll is obtained by assuming the motion to consist solely of sideslip and yaw. The rolling rate, bank angle, and rolling momentum equation are completely neglected in the usual Dutch roll approximation. Also, the change in side force with respect to yawing rate is usually neglected, because this is small and has little effect on lateral motion. Using these approximations for motion relative to level flight, Eq. (9.2.1) becomes

$$\begin{bmatrix} 1 & 0 & 0 & 0 & 0 & 0 \\ 0 & 0 & 0 & 0 & 0 & 0 \\ 0 & -\iota_{zx} & 1 & 0 & 0 & 0 \\ 0 & 0 & 0 & 1 & 0 & 0 \\ 0 & 0 & 0 & 0 & 0 & 0 \\ 0 & 0 & 0 & 0 & 0 & 1 \end{bmatrix} \begin{Bmatrix} \Delta\hat{\beta} \\ 0 \\ \Delta\hat{\bar{r}} \\ \Delta\hat{\xi}_y \\ 0 \\ \Delta\hat{\psi} \end{Bmatrix} = \begin{bmatrix} R_{y,\beta} & 0 & (R_{y,\bar{r}}-1) & 0 & 0 & 0 \\ 0 & 1 & 0 & 0 & 0 & 0 \\ R_{n,\beta} & 0 & R_{n,\bar{r}} & 0 & 0 & 0 \\ 1 & 0 & 0 & 0 & 0 & 1 \\ 0 & 0 & 0 & 0 & 1 & 0 \\ 0 & 0 & 1 & 0 & 0 & 0 \end{bmatrix} \begin{Bmatrix} \Delta\beta \\ \Delta\bar{p} \\ \Delta\bar{r} \\ \Delta\xi_y \\ \Delta\phi \\ \Delta\psi \end{Bmatrix} \tag{9.5.1}$$

The first and third equations in Eq. (9.5.1) are not coupled to the other four equations. Thus, this system of equations can be rearranged and separated to yield

$$\begin{bmatrix} (R_{y,\beta}-\lambda) & (R_{y,\bar{r}}-1) \\ R_{n,\beta} & (R_{n,\bar{r}}-\lambda) \end{bmatrix} \begin{Bmatrix} \Delta\beta \\ \Delta\bar{r} \end{Bmatrix} = \begin{Bmatrix} 0 \\ 0 \end{Bmatrix} \tag{9.5.2}$$

and

$$\begin{Bmatrix} \Delta\bar{p} \\ \Delta\bar{r} \\ \Delta\xi_y \\ \Delta\phi \\ \Delta\psi \end{Bmatrix} = \begin{Bmatrix} 0 \\ R_{n,\beta}/(\lambda - R_{n,\bar{r}}) \\ 1/\lambda + \left[R_{n,\beta}/(\lambda - R_{n,\bar{r}})\right]/\lambda^2 \\ 0 \\ \left[R_{n,\beta}/(\lambda - R_{n,\bar{r}})\right]/\lambda \end{Bmatrix} \Delta\beta \tag{9.5.3}$$

The approximate Dutch roll eigenvalues are obtained from the roots of Eq. (9.5.2), and the approximate eigenvectors are obtained by using the result in Eq. (9.5.3).

The characteristic equation for Eq. (9.5.2) is

$$\lambda^2 - (R_{y,\beta} + R_{n,\bar{r}})\lambda + (1 - R_{y,\bar{r}})R_{n,\beta} + R_{y,\beta}R_{n,\bar{r}} = 0 \tag{9.5.4}$$

From this quadratic equation the dimensionless Dutch roll eigenvalues predicted by this approximation are found to be

$$\lambda_{Dr} \cong \frac{R_{y,\beta} + R_{n,\bar{r}}}{2} \pm i\sqrt{\left(1 - R_{y,\bar{r}}\right)R_{n,\beta} + R_{y,\beta}R_{n,\bar{r}} - \left(\frac{R_{y,\beta} + R_{n,\bar{r}}}{2}\right)^2} \tag{9.5.5}$$

From Eq. (9.5.5), the approximate damped natural frequency and damping rate are

$$\omega_{d_{Dr}} \cong \frac{2V_o}{b_w}\text{imag}(\lambda_{Dr}) = \frac{2V_o}{b_w}\sqrt{(1-R_{y,\bar{r}})R_{n,\beta}+R_{y,\beta}R_{n,\bar{r}}-\left(\frac{R_{y,\beta}+R_{n,\bar{r}}}{2}\right)^2} \tag{9.5.6}$$

$$\sigma_{Dr} \cong -\frac{2V_o}{b_w}\text{real}(\lambda_{Dr}) = -\frac{V_o}{b_w}(R_{y,\beta}+R_{n,\bar{r}}) \tag{9.5.7}$$

Not surprisingly, results obtained from this commonly used approximation do not always give particularly good values for the frequency, damping, or eigenvectors that are associated with Dutch roll. The reason for poor agreement between this uncoupled Dutch roll approximation and the exact solution is that Dutch roll strongly involves all three lateral degrees of freedom, with significant coupling between sideslip, roll, and yaw. As we have seen in Example 9.2.1, the largest Dutch roll oscillations are typically in sideslip. However, the Dutch roll amplitude for rolling rate is nearly as large as that for sideslip and is about the same as that for yawing rate. Furthermore, Dutch roll oscillations in bank angle are typically as large as those in heading. Thus, it is very difficult to justify neglecting any of the three lateral degrees of freedom when attempting to develop a Dutch roll approximation. Here, we consider an improved Dutch roll approximation developed by Phillips (2000b), which includes the effects of roll as well as those of sideslip and yaw.

In this approximation, we neglect the product of inertia and the change in side force with respect to rolling rate because these values are typically small and have little effect on Dutch roll. Using these approximations for motion relative to steady level flight, the lateral equations of motion, given by Eq. (9.2.1), become

$$\begin{bmatrix}1&0&0&0&0&0\\0&1&0&0&0&0\\0&0&1&0&0&0\\0&0&0&1&0&0\\0&0&0&0&1&0\\0&0&0&0&0&1\end{bmatrix}\begin{Bmatrix}\Delta\hat{\beta}\\ \Delta\hat{\bar{p}}\\ \Delta\hat{\bar{r}}\\ \Delta\hat{\xi}_y\\ \Delta\hat{\phi}\\ \Delta\hat{\psi}\end{Bmatrix} = \begin{bmatrix}R_{y,\beta}&0&(R_{y,\bar{r}}-1)&0&R_{gy}&0\\ R_{\ell,\beta}&R_{\ell,\bar{p}}&R_{\ell,\bar{r}}&0&0&0\\ R_{n,\beta}&R_{n,\bar{p}}&R_{n,\bar{r}}&0&0&0\\ 1&0&0&0&0&1\\ 0&1&0&0&0&0\\ 0&0&1&0&0&0\end{bmatrix}\begin{Bmatrix}\Delta\beta\\ \Delta\bar{p}\\ \Delta\bar{r}\\ \Delta\xi_y\\ \Delta\phi\\ \Delta\psi\end{Bmatrix} \tag{9.5.8}$$

which results in the eigenproblem

$$\begin{bmatrix}(R_{y,\beta}-\lambda)&0&(R_{y,\bar{r}}-1)&0&R_{gy}&0\\ R_{\ell,\beta}&(R_{\ell,\bar{p}}-\lambda)&R_{\ell,\bar{r}}&0&0&0\\ R_{n,\beta}&R_{n,\bar{p}}&(R_{n,\bar{r}}-\lambda)&0&0&0\\ 1&0&0&-\lambda&0&1\\ 0&1&0&0&-\lambda&0\\ 0&0&1&0&0&-\lambda\end{bmatrix}\begin{Bmatrix}\Delta\beta\\ \Delta\bar{p}\\ \Delta\bar{r}\\ \Delta\xi_y\\ \Delta\phi\\ \Delta\psi\end{Bmatrix} = \begin{Bmatrix}0\\0\\0\\0\\0\\0\end{Bmatrix} \tag{9.5.9}$$

Using the second and fifth equations in Eq. (9.5.9), we can eliminate the rolling rate and bank angle from the first and third equations. Thus, Eq. (9.5.9) can be rearranged and separated to yield

$$\begin{bmatrix} \left(R_{y,\beta} - \dfrac{R_{gy}R_{\ell,\beta}}{(R_{\ell,\bar{p}}-\lambda)\lambda} - \lambda\right) & -\left(1 - R_{y,\bar{r}} + \dfrac{R_{gy}R_{\ell,\bar{r}}}{(R_{\ell,\bar{p}}-\lambda)\lambda}\right) \\ \left(R_{n,\beta} - \dfrac{R_{\ell,\beta}R_{n,\bar{p}}}{R_{\ell,\bar{p}}-\lambda}\right) & \left(R_{n,\bar{r}} - \dfrac{R_{\ell,\bar{r}}R_{n,\bar{p}}}{R_{\ell,\bar{p}}-\lambda} - \lambda\right) \end{bmatrix} \begin{Bmatrix} \Delta\beta \\ \Delta\bar{r} \end{Bmatrix} = \begin{Bmatrix} 0 \\ 0 \end{Bmatrix} \tag{9.5.10}$$

and

$$\begin{Bmatrix} \Delta\bar{p} \\ \Delta\bar{r} \\ \Delta\xi_y \\ \Delta\phi \\ \Delta\psi \end{Bmatrix} = \begin{Bmatrix} R_{xc} \\ R_{zc} \\ (1 + R_{zc}/\lambda)/\lambda \\ R_{xc}/\lambda \\ R_{zc}/\lambda \end{Bmatrix} \Delta\beta, \tag{9.5.11}$$

where

$$R_{xc} \equiv \frac{R_{n,\beta}R_{\ell,\bar{r}} - R_{\ell,\beta}(R_{n,\bar{r}} - \lambda)}{(R_{\ell,\bar{p}}-\lambda)(R_{n,\bar{r}}-\lambda) - R_{\ell,\bar{r}}R_{n,\bar{p}}}$$

and

$$R_{zc} \equiv \frac{R_{\ell,\beta}R_{n,\bar{p}} - R_{n,\beta}(R_{\ell,\bar{p}} - \lambda)}{(R_{\ell,\bar{p}}-\lambda)(R_{n,\bar{r}}-\lambda) - R_{\ell,\bar{r}}R_{n,\bar{p}}}$$

The characteristic equation for Eq. (9.5.10) is

$$\begin{vmatrix} \left(R_{y,\beta} - \dfrac{R_{gy}R_{\ell,\beta}}{(R_{\ell,\bar{p}}-\lambda)\lambda} - \lambda\right) & -\left(1 - R_{y,\bar{r}} + \dfrac{R_{gy}R_{\ell,\bar{r}}}{(R_{\ell,\bar{p}}-\lambda)\lambda}\right) \\ \left(R_{n,\beta} - \dfrac{R_{\ell,\beta}R_{n,\bar{p}}}{R_{\ell,\bar{p}}-\lambda}\right) & \left(R_{n,\bar{r}} - \dfrac{R_{\ell,\bar{r}}R_{n,\bar{p}}}{R_{\ell,\bar{p}}-\lambda} - \lambda\right) \end{vmatrix} = 0 \tag{9.5.12}$$

which can be expanded to give

$$\begin{aligned} &\lambda^2 - \left(R_{y,\beta} + R_{n,\bar{r}} - \frac{R_{\ell,\bar{r}}R_{n,\bar{p}}}{R_{\ell,\bar{p}}-\lambda}\right)\lambda + (1 - R_{y,\bar{r}})R_{n,\beta} + R_{y,\beta}R_{n,\bar{r}} \\ &+ \frac{R_{\ell,\beta}\left[R_{gy} - (1 - R_{y,\bar{r}})R_{n,\bar{p}}\right] - R_{y,\beta}R_{\ell,\bar{r}}R_{n,\bar{p}}}{R_{\ell,\bar{p}}-\lambda} + \frac{R_{gv}(R_{\ell,\bar{r}}R_{n,\beta} - R_{\ell,\beta}R_{n,\bar{r}})}{(R_{\ell,\bar{p}}-\lambda)\lambda} = 0 \end{aligned} \tag{9.5.13}$$

In our study of the roll mode, we found that roll is typically very heavily damped. Thus, all of those terms in Eq. (9.5.13) that are inversely proportional to the roll-damping ratio are small, but not necessarily totally negligible. This suggests that we might expand Eq. (9.5.13) in terms of a Taylor series in one over the roll-damping ratio. For this purpose we use the expansion

$$\frac{1}{R_{\ell,\bar{p}} - \lambda} = \frac{1}{R_{\ell,\bar{p}}} + \frac{\lambda}{R_{\ell,\bar{p}}^2} + \frac{\lambda^2}{R_{\ell,\bar{p}}^3} + \frac{\lambda^3}{R_{\ell,\bar{p}}^4} + \cdots \tag{9.5.14}$$

If we define λ_∞ to be the eigenvalue corresponding to an infinite roll-damping ratio,

$$R_{\ell,\bar{p}} \rightarrow \infty \tag{9.5.15}$$

then from Eq. (9.5.13), we have

$$\lambda_\infty^2 - (R_{y,\beta} + R_{n,\bar{r}})\lambda_\infty + (1 - R_{y,\bar{r}})R_{n,\beta} + R_{y,\beta}R_{n,\bar{r}} = 0 \tag{9.5.16}$$

and

$$\lambda_\infty = \frac{R_{y,\beta} + R_{n,\bar{r}}}{2} \pm i\sqrt{(1 - R_{y,\bar{r}})R_{n,\beta} + R_{y,\beta}R_{n,\bar{r}} - \left(\frac{R_{y,\beta} + R_{n,\bar{r}}}{2}\right)^2} \tag{9.5.17}$$

At this point it is interesting to note that the eigenvalues obtained from Eq. (9.5.17) are identical to those obtained from Eq. (9.5.5). Thus, we see that this earlier Dutch roll approximation is valid only in the limit as the roll-damping ratio approaches infinity. If the roll-damping ratio were large enough, the rolling motion associated with Dutch roll would be completely suppressed and the motion would indeed consist solely of sideslip and yaw. However, as the name implies, an aircraft seldom has sufficient roll damping to eliminate the rolling motion from Dutch roll. The effects of roll can be included in the Dutch roll approximation by carrying some of the low-order terms from the Taylor series in Eq. (9.5.14).

Because the roll-damping ratio is several times larger than the Dutch roll eigenvalue, all terms beyond the first in Eq. (9.5.14) are small and become smaller with increasing order. Thus, for the purpose of evaluating this Taylor series, we can replace the actual eigenvalue on the right-hand side with the approximate eigenvalue from Eq. (9.5.17),

$$\frac{1}{R_{\ell,\bar{p}} - \lambda} \cong \frac{1}{R_{\ell,\bar{p}}} + \frac{\lambda_\infty}{R_{\ell,\bar{p}}^2} + \frac{\lambda_\infty^2}{R_{\ell,\bar{p}}^3} + \frac{\lambda_\infty^3}{R_{\ell,\bar{p}}^4} + \cdots \tag{9.5.18}$$

Furthermore, because the Dutch roll damping is an order-of-magnitude less than the Dutch roll frequency, we can also neglect the damping from Eq. (9.5.17) and use the approximations

$$\frac{1}{R_{\ell,\bar{p}} - \lambda} \cong \frac{1}{R_{\ell,\bar{p}}} \pm i\frac{\varpi_\infty}{R_{\ell,\bar{p}}^2} - \frac{\varpi_\infty^2}{R_{\ell,\bar{p}}^3} \mp i\frac{\varpi_\infty^3}{R_{\ell,\bar{p}}^4} + \cdots \tag{9.5.19}$$

$$\frac{1}{(R_{\ell,\bar{p}} - \lambda)\lambda} \cong \mp i\frac{1}{\varpi_\infty R_{\ell,\bar{p}}} + \frac{1}{R_{\ell,\bar{p}}^2} \pm i\frac{\varpi_\infty}{R_{\ell,\bar{p}}^3} - \frac{\varpi_\infty^2}{R_{\ell,\bar{p}}^4} + \cdots \tag{9.5.20}$$

where

$$\varpi_\infty \equiv \sqrt{(1 - R_{y,\bar{r}})R_{n,\beta} + R_{y,\beta}R_{n,\bar{r}}} \tag{9.5.21}$$

Retaining the first two terms in each of these Taylor series and applying the results to the characteristic equation given by Eq. (9.5.13), we obtain a quadratic equation for the approximate Dutch roll eigenvalues,

$$\lambda^2 - (R_{y,\beta} + R_{n,\bar{r}} + R_{dc})\lambda + (1 - R_{y,\bar{r}})R_{n,\beta} + R_{y,\beta}R_{n,\bar{r}} + R_{fc} = 0 \tag{9.5.22}$$

where the complex coefficients R_{dc} and R_{fc} are defined as

$$R_{dc} \equiv -\frac{R_{\ell,\bar{r}}R_{n,\bar{p}}}{R_{\ell,\bar{p}}} \mp i\frac{\varpi_\infty R_{\ell,\bar{r}}R_{n,\bar{p}}}{R_{\ell,\bar{p}}^2} \tag{9.5.23}$$

and

$$\begin{aligned} R_{fc} \equiv & \left[\frac{R_{\ell,\beta}\left[R_{gy} - (1 - R_{y,\bar{r}})R_{n,\bar{p}}\right] - R_{y,\beta}R_{\ell,\bar{r}}R_{n,\bar{p}}}{R_{\ell,\bar{p}}} + \frac{R_{gy}(R_{\ell,\bar{r}}R_{n,\beta} - R_{\ell,\beta}R_{n,\bar{r}})}{R_{\ell,\bar{p}}^2}\right] \\ & \pm i\left[\frac{R_{gy}(R_{\ell,\beta}R_{n,\bar{r}} - R_{\ell,\bar{r}}R_{n,\beta})}{\varpi_\infty R_{\ell,\bar{p}}} + \frac{\varpi_\infty\left\{R_{\ell,\beta}\left[R_{gy} - (1 - R_{y,\bar{r}})R_{n,\bar{p}}\right] - R_{y,\beta}R_{\ell,\bar{r}}R_{n,\bar{p}}\right\}}{R_{\ell,\bar{p}}^2}\right] \end{aligned} \tag{9.5.24}$$

The eigenvalues obtained from Eq. (9.5.22), with the application of Eq. (9.5.21), are found to be

$$\begin{aligned} \lambda &= \frac{R_{y,\beta} + R_{n,\bar{r}} + R_{dc}}{2} \pm i\sqrt{(1 - R_{y,\bar{r}})R_{n,\beta} + R_{y,\beta}R_{n,\bar{r}} + R_{fc} - \left(\frac{R_{y,\beta} + R_{n,\bar{r}} + R_{dc}}{2}\right)^2} \\ &= \frac{R_{y,\beta} + R_{n,\bar{r}} + R_{dc}}{2} \pm i\varpi_\infty\sqrt{1 + \frac{R_{fc}}{\varpi_\infty^2} - \left(\frac{R_{y,\beta} + R_{n,\bar{r}} + R_{dc}}{2\varpi_\infty}\right)^2} \end{aligned} \tag{9.5.25}$$

Since both R_{fc} and the damping term are small compared to ϖ_∞, Eq. (9.5.25) can be further approximated as

$$\lambda \cong \frac{R_{y,\beta}+R_{n,\bar{r}}+R_{dc}}{2} \pm i\varpi_\infty \left[1+\frac{\text{real}(R_{fc})}{2\varpi_\infty^2} \pm i\frac{\text{imag}(R_{fc})}{2\varpi_\infty^2} - \frac{(R_{y,\beta}+R_{n,\bar{r}}+R_{dc})^2}{8\varpi_\infty^2}\right]$$

$$\cong \frac{R_{y,\beta}+R_{n,\bar{r}}+R_{dc}-\text{imag}(R_{fc})/\varpi_\infty}{2} \pm i\varpi_\infty \sqrt{1+\frac{\text{real}(R_{fc})}{\varpi_\infty^2} - \left(\frac{R_{y,\beta}+R_{n,\bar{r}}+R_{dc}}{2\varpi_\infty}\right)^2}$$

$$= \frac{R_{y,\beta}+R_{n,\bar{r}}+R_{dc}-\text{imag}(R_{fc})/\varpi_\infty}{2} \pm i\sqrt{\varpi_\infty^2+\text{real}(R_{fc}) - \left(\frac{R_{y,\beta}+R_{n,\bar{r}}+R_{dc}}{2}\right)^2} \tag{9.5.26}$$

Because the imaginary component of the Dutch roll eigenvalue is typically an order of magnitude larger than the real component, the second-order terms in R_{dc} and R_{fc} do not have a significant effect on the Dutch roll frequency. However, the second-order terms are crucial to an accurate determination of the much smaller Dutch roll damping rate. For this reason we retain all second-order terms in the real component of the eigenvalue but neglect second-order terms in the imaginary component. Thus, because the imaginary component of R_{dc} is second order, it can be neglected in the Dutch roll approximation. We can also neglect the second-order term in the real part of R_{fc} since it affects only the frequency. On the other hand, we must retain the second term in the imaginary part of R_{fc} because this term is part of the damping.

Thus, for this approximation, the **dimensionless Dutch roll eigenvalues** are

$$\lambda_{Dr} \cong \frac{R_{y,\beta}+R_{n,\bar{r}}-R_{Dc}+R_{Dp}}{2} \pm i\sqrt{(1-R_{y,\bar{r}})R_{n,\beta}+R_{y,\beta}R_{n,\bar{r}}+R_{Ds}-\left(\frac{R_{y,\beta}+R_{n,\bar{r}}}{2}\right)^2} \tag{9.5.27}$$

where we define the **Dutch roll stability ratio**,

$$R_{Ds} \equiv \frac{R_{\ell,\beta}\left[R_{gy}-(1-R_{y,\bar{r}})R_{n,\bar{p}}\right]-R_{y,\beta}R_{\ell,\bar{r}}R_{n,\bar{p}}}{R_{\ell,\bar{p}}} \tag{9.5.28}$$

the **Dutch roll coupling ratio**,

$$R_{Dc} \equiv \frac{R_{\ell,\bar{r}}R_{n,\bar{p}}}{R_{\ell,\bar{p}}} \tag{9.5.29}$$

and the **Dutch roll phase-divergence ratio**,

$$R_{Dp} \equiv \frac{R_{gy}(R_{\ell,\bar{r}}R_{n,\beta}-R_{\ell,\beta}R_{n,\bar{r}})}{R_{\ell,\bar{p}}(R_{n,\beta}+R_{y,\beta}R_{n,\bar{r}})} - \frac{R_{Ds}}{R_{\ell,\bar{p}}} \tag{9.5.30}$$

This gives the approximate **Dutch roll damped natural frequency**,

$$\omega_{d_{Dr}} \cong \frac{2V_o}{b_w}\sqrt{(1-R_{y,\bar{r}})R_{n,\beta}+R_{y,\beta}R_{n,\bar{r}}+R_{Ds}-\left(\frac{R_{y,\beta}+R_{n,\bar{r}}}{2}\right)^2} \tag{9.5.31}$$

and the approximate **Dutch roll damping rate**,

$$\sigma_{Dr} \cong -\frac{V_o}{b_w}\left(R_{y,\beta}+R_{n,\bar{r}}-R_{Dc}+R_{Dp}\right) \tag{9.5.32}$$

EXAMPLE 9.5.1. Using the Dutch roll approximation given by Eq. (9.5.27), find the eigenvalues, eigenvectors, damping rate, and damped natural frequency for the Dutch roll mode of the airplane described in Example 9.2.1. Compare these approximate results with the exact Dutch roll solution that was obtained in Example 9.2.1 and with the results obtained from Eq. (9.5.5).

Solution. From Example 9.2.1 we have

$$\begin{aligned} V_o &= 180 \text{ ft/sec}, & b_w &= 33 \text{ ft}, & R_{gy} &= 0.0164, \\ R_{y,\beta} &= -0.0233, & R_{y,\bar{p}} &= 0.0, & R_{y,\bar{r}} &= 0.0100, \\ R_{\ell,\beta} &= -0.1481, & R_{\ell,\bar{p}} &= -0.8099, & R_{\ell,\bar{r}} &= 0.2074, \\ R_{n,\beta} &= 0.0395, & R_{n,\bar{p}} &= -0.0325, & R_{n,\bar{r}} &= -0.0705 \end{aligned}$$

From Eq. (9.5.28), the Dutch roll stability ratio is

$$\begin{aligned} R_{Ds} &\equiv \frac{R_{\ell,\beta}\left[R_{gy}-(1-R_{y,\bar{r}})R_{n,\bar{p}}\right]-R_{y,\beta}R_{\ell,\bar{r}}R_{n,\bar{p}}}{R_{\ell,\bar{p}}} \\ &= \frac{(-0.1481)[0.0164-(0.9900)(-0.0325)]-(-0.0233)(0.2074)(-0.0325)}{-0.8099} \\ &= 0.009076 \end{aligned}$$

From Eq. (9.5.29), the Dutch roll coupling ratio is

$$R_{Dc} \equiv \frac{R_{\ell,\bar{r}}R_{n,\bar{p}}}{R_{\ell,\bar{p}}} = \frac{(0.2074)(-0.0325)}{-0.8099} = 0.008323$$

From Eq. (9.5.30), the Dutch roll phase-divergence ratio is

$$\begin{aligned} R_{Dp} &\equiv \frac{R_{gy}(R_{\ell,\bar{r}}R_{n,\beta}-R_{\ell,\beta}R_{n,\bar{r}})}{R_{\ell,\bar{p}}(R_{n,\beta}+R_{y,\beta}R_{n,\bar{r}})}-\frac{R_{Ds}}{R_{\ell,\bar{p}}} \\ &= \frac{0.0164[(0.2074)(0.0395)-(-0.1481)(-0.0705)]}{-0.8099[0.0395+(-0.0233)(-0.0705)]}-\frac{0.009076}{-0.8099} = 0.012313 \end{aligned}$$

Using these values in Eq. (9.5.27), the approximate Dutch roll eigenvalues are

$$\lambda_{Dr} \cong \frac{R_{y,\beta} + R_{n,\bar{r}} - R_{Dc} + R_{Dp}}{2} \pm i\sqrt{(1 - R_{y,\bar{r}})R_{n,\beta} + R_{y,\beta}R_{n,\bar{r}} + R_{Ds} - \left(\frac{R_{y,\beta} + R_{n,\bar{r}}}{2}\right)^2}$$

$$= \frac{-0.0233 - 0.0705 - 0.008323 + 0.012313}{2} \pm i\sqrt{0.9900(0.0395) + (-0.0233)(-0.0705) + 0.009076 - \left(\frac{-0.0233 - 0.0705}{2}\right)^2}$$

$$= -0.044904 \pm i\,0.218230$$

The damping rate and damped natural frequency of oscillation are

$$\sigma = \text{real}(\lambda)\frac{2V_o}{b_w} = 0.044904\,\frac{2(180)}{33} = 0.489862\ \text{sec}^{-1}$$

$$\omega_d = |\text{imag}(\lambda)|\frac{2V_o}{b_w} = 0.218230\,\frac{2(180)}{33} = 2.380691\ \text{rad/sec}$$

The eigenvectors for this Dutch roll approximation are found by using the complex eigenvalues in Eq. (9.5.11). This gives

$$\begin{Bmatrix} \Delta\beta \\ \Delta\bar{p} \\ \Delta\bar{r} \\ \Delta\xi_y \\ \Delta\phi \\ \Delta\psi \end{Bmatrix} = C_{1,2}\begin{Bmatrix} 0.588877 \\ -0.110484 \mp 0.001381i \\ 0.014438 \mp 0.121348i \\ 0.165221 \mp 0.228052i \\ 0.093870 \pm 0.486957i \\ -0.546529 \pm 0.046297i \end{Bmatrix} \exp[(-0.044904 \pm 0.218230i)\,\tau_y]$$

The exact solution from Example 9.2.1 is

$$\begin{Bmatrix} \Delta\beta \\ \Delta\bar{p} \\ \Delta\bar{r} \\ \Delta\xi_y \\ \Delta\phi \\ \Delta\psi \end{Bmatrix} = C_{3,4}\begin{Bmatrix} 0.589580 \\ -0.109648 \mp 0.001442i \\ 0.013967 \mp 0.121744i \\ 0.172251 \mp 0.220690i \\ 0.091681 \pm 0.484586i \\ -0.549104 \pm 0.047290i \end{Bmatrix} \exp[(-0.044202 \pm 0.217908i)\,\tau_y]$$

From Eqs. (9.5.3) and (9.5.5), the infinite roll-damping solution is

$$\begin{Bmatrix} \Delta\beta \\ \Delta\bar{p} \\ \Delta\bar{r} \\ \Delta\xi_y \\ \Delta\phi \\ \Delta\psi \end{Bmatrix} = C_{1,2} \begin{Bmatrix} 0.653476 \\ 0.000000 \\ 0.015578 \mp 0.129597\, i \\ 0.344288 \mp 0.138783\, i \\ 0.000000 \\ -0.642375 \pm 0.074105\, i \end{Bmatrix} \exp[(-0.046900 \pm 0.196337\, i)\, \tau_y]$$

Figures 9.5.1 through 9.5.5 show how the Dutch roll approximation that is given by Eq. (9.5.27) compares with that given by Eq. (9.5.5) and the exact solution for a broad range of aerodynamic parameters. Here it should be noted that as the roll-damping derivative approaches infinity, the Dutch roll stability ratio, coupling ratio, and phase-divergence ratio all approach zero. So we see that in the limit of infinite roll damping, the result that is given by Eq. (9.5.27) reduces exactly to that given by Eq. (9.5.5). Thus, as was mentioned previously, Eq. (9.5.5) represents an asymptotic solution for infinite roll damping. This can be seen graphically in Fig. 9.5.1. In this figure, all parameters except the roll-damping ratio have been held constant at those values given in Example 9.5.1. For a conventional airplane, the roll-damping derivative is large compared to the other aerodynamic derivatives. Thus, it may seem reasonable to use an asymptotic solution for large roll damping as an approximation for Dutch roll. However, the roll-damping ratio for conventional airplanes is typically somewhat less than 1.0. Figure 9.5.1 shows that this level of roll damping is not sufficient to produce the asymptotic behavior.

Figures 9.5.2 through 9.5.5 show how other aerodynamic derivatives affect Dutch roll. In Fig. 9.5.2, a comparison between Eqs. (9.5.5), (9.5.27), and the exact solution is shown for a broad range of roll-stability ratio. Figure 9.5.3 shows the same comparison for a broad range of yaw-stability ratio. Similar comparisons, showing the effects of roll and yaw coupling, are displayed in Figs. 9.5.4 and 9.5.5.

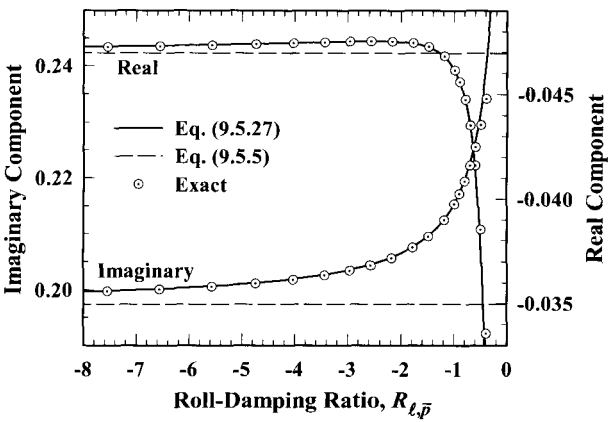


Figure 9.5.1. Effect of roll damping on the dimensionless Dutch roll eigenvalues.

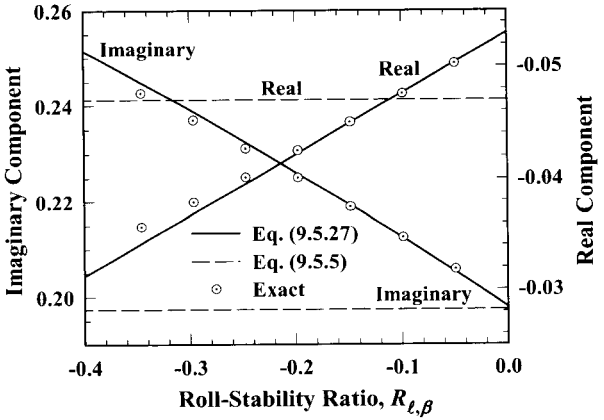


Figure 9.5.2. Effect of roll stability on the dimensionless Dutch roll eigenvalues.

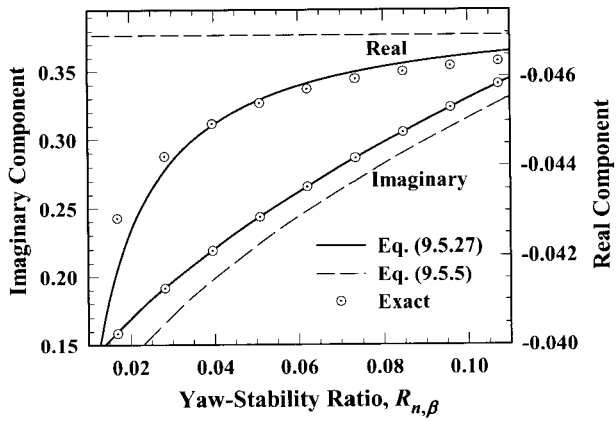


Figure 9.5.3. Effect of yaw stability on the dimensionless Dutch roll eigenvalues.

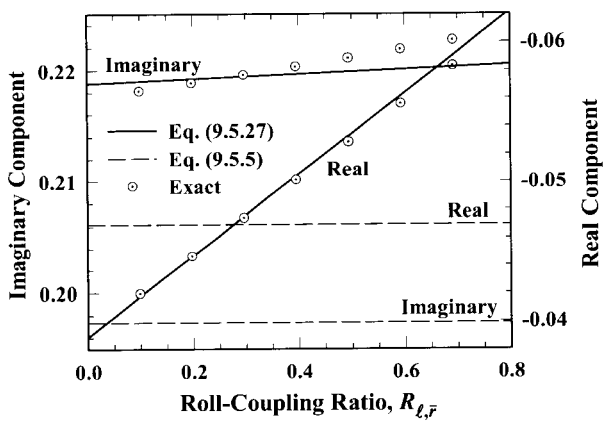


Figure 9.5.4. Effect of roll coupling on the dimensionless Dutch roll eigenvalues.

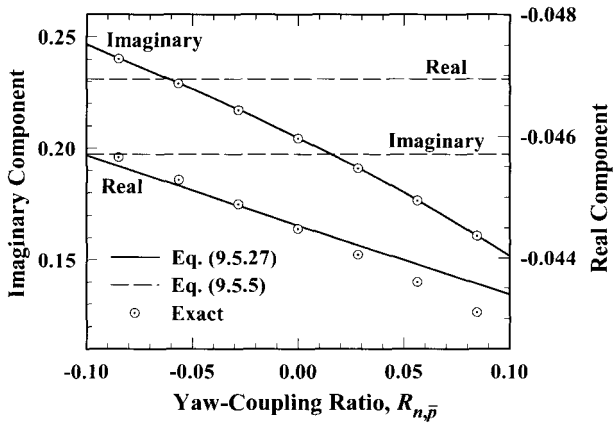


Figure 9.5.5. Effect of yaw coupling on the dimensionless Dutch roll eigenvalues.

The improved closed-form approximation allows us to see more easily how the aerodynamic coefficients and stability derivatives affect the Dutch roll motion. In order to help the student develop some insight into the genesis of Dutch roll, we shall now examine the predictions of this improved approximation in greater detail.

Damping has very little effect on the Dutch roll frequency. Thus, neglecting the damping terms in Eq. (9.5.31) and applying the definition of Dutch roll stability ratio from Eq. (9.5.28), the undamped natural frequency for Dutch roll motion is approximated as

$$\begin{aligned}\omega_{n_{Dr}} &\cong \frac{2V_o}{b_w}\sqrt{\varpi_\infty^2 + R_{Ds}} \\ &= \frac{2V_o}{b_w}\sqrt{\varpi_\infty^2 + \frac{R_{\ell,\beta}\left[R_{gy} - (1 - R_{y,\bar{r}})R_{n,\bar{p}}\right] - R_{y,\beta}R_{\ell,\bar{r}}R_{n,\bar{p}}}{R_{\ell,\bar{p}}}}\end{aligned} \tag{9.5.33}$$

where ϖ_∞ is the traditional dimensionless undamped natural frequency for infinite roll damping. The roll-damping derivative is always negative, and for a stable aircraft, the roll-stability derivative is also negative. The gravitational acceleration ratio is positive; the dimensionless change in side force with yawing rate is always less than unity; and for a conventional airplane generating positive lift, the change in yawing moment with rolling rate is typically negative. Thus, the Dutch roll stability ratio is positive, and from Eq. (9.5.33) we see that increasing roll stability will increase the Dutch roll frequency while increasing roll damping will decrease the Dutch roll frequency. Furthermore, since the change in side force with sideslip angle is negative and the change in rolling moment with yawing rate is typically positive, Eq. (9.5.33) shows that increasing the roll-yaw coupling will normally increase the Dutch roll frequency.

Using the definitions from Eqs. (9.5.28) through (9.5.30) in Eq. (9.5.32), the Dutch roll damping for the improved approximation can be written as

$$\begin{aligned}\sigma_{Dr} &\cong \sigma_\infty + \frac{V_o}{b_w}(R_{Dc} - R_{Dp}) \\ &= \sigma_\infty + \frac{V_o}{b_w}\left(\frac{R_{\ell,\bar{r}}\,R_{n,\bar{p}}}{R_{\ell,\bar{p}}} - \frac{R_{gy}(R_{\ell,\bar{r}}\,R_{n,\beta} - R_{\ell,\beta}\,R_{n,\bar{r}})}{R_{\ell,\bar{p}}(R_{n,\beta} + R_{y,\beta}\,R_{n,\bar{r}})}\right. \\ &\qquad \left. + \frac{R_{\ell,\beta}[R_{gy} - (1 - R_{y,\bar{r}})R_{n,\bar{p}}] - R_{y,\beta}\,R_{\ell,\bar{r}}\,R_{n,\bar{p}}}{R^2_{\ell,\bar{p}}}\right)\end{aligned} \tag{9.5.34}$$

where σ_∞ is the traditional yaw damping term, which provides the total Dutch roll damping for the case of infinite roll damping. The second term on the right-hand side of Eq. (9.5.34) is the Dutch roll coupling ratio. Since the roll-yaw coupling derivatives typically have opposite signs and the roll-damping derivative is always negative, the Dutch roll coupling ratio will normally increase the Dutch roll damping. However, it is possible for the roll-yaw coupling derivatives to have the same sign, in which case this Dutch roll coupling would tend to decrease the total Dutch roll damping.

The third and fourth terms on the right-hand side of Eq. (9.5.34) compose the *Dutch roll phase-divergence ratio.* This has been called the phase-divergence ratio because it results from the phase shift between the various components that comprise the Dutch roll motion and because it will typically decrease the total Dutch roll damping. For an aircraft that is stable in yaw, the denominator in the third term on the right-hand side of Eq. (9.5.34) is negative, and the denominator in the last term is always positive. Thus, since the roll-stability derivative is negative for a stable aircraft, Eq. (9.5.34) shows that increasing roll stability will decrease Dutch roll damping. In a similar manner, from further examination of Eq. (9.5.34) it can be shown that increasing yaw stability will increase Dutch roll damping.

The design of an airplane having good Dutch roll characteristics while maintaining acceptable roll, yaw, and spiral stability can present somewhat of dilemma. The aerodynamic derivatives that have greatest influence on the Dutch roll and spiral damping are the roll-stability derivative, the roll-damping derivative, the yaw-stability derivative, and the yaw-damping derivative. From the improved approximations for the Dutch roll and spiral modes, we see how each of these derivatives affect the damping for these two modes. For a conventional airplane that is stable in both roll and yaw, the influence of these derivatives is summarized as follows:

Increasing roll stability will:
- Decrease Dutch roll damping.
- Increase spiral damping.

Increasing roll damping will:
- Increase Dutch roll damping.
- Decrease spiral damping.

Increasing yaw stability will:
- Increase Dutch roll damping.
- Decrease spiral damping.

Increasing yaw damping will:
- Increase Dutch roll damping.
- Increase spiral damping.

While increasing roll stability has a favorable effect on the spiral damping, it has an adverse effect on the Dutch roll damping. On the other hand, roll damping has an

adverse effect on spiral stability while improving the Dutch roll damping. Increasing yaw stability improves the damping for Dutch roll but renders the spiral mode more unstable. Only by increasing yaw damping can we have a favorable impact on the damping for both Dutch roll and the spiral mode. Unfortunately, increasing yaw damping without increasing yaw stability is not easy to achieve through geometric design changes, without significantly increasing the drag.

The most obvious way to increase yaw damping is to increase the area of the vertical tail. However, this will add drag and increase yaw stability, which has a destabilizing effect on the spiral mode. By adding a vertical surface forward of the center of gravity, we could increase yaw damping while decreasing yaw stability. By selecting the proper combination of vertical surfaces both forward and aft of the center of gravity, it would be possible to design an airplane to have any desired combination of yaw stability and yaw damping. However, vertical surfaces placed in front of the center of gravity add unnecessarily to the drag and are not normally used. As a better solution to this problem, modern airplanes are often fitted with a feedback control system to provide additional yaw damping without the added drag and yaw stability that are produced by increasing the area of the vertical tail.

An electronic yaw damper can be constructed by using a rate gyro that produces an output signal proportional to the yawing rate of the aircraft. This output signal is multiplied by a gain coefficient and fed back into a control system to produce a rudder deflection proportional to the yawing rate. From the yawing momentum equation given by Eq. (7.7.6), we have

$$\Delta\hat{\bar{r}} - \iota_{zx}\Delta\hat{\bar{p}} - R_{n,\beta}\Delta\beta - R_{n,\bar{p}}\Delta\bar{p} - R_{n,\bar{r}}\Delta\bar{r} = R_{n,\delta_a}\Delta\delta_a + R_{n,\delta_r}\Delta\delta_r \tag{9.5.35}$$

With the yaw damper activated, the total rudder deflection is the sum of that imposed by the feedback control system and that imposed by the pilot,

$$\Delta\delta_r = K\Delta\bar{r} + (\Delta\delta_r)_{\text{pilot}} \tag{9.5.36}$$

where K is a dimensionless gain coefficient for the control system. Using Eq. (9.5.36) in Eq. (9.5.35) and rearranging gives

$$\begin{aligned}\Delta\hat{\bar{r}} - \iota_{zx}\Delta\hat{\bar{p}} - R_{n,\beta}\Delta\beta - R_{n,\bar{p}}\Delta\bar{p} - (R_{n,\bar{r}} + K\,R_{n,\delta_r})\Delta\bar{r} \\ = R_{n,\delta_a}\Delta\delta_a + R_{n,\delta_r}(\Delta\delta_r)_{\text{pilot}}\end{aligned} \tag{9.5.37}$$

Thus, the effective yaw-damping ratio for the aircraft is

$$(R_{n,\bar{r}})_{\text{effective}} = R_{n,\bar{r}} + K\,R_{n,\delta_r} \tag{9.5.38}$$

With the sign convention used in this textbook, the sign of the rudder deflection is defined such that a negative yawing moment is produced by positive rudder deflection. Thus, K must be positive to increase the effective yaw damping (i.e., to make the yaw damping derivative more negative). By adjusting the gain on the feedback control

system, we can provide any desired amount of yaw damping without affecting the yaw stability. This allows us to control the Dutch roll damping without the adverse effects associated with increasing the vertical tail area.

While the discussion above was aimed at controlling the yaw damping for an airplane, it is possible to control both the yaw damping and yaw stability. This is accomplished by producing a rudder deflection that is proportional to both the sideslip and yawing rate,

$$\Delta\delta_r = K_1\Delta\beta + K_2\Delta\bar{r} + (\Delta\delta_r)_{\text{pilot}} \tag{9.5.39}$$

Including the effects of this feedback control system, the linearized yawing momentum equation becomes

$$\begin{aligned}\Delta\hat{\bar{r}} - \iota_{zx}\Delta\hat{\bar{p}} - (R_{n,\beta} + K_1 R_{n,\delta_r})\Delta\beta - R_{n,\bar{p}}\Delta\bar{p} - (R_{n,\bar{r}} + K_2 R_{n,\delta_r})\Delta\bar{r} \\ = R_{n,\delta_a}(\Delta\delta_a)_{\text{pilot}} + R_{n,\delta_r}(\Delta\delta_r)_{\text{pilot}}\end{aligned} \tag{9.5.40}$$

The dimensionless gains for the feedback control system, K_1 and K_2, can be selected to provide any desired level of yaw damping and yaw stability. By adjusting these two gains it is possible to independently control both the Dutch roll damping and frequency. Furthermore, these gains can be varied with airspeed and flap setting to provide good Dutch roll characteristics over the full range of operating conditions. However, we must remember that both directional and spiral stability also impose constraints on the yaw stability and damping. The use of feedback control systems for stability augmentation is not a cure-all to be used in place of good geometric design. However, it does provide the designer with an additional degree of freedom, which can be used to ensure good flying qualities over the full range of operating conditions while maintaining satisfactory performance relative to other mission objectives.

9.6. Pure Rolling Motion

While pure rolling motion does not occur in free flight, a wind tunnel model could be constrained to allow motion only in pure roll. In free flight, rolling motion will always produce some sideslip and yaw. However, if a wind tunnel model is constrained as is shown in Fig. 9.6.1, the mounting sting will supply whatever moments are necessary to resist the aerodynamic moments except for those about the roll axis. With a model so constrained, it is possible to obtain information from which certain aerodynamic derivatives can be extracted.

The equation of motion for this model can be obtained from the general lateral equations by applying the constraints

$$\Delta\beta = \Delta\bar{r} = \Delta\delta_r = 0 \tag{9.6.1}$$

Using these constraints in Eq. (7.7.6) with $\Delta\bar{p} = \bar{p}$, the rolling momentum equation becomes

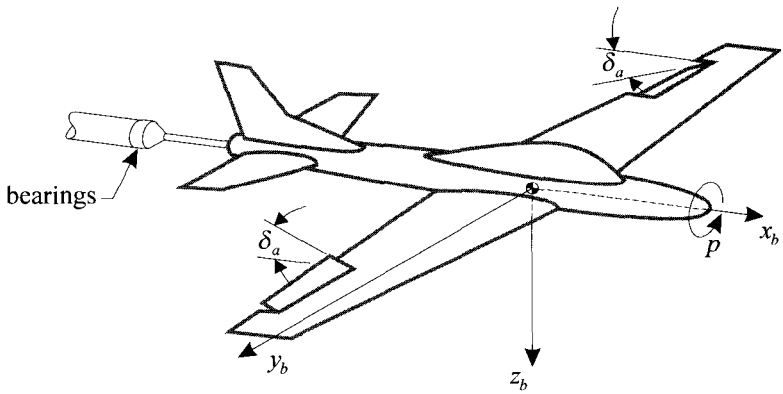


Figure 9.6.1. Wind tunnel model constrained to pure rolling motion.

$$\frac{d\bar{p}}{d\tau_y} - R_{\ell,\bar{p}}\,\bar{p} = R_{\ell,\delta_a}\,\Delta\delta_a \tag{9.6.2}$$

where

$$\bar{p} \equiv \frac{pb_w}{2V_o}, \quad \tau_y \equiv \frac{2V_o t}{b_w}, \quad R_{\ell,\bar{p}} \equiv \frac{\rho S_w b_w^3}{8I_{xx_b}} C_{\ell,\bar{p}}, \quad R_{\ell,\delta_a} \equiv \frac{\rho S_w b_w^3}{8I_{xx_b}} C_{\ell,\delta_a} \tag{9.6.3}$$

The solution to this first-order differential equation for a step change in aileron deflection is

$$\bar{p} = \frac{R_{\ell,\delta_a}\Delta\delta_a}{-R_{\ell,\bar{p}}}\left[1 - \exp(R_{\ell,\bar{p}}\,\tau_y)\right] \tag{9.6.4}$$

After applying the definitions in Eq. (9.6.3), this solution can be written as

$$\frac{pb_w}{2V_o} = \frac{C_{\ell,\delta_a}\Delta\delta_a}{-C_{\ell,\bar{p}}}\left[1 - \exp(-\sigma_r\, t)\right] \tag{9.6.5}$$

where σ_r is the roll-damping rate,

$$\sigma_r = -\frac{\rho S_w b_w^2 V_o}{4I_{xx_b}} C_{\ell,\bar{p}} \tag{9.6.6}$$

Because the roll-damping derivative is always negative, the rolling rate will exponentially approach a steady value, as shown in Fig. 9.6.2. From Eq. (9.6.5), the steady rolling rate, which develops after the rolling transient is damped out, must satisfy the equation

$$\frac{pb_w}{2V_o} = \frac{C_{\ell,\delta_a}\Delta\delta_a}{-C_{\ell,\bar{p}}} \tag{9.6.7}$$

Since the roll-damping rate is large, the transient term, $\exp(-\sigma_r t)$, decays to zero very rapidly and the rolling rate quickly approaches a constant value. This large roll-damping rate gives the pilot the impression that aileron deflection controls rolling rate rather than rolling acceleration. For this reason, the maximum rolling rate that can be attained with maximum aileron deflection is an important measure of the lateral control power available from the ailerons. Maximum rolling rate is attained when the rolling moment produced by the aileron deflection is exactly balanced by the rolling moment resulting from the rolling rate. This produces a net rolling moment of zero. The maximum dimensionless rolling rate that is attained at full aileron deflection can be used for sizing the ailerons. The **minimum requirements commonly used for aileron sizing** are:

low- to medium-maneuverability aircraft such as cargo and transport airplanes	$\left(\frac{pb_w}{2V_o}\right)_{\max} \geq 0.07$
high-maneuverability aircraft such as fighters and stunt airplanes	$\left(\frac{pb_w}{2V_o}\right)_{\max} \geq 0.09$

The rolling rate of the aircraft could be measured as a function of time using a rate gyro. By recording the roll response to a step change in aileron deflection, we could determine both the roll-damping rate and the steady rolling rate that develops after the transient has decayed. This could be done by fitting the measured response to the analytical solution given by Eq. (9.6.5). From the measured damping rate, the dimensionless roll-damping derivative could be determined by rearranging Eq. (9.6.6),

$$C_{\ell,\bar{p}} = -\frac{4I_{xx_b}\sigma_r}{\rho S_w b_w^2 V_o} \tag{9.6.8}$$

Using Eq. (9.6.8) in Eq. (9.6.7), the change in rolling moment with respect to aileron deflection could be evaluated from the measured values of the roll-damping rate and the steady rolling rate, which develops after the damping transient has decayed,

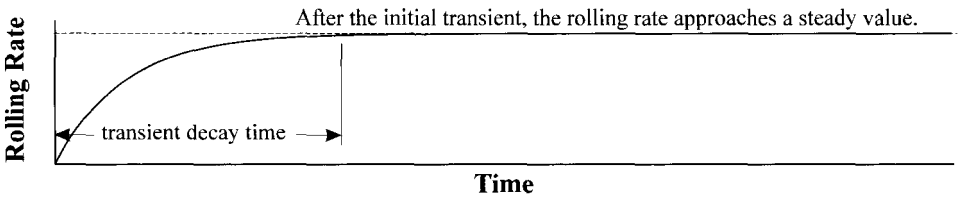


Figure 9.6.2. Roll response to a step change in aileron deflection.

$$C_{\ell,\delta_a} = \frac{2I_{xx_b}\sigma_r\, p_{\text{steady}}}{\rho S_w b_w V_o^2 \Delta\delta_a} \tag{9.6.9}$$

If the rolling moment of inertia, geometric properties of the model, and wind tunnel operating conditions are all known, Eqs. (9.6.8) and (9.6.9) can be used to determine the aerodynamic derivatives. The rolling moment of inertia for the model could be determined in a manner similar to that described in Sec. 8.5.

9.7. Pure Yawing Motion

In a similar manner, a wind tunnel model could be constrained to pure yawing motion, as shown in Fig. 9.7.1. The equation of motion for this model is obtained from the general lateral equations by applying the constraints

$$\Delta\bar{p} = \Delta\xi_y = \Delta\phi = \Delta\delta_a = 0 \tag{9.7.1}$$

$$\Delta\beta = -\Delta\psi \tag{9.7.2}$$

Using these constraints in Eq. (7.7.6) with $\Delta\bar{r} = \bar{r}$ and $\Delta\psi = \psi$, from the third and sixth rows we have

$$\frac{d\bar{r}}{d\tau_y} = R_{n,\delta_r}\Delta\delta_r - R_{n,\beta}\psi + R_{n,\bar{r}}\bar{r} \tag{9.7.3}$$

$$\frac{d\psi}{d\tau_y} = \bar{r} \tag{9.7.4}$$

where

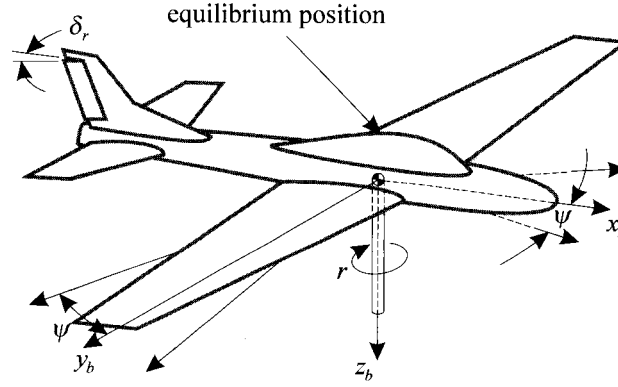


Figure 9.7.1. Wind tunnel model constrained to pure yawing motion.

$$\bar{r} \equiv \frac{rb_w}{2V_o}, \quad \tau_y \equiv \frac{2V_o t}{b_w}, \quad R_{n,\delta_r} \equiv \frac{\rho S_w b_w^3}{8I_{zz_b}} C_{n,\delta_r},$$
$$R_{n,\beta} \equiv \frac{\rho S_w b_w^3}{8I_{zz_b}} C_{n,\beta}, \quad R_{n,\bar{r}} \equiv \frac{\rho S_w b_w^3}{8I_{zz_b}} C_{n,\bar{r}} \tag{9.7.5}$$

Using Eq. (9.7.4) in Eq. (9.7.3) and rearranging, we have

$$\frac{d^2\psi}{d\tau_y^2} - R_{n,\bar{r}} \frac{d\psi}{d\tau_y} + R_{n,\beta}\psi = R_{n,\delta_r} \Delta\delta_r \tag{9.7.6}$$

The characteristic equation for Eq. (9.7.6) is

$$\lambda^2 - R_{n,\bar{r}}\lambda + R_{n,\beta} = 0 \tag{9.7.7}$$

Thus, the **eigenvalues for pure yawing motion** are

$$\lambda = \frac{R_{n,\bar{r}}}{2} \pm \sqrt{\left(\frac{R_{n,\bar{r}}}{2}\right)^2 - R_{n,\beta}} \tag{9.7.8}$$

By performing wind tunnel tests on an aircraft model that is constrained to pure yawing motion, we could determine the eigenvalues experimentally. The model's moment of inertia should be adjusted to produce underdamped motion. In the wind tunnel, the model is displaced from equilibrium and then released. The resulting oscillatory yawing motion is recorded as a function of time. By measuring the period of oscillation and the time required to reduce the amplitude of oscillation by one-half, we could determine the yaw-damping derivative as well as the yaw-stability derivative for the model.

From Eqs. (9.7.5) and (9.7.8), the 50 percent damping time is given by

$$50\% \text{ damping time} \equiv t_{50} = \frac{b_w}{2V_o}\frac{\ln(0.50)}{\text{real}(\lambda)} = \frac{b_w}{V_o}\frac{\ln(0.50)}{R_{n,\bar{r}}} = \frac{8I_{zz_b}}{\rho S_w b_w^2 V_o}\frac{\ln(0.50)}{C_{n,\bar{r}}} \tag{9.7.9}$$

and the period is

$$\text{period} \equiv t_p = \frac{b_w}{2V_o}\frac{2\pi}{|\text{imag}(\lambda)|} = \frac{\frac{\pi b_w}{V_o}}{\sqrt{R_{n,\beta} - \left(\frac{R_{n,\bar{r}}}{2}\right)^2}} = \frac{\frac{16\pi I_{zz_b}}{\rho S_w b_w^2 V_o}}{\sqrt{\frac{32 I_{zz_b}}{\rho S_w b_w^3} C_{n,\beta} - C_{n,\bar{r}}^2}} \tag{9.7.10}$$

Rearranging Eqs. (9.7.9) and (9.7.10), we have

$$C_{n,\bar{r}} = \frac{8I_{zz_b}\ln(0.50)}{\rho S_w b_w^2 V_o\, t_{50}} \tag{9.7.11}$$

$$C_{n,\beta} = \frac{2I_{zz_b}}{\rho S_w b_w V_o^2}\left[\left(\frac{2\pi}{t_p}\right)^2 + \left(\frac{\ln(0.50)}{t_{50}}\right)^2\right] \tag{9.7.12}$$

Using Eqs. (9.7.11) and (9.7.12), we could determine the yaw-damping derivative as well as the yaw-stability derivative from the measured period and 50 percent damping time, provided that we know the wind tunnel airspeed and density, along with the geometry and yawing moment of inertia for the aircraft model. Here again the yawing moment of inertia could be determined in a manner similar to that described in Sec. 8.5.

9.8. Longitudinal-Lateral Coupling

As discussed previously, the lateral equations of motion were uncoupled from the longitudinal equations of motion only as a result of imposing the small-disturbance approximation. The actual response of an aircraft to a finite lateral disturbance will involve all six degrees of freedom. Furthermore, as discussed in Sec. 7.9, inertial and gyroscopic effects can produce coupling between the lateral and longitudinal equations, even within the framework of small disturbance theory. What is normally referred to as *inertial coupling* occurs whenever the aircraft's mass is not completely symmetric about the x_b-z_b plane, and *gyroscopic coupling* occurs as a result of any net angular momentum associated with rotors spinning relative to the body-fixed coordinate system. Aircraft asymmetry can also give rise to aerodynamic coupling, because aerodynamic derivatives such as $C_{\ell,\alpha}$, $C_{n,\alpha}$, and $C_{m,\beta}$ can become nonzero. The occurrence of such first-order coupling is not unusual.

Uncoupling the longitudinal and lateral equations of motion reduces the eigenproblem associated with linearized aircraft dynamics from one 12×12 system to two 6×6 systems. Decades ago, when the theory of linearized aircraft dynamics was developed, this represented a significant computational savings. To reduce computation time even further, each of these 6×6 systems was commonly reduced algebraically to a 4×4 system. The eigenvalues obtained from the 4×4 system are identical to those obtained from the 6×6 system, except that the lower-order system does not yield the trivial rigid-body displacement modes. This represents no loss of information. However, there is a loss of information in the eigenvectors when the 6×6 systems are reduced to 4×4. Two components of each eigenvector are lost. This was a small price to pay for the computational savings that were realized in the mid-twentieth century.

Today, there are no significant computational savings to be gained by uncoupling the linearized longitudinal and lateral equations of motion. Using modern computational facilities, the solution of a 12×12 eigenproblem is trivial. Thus, it is quite simple to account for the effects of longitudinal-lateral coupling in linearized aircraft dynamics.

The Euler angle formulation of the rigid-body 6-DOF equations of motion, which was summarized in Sec. 7.4, can be modified to account for the effects of longitudinal-lateral coupling by replacing Eq. (7.4.5) with Eq. (7.9.5). Thus, **including the effects of gyroscopic and inertial coupling, the 12 first-order differential equations that govern the motion of a rigid aircraft** can be written as

$$\frac{W}{g}\begin{Bmatrix}\dot{u}\\ \dot{v}\\ \dot{w}\end{Bmatrix} = \begin{Bmatrix}F_{x_b}\\ F_{y_b}\\ F_{z_b}\end{Bmatrix} + W\begin{Bmatrix}-S_\theta\\ S_\phi C_\theta\\ C_\phi C_\theta\end{Bmatrix} + \frac{W}{g}\begin{Bmatrix}rv-qw\\ pw-ru\\ qu-pv\end{Bmatrix} \tag{9.8.1}$$

$$\begin{bmatrix}I_{xx_b} & -I_{xy_b} & -I_{xz_b}\\ -I_{xy_b} & I_{yy_b} & -I_{yz_b}\\ -I_{xz_b} & -I_{yz_b} & I_{zz_b}\end{bmatrix}\begin{Bmatrix}\dot{p}\\ \dot{q}\\ \dot{r}\end{Bmatrix} = \begin{Bmatrix}M_{x_b}\\ M_{y_b}\\ M_{z_b}\end{Bmatrix} + \begin{bmatrix}0 & -h_{z_b} & h_{y_b}\\ h_{z_b} & 0 & -h_{x_b}\\ -h_{y_b} & h_{x_b} & 0\end{bmatrix}\begin{Bmatrix}p\\ q\\ r\end{Bmatrix} + \begin{Bmatrix}(I_{yy_b}-I_{zz_b})qr + I_{yz_b}(q^2-r^2) + I_{xz_b}pq - I_{xy_b}pr\\ (I_{zz_b}-I_{xx_b})pr + I_{xz_b}(r^2-p^2) + I_{xy_b}qr - I_{yz_b}pq\\ (I_{xx_b}-I_{yy_b})pq + I_{xy_b}(p^2-q^2) + I_{yz_b}pr - I_{xz_b}qr\end{Bmatrix} \tag{9.8.2}$$

$$\begin{Bmatrix}\dot{x}_f\\ \dot{y}_f\\ \dot{z}_f\end{Bmatrix} = \begin{bmatrix}C_\theta C_\psi & S_\phi S_\theta C_\psi - C_\phi S_\psi & C_\phi S_\theta C_\psi + S_\phi S_\psi\\ C_\theta S_\psi & S_\phi S_\theta S_\psi + C_\phi C_\psi & C_\phi S_\theta S_\psi - S_\phi C_\psi\\ -S_\theta & S_\phi C_\theta & C_\phi C_\theta\end{bmatrix}\begin{Bmatrix}u\\ v\\ w\end{Bmatrix} + \begin{Bmatrix}V_{wx_f}\\ V_{wy_f}\\ V_{wz_f}\end{Bmatrix} \tag{9.8.3}$$

$$\begin{Bmatrix}\dot{\phi}\\ \dot{\theta}\\ \dot{\psi}\end{Bmatrix} = \begin{bmatrix}1 & S_\phi S_\theta / C_\theta & C_\phi S_\theta / C_\theta\\ 0 & C_\phi & -S_\phi\\ 0 & S_\phi / C_\theta & C_\phi / C_\theta\end{bmatrix}\begin{Bmatrix}p\\ q\\ r\end{Bmatrix} \tag{9.8.4}$$

To obtain the classical dynamic modes from these 12 equations, the system must be linearized relative to some equilibrium flight condition. In Sec. 7.5, the equilibrium flight condition chosen for this purpose was steady climbing flight. This condition was chosen specifically to eliminate the coupling between the longitudinal and lateral modes. However, this is not the most general equilibrium flight condition that can be used to linearize the equations of motion if we are willing to accept longitudinal-lateral coupling in the final result.

Perhaps the most common cause of longitudinal-lateral coupling is simple turning flight. In Sec. 7.5 the equations of motion were linearized relative to a flight path having both the equilibrium bank angle and azimuth angle set to zero. Since there is no force in body-fixed coordinates that depends on azimuth angle, the choice of equilibrium azimuth angle is arbitrary and has no effect on the disturbance equations. On the other hand, allowing for a nonzero equilibrium bank angle will significantly affect the disturbance equations, introducing longitudinal-lateral coupling.

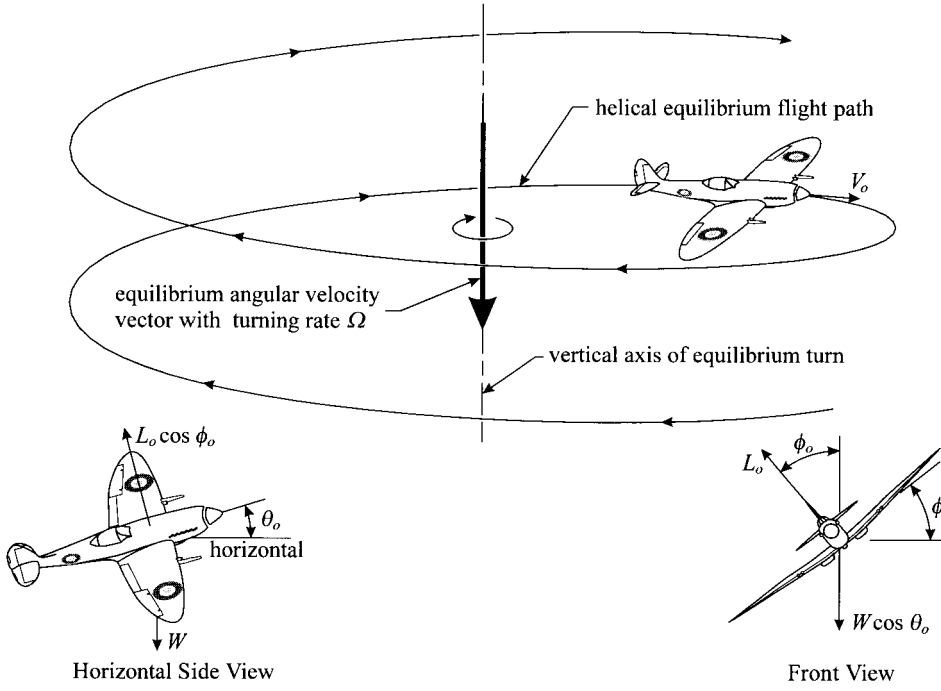


Figure 9.8.1. Equilibrium flight conditions for a steady coordinated turn.

For example, consider the steady coordinated turn shown in Fig. 9.8.1. In a steady coordinated turn the ailerons, elevator, and rudder are coordinated to maintain constant airspeed and angular acceleration while eliminating the side force. The equilibrium angular velocity vector is aligned with the z_f-axis, and by our choice of the body-fixed coordinate system, the equilibrium translational velocity vector is aligned with the x_b-axis. The equilibrium angular velocity vector in body-fixed coordinates can be determined by applying Eq. (7.3.13) to the angular velocity vector in Earth-fixed coordinates,

$$\begin{Bmatrix} p \\ q \\ r \end{Bmatrix}_o = \begin{bmatrix} C_\theta C_\psi & C_\theta S_\psi & -S_\theta \\ S_\phi S_\theta C_\psi - C_\phi S_\psi & S_\phi S_\theta S_\psi + C_\phi C_\psi & S_\phi C_\theta \\ C_\phi S_\theta C_\psi + S_\phi S_\psi & C_\phi S_\theta S_\psi - S_\phi C_\psi & C_\phi C_\theta \end{bmatrix} \begin{Bmatrix} 0 \\ 0 \\ \Omega \end{Bmatrix} = \Omega \begin{Bmatrix} -S_{\theta_o} \\ S_{\phi_o} C_{\theta_o} \\ C_{\phi_o} C_{\theta_o} \end{Bmatrix} \tag{9.8.5}$$

The translational velocity vector, in body-fixed coordinates, for this equilibrium flight condition and our choice for the body-fixed coordinate system is

$$\begin{Bmatrix} u \\ v \\ w \end{Bmatrix}_o = \begin{Bmatrix} V_o \\ 0 \\ 0 \end{Bmatrix} \tag{9.8.6}$$

From Eq. (9.8.1), constant airspeed and zero side force requires that

$$\begin{Bmatrix} 0 \\ 0 \\ 0 \end{Bmatrix} = \begin{Bmatrix} F_{x_b} \\ 0 \\ F_{z_b} \end{Bmatrix} + W \begin{Bmatrix} -S_\theta \\ S_\phi C_\theta \\ C_\phi C_\theta \end{Bmatrix} + \frac{W}{g} \begin{Bmatrix} rv - qw \\ pw - ru \\ qu - pv \end{Bmatrix} \tag{9.8.7}$$

Applying Eqs. (9.8.5) and (9.8.6) to Eq. (9.8.7), this equilibrium flight condition gives

$$\begin{Bmatrix} 0 \\ 0 \\ 0 \end{Bmatrix} = \begin{Bmatrix} F_{x_b o} \\ 0 \\ F_{z_b o} \end{Bmatrix} + W \begin{Bmatrix} -S_{\theta_o} \\ S_{\phi_o} C_{\theta_o} \\ C_{\phi_o} C_{\theta_o} \end{Bmatrix} + \frac{W \Omega V_o}{g} \begin{Bmatrix} 0 \\ -C_{\phi_o} C_{\theta_o} \\ S_{\phi_o} C_{\theta_o} \end{Bmatrix} \tag{9.8.8}$$

The second equation in Eq. (9.8.8) can be solved for the equilibrium turning rate as a function of airspeed and bank angle,

$$\Omega = \frac{g \tan \phi_o}{V_o} \tag{9.8.9}$$

From Eqs. (9.8.8) and (9.8.9), the net equilibrium aerodynamic force required to maintain a steady coordinated turn is

$$\begin{Bmatrix} F_{x_b} \\ F_{y_b} \\ F_{z_b} \end{Bmatrix}_o = W \begin{Bmatrix} S_{\theta_o} \\ 0 \\ -C_{\theta_o} / C_{\phi_o} \end{Bmatrix} \tag{9.8.10}$$

From Eqs. (9.8.4) and (9.8.5), the equilibrium Euler angle rates are readily found to be

$$\begin{Bmatrix} \dot{\phi} \\ \dot{\theta} \\ \dot{\psi} \end{Bmatrix}_o = \begin{Bmatrix} 0 \\ 0 \\ \Omega \end{Bmatrix} \tag{9.8.11}$$

Integrating Eq. (9.8.11) subject to the initial condition of zero heading at time $t = 0$, we find that the equilibrium Euler angles for a steady coordinated turn are

$$\begin{Bmatrix} \phi \\ \theta \\ \psi \end{Bmatrix}_o = \begin{Bmatrix} \phi_o \\ \theta_o \\ \Omega t \end{Bmatrix} \tag{9.8.12}$$

Similarly, using this result in Eq. (9.8.3) and integrating, the equilibrium position for the steady coordinated turn can be written as

$$\begin{Bmatrix} x_f \\ y_f \\ z_f \end{Bmatrix}_o = \begin{Bmatrix} V_{wx_f} t + V_o C_{\theta_o} S_{\Omega t}/\Omega \\ V_{wy_f} t - V_o C_{\theta_o} C_{\Omega t}/\Omega \\ (V_{wz_f} - V_o S_{\theta_o})t \end{Bmatrix} \tag{9.8.13}$$

Expanding the aircraft flight variables relative to this equilibrium state, we have

$$\begin{aligned}
u &= V_o + \Delta u, & v &= \Delta v, & w &= \Delta w, \\
p &= -gT_{\phi_o} S_{\theta_o}/V_o + \Delta p, & q &= gT_{\phi_o} S_{\phi_o} C_{\theta_o}/V_o + \Delta q, & r &= gS_{\phi_o} C_{\theta_o}/V_o + \Delta r, \\
F_{x_b} &= WS_{\theta_o} + \Delta F_{x_b}, & F_{y_b} &= \Delta F_{y_b}, & F_{z_b} &= -WC_{\theta_o}/C_{\phi_o} + \Delta F_{z_b}, \\
M_{x_b} &= M_{x_b o} + \Delta M_{x_b}, & M_{y_b} &= M_{y_b o} + \Delta M_{y_b}, & M_{z_b} &= M_{z_b o} + \Delta M_{z_b}, \\
x_f &= V_{wx_f} t + \frac{V_o^2 C_{\theta_o} S_{\Omega t}}{gT_{\phi_o}} + \Delta x_f, & y_f &= V_{wy_f} t - \frac{V_o^2 C_{\theta_o} C_{\Omega t}}{gT_{\phi_o}} + \Delta y_f, & z_f &= (V_{wz_f} - V_o S_{\theta_o})t + \Delta z_f, \\
\phi &= \phi_o + \Delta\phi, & \theta &= \theta_o + \Delta\theta, & \psi &= (g/V_o)T_{\phi_o} t + \Delta\psi
\end{aligned}$$

where T_θ is shorthand for $\tan\theta$ and the equilibrium moments are obtained by using these values in Eq. (9.8.2) with all disturbances set to zero. Equations (9.8.1) through (9.8.4) can now be linearized following Sec. 7.5 (see Phillips and Santana 2002). This gives **the general linearized 6-DOF equations of motion for aircraft dynamics,**

$$\begin{bmatrix} [\mathbf{B}]_m & [\mathbf{n}] & [\mathbf{n}] & [\mathbf{n}] \\ [\mathbf{B}]_{iv} & [\mathbf{I}] & [\mathbf{n}] & [\mathbf{n}] \\ [\mathbf{n}] & [\mathbf{n}] & [\mathbf{i}] & [\mathbf{n}] \\ [\mathbf{n}] & [\mathbf{n}] & [\mathbf{n}] & [\mathbf{i}] \end{bmatrix} \begin{Bmatrix} \Delta\dot{u} \\ \Delta\dot{v} \\ \Delta\dot{w} \\ \Delta\dot{p} \\ \Delta\dot{q} \\ \Delta\dot{r} \\ \Delta\dot{x}_c \\ \Delta\dot{y}_c \\ \Delta\dot{z}_c \\ \Delta\dot{\phi} \\ \Delta\dot{\theta} \\ \Delta\dot{\psi} \end{Bmatrix} - \begin{bmatrix} [\mathbf{A}]_{fv} & [\mathbf{A}]_{f\omega} & [\mathbf{n}] & [\mathbf{A}]_w \\ [\mathbf{A}]_{mv} & [\mathbf{A}]_{m\omega} & [\mathbf{n}] & [\mathbf{n}] \\ [\mathbf{A}]_{pv} & [\mathbf{n}] & [\mathbf{n}] & [\mathbf{A}]_{pe} \\ [\mathbf{n}] & [\mathbf{A}]_{e\omega} & [\mathbf{n}] & [\mathbf{A}]_{ee} \end{bmatrix} \begin{Bmatrix} \Delta u \\ \Delta v \\ \Delta w \\ \Delta p \\ \Delta q \\ \Delta r \\ \Delta x_c \\ \Delta y_c \\ \Delta z_c \\ \Delta\phi \\ \Delta\theta \\ \Delta\psi \end{Bmatrix} = \begin{bmatrix} [\mathbf{C}]_f \\ [\mathbf{C}]_m \\ [\mathbf{n}] \\ [\mathbf{n}] \end{bmatrix} \begin{Bmatrix} \Delta\delta_a \\ \Delta\delta_e \\ \Delta\delta_r \end{Bmatrix} \tag{9.8.14}$$

where

$$[\mathbf{B}]_m = \begin{bmatrix} \frac{W}{g} - F_{x_b,\dot{u}} & 0 & -F_{x_b,\dot{w}} \\ 0 & \frac{W}{g} & 0 \\ -F_{z_b,\dot{u}} & 0 & \frac{W}{g} - F_{z_b,\dot{w}} \end{bmatrix}$$

$$[\mathbf{B}]_{iv} = \begin{bmatrix} 0 & 0 & 0 \\ -M_{y_b,\dot{u}} & 0 & -M_{y_b,\dot{w}} \\ 0 & 0 & 0 \end{bmatrix} \qquad [\mathbf{I}] = \begin{bmatrix} I_{xx_b} & -I_{xy_b} & -I_{xz_b} \\ -I_{xy_b} & I_{yy_b} & -I_{yz_b} \\ -I_{xz_b} & -I_{yz_b} & I_{zz_b} \end{bmatrix}$$

$$[\mathbf{A}]_{fv} = \begin{bmatrix} F_{x_b,u} & \frac{WS_{\phi_o}C_{\theta_o}}{V_o} & F_{x_b,w} - \frac{WT_{\phi_o}S_{\phi_o}C_{\theta_o}}{V_o} \\ -\frac{WS_{\phi_o}C_{\theta_o}}{V_o} & F_{y_b,v} & -\frac{WT_{\phi_o}S_{\theta_o}}{V_o} \\ F_{z_b,u} + \frac{WT_{\phi_o}S_{\phi_o}C_{\theta_o}}{V_o} & \frac{WT_{\phi_o}S_{\theta_o}}{V_o} & F_{z_b,w} \end{bmatrix}$$

$$[\mathbf{A}]_{f\omega} = \begin{bmatrix} 0 & F_{x_b,q} & 0 \\ F_{y_b,p} & 0 & F_{y_b,r} - \frac{V_o W}{g} \\ 0 & F_{z_b,q} + \frac{V_o W}{g} & 0 \end{bmatrix} \qquad [\mathbf{A}]_w = \begin{bmatrix} 0 & -WC_{\theta_o} & 0 \\ WC_{\phi_o}C_{\theta_o} & -WS_{\phi_o}S_{\theta_o} & 0 \\ -WS_{\phi_o}C_{\theta_o} & -WC_{\phi_o}S_{\theta_o} & 0 \end{bmatrix}$$

$$[\mathbf{A}]_{mv} = \begin{bmatrix} 0 & M_{x_b,v} & M_{x_b,w} \\ M_{y_b,u} & M_{y_b,v} & M_{y_b,w} \\ 0 & M_{z_b,v} & M_{z_b,w} \end{bmatrix} \qquad [\mathbf{A}]_{m\omega} = \begin{bmatrix} A_{\ell p} & A_{\ell q} & A_{\ell r} \\ A_{mp} & A_{mq} & A_{mr} \\ A_{np} & A_{nq} & A_{nr} \end{bmatrix}$$

$$A_{\ell p} = M_{x_b,p} + \frac{g(I_{xz_b}T_{\phi_o}S_{\phi_o}C_{\theta_o} - I_{xy_b}S_{\phi_o}C_{\theta_o})}{V_o}$$

$$A_{\ell q} = -h_{z_b} + \frac{g[(I_{yy_b} - I_{zz_b})S_{\phi_o}C_{\theta_o} + 2I_{yz_b}T_{\phi_o}S_{\phi_o}C_{\theta_o} - I_{xz_b}T_{\phi_o}S_{\theta_o}]}{V_o}$$

$$A_{\ell r} = M_{x_b,r} + h_{y_b} + \frac{g[(I_{yy_b} - I_{zz_b})T_{\phi_o}S_{\phi_o}C_{\theta_o} - 2I_{yz_b}S_{\phi_o}C_{\theta_o} + I_{xy_b}T_{\phi_o}S_{\theta_o}]}{V_o}$$

$$A_{mp} = h_{z_b} + \frac{g[(I_{zz_b} - I_{xx_b})S_{\phi_o}C_{\theta_o} + 2I_{xz_b}T_{\phi_o}S_{\theta_o} - I_{yz_b}T_{\phi_o}S_{\phi_o}C_{\theta_o}]}{V_o}$$

$$A_{mq} = M_{y_b,q} + \frac{g(I_{xy_b}S_{\phi_o}C_{\theta_o} + I_{yz_b}T_{\phi_o}S_{\theta_o})}{V_o}$$

$$A_{mr} = -h_{x_b} + \frac{g[(I_{xx_b} - I_{zz_b})T_{\phi_o}S_{\theta_o} + 2I_{xz_b}S_{\phi_o}C_{\theta_o} + I_{xy_b}T_{\phi_o}S_{\phi_o}C_{\theta_o}]}{V_o}$$

$$A_{np} = M_{z_b,p} - h_{y_b} + \frac{g[(I_{xx_b} - I_{yy_b})T_{\phi_o}S_{\phi_o}C_{\theta_o} - 2I_{xy_b}T_{\phi_o}S_{\theta_o} + I_{yz_b}S_{\phi_o}C_{\theta_o}]}{V_o}$$

$$A_{nq} = h_{x_b} + \frac{g[(I_{yy_b} - I_{xx_b})T_{\phi_o}S_{\theta_o} - 2I_{xy_b}T_{\phi_o}S_{\phi_o}C_{\theta_o} - I_{xz_b}S_{\phi_o}C_{\theta_o}]}{V_o}$$

$$A_{nr} = M_{z_b,r} + \frac{g(-I_{yz_b}T_{\phi_o}S_{\theta_o} - I_{xz_b}T_{\phi_o}S_{\phi_o}C_{\theta_o})}{V_o}$$

$$[\mathbf{A}]_{pv} = \begin{bmatrix} C_{\theta_o} & S_{\phi_o}S_{\theta_o} & C_{\phi_o}S_{\theta_o} \\ 0 & C_{\phi_o} & -S_{\phi_o} \\ -S_{\theta_o} & S_{\phi_o}C_{\theta_o} & C_{\phi_o}C_{\theta_o} \end{bmatrix} \qquad [\mathbf{A}]_{pe} = \begin{bmatrix} 0 & -V_oS_{\theta_o} & 0 \\ 0 & 0 & V_oC_{\theta_o} \\ 0 & -V_oC_{\theta_o} & 0 \end{bmatrix}$$

$$[\mathbf{A}]_{e\omega} = \begin{bmatrix} 1 & S_{\phi_o}T_{\theta_o} & C_{\phi_o}T_{\theta_o} \\ 0 & C_{\phi_o} & -S_{\phi_o} \\ 0 & \frac{S_{\phi_o}}{C_{\theta_o}} & \frac{C_{\phi_o}}{C_{\theta_o}} \end{bmatrix} \qquad [\mathbf{A}]_{ee} = \begin{bmatrix} 0 & \frac{gT_{\phi_o}}{V_oC_{\theta_o}} & 0 \\ -\frac{gT_{\phi_o}C_{\theta_o}}{V_o} & 0 & 0 \\ 0 & \frac{gT_{\phi_o}T_{\theta_o}}{V_o} & 0 \end{bmatrix}$$

$$[\mathbf{C}]_f = \begin{bmatrix} 0 & F_{x_b,\delta_e} & 0 \\ F_{y_b,\delta_a} & 0 & F_{y_b,\delta_r} \\ 0 & F_{z_b,\delta_e} & 0 \end{bmatrix} \qquad [\mathbf{C}]_m = \begin{bmatrix} M_{x_b,\delta_a} & 0 & M_{x_b,\delta_r} \\ 0 & M_{y_b,\delta_e} & 0 \\ M_{z_b,\delta_a} & 0 & M_{z_b,\delta_r} \end{bmatrix}$$

$$\begin{Bmatrix} \Delta\dot{x}_c \\ \Delta\dot{y}_c \\ \Delta\dot{z}_c \end{Bmatrix} = \begin{bmatrix} C_{\Omega t} & S_{\Omega t} & 0 \\ -S_{\Omega t} & C_{\Omega t} & 0 \\ 0 & 0 & 1 \end{bmatrix} \begin{Bmatrix} \Delta\dot{x}_f \\ \Delta\dot{y}_f \\ \Delta\dot{z}_f \end{Bmatrix} \qquad [\mathbf{i}] = \begin{bmatrix} 1 & 0 & 0 \\ 0 & 1 & 0 \\ 0 & 0 & 1 \end{bmatrix} \qquad [\mathbf{n}] = \begin{bmatrix} 0 & 0 & 0 \\ 0 & 0 & 0 \\ 0 & 0 & 0 \end{bmatrix}$$

Equation (9.8.14) can also be used to study steady climbing flight along a linear flight path. With the equilibrium bank angle, ϕ_o, set to zero, Eq. (9.8.14) provides the linearized equations of motion for linear climbing flight, including the effects of inertial, gyroscopic, and aerodynamic coupling. Steady level flight corresponds to the special case where both ϕ_o and θ_o are zero.

As can be seen from the formulation presented here, a wide range of longitudinal-lateral coupling is introduced by simple turning flight. Gyroscopic coupling enters the linearized equations of motion only through its effect on $[\mathbf{A}]_{m\omega}$, and with no bank angle, inertial asymmetry produces coupling only through the moment of inertia tensor, $[\mathbf{I}]$. A nonzero bank angle, on the other hand, has broader effects on the linearized equations of motion. Turning flight introduces coupling in the translational velocity components as a result of the Coriolis forces seen in $[\mathbf{A}]_{fv}$. Additional translational coupling is introduced through the weight tensor, $[\mathbf{A}]_w$, when the bank angle is nonzero. Turning also produces considerable rotational coupling as a result of the gyroscopic effects seen in $[\mathbf{A}]_{m\omega}$. Finally, turning produces coupling in the position and orientation equations through $[\mathbf{A}]_{pv}$, $[\mathbf{A}]_{e\omega}$, and $[\mathbf{A}]_{ee}$.

To nondimensionalize Eq. (9.8.14), it is convenient to select a single reference length for all longitudinal and lateral variables. Retaining the equilibrium airspeed as the reference velocity, the nondimensional velocity disturbances remain,

$$\begin{aligned} \Delta\mu &\equiv \frac{\Delta u}{V_o} \\ \Delta\beta &\equiv \frac{\Delta v}{V_o} \\ \Delta\alpha &\equiv \frac{\Delta w}{V_o} \end{aligned} \tag{9.8.15}$$

Denoting the reference length as l_{ref}, the dimensionless angular rate disturbances are defined as

$$\begin{aligned} \Delta\alpha' &\equiv \frac{\Delta\dot{\alpha}\, l_{\text{ref}}}{V_o} = \frac{2l_{\text{ref}}}{\bar{c}_w}\Delta\hat{\alpha} \\ \Delta\bar{p} &\equiv \frac{\Delta p\, l_{\text{ref}}}{V_o} = \frac{2l_{\text{ref}}}{b_w}\Delta\bar{p} \\ \Delta\bar{q} &\equiv \frac{\Delta q\, l_{\text{ref}}}{V_o} = \frac{2l_{\text{ref}}}{\bar{c}_w}\Delta\bar{q} \\ \Delta\bar{r} &\equiv \frac{\Delta r\, l_{\text{ref}}}{V_o} = \frac{2l_{\text{ref}}}{b_w}\Delta\bar{r} \end{aligned} \tag{9.8.16}$$

Similarly, the disturbances in aircraft position are now nondimensionalized as

$$\begin{aligned} \Delta\varsigma_x &\equiv \frac{\Delta x_c}{l_{\text{ref}}} = \frac{\bar{c}_w}{2l_{\text{ref}}}\Delta\xi_x \\ \Delta\varsigma_y &\equiv \frac{\Delta y_c}{l_{\text{ref}}} = \frac{b_w}{2l_{\text{ref}}}\Delta\xi_y \\ \Delta\varsigma_z &\equiv \frac{\Delta z_c}{l_{\text{ref}}} = \frac{\bar{c}_w}{2l_{\text{ref}}}\Delta\xi_z \end{aligned} \tag{9.8.17}$$

For dimensionless time we define

$$\tau \equiv \frac{V_o t}{l_{\text{ref}}} = \frac{\bar{c}_w}{2l_{\text{ref}}}\tau_x = \frac{b_w}{2l_{\text{ref}}}\tau_y \tag{9.8.18}$$

and

$$f' \equiv \frac{\partial f}{\partial \tau} = \frac{l_{\text{ref}}}{V_o}\frac{\partial f}{\partial t} = \frac{2l_{\text{ref}}}{\bar{c}_w}\left(\hat{f}\right)_{\text{longitudinal}} = \frac{2l_{\text{ref}}}{b_w}\left(\hat{f}\right)_{\text{lateral}} \tag{9.8.19}$$

With these definitions, **the nondimensional linearized equations of motion** are

$$
\begin{bmatrix}
1-B_{x,\mu'} & 0 & -B_{x,\alpha'} & 0 & 0 & 0 & 0 & 0 & 0 & 0 & 0 & 0 \\
0 & 1 & 0 & 0 & 0 & 0 & 0 & 0 & 0 & 0 & 0 & 0 \\
-B_{z,\mu'} & 0 & 1-B_{z,\alpha'} & 0 & 0 & 0 & 0 & 0 & 0 & 0 & 0 & 0 \\
0 & 0 & 0 & 1 & -\iota_{xy} & -\iota_{xz} & 0 & 0 & 0 & 0 & 0 & 0 \\
-B_{m,\mu'} & 0 & -B_{m,\alpha'} & -\iota_{yx} & 1 & -\iota_{yz} & 0 & 0 & 0 & 0 & 0 & 0 \\
0 & 0 & 0 & -\iota_{zx} & -\iota_{zy} & 1 & 0 & 0 & 0 & 0 & 0 & 0 \\
0 & 0 & 0 & 0 & 0 & 0 & 1 & 0 & 0 & 0 & 0 & 0 \\
0 & 0 & 0 & 0 & 0 & 0 & 0 & 1 & 0 & 0 & 0 & 0 \\
0 & 0 & 0 & 0 & 0 & 0 & 0 & 0 & 1 & 0 & 0 & 0 \\
0 & 0 & 0 & 0 & 0 & 0 & 0 & 0 & 0 & 1 & 0 & 0 \\
0 & 0 & 0 & 0 & 0 & 0 & 0 & 0 & 0 & 0 & 1 & 0 \\
0 & 0 & 0 & 0 & 0 & 0 & 0 & 0 & 0 & 0 & 0 & 1
\end{bmatrix}
\begin{Bmatrix}
\Delta\mu' \\ \Delta\beta' \\ \Delta\alpha' \\ \Delta\bar{p}' \\ \Delta\bar{q}' \\ \Delta\bar{r}' \\ \Delta\varsigma_x' \\ \Delta\varsigma_y' \\ \Delta\varsigma_z' \\ \Delta\phi' \\ \Delta\theta' \\ \Delta\psi'
\end{Bmatrix}
=
\begin{bmatrix}
0 & D_{x,\delta_e} & 0 \\
D_{y,\delta_a} & 0 & D_{y,\delta_r} \\
0 & D_{z,\delta_e} & 0 \\
D_{\ell,\delta_a} & 0 & D_{\ell,\delta_r} \\
0 & D_{m,\delta_e} & 0 \\
D_{n,\delta_a} & 0 & D_{n,\delta_r} \\
0 & 0 & 0 \\
0 & 0 & 0 \\
0 & 0 & 0 \\
0 & 0 & 0 \\
0 & 0 & 0 \\
0 & 0 & 0
\end{bmatrix}
\begin{Bmatrix}
\Delta\delta_a \\ \Delta\delta_e \\ \Delta\delta_r
\end{Bmatrix}
\tag{9.8.20}
$$

$$
+
\begin{bmatrix}
A_{x,\mu} & A_g S_{\phi_o} C_{\theta_o} & A_{x,\alpha} - A_g T_{\phi_o} S_{\phi_o} C_{\theta_o} & 0 & A_{x,\bar{q}} & 0 & 0 & 0 & 0 & 0 & -A_g C_{\theta_0} & 0 \\
-A_g S_{\phi_o} C_{\theta_o} & A_{y,\beta} & -A_g T_{\phi_o} S_{\theta_o} & A_{y,\bar{p}} & 0 & A_{y,\bar{r}} - 1 & 0 & 0 & 0 & A_g C_{\phi_0} C_{\theta_0} & -A_g S_{\phi_0} S_{\theta_0} & 0 \\
A_{z,\mu} + A_g T_{\phi_o} S_{\phi_o} C_{\theta_o} & A_g T_{\phi_o} S_{\theta_o} & A_{z,\alpha} & 0 & A_{z,\bar{q}} + 1 & 0 & 0 & 0 & 0 & -A_g S_{\phi_0} C_{\theta_0} & -A_g C_{\phi_0} S_{\theta_0} & 0 \\
0 & A_{\ell,\beta} & A_{\ell,\alpha} & A_{\ell,\bar{p}} + \eta_{xx} & -\eta_{xy} & A_{\ell,\bar{r}} + \eta_{xz} & 0 & 0 & 0 & 0 & 0 & 0 \\
A_{m,\mu} & A_{m,\beta} & A_{m,\alpha} & \eta_{yx} & A_{m,\bar{q}} + \eta_{yy} & -\eta_{yz} & 0 & 0 & 0 & 0 & 0 & 0 \\
0 & A_{n,\beta} & A_{n,\alpha} & A_{n,\bar{p}} - \eta_{zx} & \eta_{zy} & A_{n,\bar{r}} + \eta_{zz} & 0 & 0 & 0 & 0 & 0 & 0 \\
C_{\theta_o} & S_{\phi_o} S_{\theta_o} & C_{\phi_o} S_{\theta_o} & 0 & 0 & 0 & 0 & 0 & 0 & 0 & -S_{\theta_0} & 0 \\
0 & C_{\phi_o} & -S_{\phi_o} & 0 & 0 & 0 & 0 & 0 & 0 & 0 & 0 & C_{\theta_0} \\
-S_{\theta_o} & S_{\phi_o} C_{\theta_o} & C_{\phi_o} C_{\theta_o} & 0 & 0 & 0 & 0 & 0 & 0 & 0 & -C_{\theta_0} & 0 \\
0 & 0 & 0 & 1 & S_{\phi_o} T_{\theta_o} & C_{\phi_o} T_{\theta_o} & 0 & 0 & 0 & 0 & A_g T_{\phi_o} / C_{\theta_o} & 0 \\
0 & 0 & 0 & 0 & C_{\phi_o} & -S_{\phi_o} & 0 & 0 & 0 & -A_g T_{\phi_o} C_{\theta_o} & 0 & 0 \\
0 & 0 & 0 & 0 & S_{\phi_o} / C_{\theta_o} & C_{\phi_o} / C_{\theta_o} & 0 & 0 & 0 & 0 & A_g T_{\phi_o} T_{\theta_o} & 0
\end{bmatrix}
\begin{Bmatrix}
\Delta\mu \\ \Delta\beta \\ \Delta\alpha \\ \Delta\bar{p} \\ \Delta\bar{q} \\ \Delta\bar{r} \\ \Delta\varsigma_x \\ \Delta\varsigma_y \\ \Delta\varsigma_z \\ \Delta\phi \\ \Delta\theta \\ \Delta\psi
\end{Bmatrix}
$$

where

$$\iota_{xy} \equiv \frac{I_{xy_b}}{I_{xx_b}} \quad \iota_{xz} \equiv \frac{I_{xz_b}}{I_{xx_b}} \quad \iota_{yx} \equiv \frac{I_{xy_b}}{I_{yy_b}} \quad \iota_{yz} \equiv \frac{I_{yz_b}}{I_{yy_b}} \quad \iota_{zx} \equiv \frac{I_{xz_b}}{I_{zz_b}} \quad \iota_{zy} \equiv \frac{I_{yz_b}}{I_{zz_b}}$$

$$B_{x,\mu'} \equiv \frac{\rho S_w \bar{c}_w}{4W/g} C_{X,\hat{\mu}} \quad B_{z,\mu'} \equiv \frac{\rho S_w \bar{c}_w}{4W/g} C_{Z,\hat{\mu}} \quad B_{m,\mu'} \equiv \frac{\rho S_w \bar{c}_w^2 l_{\text{ref}}}{4I_{yy_b}} C_{m,\hat{\mu}}$$

$$B_{x,\alpha'} \equiv \frac{\rho S_w \bar{c}_w}{4W/g} C_{X,\hat{\alpha}} \quad B_{z,\alpha'} \equiv \frac{\rho S_w \bar{c}_w}{4W/g} C_{Z,\hat{\alpha}} \quad B_{m,\alpha'} \equiv \frac{\rho S_w \bar{c}_w^2 l_{\text{ref}}}{4I_{yy_b}} C_{m,\hat{\alpha}}$$

$$\eta_{xx} = A_g \frac{I_{xz_b} T_{\phi_o} S_{\phi_o} C_{\theta_o} - I_{xy_b} S_{\phi_o} C_{\theta_o}}{I_{xx_b}}$$

$$\eta_{xy} = \frac{h_{z_b} l_{\text{ref}}}{I_{xx_b} V_o} + A_g \frac{(I_{zz_b} - I_{yy_b}) S_{\phi_o} C_{\theta_o} - 2I_{yz_b} T_{\phi_o} S_{\phi_o} C_{\theta_o} + I_{xz_b} T_{\phi_o} S_{\theta_o}}{I_{xx_b}}$$

$$\eta_{xz} = \frac{h_{y_b} l_{\text{ref}}}{I_{xx_b} V_o} + A_g \frac{(I_{yy_b} - I_{zz_b}) T_{\phi_o} S_{\phi_o} C_{\theta_o} - 2I_{yz_b} S_{\phi_o} C_{\theta_o} + I_{xy_b} T_{\phi_o} S_{\theta_o}}{I_{xx_b}}$$

$$\eta_{yx} = \frac{h_{z_b} l_{\text{ref}}}{I_{yy_b} V_o} + A_g \frac{(I_{zz_b} - I_{xx_b}) S_{\phi_o} C_{\theta_o} + 2I_{xz_b} T_{\phi_o} S_{\theta_o} - I_{yz_b} T_{\phi_o} S_{\phi_o} C_{\theta_o}}{I_{yy_b}}$$

$$\eta_{yy} = A_g \frac{I_{xy_b} S_{\phi_o} C_{\theta_o} + I_{yz_b} T_{\phi_o} S_{\theta_o}}{I_{yy_b}}$$

$$\eta_{yz} = \frac{h_{x_b} l_{\text{ref}}}{I_{yy_b} V_o} + A_g \frac{(I_{zz_b} - I_{xx_b}) T_{\phi_o} S_{\theta_o} - 2I_{xz_b} S_{\phi_o} C_{\theta_o} - I_{xy_b} T_{\phi_o} S_{\phi_o} C_{\theta_o}}{I_{yy_b}}$$

$$\eta_{zx} = \frac{h_{y_b} l_{\text{ref}}}{I_{zz_b} V_o} + A_g \frac{(I_{yy_b} - I_{xx_b}) T_{\phi_o} S_{\phi_o} C_{\theta_o} + 2I_{xy_b} T_{\phi_o} S_{\theta_o} - I_{yz_b} S_{\phi_o} C_{\theta_o}}{I_{zz_b}}$$

$$\eta_{zy} = \frac{h_{x_b} l_{\text{ref}}}{I_{zz_b} V_o} + A_g \frac{(I_{yy_b} - I_{xx_b}) T_{\phi_o} S_{\theta_o} - 2I_{xy_b} T_{\phi_o} S_{\phi_o} C_{\theta_o} - I_{xz_b} S_{\phi_o} C_{\theta_o}}{I_{zz_b}}$$

$$\eta_{zz} = A_g \frac{-I_{yz_b} T_{\phi_o} S_{\theta_o} - I_{xz_b} T_{\phi_o} S_{\phi_o} C_{\theta_o}}{I_{zz_b}}$$

$$A_g \equiv \frac{g l_{\text{ref}}}{V_o^2} \qquad A_{x,\mu} \equiv \frac{\rho S_w l_{\text{ref}}}{2W/g} \left(2C_X + C_{X,\mu} + \frac{T_{,V} \cos(\alpha_{T0})}{\frac{1}{2} \rho V_o S_w} \right)$$

$$A_{z,\mu} \equiv \frac{\rho S_w l_{\text{ref}}}{2W/g} \left(2C_Z + C_{Z,\mu} - \frac{T_{,V} \sin(\alpha_{T0})}{\frac{1}{2} \rho V_o S_w} \right)$$

$$A_{m,\mu} \equiv \frac{\rho S_w \bar{c}_w l_{\text{ref}}^2}{2I_{yy_b}} \left(2C_m + C_{m,\mu} + \frac{T_{,V} [z_T \cos(\alpha_{T0}) + x_T \sin(\alpha_{T0})]}{\frac{1}{2} \rho V_o S_w \bar{c}_w} \right)$$

$$A_{x,\alpha} \equiv \frac{\rho S_w l_{\text{ref}}}{2W/g} C_{X,\alpha} \quad A_{z,\alpha} \equiv \frac{\rho S_w l_{\text{ref}}}{2W/g} C_{Z,\alpha} \quad A_{m,\alpha} \equiv \frac{\rho S_w \bar{c}_w l_{\text{ref}}^2}{2I_{yy_b}} C_{m,\alpha}$$

$$A_{y,\beta} \equiv \frac{\rho S_w l_{\text{ref}}}{2W/g} C_{Y,\beta} \quad A_{\ell,\beta} \equiv \frac{\rho S_w b_w l_{\text{ref}}^2}{2I_{xx_b}} C_{\ell,\beta} \quad A_{n,\beta} \equiv \frac{\rho S_w b_w l_{\text{ref}}^2}{2I_{zz_b}} C_{n,\beta}$$

$$A_{\ell,\alpha} \equiv \frac{\rho S_w b_w l_{\text{ref}}^2}{2I_{xx_b}} C_{\ell,\alpha} \quad A_{m,\beta} \equiv \frac{\rho S_w \bar{c}_w l_{\text{ref}}^2}{2I_{yy_b}} C_{m,\beta} \quad A_{n,\alpha} \equiv \frac{\rho S_w b_w l_{\text{ref}}^2}{2I_{zz_b}} C_{n,\alpha}$$

$$A_{y,\bar{p}} \equiv \frac{\rho S_w b_w}{4W/g} C_{Y,\bar{p}} \quad A_{\ell,\bar{p}} \equiv \frac{\rho S_w b_w^2 l_{\text{ref}}}{4I_{xx_b}} C_{\ell,\bar{p}} \quad A_{n,\bar{p}} \equiv \frac{\rho S_w b_w^2 l_{\text{ref}}}{4I_{zz_b}} C_{n,\bar{p}}$$

$$A_{x,\bar{q}} \equiv \frac{\rho S_w \bar{c}_w}{4W/g} C_{X,\bar{q}} \quad A_{z,\bar{q}} \equiv \frac{\rho S_w \bar{c}_w}{4W/g} C_{Z,\bar{q}} \quad A_{m,\bar{q}} \equiv \frac{\rho S_w \bar{c}_w^2 l_{\text{ref}}}{4I_{yy_b}} C_{m,\bar{q}}$$

$$A_{y,\bar{r}} \equiv \frac{\rho S_w b_w}{4W/g} C_{Y,\bar{r}} \quad A_{\ell,\bar{r}} \equiv \frac{\rho S_w b_w^2 l_{\text{ref}}}{4I_{xx_b}} C_{\ell,\bar{r}} \quad A_{n,\bar{r}} \equiv \frac{\rho S_w b_w^2 l_{\text{ref}}}{4I_{zz_b}} C_{n,\bar{r}}$$

$$D_{y,\delta_a} \equiv \frac{\rho S_w l_{\text{ref}}}{2W/g} C_{Y,\delta_a} \quad D_{\ell,\delta_a} \equiv \frac{\rho S_w b_w l_{\text{ref}}^2}{2I_{xx_b}} C_{\ell,\delta_a} \quad D_{n,\delta_a} \equiv \frac{\rho S_w b_w l_{\text{ref}}^2}{2I_{zz_b}} C_{n,\delta_a}$$

$$D_{x,\delta_e} \equiv \frac{\rho S_w l_{\text{ref}}}{2W/g} C_{X,\delta_e} \quad D_{z,\delta_e} \equiv \frac{\rho S_w l_{\text{ref}}}{2W/g} C_{Z,\delta_e} \quad D_{m,\delta_e} \equiv \frac{\rho S_w \bar{c}_w l_{\text{ref}}^2}{2I_{yy_b}} C_{m,\delta_e}$$

$$D_{y,\delta_r} \equiv \frac{\rho S_w l_{\text{ref}}}{2W/g} C_{Y,\delta_r} \quad D_{\ell,\delta_r} \equiv \frac{\rho S_w b_w l_{\text{ref}}^2}{2I_{xx_b}} C_{\ell,\delta_r} \quad D_{n,\delta_r} \equiv \frac{\rho S_w b_w l_{\text{ref}}^2}{2I_{zz_b}} C_{n,\delta_r}$$

Even for the special case of no coupling, Eq. (9.8.20) can be used to obtain the eigenvalues and eigenvectors for both longitudinal and lateral motion. When all the coupling terms are zero, results obtained from Eq. (9.8.20) are identical to those obtained from Eqs. (7.7.5) and (7.7.6). The only advantage to be gained from using Eqs. (7.7.5) and (7.7.6) in place of Eq. (9.8.20) is computational efficiency. Two 6×6 eigenproblems can be numerically solved slightly faster than one 12×12 eigenproblem. However, with the computational hardware and software available today, when solving something as simple as a 12×12 eigenproblem, it typically takes longer to display the results than it does to perform the numerical computations. Thus, with problems of this level of complexity, computation time is no longer an issue. With current computational tools, the advantages of being able to account for inertial, gyroscopic, and aerodynamic coupling, as well as turning flight, far outweigh any computational advantage of using the uncoupled equations for longitudinal and lateral motion. Thus, when developing computer code for today's hardware, it is recommended that Eq. (9.8.20) be used instead of Eqs. (7.7.5) and (7.7.6).

When the longitudinal-lateral coupling terms in Eq. (9.8.20) are present but small, all of the traditional longitudinal and lateral modes are still observed in the solution to the associated eigenproblem. The net effect of a small amount of coupling is to produce

modest changes in the frequencies and damping rates associated with the traditional modes while introducing some lateral motion into the longitudinal modes, and vice versa. This is the case that most accurately describes the majority of conventional airplanes. At least a small amount of longitudinal-lateral coupling is usually present in any aircraft. If the coupling terms in Eq. (9.8.20) are large enough, the interactions between the longitudinal and lateral degrees of freedom can be sufficient to render the traditional longitudinal and lateral modes unrecognizable.

Aerodynamic coupling between the longitudinal and lateral modes is embodied in the linearized formulation through the inclusion of additional aerodynamic derivatives, which were not included in Eqs. (7.7.5) and (7.7.6). In the present formulation three additional aerodynamic derivatives have been included: the change in rolling moment coefficient with angle of attack, $C_{\ell,\alpha}$; the change in yawing moment coefficient with angle of attack, $C_{n,\alpha}$; and the change in pitching moment coefficient with sideslip angle, $C_{m,\beta}$. These three derivatives were included in the present formulation because they are the coupling derivatives that most commonly become significant when an airplane is flown in an asymmetric configuration. This type of aerodynamic coupling is produced by a rotating propeller and can occur whenever an aircraft is flown with an asymmetric distribution of external stores attached to the wings. This is not to say that no other longitudinal-lateral coupling derivatives can ever be significant. Additional aerodynamic coupling derivatives can easily be added to the formulation presented here. Once the first coupling term is included, adding others does not significantly increase the complexity.

Perhaps the most common cause of aerodynamic coupling between the longitudinal and lateral modes is simply a rotating propeller. No propeller-driven aircraft can be truly symmetric unless it has an even number of counterrotating propellers symmetrically distributed in the spanwise direction. An aircraft with a single rotating propeller will always display some degree of aerodynamic coupling between the longitudinal and lateral modes. Recall from Chapter 2 that a rotating propeller produces a yawing moment that is proportional to the propeller angle of attack. In Eq. (5.2.27) we found that the propeller's contribution to the change in airplane yawing moment coefficient with angle of attack can be expressed as

$$\left(\Delta C_{n,\alpha}\right)_p = \frac{2 d_p^3}{S_w b_w} (1 - \varepsilon_{d,\alpha})_p \frac{C_{n_p,\alpha}}{J^2} \tag{9.8.21}$$

Similarly, the propeller also produces a change in the airplane's pitching moment coefficient with sideslip angle, which can be expressed as

$$\left(\Delta C_{m,\beta}\right)_p = \frac{2 d_p^3}{S_w \bar{c}_w} (1 - \varepsilon_{s,\beta})_p \frac{C_{n_p,\alpha}}{J^2} \tag{9.8.22}$$

Before attempting to use Eqs. (9.8.21) and (9.8.22), the reader may wish to review the related material in Chapters 2 and 5. For airplanes with low thrust-to-weight ratio these coupling terms can usually be neglected.

EXAMPLE 9.8.1. The airplane described in Examples 8.2.1 and 9.2.1 is in a steady level coordinated turn at sea level. The airspeed is 180 ft/sec and the bank angle is 60 degrees. Determine the period and damping rate of the dynamic modes for this equilibrium flight condition, neglecting both gyroscopic and aerodynamic coupling. Compare these results with those obtained for steady level flight in Examples 8.2.1 and 9.2.1.

Solution. For this aircraft and a reference state corresponding to steady level flight at sea level, from Example 9.2.1 we have

$$S_w = 185 \text{ ft}^2, \quad b_w = 33 \text{ ft}, \quad W = 2{,}800 \text{ lbf}, \quad V_o = 180 \text{ ft/sec},$$
$$I_{xx_b} = 1{,}000 \text{ slug}\cdot\text{ft}^2, \quad I_{yy_b} = 3{,}000 \text{ slug}\cdot\text{ft}^2, \quad I_{zz_b} = 3{,}500 \text{ slug}\cdot\text{ft}^2,$$
$$I_{xy_b} = 0 \text{ slug}\cdot\text{ft}^2, \quad I_{xz_b} = 30 \text{ slug}\cdot\text{ft}^2, \quad I_{yz_b} = 0 \text{ slug}\cdot\text{ft}^2,$$
$$h_{x_b} = 0 \text{ slug}\cdot\text{ft}^2/\text{sec}, \quad h_{y_b} = 0 \text{ slug}\cdot\text{ft}^2/\text{sec}, \quad h_{z_b} = 0 \text{ slug}\cdot\text{ft}^2/\text{sec},$$
$$C_{Lo} = 0.393, \quad C_{Do} = 0.050, \quad C_{mo} = 0.000,$$
$$C_{L,\hat{\mu}} = 0.000, \quad C_{D,\hat{\mu}} = 0.000, \quad C_{m,\hat{\mu}} = 0.000,$$
$$C_{L,\hat{\alpha}} = 1.600, \quad C_{D,\hat{\alpha}} = 0.000, \quad C_{m,\hat{\alpha}} = -4.350,$$
$$C_{L,\mathrm{M}} = 0.0, \quad C_{D,\mathrm{M}} = 0.0, \quad C_{m,\mathrm{M}} = 0.0,$$
$$C_{L,\alpha} = 4.400, \quad C_{D,\alpha} = 0.350, \quad C_{\ell,\alpha} = 0.0, \quad C_{m,\alpha} = -0.680, \quad C_{n,\alpha} = 0.0,$$
$$C_{Y,\beta} = -0.560, \quad C_{\ell,\beta} = -0.075, \quad C_{m,\beta} = 0.0, \quad C_{n,\beta} = 0.070,$$
$$C_{Y,\bar{p}} = 0.000, \quad C_{\ell,\bar{p}} = -0.410, \quad C_{n,\bar{p}} = -0.0575,$$
$$C_{L,\bar{q}} = 3.800, \quad C_{D,\bar{q}} = 0.000, \quad C_{m,\bar{q}} = -9.950,$$
$$C_{Y,\bar{r}} = 0.240, \quad C_{\ell,\bar{r}} = 0.105, \quad C_{n,\bar{r}} = -0.125$$

At the level-flight reference state, the lift coefficient was found to be

$$(C_L)_{\text{ref}} = \frac{W}{\frac{1}{2}\rho V_{\text{ref}}^2 S_w} = 0.393$$

From Eq. (9.8.10), the lift coefficient in the coordinated turn is

$$C_L = \frac{W\cos\theta_o}{\frac{1}{2}\rho V_o^2 S_w \cos\phi_o} = 0.786 \tag{9.8.23}$$

The drag coefficient can be closely approximated as a linear function of the lift coefficient squared,

$$C_D = C_1 + C_2 C_L^2 \tag{9.8.24}$$

where C_1 and C_2 are constants. Thus, the change in C_D with α is given by

$$C_{D,\alpha} = 2C_2 C_L C_{L,\alpha} \tag{9.8.25}$$

From the known characteristics at the level-flight reference state, Eqs. (9.8.24) and (9.8.25) can be solved for the constants C_1 and C_2:

$$C_1 = \left(C_D - \frac{C_{D,\alpha} C_L}{2C_{L,\alpha}} \right)_{\text{ref}} \qquad C_2 = \left(\frac{C_{D,\alpha}}{2C_L C_{L,\alpha}} \right)_{\text{ref}}$$

Thus, Eqs. (9.8.24) and (9.8.25) can be written as

$$\begin{aligned} C_D &= (C_D)_{\text{ref}} + \left(\frac{C_{D,\alpha} C_L}{2C_{L,\alpha}} \right)_{\text{ref}} \left[\frac{C_L^2}{(C_L)_{\text{ref}}^2} - 1 \right] \\ &= 0.05 + \frac{(0.35)(0.393)}{2(4.40)} \left[\left(\frac{0.786}{0.393} \right)^2 - 1 \right] = 0.097 \end{aligned} \tag{9.8.26}$$

$$C_{D,\alpha} = (C_{D,\alpha})_{\text{ref}} \frac{C_L}{(C_L)_{\text{ref}}} = 0.350 \frac{0.786}{0.393} = 0.700 \tag{9.8.27}$$

and

$$C_{X,\alpha} = C_L - C_{D,\alpha} = 0.786 - 0.700 = 0.086$$

$$C_{Z,\alpha} = -C_{L,\alpha} - C_D = -4.400 - 0.097 = -4.497$$

Assuming constant lift slope, the increase in angle of attack between the level-flight reference state and the coordinated turn is

$$\Delta\alpha = \frac{C_L - (C_L)_{\text{ref}}}{C_{L,\alpha}} = \frac{0.786 - 0.393}{4.40} = 0.08932 = 5.118^\circ$$

Using the results presented in Sec. 7.8, the stability derivatives can be transformed from the stability axis for level flight to the stability axis for the coordinated turn. It should be pointed out that the lift and drag do not need to be transformed, since the required transformation is already included in Eqs. (9.8.23), (9.8.26), and (9.8.27). This is due to the fact that lift and drag are defined relative to the direction of motion. For this transformation

$$\varphi = -\Delta\alpha = -0.08932 = -5.118^\circ$$

and, after performing the required transformation, the aircraft characteristics for the coordinated turn are found to be

$$I_{xx_b} = 1{,}015 \text{ slug}\cdot\text{ft}^2, \quad I_{yy_b} = 3{,}000 \text{ slug}\cdot\text{ft}^2, \quad I_{zz_b} = 3{,}485 \text{ slug}\cdot\text{ft}^2,$$
$$I_{xy_b} = 0 \text{ slug}\cdot\text{ft}^2, \quad I_{xz_b} = -193 \text{ slug}\cdot\text{ft}^2, \quad I_{yz_b} = 0 \text{ slug}\cdot\text{ft}^2,$$
$$h_{x_b} = 0 \text{ slug}\cdot\text{ft}^2/\text{sec}, \quad h_{y_b} = 0 \text{ slug}\cdot\text{ft}^2/\text{sec}, \quad h_{z_b} = 0 \text{ slug}\cdot\text{ft}^2/\text{sec},$$
$$C_{Xo} = -0.097, \quad C_{Zo} = -0.786, \quad C_{mo} = 0.000,$$
$$C_{X,\hat{\mu}} = -0.013, \quad C_{Z,\hat{\mu}} = -0.142, \quad C_{m,\hat{\mu}} = -0.388,$$
$$C_{X,\hat{\alpha}} = -0.142, \quad C_{Z,\hat{\alpha}} = -1.587, \quad C_{m,\hat{\alpha}} = -4.333,$$
$$C_{X,\mu} = 0.0, \quad C_{Z,\mu} = 0.0, \quad C_{m,\mu} = 0.0,$$
$$C_{X,\alpha} = 0.086, \quad C_{Z,\alpha} = -4.497, \quad C_{\ell,\alpha} = 0.0, \quad C_{m,\alpha} = -0.677, \quad C_{n,\alpha} = 0.0,$$
$$C_{Y,\beta} = -0.560, \quad C_{\ell,\beta} = -0.0685, \quad C_{m,\beta} = 0.0, \quad C_{n,\beta} = 0.0764,$$
$$C_{Y,\bar{p}} = 0.0214, \quad C_{\ell,\bar{p}} = -0.4035, \quad C_{n,\bar{p}} = -0.0326,$$
$$C_{X,\bar{q}} = -0.339, \quad C_{Z,\bar{q}} = -3.785, \quad C_{m,\bar{q}} = -9.950,$$
$$C_{Y,\bar{r}} = 0.239, \quad C_{\ell,\bar{r}} = 0.130, \quad C_{n,\bar{r}} = -0.131$$

Choosing the reference length to be the square root of the wing area, $l_{\text{ref}} = 13.6$ ft, the nondimensional [**A**] and [**B**] matrices are, respectively,

$$\begin{bmatrix}
-0.0067 & 0.0117 & -0.0173 & 0.0000 & -0.0024 & 0.0000 & 0.0000 & 0.0000 & 0.0000 & 0.0000 & -0.0135 & 0.0000 \\
-0.0117 & -0.0192 & 0.0000 & 0.0009 & 0.0000 & -0.9900 & 0.0000 & 0.0000 & 0.0000 & 0.0068 & 0.0000 & 0.0000 \\
-0.0338 & 0.0000 & -0.1545 & 0.0000 & 0.9732 & 0.0000 & 0.0000 & 0.0000 & 0.0000 & -0.0117 & 0.0000 & 0.0000 \\
0.0000 & -0.0905 & 0.0000 & -0.6514 & -0.0056 & 0.1988 & 0.0000 & 0.0000 & 0.0000 & 0.0000 & 0.0000 & 0.0000 \\
0.0000 & 0.0000 & -0.0515 & 0.0096 & -0.1558 & -0.0015 & 0.0000 & 0.0000 & 0.0000 & 0.0000 & 0.0000 & 0.0000 \\
0.0000 & 0.0294 & 0.0000 & -0.0267 & 0.0006 & -0.0603 & 0.0000 & 0.0000 & 0.0000 & 0.0000 & 0.0000 & 0.0000 \\
1.0000 & 0.0000 & 0.0000 & 0.0000 & 0.0000 & 0.0000 & 0.0000 & 0.0000 & 0.0000 & 0.0000 & 0.0000 & 0.0000 \\
0.0000 & 0.5000 & -0.8660 & 0.0000 & 0.0000 & 0.0000 & 0.0000 & 0.0000 & 0.0000 & 0.0000 & 0.0000 & 1.0000 \\
0.0000 & 0.8660 & 0.5000 & 0.0000 & 0.0000 & 0.0000 & 0.0000 & 0.0000 & 0.0000 & 0.0000 & -1.0000 & 0.0000 \\
0.0000 & 0.0000 & 0.0000 & 1.0000 & 0.0000 & 0.0000 & 0.0000 & 0.0000 & 0.0000 & 0.0000 & 0.0234 & 0.0000 \\
0.0000 & 0.0000 & 0.0000 & 0.0000 & 0.5000 & -0.8660 & 0.0000 & 0.0000 & 0.0000 & -0.0234 & 0.0000 & 0.0000 \\
0.0000 & 0.0000 & 0.0000 & 0.0000 & 0.8660 & 0.5000 & 0.0000 & 0.0000 & 0.0000 & 0.0000 & 0.0000 & 0.0000
\end{bmatrix}$$

$$\begin{bmatrix}
1.0001 & 0.0000 & 0.0010 & 0.0000 & 0.0000 & 0.0000 & 0.0000 & 0.0000 & 0.0000 & 0.0000 & 0.0000 & 0.0000 \\
0.0000 & 1.0000 & 0.0000 & 0.0000 & 0.0000 & 0.0000 & 0.0000 & 0.0000 & 0.0000 & 0.0000 & 0.0000 & 0.0000 \\
0.0010 & 0.0000 & 1.0112 & 0.0000 & 0.0000 & 0.0000 & 0.0000 & 0.0000 & 0.0000 & 0.0000 & 0.0000 & 0.0000 \\
0.0000 & 0.0000 & 0.0000 & 1.0000 & 0.0000 & 0.1899 & 0.0000 & 0.0000 & 0.0000 & 0.0000 & 0.0000 & 0.0000 \\
0.0061 & 0.0000 & 0.0679 & 0.0000 & 1.0000 & 0.0000 & 0.0000 & 0.0000 & 0.0000 & 0.0000 & 0.0000 & 0.0000 \\
0.0000 & 0.0000 & 0.0000 & 0.0553 & 0.0000 & 1.0000 & 0.0000 & 0.0000 & 0.0000 & 0.0000 & 0.0000 & 0.0000 \\
0.0000 & 0.0000 & 0.0000 & 0.0000 & 0.0000 & 0.0000 & 1.0000 & 0.0000 & 0.0000 & 0.0000 & 0.0000 & 0.0000 \\
0.0000 & 0.0000 & 0.0000 & 0.0000 & 0.0000 & 0.0000 & 0.0000 & 1.0000 & 0.0000 & 0.0000 & 0.0000 & 0.0000 \\
0.0000 & 0.0000 & 0.0000 & 0.0000 & 0.0000 & 0.0000 & 0.0000 & 0.0000 & 1.0000 & 0.0000 & 0.0000 & 0.0000 \\
0.0000 & 0.0000 & 0.0000 & 0.0000 & 0.0000 & 0.0000 & 0.0000 & 0.0000 & 0.0000 & 1.0000 & 0.0000 & 0.0000 \\
0.0000 & 0.0000 & 0.0000 & 0.0000 & 0.0000 & 0.0000 & 0.0000 & 0.0000 & 0.0000 & 0.0000 & 1.0000 & 0.0000 \\
0.0000 & 0.0000 & 0.0000 & 0.0000 & 0.0000 & 0.0000 & 0.0000 & 0.0000 & 0.0000 & 0.0000 & 0.0000 & 1.0000
\end{bmatrix}$$

Using a numerical eigensolver to obtain the eigenvalues associated with this generalized eigenproblem, the dimensionless phugoid eigenvalues are found to be $\lambda = -0.000556 \pm 0.029026i$. Thus, for the phugoid we have

$$\sigma = -\text{real}(\lambda)\frac{V_o}{l_{\text{ref}}} = 0.000556\frac{180}{13.6} = 0.00736\,\text{sec}^{-1}$$

$$\omega_d = \left|\text{imag}(\lambda)\right|\frac{V_o}{l_{\text{ref}}} = 0.029026\frac{180}{13.6} = 0.384\,\text{sec}^{-1}$$

Similarly, for the other modes

	60° Bank Angle		Level Flight	
Mode	Period (sec)	Damping Rate (sec^{-1})	Period (sec)	Damping Rate (sec^{-1})
Short-period	2.44	2.48	2.42	2.47
Phugoid	16.4	0.0074	29.9	0.0169
Roll	∞	8.67	∞	8.88
Spiral	∞	0.0488	∞	0.0100
Dutch roll	2.61	0.591	2.64	0.482

From these results we see that turning flight and longitudinal-lateral coupling can have a significant effect on aircraft dynamics. For the conventional airplane used in this example, there is nothing too detrimental in the observed changes. However, for some aircraft configurations, longitudinal-lateral coupling has proven more deleterious.

9.9. Nonlinear Effects

Here again it is emphasized that the linearized analysis used in this and Chapter 8 is based on the assumption of small deviations from equilibrium flight. The linearized aerodynamic model provides a good approximation for most flight conditions when the angular rates and aerodynamic angles are small. However, many of the maneuvers executed by modern fighter aircraft and stunt planes involve high angular rates and/or large angles of attack that sometimes approach 90 degrees. Such maneuvers can produce important dynamic effects that are not predicted by linear theory. A few of these are mentioned here.

Inertial Pitch and Yaw Divergence in Roll Maneuvers

When the angular rates are large, nonlinear inertial coupling is introduced between the longitudinal and lateral degrees of freedom. This nonlinear coupling results from the product terms seen on the right-hand side of Eqs. (9.8.1) and (9.8.2). As mentioned in Sec. 7.9, the most problematic nonlinear inertial coupling results from the terms $(I_{zz_b} - I_{xx_b})pr$ and $(I_{xx_b} - I_{yy_b})pq$, which occur in the pitching and yawing momentum equations, respectively. For long slender aircraft undergoing rapid roll maneuvers, this nonlinear coupling can produce changes in angle of attack and sideslip angle that are

large enough to cause pitch and/or yaw divergence, which can result in complete control loss or even structural failure. This problem is often aggravated by the fact that to improve maneuverability, modern fighters have reduced pitch stability.

The dynamic effects of nonlinear inertial coupling were not understood or even encountered until late in World War II. On December 10, 1944, the German He-162 prototype jet fighter disintegrated during a high-speed roll maneuver just four days after its maiden flight. In spite of the fact that the incident was well recorded on film, the response of the aircraft could not be explained based on the knowledge of flight dynamics available at that time. It was not until several years later that the cause of this and other similar incidents was understood. This behavior cannot be predicted using the linearized theory presented in this chapter. To analyze such motion we must utilize the fully coupled nonlinear equations of motion.

Aerodynamic Yaw Departure at High Angles of Attack

Maneuvers involving large aerodynamic angles produce strong nonlinearity in the aerodynamic forces and moments as a result of flow separation. This flow separation can also produce nonlinear coupling between the longitudinal and lateral degrees of freedom. For example, at high angles of attack, the flow around an airplane's fuselage will separate. Separated flow around a slender body at high angles of attack can result in stable forebody vortices that are shed near the nose. As the angle of attack for a slender body is increased slightly beyond the point of separation, the cross flow generates a pair of stable symmetric vortices, as shown in Fig.9.9.1. As the angle of attack continues to

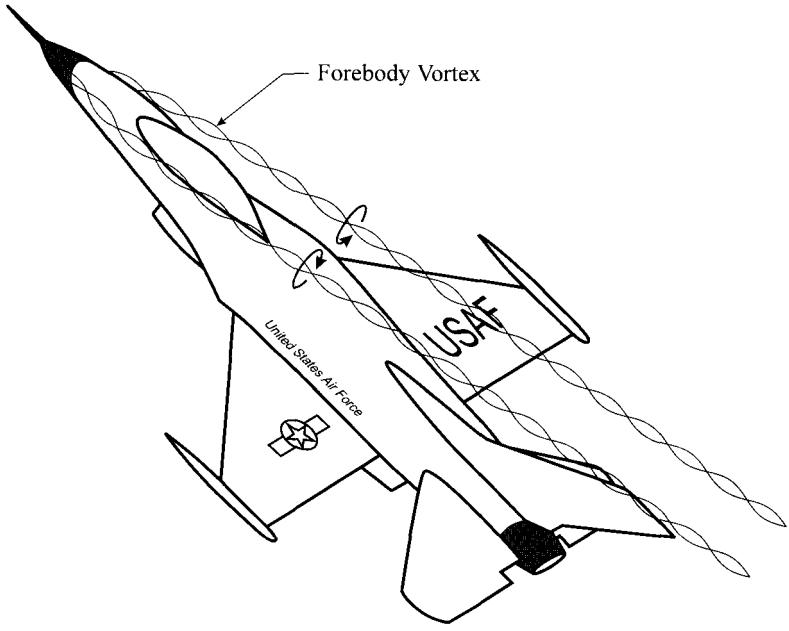


Figure 9.9.1. Forebody vortices shed from a slender fuselage at high angle of attack.

increase somewhat beyond the point of initial separation, the normal force increases nonlinearly as a result of vortex lift. At angles of attack that are only slightly above the separation point, the stable vortex pair remains symmetric and no side force is generated without sideslip. As the angle of attack is increased even further, the axial flow component remains sufficient to maintain stable vortex shedding, but the vortex pair becomes asymmetric. This can produce a large side force, even in the absence of sideslip. Since the vortex pair is shed far forward from the center of gravity, this side force also produces a strong yawing moment. The interaction of these asymmetric vortices with the wing and tail can also produce a rolling moment. At even higher angles of attack, the axial flow component is no longer adequate to maintain the stable vortex pair and the flow again becomes symmetric, as a vortex wake forms over the entire leeward side of the fuselage. At the angles of attack that produce the greatest vortex-induced yawing moment, yaw control can be drastically reduced as well, because the rudder is typically shadowed by the wake of the fuselage and wing. The problem can be reduced or eliminated with nose strakes or other reshaping that promotes symmetric vortex shedding. Clearly, the nonlinear dynamics of such high angle of attack flight cannot be studied using the method presented in this and Chapter 8.

Wing Rock

The nonlinear aerodynamics associated with high angle of attack flight can also produce dynamic oscillations that are not predicted by linear theory. One of the most common phenomena of this type is called *wing rock*. As the name implies, wing rock is an oscillatory motion, predominantly in roll. However, the motion can be very complex and typically involves several degrees of freedom. Any aircraft with highly swept wings and/or a long slender forebody is usually susceptible to wing rock at high angles of attack.

When such an aircraft is exposed to high angles of attack, a very complex vortex flow-field develops, as shown in Fig. 9.9.2. The interactions of the vortex wakes with

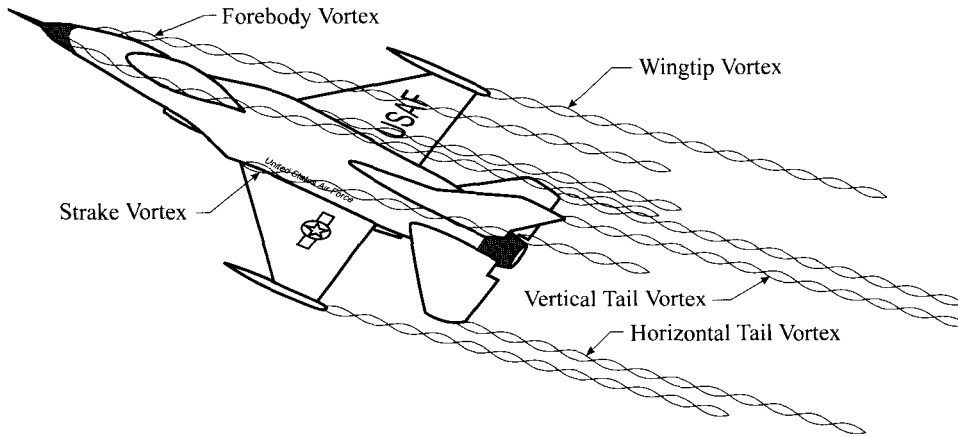


Figure 9.9.2. High angle of attack vortex wakes shed from a typical fighter aircraft.

the wing and tail can cause the aerodynamic derivatives to change very dramatically with angle of attack. For example, Fig. 9.9.3 shows how the roll-damping derivative might vary with angle of attack for a typical jet fighter. Notice that at certain angles of attack, the roll-damping derivative is positive. For angles of attack in this range, a disturbance in rolling rate produces a rolling moment in the same direction as the roll rather than opposing it. This destabilizing phenomenon results from the fact that the lift slope for the wing is negative beyond stall. At higher angles of attack the roll-damping derivative again becomes negative, because the effect of wing drag on roll damping overpowers the effect of wing lift.

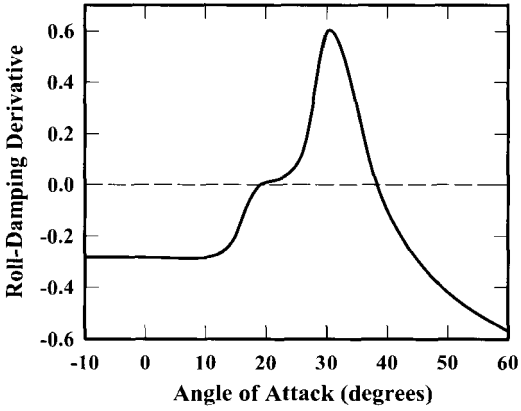


Figure 9.9.3. Loss of roll damping at high angles of attack for a typical fighter aircraft.

The presence of vortex wakes at high angles of attack also introduces aerodynamic hysteresis in the forces and moments produced on the aircraft. For example, the forebody vortices influence the forces and moments developed on the wing and tail. However, since the vortex wake is convected relative to the aircraft by the freestream, the airflow around the tail at any given instant in time depends on the motion history and vortex development as well as the instantaneous airspeed and aerodynamic angles. The vortex-induced forces and moments developed on the vertical tail depend not only on the instantaneous angle of attack, but also on the angle of attack history and the time required for the vortex wake to be transported from the nose to the tail.

The genesis of wing rock is related directly to nonlinearities and hysteresis in the aerodynamic forces and moments acting on an aircraft at high angles of attack. Oscillations that occur as a result of such nonlinear behavior can be quite different in character from those associated with the classical modes of linear dynamics. The amplitude for any classical oscillatory mode will always change exponentially with time if uncontrolled. If the mode is convergent, the amplitude of oscillation will decay exponentially to zero. If the mode is divergent, the uncontrolled oscillation will grow exponentially without limit. However, as the oscillations associated with wing rock begin to develop, the amplitude grows with an increasing rate and the frequency

decreases. After a time, the rate of amplitude growth begins to decrease and the amplitude eventually approaches a steady-state value. From this point on, the oscillations continue at constant amplitude and frequency, unless controlled in some manner. This type of motion, which is shown in Fig. 9.9.4, is called *limit-cycle oscillation.*

Since high angle of attack hysteresis and nonlinearities are the direct cause of wing rock, this and similar phenomena cannot be predicted from linear theory. To study such phenomena, we must turn to experimental methods or numerical flight simulation using the complete nonlinear equations of motion, including a model for the unsteady aerodynamics. Numerical flight simulation is treated in Chapter 11.

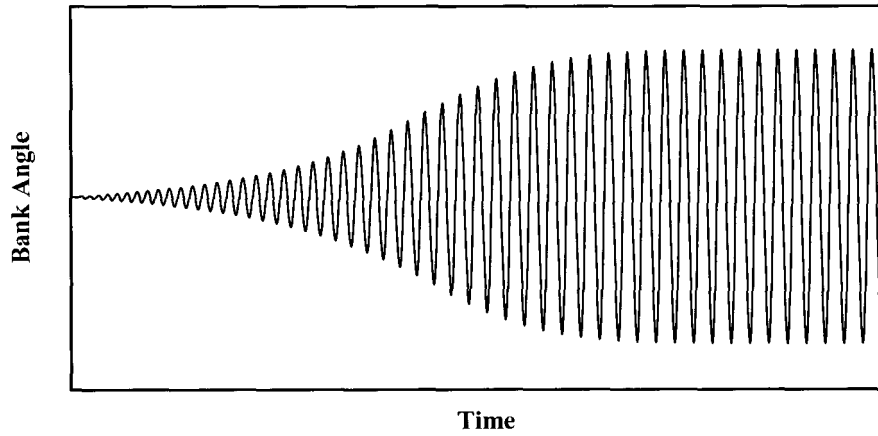


Figure 9.9.4. Limit-cycle oscillations in bank angle associated with wing rock.

9.10. Summary

In this chapter we have examined the stick-fixed lateral dynamics of an aircraft, based on the linearized rigid-body equations of motion. As was the case for longitudinal motion, the linearized lateral equations have four nonzero eigenvalues. These typically consist of one pair of distinct real eigenvalues and one complex pair. The real eigenvalues correspond to two nonoscillatory modes, the roll mode and the spiral mode. The complex pair describes an oscillatory mode called Dutch roll. For a conventional fixed-wing airplane, the roll mode is very heavily damped, with a 99 percent damping time on the order of 1 second. The spiral mode is very slowly convergent or even slightly divergent and is characterized by changes in heading and direction of travel. Even when the spiral mode is convergent, the 99 percent damping time is on the order of several minutes or longer. For an aircraft with very little wing area, the roll and spiral modes can combine to produce a long-period lateral oscillation. Dutch roll is a damped oscillatory motion that involves an out-of-phase combination of sideslip, roll, and yaw. The period for Dutch roll is typically on the order of 2 to 10 seconds, with a 99 percent damping time of 10 seconds or longer. Dutch roll is typically the most troublesome of the dynamic modes for a conventional airplane.

The reason that Dutch roll can sometimes be troublesome is because the quarter-period of oscillation is typically quite close to the response time of a human pilot, and Dutch roll is often lightly damped. The natural response of most pilots to a disturbance that causes one wing to drop is initiation of an aileron input to bring the low wing back up. However, there is always some delay between the time of the disturbance and the time of the control input, because it takes a finite length of time for the pilot to recognize the disturbance and respond. If the disturbance is periodic in nature and the quarter-period of oscillation is equal to or slightly less than the pilot's response time, then the control input to raise the low wing comes not as the wing is falling but as the wing is rising. This means that the pilot's control input will actually be applied in the direction of motion and not in the opposing direction, as the pilot intended. This control input can still feel correct to the pilot, because the aileron input to raise the low wing comes near the time when the wing is at its lowest point and the aircraft seems to respond correctly to the control input as the low wing begins to rise. However, such pilot response will actually amplify the oscillations of the airplane. This is much like pushing a child in a swing. If the push comes at or slightly after the swing reaches the apex of oscillation, the amplitude will increase. On the other hand, if the push comes just prior to the apex, the oscillation of the swing will quickly cease. In both cases the push is in a direction that returns the swing toward its equilibrium position, but the response is very different, depending on the timing.

The suitability of this analogy is demonstrated by an experience that was related to the author by Dr. Frank Redd. In the early 1960s Frank was flying KC-135s for the U.S. Air Force. Early models of the KC-135 had very light Dutch roll damping, when the yaw damper was not functioning for some reason. Since the yaw damper could be damaged and become inoperative, it was important for pilots to learn to control the aircraft with the yaw damper disengaged. For safety sake, this was done at altitude. With few exceptions, when pilots first tried to fly the KC-135 with the yaw damper disengaged, they only succeeded in aggravating the Dutch roll. To suppress the Dutch roll oscillations rather than aggravate them, a pilot needs to supply out-of-phase control inputs rather than the in-phase control inputs that result from doing what at first seems natural. One way to achieve the desired result would be to shorten pilot reaction time. However, there are human limits that place constraints on what can be done in this regard. Another option is to keep the reaction time constant, but supply the opposite control input. While this control strategy seemed counterintuitive at first, with a little practice, most pilots were able to reprogram their reflexes and compensate successfully for the disengaged yaw damper.

From this example and the analogy with pushing a child in a swing, we can see that the dynamic response of an airplane can be very closely coupled to the reaction time of the pilot, and human reaction times are widely varied. For example, a Dutch roll mode that would be totally unacceptable to one pilot might be only mildly annoying to a second pilot and go unnoticed by a third.

Because of their tailless design, hang gliders often have light Dutch roll damping. In these tiny aircraft, Dutch roll oscillations have sometimes been referred to as *pilot-induced oscillations* (PIOs). There have been many heated arguments about whether these oscillations are caused by the aircraft or the pilot. For example, Dick flies glider A

on several occasions and observes lateral oscillations on each flight. Jane, who has also flown glider A many times, has never observed such oscillations. Jane tells Dick that there is absolutely nothing wrong with the glider and that the oscillations must be entirely pilot induced, since she has never observed these oscillations while flying the same glider. The counterargument made by Dick is that the oscillations cannot possibly be pilot induced since he has flown glider B for many hours and has never observed any lateral oscillations in that glider. Thus, Dick strongly argues that he is not causing these oscillations, so they must be inherent in the aircraft. Both pilots have a strong argument from their own frame of reference, and the conflict is never resolved. The truth is that both pilots are right and both pilots are wrong. The Dutch roll oscillations are inherent in the aircraft and Dick is exciting this natural frequency with the timing of his control inputs. Most likely, Jane has a faster reaction time than Dick and is thus able to instinctively suppress the Dutch roll without even being aware of its existence.

The dynamic interaction between an aircraft and its human pilot can be a very important consideration in aircraft design. In this chapter and in Chapter 8 we confined our study of aircraft dynamics to the stick-fixed dynamic response of an aircraft to small disturbances from equilibrium flight. In so doing we have removed the pilot from the equation. To continue to ignore the pilot's influence on the human-machine system that constitutes a modern airplane would be ill advised. This is the topic of Chapter 10.

9.11 Problems

9.1. For the large jet transport and flight conditions in problem 7.34, find the eigenvalues, the eigenvectors, the damping rate, the 99 percent damping time, and the damped natural frequency and period, if underdamped, for each lateral mode. For each pair of eigenvalues, find the undamped natural frequency and the damping ratio. Compute the amplitude and phase for each component of the eigenvectors associated with the oscillatory mode.

9.2. To improve the Dutch roll characteristics, the large jet transport in problem 9.1 is to be fitted with a feedback control system to provide additional yaw damping. For the flight conditions used in problem 9.1, find the yaw-damping ratio, $R_{n,\bar{r}}$, necessary to make the Dutch roll damping rate equal to 0.35 sec^{-1}. Repeat all calculations in problem 9.1 for the modified airplane.

9.3. For the large jet transport and flight conditions in problem 7.34, using the roll mode eigenvalue approximation given by Eq. (9.3.3), find the eigenvalue and the 99 percent damping time for the roll mode. Compare this approximate result with the fully coupled roll mode solution that was obtained in problem 9.1.

9.4. For the large jet transport and flight conditions in problem 7.34, using the roll mode eigenvector approximation given by Eq. (9.3.6), find the eigenvector for the roll mode. Normalize this eigenvector according to Eq. (8.1.37). Compare this approximate eigenvector with the fully coupled roll mode solution that was obtained in problem 9.1.

9.5. For the large jet transport and flight conditions in problem 7.34, using the spiral mode eigenvalue approximation given by Eq. (9.4.3), find the eigenvalue and the 99 percent damping time for the spiral mode. Compare this approximate result with the fully coupled spiral mode solution that was obtained in problem 9.1.

9.6. For the large jet transport and flight conditions in problem 7.34, using the spiral mode eigenvector approximation given by Eq. (9.4.4), find the eigenvector for the spiral mode. Normalize this eigenvector according to Eq. (8.1.37). Compare this approximate eigenvector with the fully coupled spiral solution that was obtained in problem 9.1.

9.7. For the large jet transport and flight conditions in problem 7.34, using the spiral mode eigenvalue approximation given by Eq. (9.4.11), find the eigenvalue and the 99 percent damping time for the spiral mode. Compare this approximate result with the fully coupled spiral mode solution obtained in problem 9.1.

9.8. For the large jet transport and flight conditions in problem 7.34, using the spiral mode eigenvector approximation given by Eq. (9.4.10), find the eigenvector for the spiral mode. Normalize this eigenvector according to Eq. (8.1.37). Compare this approximate eigenvector with the fully coupled spiral solution that was obtained in problem 9.1.

9.9. For the large jet transport and flight conditions in problem 7.34, using the Dutch roll eigenvalue approximation given by Eq. (9.5.5), find the eigenvalues, the 99 percent damping time, and the period for the Dutch roll mode. Compare these approximate results with the fully coupled Dutch roll solution that was obtained in problem 9.1.

9.10. For the large jet transport and flight conditions in problem 7.34, using the Dutch roll eigenvector approximation given by Eq. (9.5.3), find the eigenvectors for the Dutch roll mode. Normalize these eigenvectors according to Eq. (8.1.37). Compare these approximate eigenvectors with the fully coupled Dutch roll solution that was obtained in problem 9.1.

9.11. For the large jet transport and flight conditions in problem 7.34, using the Dutch roll eigenvalue approximation given by Eq. (9.5.27), find the eigenvalues, the 99 percent damping time, and the period for the Dutch roll mode. Compare these approximate results with the fully coupled Dutch roll solution that was obtained in problem 9.1.

9.12. For the large jet transport and flight conditions in problem 7.34, using the Dutch roll eigenvector approximation given by Eq. (9.5.11), find the eigenvectors for the Dutch roll mode. Normalize these eigenvectors according to Eq. (8.1.37). Compare these approximate eigenvectors with the fully coupled Dutch roll solution that was obtained in problem 9.1.

9.13. For the Spitfire Mark XVIII in problems 7.36 and 7.39, find the eigenvalues, the eigenvectors, the damping rate, the 99 percent damping time, and the damped natural frequency and period, if underdamped, for each lateral mode. For each pair of eigenvalues, find the undamped natural frequency and the damping ratio. Compute the amplitude and phase for each component of the eigenvectors associated with the oscillatory mode.

9.14. For the Spitfire Mark XVIII in problems 7.36 and 7.39, using the roll mode eigenvalue approximation given by Eq. (9.3.3), find the eigenvalue and the 99% damping time for the roll mode. Compare this approximate result with the fully coupled roll mode solution that was obtained in problem 9.13.

9.15. For the Spitfire Mark XVIII in problems 7.36 and 7.39, using the roll mode eigenvector approximation given by Eq. (9.3.6), find the eigenvector for the roll mode. Normalize this eigenvector according to Eq. (8.1.37). Compare this approximate eigenvector with the fully coupled roll mode solution that was obtained in problem 9.13.

9.16. For the Spitfire Mark XVIII in problems 7.36 and 7.39, using the spiral mode eigenvalue approximation given by Eq. (9.4.3), find the eigenvalue and the 99 percent damping time for the spiral mode. Compare this approximate result with the fully coupled spiral mode solution that was obtained in problem 9.13.

9.17. For the Spitfire Mark XVIII in problems 7.36 and 7.39, using the spiral mode eigenvector approximation given by Eq. (9.4.4), find the eigenvector for the spiral mode. Normalize this eigenvector according to Eq. (8.1.37). Compare this approximate eigenvector with the fully coupled spiral solution that was obtained in problem 9.13.

9.18. For the Spitfire Mark XVIII in problems 7.36 and 7.39, using the spiral mode eigenvalue approximation given by Eq. (9.4.11), find the eigenvalue and the 99 percent damping time for the spiral mode. Compare this approximate result with the fully coupled spiral mode solution that was obtained in problem 9.13.

9.19. For the Spitfire Mark XVIII in problems 7.36 and 7.39, using the spiral mode eigenvector approximation given by Eq. (9.4.10), find the eigenvector for the spiral mode. Normalize this eigenvector according to Eq. (8.1.37). Compare this approximate eigenvector with the fully coupled spiral solution that was obtained in problem 9.13.

9.20. For the Spitfire Mark XVIII in problems 7.36 and 7.39, using the Dutch roll eigenvalue approximation given by Eq. (9.5.5), find the eigenvalues, the 99 percent damping time, and the period for the Dutch roll mode. Compare these approximate results with the fully coupled Dutch roll solution that was obtained in problem 9.13.

9.21. For the Spitfire Mark XVIII in problems 7.36 and 7.39, using the Dutch roll eigenvector approximation given by Eq. (9.5.3), find the eigenvectors for the Dutch roll mode. Normalize these eigenvectors according to Eq. (8.1.37). Compare these approximate eigenvectors with the fully coupled Dutch roll solution that was obtained in problem 9.13.

9.22. For the Spitfire Mark XVIII in problems 7.36 and 7.39, using the Dutch roll eigenvalue approximation given by Eq. (9.5.27), find the eigenvalues, the 99 percent damping time, and the period for the Dutch roll mode. Compare these approximate results with the fully coupled Dutch roll solution that was obtained in problem 9.13.

9.23. For the Spitfire Mark XVIII in problems 7.36 and 7.39, using the Dutch roll eigenvector approximation given by Eq. (9.5.11), find the eigenvectors for the Dutch roll mode. Normalize these eigenvectors according to Eq. (8.1.37). Compare these approximate eigenvectors with the fully coupled Dutch roll solution that was obtained in problem 9.13.

9.24. For the small jet transport in problems 7.37 and 7.40, find the eigenvalues, the eigenvectors, the damping rate, the 99 percent damping time, and the damped natural frequency and period, if underdamped, for each lateral mode. For each pair of eigenvalues, find the undamped natural frequency and the damping ratio. Compute the amplitude and phase for each component of the eigenvectors associated with the oscillatory mode.

9.25. For the small jet transport in problems 7.37 and 7.40, using the roll mode eigenvalue approximation given by Eq. (9.3.3), find the eigenvalue and the 99 percent damping time for the roll mode. Compare this approximate result with the fully coupled roll mode solution that was obtained in problem 9.24.

9.26. For the small jet transport in problems 7.37 and 7.40, using the roll mode eigenvector approximation given by Eq. (9.3.6), find the eigenvector for the roll mode. Normalize this eigenvector according to Eq. (8.1.37). Compare this approximate eigenvector with the fully coupled roll mode solution that was obtained in problem 9.24.

9.27. For the small jet transport in problems 7.37 and 7.40, using the spiral mode eigenvalue approximation given by Eq. (9.4.3), find the eigenvalue and the 99 percent damping time for the spiral mode. Compare this approximate result with the fully coupled spiral mode solution that was obtained in problem 9.24.

9.28. For the small jet transport in problems 7.37 and 7.40, using the spiral mode eigenvector approximation given by Eq. (9.4.4), find the eigenvector for the spiral mode. Normalize this eigenvector according to Eq. (8.1.37). Compare this approximate eigenvector with the fully coupled spiral solution that was obtained in problem 9.24.

9.29. For the small jet transport in problems 7.37 and 7.40, using the spiral mode eigenvalue approximation given by Eq. (9.4.11), find the eigenvalue and the 99 percent damping time for the spiral mode. Compare this approximate result with the fully coupled spiral mode solution that was obtained in problem 9.24.

9.30. For the small jet transport in problems 7.37 and 7.40, using the spiral mode eigenvector approximation given by Eq. (9.4.10), find the eigenvector for the spiral mode. Normalize this eigenvector according to Eq. (8.1.37). Compare this approximate eigenvector with the fully coupled spiral solution that was obtained in problem 9.24.

9.31. For the small jet transport in problems 7.37 and 7.40, using the Dutch roll eigenvalue approximation given by Eq. (9.5.5), find the eigenvalues, the 99 percent damping time, and the period for the Dutch roll mode. Compare these approximate results with the fully coupled Dutch roll solution that was obtained in problem 9.24.

9.32. For the small jet transport in problems 7.37 and 7.40, using the Dutch roll eigenvector approximation given by Eq. (9.5.3), find the eigenvectors for the Dutch roll mode. Normalize these eigenvectors according to Eq. (8.1.37). Compare these approximate eigenvectors with the fully coupled Dutch roll solution that was obtained in problem 9.24.

9.33. For the small jet transport in problems 7.37 and 7.40, using the Dutch roll eigenvalue approximation given by Eq. (9.5.27), find the eigenvalues, the 99 percent damping time, and the period for the Dutch roll mode. Compare these approximate results with the fully coupled Dutch roll solution that was obtained in problem 9.24.

9.34. For the small jet transport in problems 7.37 and 7.40, using the Dutch roll eigenvector approximation given by Eq. (9.5.11), find the eigenvectors for the Dutch roll mode. Normalize these eigenvectors according to Eq. (8.1.37). Compare these approximate eigenvectors with the fully coupled Dutch roll solution that was obtained in problem 9.24.

9.35. For the turboprop transport in problems 7.38 and 7.41, find the eigenvalues, the eigenvectors, the damping rate, the 99 percent damping time, and the damped natural frequency and period, if underdamped, for each lateral mode. For each pair of eigenvalues, find the undamped natural frequency and the damping ratio. Compute the amplitude and phase for each component of the eigenvectors associated with the oscillatory mode.

9.36. For the turboprop transport in problems 7.38 and 7.41, using the roll mode eigenvalue approximation given by Eq. (9.3.3), find the eigenvalue and the 99 percent damping time for the roll mode. Compare this approximate result with the fully coupled roll mode solution that was obtained in problem 9.35.

9.37. For the turboprop transport in problems 7.38 and 7.41, using the roll mode eigenvector approximation given by Eq. (9.3.6), find the eigenvector for the roll mode. Normalize this eigenvector according to Eq. (8.1.37). Compare this approximate eigenvector with the fully coupled roll mode solution that was obtained in problem 9.35.

9.38. For the turboprop transport in problems 7.38 and 7.41, using the spiral mode eigenvalue approximation given by Eq. (9.4.3), find the eigenvalue and the 99 percent damping time for the spiral mode. Compare this approximate result with the fully coupled spiral mode solution that was obtained in problem 9.35.

9.39. For the turboprop transport in problems 7.38 and 7.41, using the spiral mode eigenvector approximation given by Eq. (9.4.4), find the eigenvector for the spiral mode. Normalize this eigenvector according to Eq. (8.1.37). Compare this approximate eigenvector with the fully coupled spiral solution that was obtained in problem 9.35.

9.40. For the turboprop transport in problems 7.38 and 7.41, using the spiral mode eigenvalue approximation given by Eq. (9.4.11), find the eigenvalue and the 99 percent damping time for the spiral mode. Compare this approximate result with the fully coupled spiral mode solution that was obtained in problem 9.35.

9.41. For the turboprop transport in problems 7.38 and 7.41, using the spiral mode eigenvector approximation given by Eq. (9.4.10), find the eigenvector for the spiral mode. Normalize this eigenvector according to Eq. (8.1.37). Compare this approximate eigenvector with the fully coupled spiral solution that was obtained in problem 9.35.

9.42. For the turboprop transport in problems 7.38 and 7.41, using the Dutch roll eigenvalue approximation given by Eq. (9.5.5), find the eigenvalues, the 99 percent damping time, and the period for the Dutch roll mode. Compare these approximate results with the fully coupled Dutch roll solution that was obtained in problem 9.35.

9.43. For the turboprop transport in problems 7.38 and 7.41, using the Dutch roll eigenvector approximation given by Eq. (9.5.3), find the eigenvectors for the Dutch roll mode. Normalize these eigenvectors according to Eq. (8.1.37). Compare these approximate eigenvectors with the fully coupled Dutch roll solution that was obtained in problem 9.35.

9.44. For the turboprop transport in problems 7.38 and 7.41, using the Dutch roll eigenvalue approximation given by Eq. (9.5.27), find the eigenvalues, the 99 percent damping time, and the period for the Dutch roll mode. Compare these approximate results with the fully coupled Dutch roll solution that was obtained in problem 9.35.

9.45. For the turboprop transport in problems 7.38 and 7.41, using the Dutch roll eigenvector approximation given by Eq. (9.5.11), find the eigenvectors for the Dutch roll mode. Normalize these eigenvectors according to Eq. (8.1.37). Compare these approximate eigenvectors with the fully coupled Dutch roll solution that was obtained in problem 9.35.

9.46. Write a computer program that can be used to solve the 12×12 eigenproblem associated with the homogeneous form of Eq. (9.8.20). The program should import all required data from an input file of the same format as the sample file *airplane.txt*, which can be provided by your instructor. This sample data file is for the airplane and operating conditions in Example 9.8.1. Using only the data obtained from the input file, the program should fill out the two dimensionless 12×12 matrices needed for the generalized eigenproblem. The program should then use a generalized eigensolver to obtain the eigenvalues and eigenvectors from these matrices. A special eigensolver can be used if the system is first numerically reduced to the special eigenproblem. Be sure that all computations are done in double precision. Test your program by comparing results with those presented in Example 9.8.1.

9.47. Use the computer program that was written for problem 9.46 to obtain the solutions to problems 8.4 and 9.1. A formatted data file for this airplane and operation conditions is available as *B747.txt*, which can be provided by your instructor.

9.48. Use the computer program that was written for problem 9.46 to obtain the solutions to problems 8.13 and 9.13. A formatted data file for this airplane and operation conditions is available as *Spitfire.txt*, which can be provided by your instructor.

9.49. Use the computer program that was written for problem 9.46 to obtain the solutions to problems 8.22 and 9.24. A formatted data file for this airplane and operation conditions is available as *CJT001.txt*, which can be provided by your instructor.

9.50. Use the computer program that was written for problem 9.46 to obtain the solutions to problems 8.31 and 9.35. A formatted data file for this airplane and operation conditions is available as *C130H.txt*, which can be provided by your instructor.

9.51. Modify the data file *airplane.txt*, which was used in problem 9.46, to include the gyroscopic effects of the propeller and crankshaft turning at 2,350 rpm. The moment of inertia for the crankshaft and propeller combined is 4.7 slug·ft^2. Use the computer program that was written for problem 9.46 to obtain an improved solution to Example 9.8.1, including the gyroscopic effects of the rotating propeller and crankshaft.

9.52. The 2,375-horsepower, 12-cylinder Rolls-Royce Griffon engine of the Spitfire Mark XVIII in problem 9.48 is turning the five-blade, 132-inch Rotol propeller at 1,350 rpm. The effective mass moment of inertia for the crankshaft, hub, and propeller combined is 95 slug·ft^2, based on propeller speed. With a forward airspeed of 440 ft/sec, the change in propeller yawing moment coefficient with angle of attack is $C_{n_p,\alpha} = +0.296$ (the Griffon engine has left-hand rotation). Use the computer program that was written for problem 9.46 to obtain an improved solution to problem 9.48, including the gyroscopic and aerodynamic effects of the rotating propulsion system. Compare the short-period and Dutch roll eigenvectors both with and without the inclusion of the gyroscopic and aerodynamic coupling terms.

9.53. The Spitfire Mark XVIII in problem 9.48 is executing a level coordinated turn with an airspeed of 440 ft/sec and a bank angle of 60 degrees. Use the computer program that was written for problem 9.46 to obtain a solution to problem 9.48 for this operating condition. Obtain the solution both with and without the gyroscopic and aerodynamic effects of the rotating propulsion system, which were described in problem 9.52.

9.54. Repeat problem 9.52 assuming that mass moment of inertia for the crankshaft, hub, and propeller combined is doubled while all other parameters and operating conditions remain unchanged.

9.55. Four 4,910-horsepower constant-speed turboprop engines, turning at 13,820 rpm, power the transport airplane described in problem 9.50. Each engine turns a 162-inch propeller through a gear reduction assembly having a total reduction ratio of 13.54 to 1. The equivalent moment of inertia for each turbine rotor and gear reduction assembly combined is 6.5 slug·ft^2, based on turbine speed. The moment of inertia for each hub and propeller is 388 slug·ft^2. The change in propeller yawing moment coefficient with angle of attack is $C_{n_p,\alpha} = -0.154$. Assuming that all four engines turn in the same direction, use the computer program that was written for problem 9.46 to obtain a solution to problem 9.50, including the gyroscopic and aerodynamic effects of the rotating propulsion system. Compare the short-period and Dutch roll eigenvectors both with and without the inclusion of the gyroscopic and aerodynamic coupling terms.

9.56. The turboprop transport in problem 9.55 is executing a level coordinated turn with an airspeed of 440 ft/sec and a bank angle of 60 degrees. Use the computer program that was written for problem 9.46 to obtain a solution to problem 9.50 for this operating condition. Include the gyroscopic and aerodynamic effects of all four engines and propellers turning in the same direction.

Chapter 10
Aircraft Handling Qualities and Control Response

10.1. Introduction

The material presented in Chapters 8 and 9 dealt primarily with determining the eigenvalues and eigenvectors associated with the stick-fixed longitudinal and lateral modes of an airplane relative to some equilibrium flight condition. We found that longitudinal motion includes two oscillatory modes, the short-period mode and the long-period or phugoid mode. The lateral motion of a typical airplane includes two nonoscillatory modes, the roll mode and the spiral mode, as well as one oscillatory mode, Dutch roll. The damping rate for each of these modes and the damped natural frequency for the oscillatory modes can be determined from the eigenvalues. We have found that these damping rates and frequencies depend on the geometric and mass properties of the airplane as well as the aerodynamic derivatives and flight speed. The designer has some control over the characteristics of each dynamic mode through his or her selection of the airplane geometry. Furthermore, the designer can exercise additional control over the characteristics of these dynamic modes through implementation of an active feedback control system, which is referred to as *stability augmentation*.

Since the airplane designer has some control over the frequencies and damping rates associated with the longitudinal and lateral modes, a simple but important question quite naturally arises. What is considered to be good? The answer to this question is closely linked to the pilot's involvement in the control of the aircraft and has long been an important topic of research. Recent developments, such as fly-by-wire and digitally controlled aircraft, have generated renewed interest in such research, and the final statement relating to this topic has certainly not yet been expressed. It is still not uncommon to have a modern aircraft development project delayed by difficulties associated with dynamic stability and control. Such difficulties are often due, at least in part, to an insufficient understanding of the aircraft handling qualities discipline. This chapter gives only a brief introduction to aircraft handling qualities, as they apply to the dynamic modes of a typical airplane. For a more in-depth treatment of this topic, the reader is referred to Hodgkinson (1999).

10.2. Pilot Opinion

Ultimately, pilots will assess the handling qualities of any aircraft. For this reason, research on aircraft handling qualities has always centered on pilot opinion. Extensive research has been conducted by the federal government and the aviation industry to relate the static and dynamic stability characteristics of an airplane to the pilot's opinion of the aircraft's handling qualities. Since pilot opinion is subjective, it is difficult to quantify and measure. By contrast, measuring the dynamic characteristics of the aircraft itself is relatively simple.

The *Cooper-Harper rating scale* is most commonly used to quantify pilot opinion of aircraft handling qualities. The decision tree used by pilots when rating an aircraft according to the Cooper-Harper scale is shown in Fig. 10.2.1. This scale is dichotomous in that it forces the pilot to make a series of binary decisions, which ultimately lead to a quantitative rating from 1 to 10. A rating of 1 indicates excellent handling qualities, and a rating of 10 represents uncontrollable conditions. Subsequent to each dichotomous decision, the pilot further refines the rating according to the level of *pilot compensation* required. In the Cooper-Harper scale, pilot compensation is defined to be *the measure of additional pilot effort and attention required to maintain a given level of performance in the face of deficient vehicle characteristics.*

A 10-point rating scale is usually considered to be excessive for gathering subjective opinions. Perhaps for this reason, the U.S. Military Specifications for aircraft handling qualities are centered around *levels* of handling qualities, which are defined with reference to the Cooper-Harper scale. Cooper-Harper ratings of 1, 2, and 3 are defined to be *Level 1*, while *Level 2* consists of ratings 4, 5, and 6. Ratings of 7, 8, and 9 fall in *Level 3*. Common practice has unofficially labeled flying qualities having a Cooper-Harper rating of 10 as being *Level 4*. Table 10.2.1 shows the relationship between these U.S. Military Specifications for levels of handling qualities and mission effectiveness, which is reported by Hodgkinson (1999).

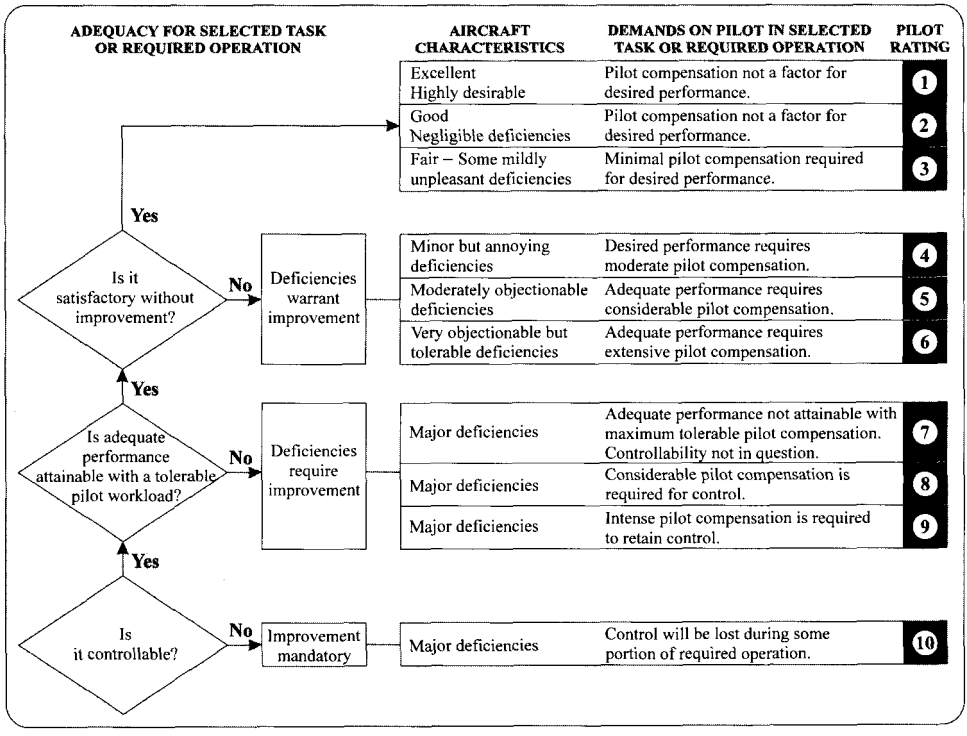


Figure 10.2.1. The Cooper-Harper handling qualities rating scale. (Cooper and Harper 1969)

	Pilot Rating	Handling Characteristics	Pilot Workload and Mission Effectiveness
Level 1	1,2,3	Satisfactory	Flying qualities clearly adequate for the mission flight phase. Desired performance is achievable with no more than minimal pilot compensation.
Level 2	4,5,6	Acceptable	Flying qualities adequate to accomplish the mission flight phase, but some increase in pilot workload or degradation in mission effectiveness, or both, exist.
Level 3	7,8,9	Controllable	Flying qualities such that the aircraft can be controlled safely in the context of the mission flight phase, but pilot workload is excessive or mission effectiveness is inadequate, or both. Category A flight phase can be terminated safely, and Category B and C flight phases can be completed.
Level 4	10	Uncontrollable	Flying qualities worse than Level 3 (unofficial).

Table 10.2.1. U.S. Military Specifications for levels of handling qualities and their relation to the Cooper-Harper scale.

It is not surprising that a pilot's opinion of an aircraft's handling qualities depends somewhat on the task that the pilot is performing. For those who have never flown an aircraft, this may be more easily understood in reference to driving a car. For example, drivers might rate the handling characteristics of a particular automobile as being excellent when referenced to high-speed highway driving. However, the same automobile may be rated as having very poor handling characteristics when drivers are ask to consider the ease of parking the car in a confined space or driving in heavy traffic. In a similar manner, pilot opinion of aircraft handling qualities must be referenced in some way to piloting task. For example, a pilot may rate an airplane as having very poor handling characteristics during takeoff. Yet, the same pilot could rate the same airplane as having good handling characteristics on landing and during the gradual coordinated maneuvers associated with climb, cruise, and descent.

The essence of piloting task definitions can be crucial to the process of gathering reliable pilot opinions on aircraft handling qualities. For many years, piloting tasks have been loosely classified into three *categories*, which are called *flight phase categories*. As reported by Nelson (1998), these categories are defined in Table 10.2.2. Today, piloting tasks are often more narrowly defined in terms of what are called *mission task elements*, which are more precisely defined tasks that can be incorporated into flight tests and flight simulations. While more precisely defined piloting tasks lead to more reliable pilot ratings, the rather loosely defined task categories specified in Table 10.2.2 are still useful for classifying pilot opinion relative to piloting task, particularly in the design phase of an aircraft development program.

Flight Phase	Piloting Task Classification
Category A	Nonterminal flight phases that require rapid maneuvering, precision tracking, or precise flight-path control. Included in the category are air-to-air combat, ground attack, weapon delivery or launch, aerial recovery, reconnaissance, in-flight refueling (receiver), terrain following, antisubmarine search, and close-formation flying.
Category B	Nonterminal flight phases that are normally accomplished using gradual maneuvers and without precision tracking, although accurate flight-path control may be required. Included in the category are climb, cruise, loiter, in-flight refueling (tanker), descent, emergency descent, emergency deceleration, and aerial delivery.
Category C	Terminal flight phases that are normally accomplished using gradual maneuvers and usually require accurate flight-path control. Included in this category are takeoff, catapult takeoff, approach, wave-off/go-around and landing.

Table 10.2.2. Flight phase categories.

The reader should likewise not be surprised to learn that the size and type of aircraft being flown has a significant effect on the handling qualities that are expected by a pilot and on the ratings that result from a particular handling characteristic. Here again we can relate this to the more commonplace experience of driving a car. For example, a handling characteristic that might be considered only mildly unpleasant in a passenger car may be considered totally unacceptable in a racing car. On the other hand, a delivery truck that exhibits exactly the same characteristic could be rated as having excellent handling qualities. Likewise, some handling characteristics that are typically considered to be excellent in a large transport aircraft may be considered to be poor in a fighter or stunt airplane. To help account for the influence of airplane size and type on pilot opinion of aircraft handling qualities, airplanes are usually classified according to size and maneuverability. Table 10.2.3 shows the classification of aircraft that was adopted in the U.S. Military Specification on flying qualities, as reported by Hodgkinson (1999).

Pilot opinion of one handling characteristic can also be influenced significantly by the presence of another. For example, if significant pilot concentration is required to compensate for poor longitudinal handling qualities, the pilot will be less tolerant of deficiencies in the lateral modes. In measuring and specifying handling qualities it is commonly assumed that any degradation in pilot opinion is the result of degrading only one handling characteristic at a time. To estimate what might be expected from the combined effects of more than one poor handling characteristic, the reader is referred to Mitchell, Aponso, and Hoh (1990).

Aircraft Classification	Aircraft Size and Type
Class I	Small, light aircraft such as: Light utility Primary trainer Light observation
Class II	Medium-weight, low- to medium-maneuverability aircraft such as: Heavy utility/search and rescue Light or medium transport/cargo/tanker Early warning/electronic countermeasures/airborne command, control or communications relay Antisubmarine Assault transport Reconnaissance Tactical bomber Heavy attack Trainer for Class II
Class III	Large, heavy, low- to medium-maneuverability aircraft such as: Heavy transport/cargo/tanker Heavy bomber Patrol/early warning/electronic countermeasures/airborne command, control or communications relay Trainer for Class III
Class IV	High-maneuverability aircraft such as: Fighter-interceptor Attack Tactical reconnaissance Observation Trainer for Class IV

Table 10.2.3. Aircraft classification, from the U.S. Military Specification on flying qualities.

Level 1 aircraft handling qualities are not necessarily required for all possible flight circumstances. Handling quality requirements for a particular situation depend to some extent on the probability that the situation will be encountered. The handling qualities that are required for a particular aircraft in a particular situation depend on what are called the *flight envelope* and the *aircraft state*.

Three nested flight envelopes are defined. The **operational flight envelope** encompasses those flight tasks that are encountered in the normal day-to-day operation of the aircraft: for example, takeoff and landing. The **service flight envelope** is defined by the service limits of the airplane, such as the service ceiling and maximum airspeed. The **permissible flight envelope** comprises all flight conditions that are allowable and possible, including stalls, spins, and other such extreme situations.

A **normal state** is defined as any normal operational configuration for the airplane, in terms of flap settings, gross weight, CG location, and so on. A **failure state** is a normal state modified by a malfunction in one or more of the airplane's components. Failure states are categorized according to the probability of occurrence.

In general, Level 1 handling qualities are always required in the operational flight envelope for an aircraft in any normal state. In a failure state, the handling qualities are allowed to degrade in accordance with the probability of occurrence for that particular state. For failure states that are very likely to occur, handling qualities must remain at Level 1. A failure state that is likely to occur more than once every 100 flights can result in handling qualities no worse than Level 2. Handling qualities as poor as Level 3 are allowed only if the failure state is likely to occur less than once in every 10,000 flights. In some cases, handling qualities have been allowed to degrade to Level 2 in moderate turbulence and to Level 3 in the presence of severe turbulence.

10.3. Dynamic Handling Quality Prediction

We have the ability to mathematically estimate the eigenvalues for the longitudinal and lateral modes associated with the dynamic response of a particular airplane design at some particular operating condition, prior to fabrication and flight testing. However, these eigenvalues do not provide a direct measure of aircraft handling qualities. What is needed is some means of predicting aircraft handling qualities from knowledge of the airplane's dynamic response eigenvalues and other design characteristics. This is one of the primary objectives of handling qualities research and is the topic of this section. Here each of the airplane's dynamic modes will be addressed separately. The handling qualities predicted for any mode are based on the assumption of Level 1 handling qualities for all other modes.

The Short-Period Mode

As discussed previously, the short-period mode is comprised primarily of high-frequency oscillations in angle of attack and vertical displacement, with little change in forward velocity. Humans are highly sensitive to acceleration but quite insensitive to small changes in position and orientation. From the pilot's viewpoint it is the acceleration associated with short-period motion that is of greatest importance. Since the forward velocity remains nearly constant for the short period, it is primarily the normal acceleration associated with this mode that pilots feel. Oscillations in angle of attack and the resulting oscillations in lift produce this normal acceleration. Thus, it is not surprising that a pilot's opinion of how the airplane's handling qualities are affected by the short-period mode depends on how the airplane's normal acceleration varies with angle of attack. The load factor, n, is the usual measure of an airplane's normal acceleration. Recall that because normal acceleration is generated by lift, the load factor can be expressed as the lift divided by the weight. The change in load factor with respect to angle of attack is called the *acceleration sensitivity*:

$$\text{acceleration sensitivity} \equiv \frac{\partial n}{\partial \alpha} = \frac{1}{W}\frac{\partial L}{\partial \alpha} = \frac{1}{C_W}\frac{\partial C_L}{\partial \alpha} \tag{10.3.1}$$

Pilot opinion of how the short-period frequency influences handling qualities has been found to vary significantly with the acceleration sensitivity of the airplane. When pilot opinion data are correlated with the short-period frequency and acceleration sensitivity, results similar to those reported by Hodgkinson (1999) and shown here in Fig. 10.3.1 are obtained. These results are based on adequate short-period damping.

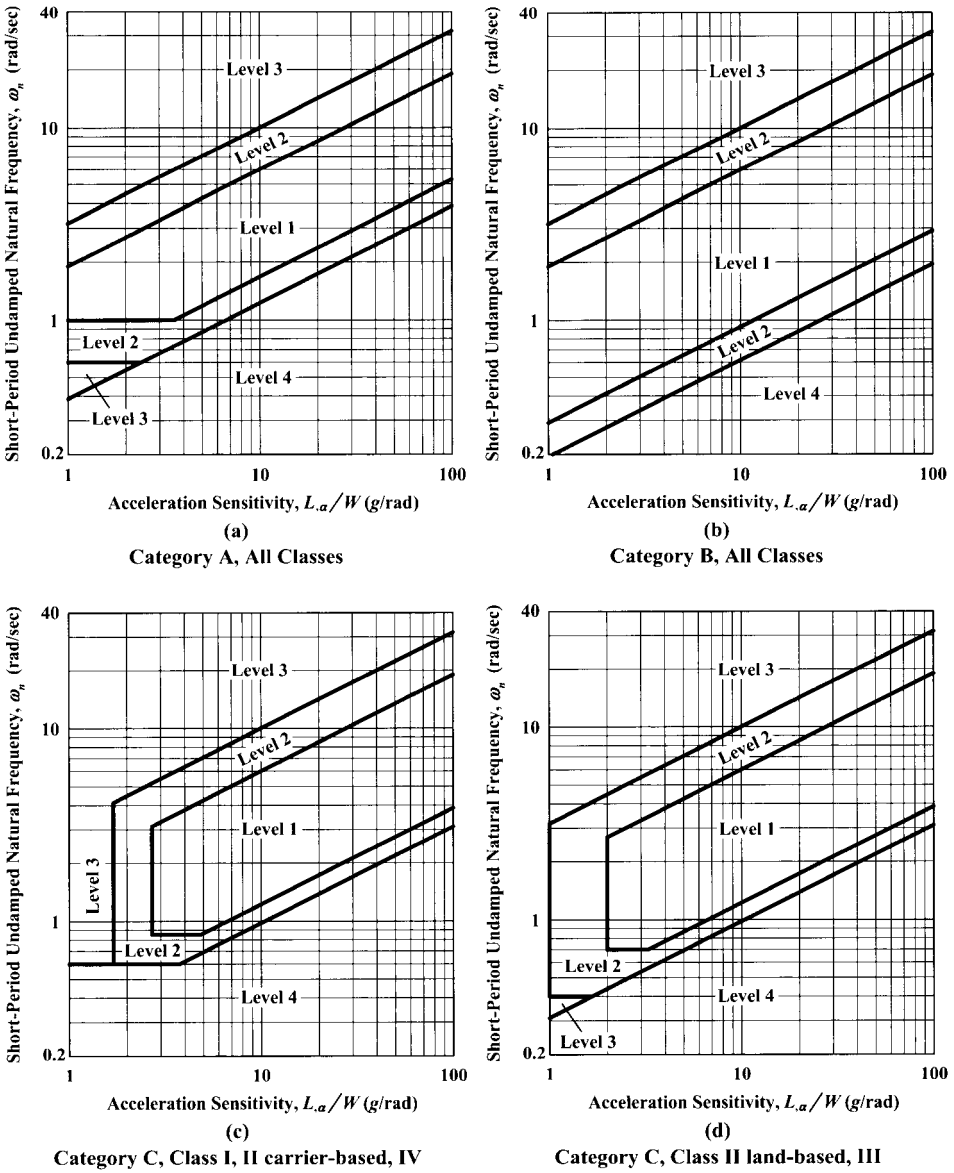


Figure 10.3.1. Short-period frequency requirements.

From Fig. 10.3.1 it can be seen that, when the acceleration sensitivity is above some minimum value, the boundaries between the different levels of handling qualities are all defined by lines of constant slope on a log-log plot. Furthermore, the slope for each of these boundary lines is exactly ½. This means that the square of the undamped natural frequency at any point along any one of these boundary lines is proportional to the acceleration sensitivity. Thus, the square of the short-period undamped natural frequency divided by the acceleration sensitivity is an important correlation parameter associated with the short-period frequency requirements. This parameter is commonly called the *control anticipation parameter* (CAP),

$$\text{CAP} \equiv (\omega_n^2)_{SP} \Big/ \frac{\partial n}{\partial \alpha} = \frac{(\omega_n^2)_{SP}}{L_{,\alpha}/W} = \frac{(\omega_n^2)_{SP}}{C_{L,\alpha}/C_W} \tag{10.3.2}$$

For the prediction of short-period frequency requirements, when the airplane's acceleration sensitivity is above some minimum value (about 3.5 to 5.0), the boundaries between different levels of handling qualities are lines of constant CAP. For example, the top two sloping lines in Fig. 10.3.1a through d have constant CAP values of 3.6 and 10.0. The lower two sloping lines have constant CAP values of 0.15 and 0.28 in Fig. 10.3.1a, 0.038 and 0.085 in Fig. 10.3.1b, and 0.096 and 0.15 in both Fig. 10.3.1c and d.

The short-period damping ratio also has a significant effect on airplane handling qualities as judged by pilot opinion. The short-period damping requirements given by Hodgkinson (1999) are listed in Table 10.3.1. The results presented in this table are based on the assumption that the short-period frequency falls within the range that would give Level 1 handling qualities according to Fig. 10.3.1.

If the acceleration sensitivity is large enough so that the short-period frequency requirements depend only on the CAP, then the short-period frequency and damping requirements can be combined in a single plot with CAP on one axis and damping ratio on the other. For example, from Fig. 10.3.1a we see that Level 1 handling qualities for Category A flight phases require a control anticipation parameter between 0.28 and 3.6, while Table 10.3.1 shows a required damping ratio between 0.35 and 1.30. These combined requirements are shown as the inner rectangle in Fig. 10.3.2. The Level 2 and 3 handling qualities boundaries are also shown in this figure. Similar results for flight phase Categories B and C are shown in Figs. 10.3.3 and 10.3.4.

Level	Category A & C Flight Phases		Category B Flight Phases	
	Minimum ζ	Maximum ζ	Minimum ζ	Maximum ζ
1	0.35	1.30	0.30	2.00
2	0.25	2.00	0.20	2.00
3	0.15	–	0.15	–

Table 10.3.1. Short-period damping ratio requirements for all aircraft classes.

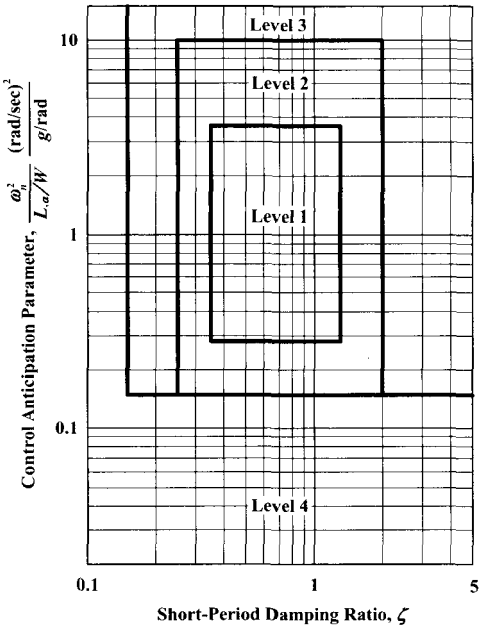


Figure 10.3.2. Short-period frequency and damping requirements for Category A flight phases and airplanes of all classes having acceleration sensitivity greater than 3.5 g/rad.

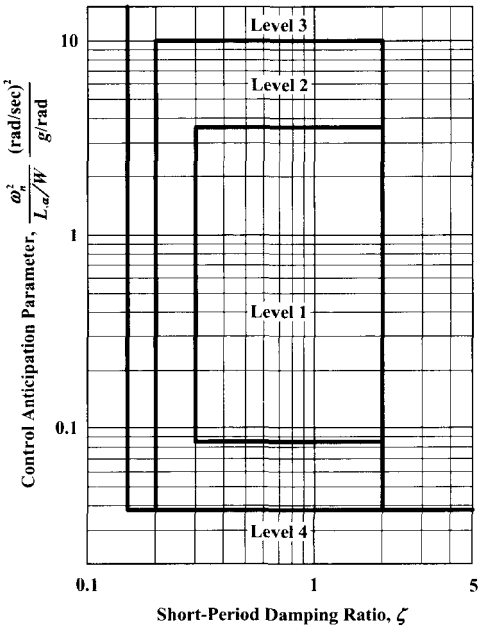


Figure 10.3.3. Short-period frequency and damping requirements for Category B flight phases and airplanes of all classes.

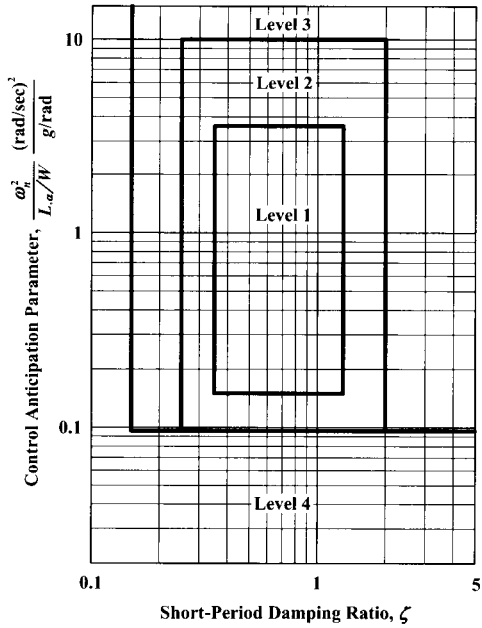


Figure 10.3.4. Short-period frequency and damping requirements for Category C flight phases and airplanes of all classes having acceleration sensitivity greater than 5 g/rad.

The Phugoid

The period of the phugoid is always long compared to a pilot's response time. Thus, pilots can easily suppress phugoid oscillations with appropriate control inputs. Because of the large difference between the phugoid period and a pilot's response time, the exact value of the phugoid frequency has almost no effect on a pilot's opinion of an airplane's handling qualities. However, if the phugoid damping is too low, suppressing the phugoid does require some pilot attention, and this makes other tasks more difficult. For this reason, aircraft handling qualities do correlate with phugoid damping. The phugoid damping requirements presented by Hodgkinson (1999) are given in Table 10.3.2. From the pilot opinion data currently available, these damping requirements appear to be independent of both aircraft class and flight phase.

Level	All Flight Phases for all Aircraft Categories Minimum Phugoid Damping
1	Damping ratio should be greater than 0.04
2	Damping ratio should be greater than 0.00
3	Time-to-double-amplitude should be greater than 55 sec

Table 10.3.2. Phugoid damping requirements for all aircraft classes.

The Roll Mode

As discussed in Chapter 9, the roll mode is a heavily overdamped motion. Thus, when a typical-fixed wing aircraft responds to a change in aileron input, the time constant is very short and the airplane quickly approaches a steady rolling rate that is proportional to aileron deflection. This gives the pilot the perception that aileron input commands the airplane's rolling rate. The time constant for any mode is defined simply as the inverse of the damping rate. For favorable handling qualities, the time constant for the roll mode is typically on the order of 1 second or slightly longer. If the roll mode time constant is much longer than a second, the transient persists well into the maneuver and the pilot begins to feel as though he or she is commanding roll acceleration instead of rolling rate. This will normally degrade the pilot's opinion of the airplane's handling qualities. Table 10.3.3 lists the minimum damping requirements for the roll mode, which are reported by Nelson (1998) in terms of maximum time constant.

Flight Phase Category	Aircraft Class	Handling Quality		
		Level 1	Level 2	Level 3
A & C	I, IV	1.0	1.4	10
	II, III	1.4	3.0	10
B	ALL	1.4	3.0	10

Table 10.3.3. Roll mode damping requirements, maximum time constant ($1/\sigma$) in seconds.

The Spiral Mode

In Chapter 9 we found that the spiral mode is usually either slowly convergent or slowly divergent. The time constant for this mode is large compared to pilot reaction time. Thus, like the phugoid, this motion is readily controlled with pilot input. Even if the spiral mode is divergent, the pilot can typically control the motion with little or no conscious effort, provided that the time required to double the disturbance amplitude is not too short. However, if the spiral divergence is too rapid, pilot attention is required that will detract from the performance of other tasks and degrade the pilot's opinion of the aircraft's handling qualities. The spiral mode damping requirements presented by Nelson (1998) are shown in Table 10.3.4.

Flight Phase Category	Aircraft Class	Handling Quality		
		Level 1	Level 2	Level 3
A	I, IV	12	12	4
	II, III	20	12	4
B & C	ALL	20	12	4

Table 10.3.4. Spiral mode damping requirements, minimum time-to-double-amplitude in seconds.

The Lateral Phugoid

Some modern aircraft have very little wing area and the roll damping for such aircraft can be quite low. For aircraft of this type, it is occasionally possible for the eigenvalues associated with the usual roll and spiral modes to combine, forming a complex pair. In this case, the aircraft will exhibit a long-period lateral oscillation, which is sometimes called the *lateral phugoid*. While this characteristic is not normally associated with good handling qualities, it can be acceptable if the damping is sufficient. Hodgkinson (1999) reports the damping requirements for this mode that are given in Table 10.3.5. The damping criteria in this table are based on the product of the undamped natural frequency, ω_n, and the damping ratio, ζ.

Level	All Flight Phases for all Aircraft Categories Minimum Damping for the Oscillatory Roll-Spiral Mode
1	The $\zeta\omega_n$ product should be greater than 0.50 rad/sec
2	The $\zeta\omega_n$ product should be greater than 0.30 rad/sec
3	The $\zeta\omega_n$ product should be greater than 0.15 rad/sec

Table 10.3.5. Total damping requirements for the seldom-encountered low-frequency mode that is sometimes called the lateral phugoid.

Dutch Roll

Dutch roll is often the most troublesome of the dynamic modes associated with the stick-fixed longitudinal and lateral response of a conventional airplane. As discussed in Chapter 9, Dutch roll is a damped oscillatory motion that involves an out-of-phase combination of sideslip, roll, and yaw. Since the period for this mode is typically on the order of 2 to 10 seconds, Dutch roll motion can be very annoying to both pilots and passengers if the damping is light. Because the quarter-period of oscillation for Dutch roll can be quite close to the response time of a human pilot, it can be extremely difficult for a pilot to suppress this motion with control inputs. In fact, as discussed in Chapter 9, the natural Dutch roll characteristics of some aircraft are such that most pilots will actually excite the Dutch roll in an attempt to suppress it. If the period of oscillation is not too short and the damping is not too light, Dutch roll motion does not require significant pilot attention. However, if the Dutch roll damping is extremely light and the period is short, the airplane can be quite difficult to handle.

As might be expected, both the Dutch roll frequency and damping ratio affect the handling qualities of an airplane. The Dutch roll frequency and damping requirements reported by Hodgkinson (1999) are presented in Table 10.3.6. Notice that this table gives a minimum value for the damping ratio, the undamped natural frequency, and the product of the damping ratio and the undamped natural frequency. All of these requirements should be met. The minimum frequency requirement is always based on the undamped natural frequency and minimum damping requirement is that which yields the largest damping ratio.

Level	Flight Phase Category	Aircraft Class	Minimum[5] ζ	Minimum[5] $\zeta\omega_n$ (rad/sec)	Minimum[6] ω_n (rad/sec)
1	A	IV-CO[1]&GA[2]	0.4	0.4	1.0
		I, IV-other	0.19	0.35	1.0
		II, III	0.19	0.35	0.4
	B	ALL	0.08	0.15	0.4
	C	I, II-C[3], IV	0.08	0.15	1.0
		II-L[4], III	0.08	0.10	0.4
2	ALL	ALL	0.02	0.05	0.4
3	ALL	ALL	0.00	—	0.4

[1]CO: combat, [2]GA: ground attack, [3]C: carrier-based, [4]L: land-based,
[5]The minimum damping requirement is that yielding the greatest damping ratio,
[6]The minimum frequency requirement is always based on the undamped natural frequency.

Table 10.3.6. The Dutch roll frequency and damping requirements.

EXAMPLE 10.3.1. For the airplane and operating condition that was described in Examples 8.2.1 and 9.2.1, compare the predicted dynamic response with the frequency and damping requirements presented in this section. What level of handling qualities should be expected for this airplane and operating condition, based on the dynamic response modes?

Solution. This is a Class I aircraft. Since the operating condition is cruise with no special requirement for precision tracking, the flight phase is in Category B.

From Example 8.2.1, the short-period damping ratio and undamped natural frequency are

$$\zeta = 0.69, \quad \omega_n = 3.59 \text{ rad/sec}$$

The lift slope and weight coefficient for this airplane and operating condition are

$$C_{L,\alpha} = 4.40, \quad C_W = 0.393$$

Thus, the acceleration sensitivity is

$$\text{acceleration sensitivity} = C_{L,\alpha}/C_W = 4.40/0.393 = 11.2 \; g/\text{rad}$$

and the control anticipation parameter is

$$\text{CAP} = \frac{(\omega_n^2)_{SP}}{C_{L,\alpha}/C_W} = \frac{3.59^2}{11.2} = 1.15 \frac{(\text{rad/sec})^2}{g/\text{rad}}$$

For this airplane and Category B flight phase, the short-period frequency and damping requirements are prescribed in Fig. 10.3.3. The damping ratio of 0.69 and CAP of 1.15 fall well within the limits for which Level 1 handling qualities would normally be expected, based on short-period requirements.

Also from Example 8.2.1, the phugoid damping ratio for this airplane and operating condition is 0.080. Based on the requirements given in Table 10.3.2, this is well over the limit needed to provide Level 1 handling qualities.

From Example 9.2.1, the predicted damping rate for the roll mode is 8.9 sec^{-1}, so the roll mode time constant is

$$\text{roll mode time constant} = 1/\sigma = 1/8.9 = 0.11 \text{ sec}$$

From Fig 10.3.7 we see that this is considerably less than the maximum time constant that would normally yield Level 1 handling qualities.

A convergent spiral mode was predicted in Example 9.2.1. Thus, from the results presented in Table 10.3.4, we see that the spiral mode should not contribute to reducing the handling qualities below Level 1.

For this airplane and operating condition, the Dutch roll damping ratio and undamped natural frequency as predicted in Example 9.2.1 are

$$\zeta = 0.20, \quad \omega_n = 2.43 \text{ rad/sec}$$

and

$$\zeta\omega_n = 0.49 \text{ rad/sec}$$

All three of these values satisfy the requirements for Level 1 handling qualities as specified in Table 10.3.6.

The frequencies and damping rates for all of the stick-fixed dynamic modes associated with this airplane and operating conditions are well within the limits that would typically provide Level 1 handling qualities. Thus, for this operating condition, we would expect that the stick-fixed dynamic response of this airplane is adequate to provide Level 1 handling qualities. However, to predict the airplane's handling qualities for all normal operation, these calculations would need to be repeated for the full range of operating conditions within the *operational flight envelope.*

10.4. Response to Control Inputs

Pilot opinion of aircraft handling qualities seems to correlate quite well with the eigenvalues for the traditional stick fixed dynamic modes, which are obtained from aircraft small-disturbance theory with all control inputs set to zero. One might ask the question: Why should results obtained using the case of no control input have such a significant effect on a pilot's ability to control the airplane? The answer is linked to the transient response of the airplane to control inputs.

As we have seen, airplane controls are used to establish trim and maneuver or accelerate an airplane from one trimmed state to another. To this point, our treatment of aircraft control and maneuverability has been mostly confined to the case of constant angular rates, which produce constant acceleration. For example, our analysis of the elevator angle and control force per g in the pull-up maneuver was based on the assumption that the maneuver had progressed to the point where the pitching rate had reached a steady value. Similarly, our analysis of the steady coordinated turn was based on the assumption that the wings were already banked at the correct angle and that the airplane was turning with a constant angular rate.

In a typical flying situation, an airplane might be flying at level trim. If the pilot wishes to climb, descend, or turn, then he or she must change the control inputs. For example, assume that the pilot wishes to change the airplane's flight path from level trimmed flight to climbing flight, without changing the throttle setting. To accomplish this, he or she must pull the stick or control yoke back. After the control has been held back for a period of time, the airplane will attain a new trim state, which then has a positive climb angle and lower airspeed. The maneuver that takes the airplane between these two trimmed states is the pull-up maneuver. However, this maneuver starts with zero pitch rate and ends with zero pitch rate. While there may be a period of time during the maneuver when the pitch rate is constant, clearly this entire maneuver cannot take place at constant pitch rate and constant airspeed. Thus, our Chapter 6 analysis for the constant-speed pull-up maneuver cannot possibly tell the whole story in regard to this common airplane maneuver.

When the pilot first initiates a pull-up maneuver from trimmed flight, the pitching moment generated by the elevator deflection produces acceleration in pitch and the pitch rate begins to rise. As the pitch rate increases, an opposing moment develops as a result of pitch damping. If this pitch rate becomes large enough, the pitch damping moment will just balance the moment produced by the elevator deflection, returning the pitch acceleration to zero. A question then naturally arises: How does the airplane respond during the transient period of angular acceleration?

We have at least superficially examined the analogous problem associated with aileron deflection. Because the roll damping is quite large for a conventional airplane, transients associated with aileron deflection are quickly damped out and the airplane rapidly approaches a constant rolling rate. This gives pilots the perception that aileron deflection commands rolling rate. However, the pitch and yaw damping for a typical airplane are much less than that for roll. Thus, the pitch and yaw controls "feel" very different from the roll control. In this section we examine the transients associated with elevator and rudder deflection.

In general, maneuvering flight with substantial translational and rotational acceleration can involve significant inertial, gravitational, and aerodynamic nonlinearities. To accurately predict the response of an airplane during such maneuvers, we must return to the nonlinear equations of motion developed in Chapter 7. These equations would need to be integrated numerically. This is the topic of Chapter 11. However, by continuing somewhat further with small disturbance theory, we can obtain some useful results that provide valuable insight into the control process. Furthermore, such results are of great value in the design of autopilot control systems.

Transfer Functions

The linearized aircraft equations of motion presented in Sec. 7.5, 7.7, or 9.8 are of the mathematical form of the generalized linear control problem,

$$[\mathbf{B}]\{\dot{\mathbf{X}}\} = [\mathbf{A}]\{\mathbf{X}\} + [\mathbf{C}]\{\mathbf{D}\}$$

where $\{\mathbf{X}\}$ is a vector of n state variables, $[\mathbf{A}]$ and $[\mathbf{B}]$ are constant $n \times n$ matrices, $\{\mathbf{D}\}$ is a vector of m control deflections, and $[\mathbf{C}]$ is a constant $n \times m$ matrix. A special case of the generalized linear control problem is of particular interest. That is the special linear control problem, where $[\mathbf{B}]$ is the identity matrix. The generalized linear control problem is easily converted to the special linear control problem by multiplying both sides of the equation by the inverse of $[\mathbf{B}]$,

$$[\mathbf{B}]^{-1}[\mathbf{B}]\{\dot{\mathbf{X}}\} = [\mathbf{B}]^{-1}[\mathbf{A}]\{\mathbf{X}\} + [\mathbf{B}]^{-1}[\mathbf{C}]\{\mathbf{D}\}$$

Thus, any generalized linear control problem is readily converted to the special linear control problem, which has the form

$$\{\dot{\mathbf{X}}\} = [\mathbf{A}]\{\mathbf{X}\} + [\mathbf{C}]\{\mathbf{D}\} \tag{10.4.1}$$

If the control deflections, $\{\mathbf{D}\}$, were known as a function of time, the solution to this linear control problem would allow us to determine the state variables, $\{\mathbf{X}\}$, as a function of time.

Linear time-invariant systems of the form given by Eq. (10.4.1) are commonly solved using the method of Laplace transforms. Recall that the Laplace transform of some function of t, say $x(t)$, is defined by

$$\bar{x}(s) \equiv \int_0^\infty x(t)e^{-st}dt \tag{10.4.2}$$

Thus, using integration by parts, the Laplace transform of the derivative of x with respect to t is given by

$$\begin{aligned}\overline{\frac{dx}{dt}} \equiv \int_0^\infty \frac{dx}{dt}e^{-st}dt &= \int_0^\infty e^{-st}dx = xe^{-st}\Big|_0^\infty - \int_0^\infty x\,d(e^{-st}) \\ &= -x(0) + s\int_0^\infty xe^{-st}dt = s\bar{x} - x(0)\end{aligned} \tag{10.4.3}$$

An important concept called the *transfer function* is widely used in the application of Laplace transforms to Eq. (10.4.1). Each element of the transfer-function matrix, $[\mathbf{G}]$, is defined to be the ratio of the Laplace transform of the response in one of the state variables to the Laplace transform of one control input, for the special case where the state variable response is zero at time $t = 0$. Specifically, $[\mathbf{G}]$ is defined to yield

$$\{\bar{\mathbf{X}}\} = [\mathbf{G}]\{\bar{\mathbf{D}}\} \tag{10.4.4}$$

If the transfer-function matrix is known, the state variable response vector in the Laplace domain can be found for any control deflections input vector by simple matrix multiplication according to Eq. (10.4.4).

The transfer-function matrix, [**G**], is readily obtained from Eq. (10.4.1). Taking the Laplace transform of Eq. (10.4.1) and applying Eq. (10.4.3) along with the null initial condition gives

$$s\{\overline{\mathbf{X}}\} = [\mathbf{A}]\{\overline{\mathbf{X}}\} + [\mathbf{C}]\{\overline{\mathbf{D}}\} \tag{10.4.5}$$

or after solving for the Laplace transform of the state variable response vector,

$$\{\overline{\mathbf{X}}\} = \left[s\,[\mathbf{i}] - [\mathbf{A}]\right]^{-1} [\mathbf{C}]\{\overline{\mathbf{D}}\} \tag{10.4.6}$$

where [**i**] is the identity matrix. By comparing Eq. (10.4.6) with Eq. (10.4.4), we see that the transfer-function matrix is given by

$$[\mathbf{G}] = \left[s\,[\mathbf{i}] - [\mathbf{A}]\right]^{-1} [\mathbf{C}] \tag{10.4.7}$$

To evaluate the inverse matrix in Eq. (10.4.7), we recall from linear algebra that if the determinant is not zero,

$$\left[s\,[\mathbf{i}] - [\mathbf{A}]\right]^{-1} = \frac{[\mathbf{M}]^T}{\left|s\,[\mathbf{i}] - [\mathbf{A}]\right|} \tag{10.4.8}$$

where $[\mathbf{M}]^T$ is the transpose of the matrix of cofactors. The components of [**M**] are defined as

$$M_{ij} = (-1)^{i+j} m_{ij} \tag{10.4.9}$$

where m_{ij} is the minor determinate of s[**i**]–[**A**], obtained from the matrix that remains after row i and column j are removed.

The significance of this mathematics is best demonstrated by example. To help the student relate the mathematics to the physics of commonplace experience, we shall begin with a simple spring-mass system.

EXAMPLE 10.4.1. Consider the spring-mass system described in Example 8.1.1. An independent time-varying control force is applied to each of the two masses as shown in Fig. 10.4.1. Find the transfer-function matrix for this system. For the special case where ΔF_1 is a unit step function and ΔF_2 is zero, find the Laplace transform of the state variable response vector.

$$m_1 = 20.0 \text{ slugs}, \quad c_1 = 30.0 \text{ lbf}\cdot\text{sec/ft}, \quad k_1 = 2.0 \text{ lbf/ft},$$
$$m_2 = 20.0 \text{ slugs}, \quad c_2 = 15.0 \text{ lbf}\cdot\text{sec/ft}, \quad k_2 = 100.0 \text{ lbf/ft}$$

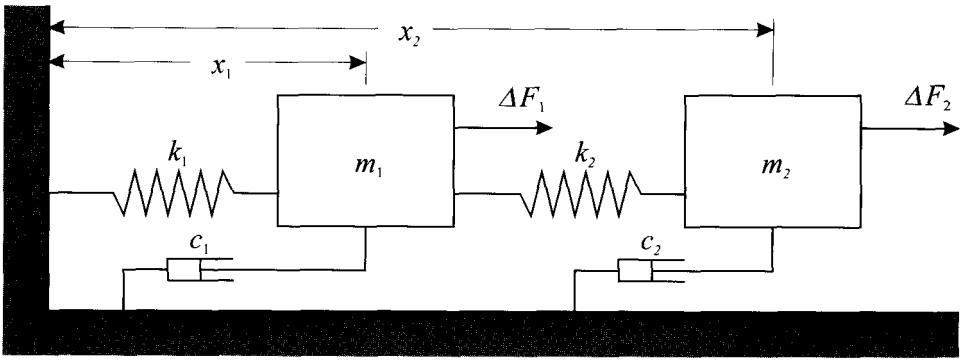


Figure 10.4.1. Damped spring-mass system with two degrees of freedom.

Solution. Following the development that led to Eq. (8.1.45) but including the control forces, we have

$$\begin{Bmatrix} \Delta\dot{V}_1 \\ \Delta\dot{V}_2 \\ \Delta\dot{x}_1 \\ \Delta\dot{x}_2 \end{Bmatrix} = \begin{bmatrix} -c_1/m_1 & 0 & -(k_1+k_2)/m_1 & k_2/m_1 \\ 0 & -c_2/m_2 & k_2/m_2 & -k_2/m_2 \\ 1 & 0 & 0 & 0 \\ 0 & 1 & 0 & 0 \end{bmatrix} \begin{Bmatrix} \Delta V_1 \\ \Delta V_2 \\ \Delta x_1 \\ \Delta x_2 \end{Bmatrix} + \begin{bmatrix} 1/m_1 & 0 \\ 0 & 1/m_2 \\ 0 & 0 \\ 0 & 0 \end{bmatrix} \begin{Bmatrix} \Delta F_1 \\ \Delta F_2 \end{Bmatrix}$$

After using the specified masses, damping coefficients, and spring constants, the special linear control problem for this system is

$$\begin{Bmatrix} \Delta\dot{V}_1 \\ \Delta\dot{V}_2 \\ \Delta\dot{x}_1 \\ \Delta\dot{x}_2 \end{Bmatrix} = \begin{bmatrix} -1.5 & 0 & -5.1 & 5.0 \\ 0 & -0.75 & 5.0 & -5.0 \\ 1 & 0 & 0 & 0 \\ 0 & 1 & 0 & 0 \end{bmatrix} \begin{Bmatrix} \Delta V_1 \\ \Delta V_2 \\ \Delta x_1 \\ \Delta x_2 \end{Bmatrix} + \begin{bmatrix} 0.05 & 0 \\ 0 & 0.05 \\ 0 & 0 \\ 0 & 0 \end{bmatrix} \begin{Bmatrix} \Delta F_1 \\ \Delta F_2 \end{Bmatrix}$$

By direct comparison with Eq. (10.4.1), we have

$$[s\,[\mathbf{i}] - [\mathbf{A}]] = \begin{bmatrix} s+1.5 & 0 & 5.1 & -5.0 \\ 0 & s+0.75 & -5.0 & 5.0 \\ -1 & 0 & s & 0 \\ 0 & -1 & 0 & s \end{bmatrix} \equiv [\mathbf{E}]$$

The cofactors of this matrix as determined from Eq. (10.4.9) are

$$
\begin{aligned}
M_{11} &= s^3 + 0.75s^2 + 5.0s \\
M_{12} &= 5.0s \\
M_{13} &= s^2 + 0.75s + 5.0 \\
M_{14} &= 5.0 \\
M_{21} &= 5.0s \\
M_{22} &= s^3 + 1.5s^2 + 5.1s \\
M_{23} &= 5.0 \\
M_{24} &= s^2 + 1.5s + 5.1 \\
M_{31} &= -5.1s^2 - 3.825s - 0.5 \\
M_{32} &= 5.0s^2 + 7.5s \\
M_{33} &= s^3 + 2.25s^2 + 6.125s + 7.5 \\
M_{34} &= 5.0s + 7.5 \\
M_{41} &= 5.0s^2 + 3.75s \\
M_{42} &= -5.0s^2 - 7.5s - 0.5 \\
M_{43} &= 5.0s + 3.75 \\
M_{44} &= s^3 + 2.25s^2 + 6.225s + 3.825
\end{aligned}
$$

From these cofactors, the determinate is found to be

$$
\begin{aligned}
\left|s\,[\mathbf{i}] - [\mathbf{A}]\right| \equiv \left|\mathbf{E}\right| &= \sum_{i=1}^{4} E_{ij} M_{ij} = \sum_{j=1}^{4} E_{ij} M_{ij} \\
&= s^4 + 2.25s^3 + 11.225s^2 + 11.325s + 0.5
\end{aligned}
$$

From Eqs. (10.4.7) and (10.4.8), the transfer-function matrix can be determined from the cofactors and the control force coefficient matrix,

$$
[\mathbf{G}] = \frac{[\mathbf{M}]^T [\mathbf{C}]}{\left|s\,[\mathbf{i}] - [\mathbf{A}]\right|}
$$

where in this case

$$
[\mathbf{C}] = \begin{bmatrix} 0.05 & 0 \\ 0 & 0.05 \\ 0 & 0 \\ 0 & 0 \end{bmatrix}
$$

After performing the indicated algebra, we have

$$[\mathbf{G}] = \frac{\begin{bmatrix} 0.05s^3 + 0.0375s^2 + 0.25s & 0.25s \\ 0.25s & 0.05s^3 + 0.075s^2 + 0.255s \\ 0.05s^2 + 0.0375s + 0.25 & 0.25 \\ 0.25 & 0.05s^2 + 0.075s + 0.255 \end{bmatrix}}{s^4 + 2.25s^3 + 11.225s^2 + 11.325s + 0.5}$$

Tables of Laplace transforms are widely available, and from any such table we would find that the Laplace transform of a unit step function is $1/s$. Thus, for the special case where ΔF_1 is a unit step function and ΔF_2 is zero,

$$\begin{Bmatrix} \overline{\Delta F_1} \\ \overline{\Delta F_2} \end{Bmatrix} = \begin{Bmatrix} 1/s \\ 0 \end{Bmatrix}$$

From Eq. (10.4.4), the Laplace transform of the state variable response vector is found to be

$$\begin{Bmatrix} \overline{\Delta V_1} \\ \overline{\Delta V_2} \\ \overline{\Delta x_1} \\ \overline{\Delta x_2} \end{Bmatrix} = [\mathbf{G}] \begin{Bmatrix} 1/s \\ 0 \end{Bmatrix} = \begin{Bmatrix} \left(\dfrac{0.05s^3 + 0.0375s^2 + 0.25s}{s(s^4 + 2.25s^3 + 11.225s^2 + 11.325s + 0.5)} \right) \\ \left(\dfrac{0.25s}{s(s^4 + 2.25s^3 + 11.225s^2 + 11.325s + 0.5)} \right) \\ \left(\dfrac{0.05s^2 + 0.0375s + 0.25}{s(s^4 + 2.25s^3 + 11.225s^2 + 11.325s + 0.5)} \right) \\ \left(\dfrac{0.25}{s(s^4 + 2.25s^3 + 11.225s^2 + 11.325s + 0.5)} \right) \end{Bmatrix}$$

Step Response

Results like those obtained in Example 10.4.1 are quite useless unless we are able to transform the solution back to the time domain. As a precursor to doing exactly that, several important observations can be made from Example 10.4.1.

First, notice that each of the transfer functions for the system is the ratio of two polynomials in s. Furthermore, it is seen that all of the transfer functions have exactly the same denominator and the order of the polynomial in the numerator is lower than that in the denominator. These characteristics hold for the solution to Eq. (10.4.1) in general, regardless of the order of the system.

The polynomial in the denominator of each transfer function is the *characteristic polynomial* for the system of equations. From Eq. (10.4.8) we see that the characteristic polynomial comes from the determinate of a characteristic matrix, which is identical to that used to obtain the eigenvalues, i.e., Eq. (8.1.63). Thus, the roots of the characteristic polynomial are the eigenvalues for the homogeneous system.

With the discussion above in mind, Eq. (10.4.8) can be used in Eq. (10.4.7) and the denominator can be factored to give

$$[\mathbf{G}] = \frac{[\mathbf{M}]^T[\mathbf{C}]}{(s-\lambda_1)(s-\lambda_2)(s-\lambda_3)\cdots(s-\lambda_n)} \tag{10.4.10}$$

where n is the order of the system. Since $[\mathbf{M}]^T$ is the transpose of the matrix of cofactors and $[\mathbf{C}]$ is a matrix of constants, each component of the numerator on the right-hand side of Eq. (10.4.10) is a polynomial of order less than n.

When the Laplace transform of some function of t is the ratio of two polynomials in s, the inverse transform can be obtained from the *Heaviside expansion theorem*. For instance, assume that the Laplace transform of $x(t)$ is given by

$$\bar{x}(s) = \frac{N(s)}{(s-r_1)(s-r_2)(s-r_3)\cdots(s-r_n)} \tag{10.4.11}$$

where $N(s)$ is a polynomial in s. In the absence of repeated roots, the inverse transform is then given by

$$x(t) = \sum_{k=1}^{n}\left[\frac{N(r_k)}{\prod_{j=1}^{n}(r_k - r_j)_{j\neq k}}\right]\exp(r_k t) \tag{10.4.12}$$

Again, the significance of the mathematics is best demonstrated by example.

EXAMPLE 10.4.2. Consider the spring-mass system in Example 10.4.1. For the special case where ΔF_1 is a unit step function and ΔF_2 is zero, obtain a time-domain expression for the Δx_1 component of the system response vector.

Solution. From Example 10.4.1,

$$\overline{\Delta x_1}(s) = \frac{0.05s^2 + 0.0375s + 0.25}{s(s^4 + 2.25s^3 + 11.225s^2 + 11.325s + 0.5)}$$

The roots of the polynomial in the denominator of this Laplace transform are the eigenvalues found in Example 8.1.1 combined with the root zero,

$$r_1 = \lambda_1 = -0.556387 + 3.098306\,i$$

$$r_2 = \lambda_2 = -0.556387 - 3.098306\,i$$

$$r_3 = \lambda_3 = -1.090975$$

$$r_4 = \lambda_4 = -0.046251$$

$$r_5 = 0.0$$

Thus, using Eq. (10.4.12),

$$\begin{aligned}\Delta x_1(t) = &\left[\frac{0.05\lambda_1^2 + 0.0375\lambda_1 + 0.25}{\lambda_1(\lambda_1-\lambda_2)(\lambda_1-\lambda_3)(\lambda_1-\lambda_4)}\right]\exp(\lambda_1 t)\\ &+\left[\frac{0.05\lambda_2^2 + 0.0375\lambda_2 + 0.25}{\lambda_2(\lambda_2-\lambda_1)(\lambda_2-\lambda_3)(\lambda_2-\lambda_4)}\right]\exp(\lambda_2 t)\\ &+\left[\frac{0.05\lambda_3^2 + 0.0375\lambda_3 + 0.25}{\lambda_3(\lambda_3-\lambda_1)(\lambda_3-\lambda_2)(\lambda_3-\lambda_4)}\right]\exp(\lambda_3 t)\\ &+\left[\frac{0.05\lambda_4^2 + 0.0375\lambda_4 + 0.25}{\lambda_4(\lambda_4-\lambda_1)(\lambda_4-\lambda_2)(\lambda_4-\lambda_3)}\right]\exp(\lambda_4 t)+\left[\frac{0.25}{(-\lambda_1)(-\lambda_2)(-\lambda_3)(-\lambda_4)}\right]\end{aligned}$$

Using the known eigenvalues and carrying out the algebra gives

$$\begin{aligned}\Delta x_1(t) = &(-0.001254 - 0.000081\,i)\exp[(-0.556387 + 3.098306\,i)t]\\ &+(-0.001254 + 0.000081\,i)\exp[(-0.556387 - 3.098306\,i)t]\\ &+0.023840\exp(-1.090975t) - 0.521332\exp(-0.046251t) + 0.500000\end{aligned}$$

The first two terms in this solution could be combined and written as a damped sinusoid. The solution for the output response to a step function input that is not of unit amplitude is found simply by multiplying this solution by the amplitude of the input step function.

We see from Example 10.4.2 that the response to a step function control input is a constant plus a weighted sum of the homogeneous solutions, which are obtained directly from the system eigenvalues independent of the control inputs. If the two matrices [**A**] and [**C**] in Eq. (10.4.1) are known, the method used in Examples 10.4.1 and 10.4.2 to obtain the system response to a step control input is very systematic and quite suitable for programming on a digital computer.

EXAMPLE 10.4.3. For steady level flight at sea level, determine the longitudinal response to a negative 1-degree step change in elevator deflection for the general aviation airplane, which was described in Example 8.2.1. Using the linearized longitudinal equations of motion, plot the angle of attack and airspeed as a function of time. For this airplane and operating condition, we have

$$S_w = 185\ \text{ft}^2,\quad b_w = 33\ \text{ft},\quad \bar{c}_w = 5.606\ \text{ft},\quad W = 2{,}800\ \text{lbf},$$

$$V_o = 180\ \text{ft/sec},\quad C_{Do} = 0.05,$$

$$I_{xx_b} = 1000\ \text{slug·ft}^2,\quad I_{yy_b} = 3000\ \text{slug·ft}^2,\quad I_{zz_b} = 3500\ \text{slug·ft}^2,$$

$$I_{xz_b} = 30\ \text{slug·ft}^2,$$

$$C_{L,\alpha} = 4.40,\quad C_{D,\alpha} = 0.35,\quad C_{m,\alpha} = -0.68,\quad C_{L,\dot{\alpha}} = 1.60,\quad C_{m,\dot{\alpha}} = -4.35,$$

$$C_{Y,\beta} = -0.560, \quad C_{\ell,\beta} = -0.075, \quad C_{n,\beta} = 0.070,$$
$$C_{D,\bar{q}} \cong 0.0, \quad C_{L,\bar{q}} = 3.80, \quad C_{m,\bar{q}} = -9.95,$$
$$C_{Y,\bar{p}} \cong 0.0, \quad C_{\ell,\bar{p}} = -0.410, \quad C_{n,\bar{p}} = -0.0575,$$
$$C_{Y,\bar{r}} = 0.240, \quad C_{\ell,\bar{r}} = 0.105, \quad C_{n,\bar{r}} = -0.125,$$
$$C_{L,\delta_e} = 0.350, \quad C_{D,\delta_e} \cong 0.00, \quad C_{m,\delta_e} = -0.920,$$
$$C_{Y,\delta_a} \cong 0.00, \quad C_{\ell,\delta_a} = -0.135, \quad C_{n,\delta_a} = 0.0035,$$
$$C_{Y,\delta_r} = 0.155, \quad C_{\ell,\delta_r} = 0.105, \quad C_{n,\delta_r} = -0.075$$

Solution. From Example 8.2.1 we have

$$\frac{\rho S_w \bar{c}_w}{4W/g} = 0.007080, \qquad \frac{\rho S_w \bar{c}_w^3}{8I_{yy_b}} = 0.003228$$

From Eq. (7.7.8), this gives

$$R_{x,\delta_e} \equiv \frac{\rho S_w \bar{c}_w}{4W/g} C_{X,\delta_e} = -\frac{\rho S_w \bar{c}_w}{4W/g} C_{D,\delta_e} = 0.00$$
$$R_{z,\delta_e} \equiv \frac{\rho S_w \bar{c}_w}{4W/g} C_{Z,\delta_e} = -\frac{\rho S_w \bar{c}_w}{4W/g} C_{L,\delta_e} = -0.00248$$
$$R_{m,\delta_e} \equiv \frac{\rho S_w \bar{c}_w^3}{8I_{yy_b}} C_{m,\delta_e} = -0.00297$$

Combining these results with those obtained in Example 8.2.1, the linearized longitudinal equations of motion as given by Eq. (7.7.5) result in a system of equations in the form of the generalized linear control problem,

$$\begin{bmatrix} 1 & 0 & 0 & 0 & 0 & 0 \\ 0 & 1.01133 & 0 & 0 & 0 & 0 \\ 0 & 0.01404 & 1 & 0 & 0 & 0 \\ 0 & 0 & 0 & 1 & 0 & 0 \\ 0 & 0 & 0 & 0 & 1 & 0 \\ 0 & 0 & 0 & 0 & 0 & 1 \end{bmatrix} \begin{Bmatrix} \Delta\hat{u} \\ \Delta\hat{\alpha} \\ \Delta\hat{\bar{q}} \\ \Delta\hat{\xi}_x \\ \Delta\hat{\xi}_z \\ \Delta\hat{\theta} \end{Bmatrix} = \begin{Bmatrix} 0 \\ -0.00248 \\ -0.00297 \\ 0 \\ 0 \\ 0 \end{Bmatrix} \Delta\delta_e$$
$$+ \begin{bmatrix} -0.00071 & 0.00030 & 0 & 0 & 0 & -0.00278 \\ -0.00556 & -0.03151 & 0.97309 & 0 & 0 & 0 \\ 0 & -0.00220 & -0.03212 & 0 & 0 & 0 \\ 1 & 0 & 0 & 0 & 0 & 0 \\ 0 & 1 & 0 & 0 & 0 & -1 \\ 0 & 0 & 1 & 0 & 0 & 0 \end{bmatrix} \begin{Bmatrix} \Delta\mu \\ \Delta\alpha \\ \Delta\bar{q} \\ \Delta\xi_x \\ \Delta\xi_z \\ \Delta\theta \end{Bmatrix}$$

Since here we are only interested in airspeed and angle of attack, and because all coefficients of $\Delta\xi_x$ and $\Delta\xi_z$ are zero, this system can be reduced to fourth order by removing the fourth and fifth rows and columns. In addition, the system is readily reduced to the special linear control problem that is in the form of Eq. (10.4.1). This gives

$$\begin{Bmatrix} \Delta\hat{u} \\ \Delta\hat{\alpha} \\ \Delta\hat{\bar{q}} \\ \Delta\hat{\theta} \end{Bmatrix} = \begin{bmatrix} -0.00071 & 0.00030 & 0 & -0.00278 \\ -0.00550 & -0.03116 & 0.9622 & 0 \\ 0.00008 & -0.00176 & -0.04563 & 0 \\ 0 & 0 & 1 & 0 \end{bmatrix} \begin{Bmatrix} \Delta u \\ \Delta\alpha \\ \Delta\bar{q} \\ \Delta\theta \end{Bmatrix} + \begin{Bmatrix} 0 \\ -0.00245 \\ -0.00294 \\ 0 \end{Bmatrix} \Delta\delta_e$$

The eigenvalues of this system are the nonzero eigenvalues that were obtained in Example 8.2.1. Only the rigid-body displacement modes are lost as a result of reducing the system to fourth order. The airspeed and angle-of-attack response to a negative 1-degree step change in elevator deflection ($\Delta\delta_e = -0.01745$), as computed from this system of equations, is shown in Fig. 10.4.2.

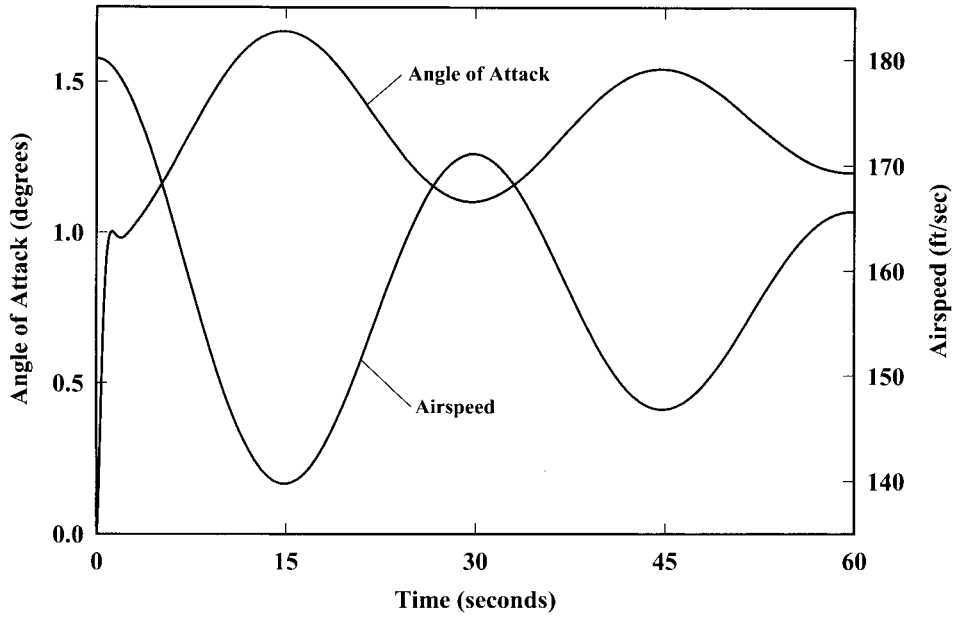


Figure 10.4.2. Response to a step change in elevator deflection for the airplane in Example 10.4.3.

A few observations should be made from the results predicted in Example 10.4.3. Here again we see that system response to a step change in control input has the same characteristic form as the homogeneous solution, which is obtained with the control input set to zero. From Fig. 10.4.2, we clearly see the nature of both the short period and the phugoid in this solution. Because the frequency of the phugoid and short period differ so greatly, for the first second or so after the elevator deflection has been applied, the response of the system depends almost entirely on the short-period characteristics. After a few seconds have passed, damping has removed all traces of the short period from this solution. However, the phugoid oscillations persist for much longer. With the elevator deflection maintained, a new trim state would eventually be reached, corresponding to climbing flight at about 160 ft/sec with an increase in angle of attack of approximately 1.3 degrees. If the elevator deflection were actually held constant, it would take several minutes for the phugoid oscillations to die out. However, if the pilot uses the stick or control yoke to hold the nose of the airplane at the desired position relative to the horizon, the phugoid oscillations will disappear almost immediately. In fact, since pilots always control an airplane by watching the horizon or an instrument, not by watching the stick or control yoke, phugoid oscillations are not normally encountered in a pull-up maneuver. The short-period characteristics, on the other hand, affect the pull-up maneuver significantly, even more so in airplanes which exhibit lower short-period damping. Figure 10.4.3 shows how reduced pitch damping affects the step response to elevator deflection.

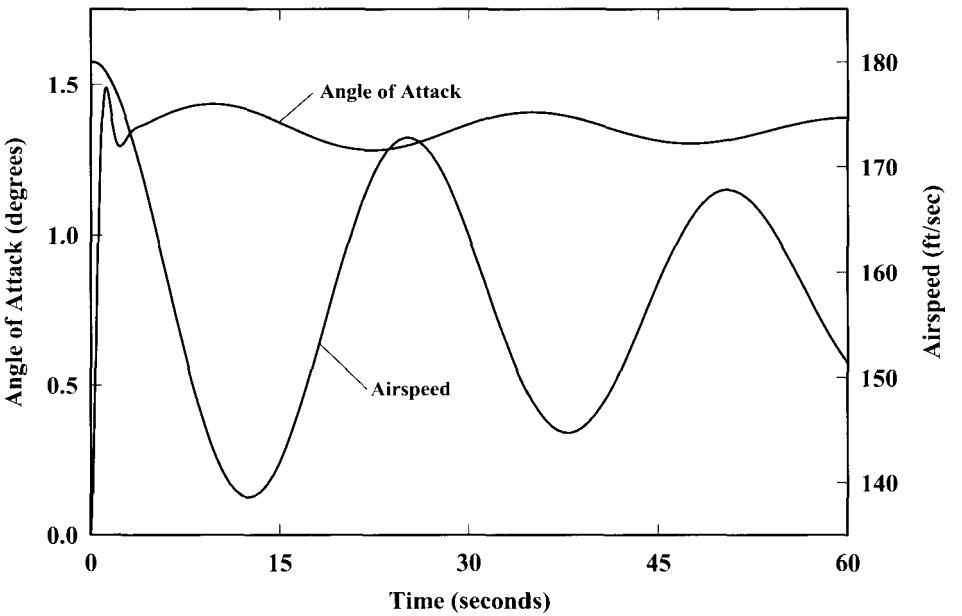


Figure 10.4.3. Response to a step change in elevator deflection for the airplane in Example 10.4.3, with a significant reduction in pitch damping.

EXAMPLE 10.4.4. For steady level flight at sea level, determine the lateral response to a 1-degree step change in rudder deflection for the general aviation airplane that was described in Example 9.2.1. Using the linearized lateral equations of motion, plot the sideslip angle and bank angle as a function of time. For this airplane and operating conditions, we have

$$S_w = 185 \text{ ft}^2, \quad b_w = 33 \text{ ft}, \quad \bar{c}_w = 5.606 \text{ ft}, \quad W = 2{,}800 \text{ lbf},$$
$$V_o = 180 \text{ ft/sec}, \quad C_{Do} = 0.05,$$
$$I_{xx_b} = 1{,}000 \text{ slug·ft}^2, \quad I_{yy_b} = 3{,}000 \text{ slug·ft}^2, \quad I_{zz_b} = 3{,}500 \text{ slug·ft}^2,$$
$$I_{xz_b} = 30 \text{ slug·ft}^2,$$
$$C_{L,\alpha} = 4.40, \quad C_{D,\alpha} = 0.35, \quad C_{m,\alpha} = -0.68, \quad C_{L,\dot{\alpha}} = 1.60, \quad C_{m,\dot{\alpha}} = -4.35,$$
$$C_{Y,\beta} = -0.560, \quad C_{\ell,\beta} = -0.075, \quad C_{n,\beta} = 0.070,$$
$$C_{D,\bar{q}} \cong 0.0, \quad C_{L,\bar{q}} = 3.80, \quad C_{m,\bar{q}} = -9.95,$$
$$C_{Y,\bar{p}} \cong 0.0, \quad C_{\ell,\bar{p}} = -0.410, \quad C_{n,\bar{p}} = -0.0575,$$
$$C_{Y,\bar{r}} = 0.240, \quad C_{\ell,\bar{r}} = 0.105, \quad C_{n,\bar{r}} = -0.125,$$
$$C_{L,\delta_e} = 0.350, \quad C_{D,\delta_e} \cong 0.00, \quad C_{m,\delta_e} = -0.920,$$
$$C_{Y,\delta_a} \cong 0.00, \quad C_{\ell,\delta_a} = -0.135, \quad C_{n,\delta_a} = 0.0035,$$
$$C_{Y,\delta_r} = 0.155, \quad C_{\ell,\delta_r} = 0.105, \quad C_{n,\delta_r} = -0.075$$

Solution. From Example 9.2.1, we have

$$\frac{\rho S_w b_w}{4W/g} = 0.041679, \qquad \frac{\rho S_w b_w^3}{8I_{xx_b}} = 1.975306, \qquad \frac{\rho S_w b_w^3}{8I_{zz_b}} = 0.564373$$

From Eq. (7.7.8), this gives

$$R_{y,\delta_a} \equiv \frac{\rho S_w b_w}{4W/g} C_{Y,\delta_a} = 0.00$$

$$R_{\ell,\delta_a} \equiv \frac{\rho S_w b_w^3}{8I_{xx_b}} C_{\ell,\delta_a} = -0.2667$$

$$R_{n,\delta_a} \equiv \frac{\rho S_w b_w^3}{8I_{zz_b}} C_{n,\delta_a} = 0.00198$$

$$R_{y,\delta_r} \equiv \frac{\rho S_w b_w}{4W/g} C_{Y,\delta_r} = 0.00646$$

$$R_{\ell,\delta_r} \equiv \frac{\rho S_w b_w^3}{8I_{xx_b}} C_{\ell,\delta_r} = 0.2074$$

$$R_{n,\delta_r} \equiv \frac{\rho S_w b_w^3}{8I_{zz_b}} C_{n,\delta_r} = -0.04233$$

Combining these results with those obtained in Example 9.2.1, the linearized lateral equations of motion as given by Eq. (7.7.6) result in a generalized linear control problem,

$$\begin{bmatrix} 1 & 0 & 0 & 0 & 0 & 0 \\ 0 & 1 & -0.0300 & 0 & 0 & 0 \\ 0 & -0.0086 & 1 & 0 & 0 & 0 \\ 0 & 0 & 0 & 1 & 0 & 0 \\ 0 & 0 & 0 & 0 & 1 & 0 \\ 0 & 0 & 0 & 0 & 0 & 1 \end{bmatrix} \begin{Bmatrix} \Delta\hat{\beta} \\ \Delta\hat{\bar{p}} \\ \Delta\hat{\bar{r}} \\ \Delta\hat{\xi}_y \\ \Delta\hat{\phi} \\ \Delta\hat{\psi} \end{Bmatrix} = \begin{bmatrix} 0 & 0.00646 \\ -0.2667 & 0.2074 \\ 0.00198 & -0.04233 \\ 0 & 0 \\ 0 & 0 \\ 0 & 0 \end{bmatrix} \begin{Bmatrix} \Delta\delta_a \\ \Delta\delta_r \end{Bmatrix}$$

$$+ \begin{bmatrix} -0.0233 & 0 & -0.9900 & 0 & 0.0164 & 0 \\ -0.1481 & -0.8099 & 0.2074 & 0 & 0 & 0 \\ 0.0395 & -0.0325 & -0.0705 & 0 & 0 & 0 \\ 1 & 0 & 0 & 0 & 0 & 1 \\ 0 & 1 & 0 & 0 & 0 & 0 \\ 0 & 0 & 1 & 0 & 0 & 0 \end{bmatrix} \begin{Bmatrix} \Delta\beta \\ \Delta\bar{p} \\ \Delta\bar{r} \\ \Delta\xi_y \\ \Delta\phi \\ \Delta\psi \end{Bmatrix}$$

Similar to Example 10.4.3, this system can also be reduced to fourth order. Notice that rows 1, 2, 3, and 5 are not coupled in any way to rows 4 and 6. Thus, removing rows and columns 4 and 6 reduces the order of the system. The result is readily reduced to the form of Eq. (10.4.1),

$$\begin{Bmatrix} \Delta\hat{\beta} \\ \Delta\hat{\bar{p}} \\ \Delta\hat{\bar{r}} \\ \Delta\hat{\phi} \end{Bmatrix} = \begin{bmatrix} -0.0233 & 0 & -0.9900 & 0.0164 \\ -0.1470 & -0.8111 & 0.2053 & 0 \\ 0.0382 & -0.0395 & -0.0687 & 0 \\ 0 & 1 & 0 & 0 \end{bmatrix} \begin{Bmatrix} \Delta\beta \\ \Delta\bar{p} \\ \Delta\bar{r} \\ \Delta\phi \end{Bmatrix}$$

$$+ \begin{bmatrix} 0 & 0.00646 \\ -0.2667 & 0.2062 \\ -0.00031 & -0.04056 \\ 0 & 0 \end{bmatrix} \begin{Bmatrix} \Delta\delta_a \\ \Delta\delta_r \end{Bmatrix}$$

The eigenvalues for this system were already obtained in Example 9.2.1. These are the eigenvalues for the roll, spiral, and Dutch roll modes, which were found in that example. The trivial rigid-body displacement modes are not found in this system of reduced order. Figure 10.4.4 shows the response in bank angle and sideslip angle to a 1-degree step change in rudder deflection, as computed from this linear system.

Despite rather heavy yaw damping, excitation of Dutch roll can clearly be seen in Fig. 10.4.4. To demonstrate how yaw damping affects control response, Fig. 10.4.5 shows similar results, as predicted with reduced yaw damping.

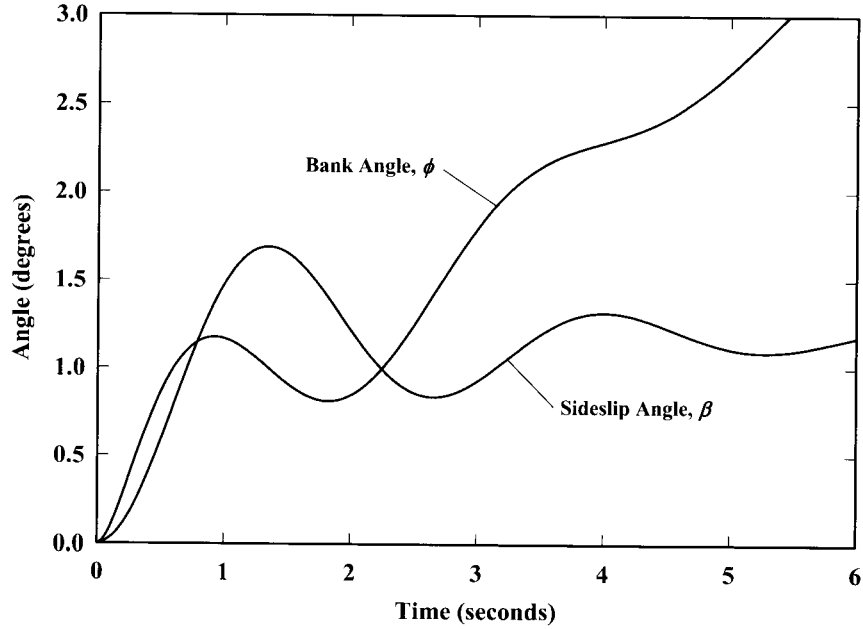


Figure 10.4.4. Response to a step change in rudder deflection for the airplane in Example 10.4.4.

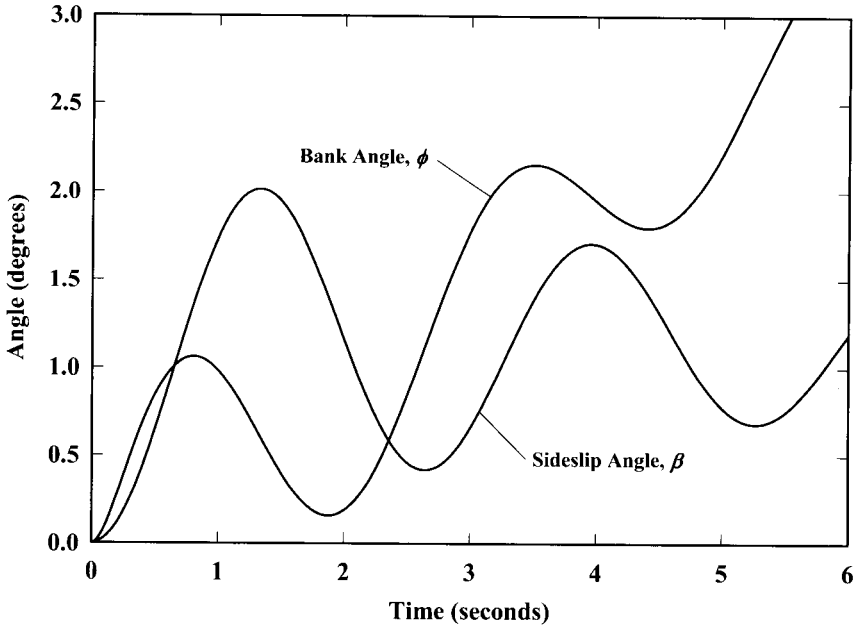


Figure 10.4.5. Response to a step change in rudder deflection for the airplane in Example 10.4.4, with a significant reduction in yaw damping.

In Examples 10.4.3 and 10.4.4, we have seen that an airplane's initial response to a change in control input has the same characteristic form as the stick-fixed dynamic modes, which are obtained from the homogeneous equations of motion with all control inputs set to zero. For this reason, the "feel" of an airplane's controls is significantly affected by the eigenvalues for the stick-fixed dynamic modes. For example, the feel of the elevator control is affected by the short-period eigenvalues, and the feel of the rudder control is affected by the Dutch roll eigenvalues. This explains why pilot opinion of aircraft handling qualities correlates so well with these eigenvalues.

Frequency Response

Another very important type of input that can be analyzed with the aid of the transfer function is the sinusoidal input. Consider a particular state variable that has a transfer function with respect to some particular input parameter, which has the usual form

$$G(s) = \frac{N(s)}{(s-\lambda_1)(s-\lambda_2)(s-\lambda_3)\cdots(s-\lambda_n)} \tag{10.4.13}$$

where $N(s)$ is a polynomial of order less than n. Now let the input be given by

$$\exp(i\omega t) = \cos(\omega t) + i\sin(\omega t) \tag{10.4.14}$$

If we multiply the Laplace transform of this input by the transfer function, the result is the Laplace transform of the response to a unit sinusoid. The real part of the result will be the Laplace transform of the response to a unit cosine input, and the imaginary part of the result will be the Laplace transform of the response to a unit sine input. From any table of Laplace transforms we find that

$$\overline{\exp(i\omega t)} = 1/(s-i\omega) \tag{10.4.15}$$

Thus, combining Eqs. (10.4.13) and (10.4.15), the Laplace transform of the response to a unit sinusoid is

$$\bar{x}(s) = G(s)\,\overline{\exp(i\omega t)} = \frac{N(s)}{(s-i\omega)(s-\lambda_1)(s-\lambda_2)\cdots(s-\lambda_n)} \tag{10.4.16}$$

After applying Eq. (10.4.12) to Eq. (10.4.16), we find that the time-domain response to a unit sinusoidal input is

$$x(t) = \sum_{k=1}^{n}\left[\frac{N(\lambda_k)}{\prod_{j=1}^{n}(\lambda_k-\lambda_j)_{j\neq k}}\right]\frac{\exp(\lambda_k t)}{(\lambda_k - i\omega)} + \frac{N(i\omega)}{(i\omega-\lambda_1)(i\omega-\lambda_2)(i\omega-\lambda_3)\cdots(i\omega-\lambda_n)}\exp(i\omega t) \tag{10.4.17}$$

Some important observations can be made from Eq. (10.4.17). Here again we see that the initial response to the control input includes a weighted sum of the homogeneous solutions that are obtained from the system eigenvalues. The last term in Eq. (10.4.17) describes a sinusoidal oscillation having the same frequency as the input. If all of the system eigenvalues are associated with convergent modes, after some time has passed, each of the homogeneous solutions will go to zero. Thus, the last term in Eq. (10.4.17) is the steady periodic response to a unit sinusoidal input. This is a sinusoidal output having the same frequency as the input but with different amplitude and phase.

Notice by comparing the transfer function in Eq. (10.4.13) with the response predicted by Eq. (10.4.17) that the steady periodic solution can simply be written as

$$x(t) \underset{t\to\infty}{=} G(i\omega)\exp(i\omega t) \tag{10.4.18}$$

The function $G(i\omega)$ is called the *complex amplitude* and is simply the transfer function evaluated at $s = i\omega$. In general, $G(i\omega)$ is a complex number that can be expressed in terms of amplitude and phase, just as we did with the eigenvectors in Chapter 8. The magnitude of $G(i\omega)$ is called the *gain* and is simply the ratio of the response amplitude to the input amplitude. When the input frequency ω is zero, Eq. (10.4.17) reduces to the step response. Thus, $G(0)$ is called the *static gain* and $|G(i\omega)|/|G(0)|$ is called the *dynamic gain*. Figure 10.4.6 shows how the dynamic gain varies with frequency and damping ratio for a second-order system.

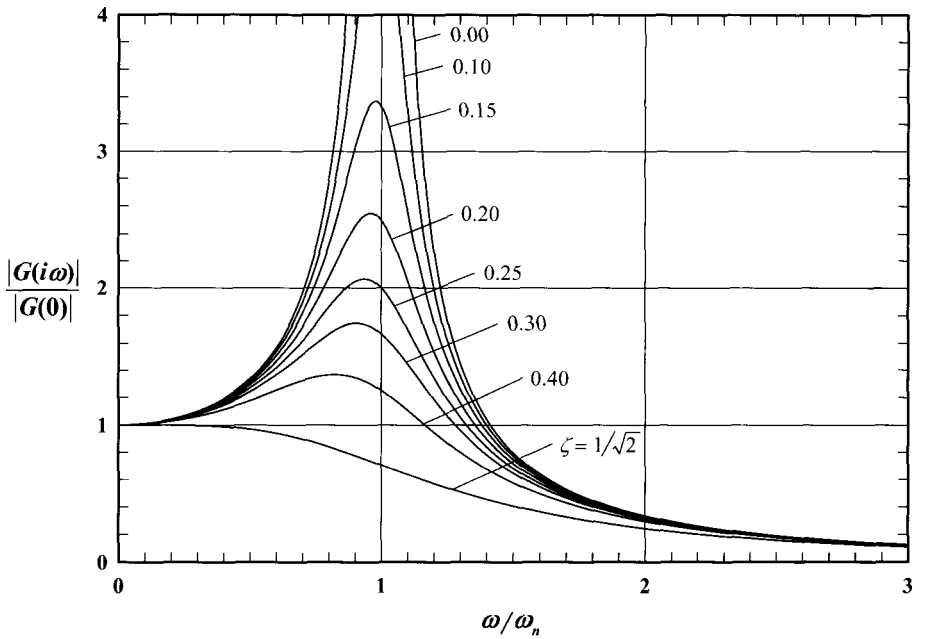


Figure 10.4.6. Dynamic frequency response for a second-order system.

Curves like those shown in Fig. 10.4.6 are commonly called *frequency-response curves*. A second-order linear-invariant system, like that used for Fig. 10.4.6, has only one undamped natural frequency and will exhibit at most one resonance peak. Higher-order linear-invariant systems, such as those associated with aircraft controls, typically have multiple natural frequencies and will commonly exhibit multiple resonance peaks. The examination of frequency-response curves for aircraft controls is left as an exercise for the student.

Autopilots and Automatic Control

The concept of transfer functions and the Laplace transform description of system dynamics are employed extensively in the application of classical automatic control theory to the design of autopilots and aircraft stability augmentation systems. To study autopilot design successfully, the student would need a good background in the fundamentals of automatic control theory as well as flight mechanics. At least one undergraduate engineering course in control theory would typically be needed to provide the minimum essential background. A detailed treatment of automatic control theory is not within the intended scope of this textbook. However, a few words on automatic control may help the interested student to decide whether or not additional coursework along these lines would be in order.

The important and exciting field of automatic control theory is commonly divided into two very broad areas, which are traditionally called *classical control theory* and *modern control theory*. The term "modern" control theory can be misleading, because it seems to imply that classical automatic control theory is obsolete and no longer used. This is not the case. To fully understand the design of autopilots and aircraft stability augmentation systems, an engineer would need to understand both the classical and modern approaches to automatic control.

Classical automatic control theory is based on the frequency-response method and utilizes the Laplace transforms and transfer functions that were briefly introduced in this section. As we have seen in Eq. (10.4.10), knowledge of the transfer functions depends on knowledge of the system's eigenvalues. Thus, the reader may begin to see why closed-form approximations for these eigenvalues would be of value in autopilot design. If the reader has made only a cursory attempt to follow the material that was presented here, he or she may have the false impression that Laplace transforms and transfer functions are very complicated and difficult to understand. However, if an honest attempt is made to follow these mathematical developments, most readers will see that describing system dynamics through the use of Laplace transforms and transfer functions is remarkably simple. In fact, the primary advantage of the classical approach to automatic control theory is the great simplification in the mathematical description of system dynamics that is afforded by the Laplace transform.

Modern automatic control theory, which is sometimes referred to as the *state space approach*, has its origins in the early 1960s with the development of the high-speed digital computer. With this approach, system dynamics is expressed directly in terms of a system of first-order linear differential equations, like those presented in Chapter 7 for aircraft dynamics. One significant advantage of this approach to automatic control has been the application of numerical optimization algorithms to the development of what is

commonly called *optimal control theory*. Modern automatic control is mathematically quite similar to digital flight simulation. Thus, an understanding of the material to be covered in Chapter 11 should be helpful in a later study of automatic control theory.

For many years autopilots have been used to relieve human pilots of the monotonous task of maintaining attitude and heading during long periods of steady level flight. Stability augmentation systems have long been used to enhance the handling qualities of airplanes and provide maneuverability that would otherwise be unattainable. Today the application of automatic control theory to the world of aviation goes far beyond these traditional applications. Totally autonomous flight is now an attainable reality. Recent developments of extremely small electromechanical systems are making flight on a very small scale possible and practicable. The next 50 years will surely see some very exciting advancements come out of the marriage between the disciplines of flight mechanics and automatic control theory.

If a student finds the topic of autopilots and aircraft stability augmentation systems to be of particular interest, he or she is encouraged to pursue this interest further with formal coursework on automatic control theory. The starting point would typically be the first undergraduate engineering course in automatic control. If interest continues, this introductory class should be followed with courses on digital and optimal control. These three classes, combined with a thorough background in fluid mechanics, aerodynamics, and flight mechanics, should find the engineering graduate well prepared to contribute to this exciting field.

10.5. Nonlinear Effects and Longitudinal-Lateral Coupling

It should be reemphasized that all of the material on aircraft handling qualities and control response that has been presented in this chapter is based on the linearized equations of motion with negligible coupling between the longitudinal and lateral degrees of freedom. Such results are restricted to low-angle-of-attack flight with relatively small departures from equilibrium. These results are also restricted to aircraft and operating conditions having little or no inertial, gyroscopic, or aerodynamic coupling between the pitch axis and the roll or yaw axes. While these conditions are satisfied for many airplanes and operating conditions, there are also important cases for which these approximations are not valid.

In Sec. 9.8, the longitudinal-lateral coupling resulting from inertial, gyroscopic, and aerodynamic asymmetry was discussed. Since coupling of this type has first-order components, it can affect aircraft handling qualities even during gradual maneuvers at low angles of attack. While these effects are not accounted for in the handling quality predictions presented in this chapter, they are of significant interest, particularly in some military application where substantial aircraft asymmetry can be encountered.

Handling qualities during very rapid maneuvers have also been ignored in this chapter. Even in a completely symmetric airplane, during very rapid maneuvers, second-order inertial coupling between roll and pitch (Secs. 7.9 and 9.8) can significantly alter control response and aircraft handling qualities. The analytical treatment of such phenomena requires numerical solution of the nonlinear equations of motion, which is discussed in Chapter 11.

Today, aircraft control and handling qualities at angles of attack beyond stall are of significant interest. For a combat aircraft, high turning rates are very critical to mission effectiveness. The maximum turning rate that can be achieved in a conventional turn is severely limited by the load factor that can be endured by an aircraft and pilot. Turning rates at low load factor can be increased substantially if the aircraft is capable of controlled flight at angles of attack well beyond stall. The cobra maneuver, which is shown in Fig. 3.9.7, is one example of how high turning rate can be achieved in such aircraft. An aircraft capable of such maneuvers has a decisive tactical advantage over an airplane that is limited to conventional turns. Because conventional airplane control surfaces become ineffective at angles of attack beyond stall, alternative methods of control have been developed for high-angle-of-attack flight. These include thrust vectoring, actuated forebody strakes, and forebody blowing and suction. Because flight dynamics becomes highly nonlinear at angles of attack beyond stall, the methods presented in this chapter do not apply. Here again, the numerical solution techniques presented in Chapter 11 provide a good alternative for the analytical investigation of such phenomena.

10.6. Problems

10.1. For the airplane and operating conditions in problem 9.47, compare the predicted dynamic response with the frequency and damping requirements presented in Sec. 10.3. What level of handling qualities should be expected for this airplane and operating conditions, based on the dynamic response modes?

10.2. For the airplane and operating conditions in problem 9.48, compare the predicted dynamic response with the frequency and damping requirements presented in Sec. 10.3. What level of handling qualities should be expected for this airplane and operating conditions, based on the dynamic response modes?

10.3. For the airplane and operating conditions in problem 9.49, compare the predicted dynamic response with the frequency and damping requirements presented in Sec. 10.3. What level of handling qualities should be expected for this airplane and operating conditions, based on the dynamic response modes?

10.4. For the airplane and operating conditions in problem 9.50, compare the predicted dynamic response with the frequency and damping requirements presented in Sec. 10.3. What level of handling qualities should be expected for this airplane and operating conditions, based on the dynamic response modes?

10.5. For the airplane and operating conditions in Example 10.4.3, find the angle-of-attack transfer function for response to elevator deflection.

10.6. From the transfer function obtained in problem 10.5, find the Laplace transform of the angle-of-attack component of the state variable response vector for a unit step change in elevator deflection.

10.7. From the Laplace transform acquired in problem 10.6, obtain a time-domain expression for the angle-of-attack response to a negative 1-degree step change in elevator deflection. Using this expression, plot the angle of attack as a function of time.

10.8. For the airplane and operating conditions in Example 10.4.4, find the sideslip angle transfer function for response to rudder deflection.

10.9. From the transfer function obtained in problem 10.8, find the Laplace transform of the sideslip angle component of the state variable response vector for a unit step change in rudder deflection.

10.10. From the Laplace transform acquired in problem 10.9, obtain a time-domain expression for the sideslip angle response to a 1-degree step change in rudder deflection. Using this expression, plot the sideslip angle as a function of time.

10.11. From the transfer function obtained in problem 10.5, examine the angle-of-attack frequency response for sinusoidal variation in elevator deflection. Plot the dynamic gain as a function of input frequency.

10.12. From the transfer function obtained in problem 10.8, examine the sideslip angle frequency response for sinusoidal variation in rudder deflection. Plot the dynamic gain as a function of input frequency.

Chapter 11
Aircraft Flight Simulation

11.1. Introduction

In Chapter 7, the six-degree-of-freedom (6-DOF) rigid-body equations of motion for an aircraft in flight were developed in terms of Euler angles. This Euler angle formulation was then linearized, and in Chapters 8, 9, and 10, we examined some aspects of aircraft dynamics as predicted from the linearized formulation. However, there are many applications in the discipline of flight dynamics to which the linearized equations of motion do not apply. For such applications, we must return to a fully coupled nonlinear formulation. For this purpose, the Euler angle formulation developed in Chapter 7 could be used. However, as we shall see, this is not the best alternative.

The Euler angle formulation contains a singularity known as *gimbal lock*, which is encountered when the nose of the airplane is pointed either straight up or straight down. While this singularity is of no concern when simulating the flight of most conventional airplanes under typical operating conditions, it does limit the general utility of a flight simulator based on the Euler angle formulation. In addition, the Euler angle formulation has significant computational disadvantages compared to other formulations that have been developed for flight simulation. In this chapter we compare some of these alternative formulations. Emphasis is placed on what is called the *quaternion formulation*, which has substantial advantages over the Euler angle formulation. For example, the computation time required for vector transformation using the Euler angle formulation is about 11 times that required with the quaternion formulation.

For simulating aircraft motion, Newton's second law is written in terms of a noninertial coordinate system fixed to the aircraft. Position and orientation are described using a coordinate frame fixed to the Earth, which for all practical purposes is an inertial coordinate system. The location and orientation of the noninertial frame relative to the inertial frame specify the aircraft's position and orientation. The noninertial or *body-fixed* coordinates are designated (x_b, y_b, z_b) and the inertial or *Earth-fixed* coordinates, which have been used to this point in the text, are denoted (x_f, y_f, z_f). The orientations of these two Cartesian coordinate systems relative to the Earth and the aircraft were shown in Fig. 7.1.2. The *flat-Earth* coordinate system (x_f, y_f, z_f) can only be used for relatively short flights that do not traverse a significant portion of the Earth's surface. For longer flights, position is described in terms of latitude, longitude, and altitude.

To develop a complete 6-DOF formulation for flight simulation, some means of transforming the components of a vector between noninertial and inertial coordinates is required. The equations used for this purpose are called the *kinematic transformation equations*. For a complete review of the literature on the mathematical formulations that have been used for aircraft kinematics the reader is referred to Phillips, Hailey, and Gebert (2000 and 2001). Much of the material presented in this chapter was taken directly from these references. The reader is cautioned that the equations in the 2001 *Journal of Aircraft* paper contain numerous typesetting errors, which are not found in the 2000 AIAA meeting paper or in the material presented in this chapter.

11.2. Euler Angle Formulations

The orientation of the noninertial reference frame relative to the inertial reference frame can be described in terms of three consecutive rotations through three *body-referenced Euler angles*. There are 12 possible ways to define three independent body-referenced Euler angles. Starting from the inertial reference frame, three consecutive rotations are performed, each about one of the three body-referenced axes, to arrive at the final noninertial reference frame. The only restriction required to provide three degrees of freedom is that no two consecutive rotations can be about the same axis. With this restriction, there are six symmetric sets of Euler angles,

$$\begin{aligned} &\varphi_x \to \varphi_y \to \varphi_x, \qquad &&\varphi_x \to \varphi_z \to \varphi_x, \\ &\varphi_y \to \varphi_x \to \varphi_y, \qquad &&\varphi_y \to \varphi_z \to \varphi_y, \\ &\varphi_z \to \varphi_x \to \varphi_z, \qquad &&\varphi_z \to \varphi_y \to \varphi_z \end{aligned}$$

and six asymmetric sets,

$$\begin{aligned} &\varphi_x \to \varphi_y \to \varphi_z, \qquad &&\varphi_x \to \varphi_z \to \varphi_y, \\ &\varphi_y \to \varphi_x \to \varphi_z, \qquad &&\varphi_y \to \varphi_z \to \varphi_x, \\ &\varphi_z \to \varphi_x \to \varphi_y, \qquad &&\varphi_z \to \varphi_y \to \varphi_x \end{aligned}$$

Tandon (1978) presents the rotation matrix for each of the 12 sets of Euler angles. Any of these 12 Euler angle sets can be used for attitude representation. For example, in the field of orbital mechanics the $\varphi_z \to \varphi_x \to \varphi_z$ sequence is typically used. The aeronautics community commonly uses the last of the rotation sequences above, $\varphi_z \to \varphi_y \to \varphi_x$. These three Euler angles, commonly written ψ, θ, and ϕ, are, respectively, the azimuth angle, elevation angle, and bank angle, which were described in detail in Sec. 7.3 and shown in Figs. 7.3.1 and 7.3.2.

With these common Euler angle definitions, in Sec. 7.3 we considered an arbitrary vector $\mathbf{v}$ having components $(v_{x_f}, v_{y_f}, v_{z_f})$ in the inertial coordinate system and having components $(v_{x_b}, v_{y_b}, v_{z_b})$ in the noninertial coordinate system. Using the shorthand notation $S_\chi = \sin(\chi)$ and $C_\chi = \cos(\chi)$, the transformation of the components of this vector from inertial coordinates to noninertial coordinates was found to be

$$\begin{Bmatrix} v_{x_b} \\ v_{y_b} \\ v_{z_b} \end{Bmatrix} = \begin{bmatrix} 1 & 0 & 0 \\ 0 & C_\phi & S_\phi \\ 0 & -S_\phi & C_\phi \end{bmatrix} \begin{bmatrix} C_\theta & 0 & -S_\theta \\ 0 & 1 & 0 \\ S_\theta & 0 & C_\theta \end{bmatrix} \begin{bmatrix} C_\psi & S_\psi & 0 \\ -S_\psi & C_\psi & 0 \\ 0 & 0 & 1 \end{bmatrix} \begin{Bmatrix} v_{x_f} \\ v_{y_f} \\ v_{z_f} \end{Bmatrix}$$

or

$$\begin{Bmatrix} v_{x_b} \\ v_{y_b} \\ v_{z_b} \end{Bmatrix} = \begin{bmatrix} C_\theta C_\psi & C_\theta S_\psi & -S_\theta \\ S_\phi S_\theta C_\psi - C_\phi S_\psi & S_\phi S_\theta S_\psi + C_\phi C_\psi & S_\phi C_\theta \\ C_\phi S_\theta C_\psi + S_\phi S_\psi & C_\phi S_\theta S_\psi - S_\phi C_\psi & C_\phi C_\theta \end{bmatrix} \begin{Bmatrix} v_{x_f} \\ v_{y_f} \\ v_{z_f} \end{Bmatrix} \tag{11.2.1}$$

The inverse of the transformation matrix in Eq. (11.2.1) is its transpose, which gives

$$\begin{Bmatrix} v_{x_f} \\ v_{y_f} \\ v_{z_f} \end{Bmatrix} = \begin{bmatrix} C_\theta C_\psi & S_\phi S_\theta C_\psi - C_\phi S_\psi & C_\phi S_\theta C_\psi + S_\phi S_\psi \\ C_\theta S_\psi & S_\phi S_\theta S_\psi + C_\phi C_\psi & C_\phi S_\theta S_\psi - S_\phi C_\psi \\ -S_\theta & S_\phi C_\theta & C_\phi C_\theta \end{bmatrix} \begin{Bmatrix} v_{x_h} \\ v_{y_h} \\ v_{z_h} \end{Bmatrix} \tag{11.2.2}$$

Since Newton's second law is written in terms of the noninertial coordinate system, the gravitational force must be expressed in terms of noninertial coordinates. Applying Eq. (11.2.1) to the weight vector, we found that

$$\begin{Bmatrix} W_{x_h} \\ W_{y_h} \\ W_{z_h} \end{Bmatrix} = \begin{bmatrix} C_\theta C_\psi & C_\theta S_\psi & -S_\theta \\ S_\phi S_\theta C_\psi - C_\phi S_\psi & S_\phi S_\theta S_\psi + C_\phi C_\psi & S_\phi C_\theta \\ C_\phi S_\theta C_\psi + S_\phi S_\psi & C_\phi S_\theta S_\psi - S_\phi C_\psi & C_\phi C_\theta \end{bmatrix} \begin{Bmatrix} 0 \\ 0 \\ W \end{Bmatrix}$$

or

$$\begin{Bmatrix} W_{x_h} \\ W_{y_h} \\ W_{z_h} \end{Bmatrix} = = W \begin{Bmatrix} -S_\theta \\ S_\phi C_\theta \\ C_\phi C_\theta \end{Bmatrix} \tag{11.2.3}$$

Similarly, from Eq. (11.2.2), the ground speed was related to the airspeed and wind by

$$\begin{Bmatrix} \dot{x}_f \\ \dot{y}_f \\ \dot{z}_f \end{Bmatrix} = \begin{Bmatrix} V_{wx_f} \\ V_{wy_f} \\ V_{wz_f} \end{Bmatrix} + \begin{bmatrix} C_\theta C_\psi & S_\phi S_\theta C_\psi - C_\phi S_\psi & C_\phi S_\theta C_\psi + S_\phi S_\psi \\ C_\theta S_\psi & S_\phi S_\theta S_\psi + C_\phi C_\psi & C_\phi S_\theta S_\psi - S_\phi C_\psi \\ -S_\theta & S_\phi C_\theta & C_\phi C_\theta \end{bmatrix} \begin{Bmatrix} u \\ v \\ w \end{Bmatrix} \tag{11.2.4}$$

Using these same Euler angle definitions, we found that the relationship between the body-fixed angular rates and the time rate of change of the Euler angles is

$$\begin{Bmatrix} \dot{\phi} \\ \dot{\theta} \\ \dot{\psi} \end{Bmatrix} = \begin{bmatrix} 1 & S_\phi S_\theta / C_\theta & C_\phi S_\theta / C_\theta \\ 0 & C_\phi & -S_\phi \\ 0 & S_\phi / C_\theta & C_\phi / C_\theta \end{bmatrix} \begin{Bmatrix} p \\ q \\ r \end{Bmatrix} \tag{11.2.5}$$

In terms of this particular set of Euler angles, Eqs. (11.2.4) and (11.2.5) provide the kinematic transformation equations, which are needed to update the position and orientation of the aircraft with time. The gimbal lock singularity is seen in the last two terms of the first and last rows of Eq. (11.2.5). Likewise, a similar set of kinematic transformation equations can be developed for any one of the other 11 Euler angle sets. However, in no case will a singularity-free formulation result. One possible means to avoid the singularity associated with an Euler angle formulation is to use two different Euler angle formulations, which have their singularities located at different orientations.

As the singularity associated with one formulation is approached, the computation algorithm is switched to the other formulation. While this avoids the gimbal lock singularity, for reasons of computational efficiency, it is not the best solution.

11.3. Direction-Cosine Formulation

The *direction-cosine matrix* can be formed from any of the symmetric or asymmetric Euler angle sets. For example, the matrix on the right side of Eq. (11.2.1) is a direction-cosine matrix. One way to avoid the singularity in Eq. (11.2.5) is to treat the nine components of this matrix as a fundamental description of orientation. The elements of this matrix are called the *direction cosines*. If these nine direction cosines are known, the components of an arbitrary vector in body-fixed coordinates are quite simply related to the components of the same vector in inertial coordinates through the definition of the direction-cosine matrix, [**C**],

$$\begin{Bmatrix} v_{x_b} \\ v_{y_b} \\ v_{z_b} \end{Bmatrix} \equiv \begin{bmatrix} C_{11} & C_{12} & C_{13} \\ C_{21} & C_{22} & C_{23} \\ C_{31} & C_{32} & C_{33} \end{bmatrix} \begin{Bmatrix} v_{x_f} \\ v_{y_f} \\ v_{z_f} \end{Bmatrix} \tag{11.3.1}$$

and the gravitational force vector, expressed in body-fixed coordinates, is

$$\begin{Bmatrix} W_{x_b} \\ W_{y_b} \\ W_{z_b} \end{Bmatrix} = W \begin{Bmatrix} C_{13} \\ C_{23} \\ C_{33} \end{Bmatrix} \tag{11.3.2}$$

The inverse of the direction-cosine matrix is simply its transpose, so the ground speed is related to the airspeed and wind by

$$\begin{Bmatrix} \dot{x}_f \\ \dot{y}_f \\ \dot{z}_f \end{Bmatrix} = \begin{Bmatrix} V_{wx_f} \\ V_{wy_f} \\ V_{wz_f} \end{Bmatrix} + \begin{bmatrix} C_{11} & C_{21} & C_{31} \\ C_{12} & C_{22} & C_{32} \\ C_{13} & C_{23} & C_{33} \end{bmatrix} \begin{Bmatrix} u \\ v \\ w \end{Bmatrix} \tag{11.3.3}$$

When the body-fixed reference frame is undergoing rotation, the elements of the direction-cosine matrix are functions of time. To complete the kinematic formulation in terms of direction cosines, a set of differential equations relating the temporal derivatives of the nine elements of the direction-cosine matrix to the body-fixed angular rates is required. These nine equations, known as *Poisson's kinematic equations*, can be written in matrix form as

$$\begin{bmatrix} \dot{C}_{11} & \dot{C}_{12} & \dot{C}_{13} \\ \dot{C}_{21} & \dot{C}_{22} & \dot{C}_{23} \\ \dot{C}_{31} & \dot{C}_{32} & \dot{C}_{33} \end{bmatrix} = \begin{bmatrix} 0 & r & -q \\ -r & 0 & p \\ q & -p & 0 \end{bmatrix} \begin{bmatrix} C_{11} & C_{12} & C_{13} \\ C_{21} & C_{22} & C_{23} \\ C_{31} & C_{32} & C_{33} \end{bmatrix} \tag{11.3.4}$$

It should be noted that there is no standard convention for numbering the direction cosines. Here, the numbering in Eq. (11.3.1) has been defined relative to the forward transformation, from Earth-fixed coordinates to body-fixed coordinates. This is the most commonly used notation. However, other authors have numbered the direction cosines relative to the inverse transformation, from body-fixed to Earth-fixed coordinates. One notation is simply the transpose of the other. Nevertheless, the reader should be careful to observe which of these notations is being used when reviewing a publication or simulation code.

There are only three degrees of freedom associated with orientation. However, there are nine components in the direction-cosine matrix. Thus, these nine components cannot be independent. There must be six levels of redundancy associated with this formulation. It can be shown that rigid-body rotation is a *proper orthogonal transformation*. Therefore, the direction-cosine matrix must be proper orthogonal, which means that the inverse of the direction-cosine matrix must be its transpose, $[\mathbf{C}]^{-1} = [\mathbf{C}]^T$. This requires the constraints

$$\begin{aligned} C_{11}^2 + C_{21}^2 + C_{31}^2 &= 1, \\ C_{12}^2 + C_{22}^2 + C_{32}^2 &= 1, \\ C_{13}^2 + C_{23}^2 + C_{33}^2 &= 1, \\ C_{11}C_{12} + C_{21}C_{22} + C_{31}C_{32} &= 0, \\ C_{11}C_{13} + C_{21}C_{23} + C_{31}C_{33} &= 0, \\ C_{12}C_{13} + C_{22}C_{23} + C_{32}C_{33} &= 0 \end{aligned} \tag{11.3.5}$$

These six constraints are usually called the *redundancy relations*. Mathematically, the relation in Eq. (11.3.4) preserves the orthogonality of the direction-cosine matrix. However, errors associated with the numerical integration of Eq. (11.3.4) can cause degradation in the orthogonality of the matrix. Furthermore, these orthogonality errors can build up with time during the simulation. A method for avoiding this error buildup with the direction-cosine formulation was first developed by Corbett and Wright (1957) and is still commonly used today.

The direction-cosine formulation contains no singularities and is frequently used by the aeronautics community to avoid the possibility of gimbal lock. However, numerical integration of Eq. (11.3.4) is excessively time-consuming and a computational penalty is paid for its use.

11.4. Euler Axis Formulation

The orientation of the noninertial reference frame relative to the inertial reference frame can also be described in terms of a single rotation through an angle, Θ, about a particular axis, $\mathbf{E}$, which is commonly called the *Euler axis* or the *eigenaxis*. This description of orientation was first introduced by Euler (1775). A comparison between this Euler axis rotation and the three Euler angle rotations that are commonly used by the aircraft community is shown in Fig. 11.4.1.

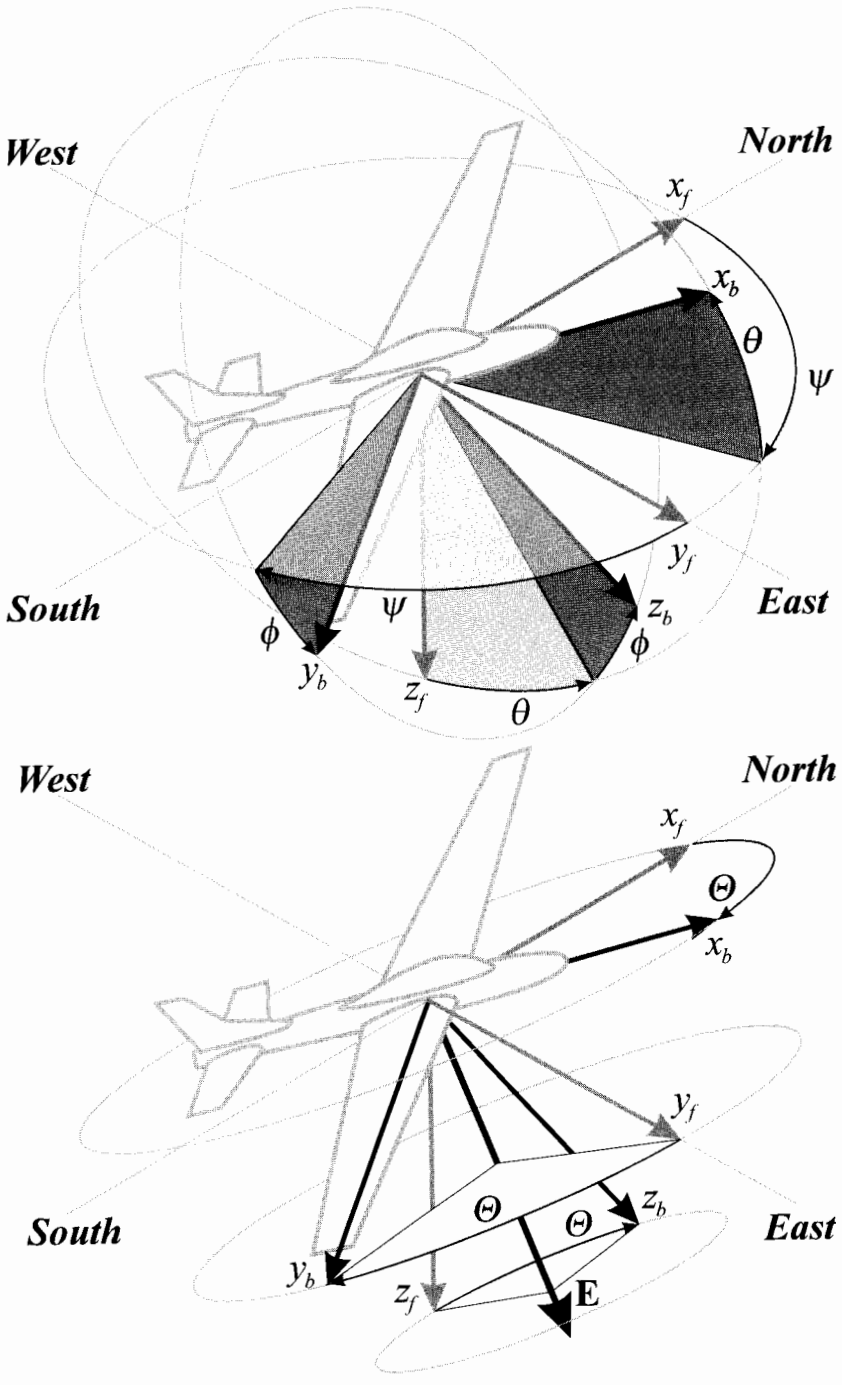


Figure 11.4.1. Comparison between the Euler angle rotations and the Euler axis rotation.

The Euler axis rotation gives rise to a four-component description of orientation. The four components in this description are the total rotation angle, Θ, and the three components of a vector directed along the Euler axis, E_x, E_y, and E_z. Since these four parameters describe an orientation having only three degrees of freedom, there is some redundancy in the Euler axis description. By describing orientation in this manner, a fourth mathematical degree of freedom has been introduced. Clearly, the length of the vector describing the orientation of the Euler axis is arbitrary. To remove this additional mathematical degree of freedom, a constraint must be applied to fix the magnitude of the Euler axis vector. While this constraint is somewhat arbitrary, the usual and most obvious solution is to require the Euler axis vector to be of unit magnitude,

$$E_x^2 + E_y^2 + E_z^2 \equiv 1 \tag{11.4.1}$$

During the Euler axis rotation, the orientation of the Euler axis is invariant. Thus, the vector, **E**, has the same components in both inertial and noninertial coordinates,

$$\begin{Bmatrix} E_{x_f} \\ E_{y_f} \\ E_{z_f} \end{Bmatrix} = \begin{Bmatrix} E_{x_b} \\ E_{y_b} \\ E_{z_b} \end{Bmatrix} \equiv \begin{Bmatrix} E_x \\ E_y \\ E_z \end{Bmatrix} \tag{11.4.2}$$

The components of an arbitrary vector, **v**, in body-fixed coordinates are related to the components of the same vector in Earth-fixed coordinates through what is commonly called *Euler's formula*,

$$\begin{Bmatrix} v_{x_b} \\ v_{y_b} \\ v_{z_b} \end{Bmatrix} = \begin{bmatrix} E_{xx} + C_\Theta & E_{xy} + E_z S_\Theta & E_{xz} - E_y S_\Theta \\ E_{xy} - E_z S_\Theta & E_{yy} + C_\Theta & E_{yz} + E_x S_\Theta \\ E_{xz} + E_y S_\Theta & E_{yz} - E_x S_\Theta & E_{zz} + C_\Theta \end{bmatrix} \begin{Bmatrix} v_{x_f} \\ v_{y_f} \\ v_{z_f} \end{Bmatrix} \tag{11.4.3}$$

where $E_{ij} = E_i E_j (1 - C_\Theta)$. The inverse of the transformation matrix in Eq. (11.4.3) is obtained by simply rotating through the negative of the total rotation angle that is used in the forward transformation (i.e., change the sign of each sine),

$$\begin{Bmatrix} v_{x_f} \\ v_{y_f} \\ v_{z_f} \end{Bmatrix} = \begin{bmatrix} E_{xx} + C_\Theta & E_{xy} - E_z S_\Theta & E_{xz} + E_y S_\Theta \\ E_{xy} + E_z S_\Theta & E_{yy} + C_\Theta & E_{yz} - E_x S_\Theta \\ E_{xz} - E_y S_\Theta & E_{yz} + E_x S_\Theta & E_{zz} + C_\Theta \end{bmatrix} \begin{Bmatrix} v_{x_b} \\ v_{y_b} \\ v_{z_b} \end{Bmatrix} \tag{11.4.4}$$

From Eq. (11.4.3) the weight vector in noninertial coordinates is

$$\begin{Bmatrix} W_{x_b} \\ W_{y_b} \\ W_{z_b} \end{Bmatrix} = W \begin{Bmatrix} E_{xz} - E_y S_\Theta \\ E_{yz} + E_x S_\Theta \\ E_{zz} + C_\Theta \end{Bmatrix} \tag{11.4.5}$$

and from Eq. (11.4.4), the ground speed can be related to the airspeed and wind by

$$\begin{Bmatrix} \dot{x}_f \\ \dot{y}_f \\ \dot{z}_f \end{Bmatrix} = \begin{Bmatrix} V_{wx_f} \\ V_{wy_f} \\ V_{wz_f} \end{Bmatrix} + \begin{bmatrix} E_{xx}+C_\Theta & E_{xy}-E_zS_\Theta & E_{xz}+E_yS_\Theta \\ E_{xy}+E_zS_\Theta & E_{yy}+C_\Theta & E_{yz}-E_xS_\Theta \\ E_{xz}-E_yS_\Theta & E_{yz}+E_xS_\Theta & E_{zz}+C_\Theta \end{bmatrix} \begin{Bmatrix} u \\ v \\ w \end{Bmatrix} \tag{11.4.6}$$

The relationship between the noninertial angular rates and the rate of change of the Euler axis rotation parameters is given by

$$\begin{Bmatrix} \dot{\Theta} \\ \dot{E}_x \\ \dot{E}_y \\ \dot{E}_z \end{Bmatrix} = \frac{1}{2} \begin{bmatrix} 2E_x & 2E_y & 2E_z \\ E'_{xx}+C/S & E'_{xy}-E_z & E'_{xz}+E_y \\ E'_{xy}+E_z & E'_{yy}+C/S & E'_{yz}-E_x \\ E'_{xz}-E_y & E'_{yz}+E_x & E'_{zz}+C/S \end{bmatrix} \begin{Bmatrix} p \\ q \\ r \end{Bmatrix} \tag{11.4.7}$$

where $E'_{ij} = -E_iE_jC/S$, $S = \sin(\Theta/2)$, and $C = \cos(\Theta/2)$. Equations (11.4.6) and (11.4.7) are the kinematic transformation equations in terms of the Euler axis rotation parameters. Notice that Eq. (11.4.7) also has a singularity. When the total rotation angle, Θ, is zero or 180 degrees, the integration of these equations is indeterminate.

The singularity in the Euler axis formulation is particularly problematic in airplane flight simulation, because it occurs when the fuselage axis is level with the ground and the aircraft is headed either due north or due south. These aircraft orientations are much more likely to occur in normal flight than the vertical orientations that give rise to the gimbal lock singularity associated with the traditional Euler angle formulation. For this reason, the Euler axis formulation is never directly applied to flight simulation. The primary reason for examining the Euler axis formulation is that it can be used with a change of variables to develop another formulation that is singularity free.

11.5. The Euler-Rodrigues Quaternion Formulation

The Euler-Rodrigues formulation is related to the Euler axis formulation through a simple change of variables. The four parameters in the Euler axis description of orientation are used to define four different parameters, which are significantly more convenient. These four new parameters are defined as

$$\begin{Bmatrix} e_0 \\ e_x \\ e_y \\ e_z \end{Bmatrix} \equiv \begin{Bmatrix} \cos(\Theta/2) \\ E_x \sin(\Theta/2) \\ E_y \sin(\Theta/2) \\ E_z \sin(\Theta/2) \end{Bmatrix} \tag{11.5.1}$$

These four parameters, known as the *Euler-Rodrigues symmetric parameters* or the quaternion of finite rotation, form the basis of a very widely used description of orientation and rigid-body rotation. The Euler-Rodrigues formulation for rigid-body

kinematics was developed well before 1844, when the well-known mathematician William R. Hamilton first developed the quaternion and the detailed theory of a noncommutative algebraic system known as quaternion algebra (see Hamilton 1844). Much has been written about the life of Hamilton and his moment of enlightenment concerning quaternion formulas while crossing a bridge with his wife (see Graves 1975, Hankins 1980, and O'Donnell 1983). Hamilton, in a letter to his son, noted that he could not resist the impulse to carve the fundamental quaternion formula into the stone on the bridge. However, it is clear that Hamilton did not develop quaternion algebra as a means of describing rotational transformations.

The brief review of the history of the Euler-Rodrigues formulation that is presented here is taken primarily from Altmann (1986 and 1989), Shuster (1993), and Cheng and Gupta (1989). An early work of Euler (1758) showed that any differential movement of a rigid body can be expressed as a translation and a rotation about some specific axis. Euler's theorem on the motion of a rigid body and Euler's formula were both published in 1775. The first publication of the derivation of the Euler angles is commonly reported as being in 1862. Although the work was published posthumously, the date is probably in error, as Euler died in 1783.

Whether or not Euler knew of the Euler-Rodrigues symmetric parameters is a subject of some debate. Euler (1770) did develop four symmetric parameters for orthogonal transformations (without the use of half angles). Roberson (1968) and Jacobi (1969) argue that Euler had presented a rotation matrix in terms of the so-called Euler-Rodrigues parameters. Shuster (1993) notes that the symmetric parameters developed by Euler in the 1770 paper contained sign errors and formed an improper orthogonal matrix. It is important to note that Euler viewed a matrix as a table. The matrix as a mathematical object would not evolve until vector space was studied by Grassman (1862 and 1878) and Gibbs (1901). As a side note, Hamilton (1884) worked out the chief properties of vectors in his investigation of quaternion algebra (see Boyer and Merzbach 1989).

Four years before Hamilton began his algebraic study of quaternions, Olinde Rodrigues (1840) published his work on the Euler-Rodrigues symmetric parameters, the rules for the compositions, and a geometrical construction for combining two rotations. Unlike Hamilton, whose accomplishments are well documented, the only detailed published article on Rodrigues did not appear until Gray (1980). Some additional historical details can be found in Van der Waerden (1985), Kline (1972), Crowe (1967), and McDuffee (1946).

There is no universal agreement on the choice of indices for the Euler-Rodrigues symmetric parameters. Most authors use the indices 1 through 4 or 0 through 3. Some authors have chosen indices 1 through 3 for the vector components while using 4 as the scalar index, whereas others have used 1 for the scalar index and 2 through 4 for the vector components. The scalar index has also been chosen as 0, with indices 1 through 3 denoting the vector components. There is not even universal agreement on the order of the vector components. Whereas most authors assign the x-, y-, and z-components in ascending order, some authors have used 4 to denote the x-component, 3 for the y-component, and 2 for the z-component. To avoid confusion in this text, the vector components are explicitly labeled using the subscripts x, y, and z, while a 0 subscript is used to denote the scalar component.

Since the four parameters defined by Eq. (11.5.1) uniquely describe an orientation having only three degrees of freedom, these four parameters must be related in some way. This relation is easily seen by squaring the four components of Eq. (11.5.1) and adding them together. This gives

$$e_0^2 + e_x^2 + e_y^2 + e_z^2 = \cos^2(\Theta/2) + (E_x^2 + E_y^2 + E_z^2)\sin^2(\Theta/2) \tag{11.5.2}$$

Since the Euler axis vector, **E**, is a unit vector and $\cos^2(\Theta/2) + \sin^2(\Theta/2) = 1$, it follows directly that

$$e_0^2 + e_x^2 + e_y^2 + e_z^2 = 1 \tag{11.5.3}$$

The transformation expressed in Eq. (11.4.3) can be written in terms of half the total rotation angle by applying the trigonometric identities, $\sin(\Theta) = 2\sin(\Theta/2)\cos(\Theta/2)$, $\cos(\Theta) = \cos^2(\Theta/2) - \sin^2(\Theta/2)$, and $1 - \cos(\Theta) = 2\sin^2(\Theta/2)$. Thus, with shorthand notation $S = \sin(\Theta/2)$, $C = \cos(\Theta/2)$, and $E_{ij} = 2E_iE_jS^2$, Eq. (11.4.3) can be rewritten as

$$\begin{Bmatrix} v_{x_b} \\ v_{y_b} \\ v_{z_b} \end{Bmatrix} = \begin{bmatrix} E_{xx} + C^2 - S^2 & E_{xy} + 2E_zSC & E_{xz} - 2E_ySC \\ E_{xy} - 2E_zSC & E_{yy} + C^2 - S^2 & E_{yz} + 2E_xSC \\ E_{xz} + 2E_ySC & E_{yz} - 2E_xSC & E_{zz} + C^2 - S^2 \end{bmatrix} \begin{Bmatrix} v_{x_f} \\ v_{y_f} \\ v_{z_f} \end{Bmatrix} \tag{11.5.4}$$

Recognizing that $E_{ij} = 2e_ie_j$ and $S^2 = (E_x^2 + E_y^2 + E_z^2)S^2 = e_x^2 + e_y^2 + e_z^2$, after applying Eq. (11.5.1) to Eq. (11.5.4), we obtain

$$\begin{Bmatrix} v_{x_b} \\ v_{y_b} \\ v_{z_b} \end{Bmatrix} = \begin{bmatrix} e_x^2 + e_0^2 - e_y^2 - e_z^2 & 2(e_xe_y + e_ze_0) & 2(e_xe_z - e_ye_0) \\ 2(e_xe_y - e_ze_0) & e_y^2 + e_0^2 - e_x^2 - e_z^2 & 2(e_ye_z + e_xe_0) \\ 2(e_xe_z + e_ye_0) & 2(e_ye_z - e_xe_0) & e_z^2 + e_0^2 - e_x^2 - e_y^2 \end{bmatrix} \begin{Bmatrix} v_{x_f} \\ v_{y_f} \\ v_{z_f} \end{Bmatrix} \tag{11.5.5}$$

The inverse of the transformation matrix in Eq. (11.5.5) is

$$\begin{Bmatrix} v_{x_f} \\ v_{y_f} \\ v_{z_f} \end{Bmatrix} = \begin{bmatrix} e_x^2 + e_0^2 - e_y^2 - e_z^2 & 2(e_xe_y - e_ze_0) & 2(e_xe_z + e_ye_0) \\ 2(e_xe_y + e_ze_0) & e_y^2 + e_0^2 - e_x^2 - e_z^2 & 2(e_ye_z - e_xe_0) \\ 2(e_xe_z - e_ye_0) & 2(e_ye_z + e_xe_0) & e_z^2 + e_0^2 - e_x^2 - e_y^2 \end{bmatrix} \begin{Bmatrix} v_{x_b} \\ v_{y_b} \\ v_{z_b} \end{Bmatrix} \tag{11.5.6}$$

The transformation equation given by Eq. (11.5.5) can be used to obtain the gravitational force vector in body-fixed coordinates,

$$\begin{Bmatrix} W_{x_b} \\ W_{y_b} \\ W_{z_b} \end{Bmatrix} = W \begin{Bmatrix} 2(e_xe_z - e_ye_0) \\ 2(e_ye_z + e_xe_0) \\ e_z^2 + e_0^2 - e_x^2 - e_y^2 \end{Bmatrix} \tag{11.5.7}$$

and from Eq. (11.5.6), the ground speed is related to the airspeed and wind by

$$\begin{Bmatrix} \dot{x}_f \\ \dot{y}_f \\ \dot{z}_f \end{Bmatrix} = \begin{Bmatrix} V_{wx_f} \\ V_{wy_f} \\ V_{wz_f} \end{Bmatrix} + \begin{bmatrix} e_x^2 + e_0^2 - e_y^2 - e_z^2 & 2(e_x e_y - e_z e_0) & 2(e_x e_z + e_y e_0) \\ 2(e_x e_y + e_z e_0) & e_y^2 + e_0^2 - e_x^2 - e_z^2 & 2(e_y e_z - e_x e_0) \\ 2(e_x e_z - e_y e_0) & 2(e_y e_z + e_x e_0) & e_z^2 + e_0^2 - e_x^2 - e_y^2 \end{bmatrix} \begin{Bmatrix} u \\ v \\ w \end{Bmatrix} \tag{11.5.8}$$

The time rate of change of the Euler-Rodrigues symmetric parameters can be related to the time rate of change of the Euler axis rotation parameters. Simply differentiating Eq. (11.5.1) with respect to time produces

$$\begin{Bmatrix} \dot{e}_0 \\ \dot{e}_x \\ \dot{e}_y \\ \dot{e}_z \end{Bmatrix} = \begin{Bmatrix} -\sin(\Theta/2) \\ E_x \cos(\Theta/2) \\ E_y \cos(\Theta/2) \\ E_z \cos(\Theta/2) \end{Bmatrix} \frac{\dot{\Theta}}{2} + \begin{Bmatrix} 0 \\ \dot{E}_x \sin(\Theta/2) \\ \dot{E}_y \sin(\Theta/2) \\ \dot{E}_z \sin(\Theta/2) \end{Bmatrix} \tag{11.5.9}$$

Using Eq. (11.4.7) to express the time rate of change of the Euler axis rotation parameters in terms of the noninertial angular rates, Eq. (11.5.9) can be written as

$$\begin{Bmatrix} \dot{e}_0 \\ \dot{e}_x \\ \dot{e}_y \\ \dot{e}_z \end{Bmatrix} = \frac{1}{2} \begin{bmatrix} -E_x S & -E_y S & -E_z S \\ C & -E_z S & E_y S \\ E_z S & C & -E_x S \\ -E_y S & E_x S & C \end{bmatrix} \begin{Bmatrix} p \\ q \\ r \end{Bmatrix} \tag{11.5.10}$$

or after applying Eq. (11.5.1),

$$\begin{Bmatrix} \dot{e}_0 \\ \dot{e}_x \\ \dot{e}_y \\ \dot{e}_z \end{Bmatrix} = \frac{1}{2} \begin{bmatrix} -e_x & -e_y & -e_z \\ e_0 & -e_z & e_y \\ e_z & e_0 & -e_x \\ -e_y & e_x & e_0 \end{bmatrix} \begin{Bmatrix} p \\ q \\ r \end{Bmatrix} \tag{11.5.11}$$

Because Eq. (11.5.11) is linear in both the noninertial angular rates and the Euler-Rodrigues symmetric parameters, it can also be written as

$$\begin{Bmatrix} \dot{e}_0 \\ \dot{e}_x \\ \dot{e}_y \\ \dot{e}_z \end{Bmatrix} = \frac{1}{2} \begin{bmatrix} 0 & -p & -q & -r \\ p & 0 & r & -q \\ q & -r & 0 & p \\ r & q & -p & 0 \end{bmatrix} \begin{Bmatrix} e_0 \\ e_x \\ e_y \\ e_z \end{Bmatrix} \tag{11.5.12}$$

Equation (11.5.8) and either Eq. (11.5.11) or Eq. (11.5.12) provide the kinematic transformation equations in terms of the Euler-Rodrigues symmetric parameters.

Robinson (1958) described the advantages of the Euler-Rodrigues quaternion formulation over the Euler angle or the direction-cosine formulation almost 50 years ago. Most of his observations, obtained on analog computers, are still valid in today's digital world. When the Euler elevation angle, θ, is $\pm 90^{\circ}$, the Euler angle integration becomes indeterminate. Despite the singularity, the Euler angle formulation is widely used because the three Euler angles have the simple interpretation of heading, elevation angle, and bank angle. The Euler-Rodrigues formulation is free of singularities. However, the physical interpretation of the quaternion is much less intuitive than that associated with the Euler angles. In a mathematical study, Stuelpnagel (1964) considered parameterization of a general three-parameter rotation group, four-parameter rotation group, and five- and six-parameter groups. He proves that the three-parameter rotation group always leads to nonlinear kinematic equations and that the Euler-Rodrigues symmetric parameters represent the smallest number of parameters (four) with linear kinematic equations. Errors associated with numerical integration of the kinematic equations for attitude have been characterized for both the quaternion and the direction-cosine parameterizations, and the superiority of the quaternion parameterization is well documented. Another advantage of the Euler-Rodrigues formulation is the application of Kalman filtering to quaternion estimation (see, for example, Shuster 1993).

A very significant advantage of the quaternion formulation over either the Euler angle formulation or the direction-cosine formulation is increased computational speed. Numerical integration of the nine component direction-cosine formulation is excessively time-consuming compared with the four component Euler-Rodrigues formulation. The trigonometric functions in the Euler angle transformation matrix make simulations that use this nonlinear formulation much more computationally intensive than those using the linear equations of the quaternion formulation. Furthermore, the computational advantage of the quaternion formulation can be extended even further through use of Hamilton's quaternion algebra. While the Euler-Rodrigues formulation was originally developed before quaternion algebra was conceived, the most computationally efficient algorithms are in fact based on this mathematical rule set, which was first introduced by Hamilton (1844). To demonstrate this computational advantage, a brief introduction to quaternion algebra is presented here.

11.6. Quaternion Algebra

A general quaternion, $\{\mathbf{Q}\}$, is defined as

$$\{\mathbf{Q}\} \equiv Q_0 + Q_x \mathbf{i}_x + Q_y \mathbf{i}_y + Q_z \mathbf{i}_z \tag{11.6.1}$$

where Q_0, Q_x, Q_y, and Q_z are scalars and $\mathbf{i}_x$, $\mathbf{i}_y$, and $\mathbf{i}_z$ are unit vectors in the Cartesian x-, y-, and z-directions, respectively. A quaternion has both vector and scalar properties. Vectors and scalars can be thought of as special cases of the more general quaternion. A scalar is a quaternion with Q_x, Q_y, and Q_z equal to zero and a vector is a quaternion where Q_0 equals zero.

For quaternion multiplication, a procedure called the *quaternion product* is defined. Since a vector is a special case of a quaternion, care should be taken to distinguish the

quaternion product from either the dot product or the cross product. Here, the quaternion product will be indicated using the operator $\otimes$. The quaternion products of the usual Cartesian unit vectors are defined according to the following rule set:

$$\begin{aligned}
&\mathbf{i}_x \otimes \mathbf{i}_x \equiv -1, \quad && \mathbf{i}_x \otimes \mathbf{i}_y \equiv \mathbf{i}_z, \quad && \mathbf{i}_x \otimes \mathbf{i}_z \equiv -\mathbf{i}_y \\
&\mathbf{i}_y \otimes \mathbf{i}_x \equiv -\mathbf{i}_z, \quad && \mathbf{i}_y \otimes \mathbf{i}_y \equiv -1, \quad && \mathbf{i}_y \otimes \mathbf{i}_z \equiv \mathbf{i}_x, \\
&\mathbf{i}_z \otimes \mathbf{i}_x \equiv \mathbf{i}_y, \quad && \mathbf{i}_z \otimes \mathbf{i}_y \equiv -\mathbf{i}_x, \quad && \mathbf{i}_z \otimes \mathbf{i}_z \equiv -1
\end{aligned} \tag{11.6.2}$$

The quaternion product simply follows the distributive law. Thus, the quaternion product of one quaternion, $\{\mathbf{A}\}$, with another quaternion, $\{\mathbf{B}\}$, is

$$\begin{aligned}
\{\mathbf{A}\} \otimes \{\mathbf{B}\} &= (A_0 + A_x\mathbf{i}_x + A_y\mathbf{i}_y + A_z\mathbf{i}_z) \otimes (B_0 + B_x\mathbf{i}_x + B_y\mathbf{i}_y + B_z\mathbf{i}_z) \\
&= (A_0B_0 - A_xB_x - A_yB_y - A_zB_z) \\
&\quad + (A_0B_x + A_xB_0 + A_yB_z - A_zB_y)\mathbf{i}_x \\
&\quad + (A_0B_y - A_xB_z + A_yB_0 + A_zB_x)\mathbf{i}_y \\
&\quad + (A_0B_z + A_xB_y - A_yB_x + A_zB_0)\mathbf{i}_z
\end{aligned} \tag{11.6.3}$$

The quaternion products defined in Eq. (11.6.2) are nearly like cross products, following the right-hand rule. However, special treatment is given to the quaternion product of a unit vector with itself. It should also be noted that, in general, $\{\mathbf{A}\} \otimes \{\mathbf{B}\} \neq \{\mathbf{B}\} \otimes \{\mathbf{A}\}$, so the quaternion product is not commutative. Also notice that the quaternion product reduces to simple multiplication for the special case when either operand is a scalar. However, it does not reduce to either the dot product or the cross product when both operands are vectors. In general, the quaternion product of two simple vectors is a four-component quaternion, equal to the negative of the dot product added to the cross product,

$$\begin{aligned}
\mathbf{A} \otimes \mathbf{B} &= -(A_xB_x + A_yB_y + A_zB_z) \\
&\quad + (A_yB_z - A_zB_y)\mathbf{i}_x \\
&\quad + (A_zB_x - A_xB_z)\mathbf{i}_y \\
&\quad + (A_xB_y - A_yB_x)\mathbf{i}_z = -\mathbf{A}\cdot\mathbf{B} + \mathbf{A}\times\mathbf{B}
\end{aligned} \tag{11.6.4}$$

Quaternions not only have properties of scalars and vectors, but quaternion algebra also has similarities to complex algebra. The magnitude of a quaternion is defined similar to that of a complex number or a vector,

$$\left|\{\mathbf{Q}\}\right| \equiv \sqrt{Q_0^2 + Q_x^2 + Q_y^2 + Q_z^2} \tag{11.6.5}$$

Also, the conjugate of a quaternion is defined as

$$\{\mathbf{Q}\}^* \equiv Q_0 - Q_x\mathbf{i}_x - Q_y\mathbf{i}_y - Q_z\mathbf{i}_z \tag{11.6.6}$$

where the asterisk indicates a quaternion conjugate. Using Eq. (11.6.6) with Eq. (11.6.3) produces

$$\{\mathbf{Q}\} \otimes \{\mathbf{Q}\}^* = Q_0^2 + Q_x^2 + Q_y^2 + Q_z^2 = \left|\{\mathbf{Q}\}\right|^2 \tag{11.6.7}$$

Thus, similar to a complex variable, the quaternion product of a quaternion with its conjugate generates a scalar equal to the square of the magnitude of the quaternion.

The Euler-Rodrigues symmetric parameters can be thought of as the components of a particular unit quaternion, $\{\mathbf{e}\}$, having components (e_0, e_x, e_y, e_z), which uniquely specifies the orientation of the noninertial coordinate system relative to the inertial coordinate system. Furthermore, the rotational transformation given by Eq. (11.5.5) can also be expressed in terms of quaternion products. Let $\mathbf{v}$ be an arbitrary vector having quaternion components $(0, v_{x_b}, v_{y_b}, v_{z_b})$ in the body-fixed coordinate system and having quaternion components $(0, v_{x_f}, v_{y_f}, v_{z_f})$ in the Earth-fixed coordinate system. The components of $\mathbf{v}$ in body-fixed coordinates are related to the components of $\mathbf{v}$ in Earth-fixed coordinates through the quaternion transformation

$$\mathbf{v}_b = \{\mathbf{e}\}^* \otimes \left(\mathbf{v}_f \otimes \{\mathbf{e}\}\right) \tag{11.6.8}$$

Expanding Eq. (11.6.8) using Eq. (11.6.3), the orthogonal transformation can be written as a two-step process using a temporary quaternion, $\{\mathbf{T}\}$,

$$\begin{aligned}\{\mathbf{T}\} = \mathbf{v}_f \otimes \{\mathbf{e}\} = {} & (-v_{x_f} e_x - v_{y_f} e_y - v_{z_f} e_z) \\ & + (v_{x_f} e_0 + v_{y_f} e_z - v_{z_f} e_y)\mathbf{i}_{x_f} \\ & + (-v_{x_f} e_z + v_{y_f} e_0 + v_{z_f} e_x)\mathbf{i}_{y_f} \\ & + (v_{x_f} e_y - v_{y_f} e_x + v_{z_f} e_0)\mathbf{i}_{z_f}\end{aligned} \tag{11.6.9}$$

$$\begin{aligned}\mathbf{v}_b = \{\mathbf{e}\}^* \otimes \{\mathbf{T}\} = {} & (e_0 T_x - e_x T_0 - e_y T_z + e_z T_y)\mathbf{i}_{x_b} \\ & + (e_0 T_y + e_x T_z - e_y T_0 - e_z T_x)\mathbf{i}_{y_b} \\ & + (e_0 T_z - e_x T_y + e_y T_x - e_z T_0)\mathbf{i}_{z_b}\end{aligned} \tag{11.6.10}$$

From Eq. (11.6.8) and the definitions in Eqs. (11.6.1) and (11.6.6), it is worth noting that **the conjugate of an Euler-Rodrigues quaternion represents the inverse rotation.**

The advantage of Eqs. (11.6.9) and (11.6.10) over Eq. (11.5.5) is a matter of reduced computation time. The rotational transformation as expressed in Eq. (11.5.5) requires 39 multiplications and 21 additions. On the other hand, computing the same transformation from Eqs. (11.6.9) and (11.6.10) requires only 24 multiplications and 17 additions. This translates to a significant computational saving. For typical modern computers, the transformation computed from Eq. (11.5.5) requires about 50 percent greater computation time than does that computed from Eqs. (11.6.9) and (11.6.10). This can be quite significant in a flight simulator, which requires a very large number of such transformations for the visual display.

For aircraft that are not all-attitude vehicles, such as transports, helicopters, and roll-stabilized missiles, Euler angles are often used to compute attitude because the singularity is not encountered. However, the computational advantage of the quaternion transformation is even more impressive when compared with the Euler angle transformation given by Eq. (11.2.1). Even when each trigonometric function in Eq. (11.2.1) is only evaluated once, the transformation computed from Eq. (11.2.1) requires about 11 times as long to evaluate as the quaternion transformation computed from Eqs. (11.6.9) and (11.6.10). Thus, even ignoring the singularity in the Euler angle formulation, the quaternion formulation is far superior to the Euler angle formulation, based on computational efficiency alone.

In the mid-1980s, algorithms were developed, which further reduced the computation time for quaternion multiplication on the hardware available at that time. For example, Dvornychenko (1985), based on the work of Winograd (1970 and 1977), presented two algorithms that were claimed to reduce computation time. The first of these algorithms requires 11 multiplications and 19 additions. The second requires 10 multiplications and 26 additions. This compares to 16 multiplications and 12 additions for the conventional quaternion multiplication described in Eq. (11.6.3). The hardware available at that time required something on the order of five instruction cycles for multiplication and only one cycle for addition. Thus, trading five multiplications for seven additions would result in a significant reduction in computation time, for the hardware of that era. However, typical modern hardware requires only one instruction cycle for multiplication and one instruction cycle for addition. Thus, the algorithms that were developed in the 1980s to speed up quaternion transformations will actually slow down the transformations when used with today's hardware. For simulations run on modern hardware, these old algorithms should be replaced with the more straightforward algorithm specified by Eq. (11.6.3).

The system of differential equations that governs the change in the transformation quaternion with time can also be written in terms of a quaternion product. This differential system, specified by either Eq. (11.5.11) or (11.5.12), can be written as

$$\{\dot{\mathbf{e}}\} = \tfrac{1}{2}\{\mathbf{e}\} \otimes \boldsymbol{\omega} \tag{11.6.11}$$

where $\boldsymbol{\omega}$ is the angular velocity vector in body-fixed coordinates. Writing the quaternion differential equation in this form provides no computational savings over the matrix form given by Eq. (11.5.12). From Eq. (11.6.3), it is observed that the quaternion product in Eq. (11.6.11) requires 16 multiplications and 12 additions. This is exactly equivalent to that required for the matrix multiplication in Eq. (11.5.12). However, the matrix multiplication in Eq. (11.5.11) requires only 12 multiplications and eight additions. Thus, the temporal derivative of the transformation quaternion should always be computed from Eq. (11.5.11).

Aircraft simulations often deal with more than two coordinate systems. For example, a single simulation could use an inertial coordinate system fixed to the center of the Earth, an Earth-fixed coordinate system at the aircraft's local latitude and longitude, an atmosphere-fixed coordinate system, and an aircraft body-fixed coordinate system. In such simulations, it is convenient to be able to efficiently combine a succession of

coordinate rotations into a single transformation. This is, of course, readily accomplished when using a direction-cosine transformation by simply multiplying the direction-cosine matrices for each successive rotation. For example, if $[\mathbf{C}]_{1\text{-}2}$ is the direction-cosine matrix for the transformation from coordinate system 1 to coordinate system 2 and $[\mathbf{C}]_{2\text{-}3}$ is the direction-cosine matrix for the transformation from coordinate system 2 to coordinate system 3, we can write

$$[\mathbf{C}]_{1\text{-}3} = [\mathbf{C}]_{2\text{-}3}[\mathbf{C}]_{1\text{-}2} \tag{11.6.12}$$

where $[\mathbf{C}]_{1\text{-}3}$ is the direction-cosine matrix for the transformation from coordinate system 1 to coordinate system 3. Since matrix multiplication is not commutative, the right-to-left order of the multiplication is important.

In an analogous manner, a succession of coordinate rotations can be combined into a single Euler-Rodrigues quaternion by making use of the quaternion product defined in Eq. (11.6.3). If $\{\mathbf{e}\}_{1\text{-}2}$ is the quaternion for the transformation from coordinate system 1 to coordinate system 2 and $\{\mathbf{e}\}_{2\text{-}3}$ is the quaternion for the transformation from coordinate system 2 to coordinate system 3, then the Euler-Rodrigues quaternion for the transformation from coordinate system 1 to coordinate system 3 is given by

$$\{\mathbf{e}\}_{1\text{-}3} = \{\mathbf{e}\}_{1\text{-}2} \otimes \{\mathbf{e}\}_{2\text{-}3} \tag{11.6.13}$$

Here again the order of multiplication is important because the quaternion product is not commutative. Notice that this quaternion product requires a left-to-right order, which contrasts with the right-to-left order required for direction-cosine matrix multiplication. The relation given by Eq. (11.6.13) is not obvious from examination of Eq. (11.6.8). Whittaker (1937) demonstrates the validity of this result.

There is some confusion in the literature regarding the order of multiplication required when using the Euler-Rodrigues quaternion for a succession of coordinate rotations. For example, Dvornychenko (1985) presents a right-to-left ordering of the quaternion product, which is opposite to that shown in Eq. (11.6.13). This is because Dvornychenko has also used an unconventional quaternion definition, which has the vector components defined as the negative of those defined in Eq. (11.5.1). The positive signs used in Eq. (11.5.1) correspond to the conventional right-hand Euler-Rodrigues quaternion, which is based on a right-hand rotation about the Euler axis. The negative signs used by Dvornychenko result in a left-hand quaternion, which is not normally used. When the right-hand Euler-Rodrigues quaternion is used, successive coordinate rotations are expressed using the left-to-right quaternion product that is shown in Eq. (11.6.13).

11.7. Relations between the Quaternion and Other Attitude Descriptors

The physical interpretation of the Euler-Rodrigues quaternion is much less intuitive than that associated with the Euler angles. For this reason it is convenient to be able to relate the Euler-Rodrigues quaternion to the Euler angles. Such a relation can be obtained by combining Eqs. (11.2.1) and (11.5.5). These two equations require that

$$\begin{bmatrix} e_x^2+e_0^2-e_y^2-e_z^2 & 2(e_xe_y+e_ze_0) & 2(e_xe_z-e_ye_0) \\ 2(e_xe_y-e_ze_0) & e_y^2+e_0^2-e_x^2-e_z^2 & 2(e_ye_z+e_xe_0) \\ 2(e_xe_z+e_ye_0) & 2(e_ye_z-e_xe_0) & e_z^2+e_0^2-e_x^2-e_y^2 \end{bmatrix} = \begin{bmatrix} C_\theta C_\psi & C_\theta S_\psi & -S_\theta \\ S_\phi S_\theta C_\psi - C_\phi S_\psi & S_\phi S_\theta S_\psi + C_\phi C_\psi & S_\phi C_\theta \\ C_\phi S_\theta C_\psi + S_\phi S_\psi & C_\phi S_\theta S_\psi - S_\phi C_\psi & C_\phi C_\theta \end{bmatrix} \tag{11.7.1}$$

This matrix equation provides nine scalar equations relating the four components of the Euler-Rodrigues quaternion, $\{\mathbf{e}\}$, to the three Euler angles, ϕ, θ, and ψ. However, the nine components of the matrices on both sides of Eq. (11.7.1) each describe a rotation having only three degrees of freedom. Thus, there are six levels of redundancy in Eq. (11.7.1). Additionally, Eq. (11.5.3) must also be satisfied, which simply requires $\{\mathbf{e}\}$ to be a unit quaternion. The three degrees of freedom in Eq. (11.7.1), combined with the requirement in Eq. (11.5.3), provide exactly the four degrees of freedom needed to solve for the four components of the quaternion $\{\mathbf{e}\}$.

Combining the diagonal components of Eq. (11.7.1) with the requirement for a unit quaternion expressed in Eq. (11.5.3), a 4×4 system of algebraic equations for the squares of the quaternion components is obtained,

$$\begin{bmatrix} 1 & 1 & -1 & -1 \\ 1 & -1 & 1 & -1 \\ 1 & -1 & -1 & 1 \\ 1 & 1 & 1 & 1 \end{bmatrix} \begin{Bmatrix} e_0^2 \\ e_x^2 \\ e_y^2 \\ e_z^2 \end{Bmatrix} = \begin{Bmatrix} C_\theta C_\psi \\ S_\phi S_\theta S_\psi + C_\phi C_\psi \\ C_\phi C_\theta \\ 1 \end{Bmatrix} \tag{11.7.2}$$

This system is readily solved by direct elimination to give

$$\begin{Bmatrix} e_0^2 \\ e_x^2 \\ e_y^2 \\ e_z^2 \end{Bmatrix} = \frac{1}{4} \begin{Bmatrix} 1+C_\theta C_\psi + S_\phi S_\theta S_\psi + C_\phi C_\theta + C_\phi C_\psi \\ 1-C_\phi C_\theta - S_\phi S_\theta S_\psi - C_\phi C_\psi + C_\theta C_\psi \\ 1-C_\theta C_\psi - C_\phi C_\theta + S_\phi S_\theta S_\psi + C_\phi C_\psi \\ 1-C_\theta C_\psi + C_\phi C_\theta - S_\phi S_\theta S_\psi - C_\phi C_\psi \end{Bmatrix} \tag{11.7.3}$$

Applying the half-angle identities, Eq. (11.7.3) is written as

$$\begin{Bmatrix} e_0^2 \\ e_x^2 \\ e_y^2 \\ e_z^2 \end{Bmatrix} = \begin{Bmatrix} (C_{\phi/2}C_{\theta/2}C_{\psi/2} + S_{\phi/2}S_{\theta/2}S_{\psi/2})^2 \\ (S_{\phi/2}C_{\theta/2}C_{\psi/2} - C_{\phi/2}S_{\theta/2}S_{\psi/2})^2 \\ (C_{\phi/2}S_{\theta/2}C_{\psi/2} + S_{\phi/2}C_{\theta/2}S_{\psi/2})^2 \\ (S_{\phi/2}S_{\theta/2}C_{\psi/2} - C_{\phi/2}C_{\theta/2}S_{\psi/2})^2 \end{Bmatrix} \tag{11.7.4}$$

Each of these component equations has two possible solutions, so the signs are indeterminate at this point.

The off-diagonal components of Eq. (11.7.1) may be extracted to produce

$$\begin{bmatrix} 0 & 0 & 2 & 2 & 0 & 0 \\ 0 & 0 & -2 & 2 & 0 & 0 \\ 0 & -2 & 0 & 0 & 2 & 0 \\ 0 & 2 & 0 & 0 & 2 & 0 \\ 2 & 0 & 0 & 0 & 0 & 2 \\ -2 & 0 & 0 & 0 & 0 & 2 \end{bmatrix} \begin{Bmatrix} e_0 e_x \\ e_0 e_y \\ e_0 e_z \\ e_x e_y \\ e_x e_z \\ e_y e_z \end{Bmatrix} = \begin{Bmatrix} C_\theta S_\psi \\ S_\phi S_\theta C_\psi - C_\phi S_\psi \\ -S_\theta \\ C_\phi S_\theta C_\psi + S_\phi S_\psi \\ S_\phi C_\theta \\ C_\phi S_\theta S_\psi - S_\phi C_\psi \end{Bmatrix} \tag{11.7.5}$$

This simple algebraic system is easily solved by adding and subtracting appropriate pairs of equations. Replacing the first and second equations with their sum and their difference and doing likewise with the other two pairs of equations results in

$$\begin{Bmatrix} e_0 e_x \\ e_0 e_y \\ e_0 e_z \\ e_x e_y \\ e_x e_z \\ e_y e_z \end{Bmatrix} = \frac{1}{4} \begin{Bmatrix} S_\phi C_\theta - C_\phi S_\theta S_\psi + S_\phi C_\psi \\ C_\phi S_\theta C_\psi + S_\phi S_\psi + S_\theta \\ C_\theta S_\psi - S_\phi S_\theta C_\psi + C_\phi S_\psi \\ C_\theta S_\psi + S_\phi S_\theta C_\psi - C_\phi S_\psi \\ C_\phi S_\theta C_\psi + S_\phi S_\psi - S_\theta \\ S_\phi C_\theta + C_\phi S_\theta S_\psi - S_\phi C_\psi \end{Bmatrix} \tag{11.7.6}$$

Using Eq. (11.7.4) in Eq. (11.7.6) and applying the half-angle identities, the off-diagonal components of Eq. (11.7.1) reduce to

$$\begin{Bmatrix} s_0 s_x (S_\phi C_\theta - C_\phi S_\theta S_\psi + S_\phi C_\psi) \\ s_0 s_y (C_\phi S_\theta C_\psi + S_\phi S_\psi + S_\theta) \\ s_0 s_z (-C_\theta S_\psi + S_\phi S_\theta C_\psi - C_\phi S_\psi) \\ s_x s_y (C_\theta S_\psi + S_\phi S_\theta C_\psi - C_\phi S_\psi) \\ s_x s_z (-C_\phi S_\theta C_\psi - S_\phi S_\psi + S_\theta) \\ s_y s_z (-S_\phi C_\theta - C_\phi S_\theta S_\psi + S_\phi C_\psi) \end{Bmatrix} = \begin{Bmatrix} S_\phi C_\theta - C_\phi S_\theta S_\psi + S_\phi C_\psi \\ C_\phi S_\theta C_\psi + S_\phi S_\psi + S_\theta \\ C_\theta S_\psi - S_\phi S_\theta C_\psi + C_\phi S_\psi \\ C_\theta S_\psi + S_\phi S_\theta C_\psi - C_\phi S_\psi \\ C_\phi S_\theta C_\psi + S_\phi S_\psi - S_\theta \\ S_\phi C_\theta + C_\phi S_\theta S_\psi - S_\phi C_\psi \end{Bmatrix} \tag{11.7.7}$$

where s_0, s_x, s_y, and s_z are the unknown signs of the quaternion components obtained from Eq. (11.7.4). Thus, the off-diagonal components of Eq. (11.7.1) provide only three additional pieces of information, $s_0 s_x = 1$, $s_0 s_y = 1$, and $s_0 s_z = -1$. Using these signs with Eq. (11.7.4), only two possible solutions to Eq. (11.7.1) exist, which are

$$\begin{Bmatrix} e_0 \\ e_x \\ e_y \\ e_z \end{Bmatrix} = \pm \begin{Bmatrix} C_{\phi/2} C_{\theta/2} C_{\psi/2} + S_{\phi/2} S_{\theta/2} S_{\psi/2} \\ S_{\phi/2} C_{\theta/2} C_{\psi/2} - C_{\phi/2} S_{\theta/2} S_{\psi/2} \\ C_{\phi/2} S_{\theta/2} C_{\psi/2} + S_{\phi/2} C_{\theta/2} S_{\psi/2} \\ C_{\phi/2} C_{\theta/2} S_{\psi/2} - S_{\phi/2} S_{\theta/2} C_{\psi/2} \end{Bmatrix} \tag{11.7.8}$$

Both solutions in Eq. (11.7.8) are valid. Any orientation of one coordinate system relative to another can be described in terms of two right-hand rotations. For example, a right-hand rotation of 90 degrees about the positive x-axis is equivalent to a right-hand rotation of 270 degrees about the negative x-axis. The two solutions in Eq. (11.7.8) represent these two equivalent rotations. Usually, the positive sign is selected.

The inverse of Eq. (11.7.8) is obtained from Eq. (11.7.1) as well. This is rather straightforward and yields

$$\begin{Bmatrix} \phi \\ \theta \\ \psi \end{Bmatrix} = \begin{Bmatrix} \text{atan2}[2(e_0 e_x + e_y e_z), (e_0^2 + e_z^2 - e_x^2 - e_y^2)] \\ \text{asin}[2(e_0 e_y - e_x e_z)] \\ \text{atan2}[2(e_0 e_z + e_x e_y), (e_0^2 + e_x^2 - e_y^2 - e_z^2)] \end{Bmatrix} \tag{11.7.9}$$

The function atan2 in Eq. (11.7.9) is a two-argument arctangent that returns a result in the proper quadrant, such as the atan2 intrinsic provided in Fortran and C. The two-argument function is not needed for the elevation angle, θ, because this angle is defined only in the range $-\pi/2$ to $\pi/2$.

The gimbal lock singularity appears again in Eq. (11.7.9). For example, consider a due north heading with an elevation angle of –90 degrees and no bank angle, i.e.,

$$\begin{Bmatrix} \phi \\ \theta \\ \psi \end{Bmatrix} = \begin{Bmatrix} 0 \\ -\pi/2 \\ 0 \end{Bmatrix}$$

Using the positive sign in Eq. (11.7.8), the quaternion representation for this attitude is

$$\begin{Bmatrix} e_0 \\ e_x \\ e_y \\ e_z \end{Bmatrix} = \begin{Bmatrix} C_{\pi/4} \\ 0 \\ -S_{\pi/4} \\ 0 \end{Bmatrix} = \begin{Bmatrix} 0.70710678 \\ 0 \\ -0.70710678 \\ 0 \end{Bmatrix}$$

Using these quaternion components in Eq. (11.7.9) to evaluate the Euler angles gives

$$\begin{Bmatrix} \phi \\ \theta \\ \psi \end{Bmatrix} = \begin{Bmatrix} \text{atan2}(0.,0.) \\ \text{asin}(-1.) \\ \text{atan2}(0.,0.) \end{Bmatrix}$$

This returns an elevation angle of –90 degrees. However, both the bank angle and the heading are indeterminate. This results from the fact that when the elevation angle is exactly ±90 degrees, the Euler angles are not unique. For example, the attitude specified by a due north heading with an elevation angle of –90 degrees and no bank angle can also be specified as a due east heading with an elevation angle of –90 degrees and a bank angle of –90 degrees, i.e.,

$$\begin{Bmatrix} \phi \\ \theta \\ \psi \end{Bmatrix} = \begin{Bmatrix} -\pi/2 \\ -\pi/2 \\ \pi/2 \end{Bmatrix}$$

Again using the positive sign in Eq. (11.7.8), this set of Euler angles also yields the quaternion representation

$$\begin{Bmatrix} e_0 \\ e_x \\ e_y \\ e_z \end{Bmatrix} = \begin{Bmatrix} C_{\pi/4}C_{\pi/4}C_{\pi/4} + S_{\pi/4}S_{\pi/4}S_{\pi/4} \\ -S_{\pi/4}C_{\pi/4}C_{\pi/4} + C_{\pi/4}S_{\pi/4}S_{\pi/4} \\ -C_{\pi/4}S_{\pi/4}C_{\pi/4} - S_{\pi/4}C_{\pi/4}S_{\pi/4} \\ C_{\pi/4}C_{\pi/4}S_{\pi/4} - S_{\pi/4}S_{\pi/4}C_{\pi/4} \end{Bmatrix} = \begin{Bmatrix} 0.70710678 \\ 0 \\ -0.70710678 \\ 0 \end{Bmatrix}$$

When the Euler elevation angle is exactly ±90 degrees, the heading angle is completely arbitrary because the orientation of the x_b-axis is fully specified by the elevation angle alone. Specifying a heading with a ±90-degree elevation angle is like specifying the longitude at the North or South Pole on the Earth's surface. When the latitude is ±90 degrees, there is no need to specify the longitude because each of these two latitudes alone uniquely describes a point on the surface of the Earth. Thus, longitude is arbitrary for latitudes of ±90 degrees.

Because of gimbal lock, the transformation given by Eq. (11.7.9) cannot be used for a completely arbitrary Euler-Rodrigues quaternion. Whenever the Euler elevation angle passes through ±90 degrees, the Euler heading and bank angle will each undergo a step change of 180 degrees. Furthermore, at an elevation angle of exactly ±90 degrees the heading angle is arbitrary and the bank angle can only be expressed as a function of this arbitrary heading. From Eq. (11.7.8), the Euler-Rodrigues quaternion at gimbal lock is found to be

$$\begin{Bmatrix} e_0 \\ e_x \\ e_y \\ e_z \end{Bmatrix} = C_{\pi/4}\begin{Bmatrix} C_{\phi/2}C_{\psi/2} \pm S_{\phi/2}S_{\psi/2} \\ S_{\phi/2}C_{\psi/2} \mp C_{\phi/2}S_{\psi/2} \\ \pm C_{\phi/2}C_{\psi/2} + S_{\phi/2}S_{\psi/2} \\ C_{\phi/2}S_{\psi/2} \mp S_{\phi/2}C_{\psi/2} \end{Bmatrix} = C_{\pi/4}\begin{Bmatrix} \cos(\phi/2 \mp \psi/2) \\ \sin(\phi/2 \mp \psi/2) \\ \pm\cos(\phi/2 \mp \psi/2) \\ \mp\sin(\phi/2 \mp \psi/2) \end{Bmatrix}, \quad \theta = \pm\frac{\pi}{2}$$

Using this result, the Euler angles at gimbal lock can be found from the Euler-Rodrigues quaternion at gimbal lock according to the relation

$$\begin{Bmatrix} \phi \\ \theta \\ \psi \end{Bmatrix} = \begin{Bmatrix} 2\,\text{asin}[e_x/\cos(\pi/4)] \pm \psi \\ \pm\pi/2 \\ \text{arbitrary} \end{Bmatrix} \tag{11.7.10}$$

Combining Eq. (11.7.9) with Eq. (11.7.10), a generalized algorithm for computing the Euler angles from the components of an arbitrary Euler-Rodrigues quaternion can be written as

$$\text{if } (e_0 e_y - e_x e_z = 0.5)$$

$$\begin{Bmatrix} \phi \\ \theta \\ \psi \end{Bmatrix} = \begin{Bmatrix} 2\,\text{asin}[e_x/\cos(\pi/4)] + \psi \\ \pi/2 \\ \text{arbitrary} \end{Bmatrix}$$

$$\text{if } (e_0 e_y - e_x e_z = -0.5)$$

$$\begin{Bmatrix} \phi \\ \theta \\ \psi \end{Bmatrix} = \begin{Bmatrix} 2\,\text{asin}[e_x/\cos(\pi/4)] - \psi \\ -\pi/2 \\ \text{arbitrary} \end{Bmatrix} \tag{11.7.11}$$

else

$$\begin{Bmatrix} \phi \\ \theta \\ \psi \end{Bmatrix} = \begin{Bmatrix} \text{atan2}[2(e_0 e_x + e_y e_z), (e_0^2 + e_z^2 - e_x^2 - e_y^2)] \\ \text{asin}[2(e_0 e_y - e_x e_z)] \\ \text{atan2}[2(e_0 e_z + e_x e_y), (e_0^2 + e_x^2 - e_y^2 - e_z^2)] \end{Bmatrix}$$

Since the heading at gimbal lock is arbitrary, any convenient value may be used.

The Euler-Rodrigues quaternion is also related to the total rotation angle and the components of the Euler axis vector through the definitions of the Euler-Rodrigues symmetric parameters,

$$\begin{Bmatrix} e_0 \\ e_x \\ e_y \\ e_z \end{Bmatrix} \equiv \begin{Bmatrix} \cos(\Theta/2) \\ E_x \sin(\Theta/2) \\ E_y \sin(\Theta/2) \\ E_z \sin(\Theta/2) \end{Bmatrix} \tag{11.7.12}$$

The inverse of Eq. (11.7.12) is readily found to be

$$\begin{Bmatrix} \Theta \\ E_x \\ E_y \\ E_z \end{Bmatrix} = \begin{Bmatrix} 2\cos^{-1}(e_0) \\ e_x/\sin(\Theta/2) \\ e_y/\sin(\Theta/2) \\ e_z/\sin(\Theta/2) \end{Bmatrix} \tag{11.7.13}$$

Thus, from the four components of the Euler-Rodrigues quaternion, the orientation of the noninertial reference frame with respect to the inertial reference frame can be expressed as a single rotation about a known axis through a known angle. For nonzero rotation angles, the three vector components of this unit quaternion compose a vector directed along the Euler axis. The scalar component of this quaternion is equal to the cosine of one half the angle of rotation about this axis, in a direction defined by the right-hand rule. If the scalar component of this quaternion is ± 1, the orientation of the Euler axis is indeterminate. However, a scalar component of ± 1 would indicate a total rotation angle of zero, making knowledge of the Euler axis unnecessary. It is important to recognize

that like the Euler axis vector, **E**, the four components of the unit quaternion, $\{\mathbf{e}\}$, are the same in both the inertial and the noninertial reference frames. Thus, a reference frame need not be specified when referring to the components of this particular quaternion.

During the 1970s the spacecraft community utilized both the direction cosines and the Euler-Rodrigues quaternion to describe attitude. For example, in space shuttle steering algorithms the command attitude was computed as a direction-cosine matrix, whereas the attitude error was more conveniently described as a quaternion. The quaternion was used to describe the attitude error because of its simpler physical interpretation. The error axis coincides with the vector part of the error quaternion and the total error is readily determined from the scalar part. To compute the error quaternion, the command-attitude quaternion was first extracted from the direction-cosine matrix. Several other space shuttle flight algorithms also required the determination of an attitude quaternion from a direction-cosine matrix. Consequently, a number of algorithms have been developed for extracting the quaternion from the direction cosines. Shepperd (1978) first published the most efficient method. The aircraft and missile community is still using both the direction cosines and the Euler-Rodrigues quaternion as attitude descriptors for aircraft flight simulation.

The direction cosines can be expressed in terms of the four components of the Euler-Rodrigues quaternion by equating the left-hand sides of Eqs. (11.3.1) and (11.5.5),

$$\begin{bmatrix} C_{11} & C_{12} & C_{13} \\ C_{21} & C_{22} & C_{23} \\ C_{31} & C_{32} & C_{33} \end{bmatrix} = \begin{bmatrix} e_x^2 + e_0^2 - e_y^2 - e_z^2 & 2(e_x e_y + e_z e_0) & 2(e_x e_z - e_y e_0) \\ 2(e_x e_y - e_z e_0) & e_y^2 + e_0^2 - e_x^2 - e_z^2 & 2(e_y e_z + e_x e_0) \\ 2(e_x e_z + e_y e_0) & 2(e_y e_z - e_x e_0) & e_z^2 + e_0^2 - e_x^2 - e_y^2 \end{bmatrix} \tag{11.7.14}$$

Combining the diagonal components of Eq. (11.7.14) with Eq. (11.5.3) provides a 4×4 system of equations that is readily solved to relate the squares of the quaternion components to the diagonal components of the direction-cosine matrix,

$$\begin{Bmatrix} e_0^2 \\ e_x^2 \\ e_y^2 \\ e_z^2 \end{Bmatrix} = \frac{1}{4} \begin{Bmatrix} 1 + C_{11} + C_{22} + C_{33} \\ 1 + C_{11} - C_{22} - C_{33} \\ 1 - C_{11} + C_{22} - C_{33} \\ 1 - C_{11} - C_{22} + C_{33} \end{Bmatrix} \tag{11.7.15}$$

The off-diagonal components of Eq. (11.7.14) can be rearranged to give

$$\begin{Bmatrix} e_0 e_x \\ e_0 e_y \\ e_0 e_z \\ e_x e_y \\ e_x e_z \\ e_y e_z \end{Bmatrix} = \frac{1}{4} \begin{Bmatrix} C_{23} - C_{32} \\ C_{31} - C_{13} \\ C_{12} - C_{21} \\ C_{12} + C_{21} \\ C_{31} + C_{13} \\ C_{23} + C_{32} \end{Bmatrix} \tag{11.7.16}$$

The components of the quaternion can be computed, without singularities, from the direction cosines by using Eqs. (11.7.15) and (11.7.16). This is done by first finding the quaternion component of greatest magnitude from Eq. (11.7.15),

$$e_{\max}^2 = \max(e_0^2, e_x^2, e_y^2, e_z^2) \tag{11.7.17}$$

Once the component of largest magnitude has been determined, the quaternion is computed from one of the following algorithms:

If $e_0^2 = e_{\max}^2$,

$$\begin{aligned} e_0 &= \pm\sqrt{1 + C_{11} + C_{22} + C_{33}}/2 \\ e_x &= (C_{23} - C_{32})/4e_0 \\ e_y &= (C_{31} - C_{13})/4e_0 \\ e_z &= (C_{12} - C_{21})/4e_0 \end{aligned} \tag{11.7.18}$$

If $e_x^2 = e_{\max}^2$,

$$\begin{aligned} e_x &= \pm\sqrt{1 + C_{11} - C_{22} - C_{33}}/2 \\ e_0 &= (C_{23} - C_{32})/4e_x \\ e_y &= (C_{12} + C_{21})/4e_x \\ e_z &= (C_{31} + C_{13})/4e_x \end{aligned} \tag{11.7.19}$$

If $e_y^2 = e_{\max}^2$,

$$\begin{aligned} e_y &= \pm\sqrt{1 - C_{11} + C_{22} - C_{33}}/2 \\ e_0 &= (C_{31} - C_{13})/4e_y \\ e_x &= (C_{12} + C_{21})/4e_y \\ e_z &= (C_{23} + C_{32})/4e_y \end{aligned} \tag{11.7.20}$$

If $e_z^2 = e_{\max}^2$,

$$\begin{aligned} e_z &= \pm\sqrt{1 - C_{11} - C_{22} + C_{33}}/2 \\ e_0 &= (C_{12} - C_{21})/4e_z \\ e_x &= (C_{31} + C_{13})/4e_z \\ e_y &= (C_{23} + C_{32})/4e_z \end{aligned} \tag{11.7.21}$$

Notice that as was the case with Eq. (11.7.1), there are two possible quaternions that will satisfy Eq. (11.7.14). These are the same two equivalent quaternions that were discussed following Eq. (11.7.8).

EXAMPLE 11.7.1. For the rocket and flight condition described in Example 7.3.2, find the Euler-Rodrigues quaternion that specifies the rocket' s orientation. Using this quaternion and the quaternion product description of rotation, determine the rocket' s velocity components in Earth-fixed coordinates.

Solution. From Example 7.3.2, the orientation of the rocket expressed in terms of Euler angles and the rocket's velocity components expressed in terms of body-fixed coordinates are

$$\begin{Bmatrix}\phi\\ \theta\\ \psi\end{Bmatrix} = \begin{Bmatrix}40^\circ\\ 20^\circ\\ 70^\circ\end{Bmatrix} \text{ and } \begin{Bmatrix}V_{x_b}\\ V_{y_b}\\ V_{z_b}\end{Bmatrix} \equiv \begin{Bmatrix}u\\ v\\ w\end{Bmatrix} = \begin{Bmatrix}825.96 \text{ ft/sec}\\ 300.63 \text{ ft/sec}\\ 476.87 \text{ ft/sec}\end{Bmatrix}$$

Using the positive sign in Eq. (11.7.8), the Euler-Rodrigues quaternion that is equivalent to this set of Euler angles is

$$\begin{Bmatrix}e_0\\ e_x\\ e_y\\ e_z\end{Bmatrix} = \begin{Bmatrix}C_{\phi/2}C_{\theta/2}C_{\psi/2} + S_{\phi/2}S_{\theta/2}S_{\psi/2}\\ S_{\phi/2}C_{\theta/2}C_{\psi/2} - C_{\phi/2}S_{\theta/2}S_{\psi/2}\\ C_{\phi/2}S_{\theta/2}C_{\psi/2} + S_{\phi/2}C_{\theta/2}S_{\psi/2}\\ C_{\phi/2}C_{\theta/2}S_{\psi/2} - S_{\phi/2}S_{\theta/2}C_{\psi/2}\end{Bmatrix} = \begin{Bmatrix}0.79212226\\ 0.18231628\\ 0.32686024\\ 0.48214674\end{Bmatrix}$$

Because the conjugate of an Euler-Rodrigues quaternion represents the inverse rotation, from Eq. (11.6.8) we have

$$\mathbf{V}_f = \{\mathbf{e}\} \otimes \left(\mathbf{V}_b \otimes \{\mathbf{e}\}^*\right)$$

or using a temporary quaternion, $\{\mathbf{T}\}$,

$$\begin{Bmatrix}T_0\\ T_x\\ T_y\\ T_z\end{Bmatrix} = \begin{Bmatrix}0\\ u\\ v\\ w\end{Bmatrix} \otimes \begin{Bmatrix}e_0\\ -e_x\\ -e_y\\ -e_z\end{Bmatrix} = \begin{Bmatrix}+ue_x + ve_y + we_z\\ +ue_0 - ve_z + we_y\\ +ue_z + ve_0 - we_x\\ -ue_y + ve_x + we_0\end{Bmatrix} = \begin{Bmatrix}478.7713 \text{ ft/sec}\\ 665.1834 \text{ ft/sec}\\ 549.4285 \text{ ft/sec}\\ 162.5756 \text{ ft/sec}\end{Bmatrix}$$

$$\begin{Bmatrix}\dot{x}_f\\ \dot{y}_f\\ \dot{z}_f\end{Bmatrix} = \begin{Bmatrix}e_0\\ e_x\\ e_y\\ e_z\end{Bmatrix} \otimes \begin{Bmatrix}T_0\\ T_x\\ T_y\\ T_z\end{Bmatrix} = \begin{Bmatrix}e_0T_x + e_xT_0 + e_yT_z - e_zT_y\\ e_0T_y - e_xT_z + e_yT_0 + e_zT_x\\ e_0T_z + e_xT_y - e_yT_x + e_zT_0\end{Bmatrix} = \begin{Bmatrix}402.43 \text{ ft/sec}\\ 882.78 \text{ ft/sec}\\ 242.37 \text{ ft/sec}\end{Bmatrix}$$

Comparing this result with that obtained in Example 7.3.2, we see that the quaternion transformation produced exactly the same result as the Euler angle transformation in a more efficient algorithm.

11.8. Applying Rotational Constraints to the Quaternion Formulation

It is occasionally desirable to simulate aircraft motion with one or more of the rotational degrees of freedom constrained. This is normally accomplished using the Euler angle formulation. However, since the quaternion transformation is more than an order of magnitude faster than the Euler angle transformation, the ability to apply rotational constraints to the quaternion formulation may be of some interest.

When applying rotational constraints, the coordinate system in which the constraint will be applied must be specified. For example, a roll constraint is very different from a bank angle constraint. The roll can be constrained very simply, in either the Euler angle formulation or the quaternion formulation, by simply replacing the x_b-component of the angular momentum equation with the **roll constraint**

$$p = 0 \tag{11.8.1}$$

However, note that constraining the roll does not constrain the bank angle. All three Euler angles can still take any possible value with the roll completely constrained.

To constrain the bank angle, using the quaternion formulation, Eq. (11.7.9) can be employed. If the bank angle is to remain zero, Eq. (11.7.9) requires that

$$e_0 e_x + e_y e_z = 0 \tag{11.8.2}$$

and

$$e_x \dot{e}_0 + e_0 \dot{e}_x + e_z \dot{e}_y + e_y \dot{e}_z = 0 \tag{11.8.3}$$

Applying Eq. (11.5.12) to Eq. (11.8.3) produces

$$\begin{aligned} &e_x(-pe_x - qe_y - re_z) + e_0(pe_0 + re_y - qe_z) \\ &+ e_z(qe_0 - re_x + pe_z) + e_y(re_0 + qe_x - pe_y) = 0 \end{aligned} \tag{11.8.4}$$

This can be simplified to yield the **quaternion bank angle constraint**

$$(e_0^2 + e_z^2 - e_x^2 - e_y^2)p + 2(e_0 e_y - e_x e_z)r = 0 \tag{11.8.5}$$

Thus, to constrain the bank angle, the roll and the yaw must be coordinated according to Eq. (11.8.5).

If the roll is to be constrained as well as the bank angle, then Eq. (11.8.5) requires

$$2(e_0 e_y - e_x e_z)r = 0 \tag{11.8.6}$$

From Eq. (11.7.9), this is equivalent to

$$\sin(\theta)r = 0 \tag{11.8.7}$$

Here it is observed that if both the roll and bank angles are to be constrained, then either the yaw or the elevation angle must also be constrained. With any nonzero elevation angle, any amount of yaw will produce a bank angle. This is not a function of the quaternion formulation. It is a simple kinematic fact.

The relationship between the body-fixed angular rates and the Euler angles, which was demonstrated here by using the roll and bank angles, is true in general. None of the Euler angles can be constrained by constraining only one of the body-fixed angular rates. The bank angle can be changed using only pitch and yaw, the elevation angle can be changed using only roll and yaw, and the azimuth angle can be changed using only roll and pitch. *Any motion having only one of the rotational degrees of freedom constrained, in body-fixed coordinates, allows for all three degrees of freedom in orientation.*

Similarly, the other rotational degrees of freedom can be constrained by using the **pitch constraint**

$$q = 0 \tag{11.8.8}$$

the **quaternion elevation angle constraint**

$$(e_0^2 + e_z^2 - e_x^2 - e_y^2)q - 2(e_0 e_x + e_y e_z)r = 0 \tag{11.8.9}$$

the **yaw constraint**

$$r = 0 \tag{11.8.10}$$

and the **quaternion azimuth angle constraint**

$$2(e_0 e_x - e_y e_z)q + (e_0^2 + e_y^2 - e_x^2 - e_z^2)r = 0 \tag{11.8.11}$$

Motion with only one rotational degree of freedom, in body-fixed coordinates, can also be simulated using the quaternion formulation. *Constraining any two rotational degrees of freedom in body-fixed coordinates will constrain two degrees of freedom in orientation.* For pure rolling motion,

$$q = r = 0 \tag{11.8.12}$$

Using these constraints in Eq. (11.5.12) gives

$$\begin{Bmatrix} \dot{e}_0 \\ \dot{e}_x \\ \dot{e}_y \\ \dot{e}_z \end{Bmatrix} = \frac{1}{2}\begin{bmatrix} 0 & -p & 0 & 0 \\ p & 0 & 0 & 0 \\ 0 & 0 & 0 & p \\ 0 & 0 & -p & 0 \end{bmatrix}\begin{Bmatrix} e_0 \\ e_x \\ e_y \\ e_z \end{Bmatrix} = \frac{p}{2}\begin{Bmatrix} -e_x \\ e_0 \\ e_z \\ -e_y \end{Bmatrix} \tag{11.8.13}$$

If the elevation angle and the azimuth angle are both initially zero, from Eq. (11.7.8), the initial condition is

$$\begin{Bmatrix} e_0 \\ e_x \\ e_y \\ e_z \end{Bmatrix}_{t=0} = \begin{Bmatrix} \cos(\phi_0/2) \\ \sin(\phi_0/2) \\ 0 \\ 0 \end{Bmatrix} \tag{11.8.14}$$

Using Eq. (11.8.14) with Eq. (11.8.13), it is noted that both e_y and e_z remain zero during this motion. Thus, **pure rolling motion** can be simulated using the constraints

$$q = r = e_y = e_z = 0 \tag{11.8.15}$$

Similarly, **pure pitching motion** can be simulated by using the quaternion constraints

$$p = r = e_x = e_z = 0 \tag{11.8.16}$$

and **pure yawing motion** results from the constraints

$$p = q = e_x = e_y = 0 \tag{11.8.17}$$

11.9. Closed-Form Quaternion Solution for Constant Rotation

It is possible to obtain a closed-form solution to the quaternion formulation for the case of constant rotation. While such a condition would frequently occur in spacecraft applications, it almost never occurs in aircraft applications. The angular rates experienced by a moving aircraft depend on the aerodynamic moments acting on the craft and are almost always changing with time. In this case, closed-form solutions to the quaternion formulation are very difficult or impossible to obtain for all but the most trivial conditions. Nevertheless, closed-form analytic solutions to the quaternion formulation for the case of constant angular rates provide an excellent mechanism for verifying the numerical algorithms used to integrate the quaternion formulation. For such verification it is useful to have a general solution that allows for rotation about any or all of the body-fixed axes. The development of such a solution, from Eq. (11.5.12), is rather straightforward.

Consider a rigid body that is rotating at a constant angular velocity. The differential equations governing the change in the components of the quaternion, $\{\mathbf{e}\}$, with time are given by Eq. (11.5.12). This system of differential equations can be written in matrix notation as

$$\{\dot{\mathbf{e}}\} - [\mathbf{M}]\{\mathbf{e}\} = 0 \tag{11.9.1}$$

$$[\mathbf{M}] = \frac{1}{2}\begin{bmatrix} 0 & -p & -q & -r \\ p & 0 & r & -q \\ q & -r & 0 & p \\ r & q & -p & 0 \end{bmatrix} \tag{11.9.2}$$

When the matrix [M] is constant, the solution to Eq. (11.9.1) is

$$\{\mathbf{e}\} = [\exp([\mathbf{M}]t)]\{\mathbf{e}\}_{t=0} \tag{11.9.3}$$

where the matrix exponential $[\exp([\mathbf{M}]t)]$ is computed from the matrix series definition

$$[\exp([\mathbf{M}]t)] \equiv [\mathbf{i}] + [\mathbf{M}]t + \frac{[\mathbf{M}][\mathbf{M}]t^2}{2!} + \frac{[\mathbf{M}][\mathbf{M}][\mathbf{M}]t^3}{3!} + \cdots \tag{11.9.4}$$

Here $\{\mathbf{e}\}_{t=0}$ is the initial value of the quaternion at time $t=0$ and [i] is the identity matrix. If the matrix [M] were completely arbitrary, the matrix exponential would need to be evaluated by summing a large number of terms in the infinite series. However, in this particular case we can take advantage of a special property of the matrix that is defined in Eq. (11.9.2).

By direct multiplication it is readily shown from Eq. (11.9.2) that

$$[\mathbf{M}][\mathbf{M}] = -\tfrac{1}{4}\omega^2[\mathbf{i}] \tag{11.9.5}$$

where $\omega^2 = p^2 + q^2 + r^2$. By making use of Eq. (11.9.5), the infinite series in Eq. (11.9.4) can be rearranged as

$$[\exp([\mathbf{M}]t)] = [\mathbf{i}]\left(1 - \frac{(\omega t/2)^2}{2!} + \frac{(\omega t/2)^4}{4!} + \cdots\right) + \frac{2}{\omega}[\mathbf{M}]\left(\frac{\omega t}{2} - \frac{(\omega t/2)^3}{3!} + \frac{(\omega t/2)^5}{5!} + \cdots\right)$$

or

$$[\exp([\mathbf{M}]t)] = [\mathbf{i}]\cos(\omega t/2) + \frac{2}{\omega}[\mathbf{M}]\sin(\omega t/2) \tag{11.9.6}$$

Using Eq. (11.9.6) in Eq. (11.9.3) yields the general solution for constant rotation

$$\{\mathbf{e}\} = \left[[\mathbf{i}]\cos(\omega t/2) + \frac{2}{\omega}[\mathbf{M}]\sin(\omega t/2)\right]\{\mathbf{e}\}_{t=0} \tag{11.9.7}$$

For the special initial condition where all three Euler angles are zero,

$$\begin{Bmatrix} e_0(0) \\ e_x(0) \\ e_y(0) \\ e_z(0) \end{Bmatrix} = \begin{Bmatrix} 1 \\ 0 \\ 0 \\ 0 \end{Bmatrix} \tag{11.9.8}$$

the solution given by Eq. (11.9.7) reduces to the rather obvious result

$$\begin{Bmatrix} e_0 \\ e_x \\ e_y \\ e_z \end{Bmatrix} = \begin{Bmatrix} \cos(\omega t/2) \\ (p/\omega)\sin(\omega t/2) \\ (q/\omega)\sin(\omega t/2) \\ (r/\omega)\sin(\omega t/2) \end{Bmatrix} \tag{11.9.9}$$

Equations (11.9.7) and (11.9.9) provide an excellent means for testing most numerical algorithms used to integrate the quaternion formulation.

EXAMPLE 11.9.1. Consider an object moving relative to the surface of the Earth under the assumption of no atmosphere. Initially, at time $t = 0$, the primary inertial axes of the body are aligned such that the Euler angles are

$$\begin{Bmatrix} \phi \\ \theta \\ \psi \end{Bmatrix}_{t=0} = \begin{Bmatrix} 0° \\ 90° \\ 0° \end{Bmatrix}$$

The initial translational and rotational velocities of the body relative to this same primary body-fixed coordinate system are

$$\begin{Bmatrix} u \\ v \\ w \end{Bmatrix}_{t=0} = \begin{Bmatrix} V_v \\ 0 \\ V_h \end{Bmatrix} \text{ and } \begin{Bmatrix} p \\ q \\ r \end{Bmatrix}_{t=0} = \begin{Bmatrix} 0 \\ \omega \\ 0 \end{Bmatrix}$$

Using the body-fixed quaternion formulation for the case where all three primary moments of inertia are equal, obtain a solution for the position and orientation of the body as a function of time.

Solution. Because we are assuming no atmosphere, the only force is gravity and there is no moment acting about the center of gravity. Applying Newton's second law as expressed in Eq. (7.2.20) and using Eq. (11.5.7) to express the gravitational force in terms of the Euler-Rodrigues quaternion, we obtain

$$\frac{W}{g}\begin{Bmatrix} \dot{u} \\ \dot{v} \\ \dot{w} \end{Bmatrix} = W\begin{Bmatrix} 2(e_x e_z - e_y e_0) \\ 2(e_y e_z + e_x e_0) \\ e_z^2 + e_0^2 - e_x^2 - e_y^2 \end{Bmatrix} + \frac{W}{g}\begin{Bmatrix} rv - qw \\ pw - ru \\ qu - pv \end{Bmatrix} \tag{11.9.10}$$

$$\begin{Bmatrix} \dot{p} \\ \dot{q} \\ \dot{r} \end{Bmatrix} = \begin{Bmatrix} 0 \\ 0 \\ 0 \end{Bmatrix} \tag{11.9.11}$$

Using the kinematic transformation equations given by Eqs. (11.5.8) and (11.5.12), for the Euler-Rodrigues formulation with no wind, we have

$$\begin{Bmatrix} \dot{x}_f \\ \dot{y}_f \\ \dot{z}_f \end{Bmatrix} = \begin{bmatrix} e_x^2 + e_0^2 - e_y^2 - e_z^2 & 2(e_x e_y - e_z e_0) & 2(e_x e_z + e_y e_0) \\ 2(e_x e_y + e_z e_0) & e_y^2 + e_0^2 - e_x^2 - e_z^2 & 2(e_y e_z - e_x e_0) \\ 2(e_x e_z - e_y e_0) & 2(e_y e_z + e_x e_0) & e_z^2 + e_0^2 - e_x^2 - e_y^2 \end{bmatrix} \begin{Bmatrix} u \\ v \\ w \end{Bmatrix} \tag{11.9.12}$$

$$\begin{Bmatrix} \dot{e}_0 \\ \dot{e}_x \\ \dot{e}_y \\ \dot{e}_z \end{Bmatrix} = \frac{1}{2} \begin{bmatrix} 0 & -p & -q & -r \\ p & 0 & r & -q \\ q & -r & 0 & p \\ r & q & -p & 0 \end{bmatrix} \begin{Bmatrix} e_0 \\ e_x \\ e_y \\ e_z \end{Bmatrix} \tag{11.9.13}$$

Choosing the positive sign from Eq. (11.7.8) and using the specified initial condition in terms of Euler angles, the initial Euler-Rodrigues quaternion is

$$\begin{Bmatrix} e_0 \\ e_x \\ e_y \\ e_z \end{Bmatrix}_{t=0} = \begin{Bmatrix} C_{\phi/2} C_{\theta/2} C_{\psi/2} + S_{\phi/2} S_{\theta/2} S_{\psi/2} \\ S_{\phi/2} C_{\theta/2} C_{\psi/2} - C_{\phi/2} S_{\theta/2} S_{\psi/2} \\ C_{\phi/2} S_{\theta/2} C_{\psi/2} + S_{\phi/2} C_{\theta/2} S_{\psi/2} \\ C_{\phi/2} C_{\theta/2} S_{\psi/2} - S_{\phi/2} S_{\theta/2} C_{\psi/2} \end{Bmatrix}_{t=0} = \begin{Bmatrix} C_{\theta/2} \\ 0 \\ S_{\theta/2} \\ 0 \end{Bmatrix}_{t=0}$$

or

$$\begin{Bmatrix} e_0 \\ e_x \\ e_y \\ e_z \end{Bmatrix}_{t=0} = \begin{Bmatrix} 1/\sqrt{2} \\ 0 \\ 1/\sqrt{2} \\ 0 \end{Bmatrix} \tag{11.9.14}$$

Defining the position of the body to be measured relative to the initial position at time $t = 0$, the initial condition for position is

$$\begin{Bmatrix} x_f \\ y_f \\ z_f \end{Bmatrix}_{t=0} = \begin{Bmatrix} 0 \\ 0 \\ 0 \end{Bmatrix} \tag{11.9.15}$$

This completes the formulation for the 13 state variables, x_f, y_f, z_f, e_0, e_x, e_y, e_z, u, v, w, p, q, and r.

From Eq. (11.9.11), it is easily seen that the body-fixed angular rates remain constant at the initial values and from Eq. (11.9.13) with the specified initial angular rates, we have

$$\begin{Bmatrix} p \\ q \\ r \end{Bmatrix} = \begin{Bmatrix} 0 \\ \omega \\ 0 \end{Bmatrix} \tag{11.9.16}$$

and

$$\begin{Bmatrix} \dot{e}_0 \\ \dot{e}_x \\ \dot{e}_y \\ \dot{e}_z \end{Bmatrix} = \frac{1}{2}\begin{bmatrix} 0 & 0 & -\omega & 0 \\ 0 & 0 & 0 & -\omega \\ \omega & 0 & 0 & 0 \\ 0 & \omega & 0 & 0 \end{bmatrix}\begin{Bmatrix} e_0 \\ e_x \\ e_y \\ e_z \end{Bmatrix} \tag{11.9.17}$$

Since ω is constant, the solution to Eq. (11.9.17) is specified by Eq. (11.9.7). Applying Eq. (11.9.14), this gives

$$\begin{Bmatrix} e_0 \\ e_x \\ e_y \\ e_z \end{Bmatrix} = \left[\begin{bmatrix} 1 & 0 & 0 & 0 \\ 0 & 1 & 0 & 0 \\ 0 & 0 & 1 & 0 \\ 0 & 0 & 0 & 1 \end{bmatrix}\cos(\omega t/2) + \frac{2}{\omega}\frac{1}{2}\begin{bmatrix} 0 & 0 & -\omega & 0 \\ 0 & 0 & 0 & -\omega \\ \omega & 0 & 0 & 0 \\ 0 & \omega & 0 & 0 \end{bmatrix}\sin(\omega t/2)\right]\begin{Bmatrix} 1/\sqrt{2} \\ 0 \\ 1/\sqrt{2} \\ 0 \end{Bmatrix}$$

or

$$\begin{Bmatrix} e_0 \\ e_x \\ e_y \\ e_z \end{Bmatrix} = \frac{1}{\sqrt{2}}\begin{Bmatrix} \cos(\omega t/2) - \sin(\omega t/2) \\ 0 \\ \cos(\omega t/2) + \sin(\omega t/2) \\ 0 \end{Bmatrix} \tag{11.9.18}$$

Using Eqs. (11.9.16) and (11.9.18) in Eq. (11.9.10) gives

$$\begin{Bmatrix} \dot{u} \\ \dot{v} \\ \dot{w} \end{Bmatrix} = \frac{g}{2}\begin{Bmatrix} -2[\cos(\omega t/2) + \sin(\omega t/2)][\cos(\omega t/2) - \sin(\omega t/2)] \\ 0 \\ [\cos(\omega t/2) - \sin(\omega t/2)]^2 - [\cos(\omega t/2) + \sin(\omega t/2)]^2 \end{Bmatrix} + \begin{Bmatrix} -\omega w \\ 0 \\ \omega u \end{Bmatrix}$$

$$= g\begin{Bmatrix} \sin^2(\omega t/2) - \cos^2(\omega t/2) \\ 0 \\ -2\cos(\omega t/2)\sin(\omega t/2) \end{Bmatrix} + \begin{Bmatrix} -\omega w \\ 0 \\ \omega u \end{Bmatrix}$$

or

$$\begin{Bmatrix} \dot{u} \\ \dot{v} \\ \dot{w} \end{Bmatrix} + \begin{Bmatrix} \omega w \\ 0 \\ -\omega u \end{Bmatrix} = g\begin{Bmatrix} -\cos(\omega t) \\ 0 \\ -\sin(\omega t) \end{Bmatrix} \tag{11.9.19}$$

The general solution to Eq. (11.9.19) is found by adding a particular solution to the homogeneous solution. This gives

$$\begin{Bmatrix} u \\ v \\ w \end{Bmatrix} = \begin{Bmatrix} C_1 \sin(\omega t) + C_2 \cos(\omega t) \\ C_3 \\ C_2 \sin(\omega t) - C_1 \cos(\omega t) \end{Bmatrix} + t \begin{Bmatrix} -g \cos(\omega t) \\ 0 \\ -g \sin(\omega t) \end{Bmatrix}$$

After applying the initial condition that is specified in the problem statement, the solution for the body-fixed velocity components is

$$\begin{Bmatrix} u \\ v \\ w \end{Bmatrix} = \begin{Bmatrix} V_v \cos(\omega t) - V_h \sin(\omega t) \\ 0 \\ V_v \sin(\omega t) + V_h \cos(\omega t) \end{Bmatrix} + t \begin{Bmatrix} -g \cos(\omega t) \\ 0 \\ -g \sin(\omega t) \end{Bmatrix} \tag{11.9.20}$$

Using Eqs. (11.9.18) and (11.9.20) in Eq. (11.9.12) results in

$$\begin{Bmatrix} \dot{x}_f \\ \dot{y}_f \\ \dot{z}_f \end{Bmatrix} = \begin{bmatrix} -\sin(\omega t) & 0 & \cos(\omega t) \\ 0 & 1 & 0 \\ -\cos(\omega t) & 0 & -\sin(\omega t) \end{bmatrix} \begin{Bmatrix} V_v \cos(\omega t) - V_h \sin(\omega t) - gt \cos(\omega t) \\ 0 \\ V_v \sin(\omega t) + V_h \cos(\omega t) - gt \sin(\omega t) \end{Bmatrix}$$

or

$$\begin{Bmatrix} \dot{x}_f \\ \dot{y}_f \\ \dot{z}_f \end{Bmatrix} = \begin{Bmatrix} V_h \\ 0 \\ -V_v + gt \end{Bmatrix} \tag{11.9.21}$$

Equation (11.9.21) is readily integrated subject to Eq. (11.9.15) to yield

$$\begin{Bmatrix} x_f \\ y_f \\ z_f \end{Bmatrix} = \begin{Bmatrix} V_h t \\ 0 \\ -V_v t + \frac{1}{2} g t^2 \end{Bmatrix} \tag{11.9.22}$$

Equation (11.9.22) specifies the position of the object as a function of time. This is the well-known parabolic solution for the trajectory of a projectile in the absence of aerodynamic drag. Equation (11.9.18) gives the object's orientation as a function of time, specified in terms of the Euler-Rodrigues quaternion.

The problem in Example 11.9.1 could have been solved more easily had it been formulated using an inertial coordinate system. However, this example does demonstrate that simple problems can be solved analytically using the quaternion formulation. Such closed-form solutions are useful for verifying computer codes that have been written for numerical integration of the quaternion formulation.

11.10. Numerical Integration of the Quaternion Formulation

When integrating Eq. (11.5.12) numerically, the zeros on the diagonal can cause some problems. Integration of this system can result in very large numerical errors if a first-order method is used. For this reason, a higher-order method, such as fourth-order Runge-Kutta or fourth-order Adams-Bashforth-Moulton (see, for example, Hoffman 1992 or Gerald and Wheatley 1999) should always be used to integrate the quaternion formulation. Since most modern numerical codes use such methods, this is not at all restrictive for simulations run on modern digital computers.

Historically, aircraft simulations using the quaternion formulation were first commonly run using analog computers. Since these analog simulations were inherently first-order, the raw quaternion formulation did not work well. When such simulations were run, the magnitude of the quaternion would grow quite rapidly with time. Since the formulation requires the magnitude of the quaternion to remain unity in order to maintain orthogonality in the attitude transformation, these large orthogonality errors would render the simulations almost useless. To remedy this problem, techniques were developed to reduce this orthogonality error. One such method, developed by Robinson (1958) and popularized by Mitchell and Rogers (1965), is based on the method first suggested by Corbett and Wright (1957) for maintaining orthogonality in the direction-cosine matrix. With this method, the kinematic equations in Eq. (11.5.12) were modified to include error reduction terms on the diagonal,

$$\begin{Bmatrix} \dot{e}_0 \\ \dot{e}_x \\ \dot{e}_y \\ \dot{e}_z \end{Bmatrix} = \frac{1}{2}\begin{bmatrix} k\varepsilon & -p & -q & -r \\ p & k\varepsilon & r & -q \\ q & -r & k\varepsilon & p \\ r & q & -p & k\varepsilon \end{bmatrix}\begin{Bmatrix} e_0 \\ e_x \\ e_y \\ e_z \end{Bmatrix} \tag{11.10.1}$$

where ε is the orthogonality error, defined as

$$\varepsilon = 1-(e_0^2+e_x^2+e_y^2+e_z^2) \tag{11.10.2}$$

and k is a gain coefficient, which Mitchell and Rogers (1965) said should be "set to a very high value." This error reduction scheme, called *Corbett-Wright orthogonality control*, worked quite well when used with the analog computers of that era.

While analog computers are no longer widely available, it is possible to demonstrate approximately how Corbett-Wright orthogonality control worked with an analog computer by integrating Eq. (11.10.1) using a first-order Euler integration scheme. Results of such integration are shown in Fig. 11.10.1. For this figure the total error was computed as the difference between the numerical integration result and the exact solution from Eq. (11.9.7). Notice that as the value of the Corbett-Wright gain coefficient approaches zero, which is the case of no orthogonality control, the total error becomes very large. For gain coefficients larger than about 0.5ω, the error is reduced to a more or less acceptable level. With the exception of the increase in error on the right, the results shown in Fig. 11.10.1 are very similar to the results reported by Mitchell and Rogers (1965) for a typical analog computer.

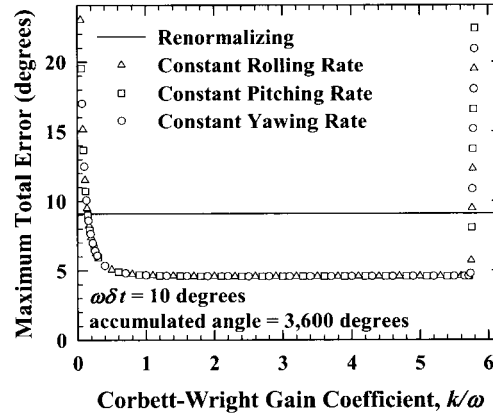


Figure 11.10.1. Effect of changing the gain coefficient on the accuracy of a first-order Euler algorithm using Corbett-Wright orthogonality control.

Unlike first-order digital integration, analog simulations were well behaved for very large values of k. The abrupt increase in error that is seen in Fig. 11.10.1 for k/ω greater than about 5.7 is a result of the well-known Euler instability that is associated with any first-order numerical integration. For Eq. (11.10.1), Fang and Zimmerman (1969) have shown that this first-order instability occurs whenever the product of the gain coefficient and the time step is greater than unity,

$$k\,\delta t > 1$$

When digital computers first became fast enough to replace analog computers for running such simulations, Corbett-Wright orthogonality control was often used in the digital solution algorithms. Furthermore, this orthogonality control is still widely used for aircraft flight simulation today. It is, however, not necessary. When a modern digital computer is used to integrate Eq. (11.5.12) with any of the prevalent fourth-order numerical methods, the orthogonality error is extremely small. Using the Corbett-Wright orthogonality control scheme with these modern numerical algorithms increases the computation time but does little to improve the accuracy of the simulation.

Even though the orthogonality error for modern numerical algorithms is very small, it can accumulate. Thus, if a simulation is to be run for long periods of time using large time steps, the quaternion should be renormalized periodically. The quaternion may be renormalized by dividing each component by the magnitude,

$$\{\mathbf{e}\}_r = \frac{\{\mathbf{e}\}}{|\{\mathbf{e}\}|} = \frac{\{\mathbf{e}\}}{\sqrt{e_0^2 + e_x^2 + e_y^2 + e_z^2}} \tag{11.10.3}$$

where the subscript r indicates renormalized. As seen in Fig. 11.10.1, renormalization is not as accurate as Corbett-Wright orthogonality control for first-order integration.

However, a different result is obtained for higher-order integration. If the time steps used with fourth-order Runge-Kutta are of a size to produce about 10 degrees of revolution per time step, it requires about 3,000,000 iterations to degrade the magnitude of the quaternion by 1 percent. Since a very long renormalization period can be used, periodic renormalization of the quaternion is much faster than using the Corbett-Wright orthogonality control scheme. However, if computation time is not a concern, Corbett-Wright orthogonality control will eliminate the growth of the orthogonality error for simulations using large time steps. If the time steps are small enough to produce about 5 degrees of rotation or less per time step, no orthogonality control whatsoever is required with fourth-order Runge-Kutta integration.

If the Corbett-Wright orthogonality control scheme is to be used for large time-step simulations, it should be remembered that this only eliminates the growth of the orthogonality error. It does not eliminate the drift error, which for modern algorithms can be much larger than the orthogonality error. In fact, when a large gain coefficient is used with fourth-order integration and Corbett-Wright orthogonality control, the drift error is increased by more than the orthogonality error is reduced, which actually increases the net error for the simulation. This is shown in Fig. 11.10.2. In contrast with the older analog simulations that used a very large gain coefficient, when Corbett-Wright orthogonality control is used with a fourth-order digital integration, a gain coefficient larger than about 2ω should not be used. As can be seen in Fig. 11.10.3, this is truly independent of the angular rate. Furthermore, as is seen in Fig. 11.10.4, decreasing the time step does not eliminate this problem. For such fourth-order numerical integration, a gain coefficient equal to the magnitude of the angular velocity will effectively eliminate the growth of the orthogonality error associated with large time steps without adversely affecting the drift error. However, for common aircraft flight simulations, the angular rates are not typically known a priori. Furthermore, the angular rate is typically changing with time and a very low angular rate requires a very low gain coefficient for accurate simulation.

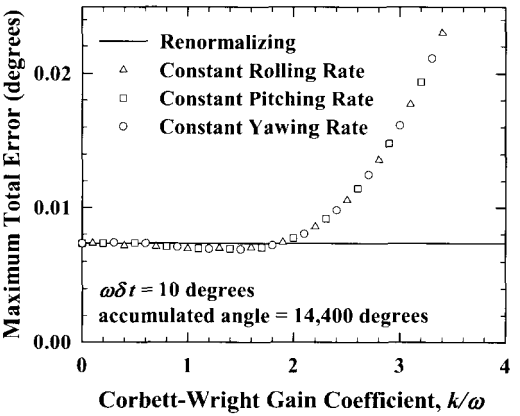


Figure 11.10.2. Effect of changing the gain coefficient on the accuracy of a fourth-order Runge-Kutta algorithm using Corbett-Wright orthogonality control.

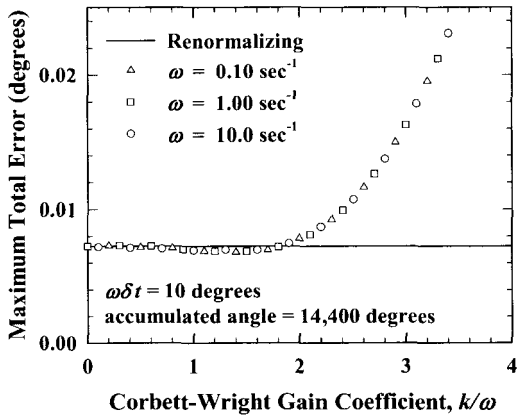


Figure 11.10.3. Effect of changing the angular rate on the accuracy of a fourth-order Runge-Kutta algorithm using Corbett-Wright orthogonality control.

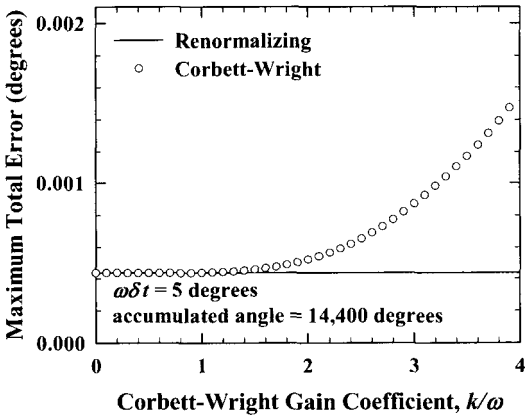


Figure 11.10.4. Effect of reducing the step size on the accuracy of a fourth-order Runge-Kutta algorithm using Corbett-Wright orthogonality control.

To avoid increasing the total error, a variable gain coefficient equal to the angular rate should be used with a fourth-order Runge-Kutta algorithm using Corbett-Wright orthogonality control,

$$k = \omega = \sqrt{p^2 + q^2 + r^2} \tag{11.10.4}$$

The implementation of Eq. (11.10.4) adds substantially to the computational burden of Corbett-Wright orthogonality control. Thus, for greatest computational efficiency, it is much preferred to use periodic renormalization of the quaternion over any use of the Corbett-Wright orthogonality control scheme.

Fang and Zimmerman (1969) proposed a pseudo fourth-order method for integrating Eq. (11.10.1). With conventional fourth-order Runge-Kutta the time rate of change of the quaternion is computed from Eq. (11.10.1) four times for each time step. With the Fang and Zimmerman algorithm, this same fourth-order numerical procedure is used to integrate Eq. (11.10.1), except that ε is held constant through all four computations in each time step. The orthogonality error is updated only once at the beginning of each full time step.

The Fang and Zimmerman algorithm exhibits features of both first- and fourth-order numerical integration. Although both the angular velocity and the quaternion on the right-hand side of Eq. (11.10.1) are estimated to fourth-order accuracy, ε is estimated only to first-order accuracy. Results of integrating Eq. (11.10.1) using the Fang and Zimmerman algorithm are shown in Fig. 11.10.5. Notice that the accuracy of the method for small values of the gain coefficient is comparable to that for full fourth-order integration. However, the method also exhibits an abrupt first-order instability when the gain coefficient is greater than 1 divided by the time step, $k > 1/\delta t$.

One striking observation that should be noted from Figs. 11.10.2 through 11.10.5 is that Corbett-Wright orthogonality control offers no significant reduction in simulation error for modern numerical integration algorithms. On the other hand, if the gain coefficient is not chosen judicially, Corbett-Wright orthogonality control can significantly increase the simulation error. Periodic renormalization of the quaternion does not present this problem and is more computationally efficient.

The computation time required for periodic renormalization of the quaternion can be reduced even further by recognizing that the orthogonality error is always very small for modern fourth-order integration algorithms. Equation (11.10.3) can be written as

$$\{\mathbf{e}\}_r = \frac{\{\mathbf{e}\}}{\sqrt{e_0^2 + e_x^2 + e_y^2 + e_z^2}} = \frac{\{\mathbf{e}\}}{\sqrt{1-\varepsilon}} \tag{11.10.5}$$

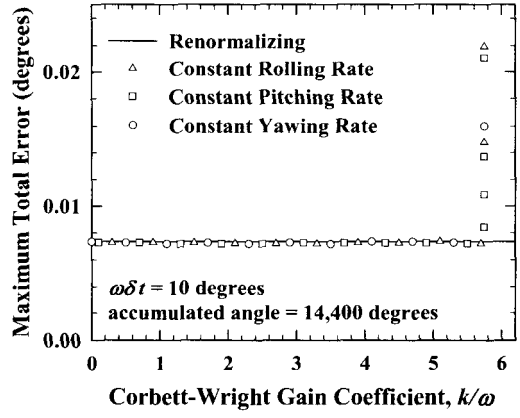


Figure 11.10.5. Effect of changing the gain coefficient on the accuracy of the numerical Fang and Zimmerman algorithm using Corbett-Wright orthogonality control.

where ε is the error in the square of the quaternion magnitude, as given by Eq. (11.10.2). Since ε is very small, Eq. (11.10.5) can be closely approximated as

$$\{\mathbf{e}\}_r \cong \{\mathbf{e}\}\left(1+\tfrac{1}{2}\varepsilon\right) \tag{11.10.6}$$

or after applying Eq. (11.10.2),

$$\{\mathbf{e}\}_r \cong \{\mathbf{e}\}\left[1.5-0.5\left(e_0^2+e_x^2+e_y^2+e_z^2\right)\right] \tag{11.10.7}$$

Periodic application of Eq. (11.10.7) is sufficient to eliminate the orthogonality error.

Renormalizing the quaternion with Eq. (11.10.7) requires nine multiplications and four additions. Using Eq. (11.10.3), on the other hand, requires eight multiplications, three additions, one square root, and one division. Typical modern hardware requires one instruction cycle for addition, one instruction cycle for multiplication, something on the order of four instruction cycles for division, and anywhere from about 4 to 30 instruction cycles for the square-root operation, depending on the processor and compiler. Therefore, renormalizing with Eq. (11.10.3) requires anywhere from 50 to 250 percent greater computation time than using Eq. (11.10.7), on typical modern hardware. Furthermore, even if future developments reduce the time required for division and square root to one instruction cycle each, Eq. (11.10.7) will be, at worst, computationally equivalent to Eq. (11.10.3).

While periodic renormalization of the quaternion using Eq. (11.10.7) provides a computationally efficient means for controlling the orthogonality error, it does not control the drift error. In fact, for higher-order algorithms, it does nothing whatsoever to reduce the total error. In Figs. 11.10.2 through 11.10.5, the points that correspond to a Corbett-Wright gain coefficient of zero were obtained using no orthogonality control at all. In each case the total error obtained with no orthogonality control was the same as that obtained when the quaternion was renormalized after each time step. From this, one may be tempted to conclude that there is no value in orthogonality control. This is not exactly true. If the orthogonality error is controlled, a small amount of drift error does not adversely affect a flight simulator, since it is constantly being corrected with virtually imperceptible pilot input. The pilot's perception of the drift error is similar to that caused by an infinitesimal change in the aerodynamics of the aircraft. The orthogonality error, on the other hand, has no counterpart in the physical world and cannot be compensated for by the pilot. When the quaternion magnitude deviates from unity, transformations obtained from Eq. (11.5.5) or Eq. (11.6.8) become nonorthogonal and vector length is not preserved through the transformation. Since rotation is an orthogonal transformation, large orthogonality errors can cause physically unrealistic distortion in the kinematic transformations. For large time-step simulations with no orthogonality control, these transformation distortions will continue to increase with time, unaffected by pilot input.

To demonstrate the effects of both orthogonality error and drift error on the visual display, Fig. 11.10.6 shows a three-dimensional image displayed after four different quaternion simulations. Each of the four simulations was carried out using fourth-order Adams-Bashforth-Moulton numerical integration. In each case all aspects of the

integration, except the error control, were the same. All four images are viewed from exactly the same position and with exactly the same perspective. The differences in the images result entirely from numerical integration errors in the transformation quaternion.

The image in Fig. 11.10.6a is essentially error-free. The orthogonality error was removed using periodic renormalization, and the drift error was eliminated with pilot input. The darker image in Fig. 11.10.6b was generated using periodic renormalization without pilot input and thus contains no orthogonality error but about 17 degrees of drift error. To emphasize the error, this image has been overlaid on an error-free image in light gray. The integration used to obtain the darker image in Fig. 11.10.6c had no orthogonality control or pilot input and produced about 8 percent orthogonality error and about 17 degrees of drift error. Again, the light gray image in this figure is error-free. By comparing Fig. 11.10.6b and c, it can be seen that orthogonality error produces a scaling distortion in the visual display. As seen in Fig. 11.10.6d, pilot input eliminates drift error but does nothing to eliminate scaling distortion caused by orthogonality error. It can readily be shown from Eq. (11.6.8) that when orthogonality error is present, all objects in the visual display are scaled by a factor of $|\{\mathbf{e}\}|^2$.

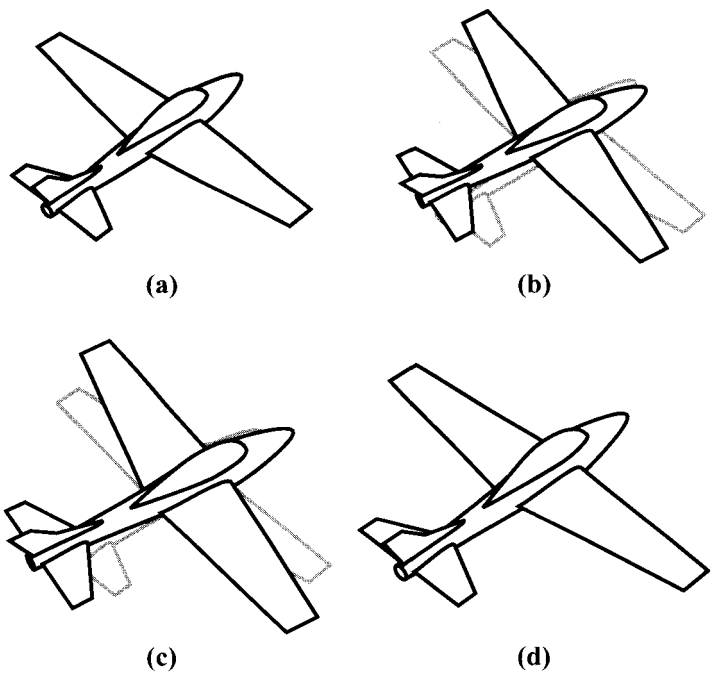


Figure 11.10.6. Effects of drift error and orthogonality error on the visual display after 2,000,000 iterations using fourth-order Adams-Bashforth-Moulton with (a) periodic renormalization, no orthogonality error, and drift error eliminated by the pilot; (b) periodic renormalization, no orthogonality error, and 17 degrees drift error; (c) no orthogonality control, 8 percent orthogonality error, and 17 degrees drift error; (d) no orthogonality control, 8 percent orthogonality error, and drift error eliminated by the pilot.

Since the orthogonality error is only a small fraction of the total error, reducing the size of the time step and/or increasing the order of the numerical integration algorithm are the only effective ways to reduce total error. The effects of time-step size on the orthogonality error and the total error for a fourth-order Runge-Kutta algorithm with no orthogonality control are shown in Figs. 11.10.7 and 11.10.8 for both single- and double-precision computations. These two figures point out a common misconception concerning the origin of the orthogonality error, which is often attributed to the *round-off error* associated with the finite word size used for numerical computation. As can be seen by comparing Fig. 11.10.7 with Fig. 11.10.8, neither the orthogonality error nor the total error is significantly affected by the computation precision for a large step size.

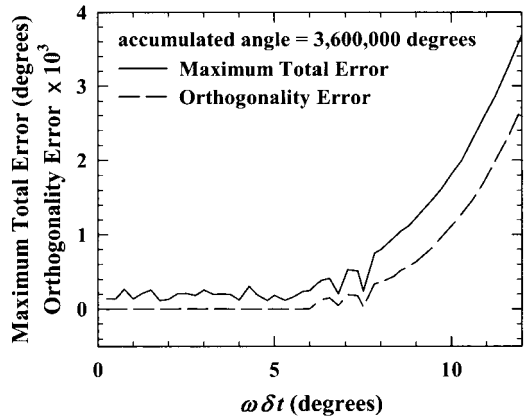


Figure 11.10.7. Effect of step size on the accuracy of a fourth-order Runge-Kutta algorithm with no orthogonality control using single-precision computations.

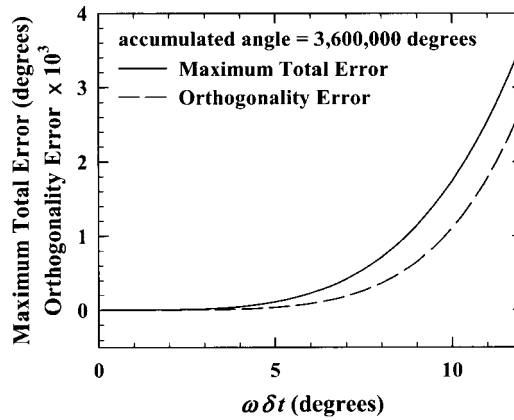


Figure 11.10.8. Effect of step size on the accuracy of a fourth-order Runge-Kutta algorithm with no orthogonality control using double-precision computations.

Furthermore, for a step size of less than about 5 degrees, the single-precision orthogonality error is exactly zero, whereas the double-precision orthogonality error is very small but finite. This is because orthogonality error does not result from the round-off error associated with word size and computation precision. It is, rather, the result of errors associated with the order of the integration algorithm. This numerical integration error is called *truncation error* because it results from truncating the Taylor series for differentiation to a finite number of terms.

In an aircraft flight simulation, computing the time derivatives of the translational and angular velocity components requires computation of the aerodynamic forces and moments. Depending on the method used, these computations can be quite time consuming. Because a digital simulation using the fourth-order Runge-Kutta algorithm requires evaluating these time derivatives four times for each time step, first- and second-order integration methods have occasionally been used in an attempt to reduce computation time. As will be demonstrated, this is not a particularly good choice.

Results of second-order Runge-Kutta integration with Corbett-Wright orthogonality control are shown in Fig. 11.10.9. Notice that as was the case for fourth-order integration, Corbett-Wright orthogonality control offers no reduction in total simulation error for this second-order integration. Furthermore, for the time step used, the accuracy of this second-order simulation is not significantly improved over that of the first-order simulation shown in Fig. 11.10.1. At first thought, this may seem counterintuitive.

From the theory of numerical methods we know that in the limit as the step size approaches zero, the global error for first-order integration should be linearly proportional to the step size, whereas the global error for the second-order integration should be proportional to the step size squared. For very small step size, this is confirmed in Fig. 11.10.10. However, for larger step size, the global error results primarily from the higher-order terms, which have been neglected in both the first- and second-order algorithms. Thus, for larger time steps, the second-order algorithm offers little increase in accuracy over the first-order algorithm. This can be seen in Fig. 11.10.11.

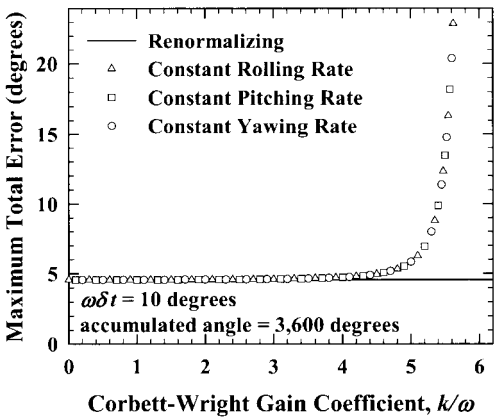


Figure 11.10.9. Effect of changing the gain coefficient on the accuracy of a second-order Runge-Kutta algorithm using Corbett-Wright orthogonality control.

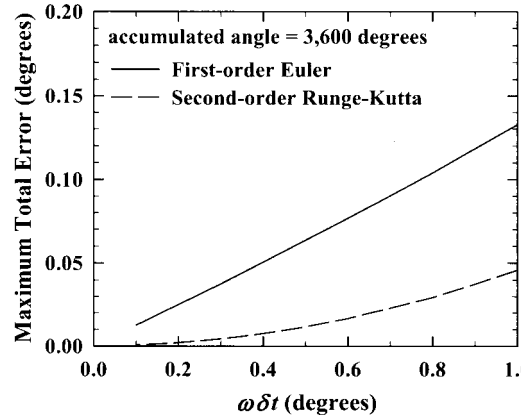


Figure 11.10.10. Comparison between first-order Euler integration and second-order Runge-Kutta integration for small time steps.

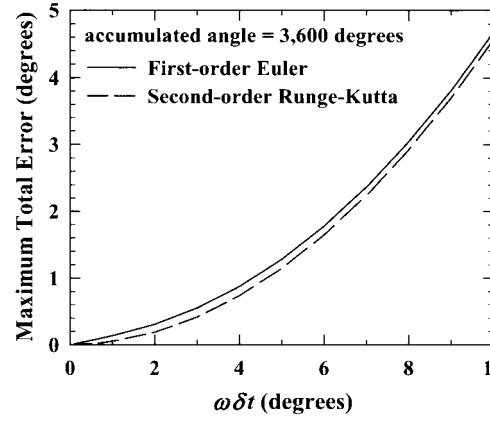


Figure 11.10.11. Comparison between first-order Euler integration and second-order Runge-Kutta integration for large time steps.

When digital computers first became practical for aircraft flight simulation, new integration algorithms were developed in an attempt to reduce computation time without sacrificing accuracy. Pope (1963) proposed one such algorithm, which was called the *exponential method*. This algorithm was first used to integrate the quaternion formulation at the NASA Langley Research Center (see Barker et al., 1973). In the aircraft community, the method is commonly known as the local linearization method. Since the method has been used in aircraft flight simulation for many years but is not commonly used elsewhere, a development of this algorithm will be presented here.

The differential equations governing the change in the components of the quaternion, $\{\mathbf{e}\}$, with time are given by Eq. (11.5.12). This system of differential equations written in matrix notation is

$$\{\dot{\mathbf{e}}\} = [\mathbf{M}]\{\mathbf{e}\} \tag{11.10.8}$$

where

$$[\mathbf{M}] = \frac{1}{2}\begin{bmatrix} 0 & -p & -q & -r \\ p & 0 & r & -q \\ q & -r & 0 & p \\ r & q & -p & 0 \end{bmatrix} \tag{11.10.9}$$

The right side of Eq. (11.10.8) can be expanded in a Taylor series about $t = t_i$ and $\{\mathbf{e}\} = \{\mathbf{e}\}_i$,

$$\begin{aligned} \{\dot{\mathbf{e}}\} &= [\mathbf{M}]_i\{\mathbf{e}\}_i + [\mathbf{M}]_i(\{\mathbf{e}\} - \{\mathbf{e}\}_i) + [\dot{\mathbf{M}}]_i\{\mathbf{e}\}_i(t - t_i) \\ &+ \frac{1}{2!}\left(2[\dot{\mathbf{M}}]_i(\{\mathbf{e}\} - \{\mathbf{e}\}_i)(t - t_i) + [\ddot{\mathbf{M}}]_i\{\mathbf{e}\}_i(t - t_i)^2\right) \\ &+ \frac{1}{3!}\left(3[\ddot{\mathbf{M}}]_i(\{\mathbf{e}\} - \{\mathbf{e}\}_i)(t - t_i)^2 + [\dddot{\mathbf{M}}]_i\{\mathbf{e}\}_i(t - t_i)^3\right) + \cdots \end{aligned} \tag{11.10.10}$$

where the subscript i indicates evaluation at time $t = t_i$.

Equation (11.10.10) forms the basis for the local linearization algorithms that have been used to integrate the quaternion formulation. These algorithms are based on the method proposed by Pope (1963), which was originally called the exponential method. Barker, Bowles, and Williams (1973) first applied this method to the quaternion formulation using a first-order approximation to Eq. (11.10.10),

$$\{\dot{\mathbf{e}}\} \cong [\mathbf{M}]_i\{\mathbf{e}\}_i + [\mathbf{M}]_i(\{\mathbf{e}\} - \{\mathbf{e}\}_i) + [\dot{\mathbf{M}}]_i\{\mathbf{e}\}_i(t - t_i) \tag{11.10.11}$$

In an attempt to improve the local linearization algorithm, Yen and Cook (1980) used the approximation

$$\{\dot{\mathbf{e}}\} \cong [\mathbf{M}]_i\{\mathbf{e}\}_i + [\mathbf{M}]_i(\{\mathbf{e}\} - \{\mathbf{e}\}_i) + [\dot{\mathbf{M}}]_i\{\mathbf{e}\}_i(t - t_i) + [\dot{\mathbf{M}}]_i[\mathbf{M}]_i\{\mathbf{e}\}_i(t - t_i)^2 \tag{11.10.12}$$

Equation (11.10.12) includes an approximation for the second term on the right-hand side of Eq. (11.10.10). Within the second term, this approximation implies that

$$(\{\mathbf{e}\} - \{\mathbf{e}\}_i) \cong \{\dot{\mathbf{e}}\}_i(t - t_i) = [\mathbf{M}]_i\{\mathbf{e}\}_i(t - t_i)$$

and

$$[\ddot{\mathbf{M}}] \cong 0$$

Since Eq. (11.10.12) completely ignores $[\ddot{\mathbf{M}}]$ in the second-order term of Eq. (11.10.10), this equation should not be expected to give higher-order accuracy than Eq. (11.10.11). This fact was confirmed by the numerical results of Yen and Cook (1980).

From Eqs. (11.10.9) and (11.10.10), we see that a full second-order approximation for the right-hand side of Eq. (11.10.10) would require knowledge of the second derivative of the angular rate vector. While the first derivative of the angular rate vector is always available from the equations of motion, its second derivative is not directly available in a six-degree-of-freedom flight simulation. For this reason, a complete second-order approximation to the right-hand side of Eq. (11.10.10) has not been used. Since the approximation given by Eq. (11.10.12) is no more accurate than that given by Eq. (11.10.11), only the local linearization algorithm based on Eq. (11.10.11) is presented here.

The local linearization algorithm of Barker, Bowles, and Williams (1973) has been used in aircraft flight simulation for many years. This algorithm is based on the closed-form solution to Eq. (11.10.11),

$$\begin{aligned}\{\mathbf{e}\}_{i+1} &= [\exp([\mathbf{M}]_i\,\delta t)]\{\mathbf{e}\}_i \\ &\quad +\left([\exp([\mathbf{M}]_i\,\delta t)]-[\mathbf{i}]-[\mathbf{M}]_i\,\delta t\right)[\mathbf{M}]_i^{-1}[\mathbf{M}]_i^{-1}[\dot{\mathbf{M}}]_i\{\mathbf{e}\}_i\end{aligned} \tag{11.10.13}$$

where $\delta t = t_{i+1} - t_i$. Applying Eq. (11.9.6) to replace the matrix exponential on the right-hand side of Eq. (11.10.13) gives

$$\begin{aligned}\{\mathbf{e}\}_{i+1} &= \cos(\omega_i\,\delta t/2)\{\mathbf{e}\}_i + (2/\omega_i)\sin(\omega_i\,\delta t/2)[\mathbf{M}]_i\{\mathbf{e}\}_i \\ &\quad +[\cos(\omega_i\,\delta t/2)-1][\mathbf{M}]_i^{-1}[\mathbf{M}]_i^{-1}[\dot{\mathbf{M}}]_i\{\mathbf{e}\}_i \\ &\quad +[(2/\omega_i)\sin(\omega_i\,\delta t/2)-\delta t][\mathbf{M}]_i[\mathbf{M}]_i^{-1}[\mathbf{M}]_i^{-1}[\dot{\mathbf{M}}]_i\{\mathbf{e}\}_i\end{aligned} \tag{11.10.14}$$

From Eq. (11.10.9), it is readily shown that the inverse of $[\mathbf{M}]$ is

$$[\mathbf{M}]^{-1} = -(4/\omega^2)[\mathbf{M}] \tag{11.10.15}$$

and

$$[\mathbf{M}]^{-1}[\mathbf{M}]^{-1} = -(4/\omega^2)[\mathbf{M}][\mathbf{M}]^{-1} = -(4/\omega^2)[\mathbf{i}] \tag{11.10.16}$$

Thus, using Eq. (11.10.16) in Eq. (11.10.14), the local linearization algorithm can be written as

$$\begin{aligned}\{\mathbf{e}\}_{i+1} &= \cos(\omega_i\,\delta t/2)\{\mathbf{e}\}_i + (2/\omega_i)\sin(\omega_i\,\delta t/2)[\mathbf{M}]_i\{\mathbf{e}\}_i \\ &\quad +(4/\omega_i^2)[1-\cos(\omega_i\,\delta t/2)][\dot{\mathbf{M}}]_i\{\mathbf{e}\}_i \\ &\quad +(4/\omega_i^2)[\delta t-(2/\omega_i)\sin(\omega_i\,\delta t/2)][\mathbf{M}]_i[\dot{\mathbf{M}}]_i\{\mathbf{e}\}_i\end{aligned} \tag{11.10.17}$$

Notice that for the special case where $[\mathbf{M}]$ is constant, Eq. (11.10.17) reduces to the exact solution given by Eq. (11.9.7).

Also note that Eq. (11.10.17) is numerically indeterminate for the special case when ω_i is zero. However, using the series expansion for the sine and the cosine, it is readily shown that when ω_i is zero, Eq. (11.10.17) reduces to

$$\{\mathbf{e}\}_{i+1} \underset{\omega_i \to 0}{=} \{\mathbf{e}\}_i + \delta t\,[\mathbf{M}]_i\{\mathbf{e}\}_i + (\delta t^2/2)[\dot{\mathbf{M}}]_i\{\mathbf{e}\}_i + (\delta t^3/6)[\mathbf{M}]_i[\dot{\mathbf{M}}]_i\{\mathbf{e}\}_i \tag{11.10.18}$$

Furthermore, from Eq. (11.10.9) we see that when ω_i is zero, all 16 components of **[M]** are also zero. Thus, even though Eq. (11.10.18) is not numerically indeterminate, it can be further simplified to give

$$\{\mathbf{e}\}_{i+1} \underset{\omega_i \to 0}{=} \{\mathbf{e}\}_i + (\delta t^2/2)[\dot{\mathbf{M}}]_i\{\mathbf{e}\}_i \tag{11.10.19}$$

Equations (11.10.17) and (11.10.19) provide the foundation for the local linearization algorithm.

The order of the truncation error associated with the local linearization algorithm can be evaluated by using the Taylor series expansion, which is defined in Eq. (11.9.4), for the matrix exponential in Eq. (11.10.13). This gives

$$\begin{aligned}\{\mathbf{e}\}_{i+1} &= \left([\mathbf{i}] + [\mathbf{M}]_i\delta t + \frac{[\mathbf{M}]_i[\mathbf{M}]_i\delta t^2}{2!} + \cdots\right)\{\mathbf{e}\}_i \\ &+ \left(\frac{[\mathbf{M}]_i[\mathbf{M}]_i\delta t^2}{2!} + \cdots\right)[\mathbf{M}]_i^{-1}[\mathbf{M}]_i^{-1}[\dot{\mathbf{M}}]_i\{\mathbf{e}\}_i\end{aligned}$$

or

$$\begin{aligned}\{\mathbf{e}\}_{i+1} &= \{\mathbf{e}\}_i + [\mathbf{M}]_i\{\mathbf{e}\}_i\delta t + \frac{[\mathbf{M}]_i[\mathbf{M}]_i + [\dot{\mathbf{M}}]_i}{2!}\{\mathbf{e}\}_i\delta t^2 \\ &+ \frac{[\mathbf{M}]_i[\mathbf{M}]_i[\mathbf{M}]_i + [\mathbf{M}]_i[\dot{\mathbf{M}}]_i}{3!}\{\mathbf{e}\}_i\delta t^3 + \cdots\end{aligned} \tag{11.10.20}$$

The Taylor series expansion of the exact solution is

$$\{\mathbf{e}\}_{i+1} = \{\mathbf{e}\}_i + \{\dot{\mathbf{e}}\}_i\delta t + \frac{\{\ddot{\mathbf{e}}\}_i}{2!}\delta t^2 + \frac{\{\dddot{\mathbf{e}}\}_i}{3!}\delta t^3 + \cdots \tag{11.10.21}$$

From Eq. (11.10.8) we have

$$\{\dot{\mathbf{e}}\}_i = [\mathbf{M}]_i\{\mathbf{e}\}_i \tag{11.10.22}$$

$$\{\ddot{\mathbf{e}}\}_i = [\mathbf{M}]_i\{\dot{\mathbf{e}}\}_i + [\dot{\mathbf{M}}]_i\{\mathbf{e}\}_i = \left([\mathbf{M}]_i[\mathbf{M}]_i + [\dot{\mathbf{M}}]_i\right)\{\mathbf{e}\}_i \tag{11.10.23}$$

and

$$\begin{aligned}\{\dddot{\mathbf{e}}\}_i &= [\mathbf{M}]_i\{\ddot{\mathbf{e}}\}_i + 2[\dot{\mathbf{M}}]_i\{\dot{\mathbf{e}}\}_i + [\ddot{\mathbf{M}}]_i\{\mathbf{e}\}_i \\ &= \left([\mathbf{M}]_i[\mathbf{M}]_i[\mathbf{M}]_i + [\mathbf{M}]_i[\dot{\mathbf{M}}]_i + 2[\dot{\mathbf{M}}]_i[\mathbf{M}]_i + [\ddot{\mathbf{M}}]_i\right)\{\mathbf{e}\}_i\end{aligned} \tag{11.10.24}$$

Using Eqs. (11.10.22) through (11.10.24) in Eq. (11.10.21) gives

$$\begin{aligned}\{\mathbf{e}\}_{i+1} &= \{\mathbf{e}\}_i + [\mathbf{M}]_i\{\mathbf{e}\}_i\delta t + \frac{[\mathbf{M}]_i[\mathbf{M}]_i + [\dot{\mathbf{M}}]_i}{2!}\{\mathbf{e}\}_i\delta t^2 \\ &+ \frac{[\mathbf{M}]_i[\mathbf{M}]_i[\mathbf{M}]_i + [\mathbf{M}]_i[\dot{\mathbf{M}}]_i + 2[\dot{\mathbf{M}}]_i[\mathbf{M}]_i + [\ddot{\mathbf{M}}]_i}{3!}\{\mathbf{e}\}_i\delta t^3 + \cdots\end{aligned} \tag{11.10.25}$$

Comparing the exact expansion from Eq. (11.10.25) with the expansion of the local linearization algorithm that is given by Eq. (11.10.20), the local truncation error for this algorithm is found to be

$$R_i = \frac{2[\dot{\mathbf{M}}]_i[\mathbf{M}]_i + [\ddot{\mathbf{M}}]_i}{3!}\{\mathbf{e}\}_i\delta t^3 + \mathcal{O}(\delta t^4) + \cdots \tag{11.10.26}$$

Thus, the method produces third-order truncation error with components proportional to both the first and second derivatives of the angular rate vector. Except for the special case of constant rotation, it does not provide an exact solution, as has sometimes been stated in the literature. Since the truncation error is of order δt^3, the local linearization method provides second-order accuracy in a single-point, single-step, numerical integration algorithm.

A more widely known integration method, which was also developed to reduce computation time over that required for fourth-order Runge-Kutta, is fourth-order Adams-Bashforth-Moulton (see, for example, Hoffman 1992). This commonly used numerical integration scheme is a four-point, two-step, backward-difference method. Because starting values at four different points are required, the method must be started using a single-point method such as fourth-order Runge-Kutta. However, after the first three time steps, this method requires evaluating the time derivatives only twice for each time step. This provides fourth-order accuracy similar to that provided by the fourth-order Runge-Kutta algorithm, but at a computational cost similar to that required for second-order Runge-Kutta. Since the development of the fourth-order Adams-Bashforth-Moulton algorithm is presented in most undergraduate textbooks on numerical methods, it will not be repeated here.

In general, simulation error can be reduced by either reducing the size of the time step used for the simulation or by increasing the order of the integration method. Both approaches require increased computation time per simulated second. Figure 11.10.12 shows how total error varies with step size for four different integration algorithms, second-order Runge-Kutta, second-order local linearization, fourth-order Runge-Kutta, and fourth-order Adams-Bashforth-Moulton. The results shown in Fig. 11.10.12 were obtained from numerical integration of the quaternion formulation for the special case of a sinusoidal rotation vector,

$$\begin{Bmatrix} p \\ q \\ r \end{Bmatrix} = \begin{Bmatrix} \omega_{ax}\sin(\omega_{fx}t) \\ \omega_{ay}\sin(\omega_{fy}t) \\ \omega_{az}\sin(\omega_{fz}t) \end{Bmatrix}$$

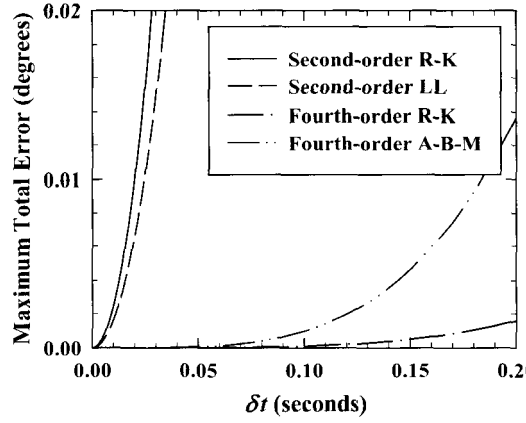


Figure 11.10.12. Comparison between second-order Runge-Kutta, second-order local linearization, fourth-order Runge-Kutta, and fourth-order Adams-Bashforth-Moulton integration.

The error was defined relative to a fourth-order Runge-Kutta solution using very small time steps. As expected, the fourth-order algorithms produce less error for a given time step than do the second-order algorithms. However, the higher-order algorithms also require a greater number of computation cycles for each time step. For this reason, it may not be directly obvious which of the four methods will result in the fastest computation for a given level of accuracy.

The second-order local linearization algorithm requires only one cycle of computation for the aerodynamic forces and moments at each time step. The second-order Runge-Kutta algorithm and the fourth-order Adams-Bashforth-Moulton algorithm each requires two computation cycles per time step, whereas the fourth-order Runge-Kutta algorithm requires four. For the same simulations that were used to produce the results in Fig. 11.10.12, the number of computation cycles per simulated second are shown as a function of step size in Fig. 11.10.13.

Because computation time depends on the method of integration as well as the step size, Fig. 11.10.12 does not present a fair comparison of the error produced by the four algorithms. Since computation time is proportional to the number of computation cycles per simulated second, a better comparison is shown in Fig. 11.10.14. In this figure, the total simulation error is plotted as a function of the number of computation cycles per simulated second. From this figure it is seen that fourth-order Adams-Bashforth-Moulton produces the smallest error for a given level of computation. Furthermore, it can be seen that a simulation using fourth-order Runge-Kutta is only slightly less efficient than one using fourth-order Adams-Bashforth-Moulton. In addition, Fig. 11.10.14 shows that the second-order algorithms are much less efficient than either of the fourth-order algorithms. These low-order algorithms should not be used, unless for some other reason very small time steps are required. The maximum total error shown in Figs. 11.10.12 and 11.10.14 was computed using

$$\omega_{ax} = \omega_{ay} = \omega_{az} = \omega_{fx} = \omega_{fy} = \omega_{fz} = 1.0 \text{ rad/sec}$$

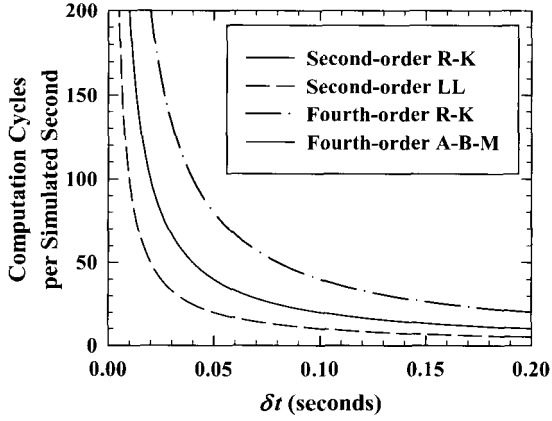


Figure 11.10.13. Computation cycles per simulated second as a function of step size for four numerical integration algorithms.

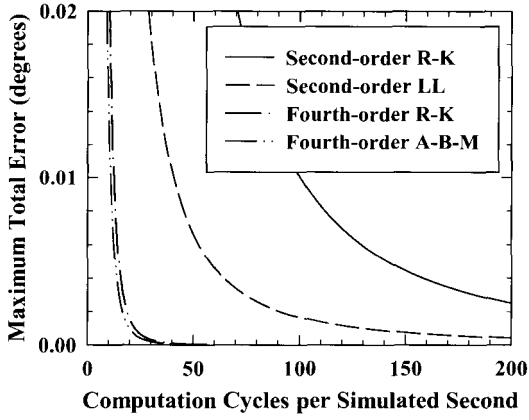


Figure 11.10.14. Simulation error as a function of computation cycles per simulated second for four numerical integration algorithms.

The absolute magnitude of the error shown in Figs. 11.10.12 and 11.10.14 depends on the angular rates. However, the relative comparison between the errors realized by the four different numerical methods is independent of these angular rates.

In some cases extremely small time steps are required for aircraft flight simulation, because of the method used to compute the aerodynamic forces and moments. When this is the case, a fourth-order integration algorithm may add unnecessarily to the computational burden. In such simulations, the second-order local linearization algorithm is by far the best alternative. Like the first-order Euler algorithm, second-order local linearization requires only one computation cycle per time step. However, it provides second-order accuracy. **In no case should a first-order Euler algorithm ever be used for aircraft flight simulation.**

11.11. Summary of the Flat-Earth Quaternion Formulation

In numerical flight simulation there is no significant advantage to neglecting any form of longitudinal-lateral coupling. Thus, starting with the Euler angle formulation presented in Eqs. (9.8.1) through (9.8.4) and expressing orientation in terms of the Euler-Rodrigues quaternion, including gyroscopic and inertial coupling, the 13 first-order differential equations that comprise this quaternion formulation for rigid-body motion are

$$\begin{Bmatrix} \dot{u} \\ \dot{v} \\ \dot{w} \end{Bmatrix} = g \begin{Bmatrix} 2(e_x e_z - e_y e_0) \\ 2(e_y e_z + e_x e_0) \\ e_z^2 + e_0^2 - e_x^2 - e_y^2 \end{Bmatrix} + \frac{g}{W} \begin{Bmatrix} X + T_{x_b} \\ Y + T_{y_b} \\ Z + T_{z_b} \end{Bmatrix} + \begin{Bmatrix} rv - qw \\ pw - ru \\ qu - pv \end{Bmatrix} \tag{11.11.1}$$

$$\begin{Bmatrix} \dot{p} \\ \dot{q} \\ \dot{r} \end{Bmatrix} = \begin{bmatrix} I_{xx_b} & -I_{xy_b} & -I_{xz_b} \\ -I_{xy_b} & I_{yy_b} & -I_{yz_b} \\ -I_{xz_b} & -I_{yz_b} & I_{zz_b} \end{bmatrix}^{-1} \left(\begin{bmatrix} 0 & -h_{z_b} & h_{y_b} \\ h_{z_b} & 0 & -h_{x_b} \\ -h_{y_b} & h_{x_b} & 0 \end{bmatrix} \begin{Bmatrix} p \\ q \\ r \end{Bmatrix} \right.$$
$$\left. + \begin{Bmatrix} \ell + T_{z_b} y_{bp} - T_{y_b} z_{bp} + (I_{yy_b} - I_{zz_b})qr + I_{yz_b}(q^2 - r^2) + I_{xz_b} pq - I_{xy_b} pr \\ m + T_{x_b} z_{bp} - T_{z_b} x_{bp} + (I_{zz_b} - I_{xx_b})pr + I_{xz_b}(r^2 - p^2) + I_{xy_b} qr - I_{yz_b} pq \\ n + T_{y_b} x_{bp} - T_{x_b} y_{bp} + (I_{xx_b} - I_{yy_b})pq + I_{xy_b}(p^2 - q^2) + I_{yz_b} pr - I_{xz_b} qr \end{Bmatrix} \right) \tag{11.11.2}$$

$$\begin{Bmatrix} \dot{x}_f \\ \dot{y}_f \\ \dot{z}_f \end{Bmatrix} = \begin{Bmatrix} e_0 \\ e_x \\ e_y \\ e_z \end{Bmatrix} \otimes \left(\begin{Bmatrix} 0 \\ u \\ v \\ w \end{Bmatrix} \otimes \begin{Bmatrix} e_0 \\ -e_x \\ -e_y \\ -e_z \end{Bmatrix} \right) + \begin{Bmatrix} V_{wx_f} \\ V_{wy_f} \\ V_{wz_f} \end{Bmatrix} \tag{11.11.3}$$

$$\begin{Bmatrix} \dot{e}_0 \\ \dot{e}_x \\ \dot{e}_y \\ \dot{e}_z \end{Bmatrix} = \frac{1}{2} \begin{bmatrix} -e_x & -e_y & -e_z \\ e_0 & -e_z & e_y \\ e_z & e_0 & -e_x \\ -e_y & e_x & e_0 \end{bmatrix} \begin{Bmatrix} p \\ q \\ r \end{Bmatrix} \tag{11.11.4}$$

Since this formulation is based on the local flat-Earth approximation, it directly applies only to short flights that do not traverse a significant fraction of the Earth's surface.

To complete the formulation, we require a model relating the aerodynamic forces, moments, and thrust to the velocity components, u, v, w, p, q, r, and their temporal derivatives. Anything from linearized aerodynamics to full CFD computations and table look-up algorithms combined with wind tunnel data can be used for this purpose.

Among some fraction of the aircraft community, the quaternion formulation has gained the somewhat undeserved reputation of being hard to understand. This reputation has more to do with the scattered nature of the literature on this topic, particularly in aircraft journals and textbooks, than it does with the raw complexity of the quaternion formulation itself.

To avoid the perceived complexity of the quaternion formulation, either the direction-cosine formulation or the Euler angle formulation has often been implemented in aircraft flight simulators. This has been done at significant computational cost. In addition to eliminating the singularity in the Euler angle formulation, the quaternion formulation is far superior to either the Euler angle formulation or the direction-cosine formulation, based on computational efficiency alone. Numerical integration of the nine component direction-cosine formulation requires more than double the computation time needed for the four component quaternion formulation. The Euler angle transformation requires about 11 times as long to evaluate as the quaternion transformation. Consequently, even in cases where the aircraft is not an all-attitude vehicle and the gimbal lock singularity is not encountered, the quaternion formulation provides important computational savings that should be seriously considered.

In order to take full advantage of the speed and accuracy of the Euler-Rodrigues quaternion formulation, it is necessary to give consideration to the numerical integration method used. Early aircraft flight simulations were run on analog computers that were inherently first-order. Numerical integration of the quaternion rate equations with a first-order method results in very large errors. Early analog programmers observed similar behavior and employed an error reduction scheme called *Corbett-Wright orthogonality control*. This orthogonality control is still found in some aircraft simulation codes that are in use today. Integration with any of today's prevalent fourth-order numerical methods produces very little orthogonality error. Using the Corbett-Wright orthogonality control scheme with modern numerical algorithms increases the computational time but does nothing to improve the accuracy of the simulation.

Even though the orthogonality error for modern numerical algorithms is very small, it can accumulate. Periodic renormalization of the quaternion eliminates this error. Corbett-Wright orthogonality control will also eliminate orthogonality error, but it does not eliminate drift error. In some cases, for certain values of the Corbett-Wright gain coefficient, the drift error is increased by more than the orthogonality error is reduced, which actually increases the total error for the simulation. Periodic renormalization of the quaternion provides a computationally efficient means for controlling orthogonality error without increasing drift error. If the orthogonality error is controlled, a small amount of drift error does not adversely affect a flight simulator, since it is constantly being corrected with virtually imperceptible pilot input. The pilot's perception of the drift error is similar to that caused by an infinitesimal change in the aerodynamics of the aircraft. Because an exact model for aircraft aerodynamics is not possible, a small amount of drift error has no significant effect on numerical flight simulation. The orthogonality error, on the other hand, has no counterpart in the physical world and cannot be compensated for by the pilot.

Reduction in size of the time step and/or increasing the order of the integration are the only effective ways to reduce total error. The fourth-order Runge-Kutta and fourth-order Adams-Bashforth-Moulton algorithms, with periodic renormalization, provide the fastest simulation for a given level of total error. If extremely small time steps are required for any reason and a single-point, single-step, algorithm is desired, the local linearization algorithm is the next best alternative. A first-order Euler algorithm should never be used for numerical integration in flight simulation.

EXAMPLE 11.11.1. Using the full 6-DOF quaternion formulation, we wish to reformulate the projectile problem in Example 7.3.3. Assume that the projectile is symmetric with respect to the pitch and yaw axes, that the products of inertia are zero, and that the rolling moment is directly proportional to the negative of the traditional dimensionless rolling rate.

Solution. From Example 7.3.3 and the symmetry of the projectile, the forces and moments are modeled as

$$\begin{Bmatrix} X \\ Y \\ Z \end{Bmatrix} \cong \tfrac{1}{2}\rho u^2 S_r \begin{Bmatrix} -k_0 - k_1(\alpha^2+\beta^2) \\ -k_2\beta \\ -k_2\alpha \end{Bmatrix} \text{ and } \begin{Bmatrix} \ell \\ m \\ n \end{Bmatrix} \cong \tfrac{1}{2}\rho u^2 S_r l_r \begin{Bmatrix} -k_5 l_r\, p/u \\ -k_3\alpha - k_4 l_r\, q/u \\ +k_3\beta - k_4 l_r\, r/u \end{Bmatrix}$$

where k_0, k_1, k_2, k_3, k_4, and k_5, are dimensionless constants, S_r is the reference area, l_r is the reference length, α is the angle of attack, and β is the sideslip angle. The aerodynamic angles will be approximated as,

$$\alpha \cong \frac{w}{u} \text{ and } \beta \cong \frac{v}{u}$$

Since there is no thrust and no wind, Eqs. (11.11.1) through (11.11.4) become

$$\begin{Bmatrix} \dot{u} \\ \dot{v} \\ \dot{w} \end{Bmatrix} = \begin{Bmatrix} -K_0u^2 - K_1(w^2+v^2) + 2g(e_xe_z - e_ye_0) + rv - qw \\ -K_2uv + 2g(e_ye_z + e_xe_0) + pw - ru \\ -K_2uw + g(e_z^2 + e_0^2 - e_x^2 - e_y^2) + qu - pv \end{Bmatrix} \tag{11.11.5}$$

$$\begin{Bmatrix} \dot{p} \\ \dot{q} \\ \dot{r} \end{Bmatrix} = \begin{Bmatrix} -K_5 pu \\ -K_3uw - K_4qu + K_6pr \\ +K_3uv - K_4ru - K_6pq \end{Bmatrix} \tag{11.11.6}$$

$$\begin{Bmatrix} \dot{x}_f \\ \dot{y}_f \\ \dot{z}_f \end{Bmatrix} = \begin{Bmatrix} e_0 \\ e_x \\ e_y \\ e_z \end{Bmatrix} \otimes \left(\begin{Bmatrix} 0 \\ u \\ v \\ w \end{Bmatrix} \otimes \begin{Bmatrix} e_0 \\ -e_x \\ -e_y \\ -e_z \end{Bmatrix} \right) \tag{11.11.7}$$

$$\begin{Bmatrix} \dot{e}_0 \\ \dot{e}_x \\ \dot{e}_y \\ \dot{e}_z \end{Bmatrix} = \frac{1}{2} \begin{bmatrix} -e_x & -e_y & -e_z \\ e_0 & -e_z & e_y \\ e_z & e_0 & -e_x \\ -e_y & e_x & e_0 \end{bmatrix} \begin{Bmatrix} p \\ q \\ r \end{Bmatrix} \tag{11.11.8}$$

where using the symmetry condition, $I_{zz_b} = I_{yy_b}$, we have

$$\begin{Bmatrix} K_0 \\ K_1 \\ K_2 \\ K_3 \\ K_4 \\ K_5 \\ K_6 \end{Bmatrix} = \begin{Bmatrix} \frac{1}{2}\rho S_r k_0\, g/W \\ \frac{1}{2}\rho S_r k_1\, g/W \\ \frac{1}{2}\rho S_r k_2\, g/W \\ \frac{1}{2}\rho S_r l_r\, k_3/I_{yy_b} \\ \frac{1}{2}\rho S_r l_r^2\, k_4/I_{yy_b} \\ \frac{1}{2}\rho S_r l_r^2\, k_5/I_{xx_b} \\ (I_{yy_b} - I_{xx_b})/I_{yy_b} \end{Bmatrix}$$

From Eq. (11.7.8) and the initial condition in Example 7.3.3, the initial condition for this formulation is

$$\begin{Bmatrix} u \\ v \\ w \\ p \\ q \\ r \\ x_f \\ y_f \\ z_f \\ e_0 \\ e_x \\ e_y \\ e_z \end{Bmatrix}_{t=0} = \begin{Bmatrix} V_0 \\ 0 \\ 0 \\ 0 \\ 0 \\ 0 \\ x_0 \\ 0 \\ z_0 \\ \cos(\theta_0/2) \\ 0 \\ \sin(\theta_0/2) \\ 0 \end{Bmatrix} \tag{11.11.9}$$

Starting with the initial values given by Eq. (11.11.9), fourth-order Runge-Kutta can be used to integrate Eqs. (11.11.5) through (11.11.8).

EXAMPLE 11.11.2. Using the quaternion formulation from Example 11.11.1, plot the elevation of the arrow in Example 7.3.4 in inches above the starting point and its airspeed in feet per second as a function of the horizontal distance downrange in yards, from zero to 100 yards. Also plot its elevation angle and angle of attack in degrees as a function of downrange distance in yards. Compare these results with those obtained in Example 7.3.4. The aerodynamic coefficients and mass properties for this specific arrow result in $K_0 = 0.00061$ ft^{-1}, $K_1 = 0.14$ ft^{-1}, $K_2 = 0.00059$ ft^{-1}, $K_3 = 0.0016$ ft^{-2}, $K_4 = 0.0064$ ft^{-1}, $K_5 = 0.19$ ft^{-1}, and $K_6 = 0.98$. The initial values are $V_0 = 210$ ft/sec, $\alpha_0 = 0$, $\beta_0 = 0$, and $\theta_0 = 5$ degrees.

Solution. Starting with this initial condition and integrating numerically with fourth-order Runge-Kutta, using 0.01-sec time steps and applying Eq. (11.10.7) to renormalize the quaternion after each full time step, we obtain

$$\begin{Bmatrix} t \\ u \\ v \\ w \\ p \\ q \\ r \\ x_f \\ y_f \\ z_f \\ e_0 \\ e_x \\ e_y \\ e_z \end{Bmatrix} = \begin{Bmatrix} 0.000000 \\ 210.000000 \\ 0.000000 \\ 0.000000 \\ 0.000000 \\ 0.000000 \\ 0.000000 \\ 0.000000 \\ 0.000000 \\ 0.000000 \\ 0.999048 \\ 0.000000 \\ 0.043619 \\ 0.000000 \end{Bmatrix} \begin{Bmatrix} 0.010000 \\ 209.703259 \\ 0.000000 \\ 0.320201 \\ 0.000000 \\ -0.000535 \\ 0.000000 \\ 2.090670 \\ 0.000000 \\ -0.181301 \\ 0.999048 \\ 0.000000 \\ 0.043618 \\ 0.000000 \end{Bmatrix} \begin{Bmatrix} 0.020000 \\ 209.406998 \\ 0.000000 \\ 0.637777 \\ 0.000000 \\ -0.002126 \\ 0.000000 \\ 4.178666 \\ 0.000000 \\ -0.359151 \\ 0.999049 \\ 0.000000 \\ 0.043612 \\ 0.000000 \end{Bmatrix}, \cdots, \begin{Bmatrix} 1.580000 \\ 176.168493 \\ 0.000000 \\ -0.141709 \\ 0.000000 \\ -0.137030 \\ 0.000000 \\ 300.310279 \\ 0.000000 \\ 11.538452 \\ 0.995957 \\ 0.000000 \\ -0.089835 \\ 0.000000 \end{Bmatrix}$$

Using Eq. (11.7.9) to convert the components of the quaternion to Euler angles, we obtain the following results:

Time (sec)	Range (yd)	Elevation (in.)	Speed (ft/sec)	θ (degrees)	α (degrees)
0.000000	0.000	0.000	210.000	5.000000	0.000000
0.010000	0.697	2.176	209.704	4.999898	0.087486
0.020000	1.393	4.310	209.408	4.999185	0.174502
⋮	⋮	⋮	⋮	⋮	⋮
1.560000	98.947	−130.998	176.434	−10.148741	−0.092663
1.570000	99.525	−134.713	176.301	−10.229081	−0.070022
1.580000	100.103	−138.461	176.169	−10.308173	−0.046088

Plotting these data duplicates the results plotted in Figs. 7.3.5 and 7.3.6.

EXAMPLE 11.11.3. The vanes of the arrow in Example 11.11.2 were mounted parallel with the axis of the shaft. With the vanes mounted in this manner, no rolling moment is produced when there is no rolling rate. Often, the vanes of an arrow are mounted with some *twist*, which causes the arrow to rotate as it moves through the air. Assume that the vanes of the arrow in Example 11.11.2 are 4.0 inches long. They are mounted such that the leading edge is twisted 10 degrees around the circumference of the shaft relative to the trailing edge. The direction of this twist is that which produces a positive rolling moment with no rolling rate.

We wish to repeat the computations made in Example 11.11.2 for the case where the vanes of the arrow are mounted in this manner. Assume that the rolling moment coefficient is independent of airspeed when there is no rolling rate.

Solution. This twist in the vanes of the arrow can be modeled simply by adding a constant term to the rolling moment coefficient. Thus, the rolling moment is

$$\ell \cong \tfrac{1}{2}\rho u^2 S_r l_r (C_{\ell 0} - k_5 l_r\, p/u) \tag{11.11.10}$$

The vanes are twisted 10 degrees in 4 inches or 30 degrees per foot. With this twist, the rolling moment should be zero when the arrow is rotating 30 degrees for each foot that it moves forward through the air (i.e., $p/u = 30$ degrees per foot). Applying this to Eq. (11.11.10) gives

$$0 = C_{\ell 0} - k_5 l_r \frac{\pi}{180^\circ} 30^\circ/\text{ft} \quad \text{or} \quad C_{\ell 0} = k_5 \frac{\pi l_r}{6\,\text{ft}}$$

Using this result in Eq. (11.11.10), the aerodynamic moments for this arrow are expressed as

$$\begin{Bmatrix} \ell \\ m \\ n \end{Bmatrix} \cong \tfrac{1}{2}\rho u^2 S_r l_r \begin{Bmatrix} k_5 l_r (\pi/6\,\text{ft} - p/u) \\ -k_3\alpha - k_4 l_r\, q/u \\ +k_3\beta - k_4 l_r\, r/u \end{Bmatrix}$$

Applying this to Eq. (11.11.2) gives

$$\begin{Bmatrix} \dot{p} \\ \dot{q} \\ \dot{r} \end{Bmatrix} = \begin{Bmatrix} K_7 u^2 - K_5 pu \\ -K_3 uw - K_4 qu + K_6 pr \\ +K_3 uv - K_4 ru - K_6 pq \end{Bmatrix} \tag{11.11.11}$$

where K_3, K_4, K_5, and K_6 are the same as in Example 11.11.2 and K_7 is given by

$$K_7 = \tfrac{1}{2}\rho S_r l_r \frac{C_{\ell 0}}{I_{xx_b}} = \frac{\pi\rho S_r l_r^2 k_5}{12\,\text{ft}\, I_{xx_b}} = \frac{\pi K_5}{6\,\text{ft}} = 0.099\,\text{ft}^{-2}$$

Replacing Eq. (11.11.6) with Eq. (11.11.11), the formulation can be integrated numerically as was done in Example 11.11.2.

Before proceeding with numerical integration, some consideration must be given to the length of the time step to be used. Because the arrow will be rotating at a substantial rate, the angular velocity must be considered in selecting the time step. From the material in Sec. 11.10, we find that a fourth-order numerical integration algorithm, with periodic renormalization of the quaternion, will provide good accuracy if the time step is selected to give about 10 steps per revolution.

For this arrow, the maximum rotation rate will be about 30 degrees per foot of travel and the maximum airspeed is 210 ft/sec. Thus, the maximum rotation rate will be somewhat less than 20 revolutions per second. With this knowledge, we shall select a time step of 0.005 second.

By using the same integration algorithm that was used in Example 11.11.2 and changing only the time step and the rolling moment equation, we obtain

$$\begin{Bmatrix} t \\ u \\ v \\ w \\ p \\ q \\ r \\ x_f \\ y_f \\ z_f \\ e_0 \\ e_x \\ e_y \\ e_z \end{Bmatrix} = \begin{Bmatrix} 0.000000 \\ 210.000000 \\ 0.000000 \\ 0.000000 \\ 0.000000 \\ 0.000000 \\ 0.000000 \\ 0.000000 \\ 0.000000 \\ 0.000000 \\ 0.999048 \\ 0.000000 \\ 0.043619 \\ 0.000000 \end{Bmatrix} \begin{Bmatrix} 0.005000 \\ 209.851551 \\ 0.008189 \\ 0.160073 \\ 19.776041 \\ -0.000134 \\ 0.000007 \\ 1.045723 \\ 0.000000 \\ -0.091086 \\ 0.998722 \\ 0.025524 \\ 0.043605 \\ -0.001114 \end{Bmatrix} \begin{Bmatrix} 0.010000 \\ 209.703258 \\ 0.061034 \\ 0.314323 \\ 35.952271 \\ -0.000526 \\ 0.000101 \\ 2.090739 \\ 0.000001 \\ -0.181306 \\ 0.994459 \\ 0.095653 \\ 0.043418 \\ -0.004176 \end{Bmatrix}, \cdots, \begin{Bmatrix} 1.580000 \\ 175.750367 \\ -1.863796 \\ 0.988304 \\ 91.793405 \\ 0.117901 \\ -0.155337 \\ 300.030653 \\ -0.108566 \\ 11.549914 \\ -0.342722 \\ 0.935250 \\ 0.024611 \\ 0.085112 \end{Bmatrix}$$

Time (sec)	Range (yd)	Elevation (in.)	θ (degrees)	α (degrees)	β (degrees)
0.000000	0.000	0.000	5.000000	0.000000	0.000000
0.005000	0.349	1.093	4.999987	0.043705	0.002236
0.010000	0.697	2.176	4.999897	0.085880	0.016676
0.015000	1.045	3.248	4.999655	0.120445	0.051740
0.020000	1.393	4.310	4.999184	0.135724	0.109670
0.025000	1.741	5.361	4.998411	0.117124	0.183424
⋮	⋮	⋮	⋮	⋮	⋮
1.555000	98.567	−129.291	−9.868364	−0.725605	0.177986
1.560000	98.856	−131.135	−9.922927	−0.718113	−0.160449
1.565000	99.145	−132.988	−9.977478	−0.563182	−0.455324
1.570000	99.433	−134.850	−10.032015	−0.297676	−0.647150
1.575000	99.722	−136.720	−10.086538	0.019859	−0.699886
1.580000	100.010	−138.599	−10.141047	0.322194	−0.607610

The airspeed and elevation of the arrow do not differ substantially from those results obtained in Example 11.11.2. However, as can be seen in Fig. 11.11.1, the aerodynamic angles are significantly affected by the rotation of the arrow.

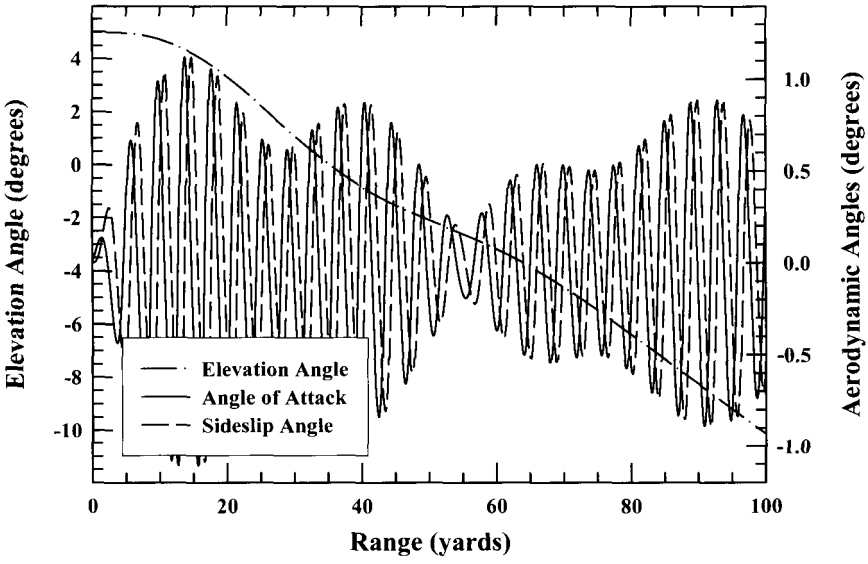


Figure 11.11.1. Effect of axial spin on the flight of an arrow.

11.12. Aircraft Position in Geographic Coordinates

The *local flat-Earth* Cartesian coordinate system (x_f, y_f, z_f) can only be used to directly describe aircraft position for relatively short flights that do not traverse a significant fraction of the Earth's surface. For longer flights, aircraft position is usually described in terms of the Earth-fixed latitude, Φ, longitude, Ψ, and geometric altitude, H. Lines of constant latitude, or parallels, are labeled in degrees north or south of the equator, with the North Pole located at 90 degrees north and the South Pole at 90 degrees south. Lines of constant longitude, or meridians, are commonly labeled in degrees east or west of the prime meridian, which runs north-south through Greenwich, England. Latitude and longitude uniquely specify any location on the Earth's surface. For example, the location of New York's, John F. Kennedy International Airport (JFK) is specified in latitude and longitude as 40 degrees 38 minutes N, 73 degrees 47 minutes W.

For the purpose of numerical computation, latitude and longitude are normally expressed in radians. North latitudes are defined to be positive and south latitudes are defined as negative. By similar convention, east longitude is defined positive and west longitude is negative. Thus, the allowable range for latitude is $-\pi/2 \le \Phi \le \pi/2$ and for longitude $-\pi \le \Psi \le \pi$. With this sign convention, the location of JFK is $\Phi = 0.709185$ and $\Psi = -1.287762$.

To transform the components of a vector from local flat-Earth coordinates (x_f, y_f, z_f) to geographic coordinates (Φ, Ψ, H), a spherical-Earth approximation is often used. The historical definition of a nautical mile is the distance along a meridian on the Earth's surface that subtends 1 minute of latitude. The nautical mile is currently defined as 1,852 meters. To be consistent with the historical definition, this implies a spherical-Earth radius of 6,366.707 kilometers. This value falls between the currently accepted polar

radius of 6,356.752 km and the accepted equatorial radius of 6,378.137 km. Thus, a value of 6,366.707 km is commonly used for the radius of the Earth, R_E, when the spherical-Earth approximation is used.

Since aircraft altitude is usually small compared with the radii of the meridian and local parallel, time derivatives of latitude, longitude, and altitude can be approximated in terms of the aircraft's velocity vector represented in local flat-Earth coordinates,

$$\begin{Bmatrix} \dot{\Phi} \\ \dot{\Psi} \\ \dot{H} \end{Bmatrix} = \begin{Bmatrix} \dot{x}_f / R_1 \\ \dot{y}_f / (R_2 \cos\Phi) \\ -\dot{z}_f \end{Bmatrix} \tag{11.12.1}$$

For the spherical-Earth approximation,

$$R_1 = R_2 = R_E = 6{,}366.707 \text{ km} \tag{11.12.2}$$

For a spheroidal-Earth model,

$$R_1 = \frac{R_{eq}(1-\varepsilon^2)}{(1-\varepsilon^2 \sin^2\Phi)^{3/2}}, \quad R_2 = \frac{R_{eq}}{\sqrt{1-\varepsilon^2 \sin^2\Phi}} \tag{11.12.3}$$

$$R_{eq} = 6{,}378.137 \text{ km}, \quad \varepsilon^2 = 6.68313865 \times 10^{-3}$$

At any time during a simulation the aircraft's velocity components in local flat-Earth coordinates can be obtained from the body-fixed velocity components and the wind vector by using Eq. (11.11.3). The geographic position rates can then be determined from Eq. (11.12.1). Numerical integration of these results yields the aircraft position as a function of time, expressed in terms of geographic coordinates. Either the spherical model given by Eq. (11.12.2) or the spheroid model described in Eq. (11.12.3) can be used with Eq. (11.12.1). The spheroid model is slightly more accurate, but a spherical model is accurate enough for most practical purposes encountered in flight simulation. Equation (11.12.1) is singular at both poles and becomes inaccurate in the close proximity of either pole. However, these singularities are not too restrictive and would not be encountered in most flight simulations.

Another important aspect of any flight simulation is *navigation*, which also makes use of the geographic coordinate system. Navigation is the art and science of getting from one point on the Earth's surface to another. One of the simplest forms of navigation is called *rhumb-line navigation*. In reality, a rhumb line is not a line at all but a curve on the surface of the Earth that traces a path of constant bearing. Rhumb-line navigation is commonly used only for traveling short distances over the Earth's surface. Even for short-distance navigation, rhumb lines are not useful for approaching locations close to either pole, because in the vicinity of a pole rhumb lines become tightly wound spirals. Some rhumb-line navigation algorithms fail completely if either the start point or the destination is a pole.

The rhumb-line bearing, or ground tract, ψ_g, from any global location (Φ, Ψ, H) to any global destination (Φ_d, Ψ_d, H_d) together with the shortest distance, d_r, measured over the Earth's surface along this path of constant bearing, can be computed from the following algorithm:

$$
\begin{aligned}
&\Delta\Psi_E = \text{mod}(\Psi_d - \Psi, 2\pi); \quad \text{if}(\Delta\Psi_E < 0.)\ \Delta\Psi_E = \Delta\Psi_E + 2\pi \\
&\Delta\Psi_W = \text{mod}(\Psi - \Psi_d, 2\pi); \quad \text{if}(\Delta\Psi_W < 0.)\ \Delta\Psi_W = \Delta\Psi_W + 2\pi \\
&\Delta\Phi = \ln\left[\tan\left(\frac{\Phi_d}{2} + \frac{\pi}{4}\right) \Big/ \tan\left(\frac{\Phi}{2} + \frac{\pi}{4}\right)\right] \\
&\text{if } \left(|\Phi_d - \Phi| < \sqrt{\varepsilon_t}\right) \\
&\qquad r = \cos(\Phi) \\
&\text{else} \\
&\qquad r = (\Phi_d - \Phi)/\Delta\Phi \\
&\text{end if} \\
&\text{if } (\Delta\Psi_W < \Delta\Psi_E) \\
&\qquad \psi_g = \text{atan2}(-\Delta\Psi_W, \Delta\Phi); \quad \text{if}(\psi_g < 0.)\ \psi_g = \psi_g + 2\pi \\
&\qquad d_r = R_E\sqrt{(r\Delta\Psi_W)^2 + (\Phi_d - \Phi)^2} \\
&\text{else} \\
&\qquad \psi_g = \text{atan2}(\Delta\Psi_E, \Delta\Phi); \quad \text{if}(\psi_g < 0.)\ \psi_g = \psi_g + 2\pi \\
&\qquad d_r = R_E\sqrt{(r\Delta\Psi_E)^2 + (\Phi_d - \Phi)^2} \\
&\text{end if}
\end{aligned}
\tag{11.12.4}
$$

where ε_t is a small tolerance on the order of machine precision, which is used as a test to avoid the indeterminate divide by zero for east-west courses.

EXAMPLE 11.12.1. Compute the rhumb-line bearing and distance from John F. Kennedy International Airport (JFK) (40° 38′ N, 73° 47′ W) to the Los Angeles International Airport (LAX) (33° 57′ N, 118° 24′ W).

Solution. For the course from JFK to LAX the coordinates of the start point and destination are

$$
\begin{aligned}
\text{JFK:} \quad & \Phi = (40 + 38/60)\pi/180 = 0.709185 \\
& \Psi = -(73 + 47/60)\pi/180 = -1.287762
\end{aligned}
$$

$$
\begin{aligned}
\text{LAX:} \quad & \Phi_d = (33 + 57/60)\pi/180 = 0.592539 \\
& \Psi_d = -(118 + 24/60)\pi/180 = -2.066470
\end{aligned}
$$

Using these values in Eq. (11.12.4) produces

$$\left.\begin{array}{l}\Delta\Psi_E = \text{mod}(\Psi_d - \Psi, 2\pi) \\ \quad \text{if}(\Delta\Psi_E < 0.)\ \Delta\Psi_E = \Delta\Psi_E + 2\pi\end{array}\right\} \quad \Delta\Psi_E = 5.504477$$

$$\left.\begin{array}{l}\Delta\Psi_W = \text{mod}(\Psi - \Psi_d, 2\pi) \\ \quad \text{if}(\Delta\Psi_W < 0.)\ \Delta\Psi_W = \Delta\Psi_W + 2\pi\end{array}\right\} \quad \Delta\Psi_W = 0.778708$$

$$\left.\Delta\Phi = \ln\left[\tan\left(\frac{\Phi_d}{2} + \frac{\pi}{4}\right) \Big/ \tan\left(\frac{\Phi}{2} + \frac{\pi}{4}\right)\right]\right\} \quad \Delta\Phi = -0.146801$$

$$\left.\begin{array}{l}\text{if } \left(\left|\Phi_d - \Phi\right| < \sqrt{\varepsilon_t}\right) \\ \quad r = \cos(\Phi) \\ \text{else} \\ \quad r = (\Phi_d - \Phi)/\Delta\Phi \\ \text{end if}\end{array}\right\} \quad r = 0.794587$$

if $(\Delta\Psi_W < \Delta\Psi_E)$

$$\left.\begin{array}{l}\psi_g = \text{atan2}(-\Delta\Psi_W, \Delta\Phi) \\ \quad \text{if}(\psi_g < 0.)\ \psi_g = \psi_g + 2\pi\end{array}\right\} \quad \psi_g = \underline{4.526057} = \underline{259.32^\circ}$$

$$\left.d_r = R_E\sqrt{(r\Delta\Psi_W)^2 + (\Phi_d - \Phi)^2}\right\} \quad d_r = \underline{4008.8 \text{ km}} = \underline{2164.6 \text{ naut mi}}$$

else

$$\left.\begin{array}{l}\psi_g = \text{atan2}(\Delta\Psi_E, \Delta\Phi) \\ \quad \text{if}(\psi_g < 0.)\ \psi_g = \psi_g + 2\pi\end{array}\right\} \quad \psi_g = 1.597459 = 91.53^\circ$$

$$\left.d_r = R_E\sqrt{(r\Delta\Psi_E)^2 + (\Phi_d - \Phi)^2}\right\} \quad d_r = 27856.5 \text{ km} = 15041.3 \text{ naut mi}$$

end if

Notice from Example 11.12.1 that the westerly course required to reach LAX from JFK along a path of constant bearing is not 180 degrees from the easterly course, which would accomplish the same result after traveling a much greater distance. This is because except for the case of north-south and east-west courses, rhumb lines are not circles, even within the approximation of a spherical Earth. A rhumb line, which is not aligned east-west or north-south, is a spiral that continues to circumnavigate the globe indefinitely in coils that are ever tightening as they approach the poles. By definition, any northeasterly rhumb line will always continue in a northeasterly direction, moving farther north with each circumvolution of the Earth's axis. However, there is no way to reach the North Pole except by traveling due north. Thus, such a rhumb line on the Earth's surface is of infinite length and never intersects itself.

From this discussion, one may begin to suspect that the shortest distance between two points on the surface of the Earth is not a path of constant bearing. Of course, the shortest distance between any two points is a straight line. However, it is not possible to travel along a straight line between two distant points on the Earth's surface without

digging a substantial tunnel. If the travel must remain above ground, the shortest path connecting any two points on the Earth's surface is a segment of what is called a *great circle*. Any great circle is the intersection of the Earth's surface with a plane passing through the Earth's center. Because any three points define a unique plane, there is one and only one plane that passes through two points on the surface of the Earth and the Earth's center. Thus, there is one and only one great circle connecting any two points on the surface of the Earth.

Since a great-circle route is the shortest path on the Earth's surface between two points, such routes are commonly used for navigation between distant locations. The initial great-circle bearing, ψ_{gc}, from any global location (Φ, Ψ, H) to any global destination (Φ_d, Ψ_d, H_d) together with the shortest great-circle distance, d_{gc}, measured over the Earth's surface, can be computed from the following algorithm:

$$\Theta = 2\sin^{-1}\left[\sqrt{\sin^2\left(\frac{\Phi_d - \Phi}{2}\right) + \cos(\Phi)\cos(\Phi_d)\sin^2\left(\frac{\Psi_d - \Psi}{2}\right)}\right]$$

if $[\sin(\Psi_d - \Psi) > 0.]$

$$\psi_{gc} = \cos^{-1}\left[\frac{\sin(\Phi_d) - \sin(\Phi)\cos(\Theta)}{\sin(\Theta)\cos(\Phi)}\right]$$

else (11.12.5)

$$\psi_{gc} = 2\pi - \cos^{-1}\left[\frac{\sin(\Phi_d) - \sin(\Phi)\cos(\Theta)}{\sin(\Theta)\cos(\Phi)}\right]$$

end if

$$d_{gc} = R_E\Theta$$

In general, the bearing does not remain constant along such great-circle routes. The bearing varies from point to point along the route, deviating from the rhumb line toward the nearest pole. Only for exact north-south routes or a route directly along the equator does the great-circle route follow the rhumb line.

EXAMPLE 11.12.2. Compute the great-circle distance and the initial bearing from JFK (40° 38′ N, 73° 47′ W) to LAX (33° 57′ N, 118° 24′ W).

Solution. For the route from JFK to LAX the coordinates are

$$\text{JFK:} \quad \Phi = (40 + 38/60)\pi/180 = 0.709185$$
$$\Psi = -(73 + 47/60)\pi/180 = -1.287762$$

$$\text{LAX:} \quad \Phi_d = (33 + 57/60)\pi/180 = 0.592539$$
$$\Psi_d = -(118 + 24/60)\pi/180 = -2.066470$$

Using these values in Eq. (11.12.5) results in

$$\Theta = 2\sin^{-1}\left[\sqrt{\sin^2\left(\frac{\Phi_d - \Phi}{2}\right) + \cos(\Phi)\cos(\Phi_d)\sin^2\left(\frac{\Psi_d - \Psi}{2}\right)}\right] = 0.623585$$

if $[\sin(\Psi_d - \Psi) > 0.]$

$$\psi_{gc} = \cos^{-1}\left[\frac{\sin(\Phi_d) - \sin(\Phi)\cos(\Theta)}{\sin(\Theta)\cos(\Phi)}\right]$$

else

$$\psi_{gc} = 2\pi - \cos^{-1}\left[\frac{\sin(\Phi_d) - \sin(\Phi)\cos(\Theta)}{\sin(\Theta)\cos(\Phi)}\right]$$

end if

$\psi_{gc} = \underline{4.779727} = \underline{273.86°}$

$d_{gc} = R_E\Theta = \underline{3970.2 \text{ km}} = \underline{2143.7 \text{ naut mi}}$

Notice from Example 11.12.1 that the path of constant bearing from JFK to LAX is more than 10 degrees south of due west. However, from Example 11.12.2, we see that the shortest route to LAX departs JFK almost 4 degrees north of due west. For this example, the difference in length between the great-circle route and the rhumb line is only about 21 nautical miles in more than 2,100. For longer routes and routes closer to the poles, the difference is much larger. For example, the rhumb-line route from Fairbanks, Alaska (64° 50′ N, 147° 43′ W) to Moscow, Russia (55° 45′ N, 37° 35′ E) is 9,601.4 km at a bearing of 263.97 degrees. The great-circle route between these same two locations is 6,594.8 km with an initial bearing of 356.54 degrees.

Since the bearing is seldom constant along a great-circle route, it is often useful to calculate the position of enroute waypoints that lie on the great circle between the start point and the destination. This is accomplished with the following algorithm:

$$\Theta = 2\sin^{-1}\left[\sqrt{\sin^2\left(\frac{\Phi_d - \Phi}{2}\right) + \cos(\Phi)\cos(\Phi_d)\sin^2\left(\frac{\Psi_d - \Psi}{2}\right)}\right]$$

$$\Theta_{wp} = d_{wp}/R_E$$

$$A = \sin(\Theta - \Theta_{wp})/\sin(\Theta)$$

$$B = \sin(\Theta_{wp})/\sin(\Theta)$$

$$x = A\cos(\Phi)\cos(\Psi) + B\cos(\Phi_d)\cos(\Psi_d) \qquad (11.12.6)$$

$$y = A\cos(\Phi)\sin(\Psi) + B\cos(\Phi_d)\sin(\Psi_d)$$

$$z = A\sin(\Phi) + B\sin(\Phi_d)$$

$$\Phi_{wp} = \text{atan2}\left(z, \sqrt{x^2 + y^2}\right)$$

$$\Psi_{wp} = \text{atan2}(y, x)$$

where Φ_{wp} and Ψ_{wp} are, respectively, the latitude and longitude of the waypoint and d_{wp} is the distance measured along the great circle from the start point to the waypoint.

EXAMPLE 11.12.3. On the great-circle route connecting JFK and LAX, find the geographic coordinates of the waypoint that is 1,000 nautical miles from JFK.

Solution. From Example 11.12.1 or 11.12.2, the geographic coordinates are

$$\text{JFK: } (0.709185, -1.287762) \qquad \text{LAX: } (0.592539, -2.066470)$$

Using these values in Eq. (11.12.6) gives

$$\Theta = 2\sin^{-1}\left[\sqrt{\sin^2\left(\frac{\Phi_d - \Phi}{2}\right) + \cos(\Phi)\cos(\Phi_d)\sin^2\left(\frac{\Psi_d - \Psi}{2}\right)}\right] = 0.623585$$

$$\Theta_{wp} = d_{wp}/R_E = 0.290888$$

$$A = \sin(\Theta - \Theta_{wp})/\sin(\Theta) = 0.559283$$

$$B = \sin(\Theta_{wp})/\sin(\Theta) = 0.491144$$

$$x = A\cos(\Phi)\cos(\Psi) + B\cos(\Phi_d)\cos(\Psi_d) = -0.075245$$

$$y = A\cos(\Phi)\sin(\Psi) + B\cos(\Phi_d)\sin(\Psi_d) = -0.765932$$

$$z = A\sin(\Phi) + B\sin(\Phi_d) = 0.638503$$

$$\left.\begin{aligned}\Phi_{wp} &= \text{atan2}\left(z, \sqrt{x^2 + y^2}\right) = 0.692551\\ \Psi_{wp} &= \text{atan2}(y, x) = -1.668721\end{aligned}\right\} \quad \underline{(39^\circ\ 40'\ 49''\ \text{N},\ 95^\circ\ 36'\ 39''\ \text{W})}$$

11.13. Problems

11.1. Write a computer subroutine to evaluate the quaternion product of two arbitrary quaternions. Use the general relation given by Eq. (11.6.3).

11.2. Write a computer subroutine to evaluate the components of the Euler-Rodriques quaternion from known values of the traditional aircraft Euler angles. Use the positive sign in Eq. (11.7.8). Test your subroutine against the result that was obtained in Example 11.7.1.

11.3. Write a computer subroutine to determine the traditional aircraft Euler angles from known values of the components of the Euler-Rodriques quaternion. Use Eq. (11.7.9) and remember that the arctangent function in most programming languages returns a value in the range $-\pi$ to π, whereas the heading angle is traditionally defined in the range 0 to 2π. Test your subroutine against the result that was obtained in Example 11.7.1.

11.4. Write a computer subroutine that uses the Euler-Rodriques quaternion and the subroutine written for problem 11.1 to transform the components of an arbitrary vector from body-fixed coordinates to Earth-fixed coordinates. Test your subroutine against the result that was obtained in Example 11.7.1.

11.5. Modify the subroutine written for problem 11.4 to eliminate all unnecessary multiplication and assignment. Test your subroutine against the result that was obtained in Example 11.7.1.

11.6. Write a computer subroutine that uses the Euler-Rodriques quaternion and the subroutine written for problem 11.1 to transform the components of an arbitrary vector from Earth-fixed coordinates to body-fixed coordinates. Test your subroutine against the result that was obtained in Example 11.7.1.

11.7. Modify the subroutine written for problem 11.6 to eliminate all unnecessary multiplication and assignment. Test your subroutine against the result that was obtained in Example 11.7.1.

11.8. Write a computer program that uses a fourth-order Runge-Kutta solution to the Euler-Rodriques quaternion formulation to solve the problem in Example 11.9.1. Apply Eq. (11.10.7) to renormalize the quaternion after each full time step. Run this code for the case $V_v = 100$ ft/sec, $V_h = 200$ ft/sec, and $\omega = 2\pi$ sec^{-1}. Compare your numerical solution with the analytical solution obtained in Example 11.9.1.

11.9. Modify the computer program written for problem 11.8 to eliminate that part of the code used to renormalize the quaternion after each full time step. Using this modified code, repeat the computations made in problem 11.8. Compare your numerical solution with the analytical solution obtained in Example 11.9.1.

11.10. Write a computer program to repeat the computations made in Example 11.11.2. Use fourth-order Runge-Kutta to integrate the Euler-Rodriques quaternion formulation. Apply Eq. (11.10.7) to renormalize the quaternion after each full time step. Test your program against the numerical results that were presented in Example 11.11.2. To test your program even further, use an initial condition that has the arrow rotated 90 degrees about the x_b-axis. Also try an initial condition that has a heading of 225 degrees. You should be able to deduce how these solutions will differ from the one presented in Example 11.11.2.

11.11. Write a computer program to repeat the computations made in Example 11.11.3. Use fourth-order Runge-Kutta to integrate the Euler-Rodriques quaternion formulation. Apply Eq. (11.10.7) to renormalize the quaternion after each full time step. Test your program against the numerical results that were presented in Example 11.11.3. To test your program even further, use an initial condition that has the arrow rotated 90 degrees about the x_b-axis. Also try an initial condition that has a heading of 225 degrees. You should be able to deduce how these solutions will differ from the one presented in Example 11.11.3.

11.12. Modify the computer program written for problem 11.11 so that it switches to the fourth-order Adams-Bashforth-Moulton algorithm after the first three time steps. Thoroughly test your program as was done in problem 11.11.

11.13. Write a computer program to simulate the flight of an airplane with conventional controls (ailerons, elevator, and rudder). Use a fourth-order Runge-Kutta algorithm to integrate the Euler-Rodriques quaternion formulation. Renormalize the quaternion after each full time step by applying Eq. (11.10.7). Use linearized aerodynamics to approximate the forces and moments, but be sure to design the program so that it is easy to change the mathematical model for the forces and moments without altering the rest of the program. Be sure that the inertia tensor is inverted only once, before the simulation is started.

11.14. Use the program that was written for problem 11.13 together with appropriate aerodynamic coefficients and mass properties to repeat the computations made in problem 11.11. Use the following properties for the arrow:

$$S_r = 0.15 \text{ ft}^2, \quad l_r = 2.0 \text{ ft}, \quad \rho = 2.0\times10^{-3} \text{ slug}\cdot\text{ft}^2, \quad W = 0.0483 \text{ lbf},$$
$$I_{xx_b} = 1.5\times10^{-5} \text{ slug}\cdot\text{ft}^2, \quad I_{yy_b} = I_{zz_b} = 7.5\times10^{-4} \text{ slug}\cdot\text{ft}^2,$$
$$k_0 = 0.0061, \quad k_1 = 1.40, \quad k_2 = 0.0059, \quad k_3 = 0.0040,$$
$$k_4 = 0.0080, \quad k_5 = 0.00475, \quad C_{\ell 0} = 0.00495$$

Thoroughly test your program as was done in problem 11.11.

11.15. Use the program that was written for problem 11.13 together with appropriate aerodynamic coefficients and mass properties to repeat the computations made in Example 10.4.3. Be sure that the airplane is trimmed for the correct airspeed before the step change in elevator deflection is applied. Compare your numerical solution with the analytical solution presented in Example 10.4.3.

11.16. Use the program that was written for problem 11.13 together with appropriate aerodynamic coefficients and mass properties to repeat the computations made in Example 10.4.4. Be sure that the airplane is trimmed for the correct airspeed before the step change in rudder deflection is applied. Compare your numerical solution with the analytical solution presented in Example 10.4.4.

11.17. Modify the computer program written for problem 11.13 so that it switches to the fourth-order Adams-Bashforth-Moulton algorithm after the first three time steps. Also modify the program to renormalize the quaternion only after each 100 time steps. Test your modified program by using it to repeat the computations made in problems 11.14 through 11.16.

11.18. Starting with the definition of a great circle on the surface of a sphere, develop the relation for the great-circle arc length, which is expressed in Eq. (11.12.5). *Hint:* Start by developing Cartesian expressions for the vectors from the Earth's center to the start and destination points.

Bibliography

Abbott, I. H., and Von Doenhoff, A. E., (1949), *Theory of Wing Sections*, Dover Publications, Inc., New York.

Abzug, M. J., (1998), *Computational Flight Dynamics*, AIAA, Reston, VA.

Abzug, M. J., and Larrabee, E. E., (1997), *Airplane Stability and Control: A History of Technologies That Made Aviation Possible*, Cambridge University Press, Cambridge.

Altmann, S. L., (1986), *Rotations, Quaternions, and Double Groups*, Oxford University Press, Oxford.

Altmann, S. L., (1989), "Hamilton, Rodrigues, and the Quaternion Scandal," *Mathematics Magazine*, **62**, 5.

Anderson, J. D., Jr., (2001), *Fundamentals of Aerodynamics*, 3rd ed., McGraw-Hill, New York.

Anderson, J. D., Jr., Corda, S., and Van Wie, D. M., (1980), "Numerical Lifting Line Theory Applied to Drooped Leading-Edge Wings Below and Above Stall," *Journal of Aircraft*, **17**, 12.

Anglin, E. L., (1965), "Analytical Study of Effects of Product of Inertia on Airplane Spin Entries, Developed Spins, and Spin Recoveries," NASA TN-D-2754.

Aramanovitch, L., (1995), "Spacecraft Orientation Based on Space Object Observations by Means of Quaternion Algebra," *Journal of Guidance, Control, and Dynamics*, **18**, 4.

Ashby, D. L., Dudley, M. R., and Iguchi, S. K., (1988), "Development and Validation of an Advanced Low-Order Panel Method," NASA TN-101024.

Ashkenas, I. L., and McRuer, D. T., (1960), "Optimization of Flight-Control, Airframe System," *Journal of Aerospace Sciences.* **27**, 3.

Babister, A. W., (1961), *Aircraft Stability and Control*, Oxford University Press, Oxford.

Babister, A. W., (1980), *Aircraft Dynamic Stability and Response*, Pergamon, Oxford.

Bairstow, L., (1939), *Applied Aerodynamics*, 2nd ed., Longmans-Green, New York.

Bar-Itzhack, I. Y., (1970), "Iterative Computation of Initial Quaternion," *Journal of Spacecraft and Rockets*, **7**, 3.

Bar-Itzhack, I. Y., (1971), "Optimum Normalization of a Computed Quaternion of Rotation," *IEEE Transactions of Aerospace and Electronic Systems*, **7**, 2.

Bar-Itzhack, I. Y., and Idan, M., (1987), "Recursive Attitude Determination from Vector Observations: Euler Angle Estimation," *Journal of Guidance, Control, and Dynamics*, **10**, 2.

Barker, L. E., Bowles, R. L., and Williams, L. H., (1973), "Development and Application of a Local Linearization Algorithm for the Integration of Quaternion Rate Equations in Real-Time Flight Simulation Problems," NASA TN D-7347.

Beatty, M. F., (1963), "Vector Representation of Rigid Body Rotation," *American Journal of Physics*, **31**, 2.

Beatty, M. F., (1967), "Kinematics of Finite, Rigid-Body Displacements," *American Journal of Physics*, **35**, 10.

Beatty, M. F., (1977), "Vector Analysis of Finite Rigid Rotations," *Journal of Applied Mechanics*, **44**, 3.

Beer, F. P., and Johnston, E. R., (1997), *Vector Mechanics for Engineers Dynamics*, 6th ed. McGraw Hill, New York.

Bertin, J. J., (2002), *Aerodynamics for Engineers*, 4th ed., Prentice-Hall, Upper Saddle River, New Jersey.

Betz, A., (1919), "Schraubenpropeller mit geringstem Energieverlust," *Nachrichten von der Gesellschaft der Wissenschaften zu Göttingen, Mathematisch-Physikalische Klasse*, **2**.

Bloy, A. W., (1998), "Thrust Offset Effect on Longitudinal Dynamic Stability," *Journal of Aircraft*, **35**, 2.

Boyer, C. B., and Merzbach, U. C., (1989), *A History of Mathematics*, 2nd ed., Wiley, New York.

Bramwell, F. H., Fage, A., Relf, E. F., and Bryant, L. W., (1914), "Experiments on Model Propellers at the National Physical Laboratory," *Reports and Memoranda*, No. 123, British Aeronautical Research Council, London.

Broucke, R. A., (1993), "On the Use of Poincaré Surfaces of Section in Rigid Body Motion," *Journal of Astronautical Sciences*, **41**, 4.

Bryan, G. H., (1911), *Stability in Aviation*, Macmillan, London.

Bush, R. H., Power, G. D., and Towne, C. E., (1998), "WIND: The Production Flow Solver of the NPARC Alliance," AIAA-1998-0935.

Campos, L. M. B. C., (1997), "Non-linear Longitudinal Stability of a Symmetric Aircraft," *Journal of Aircraft*, **34**, 3.

Campos, L. M. B. C., Fonseca, A. A., and Azinheira, J. R. C., (1995), "Some Elementary Aspects of Non-linear Airplane Speed Stability in Constrained Flight," *Progress in Aerospace Science* **31**, 2.

Cayley, A., (1845), "On Certain Results Relating to Quaternions," *Philosophical Magazine*, **26**, 1.

Cheng, H., and Gupta, K. C., (1989), "An Historical Note on Finite Rotations," *ASME Journal of Applied Mathematics*, **56**, 2.

Cheng, H. K., and Meng, S. Y., (1980), "The Oblique Wing as a Lifting-Line Problem in Transonic Flow," *Journal of Fluid Mechanics*, **97**, 3.

Chou, J. C. K., (1992), "Quaternion Kinematics and Dynamic Differential Equations," *IEEE Transactions on Robotics & Automation*, **8**, 1.

Clark, T. W. K., (1913), "Effect of Side Wind on a Propeller," *Reports and Memoranda*, No. 80, British Aeronautical Research Council, London.

Cook, M. V., (1997), *Flight Dynamics Principles*, Wiley, New York.

Cooper, G. E., and Harper, R. P., Jr. (1969), "The Use of Pilot Ratings in the Evaluation of Aircraft Handling Qualities," NASA TN D-5153.

Corbett, J. P., and Wright, F. B., (1957), "Stabilization of Computer Circuits," WADC TR 57-425, E. Hochfeld, editor, Wright-Patterson Air Force Base, OH.

Crigler, J. L., and Gilman, J., (1952), "Calculation of Aerodynamic Forces on a Propeller in Pitch or Yaw," NACA TN-2685.

Croom, M., Kenney, H., Murri, D., and Lawson, K., (2000), "Research on the F/A-18E/F Using a 22%-Dynamically-Scaled Drop Model," AIAA-2000-3913.

Crowe, M. J., (1967), *A History of Vector Analysis*, Dover, New York.

Devenport, W. J., Rife, M. C., Liapis, S. I., and Follin, G. J., (1996), "The Structure and Development of the Wing-tip Vortex," *Journal of Fluid Mechanics*, **312**.

Diederich, F. W., (1951), "Charts and Tables for Use in Calculations of Downwash of Wings of Arbitrary Plan Form," NACA TN-2353.

Diehl, W. S., (1921), "The Determination of Downwash," NACA TN-42.

Duncan, W. J., (1952), *The Principles of Control and Stability of Aircraft*, Cambridge University Press, Cambridge.

Durand, W. F., and Lesley, E., (1923), "Tests on Air Propellers in Yaw," NACA TR-113.

Durand, W. F., and Lesley, E. P., (1926), "Comparison of Tests on Air Propellers in Flight with Wind Tunnel Model Tests on Similar Forms," NACA TR-220.

Dvornychenko, V. N., (1985), "The Number of Multiplications Required to Chain Coordinate Transformations," *Journal of Guidance, Control, and Dynamics*, **8**, 1.

Etkin, B., (1972), *Dynamics of Atmospheric Flight*, Wiley, New York.

Etkin, B., and Reid L. D., (1996), *Dynamics of Flight: Stability and Control*, 3rd ed., Wiley, New York.

Euler, L., (1758), "Du Mouvement de rotation des corps solides autour d'un axe variable," *Memoires de l'Académiei des Sciences de Berlin*, **14**.

Euler, L., (1770), "Problema Algebraicum ob Affectiones Prorsus Singulares Memorabile," *Novi Commentari Academiae Scientiarum Imperialis Petropolitanae*, **15**.

Euler, L., (1775a), "Formulae Generales pro Translatione Quacunque Corporum Rigidorum," *Novi Commentari Academiae Scientiarum Imperialis Petropolitanae*, **20**.

Euler, L., (1775b), "Nova Methodus Motum Corporum Rigidorum Determinandi," *Novi Commentari Academiae Scientiarum Imperialis Petropolitanae*, **20**.

Euler, L., (1862), "De Motu Corporum Circa Punctum Fixum Mobilium," *Commentatio 825 Indicis Enestroemiani, Opera Posthuma*, **2**.

Falkner, V. M., (1943), "The Calculation of Aerodynamic Loading on Surfaces of Any Shape," *Reports and Memoranda 1910*, British Aeronautical Research Council, London.

Fallon, L., (1978), "Quaternions," *Spacecraft Attitude Determination and Control*, J. R. Wertz, editor, Kluwer Academic Publishers, Dordrecht.

Fang, A. C., and Zimmerman, B. G., (1969), "Digital Simulation of Rotational Kinematics," NASA TN D-5302.

Flachsbart, O., and Kröber, G., (1930), "Experimental Investigation of Aircraft Propellers Exposed to Oblique Air Currents," NACA TM-562.

Freeman, H. B., (1932), "The Effects of Small Angles of Yaw and Pitch on the Characteristics of Airplane Propellers," NACA TR-389.

Fremaux, C. M., (1997), "Spin-Tunnel Investigation of a 1/28-Scale Model of the NASA F-18 High Alpha Research Vehicle (HARV) With and Without Tails," NASA TR-201687.

George, L., and Vernet, J. F., (1960), *La Méchanique du vol*, Béranger, Paris.

Gerald, C. F., and Wheatley, P. O., (1999), *Applied Numerical Analysis*, 6th ed., Addison Wesley Longman, Reading, MA.

Gibbs, J. W., (1901), *Vector Analysis*, E. B. Wilson, editor, Dover, New York.

Glauert, H., (1919), "The Stability Derivative of an Airscrew," *Reports and Memoranda*, No. 642, British Aeronautical Research Council, London.

Glauert, H., (1926), *The Elements of Aerofoil and Airscrew Theory*, Cambridge University Press, London.

Glauert, H., (1935), "Aeroplane Propellers, Miscellaneous Airscrew Problems," *Aerodynamic Theory*, Vol. IV, W. F. Durand, editor, Julius Springer, Berlin.

Glauert, H., (1959), *The Elements of Aerofoil and Airscrew Theory*, 2nd ed., Cambridge University Press, Cambridge.

Goett, H. J., and Delaney, N. K., (1944), "Effect of Tilt of the Propeller Axis on the Longitudinal Stability Characteristics of Single-Engine Airplanes," NACA TR-774.

Goldstein, H., (1981), *Classical Mechanics*, 2nd ed., Addison-Wesley, Reading, MA.

Goldstein, S., (1929), "On the Vortex Theory of Screw Propellers," *Proceedings of the Royal Society* **A123**, 792.

Grassman, H. G., (1862), *Die Ausdehnungslehre: vollständig und in strenger Form bearbeitet*, T. C. F. Enslin, Berlin.

Grassman, H. G., (1878), *Die Lineare Ausdehnungslehre, Ein Neuer Zweig der Mathematik Dargestellt und durch Anwendungen auf die übrigen Zweige der Mathematik, wie auch auf die Statik, Mechanik, die Lehre vom Magnetismus und die Krystallonomie erläutert*, O. Wigand, Leipzig, Germany.

Graves, R. P. (1975), *Life of Sir William Rowan Hamilton*, Vols. 1 through 3, Arno Press, New York.

Gray, J. J., (1980), "Olinde Rodrigues' Paper of 1840 on Transformation Groups," *Archive for the History of Exact Sciences*, **21**, 4.

Green, S. I., and Acosta, A. J., (1991), "Unsteady Flow in Trailing Vortices," *Journal of Fluid Mechanics*, **227**.

Grigor'ev, V. A., and Sviatodukh, V. K., (1990), "Characteristics of the Phugoid Motion of Nonmaneuverable Aircraft," *TSAGI, Uchenye Zapiski*, **21**, 1.

Grubin, C., (1962), "Vector Representation of Rigid Body Rotation," *American Journal of Physics*, **30**, 6.

Grubin, C., (1970), "Derivation of the Quaternion Scheme via the Euler Axis and Angle," *Journal of Spacecraft and Rockets*, **7**, 10.

Grubin, C., (1979), "Quaternion Singularity Revisited," *Journal of Guidance and Control*, **2**, 3.

Hamilton, W. R., (1844), "On Quaternions: Or a New System of Imaginaries in Algebra," *Philosophical Magazine*, **25**, 3.

Hamilton, W. R., (1853), *Lectures on Quaternions*, Hodges and Smith, Dublin, Ireland.

Hamilton, W. R., (1866), *Elements of Quaternions*, Longmans-Green, London.

Hankins, T. L., (1980), *Sir William Rowan Hamilton*, Johns Hopkins University Press, Baltimore, MD.

Harris, R. G., (1918), "Forces on a Propeller Due to Sideslip," *Reports and Memoranda*, No. 427, British Aeronautical Research Council, London.

Heaviside, O., (1950), *Electromagnetic Theory*, Vol. 1, Dover, New York.

Hibbeler, R. C., (1998), *Engineering Mechanics Dynamics*, 8th ed., Prentice Hall, Upper Saddle River, NJ.

Hoak, D. E., (1960), "USAF Stability and Control Datcom," AFWAL-TR-83-3048, Wright-Patterson AFB, OH (Revised 1978).

Hodgkinson, J., (1999), *Aircraft Handling Qualities*, AIAA, Reston, VA.

Hoffman, J. D., (1992), *Numerical Methods for Engineers and Scientists*, McGraw-Hill, New York.

Hoggard, H. P., and Hagerman, J. R., (1948), "Downwash and Wake behind Untapered Wings of Various Aspect Ratios and Angle of Sweep," NACA TN-1703.

Householder, A. S., (1964), *The Theory of Matrices in Numerical Analysis*, Blaisdell, New York.

Jacobi, D. G. J., (1969), "Bemerkungen zu einer Abhandlung Eulers über die Orthogonale Substitution," *C. G. J. Jacobis Gesammelte Werke*, Vol. III, Chelsea Publishing Company, New York.

Jiang, Y. F., and Lin, Y. P., (1991), "Error Analysis of Quaternion Transformation," *IEEE Transactions on Aerospace and Electronic Systems*, **27**, 4.

Jones, D. W., (1995), "Quaternions Quickly Transform Coordinates Without Error Buildup," *EDN*, **40**, 5.

Joukowski, N. E., (1906), "Sur les Tourbillons Adjionts," *Traraux de la Section Physique de la Societé Imperiale des Amis des Sciences Naturales*, **13**, 2.

Karamcheti, K., (1966), *Principles of Ideal-Fluid Aerodynamics*, Wiley, New York.

Katz, A., (1997), *Computational Rigid Vehicle Dynamics*, Krieger, Malabar, FL.

Katz, J., and Maskew, B., (1988), "Unsteady Low-Speed Aerodynamics Model for Complete Aircraft Configurations," *Journal of Aircraft*, **25**, 4.

Katz, J., and Plotkin, A., (2001), *Low-Speed Aerodynamics*, 2nd ed., Cambridge University Press, Cambridge.

Kline, M., (1972), *Mathematical Thoughts from Ancient to Modern Times*, Oxford University Press, Oxford.

Klumpp, A. R., (1976), "Singularity-free Extraction of a Quaternion from a Direction-Cosine Matrix," *Journal of Spacecraft and Rockets*, **13**, 12.

Klumpp, A. R., (1978), "Reply to Comment on 'Singularity Extraction of a Quaternion from a Direction-Cosine Matrix'," *Journal of Spacecraft and Rockets*, **15**, 4.

Kobayashi, O., (1992), "Static and Dynamic Flight-Path Stability of Airplanes," *Japan Society for Aeronautical and Space Sciences, Journal*, **40**.

Kolk, W. R., (1961), *Modern Flight Dynamics*, Prentice-Hall, Englewood Cliffs, NJ.

Kolve, D. I., (1993), "Describing an Attitude," *Advances in the Astronautical Sciences, Proceedings of the 16th AAS Rocky Mountain Guidance and Control Conference*, Vol. 81, Univelt Inc., San Diego, CA.

Kozik, T. J., (1976), "Finite Rotations and Associated Displacement Vectors," *Journal of Applied Mechanics*, Vol. **43**, 4.

Kuipers, J. B., (1999), Quaternions and Rotation Sequences: A Primer with Applications to Orbits, Aerospace and Virtual Reality, Princeton University Press, Princeton, NJ.

Kutta, M. W., (1902), "Auftriebskräfte in Strömenden Flüssigkeiten," *Illustrierte Aeronautische Mitteilungen* **6**, 133.

Lanchester, F. W., (1908), *Aerodonetics*, Archibald Constable, London.

Lanchester, F. W., (1917), *The Flying-Machine from an Engineering Standpoint*, Constable, London.

Lecomte, P., (1962), *Méchanique du Vol*, Dunod, Paris.

Lesley, E. P., Worley, G. F., and Moy, S., (1937), "Air Propellers in Yaw," NACA TR-597.

Lotz, I., (1931), "Berechnung der Auftriebsverteilug beliebig geformter Flugel," *Zeitschrift für Flugtechnik und Motorluftschiffahrt*, **22**, 7.

Markley, F. L., (1978), "Attitude Dynamics," in *Spacecraft Attitude Determination and Control*, J. R. Wertz, editor, Kluwer Academic Publishers, Dordrecht, The Netherlands.

Markley, F. L., (1993), "New Dynamic Variables for Momentum-Bias Spacecraft," *Journal of the Astronautical Sciences*, **41**, 4.

Mathews, J., (1976), "Coordinate-free Rotation Formalism," *American Journal of Physics*, **44**, 12.

Mattingly, J. D., (1996), *Elements of Gas Turbine Propulsion*, McGraw-Hill, New York.

Mayer, A., (1960), "Rotations and Their Algebra," *SIAM Review*, **2**, 2.

Mayo, R. A., (1979), "Relative Quaternion State Transition Relation," *Journal of Guidance and Control*, **2**, 1.

McAlister, K. W., and Takahashi, R. K., (1991), "NACA 0015 Wing Pressure and Trailing Vortex Measurements," NASA TP 3151.

McCormick, B. W., (1967, 1999), *Aerodynamics of V/STOL Flight*, Dover, Mineola, NY.

McCormick, B. W., (1995), *Aerodynamics, Aeronautics, and Flight Mechanics*, 2nd ed., Wiley, New York.

McCormick, B. W., Tangler, T. L., and Sherrieb, H. E., (1968), "Structure of Trailing Vortices," *Journal of Aircraft*, **5**, 3.

McDuffee, C. C., (1946), *The Theory of Matrices*, Chelsea Publishing Company, New York.

McFarland, R. E., (1975), "A Standard Kinematic Model for Flight Simulation at NASA-Ames," NASA CR-2497.

McLemore, H. C., and Cannon, M. D., (1954), "Aerodynamic Investigation of a Four-Blade Propeller Operating through an Angle-of-Attack Range from 0 to 180 Degrees," NACA TN-3228.

McRuer, D. T., Ashkenas, I. L., and Graham, D., (1973), *Aircraft Dynamics and Automatic Control*, Princeton University Press, Princeton, NJ.

Mises, R., (1945), *Theory of Flight*, Dover, New York.

Mitchell, D. G., Aponso, B., and Hoh, R. H., (1990), "Minimum Flying Qualities, Vol. I: Pilot Simulation of Multiple Axis Flying Qualities," WRDC-TR89-3125, Wright-Patterson AFB, OH.

Mitchell, E. E. L., and Rogers, A. E., (1965), "Quaternion Parameters in the Simulation of a Spinning Rigid Body," *Simulation*, **4**, 6.

Multhopp, H., (1938), "Die Berechnung der Auftriebs Verteilung von Tragflugeln," *Luftfahrtforschung*, **15**, 14.

Multhopp, H., (1950), "Method for Calculating the Lift Distribution of Wings (Subsonic Lifting Surface Theory)," *Reports and Memoranda 2884*, British Aeronautical Research Council, London.

Munk, M. M., (1924), "Analysis of W. F. Durand's and E. P. Lesley's Propellers Tests," NACA TR-175.

Munk, M. M., and Cairo, G., (1923), "Downwash of Airplane Wings," NACA TN-124.

Nelson, R. C., (1998), *Flight Stability & Automatic Control*, 2nd ed., McGraw-Hill, New York.

O'Donnell, S., (1983), *William Rowan Hamilton, Portrait of a Prodigy*, Boole Press, Dublin, Ireland.

Painlevé, P., (1910), "Étude sur le regimé normal d'an avion," *Technique Aeronautique*, **1**, 1.

Pamadi, B. N., (1998), *Performance, Stability, Dynamics, and Control of Airplanes*, AIAA, Reston, VA.

Pearlman, N., (1967), "Vector Representation of Rigid-Body Rotations," *American Journal of Physics*, **35**, 12.

Pendley, R. E., (1945), "Effect of Propeller-Axis Angle of Attack on Thrust Distribution over the Propeller Disk in Relation to Wake-Survey Measurement of Thrust," NACA ARR-L5J02B.

Perkins, C. D., (1970), "Development of Airplane Stability and Control Technology," *Journal of Aircraft*, **7**, 4.

Perkins, C. D., and Hage, R. E., (1949), *Airplane Performance Stability & Control*, Wiley, New York.

Phillips, W. F., (2000a), "Phugoid Approximation for Conventional Airplanes," *Journal of Aircraft*, **37**, 1.

Phillips, W. F., (2000b), "Improved Closed-Form Approximation for Dutch Roll," *Journal of Aircraft*, **37**, 3.

Phillips, W. F., (2002a), "Propeller Momentum Theory with Slipstream Rotation," *Journal of Aircraft*, **39**, 1.

Phillips, W. F., (2002b), "An Analytical Solution for Wing Dihedral Effect," *Journal of Aircraft*, **39**, 3.

Phillips, W. F., (2002c), "Estimating the Low-Speed Sidewash Gradient on a Vertical Stabilizer," *Journal of Aircraft*, **39**, 6.

Phillips, W. F., (2004), "Lifting-Line Analysis for Twisted Wings and Washout-Optimized Wings," *Journal of Aircraft*, **41**, 1.

Phillips, W. F., and Anderson, E. A., (2002), "An Analytical Approximation for the Mechanics of Airplane Spin," *Journal of Aircraft*, **39**, 6.

Phillips, W. F., and Santana, B. W., (2002), "Aircraft Small-Disturbance Theory with Longitudinal-Lateral Coupling," *Journal of Aircraft*, **39**, 6.

Phillips, W. F., and Snyder, D. O., (2000), "Modern Adaptation of Prandtl's Classic Lifting-Line Theory," *Journal of Aircraft*, **37**, 4.

Phillips, W. F., Anderson, E. A., Jenkins, J. C., and Sunouchi, S., (2002), "Estimating the Low-Speed Downwash Angle on an Aft Tail," *Journal of Aircraft*, **39**, 4.

Phillips, W. F., Anderson, E. A., and Kelly, Q. J., (2003), "Predicting the Contribution of Running Propellers to Aircraft Stability Derivatives," *Journal of Aircraft*, **40**, 6.

Phillips, W. F., Hailey, C. E., and Gebert, G. A., (2000), "A Review of Attitude Kinematics for Aircraft Flight Simulation," AIAA-2000-4302.

Phillips, W. F., Hailey, C. E., and Gebert, G. A., (2001), "A Review of Attitude Representations Used for Aircraft Kinematics," *Journal of Aircraft*, **38**, 4 (also see Errata, *Journal of Aircraft*, **40**, 1).

Pistolesi, E., (1928), "Nuove Considerazioni sul Problema dell'elica in un Vento Laterale," *L'Aerotecnica*, **7**, 3.

Pope, D. A., (1963), "An Exponential Method of Numerical Integration of Ordinary Differential Equations," *Communications ACM*, **6**, 8.

Prandtl, L., (1918), "Tragflügel Theorie," *Nachricten von der Gesellschaf der Wisseschaften zu Göttingen*, Geschäeftliche Mitteilungen, Klasse.

Prandtl, L., (1921), *Applications of Modern Hydrodynamics to Aeronautics*, NACA TR-116.

Prandtl, L., and Betz, A., (1927), *Vier Abhandlungen zur Hydrodynamik und Aerodynamik*, Göttingen, Germany.

Press, W. H., Flannery, B. P., Teukolsky, S. A., and Vetterling, W. T., (1986), *Numerical Recipes—The Art of Scientific Computing*, Cambridge University Press, Cambridge.

Ramaprian, B. R., and Zheng, Y., (1997), "Measurements in Rollup Region of the Tip Vortex from a Rectangular Wing," *AIAA Journal*, **35**, 12.

Rasmussen, M. L., and Smith, D. E., (1999), "Lifting-Line Theory for Arbitrary Shaped Wings," *Journal of Aircraft*, **36**. 2.

Ribner, H. S., (1943a), "Formulas for Propellers in Yaw and Charts of the Side-Force Derivative," NACA ARR-3E19.

Ribner, H. S., (1943b). "Propellers in Yaw," NACA ARR-3L09.

Ribner, H. S., (1943c), "Proposal for a Propeller Side-Force Factor," NACA RB-3L02.

Ribner, H. S., (1945a), "Propellers in Yaw," NACA TR-820.

Ribner, H. S., (1945b), "Formulas for Propellers in Yaw and Charts of the Side-Force Derivative," NACA TR-819.

Roberson, R. E., (1968), "Kinematic Equations for Bodies Whose Rotation Is Described by the Euler-Rodrigues Parameters," *AIAA Journal*, **6**, 5.

Robinson, A. C., (1958a), "On the Use of Quaternions in the Simulation of Rigid Body Motion," WADC TR 58-17, Wright-Patterson AFB, OH.

Robinson, A. C., (1958b), "On the Use of Quaternions in the Simulation of Rigid Body Motion," *Proceedings of the Simulation Council Session of the Eastern Joint Computer Conference*, Washington, DC, Mac Millan, New York.

Rodrigues, O., (1840), "Des Lois géométriques qui régissent les déplacements d'un système solide dans l'espace, et de la variation des coordonnées provenant de ses déplacements considereés indépendamment des causes qui peuvent les produire," *Journal des Mathématiques Pures et Appliquees*, **5**.

Rolfe, J. M., and Staples, K. J., (1988), *Flight Simulation*, Cambridge University Press, Cambridge.

Roskam, J., (1990), *Airplane Design Part VI: Preliminary Calculations of Aerodynamic, Thrust and Power Characteristics*, DAR Corporation, Lawrence, KS.

Roskam, J., (1998), *Airplane Flight Dynamics and Automatic Flight Control*, DAR Corporation, Lawrence, KS.

Rumph, L. B., White, R. J., and Grummann, H. R., (1942), "Propeller Forces Due to Yaw and Their Effect on Airplane Stability," *Journal of the Aeronautical Sciences*, **9**, 12.

Runckel, J. F., (1942), "The Effect of Pitch on Force and Moment Characteristics of Full-Scale Propellers of Five Solidities," NACA WR-L-446.

Saffman, P. G., (1992), *Vortex Dynamics*, Cambridge University Press, Cambridge.

Satake, I., (1975), *Linear Algebra*, Marcel Dekker, Inc., New York.

Schmidt, L. V., (1998), *Introduction to Aircraft Flight Dynamics*, AIAA, Reston, VA.

Shepperd, S. W., (1978), "Quaternion from Rotation Matrix," *Journal of Guidance and Control*, **1**, 3.

Shuster, M. D., (1993a), "Quaternion on the Kalman Filter," *Advances in the Astronautical Sciences*, **85**, 1.

Shuster, M. D., (1993b), "A Survey of Attitude Representations," *Journal of the Astronautical Sciences*, **14**, 4.

Shuster, M. D., and Natanson, G. A., (1993), "Quaternion Computation from a Geometric Point of View," *Journal of the Astronautical Sciences*, **41**, 4.

Sidi, M. J., (1997), *Spacecraft Dynamics & Control*, Cambridge University Press, Cambridge.

Silverstein, A., and Katzoff, S., (1939), "Design Charts for Predicting Downwash Angles and Wake Characteristics behind Plain and Flapped Wings," NACA TR-648.

Silverstein, A., Katzoff, S., and Bullivant, W., K., (1939), "Downwash and Wake behind Plain and Flapped Airfoils," NACA TR-651.

Spurrier, R. A., (1978), "Comment on 'Singularity-free Extraction of a Quaternion from a Direction-Cosine Matrix,'" *Journal of Spacecraft and Rockets*, **15**, 4.

Stevens, B. L., and Lewis, F. L, (1992), *Aircraft Control & Simulation*, Wiley, New York.

Stough, H. P., DiCarlo, D. J., and Patton, J. M., (1985), "Flight Investigation of Stall, Spin, and Recovery Characteristics of a Low-Wing, Single-Engine, T-Tail Light Airplane," NASA TR-2427.

Stuelpnagel, J., (1964), "On the Parameterization of the Three-Dimensional Rotation Group," *SIAM Review*, **6**, 4.

Tandon, G. K., (1978), "Coordinate Transformations," in *Spacecraft Attitude Determination and Control*, J. R. Wertz, editor, Kluwer Academic Publishers, Dordrecht, The Netherlands.

Van Der Waerden, B. L., (1985), *A History of Algebra*, Springer-Verlag, Heidelberg, Germany.

Vathsal, S., (1991), "Derivation of the Relative Quaternion Differential Equations," *Journal of Guidance, Control, and Dynamics*, **15**, 5.

Vogeley, A. W., (1948), "Calculation of the Effect of Thrust-Axis Inclination on Propeller Disk Loading and Comparison with Flight Measurements," NACA TN-1721.

Weber, J., and Brebner, G. G., (1958), "Low-Speed Tests on 45-deg Swept-Back Wings, Part I: Pressure Measurements on Wings of Aspect Ratio 5," *Reports and Memoranda* 2882, British Aeronautical Research Council, London.

Wehage, R. A., (1984), "Quaternions and Euler Parameters—A Brief Exposition," *Computer-Aided Analysis and Optimization of Mechanical System Dynamics*, NATO ASI Series, Vol. F9, E. J. Haug, editor, Springer-Verlag, Heidelberg, Germany.

Weil, J., and Sleeman, W. C., (1949), "Prediction of the Effects of Propeller Operation on the Static Longitudinal Stability of Single-Engine Tractor Monoplanes with Flaps Retracted," NACA TR-941.

Whittaker, E. T., (1937), *A Treatise on the Analytical Dynamics of Particles and Rigid Bodies*, 4th ed., Cambridge University Press, Cambridge.

Wilkinson, J. H., (1965), *The Algebraic Eigenvalue Problem*, Clarendon Press, Oxford.

Winograd, S., (1970), "On the Number of Multiplications Necessary to Compute Certain Functions," *Communications on Pure and Applied Mathematics*, **23**, 2.

Winograd, S., (1977), "Some Bilinear Forms Whose Multiplicative Complexity Depends on the Field of Constants," *Mathematical Systems Theory*, **10**, 2.

Xu, R., (1995), "An Exploration on the Analytical-Solution for the Longitudinal Phugoid Mode of Aircraft," *Acta Aerodynamica Sinica*, **13**.

Yen, K., and Cook, G., (1980), "Improved Local Linearization Algorithm for Solving the Quaternion Equations," *Journal of Guidance and Control*, **3**, 5.

Appendix A
Standard Atmosphere, SI Units

Geometric Altitude (m)	Geopotential Altitude (m)	Temperature (K)	Pressure (N/m^2)	Density (kg/m^3)	Speed of Sound (m/sec)
0	0	288.150	1.0133E+05	1.2250E+00	340.29
2,000	1,999	275.154	7.9501E+04	1.0066E+00	332.53
4,000	3,997	262.166	6.1660E+04	8.1935E-01	324.59
6,000	5,994	249.187	4.7218E+04	6.6011E-01	316.45
8,000	7,990	236.215	3.5652E+04	5.2579E-01	308.11
10,000	9,984	223.252	2.6500E+04	4.1351E-01	299.53
12,000	11,977	216.650	1.9399E+04	3.1194E-01	295.07
14,000	13,969	216.650	1.4170E+04	2.2786E-01	295.07
16,000	15,960	216.650	1.0353E+04	1.6647E-01	295.07
18,000	17,949	216.650	7.5652E+03	1.2165E-01	295.07
20,000	19,937	216.650	5.5293E+03	8.8910E-02	295.07
22,000	21,924	218.574	4.0475E+03	6.4510E-02	296.38
24,000	23,910	220.560	2.9717E+03	4.6938E-02	297.72
26,000	25,894	222.544	2.1884E+03	3.4256E-02	299.06
28,000	27,877	224.527	1.6162E+03	2.5076E-02	300.39
30,000	29,859	226.509	1.1970E+03	1.8410E-02	301.71
32,000	31,840	228.490	8.8906E+02	1.3555E-02	303.02
34,000	33,819	233.744	6.6341E+02	9.8874E-03	306.49
36,000	35,797	239.282	4.9852E+02	7.2579E-03	310.10
38,000	37,774	244.818	3.7714E+02	5.3665E-03	313.67
40,000	39,750	250.350	2.8714E+02	3.9957E-03	317.19
42,000	41,724	255.878	2.1997E+02	2.9948E-03	320.67
44,000	43,698	261.403	1.6950E+02	2.2588E-03	324.12
46,000	45,670	266.925	1.3134E+02	1.7141E-03	327.52
48,000	47,640	270.650	1.0229E+02	1.3167E-03	329.80
50,000	49,610	270.650	7.9779E+01	1.0269E-03	329.80
52,000	51,578	270.650	6.2228E+01	8.0097E-04	329.80
54,000	53,545	267.560	4.8491E+01	6.3137E-04	327.91
56,000	55,511	263.628	3.7657E+01	4.9761E-04	325.49
58,000	57,476	259.699	2.9137E+01	3.9085E-04	323.06
60,000	59,439	255.772	2.2460E+01	3.0592E-04	320.61
62,000	61,401	251.045	1.7246E+01	2.3931E-04	317.63
64,000	63,362	243.202	1.3150E+01	1.8837E-04	312.63
66,000	65,322	235.363	9.9405E+00	1.4713E-04	307.55
68,000	67,280	227.529	7.4447E+00	1.1399E-04	302.39
70,000	69,238	219.700	5.5204E+00	8.7534E-05	297.14

Appendix B
Standard Atmosphere, English Units

Geometric Altitude (ft)	Geopotential Altitude (ft)	Temperature (°R)	Pressure (lbf/ft^2)	Density (slugs/ft^3)	Speed of Sound (ft/sec)
0	0	518.670	2.1162E+03	2.3769E−03	1116.45
5,000	4,999	500.843	1.7609E+03	2.0482E−03	1097.10
10,000	9,995	483.025	1.4556E+03	1.7555E−03	1077.40
15,000	14,989	465.216	1.1948E+03	1.4962E−03	1057.36
20,000	19,981	447.415	9.7327E+02	1.2673E−03	1036.93
25,000	24,970	429.623	7.8634E+02	1.0663E−03	1016.10
30,000	29,957	411.839	6.2967E+02	8.9068E−04	994.85
35,000	34,941	394.063	4.9935E+02	7.3820E−04	973.14
40,000	39,923	389.970	3.9313E+02	5.8728E−04	968.08
45,000	44,903	389.970	3.0945E+02	4.6227E−04	968.08
50,000	49,880	389.970	2.4361E+02	3.6392E−04	968.08
55,000	54,855	389.970	1.9180E+02	2.8652E−04	968.08
60,000	59,828	389.970	1.5103E+02	2.2561E−04	968.08
65,000	64,798	389.970	1.1893E+02	1.7767E−04	968.08
70,000	69,766	392.246	9.3727E+01	1.3920E−04	970.90
75,000	74,731	394.971	7.3990E+01	1.0913E−04	974.26
80,000	79,694	397.693	5.8511E+01	8.5710E−05	977.62
85,000	84,655	400.415	4.6350E+01	6.7434E−05	980.95
90,000	89,613	403.135	3.6778E+01	5.3147E−05	984.28
95,000	94,569	405.854	2.9232E+01	4.1959E−05	987.59
100,000	99,523	408.572	2.3272E+01	3.3182E−05	990.90
105,000	104,474	411.289	1.8557E+01	2.6285E−05	994.18
110,000	109,423	418.385	1.4837E+01	2.0659E−05	1002.72
115,000	114,369	425.983	1.1912E+01	1.6290E−05	1011.79
120,000	119,313	433.578	9.6013E+00	1.2900E−05	1020.77
125,000	124,255	441.170	7.7689E+00	1.0259E−05	1029.67
130,000	129,195	448.758	6.3095E+00	8.1907E−06	1038.48
135,000	134,132	456.342	5.1427E+00	6.5650E−06	1047.22
140,000	139,066	463.923	4.2062E+00	5.2818E−06	1055.88
145,000	143,999	471.500	3.4518E+00	4.2648E−06	1064.47
150,000	148,929	479.073	2.8419E+00	3.4558E−06	1072.99
155,000	153,857	486.643	2.3471E+00	2.8097E−06	1081.43
160,000	158,782	487.170	1.9419E+00	2.3221E−06	1082.02
165,000	163,705	487.170	1.6068E+00	1.9215E−06	1082.02
170,000	168,625	487.170	1.3297E+00	1.5901E−06	1082.02
175,000	173,544	483.944	1.1000E+00	1.3242E−06	1078.43

Index

A

Accelerating climb, 315, 317
Acceleration sensitivity, 838–841
Ackert's theory, 659
Adams-Bashfourth-Moulton, 899, 904–905, 911–912, 916
Adams-Moulton, 632
Adiabatic, 15, 93
Advance angle, 135–136, 138, 148, 181
Advance ratio, 145–154, 159, 161, 176, 187–188, 422–423, 452, 457
Adverse yaw, 77, 299, 492–493, 575
Aerodynamic, 1
  angle, 442–443, 469, 496
  angle of attack, 59, 70, 74, 76, 137, 147, 151, 181
  balance, 526, 528
  coefficients, 3, 145, 186, 224, 441, 452, 570, 605, 607, 632, 657–658
  controls, 503
  coordinates, 1–2, 462, 601
  coupling, 804, 808, 814–815, 864
  derivatives, 444, 448, 487, 652–672, 730, 794, 797, 804
  drag, 222–223, 300
  efficiency, 224, 226, 228, 351, 386
  force, 1–4, 10, 14, 24–26, 42, 45, 79, 84–92, 105, 221, 365
  force vector, 87
  hinge moment, 524
  hysteresis, 822
  moment, 1–4, 88–90, 92, 221, 365, 397, 414, 418, 441, 443, 473
  nondimensional derivatives, 676–678
  pitch angle, 131–132, 135, 137, 143–144, 147–148, 180–181
  pitch length, 132, 145, 147
  pressure, 365, 414
  properties, 22
  torsional spring, 636
  twist, 47–51, 53–54, 59, 68, 478–479
  yaw departure, 820
Aerodynamic center, 5, 26, 41, 107, 343–357, 362, 365, 373, 380, 382, 384–385, 387, 390, 396, 398, 408, 413–414, 480, 484–485 (*see also* Neutral point)
  ideal, theoretical, 26
Aerodynamics, 1, 3, 16, 24, 45, 97, 101
  compressible, 93
  inviscid, 12, 24
  inviscid compressible, 93–96
  overview, 1
Aeroelastic bending, wing, 565
Aeroelasticity, 515, 758
Aft tail, 346–347, 351–352, 356–357, 396–397, 515, 518, 522, 525–527, 549–554
  estimating downwash angle on, 371–381
Afterburner, 126, 203–204
Aileron, 68, 339, 474, 489–490, 495–496, 554, 575
  angle, 69, 489–490
  deflection, 69–72, 74, 76–78, 489–492, 495–496, 566–567
  Frise, 575
  response, 801
  reversal, 565
  reversal speed, 567
  sizing, 801
Air density, 94–95, 192, 227, 230, 234–235, 239, 241, 244, 246, 249–251, 255–256, 260–261, 266, 273, 278, 289, 293–294, 307–308
Aircraft, 1, 6–7, 10–14, 44, 49, 79, 92–93, 100, 115–130, 207, 215
  control response, 833, 854–864
  controls, 503
  design, 221, 225–226, 234, 487
  dynamics, 611
  engine, 116–117, 119, 152, 162, 198–199
  equations of motion, 599, 603
  fixed wing, 70, 567
  flight simulation, 867–926
  handling qualities, 833–864
  maneuverability, 503
  performance, 12, 221–689
  plane of symmetry, 80, 441
  position, 922
  propulsion, 115–130, 153, 215
  stability, 185, 342–343, 396, 407
  stability and control, 187, 221
  state, 837
  tailless, 413, 461, 487
  weight, 241, 254, 284, 318
Airflow, 1, 43, 93
Airfoil, 4, 22–24, 106, 280
  cambered, 105
  coordinates, 29–30
  modern, 280
  section, 3, 5, 22, 24, 28, 30, 34–46, 80–81, 85, 96, 100, 130, 346, 350, 387, 408

section geometry, 12
section moment data, 26
section theory, 46
supercritical, 101
supersonic, 100, 105, 107
symmetric, 22, 26, 105, 107, 280, 346, 350–355, 357
theory, 35
thickness, 24, 26, 34, 41
thin, 24, 96, 105, 107
Airplane
high-wing, 483–484
low-wing, 483
spin, 577–579, 587, 590
spin-resistant, 589, 590
stall, 577
Airscrew, 132 (*see also* Propeller)
Airspeed, 10, 12, 77, 120–123, 126, 133–141, 152–153, 159, 162, 178–181, 193–194, 221–330, 339–341, 349, 354–355, 359, 399, 482, 603
best climb, 243
best glide, 272–278
design, 280, 355
forward, 135–138, 149, 152, 169, 178
freestream, 167
indicated, 289, 293
liftoff, 306–307
maximum, 236–239
maximum endurance, 253–255, 261, 263
maximum range, 258–264, 267
minimum, 221, 279
minimum drag, 226, 229, 258, 261–263
minimum power, 235, 269
minimum sink, 269–270
minimum thrust, 235
optimum, 227
subsonic, 117, 127, 130
supersonic, 106, 126, 215
true, 289
VNE, 287–288
All-flying tail, 347, 568, 572
All-moveable trim adjustment, 573
Altitude, 6–8, 13, 152, 226–227, 234–235, 243–244, 251, 254, 256, 259–260, 267–269, 273, 289, 320, 339
density, 268
geometric, 6, 13
geopotential, 6–7
obstacle clearance, 315–323, 326
Ambient
pressure, 115, 165, 195–196, 208, 427
temperature, 199, 207
Amphibian, 415
Amplification factor, 701–702 (*see also* Dynamic gain)
Angle
advance, 135–136, 138, 148, 181
aerodynamic, 442–443, 469, 496
aerodynamic pitch, 131–132, 135, 137, 143–144, 147–148, 180–181
aileron, 69, 489–490
azimuth, 620, 868 (*see also* Heading)
bank, 222, 283–286, 298, 441–443, 473–474, 620, 781, 868
climb, 222, 240, 244–248, 271, 283–286, 294–296, 319–322, 348, 354, 397
crab, 257
dihedral, 80, 475, 479, 487–488
downwash, 135–136, 138, 180–181, 349, 352–353, 356–357, 371, 373, 375, 377–380, 423–424, 428, 453, 493
elevation, 397, 580, 620, 868
Euler, 619–627, 637–638, 643, 807, 867–868
ground track, 257
heading, 257, 620 (*see also* Azimuth angle)
induced, 135, 137, 143, 145, 180
Mach, 102, 104–105
orientation, 443
phase, 702
pitch, 131–132, 138, 142, 144, 147–148, 181
roll, 74
sideslip, 187, 441–447, 452–455, 460–463, 470, 473–474, 476, 482, 603, 605, 781
sidewash, 446–447, 453, 463
sweep, 80–81, 377–378
thrust, 133, 224, 227–232, 236, 240–241, 258, 282, 300
upwash, 382, 384–385, 388, 423
wind direction, 257
wind-track, 257, 270
Angle of attack, 3–5, 10–12, 24–28, 33–38, 41, 48–54, 71, 84–85, 92, 105, 147, 151, 162, 178, 181, 187, 208, 224–225, 228, 296–297, 300, 302, 306–308, 341–348, 352–365, 373, 383, 397–400, 403–404, 408–409, 413–414, 418, 420, 422, 428, 443–445, 467, 473, 509, 603
aerodynamic, 59, 70, 74, 76, 137, 147, 151, 181
blade, 151–152, 180
differential in, 476
effective, 46, 353, 371
equilibrium, 354, 614, 688
fuselage, 355, 358, 389
geometric, 47, 69–70
high, 11, 820–822, 865
induced, 46–47, 74, 81

local aerodynamic, 59, 70
local section, 46, 86, 91, 138, 145
low, 10
optimum, 311
propeller, 133–134, 163, 178–182, 184, 187, 424, 452–454, 457–459
small, 96
trim, 410
zero, 105, 353, 357–358, 366, 368, 388, 408, 410, 424, 428
zero-lift, 26–27, 36–38, 47, 55, 132, 146–147, 352, 384
Angular momentum equation, 168–169, 174
Anhedral, 80, 475
Area, 3–4
characteristic, 417
frontal, 3, 417
planform, 3, 49, 81
wing, 221, 227, 280, 307
Area rule, 101
Aspect ratio, 45, 49–50, 53, 58, 62–63, 66, 72, 81, 87, 90–91, 224, 231, 234, 237, 280, 351, 353, 372–373, 375, 380, 386–388, 408–409, 449, 471, 477, 752
apparent, 449
effective, 449, 471–472
high, 87, 227
low, 91
true, 471–472
Atmosphere, 6–10
desert, 7
polar, 7
standard, 7, 10
Atmospheric pressure, 10
Atmospheric temperature, 10
Attitude, 342, 349, 383
descriptors, 882
equilibrium, 341–343
liftoff, 299
quaternion representation, 885, 888
Autopilot, 847, 863–864
Axis of propeller rotation, 133, 135, 138, 178
Azimuth angle, 620, 868 (*see also* Heading)
constraint, 892

B

B-17 Flying Fortress, 119, 121
B-29 Superfortress, 119
Bairstow approximation, 740
Balanced field length, 315–317, 325–327
Bank angle, 222, 283–286, 298, 441–443, 473–474, 620, 781, 868
load-limited, 285–286
maximum, 284–286
stall-limited, 284–286
Beech Bonanza, 574
Bell Airacomet, 123–124
Bernoulli's equation, 165, 170
Betz condition, 141, 161, 179
Biot-Savart law, 21, 372, 377, 462
Blade
angle of attack, 151–152, 180
drag, 152, 162
interference, 121
section, 135, 137, 151, 180
wake, 161
Blade-tip vortex, 139–141, 177
helical, 177
Body, 3 (*see also* Fuselage)
axis, 1
bluff, 3, 11
streamlined, 10, 11
Body force, 556
Boeing 707, 125
Boeing 747, 127
Boundary conditions, 34
Boundary layer, 10–13, 15, 38, 96, 100, 108, 161
concept, 10
equations, 10
flow, 10, 34
separation, 11–12, 25, 38, 100
solution, 35
theory, 10, 34
viscous, 10, 12
wake, 12
Bow shock, 105
Brake power, 121, 133, 144, 146, 151–159, 167, 174–175, 255
British Fairey Delta, 496
British Spitfire, 120–121, 347, 431–432, 458, 498
Bypass ratio, 126, 207, 210–215

C

C-130 Hercules, 128, 483–484
Camber, 22–24, 35, 105–107
line, 22–24, 26–27, 33–38, 105, 107
maximum, 23, 26, 28
negative, 346
positive, 346, 352
Camber line geometry, 36–38
Camber line ordinate, 36
Cambered wing, pitch stability of, 343–346
Canard, 381–397, 409–413, 506
lift coefficient, 384, 386, 392
lift slope, 384
moveable, 554

volume ratio, 385–386, 389
Cartesian aerodynamic coordinates, 1–2, 462, 601
Ceiling
absolute, 244
service, 244
Center of gravity, 343–345, 348–357, 361–369, 382–385, 395–396, 399, 404–405, 408, 413–417, 444–445, 448–450, 484
limits, 537
low, 552
vertical position, 551
Center of pressure, 5, 25–26, 107
fuselage, 417–418
Center of thrust, 348, 357, 382, 396
Center of vorticity, 375–377
Centripetal acceleration, 556, 582
CFD, 35, 81, 90–92, 418, 426
Characteristic length, 84, 88
Characteristic polynomial, 852
Chord, 2, 23, 37
flap, 37
length, 2–3, 23, 26, 47, 50–51, 55, 59, 73, 88, 137–138, 145–148, 162, 182
line, 1–5, 22–23, 42, 83, 105, 223
root, 51
tip, 51
Chord length ratio, 145–146, 148
Circulation, 17, 20, 44, 47, 74, 79, 83, 139, 142–143
distribution, 48, 51, 71
local section, 47, 139
vector, 480
Climb, 239–249
accelerating, 315, 317
Climb angle, 222, 240, 244–248, 271, 283–286, 294–296, 319–322, 348, 354, 397
load-limited, 295–296
stall-limited, 295
steady, 320
Clustering, 28, 89
cosine, 28–29, 89–90
Cobra maneuver, 296, 865
Coefficient, 3–4
axial force, 3
drag, 3–4, 11–12, 26, 48–51, 54, 58, 92, 100, 107
induced drag, 48–51, 54–55
lift, 3, 11–12, 26, 34, 37–38, 48–59, 62, 76, 91, 97, 108, 137, 144–145, 162, 224–229, 233–234, 239, 245–246, 272, 279, 282, 284, 296, 298–302, 306, 308, 319–322, 344–345, 349–353, 358, 360, 363, 371–372, 375, 384, 409–411, 414, 506
moment, 3, 5, 25, 32, 38, 97, 107–108, 344, 349, 354, 409, 507
normal force, 3, 5
pressure, 97–99, 104–105
yawing moment, 74–77
Cofactor, 851, 853
Combustion chamber, 190, 195–197, 199, 203, 209
Complex amplitude, 862
Compressibility, 93, 121, 158
Compressible flow theory, 192
Compressible subsonic flow, 96–101
Compressor, 190, 195, 199–200, 208
inlet, 196–197
outlet, 196
Computational fluid dynamics (CFD), 35, 81, 90–92, 418, 426
Conservation of mass, 165, 170
Constant speed pull-up maneuver, 504–505
Constraint
azimuth angle, 892
design, 280
elevation angle, 892
pitch, 892
roll, 891
rotational, 891
yaw, 892
Continuity equation, 12–14, 172
Contrails, 139–140
Control, 44, 568
alternative, 554
anticipation parameter, 840
automatic, 863
derivatives, 496
inputs, 846
lateral, 554
loader, 524
longitudinal, 503, 557
orthogonality, 904–906
pitch, 68, 347, 386, 416, 503, 523, 528, 529–532, 535, 545–547, 568–572 (*see also* All-flying tail; Elevator; Stabilator; V-tail)
roll, 68–69, 489, 492, 575–576, 847 (*see also* Ailerons; Spoilers)
surface deflection, 68, 70, 384–394, 558, 560, 563
yaw, 448, 492, 576, 577, 588, 821, 847 (*see also* Rudder; V-tail)
Control derivative, 448, 456, 492, 496, 518, 567
Control force, 523
derivative, 530
gradient, 523, 528, 531, 534, 544
per g, 528, 531, 534

pitch, 503, 530, 546–547
Control point, 28–31, 84–90
Control problem
generalized linear, 848, 855, 859
special linear, 848, 850, 856
Control response, 833, 846–864
Control reversal
aileron, 565
elevator, 523
Control surface, 68
asymmetric, 68
deflection, 68, 70, 384–394, 558, 560, 563
distribution function, 70, 76
effectiveness, 385
geometry, 72
hinge moment, 524
other configurations, 568–577
sign convention, 69, 397, 457, 489, 496–497, 526, 564, 569, 798
spanwise asymmetric, 68
Control system, 524
autopilot, 847, 863–864
digital, 833
fly-by-wire, 524, 537, 576, 833
gain coefficient, 576
Control theory
automatic, 864
classical, 863
modern, 863
optimal, 864
Control volume, 115–116, 190–191
Cooper-Harper rating scale, 834–835
Coordinated
maneuver, 554, 556
turn, 284–286, 290–293, 299, 806, 807, 816–817
Coordinates, 1, 17, 467, 599–600
aerodynamic, 1–2, 462, 601
airfoil, 29–30
atmosphere-fixed, 601, 603, 610
body-fixed, 581–582, 601–602, 609, 619, 623, 625, 653, 654, 682, 806, 867, 871, 873
Cartesian, 601, 922
Earth-fixed, 601–602, 619, 623, 625, 806, 867, 871, 873
fixed, 602
flat-Earth, 922, 967
geographic, 922–928
inertial, 601, 611, 616, 618, 619, 642, 867–868, 870, 873, 880
nodal, 29
noninertial, 867–869, 873, 880
panel, 29
polar, 17
right-hand, 443
surface, lower, 23–24
surface, upper, 23–24
transformation, 97
Corbett-Wright
gain coefficient, 900–904, 907
orthogonality control, 899–904, 907, 916
Coriolis acceleration, 616
Coriolis forces, 810
Cosine clustering, 28–29, 89–90
Crab angle, 257
Critical engine failure speed, 316–317, 326–327
Curl, 12, 14, 16
Curved vortex sheet, 28
Cycle analysis, 195

D

Damped natural frequency, 698–701, 620, 723, 768, 770
Dutch roll, 771, 792
lateral mode, 768
phugoid/long period, 727, 736, 738, 746
short-period, 726, 732
Damped sinusoid, 698, 699, 709, 854
Damping
drag, 751–752
Dutch roll, 771, 775, 789, 791–792, 796–799, 819, 823–824
phase, 745, 751–752
phugoid/long period, 736, 739, 745, 751–753, 819, 842
pitch, 508, 729, 751–752, 857
rate, 698–701, 723, 737, 768, 776, 779–781, 791–792
ratio, 699–702, 723, 768, 771, 840, 842, 844
requirements, 840–846
roll, 74, 775, 789, 794, 819, 843
short-period, 729, 732, 819, 841–842, 857
spiral mode, 781, 797, 819, 843
yaw, 798, 859
Decay rate, 700 (*see also* Damping)
Deflection, 37
aileron, 69–78, 489–492, 495–496, 566–567
control surface, 68, 70, 384–394, 560, 563
efficiency, 39–40, 77
elevator, 351–362, 367–370, 398–404, 408, 504, 509
flap, 35–42, 84–85
rudder, 447–448, 454–459, 492–495, 564
Degrees of freedom, 441
lateral, 441, 495
longitudinal, 441, 495

DeHavilland Dash 8, 128
Derivatives (*see also* Gradient)
aerodynamic, 444, 448, 487, 652–672, 730, 794, 797, 804
control, 496
force and moment, 652–672
nondimensional, 676–678
Design, 41, 222, 487, 496
aircraft, 221, 225–226, 234, 487
airspeed, 280, 355
constraint, 280
final, 221–222
parameters, 221–222, 225
preliminary, 41, 92, 221–222, 350–353, 371, 378, 417, 449–450, 459, 471–472
requirements, 221
tail, 468–469
Differential equations, 97
elliptic, 97
hyperbolic, 97, 101
partial, 97, 101
Differential operator, 617
Dihedral, 48–51, 79–83, 89–90, 373, 375, 461, 463, 483
angle, 80, 475, 479, 487–488
factor, 479, 487
Dihedral effect, 473, 475, 487–488
fuselage, 487–488
vertical stabilizer, 488
Dimensionless, 3–4, 71–73, 84–89, 92
Direction cosine, 870
formulation, 870–871, 878, 916
matrix, 870
transformation, 882
Direction of flight, 223 (*see also* Heading)
Distance
acceleration, 299–300, 306–307, 311, 313, 323
braking, 313–314
FAR takeoff, 315–317, 320, 323–326
free-roll, 313–314
ground roll, 299, 315
liftoff, 299
rotation, 299–300, 306, 309, 313
Disturbance (*see also* Perturbation)
lateral, 614, 765, 784
longitudinal, 614, 765
pitch, 411–412
roll, 784
to steady equilibrium flight, 614
yaw, 444, 784
Divergence
directional, 784
drag, 100, 660
pitch, 819–820
spiral, 773–774, 777, 781, 784, 843
Divergent mode, 718–719, 740, 757, 822
Doublet, 17
Doubling time, 718, 773–774, 843
Douglas X-3 Stiletto, 468
Downwash, 44, 46, 79–81, 89, 134–139, 141, 302, 352–353, 371, 373, 375, 377–380, 409, 422, 428, 467, 486
angle, 135–136, 138, 180–181, 349, 352–353, 356–357, 371, 373, 375, 377–380, 423–424, 428, 453, 493
distribution, 352
gradient, 359, 380, 424, 428, 449, 453, 493
induced, 139, 376
uniform, 59
velocity, 353, 371–373
Drag, 2–3, 130, 133–136, 151, 178, 181–182, 190, 221–222, 229, 240, 258, 299, 301–302, 309, 341–342
aerodynamic, 222–223, 300
additive, 191–194
blade, 152, 162
coefficient, 3–4, 11–12, 26, 48–51, 54, 58, 92, 100, 107
curve, 100
damping, 751–752
divergence, 100, 660
effects of, 396–416
force, 2, 133, 136, 181, 190, 223–224, 239, 319, 343, 365, 414
induced, 46, 48–62, 133, 135, 138, 182, 224, 226, 234, 240, 301–302, 319, 342, 351, 385, 461
level flight, 240, 279
local section, 137–138
minimum, 260–261, 280–281
nacelle, 191, 194
nonlinear, 407
parasitic, 92, 133, 138, 162, 182, 224, 226–227, 234, 301
pre-entry, 191
section, 26, 107, 182
viscous, 108
wave, 107–108
zero-lift, 234, 280
Drag coefficient, 3, 138, 144–146, 162, 182, 227, 229, 298, 300, 307–309, 314, 319–322, 408–410
constant, 308
parasitic, 224, 227, 280–281
zero-lift, 281, 302, 308
Drift error, 901, 904–906, 916
Ducted fan, 127, 207

Dutch roll, 766, 773, 775, 786–799, 823–825, 844, 859, 861
amplitude, 772, 775, 787
approximation, 786–799
coupling ratio, 791, 792, 794, 797
damped natural frequency, 771, 792
damping, 771, 775, 789, 791–792, 796–799, 819, 823–824
eigenvalues, 786, 789–796, 861
eigenvectors, 771, 772, 786, 787, 793
frequency, 772, 789, 791, 796, 844
handling qualities, 844–845
mode, 766, 771, 772, 775, 792, 824
oscillation, 771, 775, 824–825
period, 773, 819
phase, 772
phase-divergence ratio, 791, 792, 794, 797
stability ratio, 791, 792, 794, 796
undamped natural frequency, 772, 796
Dynamic frequency response, 862
Dynamic gain, 862 (*see also* Amplification factor)
Dynamic handling quality predictions, 838–846
Dynamic pressure, 345, 349–350, 383
ratio, 448
Dynamics, fundamentals of, 697–720 (*see also* Eigenproblem)

E

Effective headwind, 259
Efficiency, 117, 120–121, 126–130, 153, 155, 159, 161, 207, 211–215
aerodynamic, 224, 226, 228, 351, 386
deflection, 39–40, 77
fuel, 130
hinge, 39–40, 77
ideal, 167
maximum, 121, 149, 152–153
propeller, 117, 120–121, 152–153, 162, 255
tail, 350
thermal, 198–212
thermodynamic, 130
Eigenaxis, 871
Eigenproblem, 697–720, 765
generalized, 703, 706, 710–711, 722, 767
special, 710–711, 722, 767
Eigenvalue, 698, 703–704, 707, 709–714, 718–719, 721–723, 766–768
complex, 698, 700–701, 707, 720
dimensionless, 723, 732, 737–738, 746, 749, 780
Dutch roll, 786, 789–796, 861
phugoid/long period, 727, 737, 738, 740, 743–746, 749–750
pure pitching motion, 755
pure yawing motion, 803
real, 698, 707
rigid-body displacement mode, 718, 728, 772
roll mode, 773, 776–777
short period, 726, 731–733, 861
spiral mode, 777, 778–780
Eigenvector, 703–704, 707, 708, 709, 710, 714, 719, 720, 722, 723, 728, 758, 767, 772, 804, 805, 814
complex components, 720
complex pair, 708
components, 709
Dutch roll, 771, 772, 786, 787, 793
lateral, 772
longitudinal, 728
phugoid/long period, 730, 737, 739–740, 746, 748
roll mode, 770, 777
short period, 729, 731, 733
spiral mode, 770, 778–781
Elastic deflection angle, 517
Electronic yaw damper, 798
Elevation angle, 397, 580, 620, 868
constraint, 892
Elevator, 339, 347, 352, 503, 526, 554
angle per g, 509
control reversal, 523
deflection, 351–362, 367–370, 398–404, 408, 504, 509
effectiveness, 518–522
hinge moment, 526
response, 854–857
sizing, 537, 547, 549
Empennage, 346–347, 574
Endurance, 249–257
maximum, 253–256, 261–262, 265–266, 279
specific, 254–256
Energy
equation, 167, 174
potential, 234, 319, 729–730
rotational kinetic, 729–730
translational kinetic, 730
Engine, 119–130, 133, 135, 152, 157–160, 178, 190–195, 207, 209–213, 215, 222, 239, 244, 255, 428
air-cooled piston, 117, 121
air-cooled radial, 119
aircraft, 116–117, 119, 152, 162, 198–199
bypass, 126
failure, 315–317, 323, 325, 327
failure reaction speed, 324
failure recognition speed, 324, 326–327

gas turbine, 122, 130, 190
horizontally opposed, 121
ideal, 195
internal combustion, 117–118, 120, 250
jet, 117, 122, 126, 232, 244, 426, 428–430
liquid-cooled piston, 117
piston, 120, 130, 152, 157, 159, 302
radial, 118–119
reciprocating, 244
reciprocating jet, 122
reciprocating piston, 121
Rolls-Royce Griffon, 120, 123
rotary-radial, 117–118
static-radial, 119
supercharger, 121
turbofan, 117, 126–128, 130, 207–211, 214–215, 268, 302, 426–427, 430
turbojet, 117, 122–128, 190–200, 203–204, 207, 210–211, 214, 230, 232, 236–237, 244, 248, 265, 302, 320, 323, 426–427, 430
turboprop, 128–130
turboshaft, 130
Engine-out flight configuration, 495
Engine-propeller combination, 117, 121–123, 126, 135, 158, 160, 207, 232, 244, 426, 430
Enthalpy, 116, 167, 197
freestream, 167
Equations of motion, 600, 619, 910
6-DOF, rigid body, 637
aircraft, 599, 603
general linearized, 808
lateral, 766, 823
linearized, 638–651, 823, 848, 855, 864
longitudinal, 766, 855
nondimensional linearized, 672–682, 811
nonlinear, 847, 864
rigid-body, 599–600, 637, 718, 823, 867
Equilibrium, 339–343, 348, 411
angle of attack, 354, 614, 688
neutrally stable, 341
stable, 339–341, 412
static, 339–345, 348–349, 352
unstable, 339–343, 552
Error
drift, 901, 904–906, 916
orthogonality, 899–901, 904–907, 916
quaternion, 888
round-off, 906–907
simulation, 903, 907, 912–914
truncation, 907, 911, 912
Euler angle, 619–627, 637–638, 643, 807, 867–869, 875, 878, 881–886, 891, 894–896
definitions, 619–621, 868–869
formulation, 619–637, 867–871, 874, 881, 891, 915–916
integration of, 627
rotation, 871–872
sets, 870
singularities, 627
time derivatives of, 625
transformation, 627, 881, 891, 916
Euler axis, 871–873, 887
formulation, 871–874
rotation, 871–874, 877
vector, 887–888
Euler instability, 900
Euler integration, 908, 914
Euler-Rodrigues
quaternion, 874, 878, 882, 886–890, 915
quaternion conjugate, 880
quaternion formulation, 874–883, 887–888, 895–898, 915–916
symmetric parameters, 874–875, 877–880, 887
Euler's formula, 871, 875
Euler's theorem, 875
Exhaust nozzle, 195–197
Exhaust jet, 426–428, 469
entrainment, 469
Exit nozzle, 190, 197
Exit plane, 191
Exponential method, 908–909 (*see also* Local linearization method)

F

F-14 Tomcat, 468
FAR takeoff, 315–317, 320, 323–326
Failure state, 838
Fang and Zimmerman algorithm, 903
Fan nozzle, 208–210
Feathering the prop, 151
Feedback control system, 798–799
Finite thickness, 34
Finite wing, 21, 42–45, 50, 54, 79, 82, 84, 134, 352, 480
theory, 42–79
First law of thermodynamics, 115–116, 196–197, 203, 208
Fixed-wing aircraft, 70, 567
Flap, 35–42
chord fraction, 38
chord length, 36
deflection, 35–42, 84–85
trailing-edge, 35–42, 47, 68
sealed, 39–40
Flap effectiveness, 35, 38–39, 41, 489–490

ideal section, 37–38
local section, 71
Flaperons, 554
Flat-Earth
approximation, 601, 915
coordinate system, 867, 922
quaternion formulation, 913–920
Flat vortex panels, 28
Flex-wing aircraft, 567
Flight
accelerating, 503
envelope, 287–288, 837
free, 341–342, 345, 354
gliding, 268, 271, 274, 279
level, 231, 240–241, 257–258, 279, 284, 348, 351
mechanics, 1, 215, 221–222, 599
powerless, 269–270
simulation, 221, 867, 874, 907, 910
simulator, 880
steady, 13–14
steady level, 222–225, 229–233, 236–237, 241–245, 249–252, 255, 257, 260, 268, 279, 320, 339
testing, 215
trimmed, 339, 341–342, 346, 354, 385, 404, 412–413
turning, 283–284, 558, 560
Flight envelope, 837
operational, 837, 846
permissible, 837
service, 837
Flight phase categories, 835–836
Floatplane, 458–459
Flow, 10
adiabatic, 15, 93
axisymmetric, 171
boundary layer, 10, 34
compressible, 16, 93, 96–97, 101
compressible subsonic, 96–101
core, 208, 210
doublet, 2-D, 17
entrained, 426, 469
fan, 208
field, 14, 43, 98, 371, 482
fluid, 12, 105
freestream, 13, 16, 133, 178
incompressible, 14, 16, 22, 42, 94, 96–98, 155–156, 162–165, 174
induced, 177
inviscid, 10, 11–15, 79, 93, 97
inviscid irrotational, 13
irrotational, 16, 93, 95, 101
isentropic, 15, 93, 192, 208–209
leakage, 38
lifting, 2-D, 20
over multiple lifting services, 79–92
potential, 16–21, 25–26, 28, 33–34, 45, 93, 98, 161
separation, 194, 820 (*see also* Stall)
source, 2-D, 17
stagnation, 2-D, 17
streamtube, 165, 176
subsonic, 26, 96, 101, 105, 107
supersonic, 96–101, 105
three-dimensional, 600
turbine, 195
two-dimensional, 600
uniform, 14, 16–18, 24, 28, 30, 84, 93, 95, 168–171, 174, 191, 446
viscous, 194
vortex, 2-D, 17
Fluid, 15
compressible, 15
density, 139
flow, 12, 105
inviscid, 194
statics, 6
Flying wing, 345–346
Flying qualities (*see* Handling qualities)
Force, 2, 221, 346
aerodynamic, 1–4, 10, 14, 24–26, 42, 45, 79, 84–92, 105, 365
axial, 2–4
braking, 317
buoyant, 14, 190
derivatives, 652–672
drag, 2, 133, 136, 181, 190, 223–224, 239, 319, 343, 365, 414
friction, 313
gradient, 452
lift, 223, 284–285, 343, 414
normal, 2, 134, 178, 185–189, 420–422, 424, 426–427
off-axis, 178
pressure, 10–14, 34, 100, 414, 418
resultant aerodynamic, 14
rolling friction, 302
section, 2
shear, 365, 414
side, 2, 178, 185, 187, 281, 284, 339, 343, 349, 443, 445, 450–452, 457, 470, 473, 484
thrust, 133, 178, 232, 314, 319–320
vector, 232
viscous, 34, 100
viscous shear, 10
Forced response, 697, 701

Forcing frequency, 702
Ford Tri-motor, 118–119
Forebody blowing, 865
Forebody strakes, 821, 865
Forebody suction, 865
Forward airspeed, 135–138, 149, 152, 169, 178
Forward CG limit, 370, 547
Fourier, 48
  coefficients, 48–58, 63–77
  integral, 73
  series, 48–51
Free response, 697–698, 701, 718
Freestream, 2–3, 14, 25–26, 46, 83–84, 95–96, 101–103, 105, 116, 133, 167, 178, 192–196, 348, 420, 426
  airspeed, 167
  conditions, 94
  density, 3
  dynamic pressure, 349–350
  enthalpy, 167
  flow, 13, 16, 133, 178
  Mach number, 98, 100, 101–105, 199, 659
  pressure, 116, 167, 170, 190
  static pressure, 164, 169, 172, 193
  temperature, 192
  velocity, 2, 13, 17, 31, 44, 47, 95–98, 101, 115–116, 144, 165–166, 169, 184, 198, 348, 353, 371, 373, 382, 396, 429, 480
Frequency
  Dutch roll, 772, 789, 791, 796, 844
  phugoid/long period, 738, 740, 745, 750–751, 758, 842
  response, 701, 861, 862
  response curves, 863
  short period, 730, 732, 839–842
Fuel consumption, 249, 251–252, 257, 266
  minimum, 251–253
  power-specific, 249, 279
  rate, 251–254, 265–266
  specific, 121, 249–252, 260–261, 265–266
  thrust-specific, 266, 268
  total rate, 251, 254, 265
Fuel injection, 121
Full stall landing, 543, 546
Fuselage
  angle of attack, 355, 358, 389
  bending, 518–519, 521
  center of pressure, 417–418
  contribution of, 416–420
  dihedral effect, 487–488
  effect, 449
  reference line, 223, 348, 353, 355, 357, 363, 382, 384, 396–399, 408, 423–424, 428
Fuselage-wing interaction, 483

G

Gain, 862
  coefficient, 899, 903, 907
  Corbett-Wright, coefficient, 900–904, 907
  dynamic, 862
  static, 862
Gas turbine, 122, 130, 190
Gauss elimination, 711
Geographic coordinates, 922–928
Geometric shape, 22
Geometric twist, 47–48, 51, 80, 90, 478–479
Geometric washout, 131
Gimbal lock singularity, 627, 867–871, 874, 885–887, 916
Glide ratio, 270–277
  maximum, 273–279
  zero-wind, 272–273, 279
Gliding flight, 268
Gloster Meteor, 123–124
Gloster/Whittle E28/39, 123–124
Goldstein's hypothesis, 142, 161
Goldstein's kappa factor, 142
Goldstein's vortex theory, 141–142, 147, 149, 158, 162–164, 176, 179
Gossamer Albatross, 234
Gossamer Condor, 234
Gradient, 13–15
  control force, 523, 528, 531, 534, 544
  downwash, 359, 380, 424, 428, 449, 453, 493
  moment, 452
  normal force, 422–423
  pressure, 11, 15
  sidewash, 447–449, 453, 455, 462–469
  temperature, 7, 15
  upwash, 385, 388
  velocity, 15
Great circle, 926
  navigation, 926–928
Gross weight, 221–224, 229, 252–254, 261–263, 274, 276, 280–281, 284, 288–289, 307
  maximum, 285–288
Ground control speed, 308
Ground effect, 301–302, 319–321, 537–547
Ground roll, 299–303, 306, 308, 311–312, 314, 320
  landing, 313–314
  takeoff, 315
Ground speed, 257–258, 271, 300, 316, 603
Ground track, 257
Gyroscopic coupling, 689–691, 804–805, 808, 814, 864, 915
Gyroscopic effects, 117, 690

H

Half-chord, 49, 107
Handling qualities, 339, 343, 524, 833–846, 861, 864
  aircraft, 833–865
  Dutch roll, 844–845
  lateral phugoid, 844
  phugoid/long period, 842
  roll mode, 843
  short period, 838–842
  spiral mode, 843
Heading, 257, 620 (*see also* Azimuth angle)
Headwind, 257–260, 272–278, 300
  effective, 259
Heavily damped motion, 70, 729, 766
Heaviside expansion theorem, 853
Heinkel He-162, 495
Heinkel He-178, 122
Heinkel He-280, 122
Helical
  blade-tip vortex, 177
  path, 139–141
  surface, 141
  vortex, 139, 141, 142
Helix, 132, 177
High-lift device, 280, 300, 302, 313, 387, 395, 486
High thrust vector, 416
Hinge-efficiency, 39–40, 77
Horizontal tail, 346, 348, 351, 353, 357, 371, 373, 380, 404–407, 426, 445–449
Horizontal tail volume ratio, 356–357, 448
Horseshoe vortex, 81–84, 86–89, 90
Householder method, 723

I

Ideal gas, 6, 10, 93, 192, 195
  constant, 6, 8, 15, 192, 201
  law, 103
Incompressible, 14, 167
  flow, 14, 16, 22, 42, 94, 96–98, 155–156, 162–165, 174
  inviscid flow, 14, 165
  velocity potential, 14
Induced
  angle, 135, 137, 143, 145, 180
  downwash, 139, 376
Induced drag, 46, 48–62, 133, 135, 138, 182, 224, 226, 234, 240, 301–302, 319, 342, 351, 385, 461
  minimum, 58
Inertia tensor, 601, 609, 619
Inertial coordinates, 601, 611, 616, 618, 619, 642, 867–868, 870, 873, 880
Inertial coupling, 689–691, 804–805, 808, 814, 819–820, 864, 915
Inertial cross coupling, 616
Inertial reference frame, 610
Infinite series, 25, 27
Inlet, 195
  duct, 190
  plane, 191
  pressure, 194
  velocity, 126
Inverse rotation, 880
Inverse transformation, 605–606, 853
  equations, 606
Inviscid, 10–15
  aerodynamic force, 24
  aerodynamic moment, 24
  aerodynamics, 12, 24
  adiabatic flow, 15, 93
  CFD solution, 90–92
  compressible aerodynamics, 93–96
  flow analysis, 11
  fluid, 194
  forces, 91
  lift coefficient, 32–33
  moments, 91
  panel codes, 92
  theory, 108, 161
Irrotational, 14, 16, 93, 101
Isentropic, 15, 93, 104, 195

J

Jacobian, 86
Jet engine, 117, 122, 126, 232, 244, 426, 428–430
  contribution of, 426–430
Jet propulsion, 122–123
Jet transport, 669, 678, 688

K

Kalman filtering, 878
Kinematic
  equations, 899
  formulation, 870
  transformation equations, 626, 637, 867, 869, 874, 877, 896
Kinetic energy, 115, 198, 204, 209–210, 319
Kutta, 42
  condition, 24, 30
  lift, 45
Kutta-Joukowski law, 20, 25, 44–45

L

Landing, 299–315
Landing configuration, 548

Landing gear, 300, 302, 304
tail-dragger, 300, 307, 457–458
tricycle, 300, 307–308
Landing performance, 299
Laplace
equation, 14, 94, 96–98
transform, 848–849, 852, 853, 861, 863
Lapse rate, 7
Lateral control and maneuverability, 554
Lateral disturbance, 614, 765, 784
Lateral dynamics, linearized, 765–825
Lateral equations, 766
linearized, 647, 720
Lateral mode, 838
damped natural frequency, 768
damping rate, 768
undamped natural frequency, 768
Lateral motion, 557–558, 720, 765–767
Lateral phugoid, 775, 844
handling qualities, 844
Lateral static stability, 441–497
Lateral trim, 441–497
Leading edge, 1–2, 4–5, 22–23, 29, 49, 80, 105
blunt, 105
moment coefficient, 26
sharp, 105
Length, 2–3
characteristic, 84, 88
l'Hôspital's rule, 63
Lift, 2–3, 100, 137–138, 178, 181, 221–222, 229, 239–240, 299
force, 223, 284–285, 343, 414
vector, 46, 74, 135, 138–139, 182, 281
Lift coefficient, 3, 11–12, 26, 34, 37–38, 48–59, 62, 76, 91, 97, 108, 137, 144–145, 162, 224–229, 233–234, 239, 245–246, 272, 279, 282, 284, 296, 298–302, 306, 308, 319–322, 344–345, 349–353, 358, 360, 363, 371–372, 375, 384, 409–411, 414, 506
canard, 384, 386, 392
design, 58, 77
differential, 299
inviscid, 32–33
maximum, 12, 35, 280, 289, 292–293, 304, 308, 313, 346, 370
optimum, 309, 312
section, 3, 26–27, 32–35, 42, 84–85, 91, 106, 137
tail, 350
thin airfoil, 37
wing, 350
Lift slope, 33, 35–38, 49–52, 55, 58, 73, 107, 345, 352, 356, 364, 367, 384, 535
canard, 384
in situ section, 476–479
section, 26, 38, 47, 51, 182
Lifting-line, 81–82
equation, 48, 79, 81, 471–472, 478, 480
numerical method, 81, 90–92, 353, 469–471, 477, 485, 492, 539, 574
solution, 83
theory, 44–79, 81, 90, 91, 353, 372, 374, 377, 449, 462–463, 477, 480, 491, 663, 666–667
Liftoff, 304, 308, 313, 315, 317–322
attitude, 299
speed, 304–308, 315, 323–326
Lift-to-drag ratio, 224–229, 272, 276
Linear control problem
generalized, 848, 855, 859
special, 848, 850
Linear time-invariant systems, 848
Linearized equations
coupled, 720–731, 765
lateral, 647, 720
longitudinal, 647, 720
of motion, 638–651, 823, 848, 855, 864
Linearized lateral dynamics, 765–825
Linearized longitudinal dynamics, 697–757
Load factor, 284–286, 289, 293, 295, 297, 319, 503–504, 537, 560, 838
allowable, 288–289
load-limited, 287, 289, 291, 298
maximum, 286, 288
stall-limited, 287, 289, 291, 298
Load-limit, 292–293
negative, 285, 287
positive, 285, 287–289, 292–293
Local linearization method, 908–914 (*see also* Exponential method)
Lockheed C-5 Galaxy, 127
Lockheed P-38 Lightning, 468, 493–495, 501, 522–523
Lockheed P-80, 125
Longitudinal control, 503, 557
Longitudinal disturbance, 614, 765
Longitudinal dynamics, 721
linearized, 697–757, 765
stick-fixed, 757
Longitudinal equations, 766
linearized, 647, 720
Longitudinal mode, 723, 758, 838
Longitudinal motion, 441, 495, 720–731
Longitudinal static stability, 339–430
Longitudinal trim, 339–430
Longitudinal-lateral coupling, 495–496, 804–819, 864, 915

nonlinear effects, 864–865
Long-period, 730, 736 (*see also* Phugoid)
amplitude, 727–728
approximation, 736–753
damped natural frequency, 727, 736, 738, 746
damping, 736, 739, 745, 751–753, 819, 842
damping rate, 737–738, 746, 819
eigenvalues, 727, 737, 738, 740, 743–746, 749–750
eigenvectors, 730, 737, 739–740, 746, 748
frequency, 738, 740, 745, 750–751, 758, 842
handling qualities, 842
lateral oscillation, 844
mode, 721, 726–727, 730, 740, 753, 758
motion, 730, 741, 744, 750
oscillations, 727, 758, 857
period, 727, 819
phase, 727–728
phase-divergence ratio, 745
pitch-damping-ratio, 745
stability ratio, 745, 750–753
undamped natural frequency, 727, 738, 745, 750

M

Mach angle, 102, 104–105
Mach lines, 105–106
Mach number, 14–15, 94–101, 128, 130, 158, 162, 197, 202, 204, 209, 224
critical, 96, 98–101
design, 194
design cruise, 193
exit, 203
flight, 93, 96–97, 192–194, 199–207, 211, 214–215
freestream, 98, 100, 102, 104–105, 199, 659
hypersonic, 96
inlet, 192–194
local, 98, 162
low, 32
subsonic, 96–97
supersonic, 96, 102, 104
tip, 158
transonic, 96
zero, 97
Maneuver, 287–288
cobra, 296, 865
coordinated, 554, 556
margin, 511
post-stall, 549, 296
pull-up, 503–505, 508, 524, 528, 535, 847, 857
Maneuverability, 503, 554, 568
aircraft, 503
analysis, 503
Maneuvering speed, 288–289, 292–293
Mass flow rate, 115, 116, 121, 126–127, 155, 166, 190–192, 207, 427, 611
Mass moment of inertia tensor, 609, 756
Mass transfer, 610
Maximum range, 221, 259–264, 266–268, 279
Mean chord length, 3, 345, 349, 356, 364
Messerschmitt Me-262, 123
Minimum power required, 242, 251
Minimum runway length, 315 (*see also* FAR takeoff)
Mirror image model, 539–540
Mission task elements, 835
Mode
convergent, 719, 740, 822, 862
critically damped, 700, 707
damped, 719
divergent, 718–719, 740, 757, 822
Dutch roll, 766, 771, 772, 775, 792, 824
longitudinal, 723, 758, 838
long-period, 721, 726–727, 730, 740, 753, 758
non-oscillatory, 719
oscillatory, 719, 823
overdamped, 700, 707
phugoid, 720, 726–727, 730, 740, 758, 775, 842
rigid-body, 715, 718, 719, 728, 772
roll, 766, 770–776, 789, 823, 843
short-period, 721, 726, 728–731, 758, 775, 838
spiral, 766, 770, 773–775, 777–785, 823, 843
time constant, 843
undamped, 719
underdamped, 700, 707
Moment, 1–4, 221, 346
aerodynamic, 1–4, 88–90, 92, 221, 365, 397, 414, 418, 441, 443, 473
about leading edge, 4
coefficient, 3, 5, 25, 32, 38, 97, 107–108, 344, 349, 354, 409, 507
derivatives, 652–672
gradient, 452
nondimensional derivatives, 676–678
pitching, 2, 100, 107, 178, 185, 187, 339, 343–349, 352–359, 362, 365, 380, 382, 405, 409–410, 418, 420–421, 426, 428, 441
propeller-induced, 133
propeller yawing, 452, 454, 459, 494
quarter-chord, 26, 28, 37–38, 41, 88

restoring, 444–445
rolling, 2, 68–70, 72–73, 76–78, 133, 138, 178, 339, 343, 349, 441–443, 470, 474–475, 481–486, 489–495, 765
section, 2
slope, 41, 354, 366, 419, 425
thrust, 397
yawing, 2, 74–78, 134, 178, 186–187, 339, 343, 349, 441–445, 448–454, 457, 459, 473–475, 481–485, 489–492, 587, 765
Moment coefficient, 3, 5, 25, 32, 38, 97, 107–108, 344, 349, 354, 409, 507
leading edge, 26
pitching, 3, 5, 41, 106–107, 186, 346, 352, 354, 356, 367–368, 384, 394–395, 405, 410–415, 417, 421, 423
quarter-chord, 26, 28, 37
rolling, 72–73, 78
section, 3, 88
yawing, 74–78, 186–187, 448, 473
Momentum, 79, 115, 166, 191
angular, 168–170, 173
axial, 190
downward, 79
equation, 12–14, 93, 103, 168–171, 173, 190
fluid, 135, 166
flux, 177, 190–191
theory, 166, 169, 174–178
Motion
critically damped, 699
lateral, 495
longitudinal, 441, 495, 720, 722
overdamped, 698–699
phugoid, 730, 741, 744, 750
pure pitching, 753–755, 893
underdamped, 698–699
Multiple lifting surfaces, 79–92

N

Nacelle, 190–191, 353, 356, 371, 416–417
contribution of, 416–420
drag, 191, 194
effect, 449–450
Natural frequency
damped, 698–701, 620, 723, 768, 770
undamped, 699, 702, 720, 723, 750, 768, 771
Navier-Stokes equations, 10, 94
Navigation, 923
great circle, 926–928
rhumb line, 923–925
Neutral point, 363, 365–366, 369, 388, 419, 425, 538 (*see also* Aerodynamic center)
Neutral roll stability, 784–785
Newtonian mechanics, 169, 599
Newton's corrector equation, 236
Newton's law of gravitation, 6
Newton's method, 86–87, 236–237, 278, 400
Newton's second law, 2, 79, 115, 190–191, 222, 300, 317, 324, 427, 503, 557, 609–611, 614, 616, 619, 625, 637, 641, 705, 757, 867, 895
Nodes, 28–31, 82, 84, 87, 89
Nondimensional derivatives, 676–678
Nonlinear effects, 819–823, 847, 864
Nonlinear inertial coupling, 819–820
Normal force
coefficient, 3–5
gradient, 422–423
North American XB-70, 125
Notation, 1, 600, 612–614, 624, 674, 871
Nozzle, 208
core, 208–210
exhaust, 195–197
exit, 190, 197
fan, 208–210
Numerical lifting-line method, 81, 90–92, 353, 469–471, 477, 485, 492, 539, 574
Numerical panel method, 26, 90–91

O

Operating conditions, 221
Optimum, 50, 58, 308, 311
airspeed, 227
angle of attack, 311
flight profile, 268
induced drag, 59
lift coefficient, 309, 312
thrust angle, 227–228
total washout, 58
washout, 58, 60–61, 76–78
washout distribution, 59–62, 76
washout distribution function, 65, 67
Orthogonality
control, 904–906
error, 899–901, 904–907, 916
Oscillations
Dutch roll, 771, 775, 824–825
limit-cycle, 823
long-period lateral, 775, 844
phugoid/long period, 727, 758, 857
pilot induced, 823
rolling, 766
short period, 729, 758
sideslipping, 766
sinusoidal, 862
yawing, 766
Oscillatory roll-spiral mode, 775, 844
Oswald efficiency, 224, 227, 234, 280–281

P

P-38 Lightning, 468, 493–495, 501, 522–523
P-51 Mustang, 458
Panel codes, 32, 83, 98, 426
  3-D, 81, 449
  inviscid, 92
  vortex, 99
Panel methods, 91, 418
  numerical, 26, 90–91
  vortex, 28, 32–35, 38–41, 353, 539
Panels, source, 2-D, 18–20
Panels, vortex, 2-D, 20–21
Payload-to-power ratio, 234
Performance, 12, 130, 133, 159, 165, 211
  aircraft, 12, 221–222
  characteristics, 266
  landing, 299
  takeoff, 299, 306, 308
  turning, 298
Perturbation, 95–96, 103 (*see also* Disturbance)
Phase angle, 702
Phase damping, 745, 751–752
  phugoid, 753
Phugoid, 730, 736, 842, 857 (*see also* Long-period)
  amplitude, 727–728
  approximation, 736–753
  damped natural frequency, 727, 736, 738, 746
  damping, 736, 739, 745, 751–753, 819, 842
    damping rate, 737–738, 746, 819
  eigenvalues, 727, 737, 738, 740, 743–746, 749–750
  eigenvectors, 730, 737, 739–740, 746, 748
  frequency, 738, 740, 745, 750–751, 758, 842
  handling qualities, 842
  lateral, 775, 844
  mode, 720, 726–727, 730, 740, 758, 775, 842
  motion, 730, 741, 744, 750
  oscillations, 727, 758, 857
  period, 727, 819, 842
  phase, 727–728
  phase damping, 753
  phase-divergence ratio, 745
  pitch-damping-ratio, 745
  stability ratio, 745, 750–753
  undamped natural frequency, 727, 738, 745, 750
Pilot
  compensation, 834
  opinion, 833–840, 846, 861
  reaction time, 313, 314, 325, 774, 824–824, 843
  response time, 824, 842
  technique, 319
Piloting task
  classification, 836
  definitions, 835
Pitch, 2, 68, 132, 142, 145, 147, 157, 339, 341–343, 352, 405, 473, 620–621
  angle, 131–132, 138, 142, 144, 147–148, 181
  constraint, 892
  control, 68, 347, 386, 416, 503, 523, 528, 529–532, 535, 545–547, 568–572 (*see also* All-flying tail; Elevator; Stabilator; V-tail)
  control force, 503, 530, 546–547
  damping, 508, 729, 751–752, 857
  disturbance, 411–412
  divergence, 819–820
  length, 132–133, 145, 147, 162
  rate, 505–506, 626
  stiffness, 345
Pitch-damping derivative, 508, 664
Pitch stability, 343–347, 356–357, 366, 381, 382, 384, 386, 449, 522
  derivative, 345, 359, 363, 367, 384, 407–408, 411, 414, 417, 424, 429, 444–445, 450, 475, 509, 518, 536
  static, 381, 395, 444–445
Pitching, 2
  moment, 2, 100, 107, 178, 185, 187, 339, 343–349, 352–359, 362, 365, 380, 382, 405, 409–410, 418, 420–421, 426, 428, 441
  moment of inertia, 756
  motion, pure, 753–755, 893
Pitch-to-diameter ratio, 120, 145–161, 187–188, 422
Planar, 18
  curve, 22
  segment, 18
  source sheet, 18
Planform, 3, 45, 48–51, 53–54, 56, 58, 62, 72, 81, 85, 88, 145
  arbitrary, 55, 58, 62, 73, 161
  elliptic, 45, 54, 58–59, 73, 146
  rectangular, 62–63, 65
  spanwise symmetric, 72
  tapered, 66
  wing, 56, 58, 68, 73, 76
Poisson's kinematic equations, 870
Position and orientation, 619–637 (*see also* Euler angle; Quaternion)
Position factor, 380, 388
Position vector, 637
  time rate of change, 625

Post-stall
dynamic turn, 296
maneuver, 549, 296
stability, 549, 551
Potential
energy, 274, 319, 729–730
field, 18
perturbation, 103
perturbation velocity, 95–96
scalar field, 16
scalar velocity, 94
uniform flow, 95
velocity, 14, 93–96
velocity field, 17
Potential flow, 16–21, 25–26, 28, 33–34, 45, 93, 98, 161
compressible, 94, 103
elementary, 16, 18
incompressible, 16, 97–98
linearized approximation, 96, 101
small angle, 102, 104–107
solution, 33–34, 81, 91, 538
supersonic, 102, 105, 107
theory, 34, 44, 107
Potential line, 102
Power, 115, 117, 121, 127–130, 133, 149–152, 155–159, 162, 168, 198, 207, 210
available, 236, 239, 241–246, 255, 257, 260, 265, 268, 283–284
brake, 121, 133, 144, 146, 151–159, 167, 174–175, 255
coefficient, 144, 146, 149–150, 154, 159, 163–164
distribution, 147–148
excess, 241–242, 283–284
failure, 268
full throttle, 235, 237, 241, 246
input, 116, 156
propulsive, 133, 151, 160, 167, 198, 235, 255
required, 232–239, 241–246, 250–252, 255, 257, 260, 265, 267, 269, 283–284
Power-specific fuel consumption, 249, 279, 332
Power-to-weight ratio, 117–122, 130, 236–237, 247
Prandtl-Glauert compressibility correction, 96–97, 658–660
Prandtl's tip loss factor, 143
Pressure, 11, 79, 105
aerodynamic, 365, 414
ambient, 115, 165, 195–196, 208, 427
coefficient, 97–99, 104–105
difference, 79
distribution, 33–34
dynamic, 345, 349–350, 383
force, 10–14, 34, 100, 414, 418
freestream, 116, 167, 170, 190
gradient, 11, 15
local static, 14
stagnation, 15, 93, 192, 195–197, 203
uniform, 168, 171
Pressure ratio, 127, 196, 199–200, 210
compressor, 128, 199–207, 211, 214–215
fan, 210–215
stagnation, 208
Propeller, 115–178, 215
angle of attack, 133–134, 163, 178–182, 184, 187, 424, 452–454, 457–459
blade, 130–131, 135–136, 138–139, 143, 161
blade shape, 121
blade theory, 135–164, 176
blade-tip speed, 121
brake power, 133
constant-pitch, 133, 147, 302
constant-speed, 120–121, 152–153
contribution of, 420–426
counter-rotating, 447, 468
diameter, 121, 144–145, 156, 159–161
disk, 164–166, 169–173, 177, 181, 184, 186
downwash angle, 423–424
downwash gradient, 425
effect of, 450
efficiency, 117, 120–121, 152–153, 162, 255
fixed-pitch, 133, 146, 149, 151–152, 154, 159, 250, 422
forces and moments, off-axis, 178–190
geometry, 143, 163–164
induced velocity, 134–138
momentum theory, 164–178
normal force, 421–422
performance, 133, 162–163
pitch, 153–154, 162–163, 255, 308
plane of rotation, 133–134, 178, 184–185
slipstream, 420, 446–447, 452, 457, 468, 486–487
theory, 161
thrust, 144, 146, 163, 184
variable-pitch, 120–121, 133, 151–153, 235, 255
yawing moment, 452, 454, 459, 494
Proper orthogonal transformation, 871
Propulsion, 115, 215
aircraft, 115–119, 121–122, 130, 153, 215
overview, 115–215
Propulsion system, 115, 117, 190
aircraft, 115, 117
ideal, 115–117, 121, 126

Propulsive efficiency, 116, 121, 126–127, 133, 146, 149–152, 159–160, 167–168, 175–176, 198–199, 207, 210–214, 429–430
Propulsive power, 133, 151, 160, 167, 198, 235, 255
  available, 249, 266
Pull-up maneuver, 503–505, 508, 524, 528, 535, 847, 857
  constant speed, 504–505
Pure pitching motion, 753–757, 893
  eigenvalues, 755
Pure rolling motion, 799–802, 893
Pure yawing motion, 802–803, 893
  eigenvalues, 803

Q

QR method, 723
Quarter-chord, 26, 41, 84, 90
  line, 46, 49, 80–82, 89
  moment coefficient, 26, 28, 37
  moment slope, 37–38
  wing, 352, 356, 361–362, 367–369, 377, 388
Quaternion, 875, 878–882, 887–889
  algebra, 875, 878–879, 903, 916
  attitude, 888
  bank angle constraint, 891
  closed-form solution, 891–898
  command-attitude, 888
  components, 889, 908
  conjugate, 879–880
  error, 888
  Euler-Rodrigues, 874, 878, 882, 886–890, 896, 915 (*see also* Euler-Rodrigues symmetric parameters)
  formulation, 627, 867, 881, 891–893, 898–899, 908–909, 916–918
  magnitude, 879
  numerical integration of, 897–912
  of finite rotation, 874
  product, 878–882
  relations with other attitude descriptors, 882–889
  renormalization, 900–901, 904, 916, 920
  rotational constraints, applying, 889–891
  transformation, 627, 891, 916
  unit, 887–888

R

Radius of curvature, 504
Ramjet, 122, 341
Range, 257
  maximum, 221, 259–264, 266–268, 279
  specific, 257–267
Rate gyro, 798
Rate of climb, 221–222, 239–249, 268, 283–284
  maximum, 242, 244, 246–248
  steady, 239, 268–269
Reaction force, 115
Reaction time, 313, 314, 325, 774, 824–824, 843
Redundancy relations, 871
Relative air flow, 1
Relative airspeed, 139
Relative wind, 2
  local, 46
Residual, 99
Resonance, 702, 758
Response frequency, 701, 861–862
  maximum, 720
Response time, 824, 842
Response to control inputs, 846–864
Restoring moment, 444–445
Reynolds number, 10–12, 53
Rhumb line, 923
  bearing, 924
  navigation, 923–925
Right-hand rule, 443
Rigid body, 222
  displacement, 717
  dynamics, 609–619, 720
  equations, 6-DOF, 640
  equations of motion, 599–600, 605, 637, 718, 823, 867
  mode, 715, 718–719, 728, 772
Rigid-wing aircraft, 567
Roll, 2, 68–70, 74, 76, 339, 341–343, 620–621, 765
  amplitude, 772
  acceleration, 69–70, 843
  angle, 74
  approximation, 776–777
  constraint, 891
  control, 68–69, 489, 492, 575–576, 847 (*see also* Ailerons; Spoilers)
  convergence, 773
  coupling, 795
  damping, 74, 775, 789, 794, 819, 843
  disturbance, 784
  Dutch, 766, 773, 775, 786–799, 823–825, 844, 859, 861
  eigenvalue, 773, 776–777
  eigenvector, 770, 777
  handling qualities, 843
  mode, 766, 770–776, 789, 823, 843
  moment, 2, 68–70, 72–73, 76–78, 133, 138, 178, 339, 343, 349, 474–475, 481–486, 489–495, 765

oscillations, 766
rate, 68–71, 73, 76–78, 626, 765, 776, 843
response, 70
rotation, 441
time constant, 843
trim requirements, 489–495
Roll stability, 461, 473–475, 480, 795
derivative, 474–476, 479, 482–488, 797
dihedral effect, 473–489
insufficient, 784
neutral, 784–785
ratio, 795
Roll-axis, 443, 492
Roll-damping, 74, 775, 789, 794, 819, 843
derivative, 662, 794, 797
rate, 800–801
ratio, 789, 794
Roll-spiral pair, 771, 775
Roll-yaw coupling, 564, 784, 796
derivatives, 797
Rolling friction, 300–302, 306, 308, 313
Rolls-Royce Griffon, 120, 123
Rollup, 46
Rotary-radial configuration, 117
Rotation
constant, 893–894, 912
rate, 306
triad, 613
Rotational
constraint, 891
speed, 138, 304
Round-off error, 906–907
Rudder, 339, 554
deflection, 447–448, 454–459, 492–495, 564
effectiveness, 448
response, 858–860
Runge-Kutta
fourth-order, 631, 899, 901–903, 906–907, 913, 916
second-order, 907–908, 913

S

Sailplane, 280
Scalar potential field, 16
Secant method, 99, 160
Section flap effectiveness, 35–42, 71
Section flap deflection-efficiency, 39–40
Section flap hinge-efficiency, 39–40
Section lift, 2, 48, 59, 71, 74, 91, 106, 137
Section lift coefficient, 3, 26–27, 32–35, 42, 84–85, 91, 106, 137
Segment, 18, 21–22, 82–83, 92
bound, 82, 84, 87, 89
differential, 18, 20, 25
trailing, 82
Semispan, 69–70
Shock, 100
bow, 105
waves, 100, 194
Short takeoff, 387
Short-period, 728, 729, 731, 857
amplitude, 727–728
approximation, 731–736, 739
damped natural frequency, 726, 732
damping, 729, 732, 819, 841–842, 857
damping rate, 732
damping ratio, 840
eigenvalues, 726, 731–733, 861
eigenvectors, 729, 731, 733
frequency, 730, 732, 839–842
handling qualities, 838–842
mode, 721, 726, 728–731, 758, 775, 838
oscillation, 729, 758
period, 726
phase, 727–728
undamped natural frequency, 726
Side force, 2, 178, 185, 187, 281, 284, 339, 343, 349, 443, 445, 450–452, 457, 470, 473, 484
coefficient, 186, 452, 469–470
Sideslip, 178, 185, 441, 445, 463, 468, 476, 480, 484, 492, 765
angle, 187, 441–447, 452–455, 460–463, 470, 473–474, 476, 482, 603, 605, 781
effect of, 464, 475
oscillations, 766
translation, 441
velocity, 443, 474, 476
zero, 447, 454, 456, 473
Sidewash, 446–447, 453, 457, 463, 466–467, 486, 491
angle, 446–447, 453, 463
factor, 466
Sidewash gradient, 447–448, 453, 455, 462, 465–469
induced, 465–466
Sign convention, 69, 496, 531, 922
aircraft position, 922
angles/moments, 69, 74, 441–444, 448–449, 452, 463, 474, 481, 496, 600–601
control forces, 531
control surface, 69, 397, 457, 489, 496–497, 526, 564, 569, 798
Sink, 17–18
rate, 269–270, 279
Singularity, 626, 869–870, 874, 878, 881, 916
gimbal lock, 627, 867–871, 874, 885–887, 916

Sinusoidal
input, 861
oscillation, 862
Slipstream, 115, 139, 141, 168–172, 177, 420, 446–447, 452, 457, 468, 486–487
rotation, 168–169, 174–176, 486
ultimate, 116, 167, 171–173, 175
velocity, 127, 155, 165–166, 171, 174–175
Slipstream effects, 486
Small climb angle approximation, 244–248, 284–286, 294
Small glide angle, 272
Small glide angle approximation, 276
Small thrust angle, 245, 421, 430, 451
Small thrust angle approximation, 229–232, 236, 240, 258, 282
Small-angle approximation, 36–42, 179–184, 228, 283, 349–350, 382, 463, 481
Small-disturbance theory, 638, 640, 644, 648
Sound barrier, 100
Source, 17
negative, 17
panel, 2-D, 18–20
sheet, 18
Span, 2
efficiency factor, 49, 224
finite, 42, 46
infinite, 42
Spanwise
circulation distribution, 71
coordinate, 22
differential section, 85
section lift distribution, 71
symmetric airplane, 443
variation in airspeed, 297–299
vorticity distribution, 376
Spatial vector, 21–22, 82, 84, 87–88
Specific endurance, 254–256
Specific fuel consumption, 121, 249–252, 255, 260–261, 265–266
Specific heat, 192, 195
constant, 195
Specific range, 257–267
maximum, 259–264, 267
Speed of sound, 15, 93–94, 100, 121, 192, 204
Spherical-Earth approximation, 922–923
Spin, 577–580, 584–587
airplane, 577–579, 587, 590
axis, 578
characteristics, 588–589
dynamic parameters of, 583
flat, 577–578, 589
fully developed, 581, 588
initiation, 587
recovery, 577, 587
resistance, 577
steady developed, 586, 589
steep, 577–578, 589
Spiral
amplitude, 772
approximation, 777–785
convergence, 777, 781, 784
damping, 781, 797, 819, 843
damping rate, 779, 781, 819
dive, 589, 774
divergence, 773–774, 777, 781, 784, 843
eigenvalues, 777, 778–780
eigenvectors, 770, 778–781
handling qualities, 843
instability, 774
mode, 766, 770, 773–775, 777–785, 823, 843
stability, 798
Spirit of St. Louis, 118
Spitfire Mark XVII, 120–121, 347, 431–432, 458, 498
Spoilers, 313, 575–576
Stabilator, 347, 568–569
Stability, 339, 346, 351, 396, 407, 518–521
aircraft, 185, 342–343, 396, 407
analysis, 385, 397, 416
augmentation system, 511, 833, 863–864
axes, 653, 655, 687
axes, transformation of, 682–689
derivative, 364, 408
directional, 444
dynamic, 697, 833
lateral static, 441–497
longitudinal static, 339–430
neutral, 340
pitch, 343–347, 356–357, 366, 382, 384, 386, 449, 522
post-stall, 549, 551
ratio, 745, 750–753, 791, 794, 796
roll, 461, 473–475, 480, 795
rotational, 444
static, 339, 342–346, 348, 357, 364, 371, 385–386, 416, 419, 422, 426, 429–430, 441–444, 450, 511, 833
translational, 341–342
weathercock, 444 (*see also* Yaw stability)
yaw, 444–446, 449, 454, 459, 461–462, 466, 468–469, 473, 795, 798
Stabilizer, 79
horizontal, 79–80, 347
vertical, 79
Stable
equilibrium, 339–341, 412

neutrally, 363
unconditionally, 356
Stagnation, 15
conditions, 16, 94, 196, 209
density, 15, 93
flow, 17
point, 17, 30
pressure, 15, 93, 192, 195–197, 203
temperature, 192, 196–197, 200, 203–204, 207–208, 211
Stall, 11, 38, 41, 87, 91, 231, 244, 279, 286–289, 342, 345–346, 355, 364, 549, 577
airplane, 577
asymmetric, 577
deep, 553
limit, 292
negative, 411, 413
positive, 411, 413
recovery, 549
shallow, 554
wake, 554
wingtip, 53, 297–299
Stall speed, 279, 288, 313, 392, 394–395
level flight, 279
Standard sea level, 8, 154, 159, 193, 225, 230–233, 237, 241–244, 249, 294, 320, 357
State variable response vector, 849, 852
Static equilibrium, fundamentals, 339
Static gain, 862
Static instability, 366
Static margin, 362–367, 387, 392–394, 419, 424–425, 511, 519, 548
Static pressure taps, 34
Static stability, 339, 342–346, 348, 357, 364, 371, 385–386, 416, 419, 422, 426, 429–430, 441–444, 450, 511, 833
fundamentals, 339
lateral, 441, 443
longitudinal, 339, 443
pitch, 381, 395, 444–445
Static thrust, 133, 154–159
Static-radial configuration, 118
State space approach, 863
State variable, 640
Steady flight, 13–14
Steady climbing flight, 239–240, 317
Steady coordinated turn, 281–299, 554, 555–557, 560, 563, 579, 806–807
Steady level flight, 222–225, 229–233, 236–237, 241–245, 249–252, 255, 257, 260, 268, 279, 320, 339
Steady level turning flight, 284
Step function, 853, 854
Step response, 852
Stick-fixed dynamic response, 825, 844, 861
Stick-fixed lateral dynamics, 823
Stick-fixed maneuver margin, 510
Stick-fixed maneuver point, 510–511, 514, 537
Stick-fixed neutral point, 362–365, 419, 511, 536
Stick-fixed static margin, 364
Stick-free maneuver point, 535, 537
Stick-free neutral point, 535–537
Strakes, 821, 865
Streamline, 24, 105, 164–165, 171
Streamtube, 164–165, 168–171
Strip theory, 490
Structural flexibility, 514
effects of, 514–523
Structural limit, 285, 289
Subsonic
airspeed, 117, 127, 130
flight, 194, 202
Supersonic, 81
aircraft, 100, 107
airspeed, 106, 126, 215
flight, 105, 194, 202
flow, 96–101, 105
Supersonic airfoil theory, 107
Sweep, 48, 51, 79–83, 87, 89–91, 413, 460, 463, 487
angle, 80–81, 377–378
back, 482
factor, 378, 380, 388
forward, 482
variation, 81
Symmetric
airfoil, 22, 26, 105, 107, 280, 346, 350–355
flight condition, 343
spanwise, 68–76

T

Tail, 346–362, 506
design, 468–469
effect of position, 465
efficiency, 350
lift coefficient, 350
position factor, 375
sidewash factor, 465
volume, 356
volume ratio, 357
Tail boom stiffness, 520
Tailplane, 347
Takeoff, 299–327
acceleration phase, 300, 302
distance, 12, 221
FAR, 315–317, 320, 323–326
performance, 299

Taper
linear, 61–62
ratio, 50–51, 53, 58–60, 373, 479
Temperature, 95, 104, 122, 191–192, 199–204
ambient, 199, 207
atmospheric, 10
freestream, 192
gradient, 7, 15
local, 103
ratio, 105, 192
stagnation, 192, 196–197, 200, 203–204, 207–208, 211
static, 197
turbine inlet, 128–129, 199–202, 210, 214
Thermal efficiency, 198–212
Thermodynamic cycle analysis, 190, 203, 208
Thickness, 10, 23, 24, 26, 33–35, 38, 41, 90, 105–107
airfoil, 24, 26, 34, 41
distribution, 24, 33, 35
finite, 34
maximum, 23–24
Thin airfoil approximation, 33
Thin airfoil theory, 24–42, 658–659
Thomas algorithm, 711
Throttle setting, 241, 260
Thrust, 115, 130, 138, 143–144, 151–153, 158, 165–167, 173–177, 183–184, 221–222, 229–231, 279, 283, 294–296, 300–302, 420, 427, 450
angle, 133, 224, 227–232, 236, 240–241, 258, 282, 300
asymmetric, 339
available, 190–191, 230, 235, 239–241, 244–245, 260, 295, 320
coefficient, 151, 154, 158, 160, 163, 176, 186, 421–422
equilibrium, 421
fraction, 451
full throttle, 230
installed, 190, 194
maximum, 156, 300
moment, 397
normal, 239
specific, 199–207, 210–211, 213
required, 222–234, 258, 282, 320
reversal, 313–314, 317
static, 133, 154–159
uninstalled, 191, 194, 198–199, 204, 210
vector, 222, 228, 241, 244–245, 343, 348, 397, 404–405, 408, 410, 415
vectoring, 554, 865
Thrust-specific fuel consumption, 123, 128, 130
Thrust-to-weight ratio, 117, 128, 199, 207, 230–231, 239, 241, 244, 246, 268, 425
Time constant, 700
Time domain, 852
response, 861
Time to double amplitude, 718, 773–774, 843
Time to half amplitude, 700
Torque, 133, 138, 143–144, 168–170, 174–175, 184
coefficient, 144, 146, 186
Torsional pendulum, 756–757
Torsional stiffness, wing, 565, 567
Total aircraft weight, 241
Trailing edge, 4, 22, 29–30, 43, 346
reflexed, 346
Trailing vortex sheet, 43–44, 46, 79, 81–83, 141, 161, 375
Trailing vortex filaments, 46
Trailing-edge flap, 35–42, 47, 68
Transfer function, 848, 852, 861–863
matrix, 848–849, 851
Transformation, 623
direction cosine, 627
equations, 605
Euler angle, 627, 881, 891, 916
inverse, 605–606, 853
matrices, 623
quaternion, 627
Transition phase, 317, 319
Translational coupling, 810
Transonic, 100, 659
Trim, 339–346, 348–364, 367–372, 380–401, 404–413, 416, 420, 422, 426, 429–430, 443, 568
analysis, 386, 416
lateral, 441–497
longitudinal, 339–430
level, 361
requirement, 405
residual equations, 406
stability, 385–386, 429–430
stable, 341, 345–346, 350
static, 495
tab, 523, 525–526
Trim point
conventional, 552–553
deep-stall, 552–553
Truncation error, 907, 911, 912
T-tail configuration, 469, 472, 485, 554
Turbine, 122, 128, 130, 190, 203, 207–208, 210
inlet, 197, 200, 207, 211
outlet, 203, 208
Turbofan, 115, 117, 126–128, 130, 207–215, 268, 302, 426–430

Turbomachinery, 128
Turboprop, 128–130
Turbojet, 115, 117, 122–128, 190–200, 203–204, 207, 210–211, 214, 230, 232, 236–237, 244, 248, 265, 302, 320, 323, 426–430
  afterburner, 203–207
  cycle analysis, 195–203
  thrust equation, 190–195
Turbulence, 411
Turbulent mixing, 426
Turbulent shear layer, 426
Turn, 221, 281–284, 291, 296–299
  axis, 297
  coordinated, 284–286, 290–293, 299, 806, 807, 816–817
  dynamic, 296
  level, 283, 285, 289, 294–295
  level coordinated, 283–286, 293
  steady, 282, 295
  steady coordinated, 281–285, 291
  steeply climbing, 294–296
Turning radius, 12, 282–286, 289–298, 560
  load-limited, 289–290
  minimum, 289–299
  short, 293
  stall-limited, 289–290, 298
Turning rate, 291, 295, 560
  load-limited, 291–292
  maximum, 291–293, 295, 298
  stall-limited, 291–292
Twist, 47–51, 131, 373, 375, 463 (*see also* Washout)
  aerodynamic, 47–51, 53–54, 59, 68, 478–479
  blade, 131
  geometric, 47–48, 51, 80, 90, 478–479
  wing, 53–68
Twisting moment, 566

U
Ultimate slipstream velocity, 165–166, 171, 174–175
Undamped natural frequency, 699, 702, 720, 723, 750, 768, 771
  Dutch roll, 772, 796
  lateral mode, 768
  phugoid/long period, 727, 738, 745, 750
  short-period, 726
Uniform flow, 14, 16–18, 24, 28, 30, 84, 93, 95, 168–171, 174, 191
Untwisted, 49–52, 62
Upwash, 80, 139, 384, 388, 422, 428, 483
  angle, 382, 384–385, 388, 423
  gradient, 385, 388

V
Variable, 6
  change of, 6, 24, 26–28, 53, 89, 95–97, 101
  disturbance, 641
  state, 640
Vector, 2, 65, 80, 86
  addition, 92
  calculus, 12
  circulation, 480
  correction, 87
  differential aerodynamic force, 45
  differential vortex length, 45
  dimensionless aerodynamic moment, 89
  dimensionless vortex strength, 87
  field, 16–17
  fluid velocity, 12, 103
  freestream velocity, 96, 101
  lift, 46, 74, 135, 138–139, 182, 281
  net aerodynamic force, 92
  net aerodynamic moment, 92
  notation, 12
  spatial, 21–22, 82, 84, 87–88
  thrust, 222, 228, 241, 244–245, 343, 348, 397, 404–405, 408, 410, 415
  total aerodynamic force, 87
  unit, 1–2, 17, 22, 82–85, 88, 92, 95
  velocity, 12–14, 21–22, 45, 83, 92, 95–96, 103, 135, 178, 232
  vorticity, 83, 141, 480
Velocity, 14, 16, 30–31, 84, 94–96, 103, 115, 127, 131, 144, 165, 170, 177–179, 192, 194, 198 (*see also* Airspeed)
  angular, 133, 135, 144, 169–178, 291
  axial, 169–170, 173, 177, 191
  characteristic, 144
  circumferential, 169, 171
  corner, 288 (*see also* Maneuvering speed)
  disturbance, 702 (*see also* Perturbation)
  downwash, 353, 371–373
  exhaust gas, 126, 207, 429
  exit, 204
  field, 14, 17, 93–94
  flow, 165
  fluid, 13, 45, 137, 165, 169–170
  forward, 135, 137, 141, 178
  freestream, 2, 13, 17, 31, 44, 47, 95–98, 101, 115–116, 144, 165–166, 169, 184, 198, 348, 353, 371, 373, 382, 396, 429, 480
  gradient, 15
  increment, 117, 121, 126, 155, 207
  induced, 18–22, 28–31, 44, 82–84, 134–138, 141–142, 147, 161, 164–169, 176, 178, 480
  inlet, 126

liftoff, 309
local, 94, 103
normal, 21, 30
perturbation, 95–96, 103 (*see also* Disturbance)
potential, 14, 93–96
potential field, 17
radial, 171–172
ratio, 236–237, 246–248, 256, 265, 267, 276–277, 429
rotational, 144, 637
sideslip, 443, 473, 476
slipstream, 127, 155, 165–166, 171, 174–175
tangential, 21, 30
translational, 637
vector, 12–14, 21–22, 45, 83, 92, 95–96, 103, 135, 178, 232
vector field, 16–17
Vertical offset, 396
effects of, 396–416
Vertical stabilizer, 469, 484, 491
dihedral effect, 488
Vertical tail, 346, 445, 447–449, 452, 457, 461–466
estimate lift slope for, 469–473
estimate sidewash gradient on, 462–469
volume ratio, 448
Viscous effects, 26, 33, 35, 44, 79, 91, 108
Viscous flow analysis, 34
V-n diagram, 287–288
Volume
control, 115–116, 190–191
characteristic, 356
tail, 356
Vortex, 20, 43–44, 79, 82, 84, 139, 141
blade-tip, 139–141, 177
filament, 21, 42, 44–46, 141
force, 45
forebody, 820–822
helical trailing, 139, 141, 142
horizontal tail, 821
horseshoe, 81–84, 86–89, 90
induced flow, 140
lift, 821
lifting law, 44–46, 48, 84, 139, 371, 462, 480
line segment, 3-D, 21
model, 79, 373, 376, 449, 462, 466, 469
panel, 2-D, 20–21
panel, flat, 28
panels, 29–32
segment, 21–22, 82
shedding, 821
sheet, 24–25, 28, 30, 42–44
sheet, curved, 28
sheet, trailing, 43–44, 46, 79, 81–83, 141, 161, 375
sheet, trailing helical, 142
span factor, 372, 374, 376, 463
strake, 821
strength, 21–25, 28–31, 42, 45, 82–83, 86–89, 371–372, 462–463
strength factor, 372, 374, 376
trailing, 301, 352
vertical tail, 821
wake, 821–822
wingtip, 43–44, 79, 139, 371–372, 375, 377, 446–449, 462, 464, 821
Vortex panel method, 28, 32–35, 38–41, 353, 539
Vortex segment, 21–22, 82
bound, 82, 84, 90
straight, 21–22, 84
straight semi-infinite, 22
trailing, 82–83
Vorticity, 12–13, 44, 79, 83, 139, 141, 371
bound, 46, 81, 139, 376, 480
distribution, 45, 375–376
free, 82
net, 82
shed, 89, 134, 139, 376
vector, 83, 141, 480
V-tail, 573–574

W

Wake, 11, 585
blade, 161
boundary layer, 12
trailing, 12
ultimate, 161
viscous, 161
Washout, 47, 53–71, 373, 413 (*see also* Twist)
distribution, 53–71, 76, 78
distribution function, 53, 58, 65, 67
effectiveness, 56, 61
elliptic, 78
geometric, 131
linear, 55–56
maximum total, 53
negative, 58
optimum, 58, 60–61, 76–78
positive, 58, 60
spanwise symmetric, 72
symmetric, 70
total, 53, 58, 62
Weathercock stability, 444 (*see also* Yaw stability)
Weight, 222–224, 227, 229, 234, 239, 242, 252–254

aircraft, 241, 254, 284, 318
coefficient, 508
constant, 227, 274, 301
gross, 221–224, 229, 252–254, 261–263, 274, 276, 280–281, 284, 288–289, 307
Weight-shift control, 370
Whip-stall, 387
Wind
direction, 257
local relative, 348
speed, 257–258, 271, 275
-track angle, 257, 270
Wind tunnel model, 799–800, 802
Wind tunnel test, 753, 755
Windmilling, 151
Wing
area, 221, 227, 280, 307, 345, 349
cambered, 343–346
-canard combination, 381–382, 385–387, 394–397
elliptic, 44, 49–50, 53, 58, 62, 73, 372–373, 377, 380, 463, 478
finite, 21, 42–45, 50, 54, 79, 82, 84, 134, 352, 480
finite lifting, 79
lift coefficient, 350
loading, 226, 234–235, 237, 272–275, 279–280, 293, 297, 299
planform, 56, 58, 68, 73, 76
quarter-chord, 352, 356, 361–362, 367–369, 377, 388
rectangular, 47, 68
rock, 821–823
sweep, 551
sweep factor, 378
swept, 376–377, 461
tapered, 50–61, 68, 73, 373, 377, 463, 479
twist, 53–68 (*see also* Washout)
unswept, 62, 373, 445, 459, 463
Wing dihedral, 475–476, 479, 487
effect of, 475
Wing sweep, 479–482
effect of, 479
Wing-canard, 381–382, 385–387, 394–397, 408
Wing-canard combination
simplified pitch stability analysis, 381–396
Winglet, 449, 469
Wing-tail, 346, 363–369, 380, 382, 397–400, 405, 466
Wing-tail combination
Simplified pitch stability analysis, 346–362
Wingtip, 42–43
stall, 53, 297–299
vortex, 43–44, 79, 371–372, 375–376, 446–449, 462, 464, 821
Wright Flyer, 117, 130
Wright R-3350-23 Cyclone, 120
Wright Whirlwind, 118–119

X

X-3 Stiletto, 467
XB-70, 125

Y

Yaw, 2, 74, 299, 339, 342, 450, 620–621, 765
adverse, 77, 299, 492–493, 575
constraint, 892
control, 448, 492, 576, 577, 588, 821, 847 (*see also* Rudder; V-tail)
control derivative, 448, 456
coupling, 796
damping, 798, 859
disturbance, 444, 784
divergence, 819–820
rate, 626, 776
stiffness, 444, 448
trim, 444, 454
Yaw-damping derivative, 564, 666, 797, 804
Yaw stability, 444–446, 448–450, 453–455, 459, 460–462, 466, 468–469, 473, 795, 798
derivative, 444–445, 448, 449, 453, 455, 459–461, 468, 475, 487, 797, 804
excess, 784
insufficient, 784
ratio, 795
Yawing, 2
moment, 2, 74, 76–77, 134, 178, 186–187, 339, 343, 349, 441–445, 448–454, 457, 459, 473–475, 481–485, 489–492, 587, 765
moment gradient, 452
motion, pure, 802–803, 893
oscillations, 766
rate, 560, 577, 765
rotation, 441

Z

Zero lift, 55, 226, 229
Zero-lift angle of attack, 26–27, 36–38, 47, 55, 132, 146–147, 352, 384
Zero-lift line, 131–132, 135, 137, 147, 180, 348, 456, 493